Design Aids in Soil Mechanics and Foundation Engineering

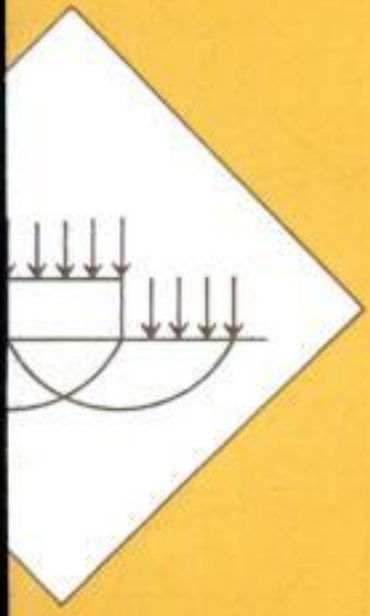

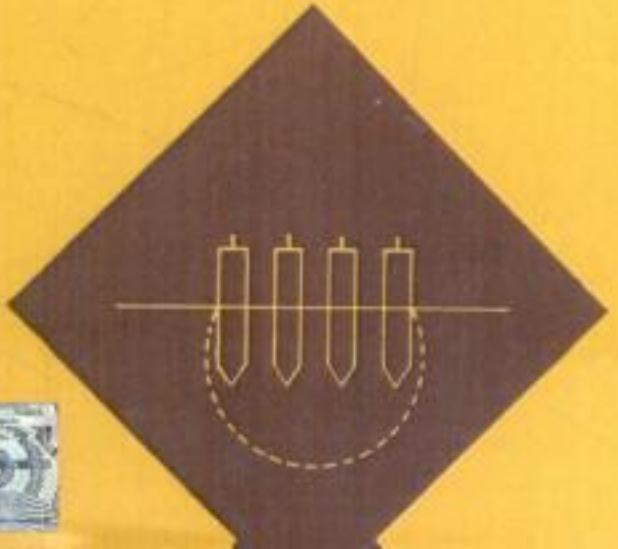

SHENBAGA R KANIRAJ

Design Aids in
SOIL MECHANICS AND
FOUNDATION ENGINEERING

Design Aids in SOIL MECHANICS AND FOUNDATION ENGINEERING

Shenbaga R Kaniraj
Indian Institute of Technology
Delhi

TATA McGRAW-HILL
Publishing Company Limited
NEW DELHI

McGraw-Hill Offices
New Delhi New York St Louis San Francisco Auckland Bogotà
Guatemala Hamburg Lisbon London Madrid Mexico Milan Montreal
Panama Paris San Juan São Paulo Singapore Sydney Tokyo Toronto

Tata McGraw-Hill

Tenth reprint 2008
RDALCRYXDZZLB

ISBN-13: 978-0-07-451714-7
ISBN-10: 0-07-451714-7

Published by Tata McGraw-Hill Publishing Company Limited,
7 West Patel Nagar, New Delhi 110 008, and printed at
Sai Printo Pack Pvt. Ltd., New Delhi 110 020

The McGraw-Hill Companies

To

Mangalam
Samrat
Samyukth 5

PREFACE

"Why shouldn't I write a book?" The question haunted me for several years, born out of the conviction that there still was scope in India to write a book on soil mechanics and foundation engineering for designers. Convinced rather erroneously, as some might say and as I too realised soon! "Most of the books published in India have their prime target as the undergraduate students. Engineers depend mainly on these books for design. A book addressed to undergraduate students is, perforce, limited in scope, content and presentation. But the designers are a different kettle of fish altogether. They need current and advanced information, preferably in an easily digestible capsule form. And definitely they don't need to pass any examination!" So went my thoughts reinforcing my convictions and I began to sift information and assemble them together for a possible book in the distant future. When one does that, he reads more books and starts looking at them from a different perspective. I soon turned around and started questioning myself, "Why should I write a book?" The apprehensions became menacing, every time after I came across an excellently written book, of which there happened to be many, from abroad. But the persisting desire to organise and present the information in the manner I liked best made me persevere and complete the exercise. Having tendered my apologies for "Why the book" let me proceed to explain "What it is".

The book may be divided into two parts. The first nine chapters which constitute about one-fourth of the book belong to soil mechanics, and the rest to soil engineering. In both parts, emphasis is laid on problem solving. However, the principles and assumptions involved in the design steps and equations are invariably presented in such an order that the user would be able to appreciate the solutions better and understand their limitations too.

The *soil mechanics* part begins with the fundamental definitions in Chapter 1. The engineering classification of soil, the index properties required for the same, and the engineering use of soil classification are explained in Chapters 2 and 3. The engineering behaviour of soils and their engineering properties are presented in Chapters 4 through 9. Engineering properties such as permeability and strength are described. The methods of determining the different parameters, their range of values for different soil types and their selection are explained. This information, it is hoped, would help designers in better interpretation of soil investigation reports, and in judicious selection of the parameters required for design.

The *soil engineering* part of the book, Chapters 10 to 20, caters to a wide variety of problems faced in the design of shallow foundations, pile foundations, earth retaining structures, slopes, and machine foundations. In soil engineering design, one often comes across a bewildering variety of solutions ranging from an intricate finite element analysis to an unsophisticated empirical equation. Not only that, even within a particular kind of

approach itself, there are dissimilar and vastly varying recommendations. The spectrum at times may be so vast that the conservatives, the moderates and the radicals in design offices can all be at ease with the spread before them. However, an ordinary designer is ordinarily confused. The very nature of the material with which one deals with in soil engineering makes it imperative that differing recommendations be made. Soil is a natural material, highly variable, and affected by numerous factors so that, even for a simple problem, it is far too difficult to account for all these comprehensively and yet look for a unique solution. This sometimes gives rise to a feeling among fellow civil engineers that anything and everything is all right in soil engineering! This view would be an abdication of responsibility by the designer. Time and again, it has been stressed that the designer should draw upon his experience in such situations and make a sound engineering judgement. As is rightly said, "It is not the function of the designers to compute accurately, but to judge correctly!" It may appear at times that after presenting widely varying recommendations, the book leaves a situation open-ended. It is expected that in such instances the designer will make a judicious choice based on his experience and the facts before him. However, it is visualised that the more reliable and useful of the recommendations will stand the test of time and, eventually, the scatter will narrow down to a manageable range.

I have used, partly and substantially, the contents of the book to teach undergraduate courses on Soil Mechanics, Earth and Earth Retaining Structures and postgraduate courses on Foundation Engineering, Flow Through Porous Media, Soil Dynamics and Machine Foundations. Though intended primarily for designers, the teachers and students as well may find the book useful.

Many have rendered valuable help in the preparation of the book. I gratefully acknowledge their services. Prof. A P Gupta, IIT Kharagpur and Prof. A Varadarajan, IIT Delhi reviewed parts of the manuscript and offered their comments. Mr R Nagarajan typed the entire manuscript with a commendable degree of excellence. Mr N L Arora, and Mr Rajvir Agarwal drew all the figures with the touch of their professional competence. The Curriculum Development Cell of the Civil Engineering Department at the Indian Institute of Technology, Delhi financially supported the preparation of the book.

Credit is due to Prof. B V Ranganatham, Civil Engineering Department, Indian Institute of Science, Bangalore, who in the late sixties inducted the rather unwilling author into the realms of soil mechanics and foundation engineering and inculcated in him a sense of critical inquiry.

Full marks to the woman behind the man, Mangalam, and our boys, Samrat and Samyukth! The efforts were all very ably supported, shared and enjoyed by them. They all proved to be great proofreaders! I very fondly dedicate this book to them.

SHENBAGA R KANIRAJ

CONTENTS

SI UNITS

The Systéme International d'Unités—The International System of Units, abbreviated as SI Units, is being increasingly used by engineers. The following gives some fundamental definitions and factors for conversion of metric units into SI units and vice versa.

Definitions

Newton (N) is that force which, when applied to a mass of 1 kg gives it an acceleration of 1 m/s^2.

Pascal (Pa) is the pressure produced by a force of 1 N applied, uniformly distributed, over an area of 1 m^2.

1 kPa = 1000 Pa

Conversion Factors

To convert metric	Into SI	Multiply by	Conversely multiply by
kg	N	9.807	0.1020
T	kN	9.807	0.1020
kg/m^3	Pa	9.807	0.1020
kg/cm^3	kPa	98.07	0.0102
T/m^3	kPa	9.807	0.1020
kg m	Nm	9.807	0.1020
Tm	kNm	9.807	0.1020
g/cm^3	kN/m^3	9.807	0.1020
T/m^3	kN/m^3	9.807	0.1020

1

FUNDAMENTAL DEFINITIONS, RELATIONSHIPS AND INTER-RELATIONSHIPS

For engineering purposes soil is considered as the natural product of weathering of rocks which forms the outer crust of earth. It is an aggregate of mineral grains and may occur with or without organic constituents.

Soil is a three-phase material. In any given volume of soil we can generally find some solid particles, some moisture and some air voids. If there is no moisture present then it is a *dry* soil. If the air voids are completely occupied by water it is called a *saturated* soil. Soils in which water does not completely fill the voids are known as *unsaturated* soils. In a schematic representation of the three phases of soil, the volume or weight of each phase is lumped together and shown separately, as in Fig. 1.1.

1.1 DEFINITIONS AND FUNDAMENTAL RELATIONSHIPS

1.1.1 Volume-Volume Relationships

The three volume-volume relationships are: (i) void ratio, (ii) porosity, and (iii) degree of saturation.

Void ratio,
$$e = \frac{V_v}{V_s} \tag{1.1}$$

The terms V_v and V_s are explained in Fig. 1.1.
Void ratio is greater than zero and can be greater than 1. Table 1.1 gives typical values of void ratio for different types of soil. The values are indicative of the large variation of e in different types of soil and may not be construed as unique representative values. In natural soils void ratio should be determined by appropriate tests.

Porosity,
$$n = \frac{V_v}{V} \tag{1.2}$$

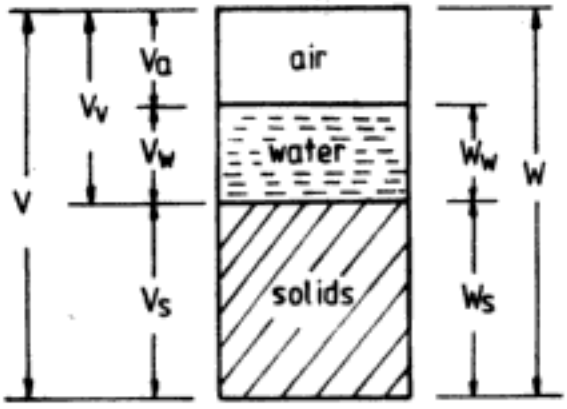

In a given volume of soil :

V = Total volume of soil = $V_a + V_w + V_s$

V_a = Volume of air

V_w = Volume of water

V_s = Volume of solids

V_v = Volume of voids = $V_w + V_a$

W = Total weight of soil = $W_w + W_s$

W_w = Weight of water in voids

W_s = Weight of solids

Air can be considered weightless

Fig. 1.1 Three phases of soil

Table 1.1 Typical Values of Void Ratio, Saturation Water Content and Densities

Soil description	Void ratio e	Saturation water content w_{sat}, %	Density γ_d g/cc	Density γ_{sat} g/cc
Dense, uniform sand	0.50	19	1.75	2.10
Loose, uniform sand	0.85	32	1.43	1.90
Dense, mixed grained sand	0.42	16	1.86	2.16
Loose, mixed grained sand	0.66	25	1.59	2.00
Windblown silt (loess)	0.99	21	1.36	1.86
Soft clay (glacial)	1.20	45	1.22	1.77
Soft slightly organic clay	1.90	70	0.93	1.58
Soft very organic clay	3.0	110	0.68	1.43
Soft Bentonite	5.2	195	0.43	1.27

Porosity is also greater than zero, as there are always some voids present in the soil, but it is always less than 1 since volume of voids cannot exceed the total volume itself.

Degree of saturation, $$S = \frac{V_w}{V} \tag{1.3}$$

Degree of saturation varies between 0 and 1.

$S = 0$	dry soil ($V_w = 0$)
$S = 1$	saturated soil ($V_w = V_v$)
$0 < S < 1$	unsaturated soil

Degree of saturation is also often expressed in per cent.

Then, $$S\% = \frac{V_w}{V_v} \times 100 \tag{1.4}$$

S in per cent varies from 0 to 100.

$S = 0\%$	dry soil
$S = 100\%$	saturated soil
$0\% < S < 100\%$	unsaturated soil

1.1.2 Weight-Volume Relationships

The two weight-volume relationships are (i) *total density* or *bulk density*, and (ii) *dry density*.

Total or bulk density, $$\gamma_t = \frac{W}{V} \tag{1.5}$$

Typical values of γ_t for granular soils are shown in Table 4.5. γ_t is also referred to as wet density or moist density.

Dry density, $$\gamma_d = \frac{W_s}{V} \tag{1.6}$$

Tables 1.1 and 4.4 give typical values of γ_d.

A particular case of total density is when the soil is saturated. The total density when $S = 1$ is known as *saturated density*, γ_{sat}. Typical values of γ_{sat} are given in Table 1.1.

Another density of interest is the *submerged* or *buoyant density*, γ_b. This is the density of soil below groundwater level or when the soil is submerged in water. γ_b is given by the relationship,

$$\gamma_b = \gamma_t - \gamma_w \tag{1.7}$$

where γ_w is the density of water which can be taken as 1 g/cc or 1 T/m^3 in engineering calculations. Mostly soils submerged in water are saturated. Then γ_t in Eq. 1.7 is replaced by γ_{sat}. That is, for saturated soils,

$$\gamma_b = \gamma_{sat} - \gamma_w \tag{1.8}$$

1.1.3 Weight-Weight Relationship

The only important weight-weight relationship is *water content*, which is defined as,

$$w\% = \frac{W_w}{W_s} \times 100 \tag{1.9}$$

Water content is generally expressed in per cent. Value of water content can be rounded off to the nearest whole number without affecting the accuracy of results. For dry soils $w = 0$. The water content at which a given soil will become saturated is known as *saturation water*

content, w_{sat}. Table 1.1 gives typical values of w_{sat} for different soils. The value of water content can exceed 100%, as per definition in Eq. 1.9.

1.2 INTER-RELATIONSHIPS

By simple mathematical manipulations inter-relationships between the fundamental relationships given in Eqs. 1.1 to 1.9 can be established. Some of the commonly used inter-relationships are given below:

$$n = \frac{e}{(1 + e)} \tag{1.10}$$

$$w = \frac{Se}{G_s} \tag{1.11}$$

where G_s is the specific gravity of soil solids.

$$G_s = \frac{W_s}{V_s \gamma_w} \tag{1.12}$$

Table 1.2 gives values of G_s for different soil types. For inorganic soils G_s varies from 2.6 to 2.7 and in these soils G_s can be taken as 2.65.

Table 1.2 Typical Values of G_s (Specific Gravity of Solids)

Soil type	G_s
Quartz sand	2.64–2.65
Quartzite	2.65
Silt	2.68–2.72
Silt with organic matter	2.40–2.50
Loess	2.65–2.75
Lime	2.70
Clay	2.44–2.92
Kaolin	2.47–2.58
Chalk	2.63–2.81
Bentonite clay	2.34
Peat	1.26–1.80
Humus	1.37

Some other useful inter-relationships are,

$$S = \frac{(w\gamma_t)}{[n(1 + w)\gamma_w]} \tag{1.13}$$

$$w_{sat} = \left(\frac{1}{\gamma_d} - \frac{1}{G_s\gamma_w}\right)\gamma_w \tag{1.14}$$

$$\gamma_t = \frac{(Se + G_s)}{(1 + e)}\gamma_w \quad S \textit{ not} \text{ in } \% \text{ but varies from 0 to 1} \tag{1.15}$$

$$\gamma_t = \frac{(1 + w)}{(1 + e)} G_s \gamma_w \qquad w \textit{ not} \text{ in } \% \tag{1.16}$$

$$\gamma_d = \frac{\gamma_t}{(1 + w)} \qquad w \textit{ not} \text{ in } \% \tag{1.17}$$

$$\gamma_b = \frac{(G_s - 1) + (S - 1)e}{1 + e} \gamma_w \tag{1.18}$$

S *not* in % but varies from 0 to 1

More such inter-relationships are given in Table 1.3.

Q 1.1: A saturated soil sample has a water content of 49 per cent. If specific gravity of solids is 2.7, compute the void ratio, porosity and the saturated density of soil sample.

Ans: To compute void ratio, use Eq. 1.11 in which $S = 100\%$

$$e = \frac{49}{100} \times 2.7 = 1.32$$

From Eq. 1.10, porosity is

$$n = \frac{1.32}{1 + 1.32} = 0.57$$

Saturated density can be calculated using Eq. 1.15 with $S = 1$ and $\gamma_w = 1$ g/cc

$$\gamma_{sat} = \frac{(1.32 + 2.7)}{(1 + 1.32)} \times 1$$

$$= 1.73 \text{ g/cc} = 1.73 \text{ T/m}^3$$

Alternatively γ_{sat} can also be calculated using Eq. 1.16.

Q 1.2: A 10-cm diameter and 30-cm long soil sample extracted from ground weighs 4.125 kg. A moist specimen of the sample weighs 12.7 g and after oven drying 9.2 g. Specific gravity of solids = 2.65. Determine the (i) total density, (ii) water content, (iii) void ratio, (iv) degree of saturation, and (v) the dry density of the soil sample.

Ans: Volume of soil sample, $V = \pi \times \frac{10^2}{4} \times 30$

$$= 2356.2 \text{ cm}^3$$

(i) Total weight of soil sample, $W = 4125$ g

Total density, $\gamma_t = \frac{4125}{2356.2} = 1.75$ g/cc

(ii) Initial weight of specimen = 12.7 g

Dry weight = Weight of solids = $W_s = 9.2$ g

Weight of water = $W_w = 12.7 - 9.2 = 3.5$ g

Water content = $w = \frac{3.5}{9.2} = 0.38$ or 38%

Table 1.3 Inter-relationships between Physical Quantities
(Adapted from Jumkis, A.R., **Soil Mechanics**, pp 90–91, D.Van Nostrand Co. Inc., Princeton, New Jersey)

Given γ_w and:	To obtain: Specific gravity G_s	Dry density γ_d	Saturated density γ_{sat}	Saturation water content w_{sat}	Porosity n	Void ratio e	Remarks
G_s; γ_d			$\left(1-\frac{1}{G_s}\right)\gamma_d+\gamma_w$	$\left(\frac{1}{\gamma_d}-\frac{1}{G_s\gamma_w}\right)\gamma_w$	$1-\frac{\gamma_d}{G_s\gamma_w}$	$\frac{G_s\gamma_w}{\gamma_d}-1$	
G_s; γ_{sat}		$\frac{\gamma_{sat}-\gamma_w}{G_s-1}G_s$		$\frac{G_s\gamma_w-\gamma_{sat}}{(\gamma_{sat}-\gamma_w)G_s}$	$\frac{G_s\gamma_w-\gamma_{sat}}{(G_s-1)\gamma_w}$	$\frac{G_s\gamma_w-\gamma_{sat}}{\gamma_{sat}-\gamma_w}$	
G_s; w; S		$\frac{SG_s}{S+wG_s}\gamma_w$	$\frac{1+(w/S)}{S+wG_s}G_s\gamma_w S$	w/S	$\frac{wG_s}{S+wG_s}$	wG_s/S	w and S both in % or both not in %
G_s; n		$G_s(1-n)\gamma_w$	$[G_s-n(G_s-1)]\gamma_w$	$\frac{n}{G_s(1-n)}$		$\frac{n}{1-n}$	
G_s; e		$\frac{G_s}{1+e}\gamma_w$	$\frac{G_s+e}{1+e}\gamma_w$	$\frac{e}{G_s}$	$\frac{e}{1+e}$		
γ_d; γ_{sat}	$\frac{\gamma_d}{\gamma_w+\gamma_d-\gamma_{sat}}$			$\frac{\gamma_{sat}}{\gamma_d}-1$	$\frac{\gamma_{sat}-\gamma_d}{\gamma_w}$	$\frac{\gamma_{sat}-\gamma_d}{\gamma_w+\gamma_d-\gamma_{sat}}$	
γ_d; w; S	$\frac{S\gamma_d}{S\gamma_w-w\gamma_d}$		$\left(1+\frac{w}{S}\right)\gamma_d$	w/S	$\frac{w}{S}\frac{\gamma_d}{\gamma_w}$	$\frac{w\gamma_d}{S\gamma_w-w\gamma_d}$	w and S both in % or both not in %
γ_d; n	$\frac{\gamma_d}{(1-n)\gamma_w}$		$\gamma_d+n\gamma_w$	$\frac{n\gamma_w}{\gamma_d}$		$\frac{n}{1-n}$	
γ_d; e	$(1+e)\frac{\gamma_d}{\gamma_w}$		$\frac{e\gamma_w}{1+e}+\gamma_d$	$\frac{e}{1+e}\frac{\gamma_w}{\gamma_d}$	$\frac{e}{1+e}$		
γ_{sat}; w_{sat}	$\frac{\gamma_{sat}}{\gamma_w-w_{sat}(\gamma_{sat}-\gamma_w)}$	$\frac{\gamma_{sat}}{1+w_{sat}}$			$\frac{w_{sat}\gamma_{sat}}{(1+w_{sat})\gamma_w}$	$\frac{w_{sat}\gamma_{sat}}{\gamma_w-w_{sat}(\gamma_{sat}-\gamma_w)}$	w_{sat} not in %
γ_{sat}; n	$\frac{\gamma_{sat}-n\gamma_w}{(1-n)\gamma_w}$	$\gamma_{sat}-n\gamma_w$		$\frac{n\gamma_w}{\gamma_{sat}-n\gamma_w}$		$\frac{n}{1-n}$	
γ_{sat}; e	$(1+e)\frac{\gamma_{sat}}{\gamma_w}-e$	$\gamma_{sat}-\frac{e}{1+e}\gamma_w$		$\frac{e\gamma_w}{\gamma_{sat}+e(\gamma_{sat}-\gamma_w)}$	$\frac{e}{1+e}$		
w; n; S	$\frac{Sn}{(1-n)w}$	$\frac{nS}{w}\gamma_w$	$n\frac{1+(w/S)}{(w/S)}\gamma_w$	w/S		$\frac{n}{1-n}$	w and S both in %
w; e; S	$\frac{Se}{w}$	$\frac{Se}{(1+e)w}\gamma_w$	$\frac{Se}{w}\frac{(1+w/S)}{(1+e)}\gamma_w$	w/S	$\frac{e}{1+e}$		or both not in %

(iii) Rearranging Eq. 1.16

$$e = \frac{(1 + w)}{\gamma_t} G_s \gamma_w - 1$$

$$= \frac{(1 + 0.38)}{1.75} \times 2.65 \times 1 - 1$$

$$= 1.09$$

(iv) From Eq. 1.11

$$S = \frac{G_s w}{e}$$

$$= \frac{2.65 \times 0.38}{1.09}$$

$$= 0.92 \quad \text{or} \quad 92\%$$

(v) Using Eq. 1.17

$$\gamma_d = \frac{1.75}{1 + 0.38} = 1.27 \text{ g/cc}$$

Q 1.3: A soil in its natural state has a void ratio of 0.65 and a water content of 21 per cent. Specific gravity of solids is 2.65. How many additional litres of water per cubic metre of soil is needed to make it a saturated soil with no change in void ratio?

Ans. Using Eq. 1.11, the saturation water content of soil is

$$w_{sat} = \frac{1 \times 0.65}{2.65}$$

$$= 0.245 \quad \text{or} \quad 24.5\%$$

The total density of soil at 21% water content (using Eq. 1.16)

$$= \frac{1 + 0.21}{1 + 0.65} \times 2.65 \times 1 = 1.943 \text{ g/cc}$$

The saturated density of soil at 24.5% water content

$$= \frac{1 + 0.245}{1 + 0.65} \times 2.65 \times 1 = 2 \text{ g/cc}$$

The increase in density is only due to the addition of water. Additional water required per cubic centimetre of soil to saturate it

$$= 2 - 1.943 = 0.057 \text{ cc}$$

Therefore, for 1 cubic metre of soil, additional water required

$$= 0.057 \times \frac{10^6}{10^3}$$

$$= 57 \text{ litres}$$

Q 1.4: A land development project requires construction of a compacted fill. The potential borrow areas are Site A and Site B. The in-place properties of soil at these sites are as below:

	Site A	*Site B*
in-place void ratio	0.79	0.65
in-place water content, %	18	15

The fill at the end of construction will have a total volume of 40,000 m³, a total density of 2 T/m³, and a placement water content of 21 per cent.

Soil from either site is to be excavated and transported to the site in trucks of 10 m³ capacity. During excavation and placing of soil in truck the soil bulks in volume by 10 per cent. At the site the required amount of water is added and compacted to the required extent using rollers.

The cost of excavation of soil, its transportation, and its compaction excluding water charges is Rs 225 per truck for Site A, and Rs 260 per truck for Site B. Water charges per truck is Rs 100. Specific gravity of solids is 2.65.

Which of the two sites is more economical?

Ans:

Data for the fill at the end of construction:

Total weight of soil $= \gamma_t \times V = 2 \times 40{,}000 = 80{,}000$ T

Total dry weight of soil (solids) $= \gamma_d \times V$

$$= \frac{2}{(1 + 0.21)} \times 40{,}000 = 66{,}115 \text{ T}$$

Weight of water $= 80{,}000 - 66{,}115 = 13{,}885$ T

Cost of using Site A as borrow area:

Volume of soil needed from Site A for 66,115 T of dry soil

$$= \frac{66{,}115}{(2.65 \times 1)/(1 + 0.79)} = 44{,}658.8 \text{ m}^3$$

Total number of truck trips required to transport 44,658.8 m³ of soil with 10% allowance for bulking

$$= \frac{(44658.8 \times 1.1)}{10}$$

$$= 4913$$

Amount of water present in 44,658.8 m³ of soil

$$= wW_s = 0.18 \times 66{,}115 = 11{,}900.7 \text{ T}$$

Additional amount of water needed $= 13{,}885 - 11{,}900.7$

$$= 1984.3 \text{ T}$$

Number of truck trips required to transport water $= 1984.3/10 = 199$

Cost of excavating, transporting and placing of soil excluding water charges

$$= 4913 \times 225$$

$$= \text{Rs } 11{,}05{,}425$$

Cost of transporting water $= 199 \times 100$

$$= \text{Rs } 19{,}900$$

Total cost of using soil from Site A

$$= \text{Rs } 11,05,425 + \text{Rs } 19,900$$
$$= \text{Rs } 11,25,325$$

Cost of using Site B as borrow area:

Volume of soil needed from Site B for 66,115 T of dry soil

$$= \frac{66,115}{(2.65 \times 1)/(1 + 0.65)}$$
$$= 41,165.9 \text{ m}^3$$

Total number of truck trips required to transport 41,165.9 m^3 of soil with 10% allowance for bulking

$$= \frac{41,165.9 \times 1.1}{10} = 4529$$

Amount of water present in 41,165.9 m^3 of soil

$$= 0.15 \times 66,115 = 9917.25 \text{ T}$$

Additional amount of water needed = 13885 − 9917.25 = 3967.75 T

Number of truck trips required to transport water

$$= \frac{3967.75}{10} = 397$$

Cost of excavating, transporting, and placing of soil excluding water charges

$$= 4529 \times 260$$
$$= \text{Rs } 11,77,540$$

Cost of transporting water = 397×100 = Rs 39,700

Total cost of using soil from Site B

$$= \text{Rs } 11,77,540 + \text{Rs } 39,700$$
$$= \text{Rs } 12,17,240$$

Site A is more economical than Site B.

The saving in cost in using Site A is

$$= \text{Rs } 12,17,240 - \text{Rs } 11,25,325$$
$$= \text{Rs } 91,915$$

2

INDEX PROPERTIES

Natural soils occur in many varieties and types. For engineering purposes the soils may be broadly grouped into two categories, namely,

1. Coarse grained soils
2. Fine grained soils

Obviously, the basis of such grouping is the size of individual soil grains. Gravels and sands are examples of coarse grained soils, and silts and clays are examples of fine grained soils. Index properties help in proper identification and classification of different types of soils. An immediate appreciation of the general soil behaviour is also possible from a knowledge of the index properties. These index properties are obtained from the results of experiments for (i) grain size distribution, and (ii) Atterberg limits.

2.1 GRAIN SIZE DISTRIBUTION

Soil consists of different sizes of particles. The amount of a given size of particle (in a particular quantity of soil) varies from one soil to another. Particle size analysis in soil is carried out by using (i) sieve analysis, and (ii) sedimentation tests. Sieve analysis is useful for coarse grained soils. Silt and clay particle sizes cannot be separated by sieving. For these soil types sedimentation tests are used. Hydrometer test and pippette test are the common sedimentation tests. The results of grain-size analysis are presented in a semilogarithmic plot as shown in Fig. 2.1. For convenience, the size of soil particle is expressed in equivalent diameter which corresponds to the size of sieve opening or the size of a spherical particle falling through a soil suspension in sedimentation test.

Figure 2.1 shows grain size distribution curves for three soils which are marked A–A, B–B, and C–C. On curve B–B, sizes corresponding to 10% finer by weight, 30% finer by weight, and 60% finer by weight have been marked and are designated D_{10}, D_{30} and D_{60} respectively. Size D_{10} is known as *effective size* or *effective diameter*. With these sizes the following quantities are defined.

Coefficient of uniformity,
$$C_u = \frac{D_{60}}{D_{10}} \tag{2.1}$$

Coefficient of curvature, or

Coefficient of gradation,

$$C_c = \frac{D_{30}^2}{D_{60} D_{10}} \tag{2.2}$$

Coefficients C_u and C_c are useful in defining the gradation characteristics of soils. In Fig. 2.1 it can be observed that curve B–B spreads over a large range of particle sizes. Such soils are called *well graded*. Curve A–A is confined to a narrow range of particle sizes and is hence called *uniformly graded* or *poorly graded*. In the soil corresponding to curve C–C particle sizes over a range C'–C'' are missing. There is a gap in gradation, hence, it is called *gap graded*. The range of values of C_u and C_c for uniformly and well graded soils is given in Table 2.1.

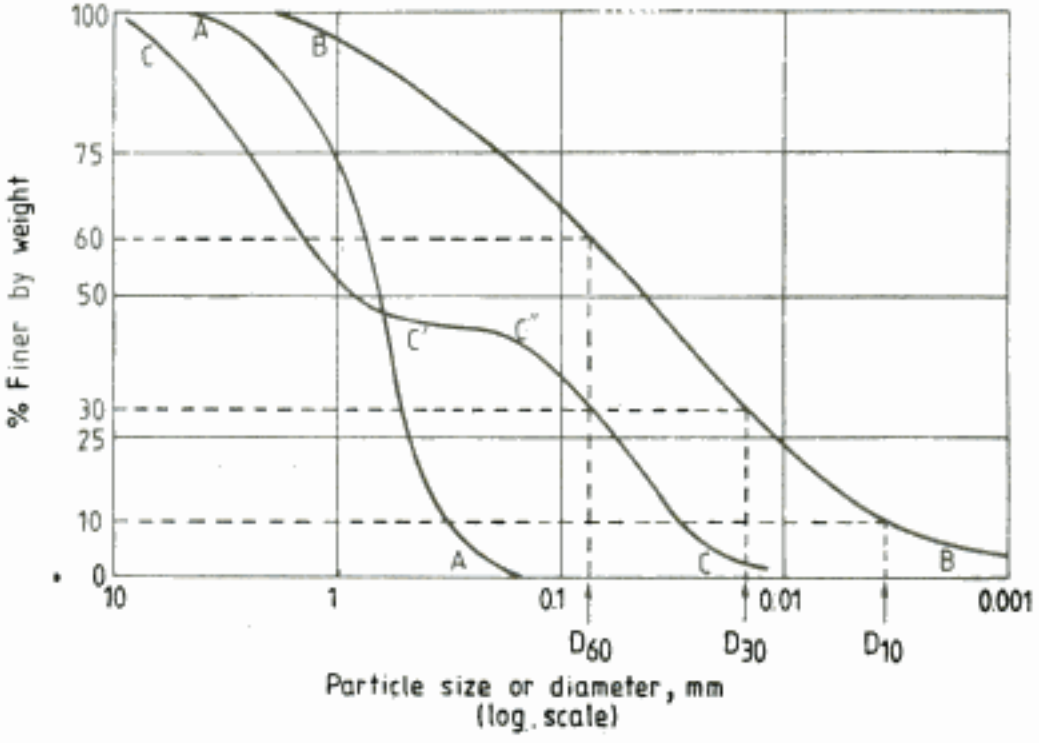

Fig. 2.1 Grain size distribution curves

Table 2.1 Gradation Characteristics based on C_u and C_c

Soil type	Soil gradation	C_u	C_c
Gravel	Well graded	>4	$1 < C_c < 3$
"	Poorly graded	not meeting the above requirements	
Sand	Well graded	>6	$1 < C_c < 3$
"	Poorly graded	not meeting the above requirements	

Grain size distribution curves, C_u and C_c are more useful for coarse grained soils than for fine grained soils. For fine grained soils, the useful index properties are Atterberg limits.

2.2 ATTERBERG LIMITS

With continuous change in water content the consistency of soil passes from one state to another. Figure. 2.2 shows the different consistency states in which soil can exist. A soil with a lot of water can flow like a liquid. It exists in a liquid state. If this soil is dried or water is removed by other means the water content decreases and reaches a stage when soil can be remoulded by hand. The soil is then plastic and is in plastic state. With further drying a stage is reached when water content is so small that it cannot be remoulded by hand. The soil has reached the semi-solid state. With further decrease in water content, solid state is reached and further drying produces no change in the total volume of the soil. The boundaries of these limits are known as, (i) *liquid limit*, (ii) *plastic limit*, and (iii) *shrinkage limit* and are called Atterberg limits. A detailed definition of these limits is provided below:

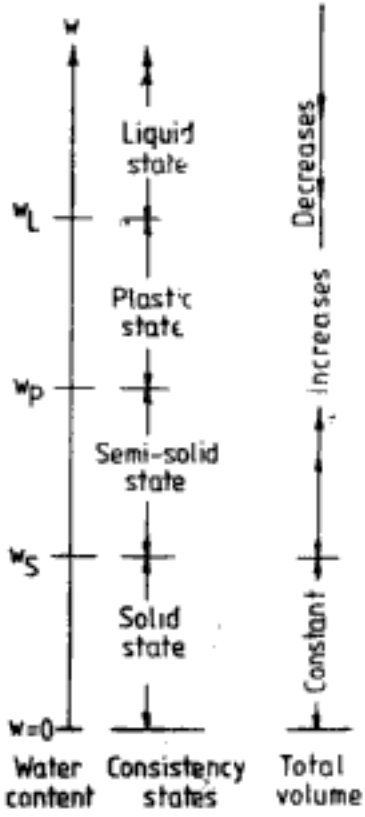

Fig. 2.2 Consistency states and Atterberg limits

Liquid limit (w_L): Water content at which,

1. the soil has negligibly small shear strength
2. the consistency of soil reaches the boundary between liquid state and plastic state
3. a standard groove made in soil in a liquid limit apparatus closes over a length of 12 mm for 25 blows

Plastic limit (w_P): Water content at which,

1. the consistency of soil reaches the boundary between plastic state and semi-solid state
2. the soil when rolled into a thread crumbles at a diameter of 3 mm

Shrinkage limit (w_S): Water content at which,

1. the consistency of soil reaches the boundary between semi-solid state and solid state
2. regardless of further drying the soil remains at constant volume

Using Atterberg limits three soil indices can be defined. These are: (i) *plasticity index*. (ii) *liquidity index*, and (iii) *consistency index*.

Plasticity index, $$I_P = w_L - w_P \tag{2.3}$$

Thus plasticity index indicates the magnitude of water content over which the soil remains in plastic state. The composition and the Atterberg limits of a few Indian soils are given in Table 2.2. Atterberg limits and plasticity index are rounded off to nearest whole number. It will not be necessary to do so if rounding off had been already done for water content.

Table 2.2 Composition and Atterberg Limits of Some Indian Soils

Soil	Sand size %	Silt size %	Clay size %	w_L %	w_P %	I_P %
Black cotton soil	15	55	30	101	28	73
Delhi silt	15	70	15	32	22	10
Ghaggar clay	4	58	38	51	25	26
Dhanouri clay	1	64	35	51	30	21
Beas shale	2	68	30	35	19	16
Bombay marine clay	2	32	66	90	40	50
Farakka clay	3	32	65	105	35	70

Atterberg limits depend on the amount and type of clay in the soil. The limits form the basis for classification and identification of fine grained soils which is explained in Ch. 3. An experienced engineer is able to get a picture of the engineering behaviour of the soil knowing its Atterberg limits. There also exist extensive empirical correlations between Atterberg limits and a number of engineering properties like compressibility, permeability, strength, etc. Some general relationships between Atterberg limits and engineering properties are given in Table 2.3.

Table 2.3 General Relationships between Atterberg Limits and Engineering Properties

Characteristics	Comparing soils at equal liquid limit with plasticity index increasing	Comparing soils at equal plasticity index with liquid limit increasing
Compressibility	About the same	Increases
Permeability	Decreases	Increases
Rate of volume change	Decreases	—
Toughness near plastic limit	Increases	Decreases
Dry strength	Increases	Decreases

Liquidity index, $$I_L = \frac{w_n - w_P}{I_P} \tag{2.4}$$

where w_n = natural or in-place water content of soil

For a soil in plastic state I_L varies from 0 to 1.

Consistency index, $$I_c = \frac{w_L - w_n}{I_P} = 1 - I_L \tag{2.5}$$

Guidelines for defining soil consistency using I_L and I_c are given in Table 2.4.

Table 2.4 Consistency of Cohesive Soils Using Liquidity and Consistency Indices

Soil consistency		I_L	I_C
Solid	very hard	< 0	> 1
	hard or very stiff	< 0	> 1
Plastic	stiff	0–0.25	0.75–1
	firm or medium stiff	0.25–0.5	0.5–0.75
	soft	0.5–0.75	0.25–0.5
	very soft	0.75–1	0–0.25
Liquid	liquid	> 1	< 0

Note: More guidelines for defining consistency of cohesive soils on the basis of standard penetration number (N) and undrained cohesion (c_u) are given in Table 9.10.

Plasticity index of soil is dependent on (i) the type of clay mineral, and (ii) the amount of clay mineral present in the soil. Skempton (1953) observed that I_P is directly proportional to per cent of clay-size particles (less than 0.002 mm) by weight. This observation can be represented as shown in Fig. 2.3. On the basis of this behaviour an index property called *activity* is defined as,

Activity, $$A = \frac{I_P}{C} \tag{2.6}$$

where C = per cent clay size particles (<0.002 mm) by weight

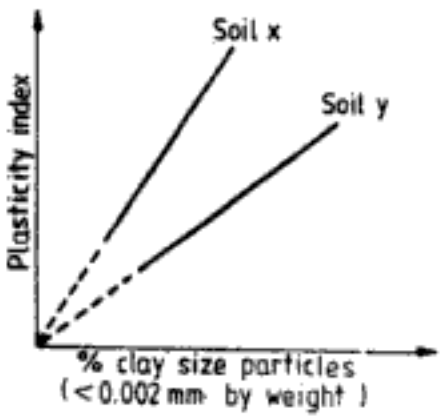

Fig. 2.3 Activity of soil

Table 2.5 gives typical values of activity of pure clay minerals.

Table 2.5 Activity of Pure Clay Minerals

Clay mineral	Activity
Sodium montmorillonite	7.2
Illite	0.9
Kaolinite	0.38

We can expect higher volume change in soils (like higher compressibility and higher swelling) with higher values of activity. Thus, two soils X and Y may have comparable plasticity index. But if soil X has a higher activity than Y, then soil X is more susceptible to shrink or swell than soil Y.

Q 2.1: Compare the characteristics of Ghaggar clay and Dhanouri clay from their composition and Atterberg limits given in Table 2.2.

Ans:

	Ghaggar clay	*Dhanouri clay*
w_L, per cent	51	51
w_P, per cent	25	30
I_P, per cent	26	21
C (clay size)	38	35
A (activity)	0.68	0.6

A qualitative comparison of the characteristics of the two soils is as follows (assuming otherwise identical conditions for the two soils):

The dry strength and toughness near plastic limit are more for Ghaggar clay than for Dhanouri clay. However, the permeability and rate of volume change are more for Dhanouri clay than for Ghaggar clay. The compressibility of the two soils is nearly the same. Ghaggar clay is susceptible to undergo higher volume change than Dhanouri clay.

Note: Activity as an index to indicate the susceptibility of a soil to undergo volume change is strikingly revealed when black cotton soil and Farakka clay of Table 2.2 are compared. Both have nearly equal liquid limit and plasticity index. But the activity of black cotton soil is 2.43 and that of Farakka clay is only 1.08. The black cotton soil has high susceptibility for volume change, as is generally well known.

3

SOIL CLASSIFICATION

If someone describes a soil as "Madras soil", to those who are not familiar with the Madras region the description tells very little about the soil other than its location. Similarly a "black soil" is black in colour and nothing more could be inferred about its other characteristics. People also identify soil by some local terminologies. Description of soil by place or colour or some local terminology does not help to establish communication between engineers. It does not tell a person of the possible characteristics and behaviour of the soil, the suitability or otherwise of it for a particular purpose, its constituents, etc. Soil classification is an attempt to overcome the defects of arbitrary description of soil.

Soil classification establishes standard terminologies and symbols for soils. The types of soils and their symbols are,

Gravel—G	Clay —C
Sand —S	Organic soil—O
Silt —M	Peat —Pt

For more details of these symbols Table 3.2 can be referred.

Coarse grained soils are classified by their gradation characteristics, namely,

Well graded —W

Poorly graded—P

Fine grained soils are distinguished by their plasticity characteristics, as

Low plasticity —L

High plasticity—H

Two symbols are used to designate a soil type. From the symbols explained above it is possible to have different combinations of these symbols. For example, GW, SW, GP, GM, SP, CH, ML, etc. In all the combinations the principal soil type symbol is followed by the characteristics symbol. Thus,

GW—means well graded gravel

CH—means highly plastic clay

Tables 3.1 to 3.4 give more detailed description of soils designated by these symbols.

3.1 SOIL CLASSIFICATION SYSTEMS

Soil classification systems serve two purposes.

1. They help to properly classify the soils.
2. They identify the suitability of soils for various purposes. Many agencies are interested in the suitability of soils for some specific purposes. For example, highway organisations are interested to know the suitability of soil for use in pavement. A number of classification systems have been developed to serve appropriate end uses.

3.1.1 Unified Classification System (UCS)

Table 3.1 gives the details af UCS. It explains how the soils are classified into different groups on the basis of some experiments conducted on soils. Table 3.2 describes the soil components used in Unified Soil Classification System (Wagner, 1957) and their significant properties. After a soil has been classified according to UCS, its important properties and relative desirabilily for various uses can be identified from the engineering use chart in Table 3.3 (Wagner, 1957).

Q 3.1: The salient features of sieve analysis and Atterberg limits experiments of a soil are as given below:
Total weight of soil sieved = 250 g

Sieve size	*Cumulative weight retained*
mm	g
4	40
0.075	190

$D_{60} = 2$ mm; $D_{10} = 0.06$ mm; $D_{30} = 0.1$ mm

From Atterberg limit tests on fractions less than 0.38 mm size: $w_L = 35$; $w_P = 27$.
Classify the soil according to UCS and indicate the suitability of soil as "foundation for structures".

Ans:

From sieve analysis results:

$$\text{weight of soil finer than 0.075 mm} = 250 - 190$$
$$= 60 \text{ g}$$
$$\% \text{ finer than 0.075 mm} = \frac{60}{250} \times 100 = 24$$

Soil belongs to group of "coarse grained soils" since more than half of soil particles are larger than 0.075 mm. From laboratory classification criteria, since percentage fines (fraction smaller than 0.075 mm) is more than 12%, the soil belongs to one of the following groups, namely

GM, GC, SM, SC

Total weight of soil particles larger than 0.075 mm size = 190 g
Within this coarse fraction % larger than 4 mm, i.e.,

$$\text{per cent gravel size} = \frac{40}{190} \times 100 = 21$$

and

$$\% \text{ finer than 4 mm} = 100 - 21 = 79$$

(i.e., % sand size)

Table 3.2 Soil Components and Fractions

Soil component	Symbol	Grain size range and description	Significant properties
Boulder	None	Rounded to angular, bulky, hard, rock particle, average diameter more than 300 mm	Boulders and cobbles are very stable components, used for fills, ballast, and to stabilize slopes (riprap). Because of size and weight, their occurrence in natural deposits tends to improve the stability of foundations. Angularity of particles increases stability.
Cobble	None	Rounded to angular, bulky, hard, rock particle, average diameter smaller than 300 mm but larger than 150 mm	
Gravel	*G*	Rounded to angular, bulky, hard, rock particle, passing 75 mm sieve retained on 4 mm sieve	Gravel and sand have essentially same engineering properties differing mainly in degree. The 4 mm sieve is arbitrary division, and does not correspond to significant change in properties. They are easy to compact, little affected by moisture, not subject to frost action. Gravels are generally more perviously stable, resistant to erosion and piping than are sands. The well-graded sands and gravels are generally less pervious and more stable than those which are poorly graded (uniform gradation). Irregularity of particles increases the stability slightly. Finer, uniform sand approaches the characteristics of silt: i.e. decrease in permeability and reduction in stability with increase in moisture.
Coarse		75 to 19 mm	
Fine		19 to 4 mm	
Sand	*S*	Rounded to angular, bulky, hard, rock particle, passing 4 mm sieve retrained on 75 μm sieve	
Coarse		4 to 1.7 mm sieves	
Medium		1.7 mm to 380 μm sieves	
Fine		380 to 75 μm sieves	
Silt	*M*	Particles smaller than 75 μm sieve identified by behaviour; that is, slightly or non-plastic regardless of moisture and exhibits little or no strength when air dried	Silt is inherently unstable, particularly when moisture is increased, with a tendency to become quick when saturated. It is relatively impervious, difficult to compact, highly susceptible to frost heave, easily erodible and subject to piping and boiling. Bulky grains reduce compressibility; flaky grains, i.e., mica, diatoms, increase compressibility, produce an "elastic" silt.
Clay	*C*	Particles smaller than 75 μm sieve identified by behaviour; that is, it can be made to exhibit plastic properties within a certain range of moisture and exhibits considerable strength when air dried	The distinguishing characteristic of clay is cohesion or cohesive strength, which increases with decrease in moisture. The permeability of clay is very low, it is difficult to compact when wet and impossible to drain by ordinary means, when compacted is resistant to erosion and piping, is

Soil component	Symbol	Grain size range and description	Significant properties
			not susceptible to frost heave, is subject to expansion and shrinkage with changes in moisture. The properties are influenced not only by the size and shape (flat, plate like particles) but also by their mineral composition; i.e., the type of clay-mineral, and chemical environment or base exchange capacity. In general, the montmorillonite clay mineral has greatest, illite and kaolinite the least, adverse effect on the properties.
Organic matter	*O*	Organic matter in various sizes and stages of decomposition	Organic matter present even in moderate amounts increases the compressibility and reduces the stability of the fine-grained components. It may decay causing voids or by chemical alteration change the properties of a soil, hence organic soils are not desirable for engineering uses.

Note: The symbols and fractions were developed for the Unified Classification System. The sand fractions are not equal divisions on a logarithmic plot; the 1.7 mm was selected because of the significance attached to that size by some investigators. The 380 μm size was chosen because the "Atterberg limits" tests are performed on the fraction of soil finer than the 380 μm.

(After Wagner, 1957. Reprinted by permission of Butterworth Scientific, Survey, U.K.)

Since more than half of coarse fraction is finer than 4 mm, the soil belongs to category of "sands" and possible group symbols narrow down to SM and SC.
Again from laboratory classification criteria:

$$I_P = 35 - 27 = 8$$

In the plasticity chart, point $w_P = 35$, $I_P = 8$ is below '*A*-line'. With the Atterberg limits below *A*-line the classification symbol for soil is 'SM'

Note: Table 3.1 has been used for classification purposes. Data about D_{10}, D_{30}, and D_{60} sizes have not been used since the soil groups identified in this particular example are not governed by index properties C_u and C_c.

Suitability of soil for foundation:

From Table 3.3 the soil SM can be rated as "average" in suitability if seepage is no consideration, since it is given a rating of 7 on a scale of 14. But if seepage is an important consideration the soil can be rated as "good" since it has a better rating of 3 on a scale of 10.

3.1.2 Indian Standard Classification System (IS: 1498—1970)

Indian soil classification system is shown in Table 3.4. The laboratory classification criterion for coarse grained soils is the same as for Unified System (Table 3.1). The plasticity chart recommended for classification of fine grained soil is shown in Fig. 3.1. While UCS identifies

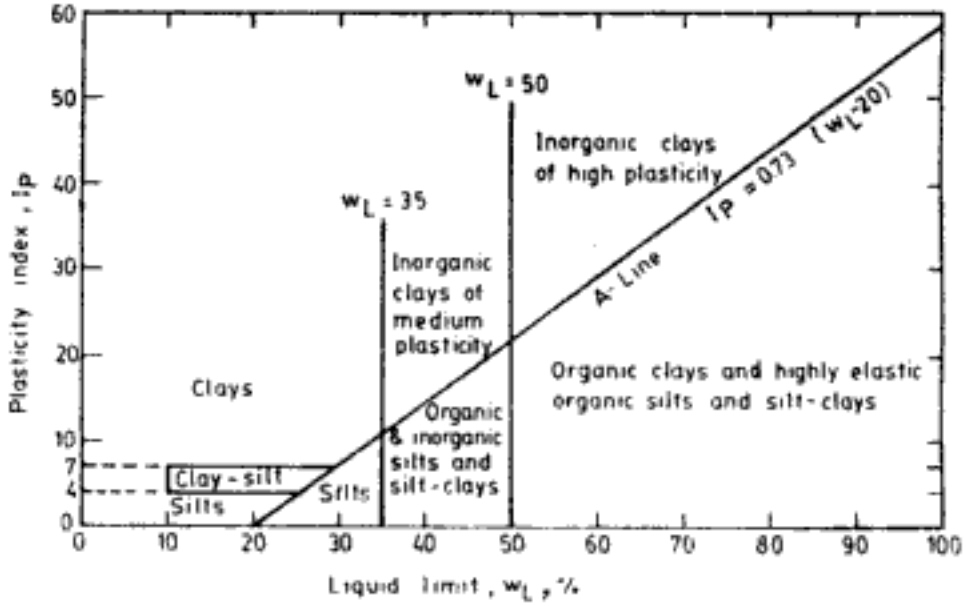

Fig. 3.1 Indian standard plasticity chart

(After IS: 1498—1970. By permission of Indian Standards Institution, New Delhi)

only high and low plasticity characteristics depending on whether liquid limit is above or below 50, IS classification system identifies three different ranges of compressibility as below.

High → H → w_L above 50

Intermediate or medium → I → $50 > w_L > 35$

Low → L → $w_L < 35$

Tables 3.5, 3.6, and 3.7 indicate the suitability of soil for different purposes.

3.1.3 Highway Research Board (HRB) or Public Roads Administration (PRA) Classification System

This classification system is devised to evaluate the suitability of soils for use in highway pavements. Table 3.8 gives the classification system. Soils are divided into seven primary groups A-1 to A-7 and into subgroups among primary groups. Grain size analysis and Atterberg limits are used to identify the group to which soil belongs.

A general rating of the soil for use in pavement can then be obtained. Within a given soil group the relative quality of material can be determined by computing *group index* of the soil. The group index depends upon (i) the percentage of soil finer than 0.075 mm, (ii) liquid limit, and (iii) plastic limit. Group index can be computed from,

$$\text{Group index} = 0.2a + 0.005ac + 0.01bd \qquad (3.1)$$

where a = that portion of percentage passing 75-micron sieve greater than 35 and not exceeding 75 expressed as a whole number (0 to 40)

i.e., $a = (X - 35) \geqslant 0$, but $\leqslant 40$

X = percent finer than 0.075 mm

when $X \geqslant 75$ $a = 40$

$X \leqslant 35$ $a = 0$

Table 3.6 Characteristics Pertinent to Embankments and Foundations

Soil group	Value of embankment	Coefficient of permeability cm/s	Compaction characteristics	Dry density g/cm³	Value of foundation	Requirement for seepage control
(1)	(2)	(3)	(4)	(5)	(6)	(7)
GW	Very stable; pervious shells of dikes and dams	$> 10^{-3}$	Good; tractor, rubber tyred, steel-wheeled roller	2.00-2.16	Good bearing value	Positive cutoff
GP	Reasonably stable; pervious shells of dikes and dams	$> 10^{-3}$	do	1.84-2.00	do	do
GM	Reasonably stable; not particularly suited to shells, but may be used for impervious cores or blankets	10^{-3} to 10^{-6}	Good; with close control, rubber-tyred, sheeps-foot roller	1.92-2.16	do	Toe trench to none
GC	Fairly stable; may be used for impervious core	10 to 10^{-6}	Fair; rubber-tyred, sheeps-foot roller	1.84-2.08	do	None
SW	Very stable; pervious sections, slope protection required	$> 10^{-3}$	Good; tractor	1.76-2.08	do	Upstream blanket and toe drainage or well
SP	Reasonably stable; may be used in dike section with flat slopes	$> 10^{-3}$	Good; tractor	1.60-1.92	Good to poor bearing value depending on density	do
SM	Fairly stable; not particularly suited to shells, but may be used for impervious cores or dikes	10^{-3} to 10^{-6}	Good; with close control, rubber-tyred, sheeps-foot roller	1.76-2.00	do	do
SC	Fairly stable; use for impervious core for flood control structures	10^{-6} to 10^{-3}	Fair; sheeps-foot roller, rubber-tyred	1.68-2.00	Good to poor bearing value	None
ML, MI	Poor stability; may be used for embankments with proper control	10^{-3} to 10^{-6}	Good to poor, close control essential; rubber-tyred roller, sheeps-foot roller	1.52-1.92	Very poor, susceptible to liquefaction	Toe trench to none
CL, CI	Stable; impervious cores and blankets	10^{-6} to 10^{-3}	Fair to good; sheeps-foot roller, rubber-tyred	1.52-1.92	Good to poor bearing	None

(Contd.)

Table 3.6 (Contd.)

(1)	(2)	(3)	(4)	(5)	(6)	(7)
OL, OI	Not suitable for embankments	10^{-4} to 10^{-6}	Fair to poor; sheeps-foot roller	1.28-1.60	Fair to poor bearing, may have excessive settlements	None
MH	Poor stability; core of hydraulic fill dams not desirable in rolled fill construction	10^{-4} to 10^{-6}	Poor to very poor; sheeps-foot roller	1.12-1.52	Poor bearing	do
CH	Fair stability with flat slopes; thin cores, blankets and dike sections	10^{-6} to 10^{-8}	Fair to poor; sheeps-foot roller	1.20-1.68	Fair to poor bearing	do
OH	Not suitable for embankments	10^{-4} to 10^{-6}	Poor to very poor; sheeps-foot roller	1.04-1.60	Very poor bearing	do
Pt	Not used for construction	—	Compaction not practical	—	Remove from foundation	—

Note 1: Values in Columns 2 and 6 are for guidance only. Design should be based on test results.

Note 2: The equipment listed in Column 4 will usually produce densities with a reasonable number of passes when moisture conditions and thickness of lift are properly controlled.

Note 3: Dry densities in Column 5 are for compacted soil at optimum moisture content for Indian Standard light compaction effort [*see* IS: 2720 (Part VII)—1965*].

*Methods of test for soils: Part VII Determination of moisture content-dry density relation using light compaction

(After IS: 1498—1970. Reprinted by permission of Indian Standards Institution, New Delhi.)

Table 3.7 Suitability for Canal Sections, Compressibility, Workability as a Construction Material and Shear Strength

Soil group	Relative suitability for canal sections*		Compressibility when compacted and saturated	Workability as a construction material	Shearing strength when compacted and saturated
	Erosion resistance	Compacted earth lining			
GW	1	—	Negligible	Excellent	Excellent
GP	2	—	Negligible	Good	Good
GM	4	4	Negligible	Good	Good
GC	3	1	Very low	Good	Good to Fair
SW	6	—	Negligible	Excellent	Excellent
SP	7, if gravelly	—	Very low	Fair	Good
SM	8, if gravelly	5 (Erosion critical)	Low	Fair	Good
SC	5	2	Low	Good	Good to Fair
ML, MI	—	6 (Erosion critical)	Medium	Fair	Fair
CL, CI	9	3	Medium	Good to Fair	Fair
OL, OI	—	7 (Erosion critical)	Medium	Fair	Poor
MH	—	—	High	Poor	Fair to Poor
CH	10	8 (Volume change critical)	High	Poor	Poor
OH	—	—	High	Poor	Poor
Pt	—	—	—	—	—

*Number 1 is the best.

(After IS: 1498—1970. Reprinted by permission of Indian Standards Institution, New Delhi.)

b = that portion of percentage passing 75-micron sieve greater than 15 and not exceeding 55 expressed as a whole number (0 to 40)

i.e., $b = (X - 15) \geqslant 0$, but $\leqslant 40$

when $X \geqslant 55$ $\quad b = 40$

$X \leqslant 15$ $\quad b = 0$

c = that portion of the numerical value of liquid limit greater than 40 and not exceeding 60 expressed as a positive whole number (0 to 20)

i.e., $c = (w_L - 40) \geqslant 0$, but $\leqslant 20$

if $w_L \leqslant 40$ $\quad c = 0$

$w_L \geqslant 60$ $\quad c = 20$

d = that portion of numerical value of plasticity index greater than 10 and not exceeding 30 expressed as a positive whole number (0 to 20)

i.e., $d = (I_P - 10) \geqslant 0$, but $\leqslant 20$

if $I_P \leqslant 10$ $\quad d = 0$

$I_P \geqslant 30$ $\quad d = 20$

The higher the group index of a soil the poorer is its quality within a group.

Table 3.8 HRB Classification of Soil and Soil Aggregate Mixtures

General description	Granuler material (35% or less passing 75 micron IS sieve)							Silt-clay materials (more than 35% passing 75 micron IS sieve)			
Group classification	A-1		A-3	A-2				A-4	A-5	A-6	A-7
	A-1-a	A-1-b		A-2-4	A-2-5	A-2-6	A-2-7				A-7-5 A-7-6
Sieve analysis, per cent passing											
2.0 mm IS sieve	50 max										
425-micron sieve	30 max	50 max	51 min								
75-micron sieve	15 max	25 max	10 max	35 max	35 max	35 max	35 max	36 min	36 min	36 min	36 min
Characteristics of fraction passing 425-micron sieve:											
Liquid Limit				40 max	41 min	40 max	41 min	40 max	41 min	40 max	41 min
Plasticity Index	6 max		NP	10 max	10 max	11 min	11 max	10 max	10 max	11 min	11 min
Group index	Zero			4 max				8 max	12 max	16 max	20 max
Usual types of significant constituent materials	Stone fragments gravel and sand		Fine sand	Silty or clayey gravel and sand				Silty soil		Clayey soils	
General rating as subgrade	Excellent to good			Fair to poor							

Q 3.2: Classify the soil in Q 3.1 by HRB/PRA classification system and find its suitability for use in subgrade.

Ans: Since % finer than 0.075 mm is only 24 (< 35) the soil belongs to one of the groups of A-1, A-2 and A-3.

Again from the same consideration that 24% is finer than 0.075 mm, the soil groups narrow down to A-1-b and subgroups of A-2, since for A-3 and A-1-a the maximum percentage finer than 0.075 mm is only 10 and 15 respectively.

Since plasticity index is 8 (> 6) the soil now belongs to one of the subgroups of A-2. It is important to note here that Atterberg limits in Q 3.1 have been determined on the fraction of soil finer than 0.38 mm. However, to use Table 3.8, tests for Atterberg limits should be carried out on the soil fraction finer than 0.425 mm. Due to paucity of data, same Atterberg limits as in Q 3.1 have been assumed here, which is not strictly correct.

For $w_L = 35$ and $I_P = 8$ the group to which the soil belongs is A-2-4.

The group index of soil is zero, since

$$a = 0, \quad b = 9, \quad c = 0, \quad d = 0$$

A-2-4 group of soil may be described as silty or clayey gravel and sand which is in conformity with the description in Q 3.1 as silty sand, thereby indicating that the assumption regarding Atterberg limits is not much in error.

The general rating as subgrade is excellent to good. But since the soil is towards last in the order of arrangement of groups for such a rating, the rating for use in subgrade can be considered as "good".

For Indian black cotton soils, Central Road Research Laboratory, New Delhi, has extended the HRB/PRA classification system as shown in Table 3.9. To find out group index in Table 3.9, Eq. 3.1 has been recommended with the following modifications for a, b, c and d.

$$a = (X - 35) \geqslant 0, \quad \text{but} \quad \leqslant 65$$

$$\text{if } X \leqslant 35 \qquad a = 0$$

$$X \geqslant 100 \qquad a = 65$$

$$b = (X - 15) \geqslant 0 \quad \text{but} \quad \leqslant 65$$

$$\text{if } X \leqslant 15 \qquad b = 0$$

$$X \geqslant 80 \qquad b = 65$$

$$c = (w_L - 40) \geqslant 0, \quad \text{but} \quad \leqslant 45$$

$$\text{if } w_L \leqslant 40 \qquad c = 0$$

$$w_L \geqslant 85 \qquad c = 45$$

$$d = (I_P - 10) \geqslant 0, \quad \text{but} \quad \leqslant 34$$

$$\text{if } I_P \leqslant 10 \qquad d = 0$$

$$I_P \geqslant 44 \qquad d = 34$$

Without having to go through computations it is evident from Table 3.9 that black cotton soils do not form good subgrade material.

Table 3.9 Extension of HRB Classification for Indian Black Cotton Soils

Group	A–7	A–7a	A–7b	A–7c
Per cent passing 75-micron sieve	up to 75	55–95	80–95	85–100
Characteristics of fraction passing 425-micron sieve				
Liquid limit	below 55	below 65	above 65	above 65
Plasticity index	below 25	below 42	below 42	above 42
Group index	20 max	20–30	30–40	40–50
Usual type of significant constituent material		Clayey soils		
General rating as subgrade	Fair to poor		Poor	

3.2 POINTS TO REMEMBER ABOUT SOIL CLASSIFICATION SYSTEMS

1. Grain size for demarcation of soil types

Different classification systems choose different grain sizes, rather arbitrarily, to demarcate the soil types. Figure 3.2 shows the classification on the basis of grain size in UCS. Figure 3.3 shows recommendations due to Indian Standard—IS: 1498—1970. A rather convenient classification is due to MIT (Massachusetts Institute of Technology) system shown in Fig. 3.4 and also due to British Standard Practice shown in Fig. 3.5 in which numbers 2 and 6 appear alternately. If the limiting size for clay-size fractions is remembered as 0.002 mm, the other boundaries can be easily obtained as the next immediate higher value alternately in 6 and 2.

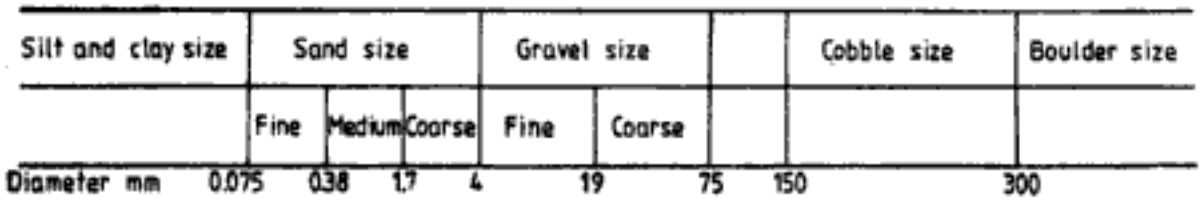

Fig. 3.2 Grain sizes for Unified Classification System

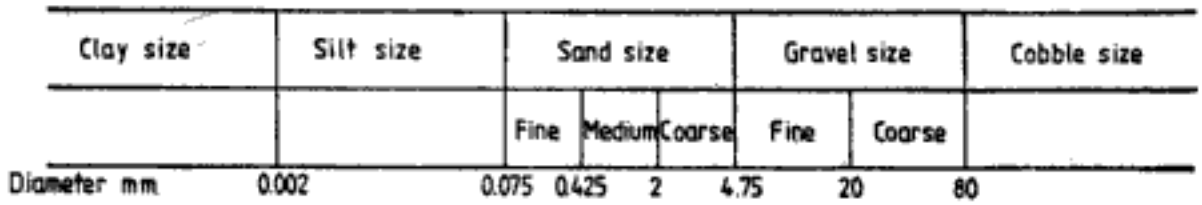

Fig. 3.3 Grain sizes for Indian Standard System

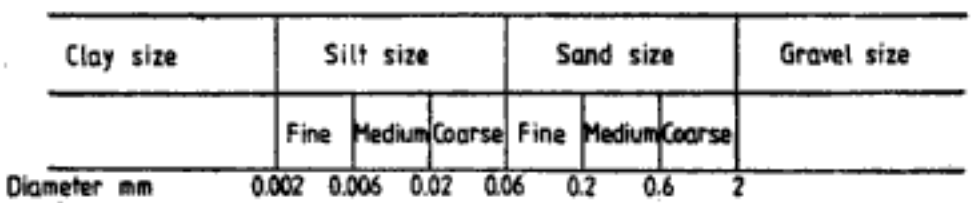

Fig. 3.4 Grain sizes for MIT Classification System

Clay size	Silt size			Sand size			Gravel size			Cobble size	Boulder size
	Fine	Medium	Coarse	Fine	Medium	Coarse	Fine	Medium	Coarse		
Diameter mm	0.002	0.006	0.02	0.06	0.2	0.6	2	6	20	60	200

Fig. 3.5 Grain sizes for British Standard Classification System

It must be pointed out here that clayey type of soils cannot be identified by particle size alone. Their behaviour is controlled by the nature of clay minerals. While coarse grained soils can be effectively separated and identified by sieving, the fine grained soils are distinguished by means of plasticity characteristics.

2. Errors in classification

Different classification systems use different criteria as distinguishing boundaries between various soil types. Naturally, one can expect that the same soil may be classified differently by different systems. But this error is tolerable, for soil classification can help only in a qualitative appreciation or evaluation of the general behaviour of the soil.

3. Use in design

Soil classification is never a substitute for detailed investigations like laboratory or field testing. Designs should never be based on soil classification alone. Soil classification indicates the further direction in which the detailed investigations must be carried out. In the initial phases of project design and in preliminary designs, soil classification plays an important role in effective decision making.

4

SOIL COMPACTION

Soil compaction is one of the soil improvement techniques. It is a process in which by expending compactive energy on soil the soil grains are more closely rearranged. Compaction increases the shear strength of soil and reduces its compressibility. Compaction should not be confused with consolidation. The similarities and differences between compaction and consolidation are explained in Table 4.1. Consolidation is described separately in Ch. 7.

Table 4.1 Compaction Vs. Consolidation

Compaction	Consolidation
Similarities	
At the end of the process a closer packing of soil grains results. Shear strength increases. Compressibility and permeability decrease.	
Differences:	
1. Compaction is almost instantaneous	1. Consolidation is time dependent
2. Densification is due to reduction of air voids	2. Consolidation is due to expulsion of pore water from voids
3. Soil is always unsaturated	3. Soil is saturated
4. For a specified compactive effort densification takes place only up to a certain limiting water content called optimum moisture content	4. No such limiting value of moisture content

4.1 THEORY OF COMPACTION

For a given soil and for a given compactive effort Fig. 4.1 shows the variation of dry density with moisture content (curve ABC). Also shown in the figure are γ_d versus w curves for $S = 100\%$ (zero air void curve) and $S = 90\%$. The density–moisture content relationship curve ABC for a soil is obtained from experiments. The other curves of γ_d versus w for different degrees of saturation can be drawn using the relationship,

$$\gamma_d = \frac{SG_s}{S + wG_s}\gamma_w \tag{4.1}$$

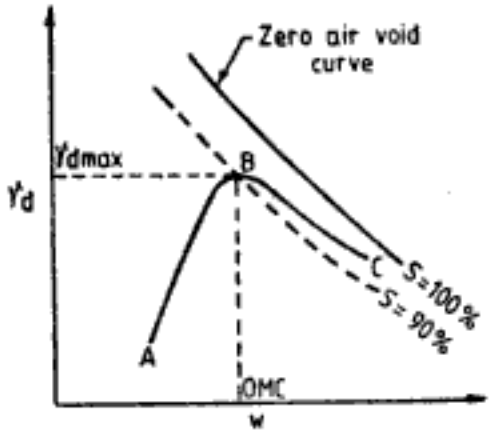

Fig. 4.1 Moisture content–dry density relationship for compacted soil

From Fig. 4.1 the following points can be noted:

1. For a given compactive effort the dry density of soil first increases with increase in water content. Beyond a certain value of water content the trend is reversed.
2. The degree of saturation is always less than 100% even at high value of water content.

The reason for the increase and then decrease in dry density can be explained as follows. Addition of water to begin with facilitates easier movement of particles and their closer packing. Hence, an increase in density. However, beyond a certain limit the water becomes excessive and tends to occupy space which otherwise would have been occupied by solid particles. Hence, a decrease in dry density due to additional void space.

Water content corresponding to maximum value of dry density (γ_{dmax}) is called optimum moisture content, OMC. Limb *AB* of the curve is said to be on the dry side of OMC and the portion *BC* on the wet side of OMC.

Figure 4.2 shows the effect of compactive effort on the dry density–moisture content relationship for soils in general. It is evident from the figure that increase in compactive effort increases the maximum dry density and decreases the optimum moisture content.

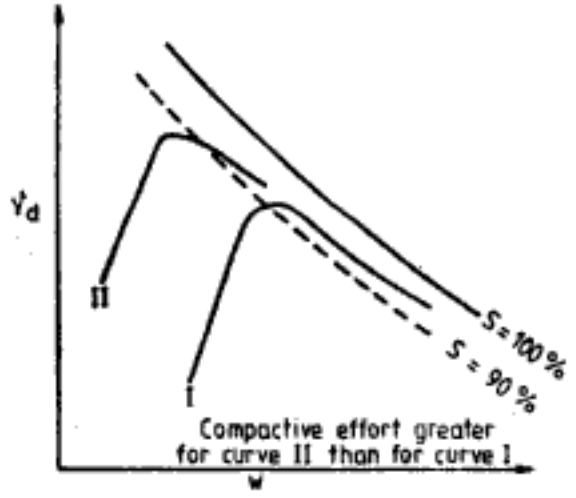

Fig. 4.2 Effect of compactive effort on moisture content–dry density relationship

The physical and behavioural characteristics of a compacted soil depend on whether it is on the dry or wet side of OMC. Table 4.2 gives an account of these differences.

Table 4.2 Characteristics of Soil on Dry and Wet Side of OMC

Soil characteristics	Dry side of OMC	Wet side of OMC
Soil structure	flocculated	dispersed
Coefficient of permeability upon saturation	more	less
Shear strength	high	low
Stress-strain behaviour	brittle	ductile
Compressibility	more	less

On account of the differences in soil characteristics the soil may be compacted at dry or wet of optimum moisture content depending upon the performance required from soil. Table 4.3 gives some typical examples.

Table 4.3 Selection of Compaction Moisture Content

For use in	Compact soil at	For reasons
Homogeneous earth dams	dry of OMC	to prevent building up of high pore water pressure
Core of earth dams	wet of OMC	to reduce coefficient of permeability and to prevent cracking of core
Subgrade for pavements	dry of OMC	to limit volume change in subgrade
Fills	dry of OMC	to facilitate easy working conditions

4.1.1 Compaction of Sands

While the foregoing discussions apply to all soils containing sufficient amount of fine grained soils, in case of purely sandy soils the dry density–water content relationship will be as shown in Fig. 4.3. Initially there is some decrease in dry density due to *bulking* of sand. The surface tension forces due to capillary water resist closer arrangement of sand particles. The trend reverses when sufficient quantity of water becomes available.

The following additional observations also can be made from Fig. 4.3:

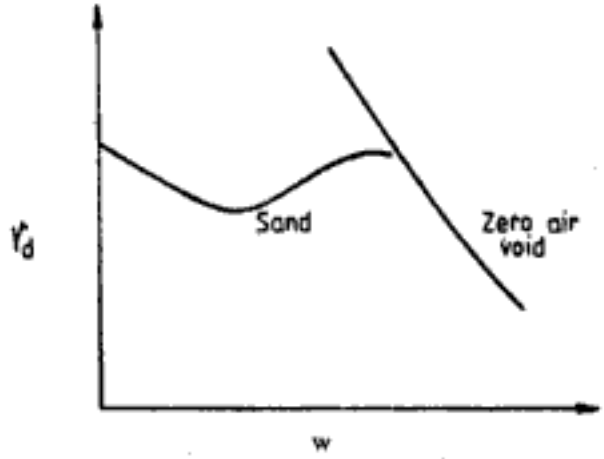

Fig. 4.3 Compaction curve for sands

1. Maximum dry density results when the soil is either dry or saturated. Therefore to achieve maximum compaction in sand it must be compacted either in a dry state or in a saturated state by flooding it with water.
2. The difference in dry density for sand with water content is very small. This implies that sand can be compacted to high density even at natural moisture content.

4.1.2 Degree of Compaction of Sands

The degree of compaction of fine grained soils is measured in relation to maximum dry density for a certain compactive effort, like 90% of light compaction density or Proctor density. But in case of coarse grained soils a different sort of index is used. Depending upon the shape, size, and gradation of soil grains, coarse grained soils can remain in two extreme states of compaction, namely in the loosest and densest states. Any intermediate state of compaction can be compared to these two extreme states using an index called *relative density* or *density index*. Relative density (I_D) is usually expressed in per cent and can be defined using void ratio, or dry density, or porosity as follows

$$I_D = \frac{e_{max} - e}{e_{max} - e_{min}} \times 100 \tag{4.2}$$

where e = in-place void ratio
e_{max} = void ratio in loosest state
e_{min} = void ratio in densest or most compact state

$$I_D = \frac{\gamma_{dmax}(\gamma_d - \gamma_{dmin})}{\gamma_d(\gamma_{dmax} - \gamma_{dmin})} \times 100 \tag{4.3}$$

where γ_d = in-place dry density
γ_{dmax} = maximum dry density or dry density corresponding to most compact state
γ_{dmin} = minimum dry density or dry density corresponding to loosest state

$$I_D = \frac{(n_{max} - n)(1 - n_{min})}{(n_{max} - n_{min})(1 - n)} \times 100 \tag{4.4}$$

where n = in-place porosity
n_{max} = maximum porosity at loosest state
n_{min} = minimum porosity at densest state

Table 4.4 shows typical values of maximum and minimum void ratio and dry density of sandy soils compiled from the data of Hough (1957) and Das (1983).

Relative density is a useful parameter to describe soil's characteristics. Empirical correlations for angle of shearing resistance, liquefaction potential, etc., in terms of relative density have been suggested. Table 4.5 gives a few of the soil's characteristics based on relative density.

Another index called *relative compaction*, R_c, is also sometimes used to define degree of compaction. Relative compaction is defined as,

$$R_c = \frac{\gamma_d}{\gamma_{dmax}} \tag{4.5}$$

Table 4.4 Maximum and Minimum Void Ratio and Dry Density of Sandy Soils

Soil type	Void ratio		Dry density g/cc	
	Maximum	Minimum	Maximum	Minimum
Gravel	0.60	0.30	2.03	1.65
Coarse sand	0.75	0.35	1.97	1.52
Fine to coarse sand	0.95	0.20	2.17	1.34
Fine sand	0.85	0.40	1.89	1.44
Gravelly sand	0.70	0.20	2.21	1.55
Silty sand	1.00	0.40	1.89	1.33
Micaceous sand	1.20	0.40	1.89	1.19
Silty sand and gravel	0.85	0.15	2.33	1.44

Table 4.5 Soil Characteristics by Relative Density†

Relative density I_D%	Soil compactness	*Angle of shearing resistance, $\phi°$	Moist or total density γ_t, g/cc	Buoyant density γ_b, g/cc
0-15	Very loose	< 28	< 1.6	< 0.96
15-35	Loose	28-30	1.52-2.00	0.88-1.04
35-65	Medium	30-36	1.76-2.10	0.96-1.12
65-85	Dense	36-41	1.76-2.25	1.04-1.36
85-100	Very dense	> 41	> 2.10	> 1.2

*Increase 5° for soils containing less than 5% silt

Meyerhof (1956): $\phi° = 25 + 0.15I_D$ for granular soils with more than 5% silt

$\phi° = 30 + 0.15I_D$ for granular soils with less than 5% silt

†Adapted from Teng, 1962. By permission of Prentice-Hall Inc., (Englewood Cliffs, NJ.)

In terms of relative density, relative compaction can be expressed as,

$$R_c = \frac{R_o}{1 - I_D(1 - R_o)} \tag{4.6}$$

where $R_o = \gamma_{dmin}/\gamma_{dmax}$ and I_D and R_c are *not* in per cent. Lee and Singh (1971) give the following approximate relationship between relative compaction and relative density,

$$R_c = 80 + 0.2I_D \tag{4.7}$$

In Eq. 4.7, R_c and I_D are both in per cent. From this equation the minimum value of R_c is 80% corresponding to $I_D = 0\%$ (at the loosest state) and $R_c = 100\%$ when $I_D = 100\%$ (at the densest state).

4.2 LABORATORY TESTS

Compaction characteristics and degree of compaction can be obtained from laboratory experiments.

4.2.1 Compaction Tests

Proctor (1933) devised a compaction test. A standard volume (944 cc) mould is filled up with soil in three layers. Each layer is compacted by delivering 25 blows with a standard hammer of weight 2.494 kg falling through 30.48 cm. Knowing the wet weight of compacted soil and its water content, dry density can be calculated. The test is repeated at different water contents to obtain the dry density *versus* water content relationship. This test is commonly known as *Standard Proctor Test.*

With the development of heavier compaction, Proctor test was modified to simulate the field compaction more realistically. This test known as *Modified Proctor Test* differs from standard proctor test only in weight of hammer and its drop. The weight of hammer is now 4.54 kg and height of fall is 45.72 cm.

Indian Standards equivalence of standard proctor test is called *light compaction test* (IS: 2720, Part VII—1974). Volume of mould is 1000 cc. Hammer weight is 2.6 kg and drop 31 cm.

Indian Standards equivalence of modified proctor test is *heavy compaction test* (IS: 2720, Part VIII—1983). Weight of hammer in this case is 4.9 kg and its height of fall is 45 cm.

By comparison it can be observed that Indian Standards experiments are not significantly different from the original tests. Hence, no appreciable difference in the test results can be expected if IS tests are substituted by original tests or *vice versa.*

4.2.2 Degree of Compaction of Sands

The minimum and maximum dry density of soil can be determined by conducting experiments according to procedures explained in IS: 2720, Part XIV—1983. The *in situ* dry density of soil can be determined either by core cutter method (IS: 2720, Part XXIX—1975) or sand displacement method (IS: 2720, Part XXVIII—1974). Relative density can then be computed using Eq. 4.3. Core cutter method or sand displacement method is useful only at shallow depths. For deeper locations, correlations with other field tests have to be used since it is difficult to take out undisturbed soil samples in sandy soil. One such correlation between standard penetration number, and relative density is given in Fig. 12.45.

4.3 FIELD COMPACTION

The equipments used for compaction of soil can be broadly classified into the following three categories:

1. Rolling equipments
2. Ramming equipments
3. Vibrating equipments

Smooth wheel rollers, pneumatic-tyred rollers, and sheep foot rollers come under the category of rolling equipments. Ramming equipments can be of impact type, internal combustion type, or pneumatic type. Vibrating equipments consist of vibrating unit mounted on a screed, plate, or roller. Vibration may be induced by rotating unbalanced mass or by pulsating hydraulic system.

The degree of compaction achieved in the field depends mainly on the following factors:

1. Thickness of lift
2. Type of roller used
3. Number of roller passes
4. Area over which the roller exerts compactive effort
5. Intensity of pressure applied to the soil

Table 4.6 provides guidelines for selection of equipment depending on soil type.

Table 4.6 Selection of Equipments for Effective Compaction in Soils

Type of equipment	For effective compaction in
Smooth wheel roller	Crushed rocks, gravels, sands
Rubber tyred roller	Gravels, sands
Pneumatic tyred roller	Sands, gravels, silty soils, clayey soils
Sheep foot roller	Silty soils, clayey soils
Rammers	Soils in confined zones
Vibratory rollers	Sands

4.3.1 Determination of Extent of Compaction Required in Clayey Soils

The degree of compaction increases markedly for the first few passes of a roller. The rate of increase, however, significantly decreases with more passes. In general it can be said that the economical number of passes in clayey soils is about 10.

4.3.2 Determination of Extent of Compaction Required in Sands

Vibratory rollers are the most suited for compaction of sands. Figure 4.4 shows the variation of degree of compaction with depth in sands when vibratory rollers are used. The following observations can be made from this figure.

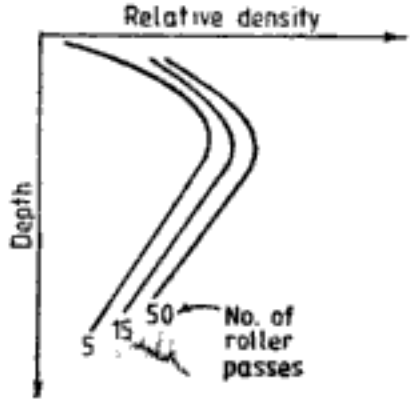

Fig. 4.4 Variation of degree of compaction with depth in sands

1. For a given number of roller passes degree of compaction is maximum at some depth below surface. The lower compaction near the surface is due to lack of confining pressure and disturbance due to agitation during compaction.

2. With increasing number of passes the degree of compaction improves but at a diminishing rate. Also the location of maximum compaction shifts downwards. After about five passes there is no significant gain in compaction.

The degree of compaction required is usually defined in terms of achieving a minimum specified value of relative density at all locations in the compacted deposit. Figure 4.5 explains an approximate procedure (D'Appolonia *et al.*, 1969) of determining the thickness of lift that must be used to fulfil this requirement. To do this,

1. First fix the number of passes per layer.
2. For a large lift obtain the relative density *versus* depth curve [shown in Fig. 4.5(a)] for the fixed number of passes. From this, the depth at which maximum compaction occurs d_{max} can be determined.
3. The actual placement lift height d should be small enough so that a loose layer is not trapped near the interface between lifts. This can be achieved by choosing d to be not significantly greater than d_{max}.
4. Placement lift height d should not be significantly less than d_{max} or else much of the compactive effort is wasted.

The curve in solid line in Fig. 4.5(b) shows the relative density-depth profile for the placement lift height d, kept equal to d_{max}.

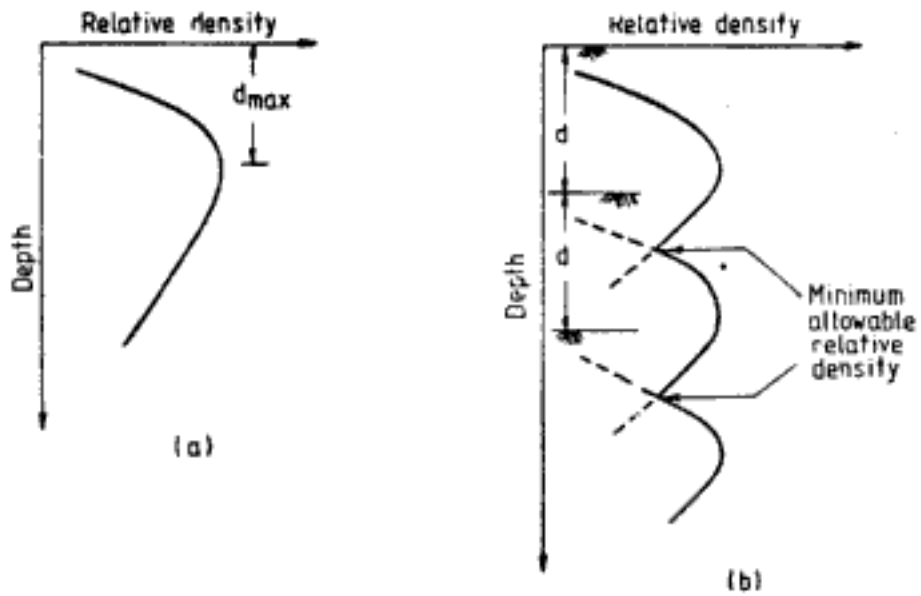

Fig. 4.5 Determination of thickness of lift for compaction of sands: (a) Relative density—depth relationship for large lift height for a fixed number of passes, d_{max} = depth of maximum compaction and (b) Relative density–depth profile (in solid line) for sand compacted in lift depth of d

4.3.3 Compaction Control

For proper control of compaction in field, frequent measurements of compaction water content and dry density must be made. In sands compaction control is by means of determining the relative density of compacted soil.

Water content in field can be determined rapidly (i) by calcium carbide method (IS: 2720, Part II—1973), or (ii) by proctor needle method. The proctor needle consists of a needle point, attached to a graduated shank which in turn is attached to a graduate plunger. Needle points of different cross-sectional area can be used depending upon the range of penetration resistance to be measured. The proctor needle is used to measure the penetration resistance in the field and this resistance is compared with a calibration chart (Fig. 4.6) prepared in the laboratory. The calibration chart is prepared by penetrating the needle into the compacted soil in the mould prepared at the time of carrying out compaction tests. The variation of penetration resistance with water content can thus be obtained and plotted. For a measured penetration resistance in field the water content can be read off from the chart.

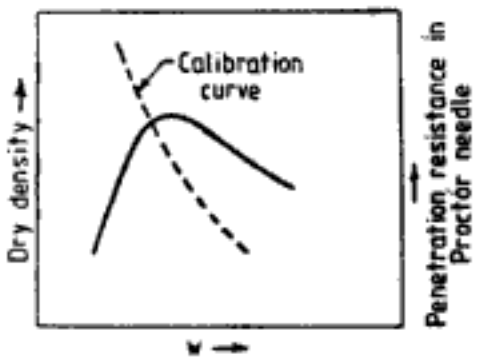

Fig. 4.6 Calibration curve for proctor needle

The in-place dry density can be determined using the tests for field density determination explained in Sec. 4.2.2.

Q 4.1: A sand deposit was compacted dry to an in-place void ratio of 0.45. For this sand $e_{max} = 0.7$ and $e_{min} = 0.3$. Determine relative density and relative compaction of this sand deposit. $G_s = 2.65$.

Ans: Using Eq. 4.2 relative density is,

$$I_D = \frac{0.7 - 0.45}{0.7 - 0.3} \times 100 = 62.5\%$$

From Table 4.5 it may be seen that the state of compaction is medium dense.
Using the relationship for γ_d, given G_s and e (from Table 1.3)

$$\gamma_{dmax} = \frac{G_s \gamma_w}{1 + e_{min}} = \frac{2.65 \times 1}{1 + 0.3} = 2.04 \text{ T/m}^3$$

$$\gamma_{dmin} = \frac{G_s \gamma_w}{1 + e_{max}} = \frac{2.65 \times 1}{1 + 0.7} = 1.56 \text{ T/m}^3$$

$$\text{in-place } \gamma_d = \frac{2.65 \times 1}{1 + 0.45} = 1.83 \text{ T/m}^3$$

From Eq. 4.5 relative compaction is,

$$R_c = \frac{1.83}{2.04} \times 100 = 89.7\%$$

5

FLOW THROUGH SOILS (STEADY STATE)

There are many situations in which flow of water through soils must be given adequate consideration in civil engineering design. Some typical examples of flow through soil are shown in Figs. 5.1 to 5.4.

Fig. 5.1 Flow through homogeneous earth dam

Figure 5.1 shows the example of flow through an earth dam. The flow characteristics must be understood in order to investigate:

1. Seepage losses through the dam
2. The stability of upstream and downstream slopes of the dam
3. The filter or drain requirements

Figure 5.2 illustrates the situation of flow under a concrete dam. Investigations here will include:

1. Seepage losses
2. Uplift pressure on the dam
3. Exit gradient at the downstream end of dam

Consider a sheet pile, for example, used in an excavation to make room for some construction work. Because of the differential water level on the two sides of the sheet pile as shown in Fig. 5.3 water flows around the sheet pile. Then the effect of flow should be considered in the determination of

1. Stability of the excavation
2. Lateral pressure acting on sheet pile

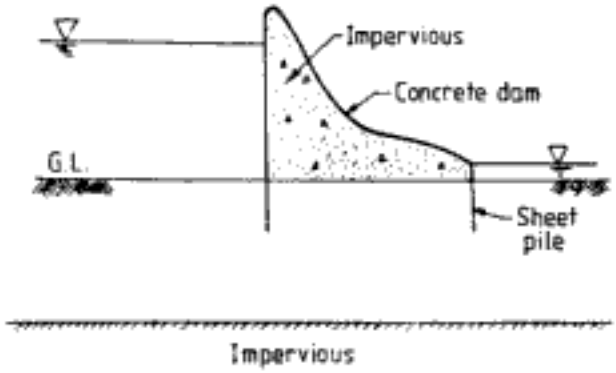

Fig. 5.2 Flow under an impervious dam

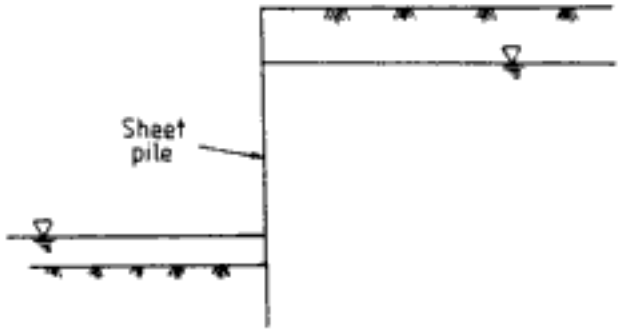

Fig. 5.3 Flow around sheet pile

Figure. 5.4 depicts the case of water flow into wells. Water is required to be pumped from well point installations, from wells for field permeability determination and in many other applications. Study of flow through soils in these cases is a requirement to

1. Determine and plan for rate of pumping
2. Plan and design well point installations

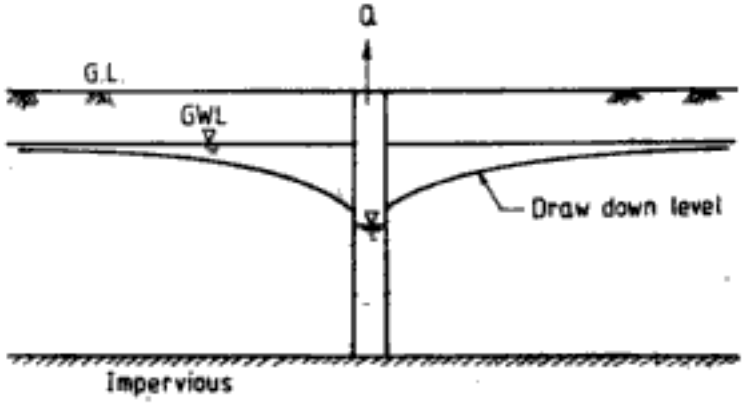

Fig. 5.4 Flow into a well

5.1 TYPES OF FLOW THROUGH SOIL

The different types of flow can be classified based on (i) time, (ii) the nature of flow, (iii) boundaries of flow, and (iv) the direction of flow.

Based on time

Steady flow : In steady flow, at any point there is no change in velocity or pressure head with respect to time.

Transient flow : At any point velocity or pressure head varies with time.

Flow through earth dam in Fig. 5.1 after the top flow line has stabilised is an example of steady flow. Flow of water during the process of consolidation, explained in Ch. 7 is an example of transient flow.

Based on nature of flow

Laminar flow : The pressure head loss is directly proportional to velocity of flow ($h_f \propto v$) and the flow is free of eddies.

Turbulent flow : The pressure head loss is proportional to velocity of flow raised to an exponent ($h_f \propto v^N$). Flow is a local phenomenon and contains eddies.

Flow through soils is mostly laminar in nature.

Based on boundaries of flow

Confined flow : In confined flow, the flow occurs under pressure. The flow takes place between non-leaky or impervious boundaries.

Unconfined flow : The flow occurs under gravity and there is a phreatic surface of flow which is open to atmosphere.

Flow under a concrete dam as shown in Fig. 5.2 is an example of confined flow. Figure 5.1 illustrates unconfined flow in which the top flow line in the flow through earth dam is the phreatic surface.

Based on direction of flow

One-dimensional flow : The velocity or pressure is a function of only one direction, say $f(x)$

Two-dimensional flow : The velocity or pressure is a function of two orthogonal directions, say $f(x, y)$

Three-dimensional flow : The velocity or pressure is a function of three orthogonal directions, say $f(x, y, z)$

5.2 CONCEPT OF HEADS

Figures 5.5 and 5.6 show two cases of hydrostatic condition where there is no flow but the water remains static. Figure 5.5 is a case of static groundwater obtained below ground. Figure 5.6 shows the case of water in a lake. If we insert two stand pipes 1 at A and 2 at B as shown in these figures, the water will rise in the stand pipes and will ultimately stabilise at the elevation of GWL (in Fig. 5.5) or at lake water level (in Fig. 5.6). To define the water head at a point the following three heads must be considered:

1. *Pressure head*, h_p, is the pressure divided by unit weight or density of water. Or simply, it is the height to which the water will rise in the stand pipe from its point of insertion. Thus, h_{pA} is the pressure head at point A and h_{pB} at point B.

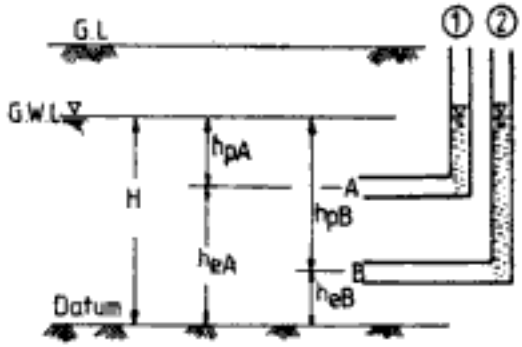

Fig. 5.5 Static groundwater

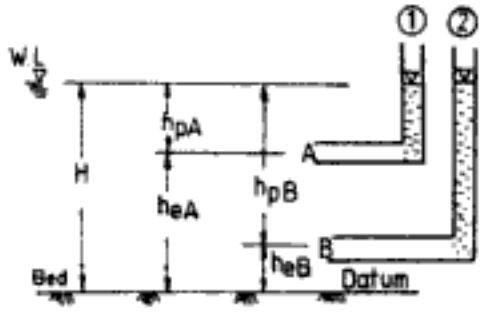

Fig. 5.6 Water body above ground level

2. *Elevation head*, h_e, is the distance of the point from a chosen datum.
3. *Total head*, h, is the sum of pressure head and elevation head. Thus $h = h_p + h_e$.

Now, consider the case of water flowing through soil.

Figures 5.7 and 5.8 are examples of one-dimensional flow through soils. In Fig. 5.7 water flows vertically upwards through a column of soil. The water levels at D and C are kept constant. The elevation heads with reference to a common datum and the pressure heads at the bottom and top of soil column, A and B respectively, are shown in Fig. 5.7. In Fig. 5.8 the water flow is parallel to the impervious bed. This figure also shows the elevation and pressure heads for two points A and B. The total head for the hydrostatic and hydrodynamic cases are compared now.

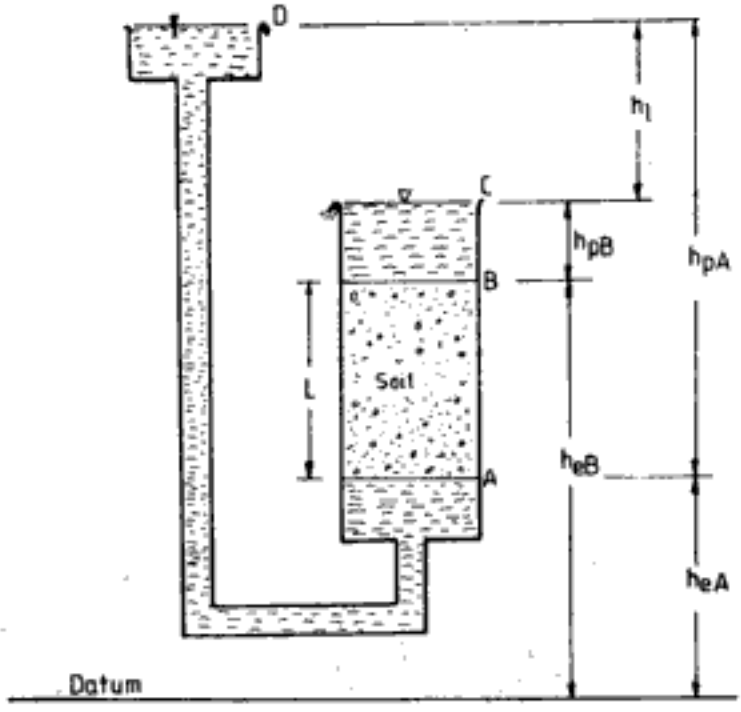

Fig. 5.7 One-dimensional upward flow

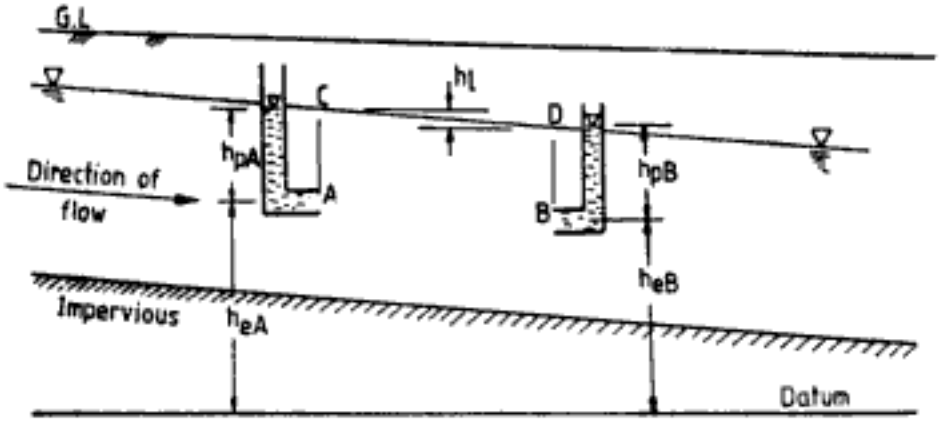

Fig. 5.8 Flow parallel to impervious boundary

5.2.1 Hydrostatic Case—No Flow (Figs. 5.5 and 5.6)

If we denote h_A = total head at A

h_B = total head at B

then referring to figures,

$$h_A = h_{eA} + h_{pA}$$
$$h_B = h_{eB} + h_{pB}$$
$$h_A = h_B$$

When there is no water flow the total head at all points is the same.

5.2.2 Hydrodynamic Case—Flow (Figs. 5.7 and 5.8)

Referring to Figs. 5.7 and 5.8

$$h_A = h_{eA} + h_{pA}$$
$$h_B = h_{eB} + h_{pB}$$
$$h_A \neq h_B$$
$$h_B < h_A$$
$$h_A - h_B = h_l$$

The total head at *corresponding points* in the *direction* of flow are not equal. The difference of the total heads between these points is known as the "head loss", h_l.

5.2.3 Points to Note

1. While considering the total head in hydrodynamic situation the velocity head has been ignored because of its very low value.
2. The datum chosen for measurement of elevation head must have a common level. For example, the impervious boundary has not been considered as datum because of its inclination and varying levels along the direction of flow.

3. Any common level can be selected as datum, since in flow problems absolute value of total head or elevation head is of little use. Rather the difference in total head (h_l) is of interest and h_l is same irrespective of where we choose the datum.

5.3 DARCY'S LAW

Consider Fig. 5.7. Let the length of soil column AB be L and its cross-sectional area A. If we measure the rate of flow q of water through the soil column, it is possible to express q as

$$q = -k\frac{h_B - h_A}{L}A \tag{5.1}$$

If rate of flow is expressed as

$$q = vA \tag{5.2}$$

where v = superficial velocity of flow, i.e., velocity of flow with respect to gross-cross-sectional area (A) of soil

then from Eqs. 5.1 and 5.2

$$v = -k\frac{h_B - h_A}{L} = k\frac{h_l}{L}$$

or

$$v = -kl \tag{5.3}$$

whete i = hydraulic gradient, i.e., the ratio of head loss to the flow path of length L

k = coefficient of permeability (with units of velocity, like cm/s)

Equation 5.3 is commonly known as Darcy's law. Value of k varies over a large range and depends mainly on soil type. Table 5.1 shows typical values of k for different soil types. Very small quantities of fine grained soils can block the voids between coarse particles which will greatly reduce the permeability of coarse grained soils. Fissured clays have higher values of k (between 10^{-2} to 10^{-6} cm/s) than similar intact clays ($k < 10^{-6}$ cm/s), because much of the flow takes place through fissures than through the soil.

The actual velocity of flow through the pores of the soil referred to as seepage velocity (v_s) is rarely considered in soil mechanics. The concept of seepage velocity in illustrated in Fig. 5.9.

$$v_s = \frac{v}{n} \tag{5.4}$$

where v_s = seepage velocity, i.e., velocity of flow through the proportion of area of voids

v = superficial velocity

n = soil porosity

Q 5.1: Determine the rate of flow through soil shown in Fig. 5.10. k of soil = 10^{-3} cm/s. Area of cross-section of soil = 100 cm². Determine also the total discharge in 30 minutes.

Ans: Irrespective of any chosen datum it can be shown that total head loss in soil = 1 m

$$L = 2 \text{ m}$$

$$\text{Hydraulic gradient} = \frac{1}{2} = 0.5$$

Hence, $v = 10^{-3} \times 0.5$

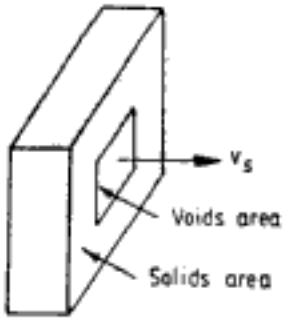

Fig. 5.9 Seepage velocity

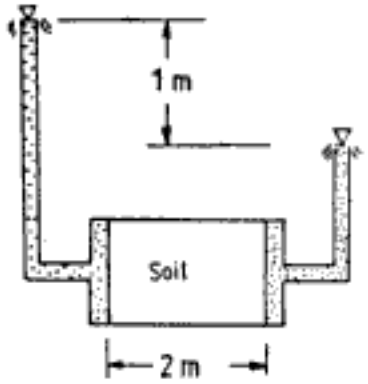

Fig. 5.10 Q 5.1

Rate of flow $= q = 10^{-3} \times 0.5 \times 100 = 5 \times 10^{-2}$ cm^3/s

Total discharge (Q) in 30 minutes

$$= 5 \times 10^{-2} \times 30 \times 60$$
$$= 90 \text{ cc}$$

5.4 FACTORS INFLUENCING COEFFICIENT OF PERMEABILITY

The factors and the manner in which they influence k are briefly discussed below.

1. The size and shape of soil particles—the soil type

Values of k in Table 5.1 show the influence of soil type on coefficient of permeability. Hazen gives the following empirical formula for clean filter sands in loose state:

$$k \text{ (cm/s)} = C_1 D_{10}^2 \tag{5.5}$$

where D_{10} = effective size in cm

C_1 = empirical coefficient which varies from 90 to 120, often assumed as 100.

2. The soil density or void ratio

Permeability of soil decreases as the soil density increases or as the void ratio decreases. Figure 5.11 shows the typical variation of k with void ratio. This variation can be mathematically described as

$$e \propto \log k \tag{5.6}$$

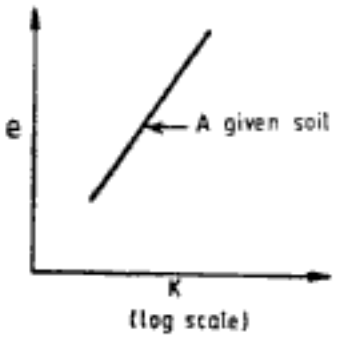

Fig. 5.11 Variation of coefficient of permeability with void ratio

3. The detailed arrangement of the individual soil grains—the structure or soil fabric
The coefficient of permeability is different in different directions. It also depends upon the nature of formation of soil.

$k_h > k_v$ for water deposited soil
$k_v > k_h$ for wind blown deposits

k_h and k_v are coefficients of permeability in horizontal and vertical directions, respectively. Further,

k for soil placed in a relatively dry state $>$ k for soil placed in a relatively moist state

4. The permeant, its viscosity or temperature
It is customary to standardise the value of k at 20°C.

$$k_{20} = \frac{\mu_T}{\mu_{20}} \frac{\gamma_{20}}{\gamma_T} k_T \tag{5.7}$$

where k_{20} = value of k at 20°C
k_T = value of k at T°C
μ_{20} = viscosity of permeant at 20°C
μ_T = viscosity of permeant at T°C
γ_{20} = unit weight or density of permeant at 20°C
γ_T = unit weight or density of permeant at T°C

The values of μ_T/μ_{20} for water for different temperatures are given in Table 5.2. Value of γ_{20}/γ_T is approximately 1.

Table 5.2 Values of μ_T/μ_{20} for Water for Different Temperatures

Temperature T°C	μ_T/μ_{20}	Temperature T°C	μ_T/μ_{20}
10	1.298	21	0.975
11	1.263	22	0.952
12	1.228	23	0.930
13	1.195	24	0.908
14	1.165	25	0.887
15	1.135	26	0.867
16	1.106	27	0.847
17	1.078	28	0.829
18	1.051	29	0.811
19	1.025	30	0.793
20	1.000		

5. The presence of discontinuities

Presence of air in soil makes it unsaturated and,

$k_{unsat} < k_{sat}$
k_{unsat} value of k for unsaturated soil
k_{sat} = value of k for saturated soil

n general,

$$\left(\frac{k_{unsat}}{k_{sat}}\right)_{\text{at same void ratio}} = \left(\frac{S}{100}\right)^{3.5} \tag{5.8}$$

where S = degree of saturation, 0-100%

For S = 80 to 100 per cent,

$$\frac{k_{unsat}}{k_{sat}} = 1 - m\left(\frac{1 - S}{100}\right) \tag{5.9}$$

where m = a constant which varies from 2 to 4 = 3.5 for S = 80 to 100 per cent.

Lower value of m holds for soils of uniform grain size and m increases in well graded materials.

Table 5.3 gives values of (k_{unsat}/k_{sat}) according to Eqs. 5.8 and 5.9, from which it can be seen that even a small amount of air present in soil can greatly reduce its permeability.

Table 5.3 Values of k_{unsat}/k_{sat}

S %	Eq. 5.8	Eq. 5.9		
		$m = 2$	$m = 3.5$	$m = 4$
30	0.01	—	—	—
50	0.09	—	—	—
70	0.29	—	—	—
75	0.37	—	—	—
80	0.46	0.60	0.30	0.20
85	0.57	0.70	0.48	0.40
90	0.69	0.80	0.65	0.60
95	0.84	0.90	0.82	0.80
100	1.00	1.00	1.00	1.00

5.5 FLOW THROUGH STRATIFIED SOIL DEPOSITS

5.5.1 Flow along Direction of Stratification

Figure 5.12 illustrates flow along direction of stratification. This layered system can now be converted into a single layer of thickness D having an equivalent coefficient of permeability k_h. The results are obtained from following two considerations: (i) the head loss over a given distance of flow is same in all layers, and (ii) total rate of flow is the sum of rate of flow in each layer.

$$k_h = \frac{\sum_{n=1}^{m} k_n d_n}{\sum_{n=1}^{m} d_n} \simeq \frac{k_p d_p}{\sum_{n=1}^{m} d_n} \tag{5.10}$$

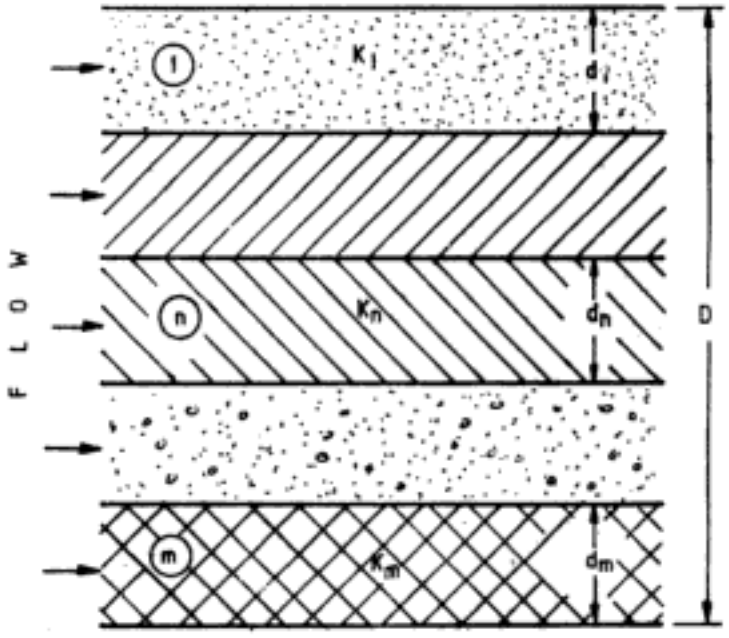

Fig. 5.12 Flow along direction of stratification

where k_h = equivalent coefficient of permeability along direction of stratification for an equivalent layer of thickness D

k_n = k of nth layer

d_n = thickness of nth layer

k_p = k of the most pervious layer

d_p = thickness of the most pervious layer

m = the total number of soil layers

$D = \sum_{n=1}^{m} d_n$ = sum of thickness of all layers

5.5.2 Flow Perpendicular to the Direction of Stratification

In the case of flow normal to direction of stratification (Fig. 5.13) the equivalent coefficient of permeability k_v can be worked out from the following considerations: (i) rate of flow in each layer is same, and (ii) total head loss is sum of head loss in all layers.

$$k_v = \frac{\sum_{n=1}^{m} d_n}{\sum_{n=1}^{m} \frac{d_n}{k_n}} \simeq \frac{\sum_{n=1}^{m} d_n}{\frac{d_l}{k_l}} \tag{5.11}$$

where k_v = equivalent coefficient of permeability perpendicular to direction of stratification for an equivalent layer of thickness D

k_l = k of least pervious layer

d_l = thickness of least pervious layer

$D = \sum_{n=1}^{m} d_n$ = sum of thickness of all layers

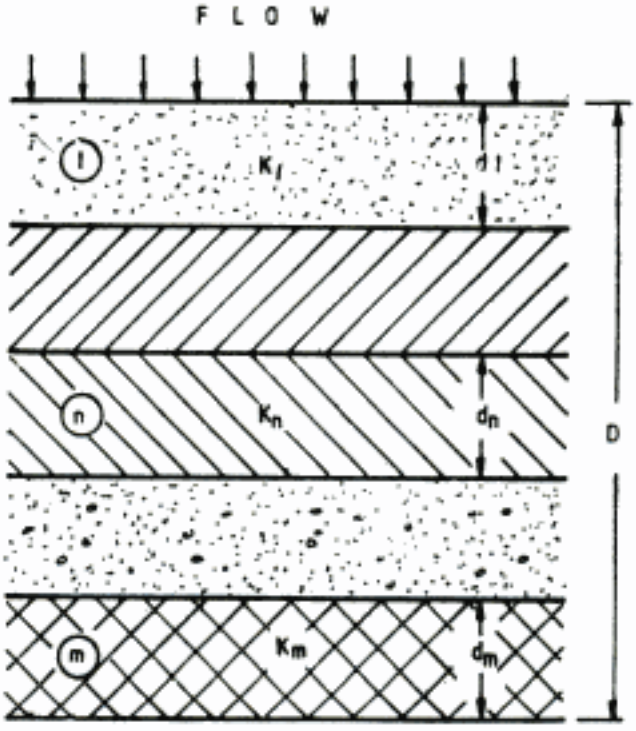

Fig. 5.13 Flow perpendicular to direction of stratification

Equations 5.10 and 5.11 give rigorous and approximate expressions for equivalent coefficients of permeability. The approximate relationships indicate that k_h is governed by the most pervious layer and k_v is governed by the most impervious layer. The approximate expression for k_v gives good results when the k-values of individual layers are significantly different. The results obtained for k_h by the approximate expression are not, however, as good as those obtained for k_v. In general $k_h > k_v$.

Q 5.2: Figure 5.14 shows flow occurring along the horizontal direction of a three-layer deposit. The two-stand pipes shown in the figure are at the same elevation. Determine the following:

(a) the equivalent coefficient of permeability, and
(b) the rate of flow

Ans:

(a) Equivalent coefficient of permeability:

$$k_h = \frac{(3\times3\times10^{-3}) + (2\times6.5\times10^{-2}) + (4\times7\times10^{-4})}{3+2+4}$$

$$= 1.58\times10^{-2} \text{ cm/s}$$

By approximate relationship,

$$k_h \simeq \frac{2\times6.5\times10^{-2}}{3+2+4} = 1.44\times10^{-2} \text{ cm/s}$$

which is lower than the solution by rigorous method by 9 per cent.

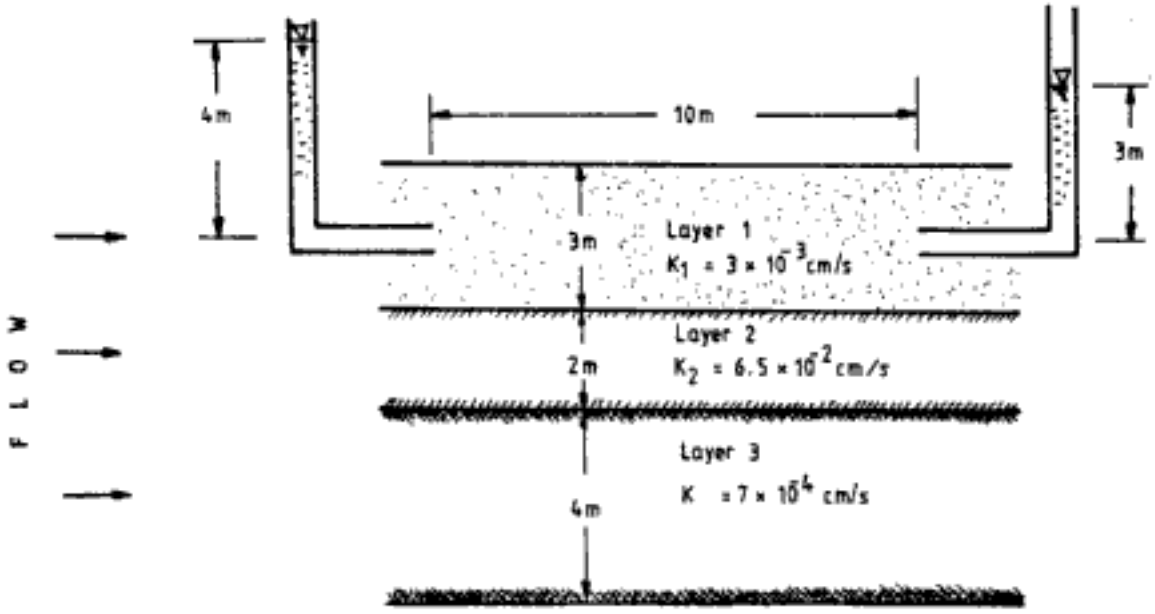

Fig. 5.14 Q 5.2

(b) Rate of flow:

$$h_l = 1 \text{ m} \qquad L = 10 \text{ m}$$

$$v = 1.58 \times 10^{-2} \times \frac{1}{10} = 1.58 \times 10^{-3} \text{ cm/s}$$

$$q = 1.58 \times 10^{-3} \times 900 \times 100 = 142.2 \text{ cc/s/m width of deposit}$$

Q 5.3: Figure 5.15 shows flow occurring normal to the direction of stratification. Determine the following:

(i) the equivalent coefficient of permeability,
(ii) the rate of flow, and
(iii) the total head loss in the three layers

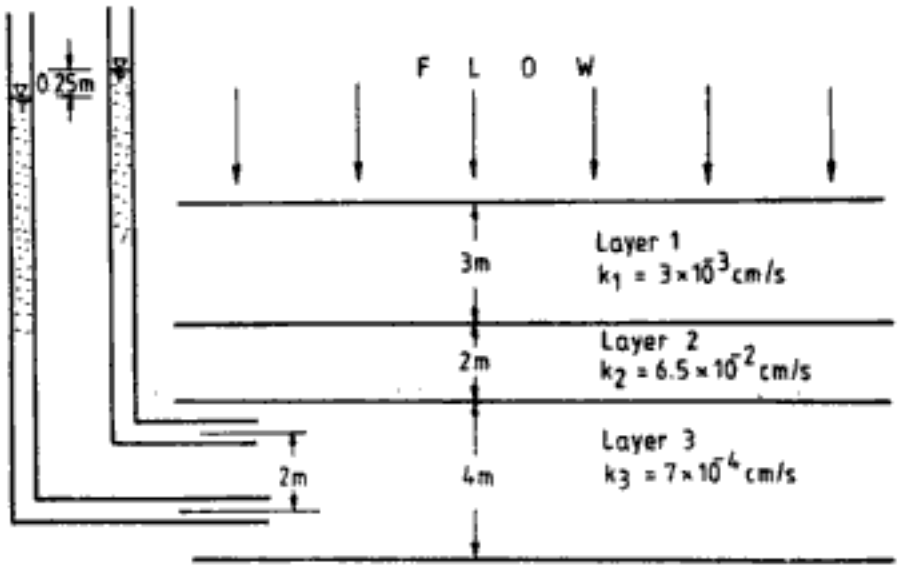

Fig. 5.15 Q 5.3

Ans:

(i) *Equivalent coefficient of permeability:*

$$k_v = \frac{3 + 2 + 4}{\frac{3}{3\times10^{-3}} + \frac{2}{6.5\times10^{-2}} + \frac{4}{7\times10^{-4}}}$$

$$= 1.33\times10^{-3} \text{ cm/s}$$

By approximate relationship

$$k_v \simeq \frac{3 + 2 + 4}{4/7\times10^{-4}} = 1.58\times10^{-3} \text{ cm/s}$$

which is higher than the solution by rigorous method by 19 per cent.

(ii) *Rate of flow:*

In layer 3: $h_l = 0.25$ m; $L = 2$ m

$$v = 7\times10^{-4}\times\frac{0.25}{2} = 0.875\times10^{-4} \text{ cm/s}$$

$$q = 0.875\times10^{-4}\times100\times100$$

$$= 0.875 \text{ cc/s/m}^2 \text{ of plan area.}$$

(iii) *Total head loss:*

For continuity of flow

$$v = -k_3 i_3 = -k_{eq} i_{eq}$$

$$-i_{eq} = \frac{\text{(total head loss in 9 m)}}{9}$$

$$\text{Total head loss in 9 m} = \frac{0.875\times10^{-4}}{1.33\times10^{-3}}\times9$$

$$= 0.5921 \text{ m}$$

5.6 TWO-DIMENSIONAL FLOW

There are a number of situations in soil mechanics where the flow through soil is two-dimensional. For example, the illustrations in Figs. 5.1, 5.2 and 5.3 show two-dimensional flow problems.

5.6.1 Laplace's Equation

In a three-dimensional space of x, y, z orthogonal coordinates, from consideration of satisfying the condition of continuity of flow at any point in the flow region, the following equation can be derived,

$$k_x \frac{\partial^2 h}{\partial x^2} + k_y \frac{\partial^2 h}{\partial y^2} + k_z \frac{\partial^2 h}{\partial z^2} = 0 \qquad (5.12)$$

where, h is the total head, and k_x, k_y, and k_z are coefficients of permeability in x, y and z directions respectively. In an isotropic soil where the properties are same in all directions,

$$k_x = k_y = k_z$$

Then Eq. 5.12 reduces to the form,

$$\frac{\partial^2 h}{\partial x^2} + \frac{\partial^2 h}{\partial y^2} + \frac{\partial^2 h}{\partial z^2} = 0 \tag{5.13}$$

Equation 5.13 becomes, for two-dimensional flow situations, as

$$\frac{\partial^2 h}{\partial x^2} + \frac{\partial^2 h}{\partial y^2} = 0 \tag{5.14}$$

Equation 5.14 is commonly referred to as Laplace's equation, the solution of which defines the flow characteristics in the region of flow.

5.6.2 Graphical Solution

The graphical solution to Laplace equation is called as *flow net*. Figure 5.16 shows the flow net for flow around a sheet pile. A flow net is a network of two sets of orthogonal lines. In Fig. 5.16 lines 1–1–1, 2–2–2, and 3–3–3, are one set of lines called as *stream lines* or *flow lines*. Flow occurs along stream lines and there is no flow across a stream line. The other set of lines are orthogonal to the streamlines and are known as *equipotential lines*. Along an equipotential line the total head is constant. The space between two adjacent stream lines is known as *flow channel*. A flow net is very useful in analysis of flow problem.

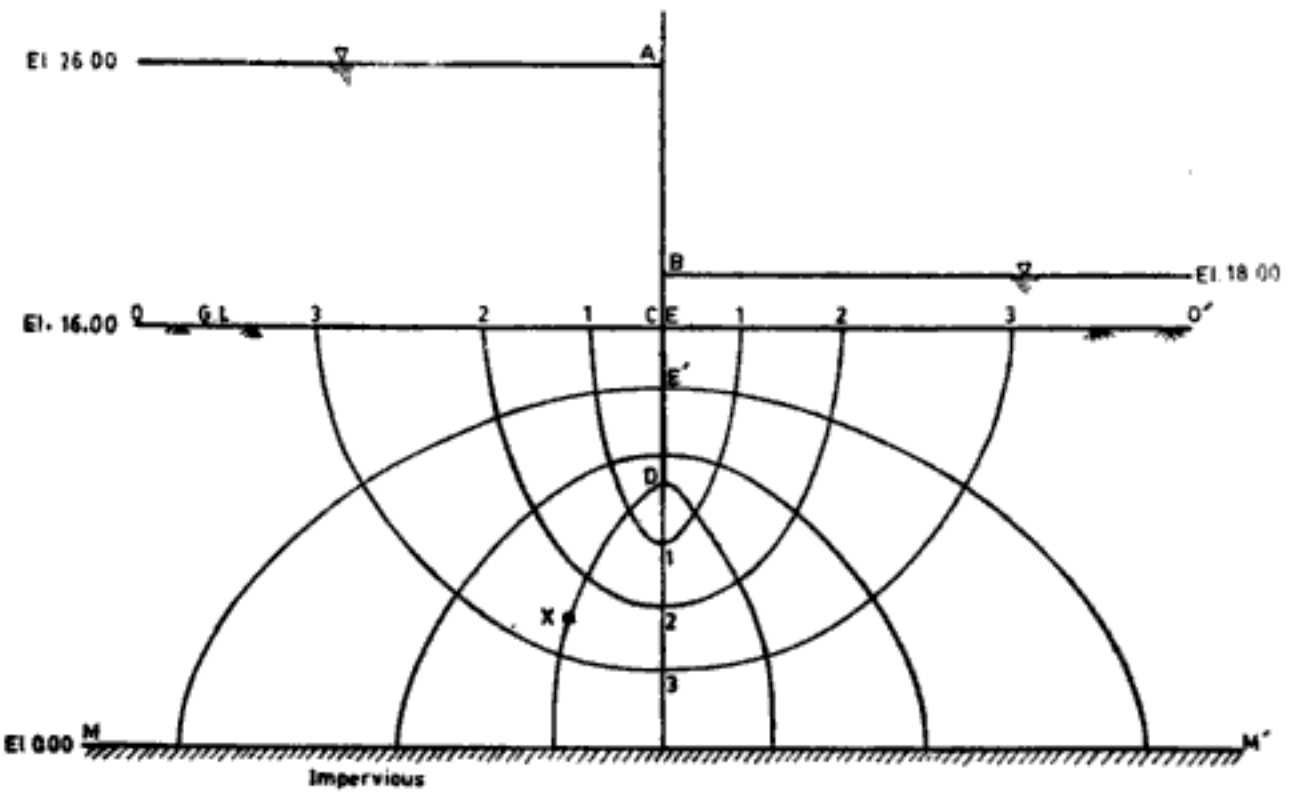

Fig. 5.16 Flow net for flow around sheet pile

Drawing of flow net: To draw a flow net the following procedure may be followed.

1. Determine the flow boundaries. In Fig. 5.16 for example

   CDE is a flow line
   MM' is a flow line
   OC is an equipotential line
   EO' is an equipotential line

2. Draw a set of stream lines and equipotential lines within the boundaries, keeping in mind the two points that (i) stream lines do not intersect each other, and (ii) stream lines and equipotential lines intersect each other at right angles.
3. Adjust the number of equipotential lines and flow lines such that the network is made of curvilinear squares. Though a network may be constructed with curvilinear rectangles also, a square network is convenient and useful for the following reasons. In a square network the flow through each flow channel is equal and also the head loss between successive equipotential lines is equal.

Flow net construction is a painstaking and time-consuming trial-and-error process. The flow net can also have fractional flow channel.

Uses of flow net: The flow net can be used to determine the following:

1. *The quantity of flow*: The rate of flow, q, per unit length of structure is given by the relationship,

$$q = kh \frac{n_f}{n_d} \tag{5.15}$$

where n_f = number of flow channels

n_d = number of head drops $= (N_p - 1)$

N_p = number of equipotential lines

h = total head loss from the first to the last equipotential line

2. *Uplift pressure*: The uplift pressure diagram under a hydraulic structure can be constructed knowing the pressure heads of equipotential lines terminating at the bottom of the structure. The area of the uplift pressure diagram gives the total uplift force on the structure.
3. *Exit gradient*: Near the downstream end of the hydraulic structure the water exits with a high velocity. To avoid piping failure the exit gradient must be kept within the critical hydraulic gradient. The exit gradient at exit points can be determined using flow net diagram.

In addition to the above uses, at any point within the flow region the total and pressure heads, velocity of flow and its direction can also be determined using flow net diagram.

Q 5.4: For the flow around sheet pile shown in Fig. 5.16 determine (i) the total quantity of seepage for a day over a length of 40 m, (ii) the exit gradient at point E, (iii) the elevation to which water will rise in a stand pipe inserted at x.

k of soil $= 5.5 \times 10^{-4}$ cm/s

Ans:

(i) *Quantity of seepage*:

No. of flow channels $= n_f = 4$

No. of potential drops $= n_d = 8$

Total head loss $= 26.00 - 18.00 = 8$ m

Rate of flow, q per metre length $= 5.5 \times 10^{-4} \times 800 \times 4/8 \times 100$

$= 22$ cm^3/s/m

Quantity of seepage in a day over a length of 40 m,

$$Q = 22 \times 40 \times 24 \times 60 \times 60 \times 10^{-6}$$

$= 76.032$ m^3/day

$= 76{,}032$ l/day

(ii) *Exit gradient at E*

Length of flow path $E'E = 2.5$ m

Head drop over $E'E = \frac{1}{8} \times 8$ m

Exit gradient, $i_{exit} = \frac{8/8}{2.5} = 0.4$

(iii) *Pressure head at x*:

No. of equipotential drops till $x = 3$

$\therefore$ the head loss till point $x = 3 \times \frac{8}{8} = 3$ m

The elevation to which water will rise in a stand pipe at x

$= 26.00 - 3 = 23$ m

Q 5.5: Determine the uplift force per metre width of the dam shown in Fig. 5.17.

Ans: The flow net is drawn as shown in Fig. 5.17. The flow net consists of 4 flow channels and 12 equipotential drops. Total head drop is 10 m. The uplift pressure is determined at points C, K, L, M and D.

Point C: The head drop till $C' = \frac{10}{12} \times 7 = 5.833$ m

Length of $C'CK = 10$ m

Head loss over $C'CK = \frac{10}{12} = 0.833$ m

Length of $C'C = 2.8$ m

Head loss over $C'C = 0.833 \times \frac{2.8}{10} = 0.233$ m

Total head loss till $C = 5.833 + 0.233 = 6.067$ m

Elevation to which water will rise in standpipe in C

$= 28.00 - 6.067 = 21.933$ m

Pressure head at $C = 21.933 - 16 = 5.933$ m

Uplift pressure at $C = 5.933 \times 1 = 5.933$ T/m^2

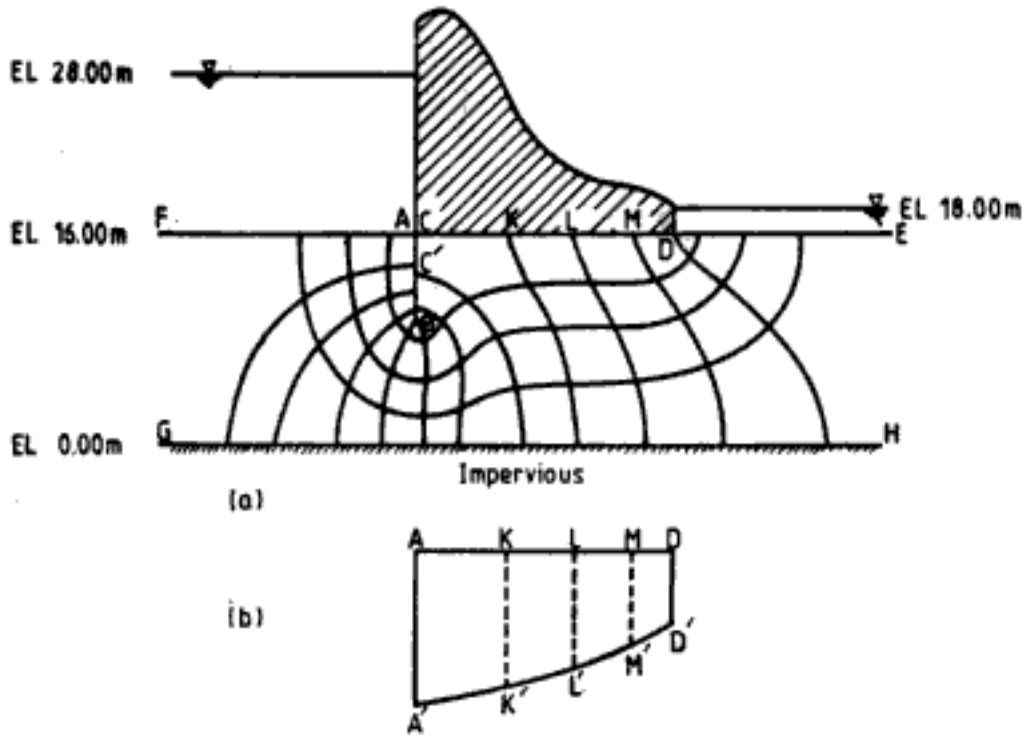

Fig. 5.17 Q 5.5

Table 5.4 shows the calculated values for other points.

Table 5.4 Uplift Pressure Calculations for Fig. 5.17(b)

Point	Elevation of water rise in stand pipe, m	Pressure head m	Uplift pressure T/m^2
A	21.933	5.933	5.933 (*AA'*)
K	21.330	5.330	5.330 (*KK'*)
L	20.500	4.500	4.500 (*LL'*)
M	21.667	3.667	3.667 (*MM'*)
D	18.833	2.833	2.833 (*DD'*)

The uplift pressure diagram is shown in Fig. 5.17(b). Uplift force can now be calculated by determining the area of the uplift pressure diagram. In the figure $AK = 7.2$ m; $KL = 5.2$ m; $LM = 4.4$ m; $MD = 3.2$ m.

Uplift force P_{up} per metre width of dam

$$= \frac{(5.933 + 5.330)}{2} \times 7.2 \times 1 + \frac{(5.330 + 4.500)}{2} \times 5.2 \times 1$$

$$+ \frac{(4.500 + 3.667)}{2} \times 4.4 \times 1 + \frac{(3.667 + 2.833)}{2} \times 3.2 \times 1$$

$$P_{up} = 94.5 \text{ T/m}$$

5.7 DETERMINATION OF COEFFICIENT OF PERMEABILITY

Coefficient of permeability can be determined by conducting (i) laboratory tests, and/or (ii) field tests. Laboratory tests are conducted on small undisturbed soil samples which may not represent the field conditions in entirety. For very important projects k must be determined by field tests.

5.7.1 Laboratory Tests

The two tests commonly used in laboratory are:

1. Constant head permeability test
2. Variable head permeability test.

Where the quantity of flow through soil is considerable such as sands, constant head permeability test can be used, in which a measurable quantity of water is collected over a small interval of time.

Where the quantity of flow through soil is small and is not adequate enough for measurement in reasonable time limits, such as in the case of clays, variable head (or falling head) permeability test is used. The test results of consolidation test described in Ch. 7 can also be used for evaluation of k in such types of soil.

The applicability and limitations of the laboratory tests to different soil types are explained in Table 5.1. IS: 2720, Part XVII—1966 and IS: 2720, Part XXXVI—1975 explain the procedures for conducting laboratory tests for determination of coefficient of permeability.

1. *Constant head permeability test*: Figure 5.18 shows three possible variations in the test. Figures 5.18(a) and (b) show the arrangement in which the flow is one-dimensional and is downwards. Figure 5.18(c) shows the arrangement in which flow is one-dimensional but upwards. In this set-up (Fig. 5.18c) (with the help of valve C the rate of flow through soil can be regulated. The figures also indicate the head loss (h_l) and the corresponding length of soil, L, over which the head loss occurs.

The experimental data consist of a measured quantity of discharge Q during a time interval t, under steady state conditions of flow. The head loss h_l is also noted. k can be computed from the formula,

$$k = \frac{QL}{h_l A t} \tag{5.16}$$

where Q = quantity of discharge in time t
h_l = head loss over length L
A = area of cross-section of soil sample

Q. 5.6: The observations made in a constant head permeability test of type shown in Fig. 5.18(c) are given below:

Q cc	t s	h_1 cm	h_2 cm
100	128	68.5	46
100	109	78.5	55
100	86	87	61

Other data are: L = 15 cm; diameter of soil sample = 10 cm. Compute the coefficient of permeability of soil.

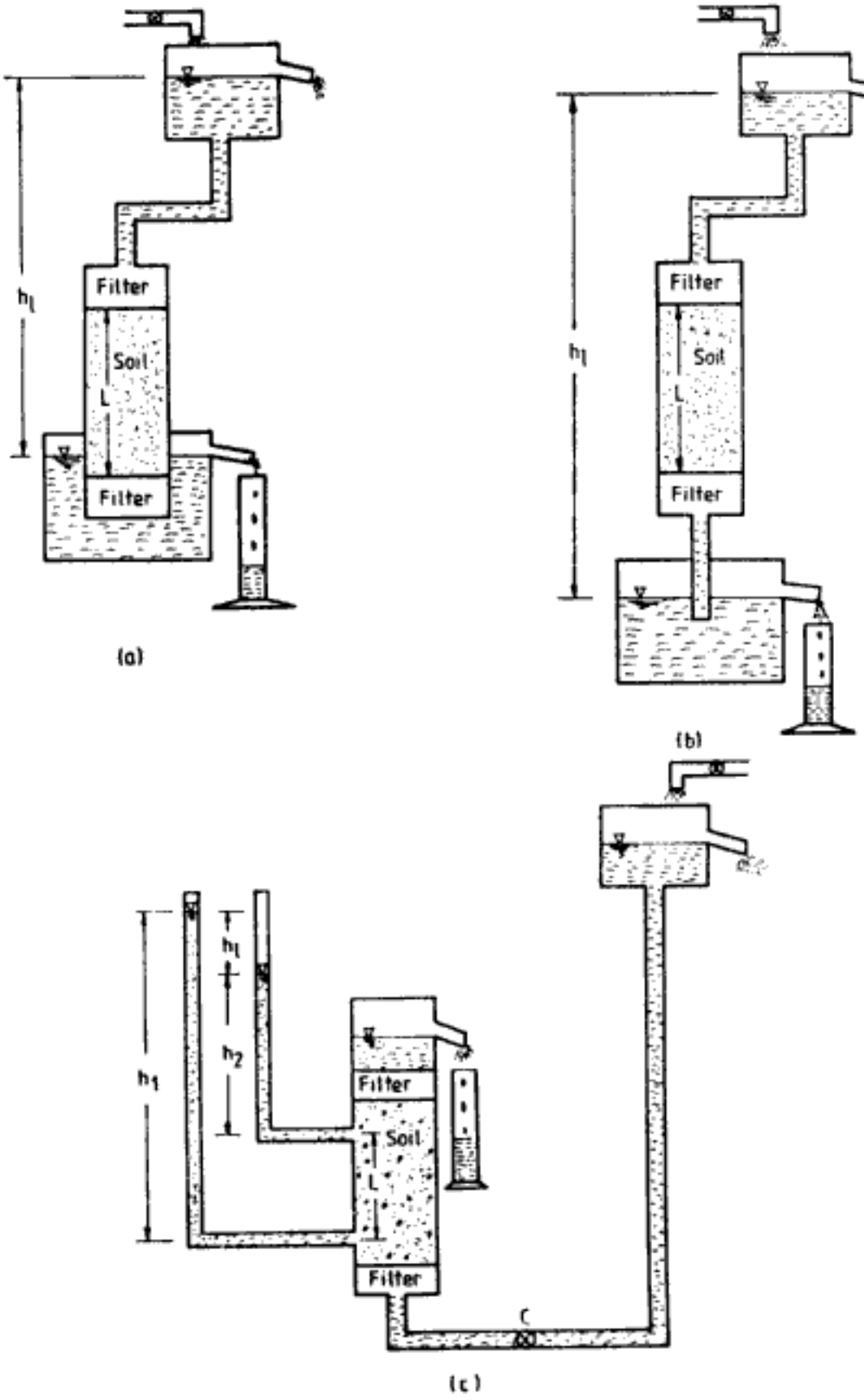

Fig. 5.18 Different arrangements for constant head permeability test

Ans: Area of soil sample $= \pi \times \frac{10^2}{4} = 78.54 \text{ cm}^2$

For first set of data:

$$h_1 = 68.5 - (46 + 15) = 7.5 \text{ cm}$$

Using Eq. 5.16 $$k = \frac{100 \times 15}{7.5 \times 78.54 \times 128} = 1.99 \times 10^{-2} \text{ cm/s}$$

Similarly,
with second set of data, $k = 2.06 \times 10^{-2}$ cm/s
with third set of data, $k = 2.02 \times 10^{-2}$ cm/s
Average value of $k = 2 \times 10^{-2}$ cm/s

2. *Variable head permeability test*: A typical set-up for falling head permeability test is shown in Fig. 5.19. The water level in the stand pipe is observed from time to time. Let A be the area of soil sample, a the area of stand pipe and L the length of soil sample. If the head difference at time t_1 is h_1 and at time t_2 is h_2, then coefficient of permeability is calculated from the expression

$$k = \frac{aL}{A(t_2 - t_1)} \log_e \left(\frac{h_1}{h_2}\right) \tag{5.17}$$

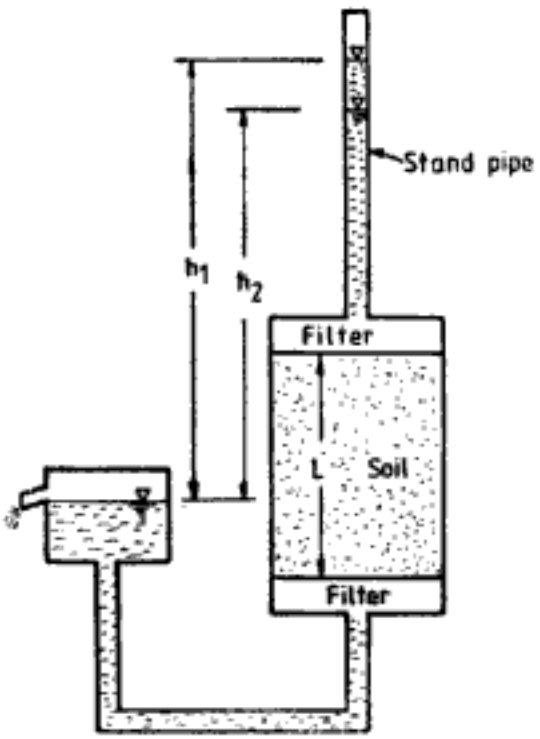

Fig. 5.19 Arrangement for variable-head permeability test

Q 5.7: Compute the coefficient of permeability of a soil on which a falling head test has been carried out. Area of soil sample = 80 cm²; area of stand pipe = 4 cm²; length of soil sample = 15 cm. Time *v.* head difference readings are as given below:

	Time (minutes)	Head difference h (cm)
(i)	0	107
(ii)	27	105
(iii)	60	103

Ans: For the combination of readings (i) and (ii)

$$k = \frac{4 \times 15}{80 \times (27 - 0) \times 60} \log_e \frac{107}{105}$$
$$= 8.74 \times 10^{-6} \text{ cm/s}$$

Similarly, for combination of readings (ii) and (iii) $k = 7.29 \times 10^{-6}$ cm/s
For combination of readings (i) and (iii) $k = 7.94 \times 10^{-6}$ cm/s
Average value of $k = 8 \times 10^{-6}$ cm/s.

5.7.2 Field Tests

Field tests to determine coefficient of permeability can be broadly grouped into three categories as below:

1. Pumping test (Pump-out test)
2. Borehole test (Pump-in test)
3. Variable head test

1. *Pumping test*
In this test water is pumped out of wells at a constant rate. When steady-state conditions are reached the data collected from field are used to determine k. Three cases of such test are discussed below.

(a) *Fully penetrating gravity well*: Figure 5.20 shows the arrangement for a fully penetrating gravity well. Water is pumped from pumping well at a steady rate. The natural groundwater level gets lowered and the change in water level is observed in the observation

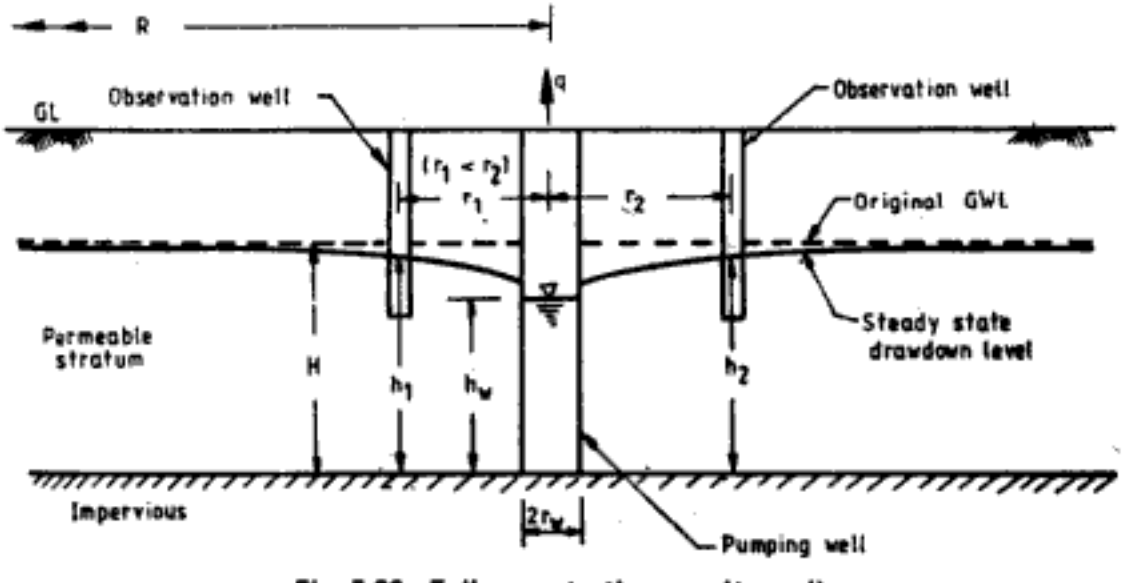

Fig. 5.20 Fully penetrating gravity well

wells. When steady state conditions are reached, data are collected from the pumping well and the observation wells. From the observations recorded, k can be computed as

$$k = \frac{q \log_e (r_2/r_1)}{\pi(h_2^2 - h_1^2)} \tag{5.18}$$

where q = constant rate of pumping

r_1, r_2 = radial distance of observation wells 1 and 2 respectively from pumping well, $r_1 < r_2$

h_1, h_2 = depth of water above impervious stratum in observation wells 1 and 2 respectively

k can be alternatively obtained from,

$$k = \frac{q \log_e (R/r_w)}{\pi(H^2 - h_w^2)} \tag{5.19}$$

where R = radius of influence, i.e., the radial distance from pumping well where the original GWL and draw-down water level merge with each other

H = natural depth of groundwater above impervious stratum

r_w = radius of well

h_w = depth of water in pumping well above impervious stratum after draw-down

According to Kozeny (1933), R can be expressed as,

$$R = \left\{\frac{12t}{n}\left(\frac{qk}{\pi}\right)^{1/2}\right\}^{1/2} \tag{5.20}$$

where n = soil porosity

t = time required to establish steady conditions

Recommendations for values of R made by U.S. Department of Agriculture—Bureau of Soils are shown in Table 5.5.

Table 5.5 Values of Radius of Influence, R

Soil description	Particle size mm	R m
Coarse gravel	> 10	> 1500
Medium gravel	2–10	500–1500
Fine gravel	1–2	400–500
Coarse sand	0.5–1	200–400
Medium sand	0.25–0.5	100–200
Fine sand	0.1–0.25	50–100
Very fine sand	0.05–0.1	10–50
Silty sand	0.025–0.05	5–10

Q 5.8: A pump-out test is carried out with a fully penetrating gravity well. Steady state conditions are reached after 27 hours of pumping at a constant rate of 1320 l/minute. The depth of groundwater is 7.8 m. The draw-down water depth in the well of 30 cm diameter is 6.15 m. Void ratio of in-place soil is 0.45. Compute the coefficient of permeability of the soil.

Ans: $r_w = 15$ cm $\quad n = \dfrac{0.45}{1 + 0.45} = 0.31$

Since no observation well data have been provided k will be calculated using Eqs. 5.19 and 5.20. A trial and error procedure is adopted as explained below.

Trial I: Assuming $k = 10^{-3}$ cm/s, from Eq. 5.20

$$R = \left\{\frac{12 \times 27 \times 60 \times 60}{0.31}\left(\frac{1320 \times 10^3 \times 10^{-3}}{\pi \times 60}\right)^{1/2}\right\}^{1/2} = 3155 \text{ cm}$$

Substituting in Eq. 5.19

$$k = \frac{1320 \times 10^3 \times \log_e (3155/15)}{60 \times \pi \times (780^2 - 615^2)} = 1.63 \times 10^{-1} \text{ cm/s}$$

Due to large difference between assumed and computed values another trial is necessary.

Trial II: Assume $k = 10^{-2}$ cm/s, then

$$R = \left\{\frac{12 \times 27 \times 60 \times 60}{0.31}\left(\frac{1320 \times 10^3 \times 10^{-2}}{\pi \times 60}\right)^{1/2}\right\}^{1/2} = 5610 \text{ cm}$$

$$k = \frac{1320 \times 10^3 \times \log_e (5610/15)}{60 \times \pi \times (780^2 - 675^2)} = 1.8 \times 10^{-1} \text{ cm/s}$$

Trial III: Assume $k = 2 \times 10^{-1}$ cm/s. From calculations,

$$R = 11870 \text{ cm}$$

and $\quad k = 2.03 \times 10^{-1}$ cm/s $\quad O.K.$

The coefficient of permeability of soil deposit is *0.2 cm/s*. It can be noted that k is not very sensitive to value of R. Hence, a reasonable value of R can be used in the calculations.

(b) *Partially penetrating gravity well*: A pump-out test from partially penetrating gravity well is shown in Fig. 5.21. k is expressed by the relationship (Mansur and Kaufman, 1962)

$$k = \frac{q \log_e (R/r_w)}{\pi\{(H - s)^2 - h_w^2\}m} \tag{5.21}$$

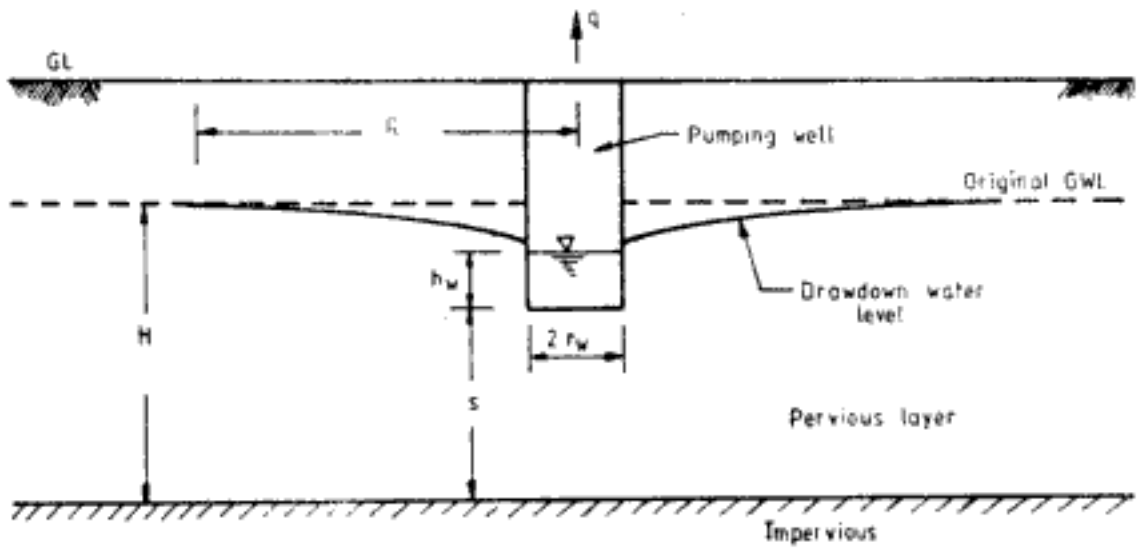

Fig. 5.21 Partially penetrating gravity well

where $m = \left\{1 + \left(0.30 + \frac{10\,r_w}{H}\right) \sin \frac{1.8\,s}{H}\right\}$

s = depth below bottom of well to impervious stratum

(c) *Fully penetrating artesian well*: Artesian conditions can exist in a confined aquifer sandwiched between two impervious layers. A well fully penetrating the pervious aquifer is shown in Fig. 5.22. When steady state conditions are reached at a constant pumping rate of q, coefficient of permeability can be determined from the equation

$$k = \frac{q \log_e (r_2/r_1)}{2\pi T(h_2 - h_1)} \tag{5.22}$$

where T = thickness of pervious aquifer and $r_2 > r_1$
Other details are as shown in Fig. 5.22. Alternatively, k can be determined from,

$$k = \frac{q \log_e (R/r_w)}{2\pi T(H - h_w)} \tag{5.23}$$

In Eq. 5.22 H is the pressure head due to artesian pressure as shown in Fig. 5.22.

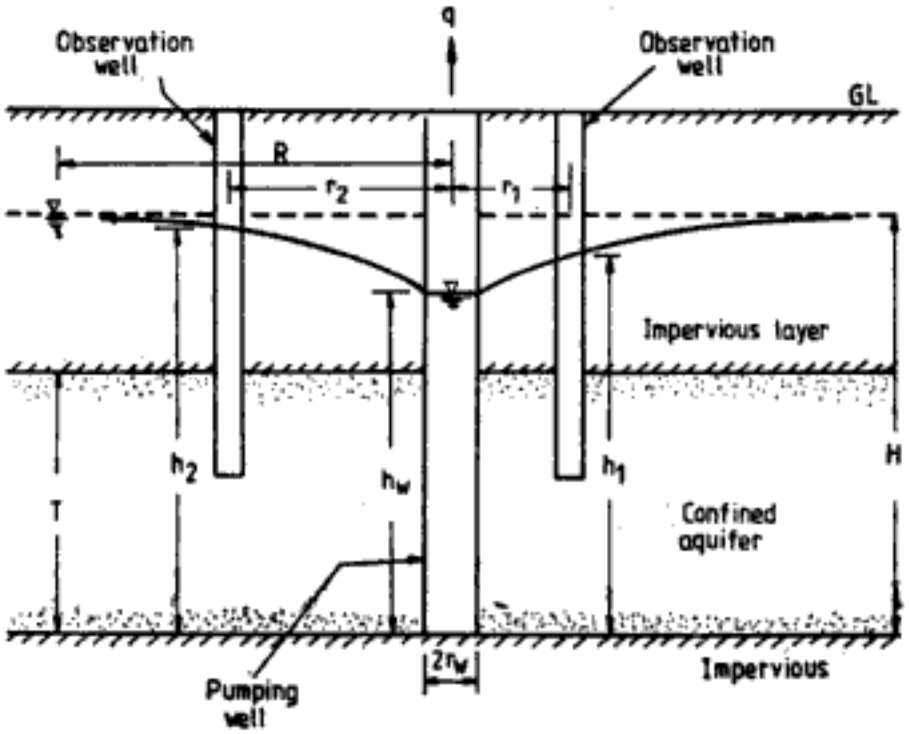

Fig. 5.22 Fully penetrating artesian well

2. *Borehole tests*

Pump-out tests are expensive and time consuming. Borehole tests which are relatively economical and easy to conduct have been recommended by USBR (U.S. Bureau of Reclamation, 1961). There are two different types of borehole tests. These are:

(a) Open-end test
(b) Packer test

Borehole tests are carried out using standard casing pipes. The dimensions of USBR standard casings are given in Table 5.6.

Table 5.6 Dimensions of USBR Casings

Casing designation	Inside diameter in. (mm)	Outside diameter in. (mm)
EX	$1\frac{1}{2}$(38.1)	$1\frac{13}{16}$ (46)
AX	$1\frac{29}{32}$ (48.4)	$2\frac{1}{4}$ (57.2)
BX	$2\frac{3}{8}$ (60.3)	$2\frac{7}{8}$ (73)
NX	3 (76.2)	$3\frac{1}{2}$ (88.9)

(a) *Open-end test*: The casing is inserted into the soil to the depth where k is required to be determined. The bottom end of the casing is open and can be kept either above or below groundwater table. In case of more pervious soils water level inside the casing is always maintained at the top of the casing. Due to gravity the water flows into the soil from the casing. The rate of flow of water required to maintain the water constantly at the top of the casing can be recorded.

In less pervious soils in addition to gravity head, pressure head also can be applied and the corresponding rate of discharge to maintain a constant total head can be recorded. Figure 5.23 shows the different situations in open-end tests. For all the situations shown in the figure k can be determined from the equation

$$k = \frac{q}{5.5\,rh} \tag{5.24}$$

where r = inside radius of casing
h = head of water = $h_p + h_{gr}$
h_p = pressure head over gravity head
h_{gr} = gravity head (Fig. 5.23)
q = rate of supply of water to maintain head h

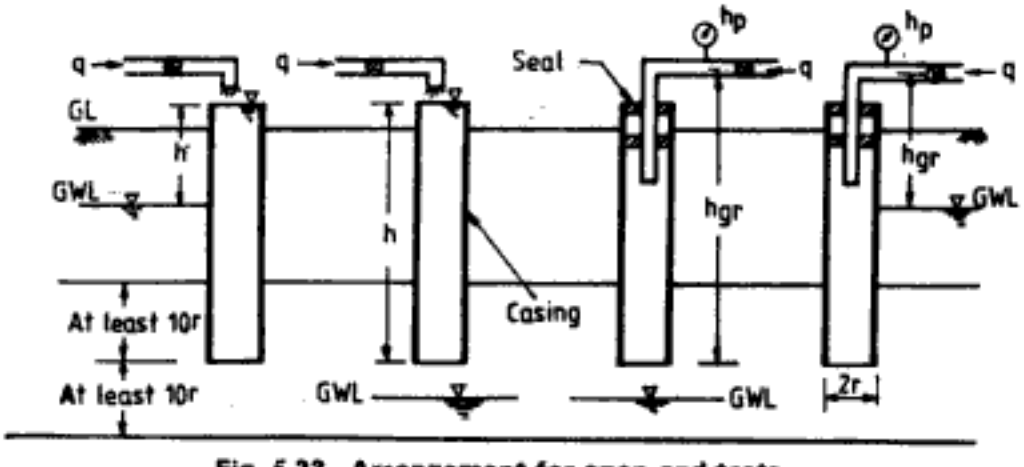

Fig. 5.23 Arrangement for open-end tests
(After U.S. Bureau of Reclamation, 1961)

Any consistent set of units can be used in Eq. 5.24. For q in gallons per minute, k in ft/year and h in ft, k is expressed as

$$k = C_1 \frac{q}{h} \tag{5.25}$$

where C_1 is an empirical constant. Table 5.7 gives the values of C_1 for different standard casings after USBR (1961).

Table 5.7 Values of C_1 (Eq. 5.25)

Casing designation	C_1
EX	204,000
AX	160,000
BX	179,000
NX	102,000

(After U.S. Bureau of Reclamation, 1961. Reprinted by permission of United States Bureau of Reclamation, Denver.)

(b) *Packer test*: In packer test (Fig. 5.24) the rate of flow of water required to maintain a constant head over the desired length of soil stratum is observed. The test can be carried out either while drilling of bore-hole [Fig. 5.24(a) and (b)] or after completion of bore-hole [Fig. 5.24(c) and (d)]. In the first procedure

(i) the borehole is drilled up to the required depth
(ii) a packer is inserted to seal off the test length (L)
(iii) water is let in and maintained under pressure over the test length and discharge for constant head is noted.

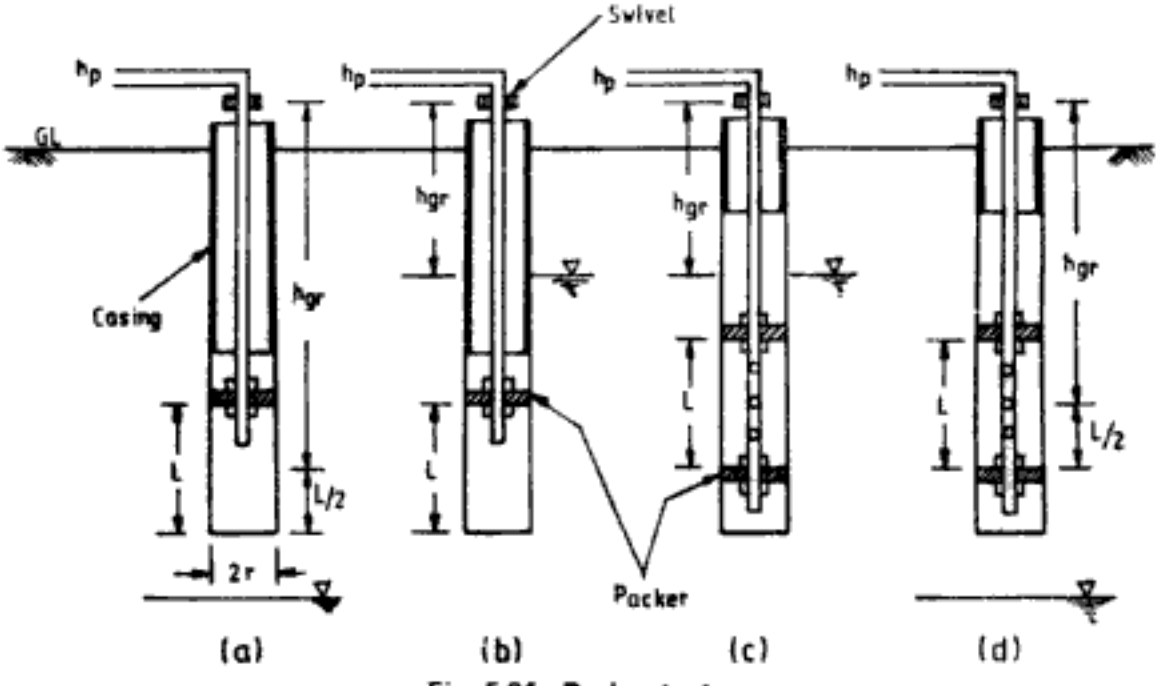

Fig. 5.24 Packer tests
(After U.S. Bureau of Reclamation, (1961)

The test proceeds from top to bottom as the boring operations proceed. Where the soil is firm and the borehole can remain unsupported the second procedure can be used. In this,

(i) the borehole is first completed
(ii) two packers are inserted adjusted over the desired length of test section (L)
(iii) water is maintained under pressure over test section and discharge for constant head is noted.

The test proceeds from bottom to top.
In both cases k is determined from the following formulae,

$$k = \frac{q}{2\pi Lh} \log_{10} \frac{L}{r} \qquad \text{for } L \geqslant 10\,r \tag{5.26}$$

and

$$k = \frac{q}{2\pi Lh} \sinh^{-1} \frac{L}{2r} \qquad \text{for } 10\,r > L \geqslant r \tag{5.27}$$

where q = constant rate of flow

h = head of water = $h_p + h_{gr}$

L = length of test section

r = radius of borehole

Any consistent units can be used in Eqs. 5.26 and 5.27. For q in gallons per minute, h in ft, k will be given in ft/year by the following equation (USBR, 1961)

$$k = C_p \frac{q}{h} \tag{5.28}$$

Table 5.8 gives the values of empirical constant C_p for standard size casings.

Table 5.8 Values of C_p (Eq. 5.28)

L (ft)	Casing designation			
	EX	AX	BX	NX
1	31000	28500	25800	23300
2	19400	18100	16800	15500
3	14400	13600	12700	11800
4	11600	11000	10300	9700
5	9800	9300	8800	8200
6	8500	8100	7600	7200
7	7500	7200	6800	6400
8	6800	6500	6100	5800
9	6200	5900	5600	5300
10	5700	5400	5200	4900
15	4100	3900	3700	3600
20	3200	3100	3000	2800

(After U.S. Bureau of Reclamation, 1961. Reprinted by permission of United States Bureau of Reclamation, Denver.)

3. *Variable head tests*

The principle of variable head test is as follows: An observation well or piezometer is constructed in the soil stratum. The well may be uncased, partially cased or fully cased. It can also have different conditions at the bottom intake point, for example the soil can be flush with the bottom of the casing or there can be a soil plug inside the casing or it can be an enlarged intake point, etc. The water level in the observation well or piezometer is at first lowered below the natural groundwater level. With passage of time the water level in the well rises and ultimately reaches the natural groundwater level. The rate of rise of water in the well is indicative of the coefficient of permeability of soil. The water level in the observation well is observed at different time intervals. This data are used to calculate the coefficient of permeability of soil.

U.S. Department of Navy (1971) has developed variable head tests in piezometer observation wells. Table 5.9 explains these methods. For condition A (uncased hole) given in Table 5.9 the shape factor coefficient S' can be obtained from Fig. 5.25. Figure 5.26 gives the shape factor coefficient C_s for use in condition F-1 of Table 5.9. The procedure of analysis in case of variable head tests is explained in Fig. 5.27.

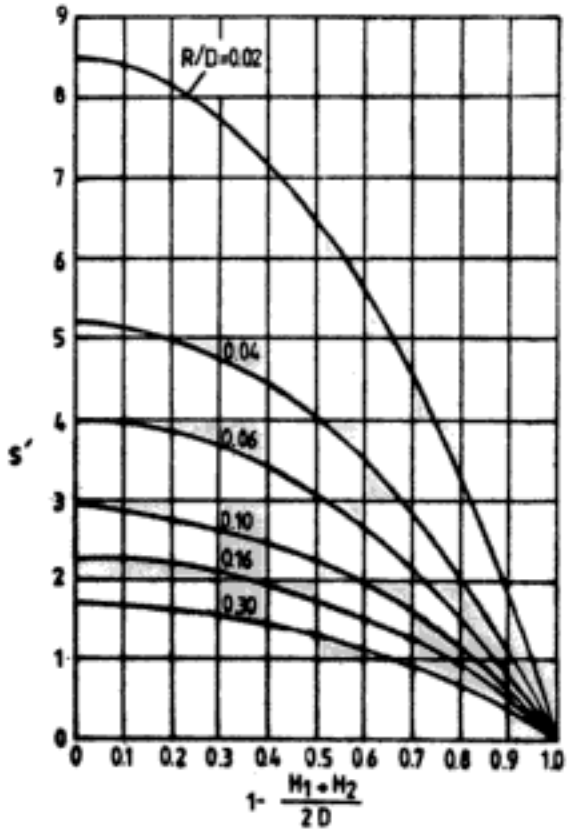

Fig. 5.25 Shape factor coefficient S' used for (A) of Table 5.9
(After U.S. Navy, 1971; by permission of Department of Navy, Alexandria)

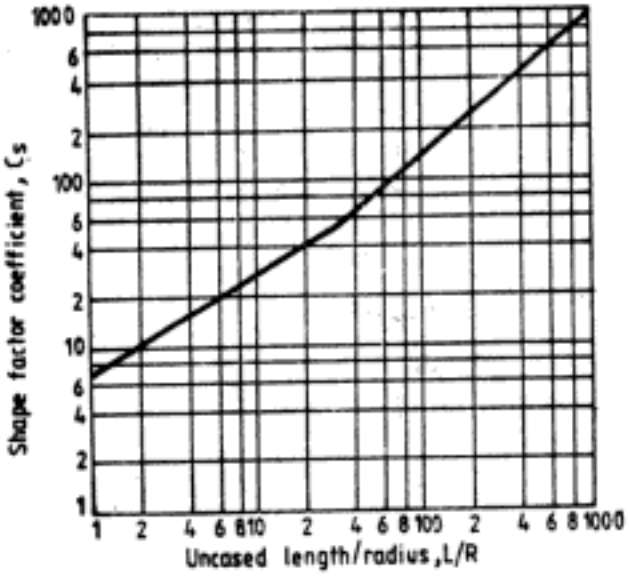

Fig. 5.26 Shape factor coefficient C_s for condition (F—1) of Table 5.9
(After U.S. Navy, 1971; from Spangler, 1963)

In general:

$$k = \frac{A}{F(t_2 - t_1)} \ln \frac{H_1}{H_2}$$

F = shape factor of intake point
A = standpipe area
k = mean permeability
$\ln(H_1/H_2)$, and $t_2 - t_1$ are obtained from plot of observations

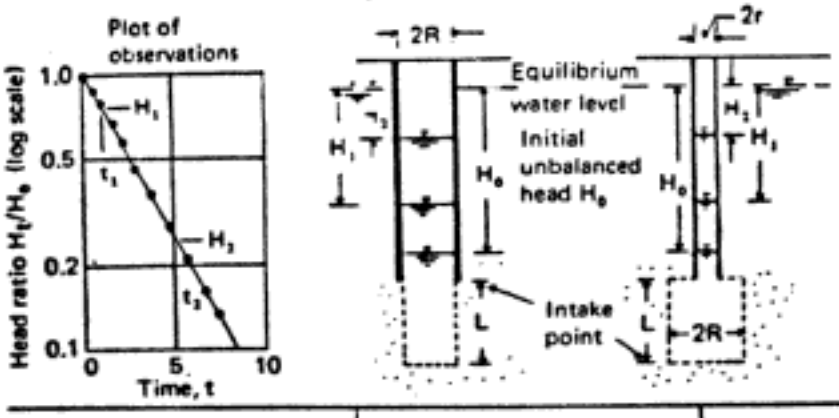

Observation well in isotropic soil:

Obtain shape factor from Table 5.9
For condition (F—1):

$$F = \frac{2\pi L}{\ln (L/R)}$$

$$k = \frac{R^2}{2L(t_2 - t_1)} \ln \frac{L}{R} \ln \frac{H_1}{H_2}$$

Piezometer in isotropic soil:

Radius of intake point, R, differs from radius of standpipe, r

$$F = \frac{2\pi L}{\ln (L/R)}; \quad A = \pi r^2$$

$$k = \frac{A}{F(t_2 - t_1)} \ln \frac{H_1}{H_2}$$

$$k = \frac{r^2}{2L(t_2 - t_1)} \ln \frac{L}{R} \ln \frac{H_1}{H_2}$$

Test in anisotropic soil:

Estimate ratio of horizontal to vertical permeability and divide horizontal dimensions of the intake point by:

$m = \sqrt{k_h/k_v}$ to compute mean permeability $k = \sqrt{k_h k_v}$. For condition (C), Table 5.9

$$F = \frac{2\pi L}{\ln (mL/R)}$$

$$k = \frac{r^2}{2L(t_2 - t_1)} \ln \frac{mL}{R} \ln \frac{H_1}{H_2}$$

Fig. 5.27 Analysis of coefficient of permeability by variable head tests
(After U.S. Navy, 1971; by permission of Department of Navy, Alexandria)

5.8 QUICK CONDITION AND LIQUEFACTION

5.8.1 Critical Hydraulic Gradient

When water flows upwards in soil, at a certain hydraulic gradient the upward forces neutralise the downward gravitational forces. This particular gradient of flow is called critical hydraulic gradient, i_{cr}. i_{cr} is given by the equation

$$i_{cr} = \frac{G_s - 1}{1 + e} = \frac{\gamma_b}{\gamma_w} \simeq 1 \tag{5.29}$$

Quick condition is a state or hydraulic condition of the soil when water flows upwards at the critical hydraulic gradient. For safety of hydraulic structures against piping the upward hydraulic gradient must be within safe limits. The factor of safety for exit gradient (FS) is defined as

$$\text{FS} = \frac{i_{cr}}{i_{exit}} \tag{5.30}$$

where, i_{exit} = maximum exit gradient
Maximum exit gradient can be determined from flow net (See Q 5.4). A factor of safety of 3 to 4 must be obtained for the safe performance of structure. Lambe and Whitman (1979) recommend a factor of safety even greater than 3 to 4 due to the fact that the consequences of quick conditions are very serious and minor variations in soil might cause relatively large errors in the computation for exit gradient.

It may be mentioned here that, the commonly known 'quick sand' is only a particular state of sand at quick condition. It is not a type of sand.

5.8.2 Liquefaction

Liquefaction is again a state or condition of soil when it becomes unstable. When effective stress (Ch. 6) in soil is reduced to zero, the soil loses its shear strength (Ch. 9). It behaves like a thick slurry and flows like a liquid. This is known as liquefaction.

Liquefaction is usually associated with earthquakes. Due to vibration the pore water pressure in soil builds up and effective stress decreases. Liquefaction does not occur in very fine soils like silts and clays or in very coarse soils like gravels. It usually occurs in loose fine sands.

5.9 CAPILLARITY IN SOILS

Due to surface tension effects water rises in the voids of soil above the groundwater level or above phreatic surface in unconfined flow. The principle of capillary rise is shown in Fig. 5.28 from which,

$$h_c = 2\sigma \cos \alpha / R\gamma \tag{5.31}$$

where h_c = height of capillary rise
σ = surface tension of liquid
α = contact angle between liquid and tube
R = radius of tube
γ = unit weight or density of liquid

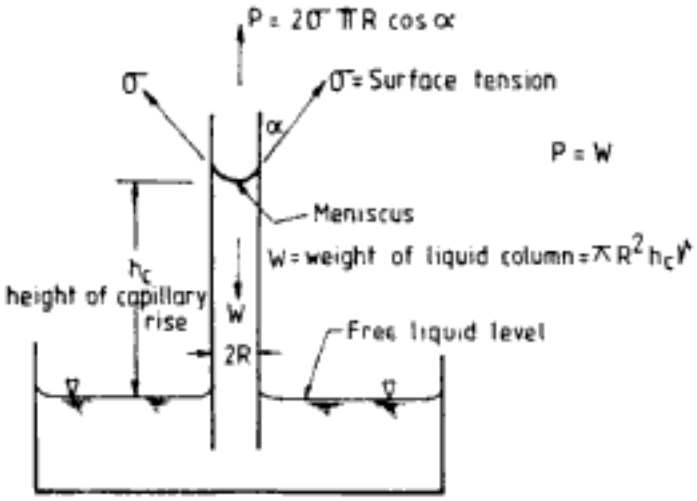

Fig. 5.28 Capillary rise in soils

Surface tension σ decreases slightly with increase in temperature. For water σ is about 0.075 g/cm at room temperature. α may be taken as 0° for clean sand and 15° for dirty sand. The average diameter of voids should be used to calculate capillary rise in soils.
The following two points are noteworthy here:

1. The capillary rise in soils depends on
   (a) the size of void that is effective. It varies inversely with the size of voids
   (b) the particle size and density of soil
2. The capillary rise is most pronounced in soils composed mainly of fine sands, silts, silty clays and colloids.

Tables 5.10 and 5.11 show typical values of height of capillary rise in different types of soil. Capillary rise has the following two effects on soils: (i) it increases the degree of saturation and total density of soil within the capillary zone, (ii) within the capillary zone the effective stress increases.

Table 5.10 Capillary Height of Water in Soils (Jumkis, 1967)
(Average values for average conditions)

Soil	Size of particles (mm)	Capillary height h_c (cm)
Fine gravel	2–1	2–10
Coarse sand	1–0.5	10–15
Medium sand	0.5–0.25	15–30
Fine sand	0.25–0.05	30–100
Silt	0.05–0.005	100–1000
Clay	0.005–0.0005	1000–3000
Colloids	<0.0005	>3000

Table 5.11 Capillary Height of Water in Cohesionless Soils (Lane and Washburn, 1946)

Soil	Effective diameter D_{10} (mm)	Void ratio	Capillary height h_c (cm)
Coarse gravel	0.82	0.27	5–6
Sandy gravel	0.20	0.45	20–28
Fine gravel	0.30	0.29	19–20
Silty gravel	0.06	0.45	68–106
Coarse sand	0.11	0.27	60–82
Medium sand	0.02	0.48–0.66	120–240
Fine sand	0.03	0.36	112–166
Silt	0.006	0.93–0.95	180–360

Terzaghi and Peck (1948) give an approximate relationship for h_c in granular soils in terms of void ratio e as,

$$h_c = \frac{C}{eD_{10}} \tag{5.32}$$

where h_c is in cm, D_{10} is effective size in cm, and C is an empirical coefficient. Value of C depends on shape of grains and the impurities on surface. Generally C ranges between 0.1 and 0.5 sq cm.

In routine design problems the effect of capillary rise in soils is ignored. But in small scale model tests to investigate the flow characteristics through soils, capillarity will cause significant differences. Because in these tests the capillary height will be comparable to the dimensions of the models themselves.

6

EFFECTIVE STRESS PRINCIPLE

Effective stress principle enunciated by Terzaghi (1925, 1936) is an important event in the annals of soil mechanics. Now it is well recognised that important engineering properties of soil like shear strength, compressibility, and lateral earth pressure depend on the state of effective stress in soil.

6.1 EFFECTIVE STRESS IN SATURATED SOILS

Figure 6.1 is a magnification of the arrangement of soil grains in a deposit. The voids are filled with water in saturated soils. XX is a wavy plane passing through the points of particle contacts. Let the area of this plane XX be A. Part of this area is the area of grain contacts (A_c) and the rest is the area of water (A_w). If we lump the discrete areas at grain contacts together and similarly lump the discrete water areas together, they can be represented as shown in Fig. 6.2. It is evident from this figure that $A_c \ll A_w$ and $A_w \simeq A$. Let F be the total force on A.

Then,
$$F = F_S + F_W \tag{6.1}$$

where F_S = total force transmitted through soil grains

F_W = total force transmitted through water

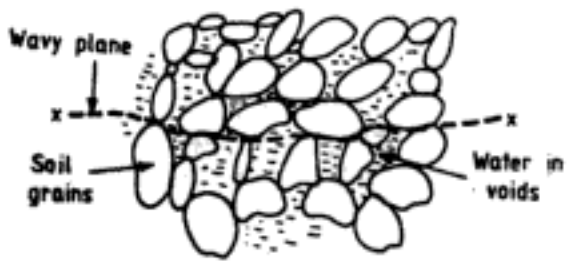

Fig. 6.1 Wavy plane through particle contact points

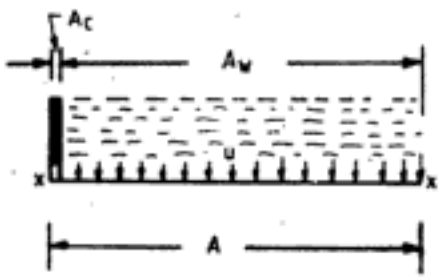

Fig. 6.2 Lumped contact area and water area on plane XX

If the pressure in water is u, then

$$F_W = u\,A_w \tag{6.2}$$

The *total stress* on the plane is then

$$\frac{F}{A} = \frac{F_S}{A} + \frac{uA_w}{A} \tag{6.3}$$

i.e.,
$$\sigma = \bar{\sigma} + u \tag{6.4}$$

where σ = total stress

$\bar{\sigma}$ = effective stress

u = pore water pressure

$$\frac{uA_w}{A} = u \qquad \text{since } A_w \simeq A$$

From Eq. 6.4

$$\bar{\sigma} = \sigma - u \tag{6.5}$$

Equation 6.5 defines the effective stress principle. Stated in words,

Effective stress = Total stress − Pore water pressure.

The following points must be noted about the effective stress concept explained so far:

1. Effective stress is also referred to as *intergranular stress*. But it is *not* the *contact stress*. Contact stress will be F_S/A_c which will be much higher than effective stress.
2. Effective stress cannot be measured. It is not a physical reality but only a conceptual quantity. Total stress and pore water pressure can be measured, at any point. Thus effective stress can be calculated from these values using Eq. 6.5.
3. Equation 6.5 will have to be modified in the case of soils made of surface active minerals. Clay minerals like montmorillonite have appreciable repulsive and attractive forces. Modifications for such situations are considered later in this chapter. But for most of the engineering design problems use of Eq. 6.5 will be sufficient.

6.1.1 Determination of Effective Stress

The determination of effective stress is explained first only for soil below groundwater level. It is assumed that there is no capillary action of water in soil. The effect of capillary action is considered later. The soil below groundwater is usually saturated and hence effective stress equation (Eq. 6.5) is applicable. The effective stress determination when water body is present above ground level is explained through an example problem.

1. *Hydrostatic case:* Figure 6.3 presents the details of calculation of effective stress in this case. Total stress, pore water pressure, effective stress all increase with depth.
2. *Hydrodynamic case:* The details of calculation of effective stress when flow takes place upwards in a soil deposit are shown in Fig. 6.4. Such an upward flow results, for example, where artesian condition prevails in a lower layer. Compared to hydrostatic conditions, upward flow of water decreases the effective stress in soil. This is demonstrated through a worked out example in Q 6.4.

Another case of flow is the downward flow of water through the soil layers. Such a type of flow can be expected to occur when large quantity of water is pumped out from some of

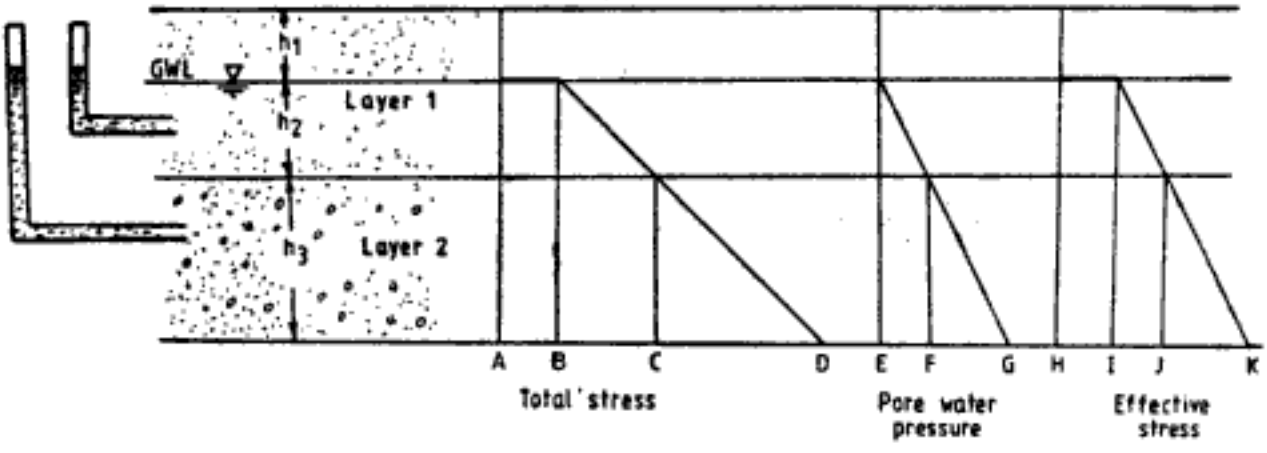

γ_{t1} = Total density of soil layer 1 above ground water level

$\gamma_{sat1}, \gamma_{sat2}$ = Saturated density of soil layer 1 below GWL and soil layer 2 respectively

Fig. 6.3 Total stress, pore water pressure, and effective-stress diagrams for hydrostatic conditions

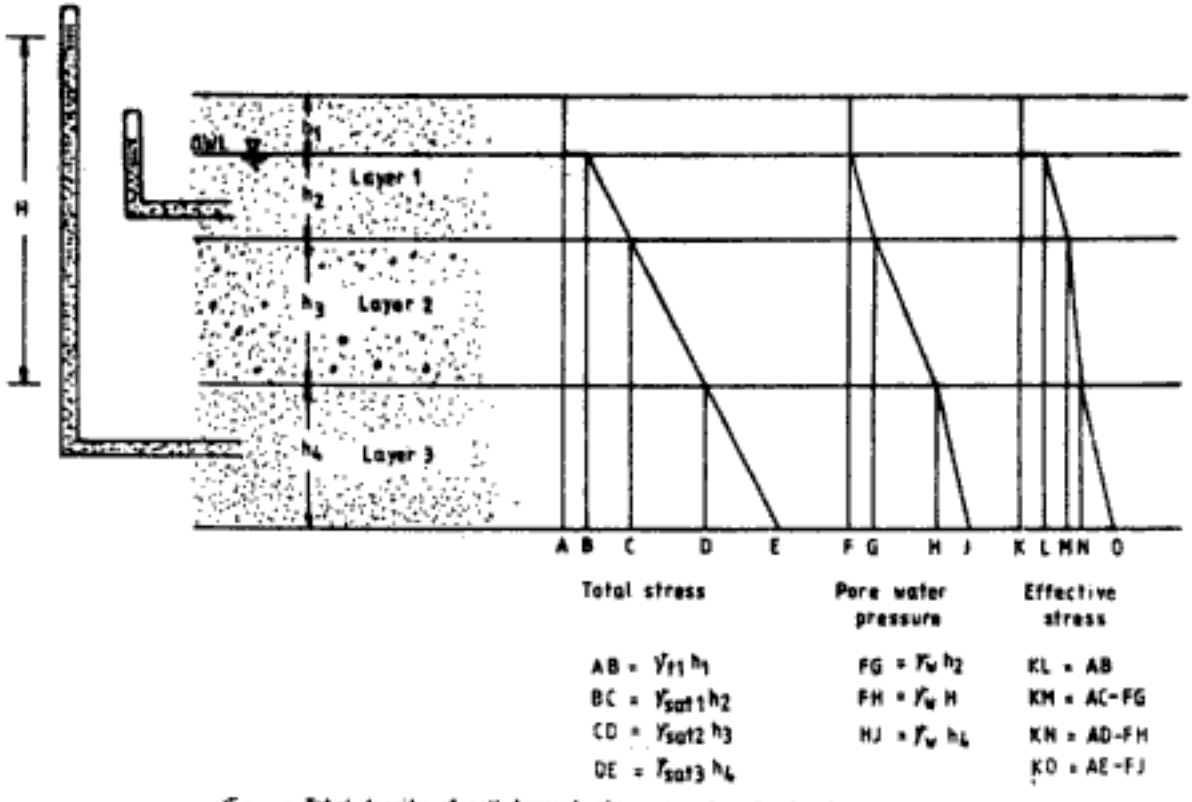

γ_{t1} = Total density of soil layer 1 above ground water level

$\gamma_{sat1}, \gamma_{sat2}, \gamma_{sat3}$ = Saturated density of soil layer 1 below GWL, soil layer 2, and soil layer 3 respectively

Fig. 6.4 Total stress, pore water pressure, and effective-stress diagrams for conditions of upward flow of water

the lower layers releasing the pressure in these layers as a result of which the groundwater level in the upper layers tends to go down. The procedure of calculation of effective stress in this case is explained in Fig. 6.5. Compared to hydrostatic conditions downward flow of water increases the effective stress in soil. This is demonstrated in Q 6.5.

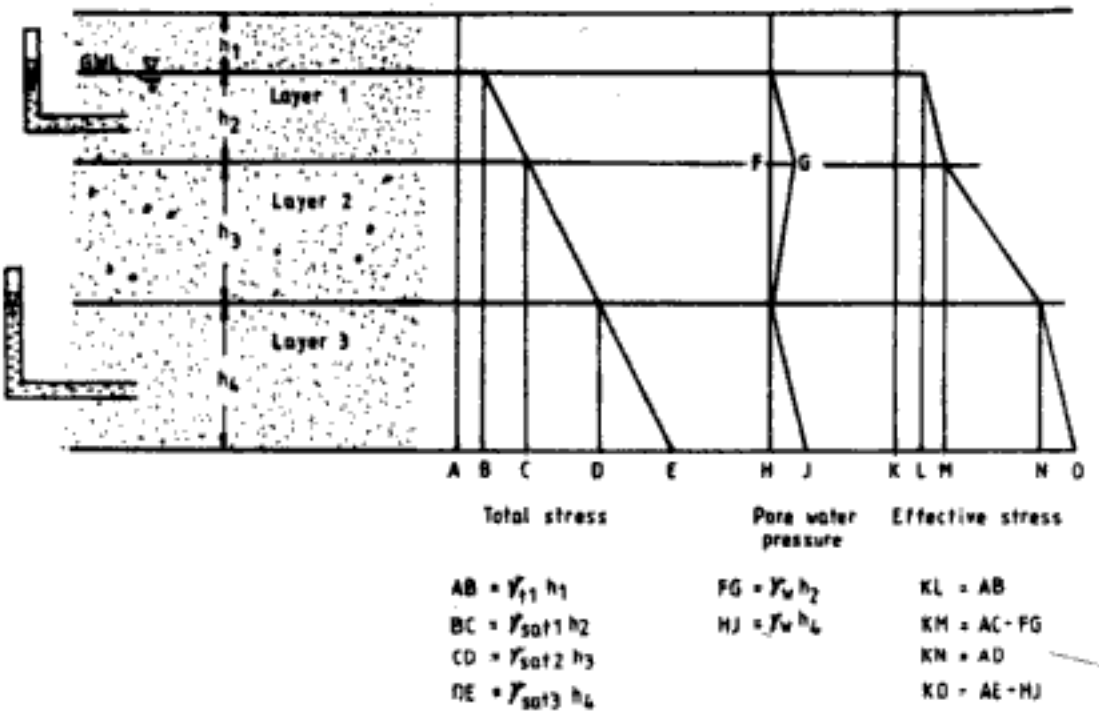

γ_{t1} = Total density of soil layer 1 above ground water level

$\gamma_{sat1}, \gamma_{sat2}, \gamma_{sat3}$ = Saturated density of soil layer 1 below GWL, soil layer 2, and soil layer 3 respectively

Fig. 6.5 Total stress, pore water pressure, and effective-stress diagrams for conditions of downward flow of water

Q 6.1: For the soil deposit shown in Fig. 6.6(a) draw the total stress, pore water pressure, and effective stress diagrams. The groundwater level is at elevation (El.) 0.0 m.

Ans: The total stress, pore water pressure and effective stress diagrams are shown in Fig. 6.6(b), (c), and (d) respectively. The computations are as below:

Computations for total stress

At El. -4 $AB = 1.92 \times 4 = 7.68$ T/m^2

At El. -11 $AC = 7.68 + (2.1 \times 7) = 22.38$ T/m^2

Computations for pore water pressure

At El. -4 $DE = 1 \times 4 = 4$ T/m^2

At El. -11 $DF = 4 + (1 \times 7) = 11$ T/m^2

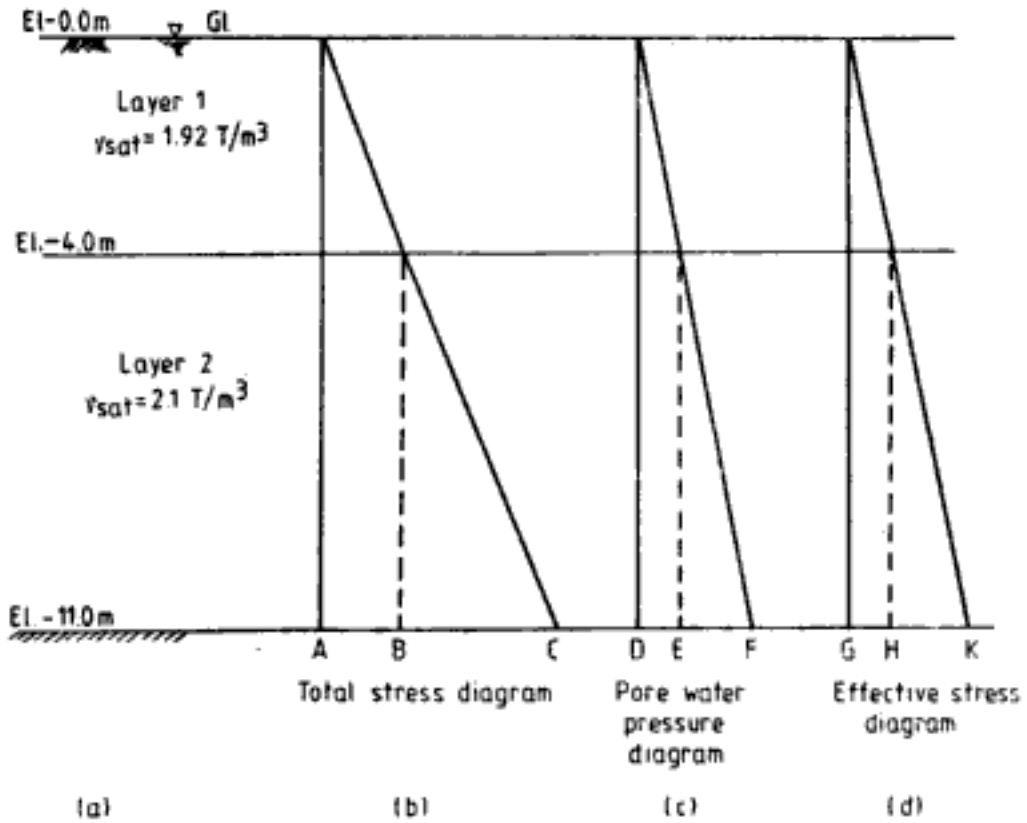

Fig. 6.6 Q 6.1

Computations for effective stress

$$\text{At El. } -4 \quad GH = AB - DE = 7.68 - 4 = 3.68 \text{ T/m}^2$$

$$\text{At El. } -11 \quad GK = AC - DF = 22.38 - 11 = 11.38 \text{ T/m}^2$$

Q 6.2: For the soil deposit shown in Fig. 6.7(a), draw the total stress, pore water pressure and effective stress diagrams. There is a standing water of 3 m above ground level (at El. +3.0 m). Compare the solution with that for Q 6.1.

Ans: The total stress, pore water pressure, and effective stress diagrams are shown in Fig. 6.7(b), (c) and (d) respectively. The computations are as below:

Total stress

$$\text{At El. } 0 \quad AB = 1 \times 3 = 3 \text{ T/m}^2$$

$$\text{At El. } -4 \quad AC = 3 + (1.92 \times 4) = 10.68 \text{ T/m}^2$$

$$\text{At El. } -11 \quad AD = 10.68 + (2.1 \times 7) = 25.38 \text{ T/m}^2$$

Pore water pressure

$$\text{At El. } 0 \quad EF = 1 \times 3 = 3 \text{ T/m}^2$$

$$\text{At El. } -4 \quad EG = 3 + (1 \times 4) = 7 \text{ T/m}^2$$

$$\text{At El. } -11 \quad EH = 7 + (1 \times 7) = 14 \text{ T/m}^2$$

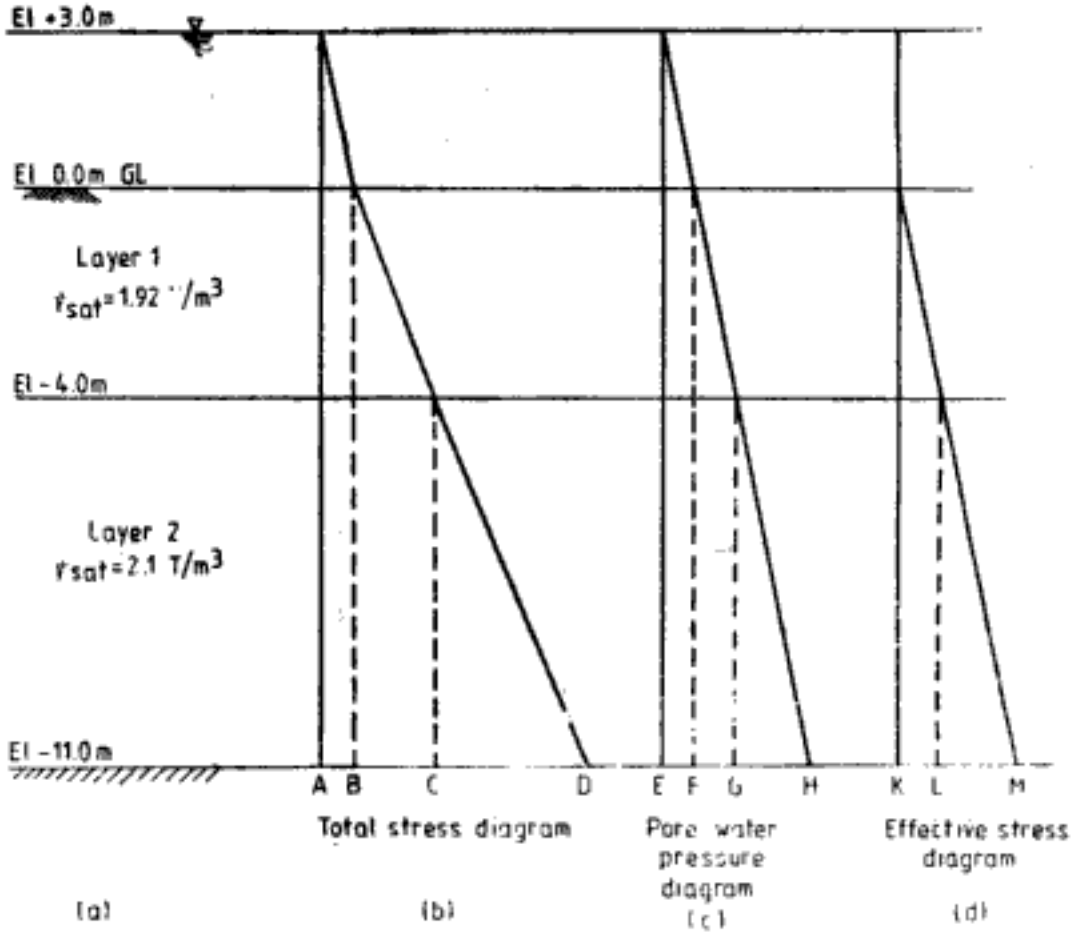

Fig. 6.7 Q 6.2

Effective stress

At El. 0 $AB - EF = 3 - 3 = 0$ T/m²
At El. −4 $KL = AC - EG = 10.68 - 7 = 3.68$ T/m²
At El. −11 $KM = AD - EH = 25.38 - 14 = 11.38$ T/m²

From a comparison with solution to Q 6.1 it can be observed that effective stresses in the soil are the same. Thus, change in water level above ground level does not affect effective stresses in soil. However, total stress and pore water pressure at a point change, both by the same amount.

Q 6.3: Figure 6.8(a) shows the same soil profile as in Fig. 6.6(a) with the water-table lowered down to El. − 2.0 m. Due to lowering of water-table the soil between elevations 0.0 m and −2.0 m is not saturated. Draw the total stress, pore water pressure and effective stress diagrams. Compare the solution with that for Q 6.1.

Ans: The total stress, pore water pressure, and effective stress diagrams are shown in Fig. 6.8(b), (c) and (d) respectively. The computations are as below:

Total stress

At El. −2 $AB = 1.85 \times 2 = 3.70$ T/m²
At El. −4 $AC = 3.70 + (1.92 \times 2) = 7.54$ T/m²
At El. −11 $AD = 7.54 + (2.1 \times 7) = 22.24$ T/m²

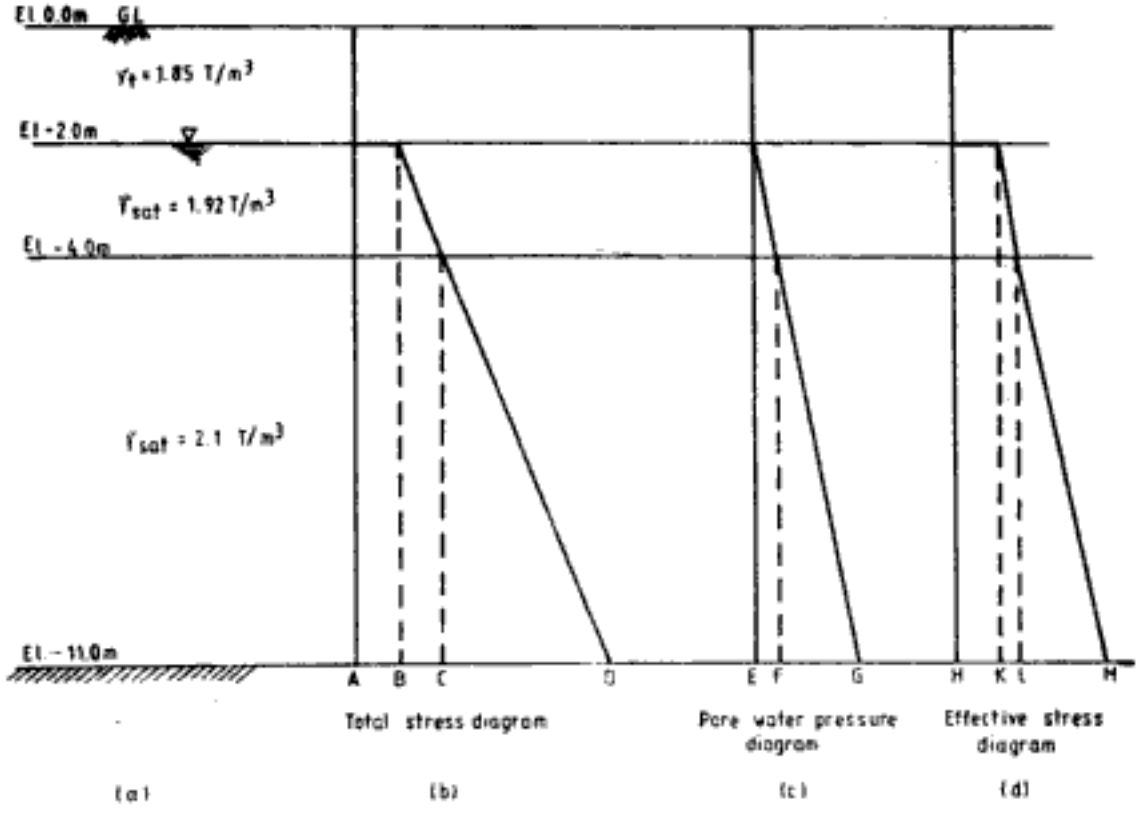

Fig. 6.8 Q 6.3

Pore water pressure

At El. -4 $EF = 1 \times 2 = 2$ T/m²

At El. -11 $EG = 2 + (1 \times 7) = 9$ T/m²

Effective stress

At El. -2 $HK = AB = 3.7$ T/m²

At El. -4 $HL = AC - EF = 7.54 - 2 = 5.54$ T/m²

At El. -11 $HM = AD - EG = 22.24 - 9 = 13.24$ T/m²

Comparing the solution with that for Q 6.1 it is seen that the effective stress in soil increases due to lowering of water-table. This is due to the decrease in pore water pressure.

Q 6.4: Figure 6.9(a) shows the same soil profile as in Fig. 6.6(a) but with artesian conditions prevailing in Layer 2. Groundwater level is at El. 0.0 m. Water rises to El. +2.0 m in stand pipe inserted in Layer 2. Draw the total stress, pore water pressure, and effective stress diagrams. Compare the solution with the solution obtained for hydrostatic case in Q 6.1.

Ans: Total stress, pore water pressure, and effective stress diagrams are shown in Fig. 6.9(b), (c) and (d) respectively. The calculations are as below:

Total stress

At El. -3 $AB = 1.92 \times 4 = 7.68$ T/m²

At El. -11 $AC = 7.68 + (2.1 \times 7) = 22.38$ T/m²

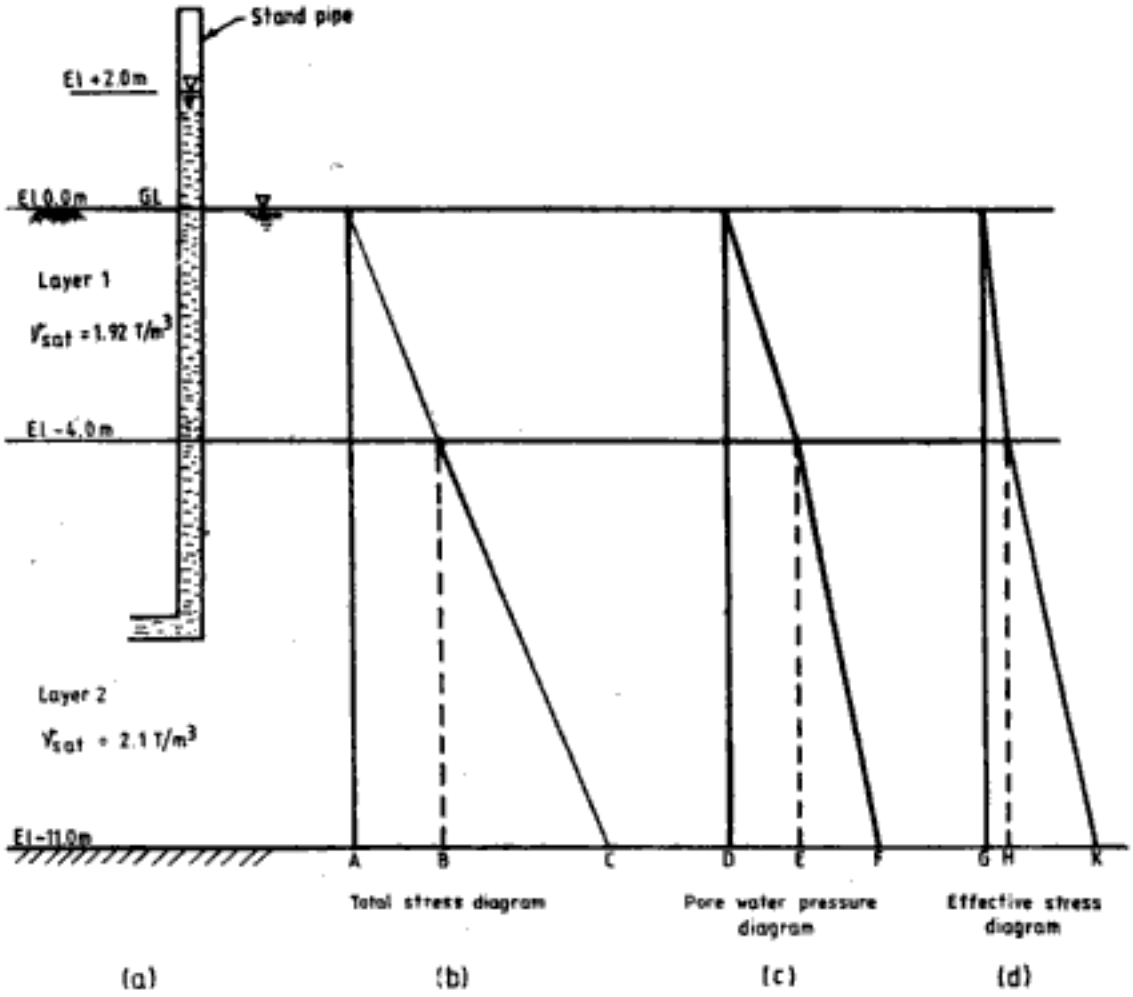

Fig. 6.9 Q 6.4

Pore water pressure

At El. -4 $DE = 1 \times 6 = 6$ T/m² which is the artesian pressure at this level

At El. -11 $DF = 6 + (1 \times 7) = 13$ T/m²

Effective stress

At El. -4 $GH = AB - DE = 7.68 - 6 = 1.68$ T/m²

At El. -11 $GK = AC - DF = 22.38 - 13 = 9.38$ T/m²

Comparing this with the solution for Q 6.1 the following observations can be made:

(i) Due to artesian conditions prevailing in lower layer there is an upward water flow in Layer 1. This results in a significant reduction in effective stress in Layer 1.

(ii) The effective stress in Layer 2 is also reduced due to increase in pore water pressure.

Q 6.5: Figure 6.10(a) shows the same soil profile as in Fig. 6.6(a) but with large-scale pumping operation from Layer 2. Groundwater level is at El. 0.0 m. Due to pumping operation the water level in a stand pipe inserted in Layer 2 rises to El. -2.0 m. Draw the total stress, pore water pressure, and effective stress diagrams. Compare the solution to hydrostatic conditions of Q 6.1.

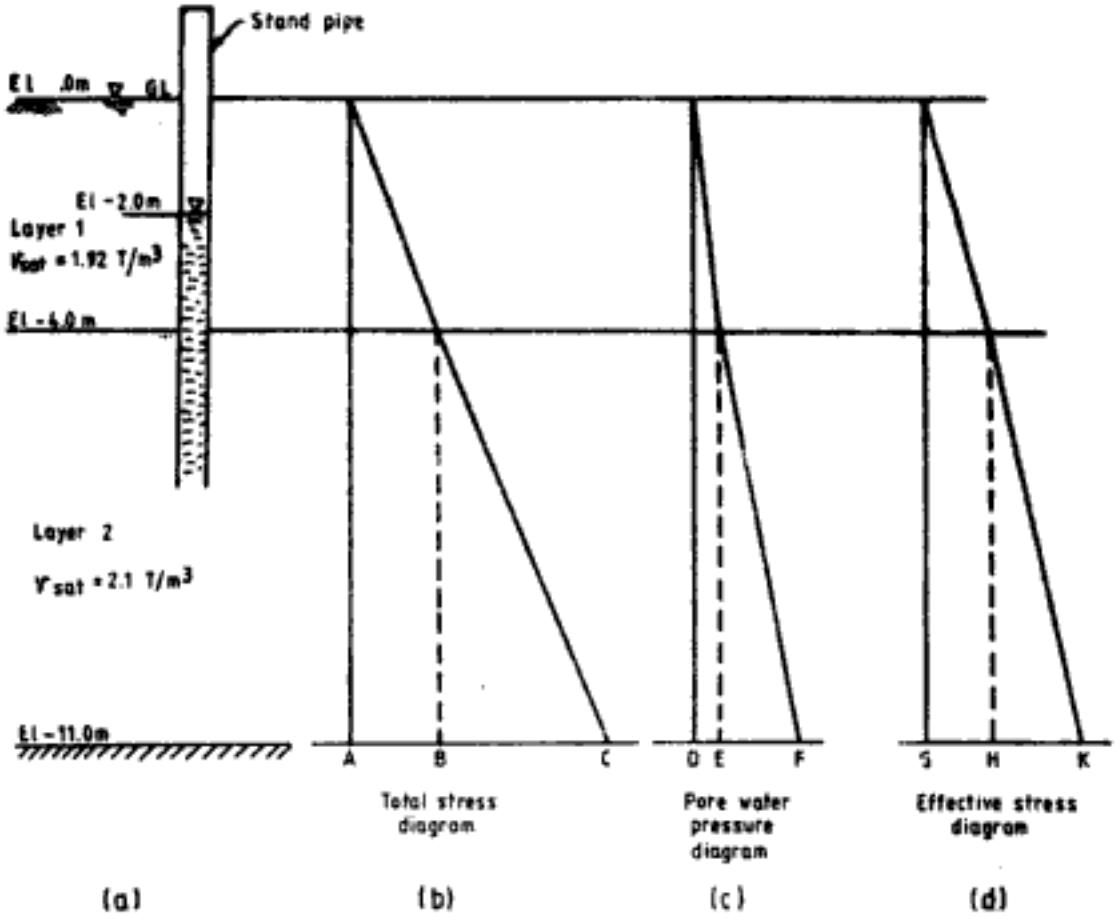

Fig. 6.10 Q 6.5

Ans: Total stress, pore water pressure and effective stress diagrams are shown in Fig. 6.10 (b), (c) and (d) respectively. The calculations are as below:

Total stress

At El. -4 $AB = 1.92 \times 4 = 7.68$ T/m²

At El. -11 $AC = 7.68 + (2.1 \times 7) = 22.38$ T/m²

Pore water pressure

At El. -4 $DE = 1 \times 2 = 2$ T/m² due to reduced pressure in Layer 2 because of pumping

At El. -11 $DF = 2 + (1 \times 7) = 9$ T/m²

Effective stress

At El. -4 $GH = AB - DE = 7.68 - 2 = 5.68$ T/m²

At El. -11 $GK = AC - DF = 22.38 - 9 = 13.38$ T/m²

Comparing this with solution for Q 6.1,

(i) Due to downward flow of water in Layer 1 effective stress in that layer increases.

(ii) Due to reduced pore water pressure in Layer 2 the effective stress in this layer also increases.

6.1.2 Effect of Capillarity on Effective Stress

The discussions till now disregard the effect of capillary rise in voids of soil above groundwater level. The capillary phenomenon, however, exists and leads to two important effects.

1. The capillary rise tends to saturate the soil in the capillary zone which in turn results in higher density for soil in this zone. This will have a corresponding effect in increasing the total stress and effective stress in soil below groundwater level.

2. The water in the capillary zone is in tension. The pore water pressure at any point in this zone is negative and is given by

$$u = -\gamma_w z \tag{6.6}$$

where z is height above groundwater level.
Because u is negative, it increases effective stress in this capillary zone.

Figure 6.11 shows the total stress, pore water pressure, and effective stress diagrams considering capillarity. The pore water pressure varies linearly in capillary zone.

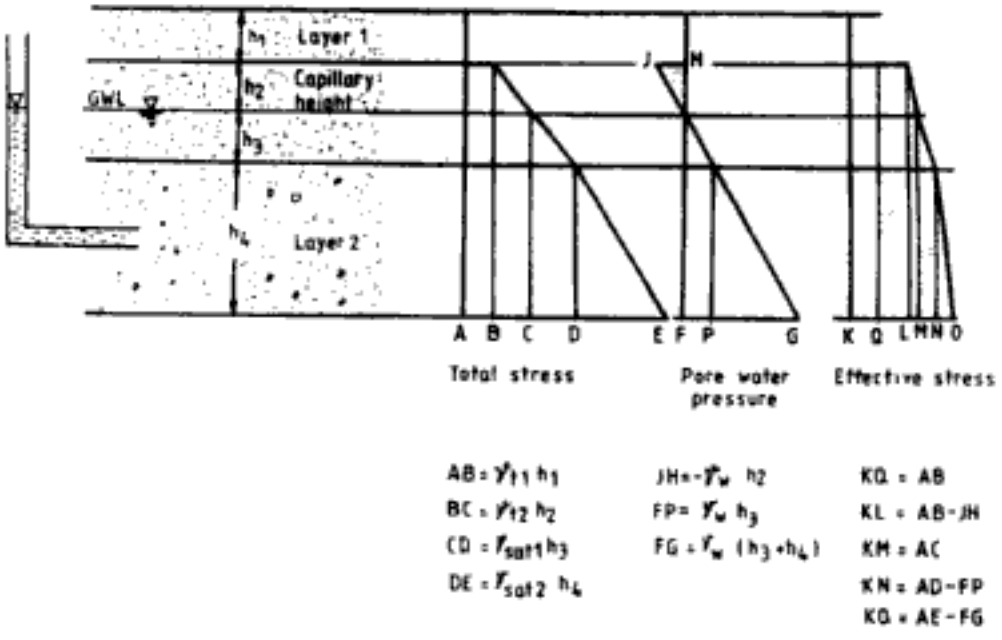

Fig. 6.11 Effect of capillarity on effective stress

The capillary effects will disappear when the soil is submerged in water or if the groundwater table rises. Hence, it may not be advisable to consider the favourable increase in effective stress due to capillary action as it is not of a permanent nature.
Questions 6.6 demonstrates the calculation for effective stress including capillary stresses.

Q 6.6: Figure 6.12(a) shows the same soil profile as in Fig. 6.8(a) but with a capillary zone 1 m above groundwater level. The soil in capillary zone may be assumed to be saturated. Draw the total stress, pore water pressure and effective stress diagrams.

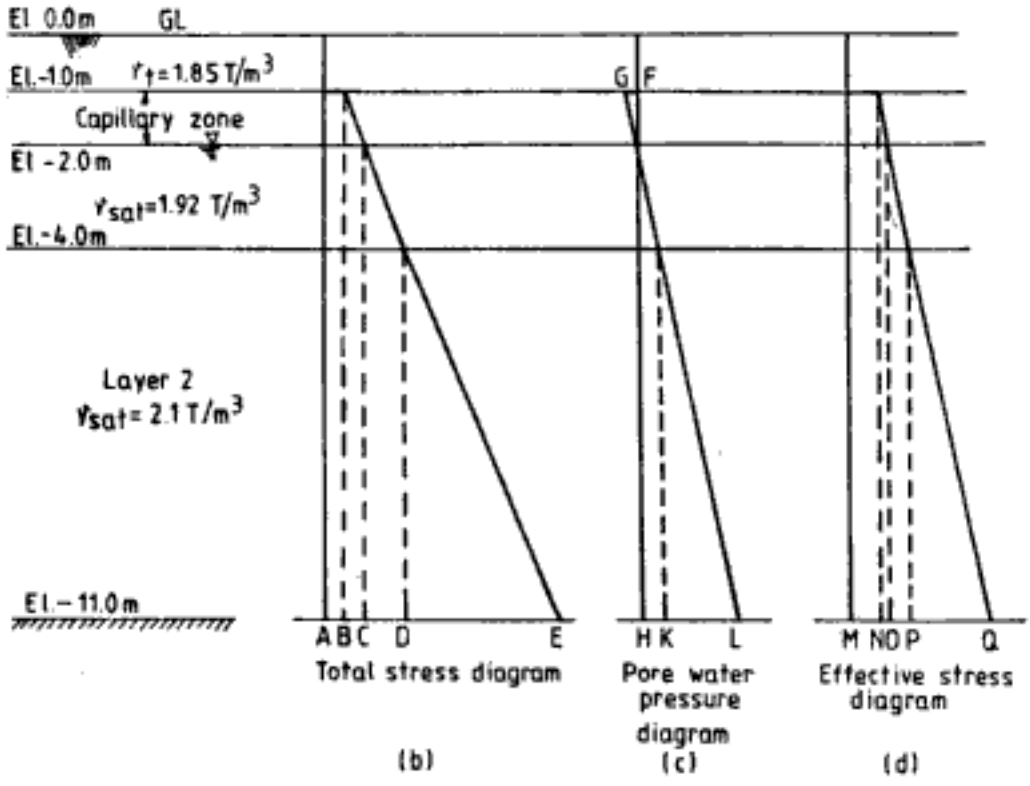

Fig. 6.12 Q 6.6

Ans: Total stress, pore water pressure and effective stress diagrams are shown in Fig. 6.12 (b), (c) and (d) respectively. Calculations are as below:

Total stress

At El. -1 $AB = 1.85 \times 1 = 1.85$ T/m^2

At El. -2 $AC = 1.85 + (1.92 \times 1) = 3.77$ T/m^2

At El. -4 $AD = 3.77 + (1.92 \times 2) = 7.61$ T/m^2

At El. -11 $AE = 7.61 + (2.1 \times 7) = 22.31$ T/m^2

Pore water pressure

At El. -1 $FG = -(1 \times 1) = -1$ T/m^2 from Eq. 6.6

At El. -2 $u = 0$

At El. -4 $HK = 1 \times 2 = 2$ T/m^2

At El. -11 $HL = 2 + (1 \times 7) = 9$ T/m^2

Effective stress

At El. -1 $MN = AB - FG = 1.85 + 1 = 2.85$ T/m^2

At El. -2 $MO = AC = 3.77$ T/m^2

At El. -4 $MP = AD - HK = 7.61 - 2 = 5.61$ T/m^2

At El. -11 $MQ = AE - HL = 22.31 - 9 = 13.31$ T/m^2

6.1.3 Modification to Effective Stress Equation in Soils Composed of Surface Active Minerals

In case of soils composed of surface active minerals the effective stress equation (Eq. 6.5) will have to be modified to account for the attractive and repulsive forces at the interparticle level. The effective stress equation will then be written as,

$$\bar{\sigma} = \sigma - u + (A' - R') \tag{6.7}$$

where A' = attractive force per unit cross-sectional area of soil

R' = repulsive force per unit cross-sectional area of soil

Due to difficulties in proper quantification of A' and R' forces, Eq. 6.7 is not popularly used in design calculations.

6.2 EFFECTIVE STRESS IN UNSATURATED SOILS

In unsaturated wet soils part of void space is occupied by air. Hence, in these soils in addition to pore water pressure pore air pressure is also present. The effective stress equation in the general form can be written as,

$$\bar{\sigma} = \sigma - u_a + \chi(u_a - u_w) \tag{6.8}$$

where u_a = pore air pressure

u_w = pore water pressure

χ = fraction of unit cross-sectional area occupied by water = A_w/A

A_w = area of water

A = area of cross-section of soil

Due to difficulties in the determination of pore air pressure and its quantification, Eq. 6.8 is also not popularly used. Bishop (1961) gives the variation of χ with degree of saturation S. This is shown in Fig. 6.13. χ is also influenced by other factors, like soil structure and the process by which the present degree of saturation has been reached. It is recommended that for degree of saturation near unity ($S \geqslant 90\%$) χ may be assumed as 1. Then effective stress equation (Eq. 6.5) may be used which is reasonably accurate for engineering purposes.

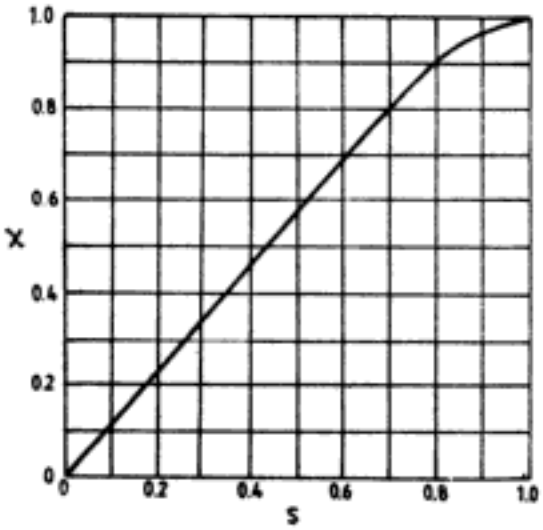

Fig. 6.13 Variation of χ with degree of saturation S (After Bishop, 1961)

7

CONSOLIDATION

Consider a small cylindrical piece of saturated soil sample enclosed in a close fitting metallic ring having smooth inner surface. With two free draining porous stones, one at top and the other at the bottom of the sample, let the entire assembly be kept immersed in water in a container as shown in Fig. 7.1. We may now conduct a few experiments on the sample.

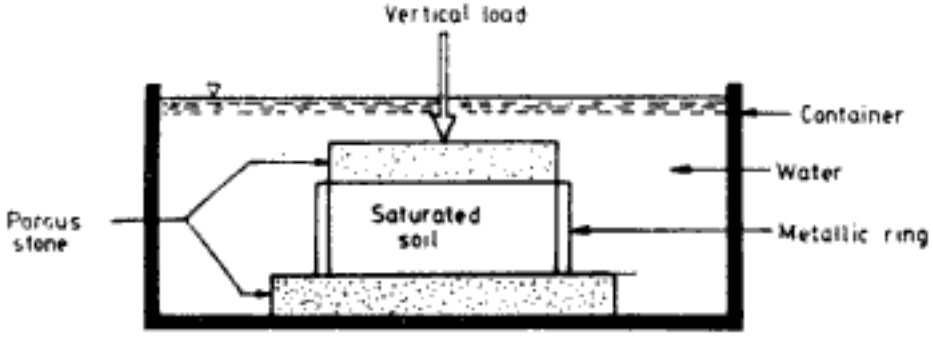

Fig. 7.1 Experimental set-up for one-dimensional consolidation

Experiment No. 1

Let a vertical load be now applied on the soil sample through the top porous stone. As can be expected, the soil sample will compress and reduce in thickness. But the reduction in thickness will not be instantaneous or immediate like the elastic compression of a steel rod subjected to compressive load. If we observe the vertical deformation of the soil sample over a period of time at the same constant vertical load and make a plot of deformation against time, a curve similar to the one shown in Fig. 7.2 will be obtained. From this figure the following points are evident:

1. The vertical deformation is time dependent
2. Compression of soil means reduction in void space, hence reduction in void ratio. Therefore, application of load on the soil sample decreases the void ratio, the decrease occurring over a period of time.
3. The soil compression comes to an end after some time.

The natural question is, why compression in the soil is not instantaneous, but time dependent. The following explanation has now universal acceptance:

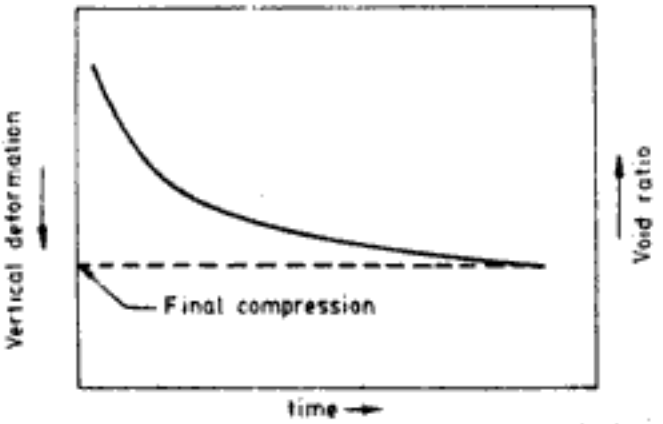

Fig. 7.2 Deformation-time-void ratio variation for consolidation experiment

When the load is applied on saturated soil, immediately the load is carried by pore water, i.e., an excess pore water pressure is developed. But if some suitable drainage for this excess pore water pressure is available (like the porous stones in the experiment) the excess pore water pressure cannot be sustained indefinitely. It will have to return to hydrostatic conditions. Through the drainage, the excess pore water pressure will be dissipated slowly. To maintain static equilibrium whatever excess pore water pressure has been dissipated will be transferred on to the soil grains or in otherwords the effective stress will increase by the same amount by which the excess pore water pressure decreases. The pore water pressure dissipation is not simply a release of pressure. The dissipation is by means of expulsion of some quantity of pore water itself from voids to accommodate for the compression of soil. The void space decreases and the water corresponding to this decrease in volume is expelled. After some time the entire excess pore water pressure will be dissipated and all the externally imposed stress will be transferred to soil grains as effective stress. There will be no further reduction in volume of voids or there will be no further reduction in void ratio.

"Consolidation" is a single powerful word in soil mechanics which stands for all which have been said in the previous paragraph.

Figure 7.2 and the associated discussions are valid for all types of soil even though there can be variations in details. The deformation will be time dependent, but the time required for full dissipation of pore water pressure will depend upon the following factors.

1. *Coefficient of permeability*: Water can be expelled more easily from soils which have a high coefficient of permeability than from soils with low coefficient of permeability. Therefore, time required for consolidation will be more for clays than for silts. But in the case of sands and gravels, the coefficient of permeability is so high that the pore water pressure is dissipated almost immediately upon application of load. In such types of soils, unless the free drainage is blocked, for all practical purposes, the compression can be considered to occur instantaneously.

2. *Thickness of soil*: If consolidation experiments are conducted on two samples of the same soil but having different thicknesses, the results of the experiments will be as shown in Fig. 7.3.

This figure explains that (i) the thick soil sample deforms more than the thin sample because more thickness means more void space available for compression, (ii) the time for

completion of consolidation, i.e., full dissipation of pore water pressure, is more for thick sample than for thin sample. This is because, the maximum distance which the water particles have to travel to reach the drainage surface in order to be expelled out of soil is more for thick soil sample than for thin sample. This maximum distance is called *drainage path*. Therefore, as length of drainage path increases time required for consolidation also increases.

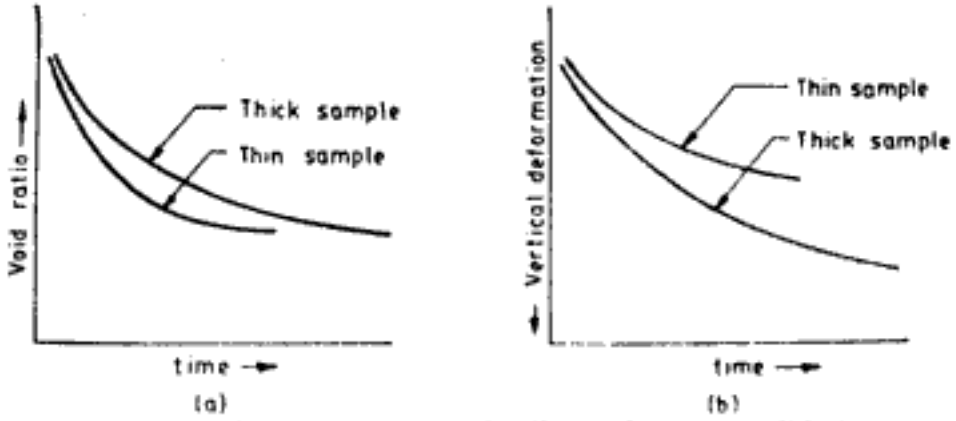

Fig. 7.3 Effect of thickness of soil sample on consolidation

In Fig. 7.1 length of drainage path is half the thickness of soil sample, since it is free draining at both top and bottom. The maximum distance the water particles have to travel is from the middle of the soil sample to either the top or bottom drainage surface. The length of drainage path will double if at one end we replace porous stone with an impervious disc (metallic or perspex) in which case water will have to travel from the impervious boundary to the free draining boundary.

Experiment No. 2

Let the experiment on the soil sample continue after getting the data to draw Fig. 7.2. After full consolidation has occurred the vertical load is released. The soil sample will rebound, which will again depend on time. The soil compression and rebound curve will be as shown in Fig. 7.4. It is evident from this figure that the deformation in soil during consolidation is not completely recoverable. Only a part of it is recoverable. This is due to the fact that during consolidation there is structural rearrangement of soil particles when reduction in void space occurs. Upon release of load the rearranged soil particles do not spring back to their initial arrangement before loading.

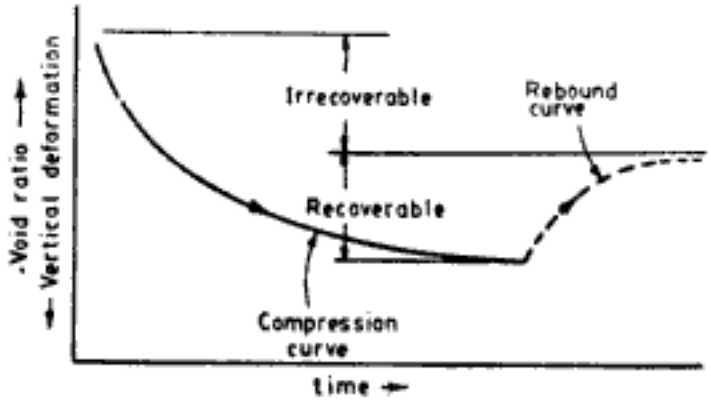

Fig. 7.4 Compression and rebound curves

Experiment No. 3

Let the experiment on the soil sample be conducted in a different fashion now. Let the sample be subjected to a vertical stress, say σ_A, first. At the end of consolidation under this stress, let the vertical stress be increased to some other value, say σ_B and the sample be allowed to consolidate. Like this the sample is consolidated at four stress levels, say σ_A, σ_B, σ_C and σ_D. Ther esulting compression—time diagram will be as shown in Fig. 7.5. From this figure the following can be inferred:

1. At the end of consolidation the effective stress becomes equal to total stress on the soil.
2. At this effective stress the soil reaches a certain equilibrium value of void ratio.

These data can be now used to define the compressibility parameters of soil.

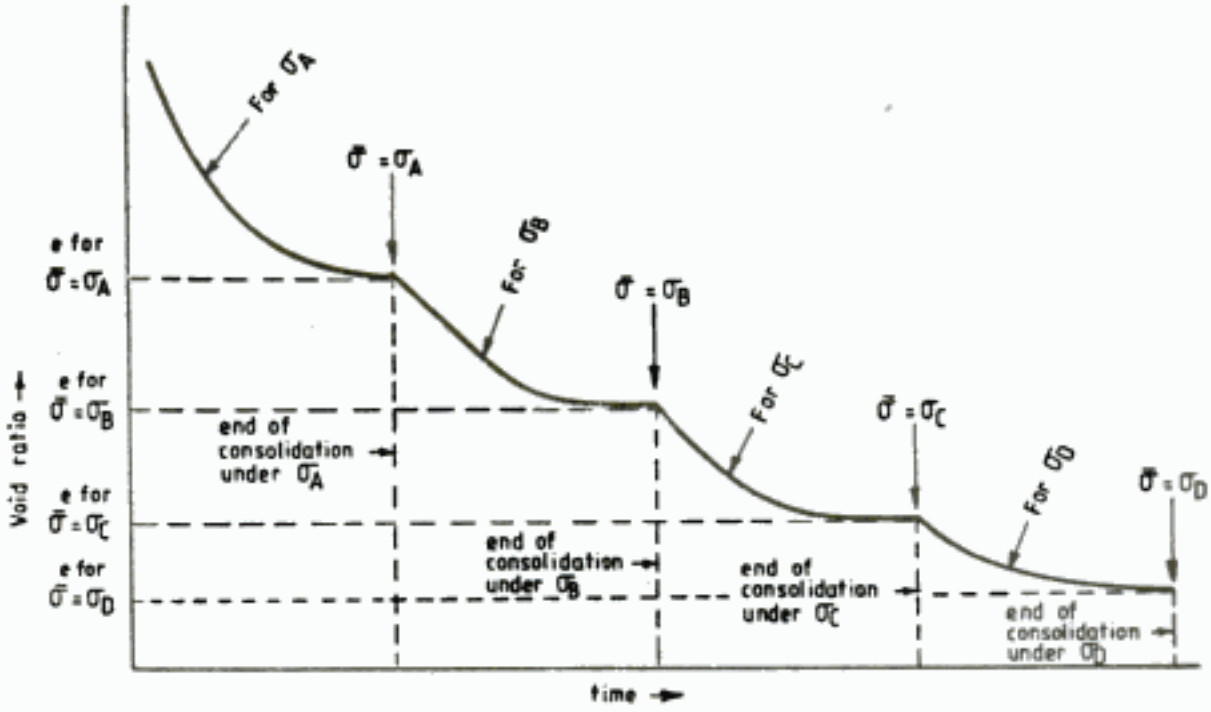

Fig. 7.5 Compression curves for different stress levels

7.1 COMPRESSIBILITY PARAMETERS

The compressibility parameters of a soil are obtained in the laboratory by conducting an experiment on a small soil sample. The soil sample must be an undisturbed sample if it were to represent the *in situ* compressibility characteristics of soil. Such a laboratory experiment is called ***consolidation test***, or *oedometer test*. Experiments No. 1 to 3 described in the previous section are merely a loose description of this laboratory test. In a laboratory test, however, the procedures are standardised. IS : 2720 (Part XV)-1965 specifies the procedure for this test. In brief, the salient features of this standard are:

1. A cyclindrical soil sample with a diameter to thickness ratio of minimum 3 is used in the test. Sixty mm is the diameter for normal testing. In special cases 50 mm, 70 mm, 100 mm diameter samples can also be used.

2. The sample is subjected to a seating pressure of 0.05 kg/cm² for 24 hours.
3. The sample is then subjected to a series of loading. The recommended stresses are 0.1, 0.2, 0.4, 0.8, 1.6, 3.2 and 6.4 kg/cm². Each stress level is maintained for 24 hours to facilitate full consolidation. Then the stress level is increased to the next higher level.
4. Time versus deformation readings are noted to obtain the necessary results. For each pressure increment the deformation readings are taken at the following total elapsed time in minutes: 0.25, 1, 2.25, 4, 6.25, 9, 16, 20.25, 25, 36, 49, 64, 81, 100, 121, 144, 1440 (24 h).

In a condensed and useful form the data obtained from consolidation test can be represented as shown in Fig. 7.6. This figure is an abstracted version of Fig. 7.5 showing the variation of void ratio (at the end of consolidation) with effective stress. With this curve shown in Fig. 7.6, *coefficient of compressibility*, a_v can be defined as follows:

$$a_v = -\frac{e_i - e_f}{\bar{\sigma}_i - \bar{\sigma}_f} = \frac{\Delta e}{\Delta \bar{\sigma}} \tag{7.1}$$

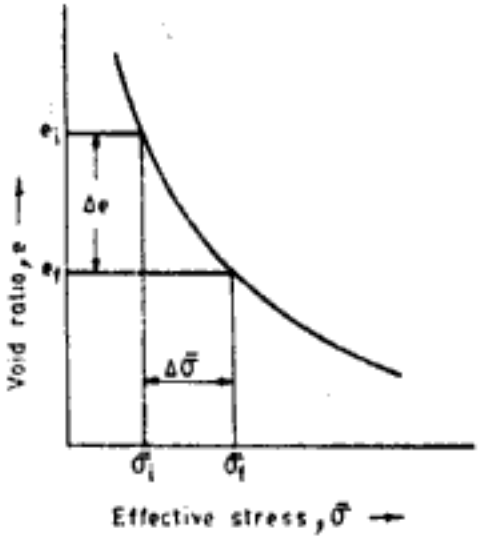

Fig. 7.6 Variation of void ratio with effective stress

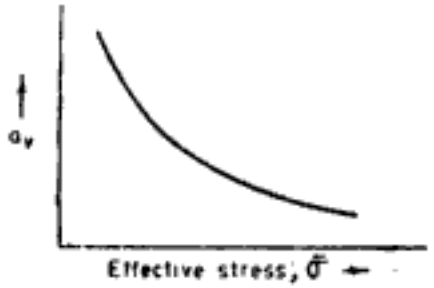

Fig. 7.7 Variation of coefficient of compressibility with effective stress

a_v, in other words, defines the rate of change of void ratio with effective stress. This rate of change is not constant as can be inferred from Fig. 7.6. It decreases with increasing effective stress. The trend of variation of a_v with effective stress is shown in Fig. 7.7. Since a_v is not a constant quantity, its value must be specified over the appropriate stress ranges. Another parameter known as *coefficient of volume compressibility*, m_v, is defined as follows

$$m_v = \frac{a_v}{1 + e_i} \tag{7.2}$$

m_v is also known as *modulus of volume change* or *coefficient of volume decrease*. Figure 7.8 shows the variation of m_v with effective stress. As is evident m_v is not a constant quantity, but decreases with increasing effective stress. Therefore, like coefficient of compressibility (a_v),

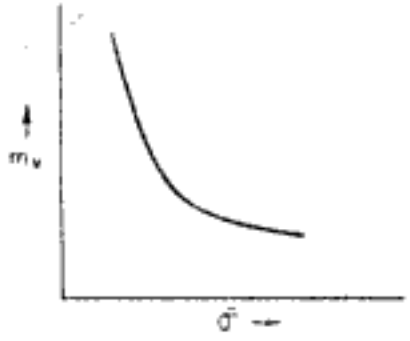

Fig. 7.8 Variation of coefficient of volume compressibility with effective stress

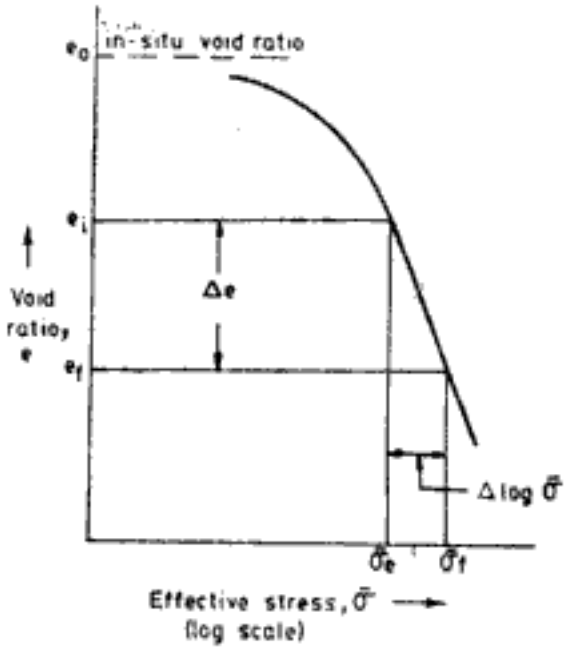

Fig. 7.9 e–log $\bar{\sigma}$ curve

m_v also should be specified over particular stress ranges.

The data in Fig. 7.6 can be represented in another form if we plot effective stress to logarithmic scale. The data will then be represented typically as shown in Fig. 7.9. Generally a curved and flatter portion is followed by a steeper straight line portion. With respect to the straight line portion, yet another compressibility parameter known as *compression index*, C_c, can be defined as follows,

$$C_c = -\frac{e_i - e_f}{\log \bar{\sigma}_i - \log \bar{\sigma}_f} = \frac{\Delta e}{\Delta \log \bar{\sigma}} \tag{7.3}$$

C_c is a dimensionless constant quantity.

Several empirical correlations for C_c are available in literature. Some of these are given below.

For natural and plastic normally-consolidated clays of low to medium sensitivity, Terzaghi and Peck (1967) give the correlation as,

$$C_c = 0.009\,(w_L - 10) \tag{7.4}$$

where w_L, the liquid limit, is in per cent. Equation 7.4 is not applicable for clays with sensitivity ratio greater than 4. For remoulded clays of low to medium sensitivity, Terzaghi and Peck suggest,

$$C_c = 0.007\,(w_L - 10) \tag{7.5}$$

where w_L is in per cent.

A correlation in terms of *in situ* (natural) void ratio, e_0, of the soil is as follows,

$$C_c = a(e_0 - b) \tag{7.6}$$

where a and b are constants. Table 7.1 gives the values of a and b for different types of soils.

Table 7.1 Values of a and b in Eq. 7.6

Type of soil	Value of	
	a	b
Uniform soil ($C_u \leqslant 2$) or coarse grained sands and gravels	0.10	e_{min}
Well graded fine to medium sand, silty sand, and inorganic silt	0.15	e_{min}
Inorganic silty clay or clay	0.30	0.27

Another correlation for organic soils and peats in terms of *insitu* (natural) moisture content w_n is as below,

$$C_c = 0.0115\, w_n \tag{7.7}$$

Azzouz *et al.* (1976) give the following correlation

$$C_c = 0.37\,(e_0 + 0.003\, w_L + 0.0004\, w_n - 0.34) \tag{7.8}$$

Compression ratio, C_R, is another compressibility parameter and is defined as

$$C_R = \frac{C_c}{1 + e_0} \tag{7.9}$$

where e_0 is the initial/*in situ* void ratio. Azzouz *et al.* (1976) give the correlation for C_R as,

$$C_R = 0.135\,(e_0 + 0.01\, w_L - 0.002\, w_n - 0.06) \tag{7.10}$$

It must be cautioned here that the empirical correlations cannot be depended on for evaluation of soil parameters. They can be considered only as rough guides. For preliminary and approximate calculations they may be useful. For design purposes compressibility parameters must be obtained from carefully conducted experiments on undisturbed soil samples.

The nature of rebound in soils is explained in Experiment No. 2 and in Fig. 7.4 of the previous section. Let the consolidation test be carried out in the following manner,

1. first the sample is successively loaded,
2. at some stress level it is partially unloaded,
3. after rebound the sample is reloaded.

The e—log $\bar{\sigma}$ curve plotted for the experiment carried out in this manner will be as shown in Fig. 7.10. The behaviour during unloading of the soil sample represented by portion BC of the curve can be used to define the swelling characteristics of the soil. The slope of this line defines the swelling index.

Swelling index,
$$C_s = -\frac{e_i - e_f}{\log \bar{\sigma}_i - \log \bar{\sigma}_f} \tag{7.11}$$

e_i, e_f, $\bar{\sigma}_i$ and $\bar{\sigma}_f$ are explained in Fig. 7.10.

Some of the important points about C_s are:

1. Numerically C_s is much smaller than C_c ($C_s \ll C_c$) as is evident in Fig. 7.10.
2. C_s is more or less same for all stages of unloading. It means that we can evaluate C_s at any stress level in consolidation test. But it must be done when the stress level has reached the straight line portion of e—log $\bar{\sigma}$ curve.
3. The slope of recompression curve (CD in Fig. 7.10) is nearly the same as C_s. That is, on reloading the change in void ratio of soil is very small till the stress level reaches the previous maximum level before unloading.

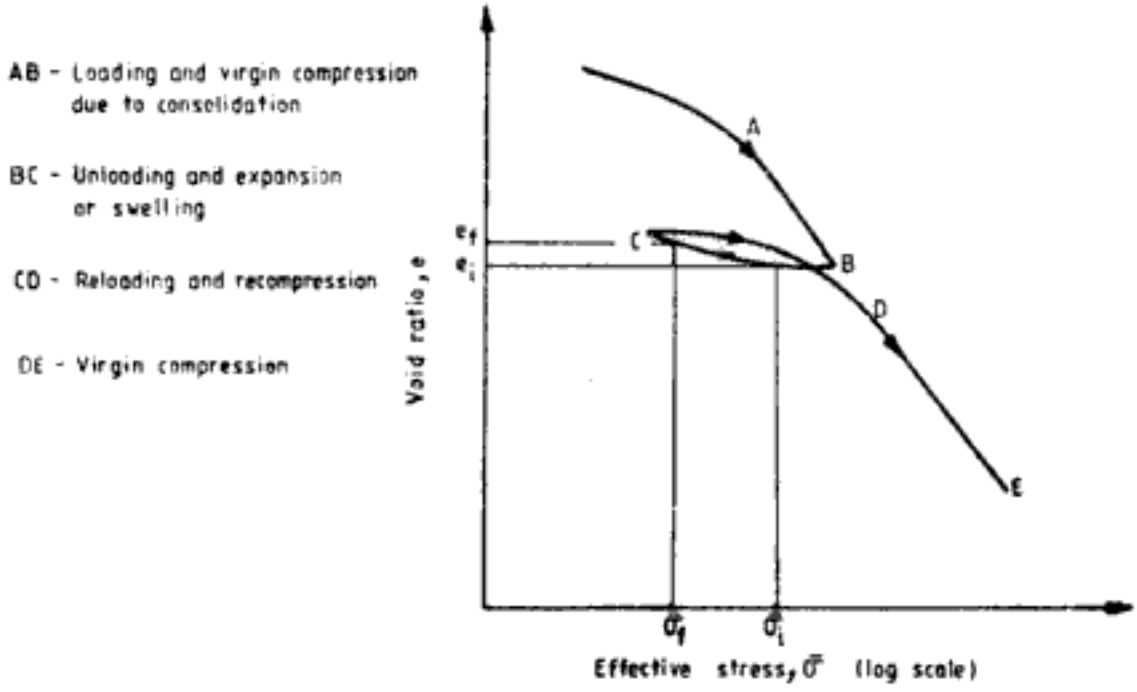

Fig. 7.10 e-log $\bar{\sigma}$ curve for loading-unloading-reloading cycle

4. C_s increases with increasing liquid limit. Variation of C_s with liquid limit is shown in Fig. 7.11.

Another useful compressibility parameter, *coefficient of consolidation* (c_v) is defined as,

$$c_v = \frac{k(1 + e_i)}{\gamma_w a_v} = \frac{k}{\gamma_w m_v} \tag{7.12}$$

where k = coefficient of permeability of soil

γ_w = density of water

e_i = initial void ratio in the stress range over which c_v is specified

It can be easily appreciated that c_v is not a constant quantity, since m_v is not a constant. Hence, c_v must also be specified over the same stress range in which m_v is specified. Equation 7.12 can be rearranged and written as follows,

$$k = \gamma_w m_v c_v \tag{7.13}$$

We can expect the coefficient of permeability to decrease with increasing effective stress because of continuous reduction in void space. It means then that since γ_w is a constant quantity, the product $m_v c_v$ decreases with increasing stress levels.

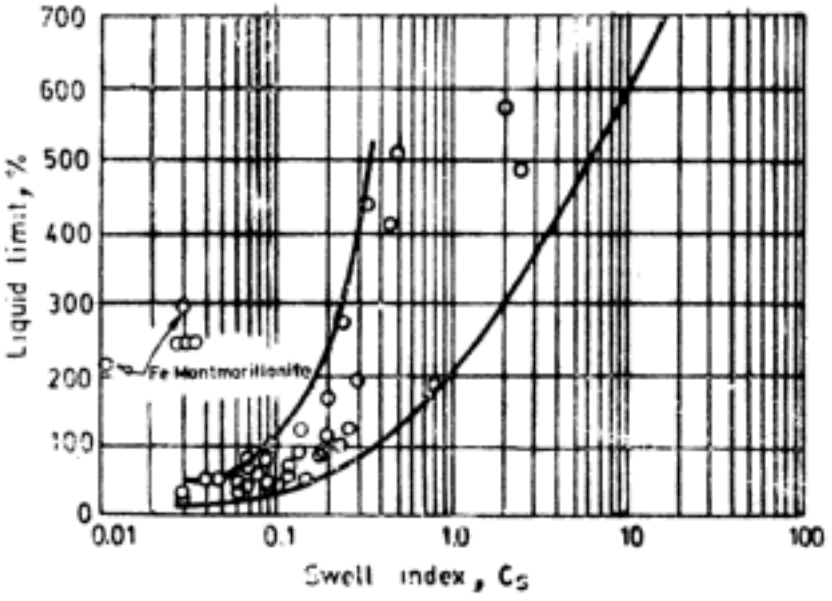

Fig. 7.11 Variation of swell index with liquid limit (after Lambe and Whitman, 1979; reprinted by permission of John Wiley and Sons, Inc., New York)

7.1.1 Uses of Compressibility Parameters

Parameters a_v, m_v, and C_c are used to determine the amount of total compression of soil. When a foundation imposes load on soil, excess pore water pressure is generated leading to consolidation of soil. The soil deforms and the foundation settles down by the same amount. This amount of settlement called *consolidation settlement* can be calculated using a_v, m_v, and C_c. The procedures are explained in more detail in Ch. 14 with illustrative examples.

Parameter C_s can be similarly used to determine upheaval movement when the load is released. For example, when an excavation is made in soil, the overburden pressure is released, as a result of which the bottom of excavation heaves up. This can be determined with C_s.

Dissipation of excess pore water pressure, and occurrence of consolidation settlement are dependent on time. It is of interest to know how much excess pore water pressure is still left to be dissipated at a given time and also how much of the total consolidation settlement has occurred till that time. These, namely, *degree of consolidation* and *rate of consolidation* can be determined with c_v. The evaluation of c_v from consolidation experiment data and the procedures of determining rate and degree of consolidation are explained in Sec. 7.2.

7.2 DEGREE OF CONSOLIDATION—ONE-DIMENSIONAL CONSOLIDATION

7.2.1 One-Dimensional Consolidation

The consolidation which occurs in the soil sample in experimental set-up shown in Fig. 7.1 and in the experiments described subsequently is one dimensional in nature. Because, the soil compression is in one direction (vertical) and the water particles also migrate in only

one direction, namely, vertically towards the free draining boundaries. Such a consolidation process is known as one-dimensional consolidation.

One-dimensional consolidation is frequently encountered in engineering practice, examples of which are shown in Fig. 7.12. When the breadth of foundation is large and the thickness of the compressible soil is small consolidation is one dimensional in nature. This condition is shown in Fig. 7.12(a). Similarly as shown in Fig. 7.12(b), if an extensive soil fill is placed over a compressible soil the soil will undergo one-dimensional consolidation.

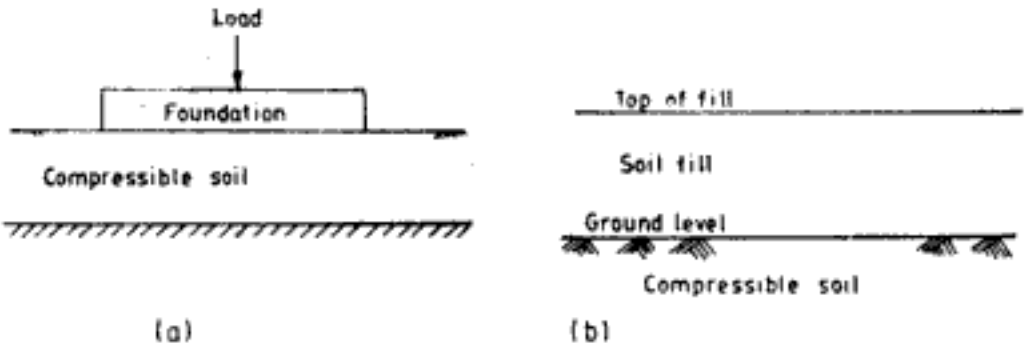

Fig. 7.12 Situations of one-dimensional consolidation

One-dimensional consolidation problems are easy to treat both analytically and experimentally. For most field problems which differ from one-dimensional consolidation, the approximate approach is to treat the problem as a one-dimensional consolidation problem and then to apply correction factors for other effects or deviations.

In the discussions to follow in this section only one-dimensional consolidation is considered.

7.2.2 Consolidation Equation

Consider a compressible layer sandwiched between two drainage layers as shown in Fig. 7.13. Let there be a uniform surcharge loading (q) at the top. In the drainage layers the pore water pressure will be dissipated simultaneously with the application of surcharge pressure. In the compressible layer, however, the surcharge pressure will be instantaneously borne by the pore water. Since the surcharge pressure is uniform the pore water pressure at all points in the compressible soil will increase by an amount equal to the value of surcharge pressure. This increase is shown in Fig. 7.13 by $ABDC$. AC denotes the initial hydrostatic base, BD stands for the new level of pore water pressure. Thus, $AB = CD =$ initial excess pore water pressure (u_{ei}) $= q$. Soon after the loading, however, the excess pore water pressure will begin to dissipate. At the interface of drainage layer and compressible layer the entire excess pore water pressure will dissipate in no time. At places nearer to drainage layer, dissipation will be faster than the dissipation at places away from drainage layer because of the distance which water has to travel. Some time after the application of surcharge pressure q (but before completion of consolidation), say at time t, the distribution of excess pore water pressure within the compressible layer will be typically as shown by curve AEC. The area shaded in the diagram, $ABDCEA$, is the total excess pore water pressure which has been dissipated and the unshaded area $AECA$ is the total excess pore water pressure which still remains to be dissipated. From any point on AC the horizontal distance to curve AEC gives the excess pore-

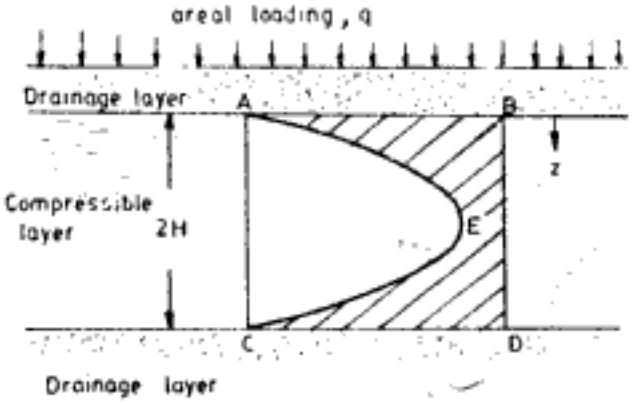

Fig. 7.13 Compressible soil layer with free drainage surfaces at top and bottom

water pressure at that point (say z) at that time, t, namely $u_{e,z,t}$. Theoretically at infinite time all the excess pore water pressure will be dissipated and curve AEC will merge with line AC. For illustration purposes the process of dissipation of excess pore water pressure has been explained with an initial uniform increase in excess pore water pressure. The initial increase in pore water pressure can vary with depth also. However, a similar process of dissipation of pore water pressure will be obtained in that case also. This process of dissipation of excess pore water pressure is defined by the following differential equation,

$$\frac{\partial u_e}{\partial t} = c_v \frac{\partial^2 u_e}{\partial z^2} \tag{7.14}$$

where u_e = excess pore water pressure
t = time
z = distance (see Fig. 7.13)

Equation 7.14 is called Terzaghi's consolidation equation, which describes the variation of excess pore water pressure with time and with depth within the compressible layer. Some of the important assumptions in the derivation of Eq. 7.14 are:

1. The compressible layer is homogeneous and saturated.
2. Darcy's law is valid.
3. Soil particles and pore water are incompressible.
4. The external stress is applied instantaneously and held constant during consolidation.

7.2.3 Degree of Consolidation

The distribution of excess pore water pressure in a soil deposit with depth at different times during consolidation can be obtained by solving Eq. 7.14 for known boundary conditions. For the situation shown in Fig. 7.13, for example, the three boundary conditions are:

1. At $t = 0$, $u_{e,z,o} = u_i$ for $z \geqslant 0$
   i.e., when consolidation starts the excess pore water pressure at all depths is same equal to some value u_i (in Fig. 7.13, $u_i = q$)
2. At $t > 0$, $u_{e,z,t} = 0$ for $z = 0$, and $z = 2H$
   i.e., immediately after consolidation starts, at the interfaces between compressible layer the excess pore water pressure is zero.

3. $\frac{\partial u_{e,z,t}}{\partial z} = 0$ for $t > 0$ and $z = H$

i.e., immediately after consolidation starts the excess pore water pressure is always maximum at the centre of the compressible layer since the longest drainage path is from the centre.

Equation 7.14 when solved for known boundary conditions will result in an expression for excess pore water pressure as a function of z and t,

That is, $$u_e = f(z, t) \tag{7.15}$$

For example, for the situation in Fig. 7.13 with the already explained boundary conditions, Eq. 7.14 can be solved to give,

$$u_e = \sum_{m=0}^{\infty} \frac{4u_i}{(2m+1)\pi} \sin \frac{(2m+1)\pi z}{2H} \exp\left\{-\frac{(2m+1)^2\pi^2}{4}\frac{c_v t}{H^2}\right\} \tag{7.16}$$

where $u_i = q$

With the solution for u_e the distribution of excess pore water pressure with depth in the compressible layer can be obtained for any given time. But it is found convenient to express the solution in terms of non-dimensional parameters. The two such parameters used are,

$$Z = \frac{z}{H} \tag{7.17}$$

Time factor, $$T = \frac{c_v t}{H^2} \tag{7.18}$$

In Eqs. 7.17 and 7.18 H is the longest drainage path. On substituting this in Eq. 7.16 the solution for u_e for situation in Fig. 7.13 will read as,

$$u_e = \sum_{m=0}^{\infty} \frac{4u_i}{(2m+1)\pi} \sin \frac{(2m+1)\pi}{2} Z \exp\left\{-\frac{(2m+1)^2\pi^2}{4}T\right\} \tag{7.19}$$

But, u_e which is still a dimensional quantity in Eq. 7.19 can be expressed in a non-dimensional form.

For this *consolidation ratio* or *degree of consolidation* $U_{Z,T}$ at any depth z is defined as,

$$U_{Z,T} = \frac{\text{excess pore water pressure dissipated}}{\text{initial excess pore water pressure}} \tag{7.20}$$

$$= \frac{u_i - u_e}{u_i} = 1 - \frac{u_e}{u_i} = \frac{\Delta\bar{\sigma}}{u_i}$$

where $\Delta\bar{\sigma}$ is the increase in effective stress at depth z due to consolidation. For situation in Fig. 7.13,

$$U_{Z,T} = 1 - \sum_{m=0}^{\infty} \frac{4}{(2m+1)\pi} \sin \frac{(2m+1)\pi}{2H} Z \exp\left\{-\frac{(2m+1)^2\pi^2}{4}T\right\} \tag{7.21}$$

A series of curves $U_{Z,T}$ versus Z can be drawn now for different values of T (see Fig. 7.17). Each curve in such a diagram is called an *isochrone*. The series of curves can be used to determine the distribution of excess or dissipated pore water pressure with depth at any instant. This is later illustrated in Qs 7.1 to 7.3.

Average degree of consolidation, $U_{av,T}$ corresponding to any time factor T for the entire compressible layer is defined as

$$U_{av,T} = \frac{\int_0^{H_t} u_i\,dz - \int_0^{H_t} u_e\,dz}{\int_0^{H_t} u_i\,dz} \times 100 \tag{7.22}$$

where H_t = total thickness of compressible layer
($H_t = 2H$ in Fig. 7.13)

$U_{av,T}$ is generally expressed in per cent.

With reference to Fig. 7.13 $U_{av,T}$ in Eq. 7.22 is nothing but,

$$U_{av,T} = \frac{\text{area } ABDCEA}{\text{area } ABDCA} \times 100 \tag{7.23}$$

More importantly the average degree of consolidation is also,

$$U_{av,T} = \frac{\text{consolidation settlement at any time}}{\text{total consolidation settlement}} \times 100 \tag{7.24}$$

Thus $U_{av,T}$ can be used to determine the rate of consolidation settlement. For the situation in Fig. 7.13, $U_{av,T}$ by definition of Eq. 7.22 can be worked out to give

$$U_{av,T} = 1 - \sum_{m=0}^{\infty} \frac{8}{(2m+1)^2\pi^2} \exp\left\{-\frac{(2m+1)^2\pi^2}{4}T\right\} \tag{7.25}$$

A graph of $U_{av,T}$ versus T can be plotted (see Fig. 7.18).

7.2.4 Consolidation Ratio and Average Degree of Consolidation for Some Particular Cases

Case 1: Semi-infinite compressible soil stratum with uniform initial excess pore water pressure distribution

The case of semi-infinite compressible stratum with a uniform surcharge load is shown in Fig. 7.14 which also shows the boundary conditions. Since the deposit is semi-infinite the drainage is only at the top.

Consolidation ratio, $U_{Z,T}$ in this case is given by

$$U_{Z,T} = 1 - erf\left(\frac{Z}{2\sqrt{T}}\right) \tag{7.26}$$

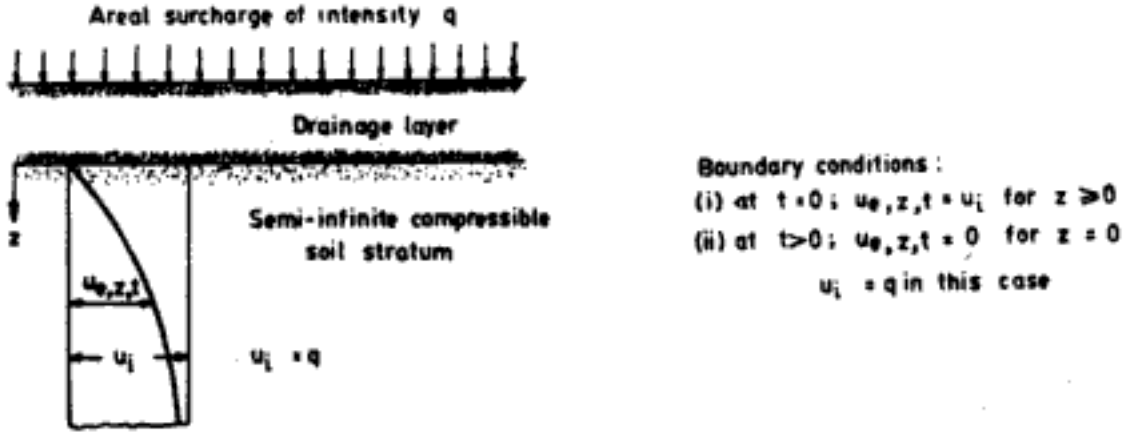

Fig. 7.14 Semi-infinite compressible soil stratum

For Z and T in this expression any arbitrary value of H can be chosen. This is because when converted to dimensional form, H will vanish from the expression. Table 7.2 gives the values for $erf(Z/2\sqrt{T})$.

Table 7.2 Values of $erf\ (Z/2\sqrt{T})$

$\frac{Z}{2\sqrt{T}}$	$erf\left(\frac{Z}{2\sqrt{T}}\right)$	$\frac{Z}{2\sqrt{T}}$	$erf\left(\frac{Z}{2\sqrt{T}}\right)$
0	0	1.1	0.8802
0.1	0.1125	1.2	0.9103
0.2	0.2227	1.3	0.9340
0.3	0.3286	1.4	0.9523
0.4	0.4284	1.5	0.9661
0.5	0.5205	1.6	0.9763
0.6	0.6039	1.7	0.9838
0.7	0.6778	1.8	0.9891
0.8	0.7421	1.9	0.9928
0.9	0.7969	2.0	0.9953
1.0	0.8427		

Since the soil is semi-infinite in depth, the value of consolidation settlement is also infinite. Hence, there is no expression for $U_{av,T}$ in this case. Use of Eq. 7.26 is illustrated in Q 7.1.

Q. 7.1: On the surface of a saturated semi-infinite compressible medium a uniform surcharge load of intensity 4.2 kg/cm² is applied. If the c_v of soil is 1.8×10^{-3} cm²/s, find the excess pore water pressure at a depth of 5 m, 400 days after application of surcharge pressure.

Ans. From Eqs. 7.20 and 7.26

$$U_{Z,T} = 1 - \frac{u_e}{u_i} = 1 - erf\left(\frac{Z}{2\sqrt{T}}\right)$$

$$\therefore \quad \frac{u_e}{u_i} = erf\left(\frac{Z}{2\sqrt{T}}\right)$$

Assume $H = 5$ m

$$\therefore \quad Z = 5/5 = 1$$

$$T = \frac{1.8\times10^{-3}\times400\times24\times60\times60}{500^2}, \quad \text{since } t = 400 \text{ days}$$

$$= 0.25$$

$$\frac{Z}{2\sqrt{T}} = \frac{1}{2\sqrt{0.25}} = 1$$

From Table 7.2 $erf\,(1) = 0.8427$

$$u_i = 4.2 \text{ kg/cm}^2$$

$$u_{e,5\text{m, 400 days}} = 0.8427\times4.2 = 3.54 \text{ kg/cm}^2$$

Case 2: Compressible soil layer with drainage at top and bottom under uniform initial excess pore water pressure distribution

Figure 7.15 shows this case. The drainage path and the notation for thickness of soil layer are shown in this figure.

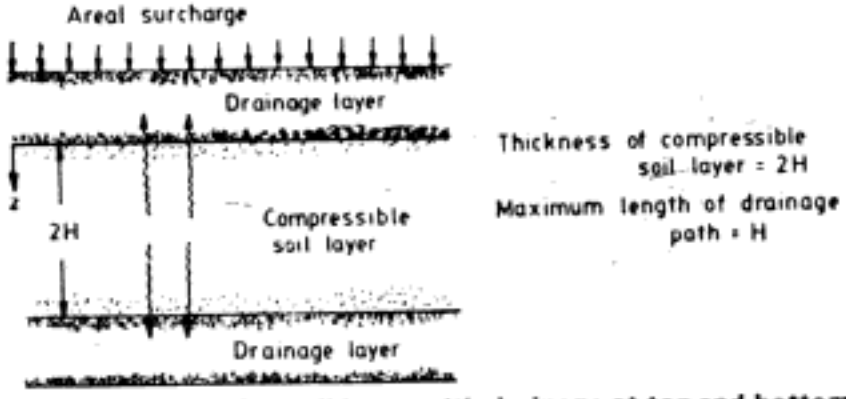

Fig. 7.15 Compressible soil layer with drainage at top and bottom

Figure 7.16 shows the boundary conditions for Case 2. Also the excess pore water pressure distribution initially and at time t are shown in this figure.

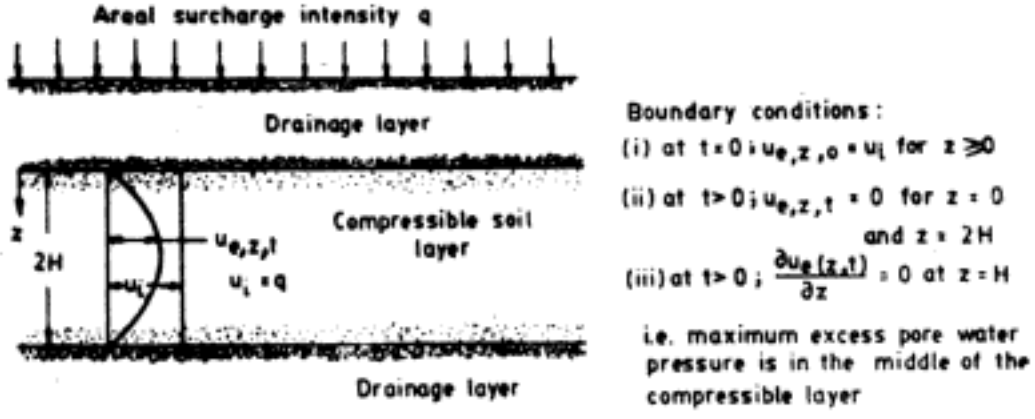

Fig. 7.16 Boundary conditions for Case 2

In fact Case 2 is the same as in Fig. 7.13 which is used to explain degree of consolidation and average degree of consolidation. Hence $U_{Z,T}$ and $U_{av,T}$ for this case are given by Eqs. 7.21 and 7.25 respectively. But these equations are not easy to use since they contain, theoretically, infinite series of terms. Hence, simple enough approximate expressions are generally used in practice. One set of such solutions are, for consolidation ratio,

$$U_{Z,T} = 1 - erf\left(\frac{Z}{2\sqrt{T}}\right) \qquad \text{for} \quad T \leq 0.2 \qquad (7.27)$$

$$U_{Z,T} = 1 - \frac{4}{\pi} \sin \frac{\pi Z}{2} \exp\left(-\frac{\pi^2 T}{4}\right) \qquad \text{for} \quad T > 0.2 \qquad (7.28)$$

and for average degree of consolidation,

$$U_{av,T} = \sqrt{\frac{4T}{\pi}} \qquad \text{for} \quad T \leq 0.2 \qquad (7.29)$$

$$U_{av,T} = 1 - \frac{8}{\pi^2} \exp\left(-\frac{\pi^2 T}{4}\right) \qquad \text{for} \quad T > 0.2 \qquad (7.30)$$

Equations 7.29 and 7.30 must be multiplied by 100 to get $U_{av,T}$ in per cent. Figure 7.17 depicts the variation of consolidation ratio with Z for different values of time factor T. Figure 7.18 gives the variation of $U_{av,T}$ with time factor T. This variation is also tabulated in Table 7.3.

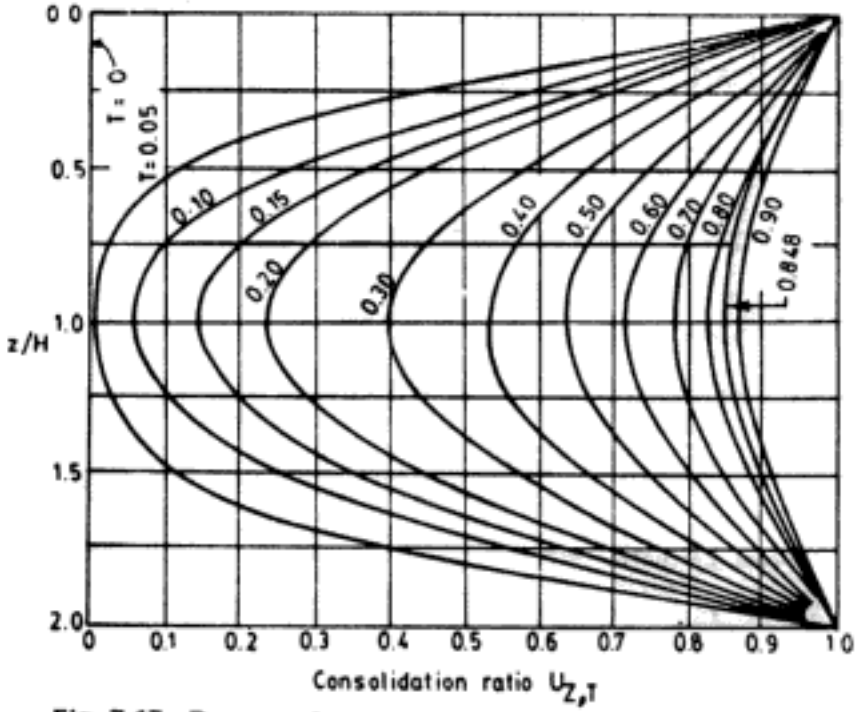

Fig. 7.17 Degree of consolidation as a function of depth ratio and time factor

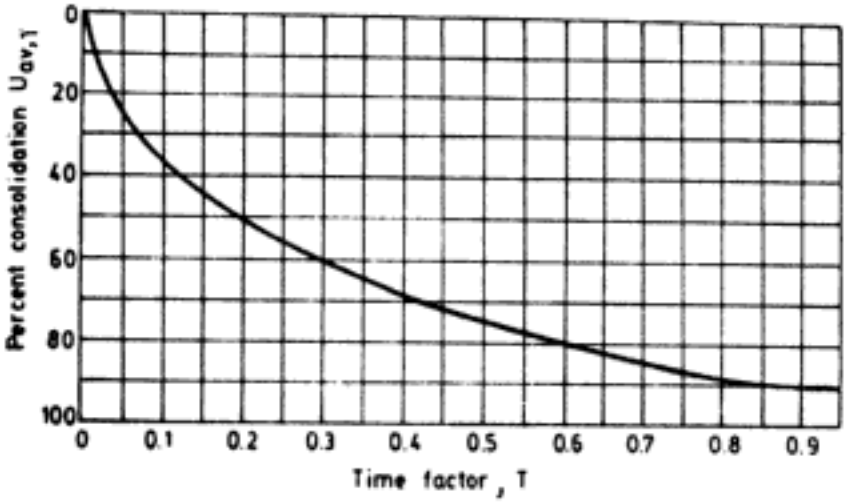

Fig. 7.18 Average degree of consolidation as a function of time factor

Terzaghi suggests the following approximate relationships between $U_{av,T}$ and T,

$$T = \frac{\pi}{4}(U_{av,T})^2 \qquad \text{for} \quad U_{av,T} = 0 \text{ to } 0.53 \qquad (7.31)$$

and

$$T = 1.781 - 0.933\,\{\log_{10}(1 - U_{av,T})\} \qquad \text{for} \quad U_{av,T} = 0.53 \text{ to } 1 \qquad (7.32)$$

Table 7.3 $U_{av,T}$ vs. T

$U_{av,T}$	T	$U_{av,T}$	T
0	0	0.55	0.238
0.05	0.0017	0.60	0.286
0.10	0.0077	0.65	0.342
0.15	0.0177	0.70	0.403
0.20	0.0314	0.75	0.477
0.25	0.0491	0.80	0.567
0.30	0.0707	0.85	0.684
0.35	0.0962	0.90	0.848
0.40	0.126	0.95	1.129
0.45	0.159	1.00	∞
0.50	0.196		

Sivaram and Swamee (1977) give the following equations for $U_{av,T}$ varying from 0 to 1

$$U_{av,T} = \frac{\sqrt{4T/\pi}}{\{1 + (4T/\pi)^{2.8}\}^{0.179}} \tag{7.33}$$

or

$$T = \frac{(\pi/4)U_{av,T}^2}{(1 - U_{av,T}^{5.6})^{0.357}} \tag{7.34}$$

Q. 7.2: A 7.5 m thick saturated compressible soil layer has drainage at top and bottom. c_v of the layer is 1.65×10^{-3} cm²/s. Determine the excess pore water pressure in the middle of the layer 400 days after application of areal surcharge of intensity 2 kg/cm². What is the average degree of consolidation at that time?

Ans. $2H = 7.5$ m $\quad \therefore H = 3.75$ m

At the middle of the layer, $z = 3.75$ m

$$Z = \frac{3.75}{3.75} = 1$$

For 400 days,
$$T = \frac{1.65 \times 10^{-3} \times 400 \times 24 \times 60 \times 60}{375 \times 375} = 0.406$$

From Fig. 7.17,
$$U_{Z,T} = 0.54 = 1 - \frac{u_e}{u_i}$$

$\therefore$
$$u_e = (1 - 0.54)u_i$$
$$u_i = 2 \text{ kg/cm}^2$$
$$u_{e,3.75\text{m},\ 400\text{ days}} = (1 - 0.54) \times 2 = 0.92 \text{ kg/cm}^2$$

From Fig. 7.18 or Table 7.3 average degree of consolidation for $T = 0.406$ is,

$$U_{av,T} = 70\%$$

Case 3: Compressible soil layer with drainage only at top under uniform initial excess pore water pressure distribution

Figure 7.19 shows the drainage path and the notation for thickness of layer in this case. Figure 7.20 shows the boundary conditions for Case 3. Also the excess pore water pressure distribution initially and at time t are shown in this figure.

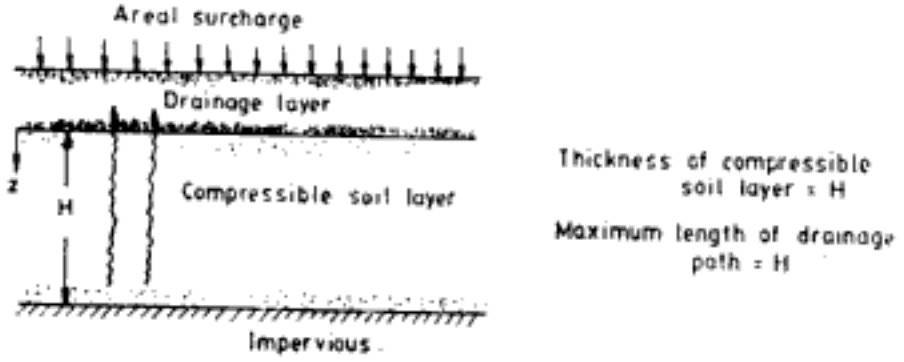

Fig. 7.19 Compressible soil layer with drainage only at top

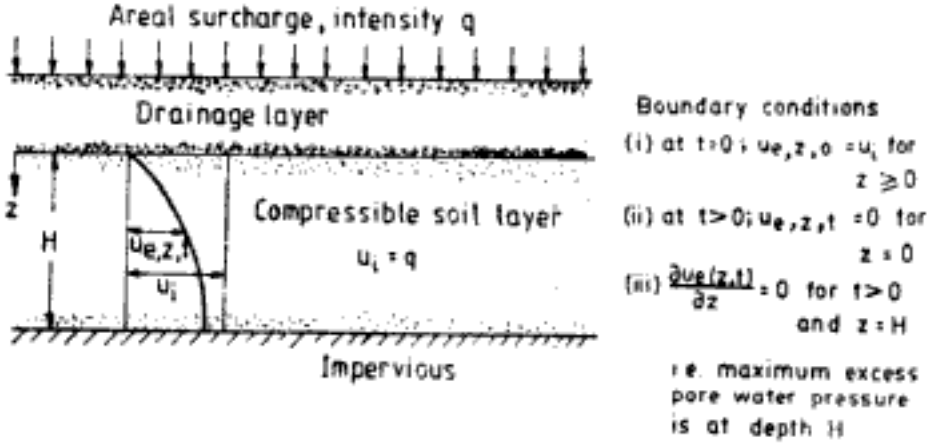

Fig. 7.20 Boundary conditions for Case 3

In this case also $U_{Z,T}$ is given by the same equations as for Case 2, namely Eqs. 7.27 and 7.28. Hence, Fig. 7.17 is applicable for consolidation ratio in this case also. However, only top half of the figure is relevant here, since in this case Z has a maximum value of 1.

Equations for average degree of consolidation $U_{av,T}$ in this case are also the same as those for Case 2 (Eqs. 7.25, 7.29, and 7.30). Figure 7.18 and Table 7.3 can then be used for $U_{av,T}$.

Q. 7.3: Redo Q 7.2 if the compressible layer has drainage only at top.

Ans. $H = 7.5$ m; $z = 3.75$ m

$Z = 3.75/7.5 = 0.5$

For 400 days, $$T = \frac{1.65 \times 10^{-3} \times 400 \times 24 \times 60 \times 60}{750 \times 750} = 0.101$$

From Fig. 7.17 $$U_{Z,T} = 0.265 = 1 - \frac{u_e}{u_i}$$

$$u_e = (1 - 0.265) \times 2$$

$$u_{e,3.75\text{ m},\ 400\text{ days}} = 1.47 \text{ kg/cm}^2$$

From Fig. 7.18 average degree of consolidation for $T = 0.101$ is,

$$U_{av,T} = 36\%$$

Case 4: Compressible soil layer with drainage only at bottom under uniform initial excess pore water pressure distribution

This case is the same as Case 3 with the direction for distance z modified as shown in Fig. 7.21. All discussions made in Case 3 are valid for Case 4 also with this modification for direction of z.

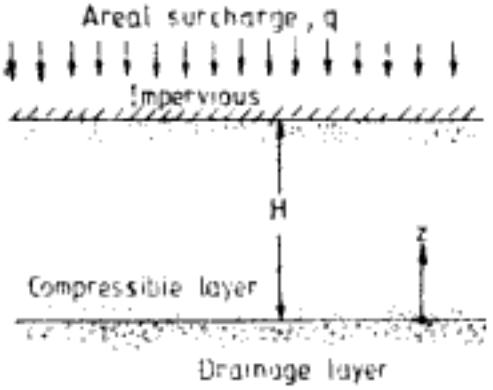

Fig. 7.21 Compressible soil layer with drainage only at bottom

Case 5: Compressible soil layer with drainage at top and bottom under linearly varying initial excess pore water pressure distribution.

A linear increase of initial excess pore water pressure with depth is shown in Fig. 7.22(a) and the linear decrease with depth is shown in Fig. 7.22(b). By reversing the direction of z as shown in these figures both can be treated as one and the same case. The linear variation in initial excess pore water pressure u_i is given by the equation,

$$u_i = u_1 - u_2\left(\frac{H - z}{H}\right) \tag{7.35}$$

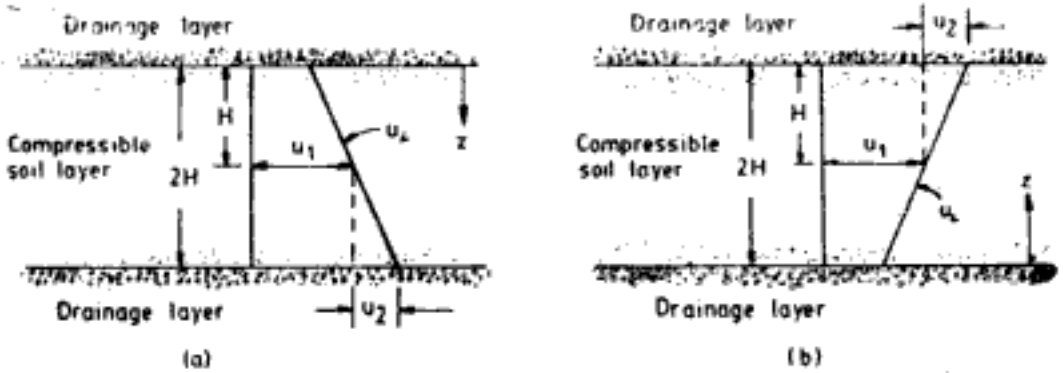

Fig. 7.22 Compressible soil layer with two-way drainage and having linearly varying initial excess pore water pressure distribution

where u_1 and u_2 are as shown in Fig. 7.22. The solution for average degree of consolidation $U_{av,T}$ for this case also is given by Eqs. 7.25, 7.29 and 7.30. So, for this case also Fig. 7.18 and Table 7.3 can be used to determine $U_{av,T}$.

Case 6: Compressible soil layer with drainage at top and bottom under sinusoidal (full) initial excess pore water pressure distribution

Figure 7.23 presents this case. Initial excess pore water pressure distribution, u_i, is given by,

$$u_i = u_0 \sin \frac{\pi z}{2H} \tag{7.36}$$

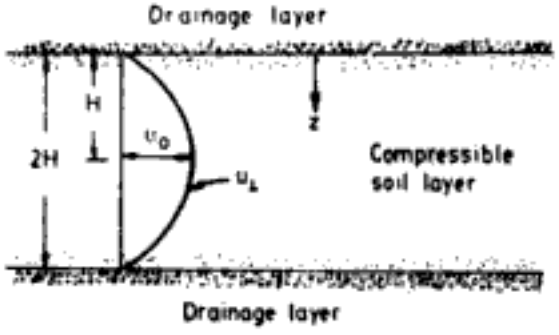

Fig. 7.23 Compressible soil layer with two-way drainage and having sinusoidal (full) initial excess pore water pressure distribution

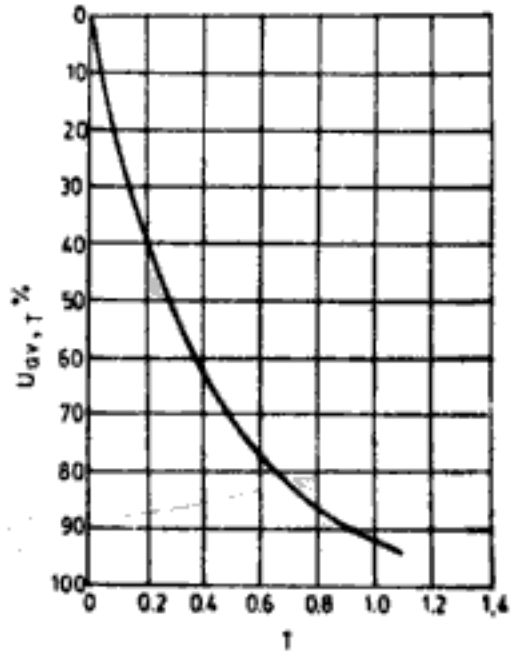

Fig. 7.24 Average degree of consolidation as a function of time factor for Case 6

The solution for average degree of consolidation for this type of distribution is given by,

$$U_{av,T} = 1 - \exp\left(-\frac{\pi^2 T}{4}\right) \tag{7.37}$$

Figure 7.24 presents the variation of $U_{av,T}$ with T.

Case 7: Compressible soil layer with drainage at top and bottom under sinusoidal (half) initial excess pore water pressure distribution

The case is shown in Fig. 7.25. In the compressible soil layer, initial excess pore water pressure distribution is given by,

$$u_i = u_0 \sin \frac{\pi z}{4H} \tag{7.38}$$

The variation of average degree of consolidation $U_{av,T}$ with time factor T, for such a distribution is shown in Fig. 7.26.

Case 8: Compressible soil layer under triangular initial excess pore water pressure distribution

Figure 7.27 shows some typical situations of compressible soil layer with triangular excess pore water pressure distribution. In Fig. 7.27 (*a*)-(*d*) the initial distribution u_i is given by,

$$u_i = u_0 \frac{z}{H} \tag{7.39}$$

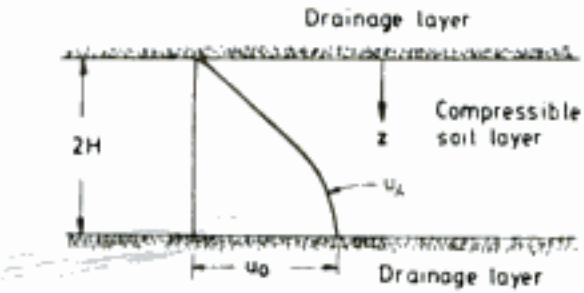

Fig. 7.25 Compressible soil layer with two-way drainage and having sinusoidal (half) initial excess pore water pressure distribution

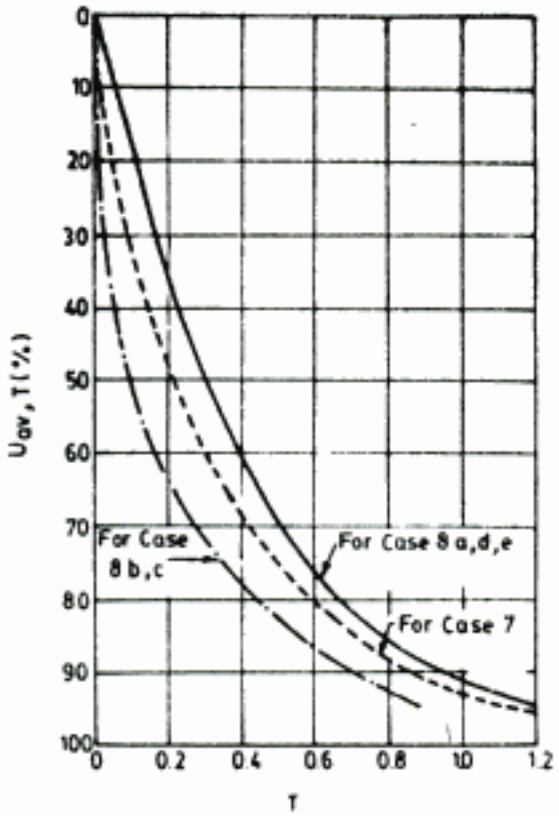

Fig. 7.26 Average degree of consolidation as a function of time factor for Cases 7 and 8

Direction of z is marked in these figures. For Fig. 7.27(e), u_i is given by

$$u_i = u_0 \frac{z}{H} \qquad \text{for } z = 0 \text{ to } H \tag{7.40}$$

and

$$u_i = u_0\left(2 - \frac{z}{H}\right) \qquad \text{for } z = H \text{ to } 2H \tag{7.41}$$

The variations of average degree of consolidation $U_{av,T}$ with time factor T, for all these types of triangular distributions are shown in Fig. 7.26.

7.2.5 Average Degree of Consolidation for Time Dependent Loading

In the discussions till now the external load is assumed to be applied instantaneously. In other words, the initial excess pore water pressure distribution develops instantaneously. But in practice, the load is built up gradually and during this construction time there is also some generation and dissipation of excess pore water pressure.

A typical type of time dependent loading is shown in Fig. 7.28 called *ramp loading*. Over a construction period t_c the final load intensity q is built up linearly. For a compressible soil layer with drainage at top and bottom as shown in Fig. 7.29, Olson (1977) gives the solution

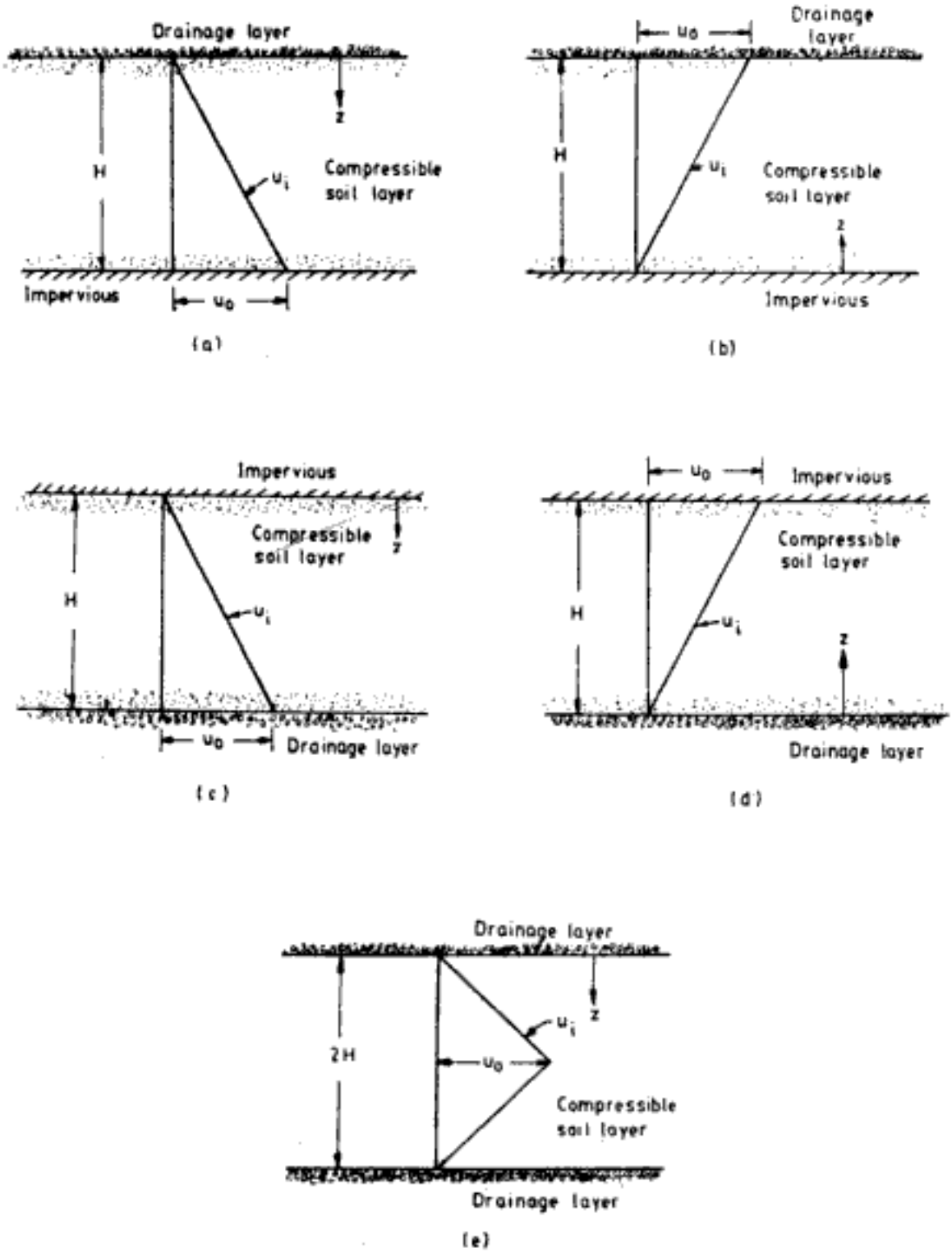

Fig. 7.27 Cases of compressible soil layer having triangular initial excess pore water pressure distribution

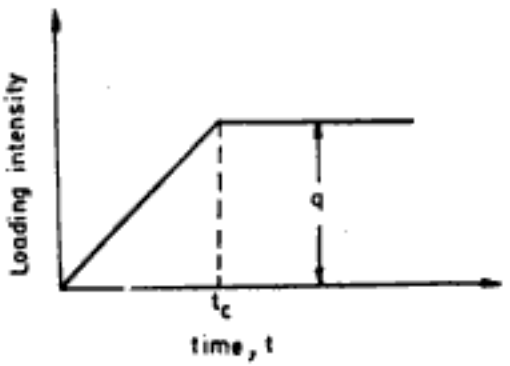

Fig. 7.28 Ramp loading

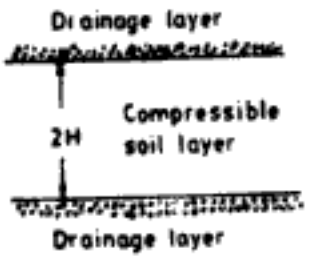

Fig. 7.29 Compressible soil layer with two-way drainage and subjected to ramp loading

for average degree of consolidation considering ramp loading. For this, one more non-dimensional time factor, called *construction time factor*, T_c, is defined as,

$$T_c = \frac{c_v t_c}{H^2} \tag{7.42}$$

where t_c is as shown in Fig. 7.28.

Average degree of consolidation, $U_{av,T}$, is given by the following equations:

For $T \leqslant T_c$,

$$U_{av,T} = \frac{T}{T_c}\left(1 - \frac{2}{T}\sum_{m=0}^{\infty}\frac{16}{\{(2m+1)\pi\}^4}\left[1 - \exp\left\{-\frac{4T}{(2m+1)^2\pi^2}\right\}\right]\right) \tag{7.43}$$

For $T \geqslant T_c$,

$$U_{av,T} = 1 - \frac{2}{T_c}\sum_{m=0}^{\infty}\frac{16}{\{(2m+1)\pi\}^4}\left[\exp\left\{\frac{4T_c}{(2m+1)^2\pi^2}\right\} - 1\right]\exp\left\{-\frac{4T}{(2m+1)^2\pi^2}\right\} \tag{7.44}$$

Variation of $U_{av,T}$ with T for different values of construction time factors T_c, is shown in Fig. 7.30.

Q 7.4: Over a saturated 7.5 m thick clay layer with drainage at top and bottom, surcharge pressure is built up at a daily rate of 0.03 kg/cm^2 to a final value of 4.5 kg/cm^2. c_v of the clay layer is 1.65×10^{-3} cm^2/s. Determine the average degree of consolidation 60 days and 450 days from the beginning of construction?

Ans: $2H = 7.5$ m; $\therefore \quad H = 3.75$ m

Time for construction, $t_c = \dfrac{4.5}{0.03} = 150$ days

Construction time factor, $T_c = \dfrac{1.65 \times 10^{-3} \times 150 \times 24 \times 60 \times 60}{375 \times 375}$

$= 0.152$

For $t = 60$ days

$$T = \frac{1.65 \times 10^{-3} \times 60 \times 24 \times 60 \times 60}{375 \times 375} = 0.061 < T_c$$

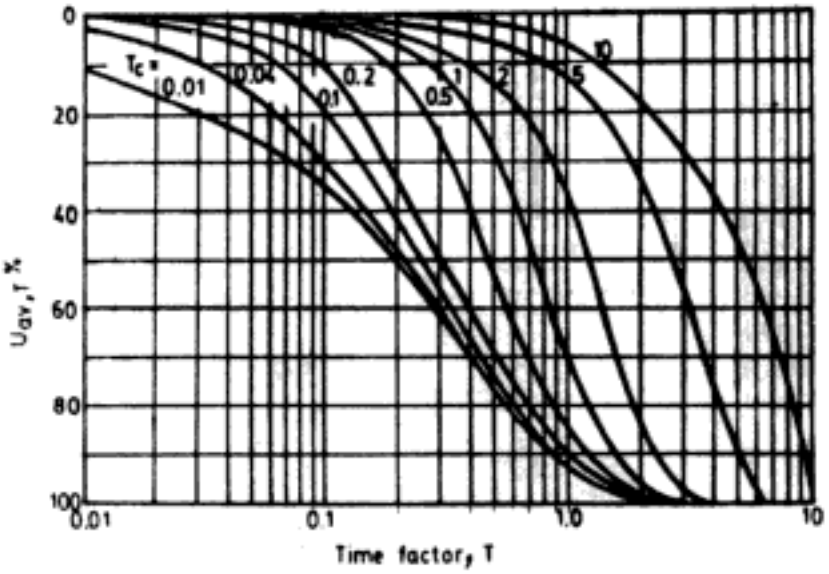

Fig. 7.30 Average degree of consolidation as function of time factor for single ramp load (after Olson, 1977. Reprinted by permission of American Society of Civil Engineers, New York)

From Fig. 7.30

$$U_{av,T} = 7\%$$

For $t = 450$ *days*

$$T = \frac{1.65 \times 10^{-3} \times 450 \times 24 \times 60 \times 60}{375 \times 375} = 0.456 > T_c$$

From Fig. 7.30 $U_{av,T} = 67\%$

Note: It is significant to note that the average degree of consolidation at the end of construction ($t = 150$ days, $T = 0.152$) is nearly 28%.

7.2.6 Degree of Consolidation in Layered Soils

Because of the different thicknesses, different coefficients of permeability, and the different coefficients of consolidation of the soil layers, it is difficult to get closed form solution in case of layered soils. A solution for a two-layer system shown in Fig. 7.31 has been given by Luscher (1965).

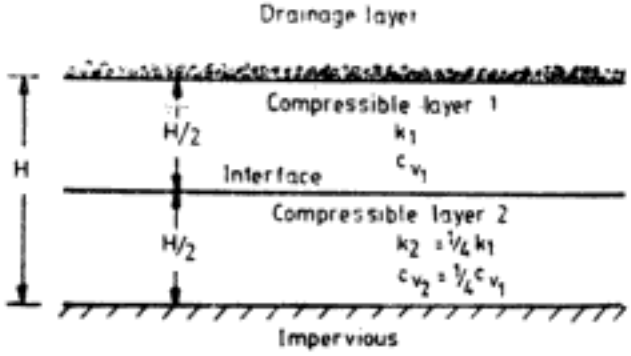

Fig. 7.31 Two-layer system subjected to uniform initial excess pore water pressure distribution

Time factor in this case is defined as

$$T = \frac{c_{v1} t}{H^2} \tag{7.45}$$

The solution for degree of consolidation $U_{Z,T}$ is shown in Fig. 7.32.

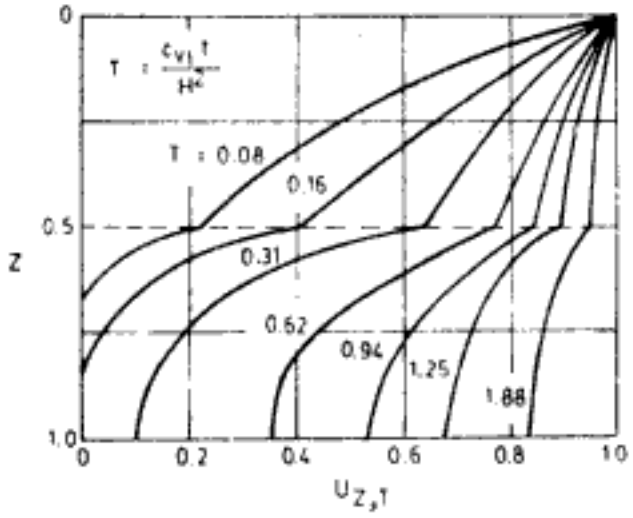

Fig. 7.32 Degree of consolidation as a function of depth ratio and time factor in twolayered soil (after Luscher, 1965. Reprinted by permission of American Society of Civil Engineers, New York)

The average degree of consolidation of layered soils can be determined by an approximat procedure suggested by Palmer (1953). If there are two layers of soil, one above and another as shown in Fig. 7.33, the top layer can be replaced by an equivalent layer having coefficient of consolidation same as the bottom layer. The thickness of the equivalent layer H_1' is given by

$$H_1' = H_1 \sqrt{\frac{c_{v2}}{c_{v1}}} \tag{7.46}$$

where H_1 = thickness of top layer

c_{v1}, c_{v2} = coefficients of consolidation of top and bottom layer, respectively

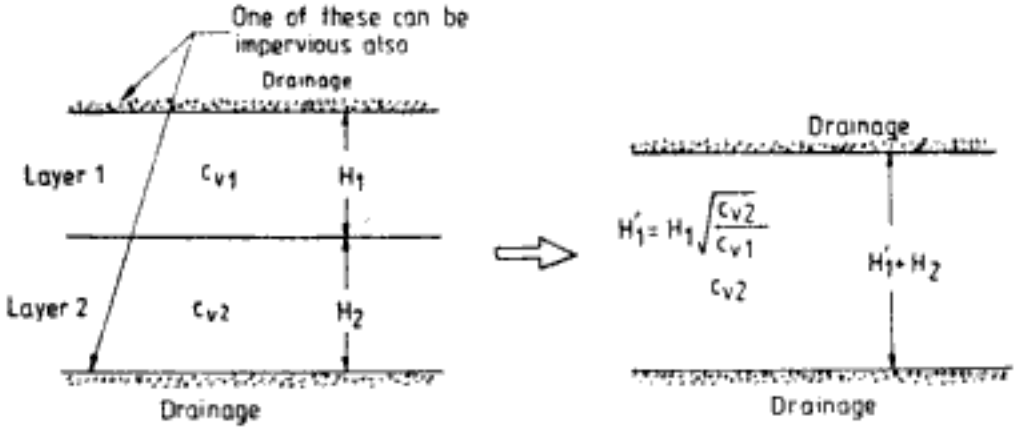

Fig. 7.33 Single equivalent layer for two-layered soil

Now the two layers can be treated as one single layer of total thickness $H_1' + H_2$ having coefficient of consolidation as c_{v2}. This equivalence is also shown in Fig. 7.33. From the figure it may *not* be inferred that H_1' is always less than H_1. The relationship depends upon values of c_{v1} and c_{v2}. The equivalent single layer with coefficient of consolidation c_{v1} can also be obtained, in which case the total thickness of equivelent layer is $H_1 + H_2'$ where H_2' is

$$H_2 \sqrt{\frac{c_{v1}}{c_{v2}}}.$$

The procedure suggested by Palmer can be applied to any number of layers, by successive reductions in number of layers. Question 7.5 demonstrates the application of Palmer's procedure.

Another kind of stratification often encountered in field is shown in Fig. 7.34. In such a situation the two layers undergo consolidation simultaneously and independently of each other. The average degree of consolidation of each layer is determined separately, from which the average degree of consolidation of the total system can be computed.

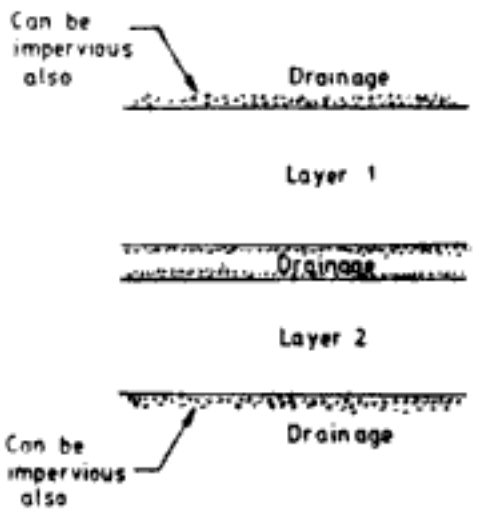

Fig. 7.34 Drainage between two compressible layers

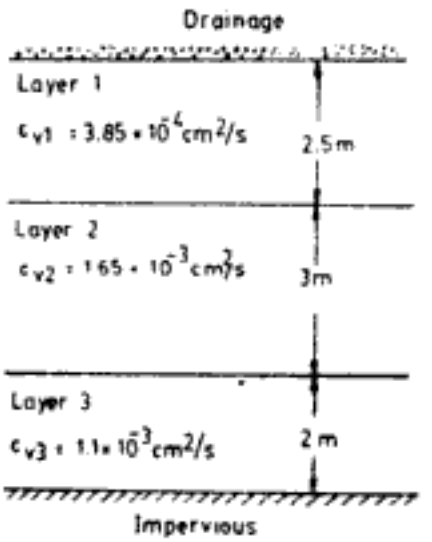

Fig. 7.35 Q 7.5

Q. 7.5 Determine the average degree of consolidation for the three-layer system shown in Fig. 7.35, 1250 days after an initial uniform increase in pore water pressure of 1 kg/cm².

Ans: Considering layers 1 and 2, equivalent height of layer 1 with c_v as c_{v2}

$$H_1' = 2.5 \sqrt{\frac{1.65 \times 10^{-3}}{3.85 \times 10^{-4}}}$$

$$= 5.18 \text{ m}$$

Now the system is reduced to a two-layer system as shown in Fig. 7.36.
Equivalent thickness of the top layer in Fig. 7.36 with c_v as c_{v3},

$$= 8.18 \sqrt{\frac{1.1 \times 10^{-3}}{1.65 \times 10^{-3}}}$$

$$= 6.68 \text{ m}$$

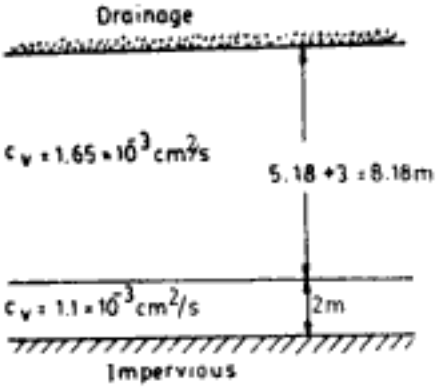

Fig. 7.36 Q. 7.5

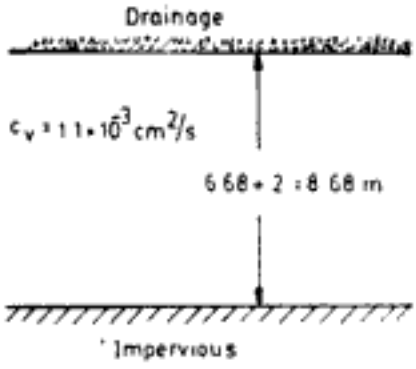

Fig. 7.37 Q. 7.5

The equivalent single layer for the three-layer system is shown in Fig. 7.37. For a uniform increase in pore water pressure solution can be obtained from Case 3.

For 1250 days, $$T = \frac{1.1 \times 10^{-3} \times 1250 \times 24 \times 60 \times 60}{868 \times 868}$$

$$= 0.158$$

From Eq. 7.29 average degree of consolidation is,

$$U_{av,T} = \sqrt{\frac{4 \times 0.158}{\pi}} \times 100 = 45\%$$

7.2.7 Determination of c_v

It is explained in Sec. 7.1 that consolidation test consists of applying a series of increasing loads on a soil sample. The vertical deformation dial gauge—elapsed time readings taken during each step of load application are used to determine c_v.

Logarithm of time method

Figure 7.38 shows the typical trend of dial gauge reading vs. logarithm of time plot.

The procedure proposed by Casagrande and Fadum (1940), for the determination of c_v is as follows:

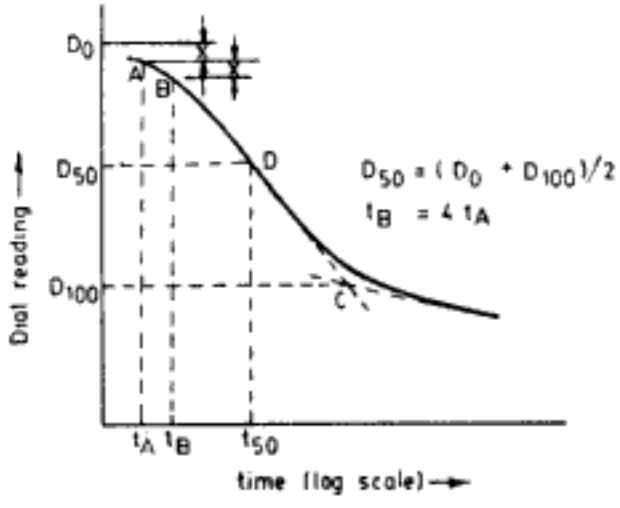

Fig. 7.38 Dial gauge reading *vs.* log *t* curve for one-dimensional consolidation test

1. Draw the dial gauge vs. logarithm of time curve (Fig. 7.38). The curve consists of a parabolic portion in the beginning, a nearly straight line portion in the middle and again a curved portion in the end. The vertical scale will have to be changed to get a pronounced pattern like this if it is not clearly discernible.
2. In the top parabolic portion of the curve plot two points A and B such that the time for point B (t_B) is four times that for point A(t_A). i.e., $t_B = 4t_A$.
3. Measure the vertical distance between points A and B. Let this be x.
4. Set off a vertical distance x above point A and draw a horizontal line through this point to intersect the ordinate axis. The reading corresponding to this point of intersection is the corrected initial dial gauge reading, D_0, at which the average degree of consolidation is 0%.
5. Draw the tangents at the lower part of the curve. Their point of intersection C is taken to define 100% primary consolidation. Hence, the dial gauge reading corresponding to this point is D_{100}.
6. Determine the 50% consolidation dial gauge reading D_{50} as,

$$D_{50} = \frac{D_0 + D_{100}}{2} \tag{7.47}$$

7. For D_{50} obtain the corresponding point D on the curve from which time for 50% consolidation of the soil sample can be obtained as t_{50}.
8. Determine c_v from the relationship $T = (c_v t/H^2)$. The laboratory soil sample has drainage at top and bottom and is an example of Case 2. From Table 7.3 time factor for 50% average degree of consolidation is 0.196.

   Therefore, $$c_v = \frac{0.196H^2}{t_{50}} \tag{7.48}$$

   where $2H$ is the average thickness of the soil sample.

Square-root of time method

This method is proposed by Taylor (1942). The procedure is as follows:

1. Draw the dial gauge vs. $\sqrt{t}$ curve (Fig. 7.39).

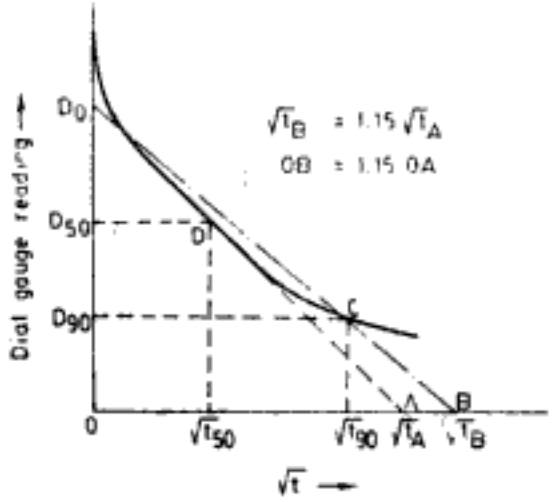

Fig. 7.39 Dial gauge reading *vs.* $\sqrt{t}$ curve for one-dimensional consolidation test

2. Extend the middle straight line portion of the curve to intersect the abcissa at A. The point where the straight line intersects the ordinate is taken as the corrected zero point with dial gauge reading D_0.
3. Mark off point B on abcissa such that $OB = 1.15\ OA$.
4. Draw a straight line joining corrected zero point D_0 and point B. This will intersect the curve at point C which is taken as the point defining 90% average degree of consolidation. From Table 7.3 for 90% consolidation $T = 0.848$. Therefore,

$$c_v = \frac{0.848H^2}{t_{90}} \tag{7.49}$$

Alternatively D_{100} can be determined as follows,

$$D_{100} = D_0 - 1.1(D_0 - D_{90}) \tag{7.50}$$

Knowing D_0 and D_{100}, D_{50} can be determined from Eq. 7.47. Point D on the curve corresponding to D_{50} can be obtained and t_{50} can be determined. Using Eq. 7.48, c_v can be computed.

Maximum slope method

This method is suggested by Su (1958) and is useful in situations where the end portion of the curve explained in logarithm of time method (Fig. 7.38) cannot be clearly distinguished. The procedure is as follows:

1. Draw the dial gauge reading vs. logarithm of time plot.
2. Determine D_0 as explained in logarithm of time method.
3. Draw a tangent AB to the steepest part of the curve as in Fig. 7.40.
4. Mark two convenient points X and Y on the tangent AB and determine its slope h, as,

$$h = \frac{D_X - D_Y}{\log(t_Y) - \log(t_X)} = \frac{D_X - D_Y}{\log(t_Y/t_X)} \tag{7.51}$$

5. The dial gauge reading D_U for any required average degree of consolidation $U_{av,T}$ is computed by the formula,

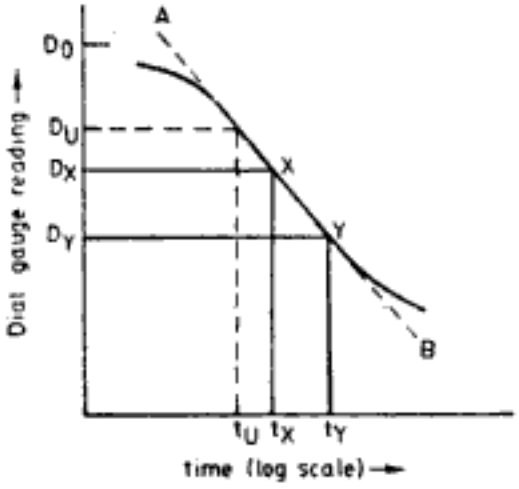

Fig. 7.40 Determination of coefficient of consolidation by maximum slope method

$$D_U = D_0 - \frac{h}{0.688} U_{av,T} \tag{7.52}$$

Choose a value of average degree of consolidation and compute D_U.

6. Time t_U corresponding to D_U can be determined from the curve. Time factor T, corresponding to chosen $U_{av,T}$ can be obtained from Table 7.3 or Fig. 7.18. c_v can then be determined from,

$$c_v = \frac{TH^2}{t_U} \tag{7.53}$$

Computational method

This method proposed by Sivaram and Swamee (1977) is as follows.

1. Note two dial readings, say D_1 and D_2 and their corresponding times, t_1 and t_2. These readings must be noted in the range of readings where average degree of consolidation is less than 53%.
2. Note another dial reading D_3 at time t_3 after considerable settlement has occurred.
3. Determine D_0 as,

$$D_0 = \frac{D_1 - D_2\sqrt{t_1/t_2}}{1 - \sqrt{t_1/t_2}} \tag{7.54}$$

4. Determine D_{100} as,

$$D_{100} = D_0 - \frac{D_0 - D_3}{[1 - \{(D_0 - D_3)(\sqrt{t_2} - \sqrt{t_1})/(d_1 - d_2)\sqrt{t_3}\}^{5.6}]^{0.179}} \tag{7.55}$$

5. Determine c_v as

$$c_v = \frac{\pi}{4}\left(\frac{D_1 - D_2}{D_0 - D_{100}} \frac{H}{\sqrt{t_2} - \sqrt{t_1}}\right)^2 \tag{7.56}$$

Considerable experience and judgement is required for a proper determination of c_v. All procedures described are empirical and hence may give different results for the same set of data. The differences can be quite large at times. While the determination of c_v is not exact, so also is the phenomenon which it explains, namely, rate of consolidation. The amount of total consolidation settlement predicted by theory is reasonably accurate. But the rate of consolidation predicted by theory is generally much slower than the rate at which it really occurs in the field. An important reason for this is the presence of thin seams of drainage material within the soil layers which will reduce drainage path and accelerate consolidation.

7.3 UNDER-, NORMALLY-, AND OVER-CONSOLIDATED SOILS

The e-log $\bar{\sigma}$ curve in Fig. 7.9 has a curved portion in the beginning and then a straight line portion. The curved portion has a flatter slope than the straight line portion. Conceptually this means that the soil undergoes little compression or void ratio change till a particular value of loading on the soil is reached. The reason for this is that in the field the soil sample exists at some effective stress level. When the sample is removed from the ground and taken to the laboratory this *in situ* effective stress level has been released. So, upon reloading in

the laboratory the sample undergoes very little deformation until its previous effective stress level is reached. This maximum effective stress which the soil has experienced in the past is known as *preconsolidation pressure*, $\bar{p}_c$. Once the applied stress exceeds $\bar{p}_c$ we can expect larger deformation to occur in soil. This is clearly illustrated in Fig. 7.10. In this figure, after reaching up to stress level corresponding to point B the sample is partially unloaded to stress level of C. On reloading the sample exhibits very little change in void ratio until stress level for point B is exceeded. (Note that the slope of recompression curve is very much smaller than C_c).

Different empirical procedures are available to determine the preconsolidation pressure of soil sample using e—log $\bar{\sigma}$ curve. A procedure suggested by Casagrande (1936) is explained in detail in Ch. 14.

In natural soils the preconsolidation pressure and the effective stress computed on the basis of weight of overburden material ($\bar{p}_o$) need not be the same. The two can be different. It means that the soil could have experienced an effective stress more than or less than the effective stress due to the weight of the overburden itself.

The situation when the preconsolidation pressure and the present effective overburden pressure are same, i.e., $\bar{p}_c = \bar{p}_o$ the soil is said to be *normally consolidated.*

Consider another situation when some considerable thickness of top soil in a normally consolidated soil is eroded away. This is in effect a removal of load. The soil exists now in a state where it has been subjected in the past to a higher effective stress than the present overburden effective stress. Such types of deposits which have experienced in the past higher than present effective overburden stress, i.e., $\bar{p}_c > \bar{p}_o$, are said to be *over-consolidated. Over-consolidation ratio, OCR,* is defined as,

$$OCR = \frac{\text{preconsolidation pressure}}{\text{present effective overburden stress}} = \frac{\bar{p}_c}{\bar{p}_o} \tag{7.57}$$

Consider yet another situation when upon a normally consolidated soil a fill has been built recently. Until the excess pore water pressure developed due to this is fully dissipated the soil will exist in a state where the effective stress will be less than the effective overburden pressure (overburden includes fill). Soil in which preconsolidation pressure is less than present effective overburden pressure, $\bar{p}_c < \bar{p}_o$, is known as *under-consolidated soil.*

To determine whether a soil deposit is under- or, normally-, or over-consolidated, the following procedure can be followed:

1. In the soil layer undisturbed samples are taken at different elevations. From consolidation experiments, the pre-consolidation pressure at these elevations ($\bar{p}_{cz}$) can be determined.
2. Based on information such as the density of soil, elevation of water-table, thickness of soil layers, etc., the effective overburden stress at the elevations of soil samples ($\bar{p}_{oz}$) can be calculated. This is explained in Fig. 7.41.
3. Profiles of preconsolidation pressure, and effective overburden stress with depth can be drawn as shown in Fig. 7.42. From a comparison of the two profiles the soil can be classified as under-, or normally-, or over-consolidated.

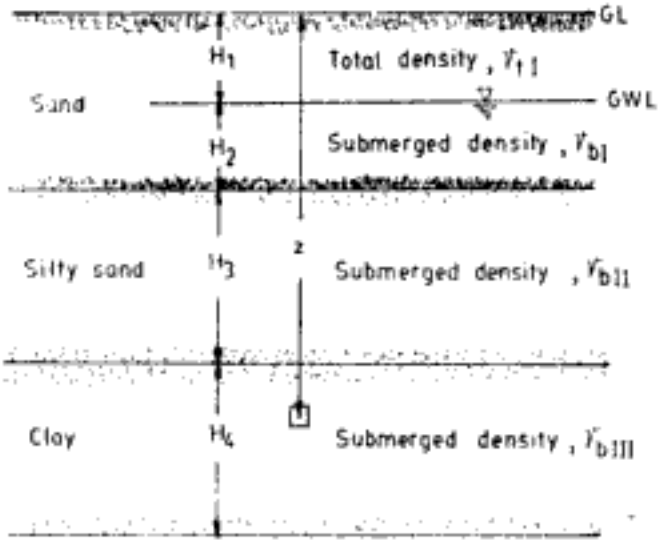

Fig. 7.41 Effective overburden pressure

$\bar{p}_{oz}$ = present effective overburden stress in clay at depth z from GL

$$= \gamma_{tI} H_1 + \gamma_{bI} H_2 + \gamma_{bII} H_3 + \gamma_{bIII} (z - H_1 - H_2 - H_3)$$

$\bar{p}_{cz}$ = preconsolidation pressure at depth z; i.e. maximum effective stress which the clay has experienced in the past

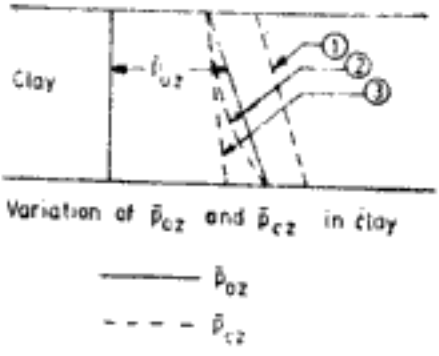

Fig. 7.42 Comparison of preconsolidation pressure and effective overburden pressure

$\bar{p}_{cz} = \bar{p}_{oz}$: normally consolidated soil

$\bar{p}_{cz} > \bar{p}_{oz}$: overconsolidated soil–curve 1 for $\bar{p}_{cz}$

$\bar{p}_{cz} > \bar{p}_{oz}$: underconsolidated soil

Curve 2 : drainage at top and bottom

Curve 3 : (a) drainage at top only, or (b) drainage at top and bottom with artesian conditions prevailing

8

DEVELOPMENT OF PORE WATER PRESSURE AND PORE WATER PRESSURE PARAMETERS

The pore water pressure under hydrostatic and hydrodynamic conditions can be computed on the basis of principles explained in Ch. 6. It is explained in Ch. 7 that when a load is imposed upon saturated soils the load is instantaneously borne by the pore water. In other words simultaneously with the application of load there is a concomittant increase in pore water pressure. If this excess pore water pressure is not allowed to dissipate or water is not allowed to drain out, the excess pore water pressure will continue to remain. This type of loading is known as *undrained loading*. In soil mechanics practice a soil element is subjected to different forms of loading. Most common among these are:

1. One-dimensional compression
2. Three-dimensional uniform loading or isotropic loading
3. Three-dimensional uniform loading followed by one dimensional loading

The pore water pressure developed in saturated soil is different for different types of loading. The excess pore water pressure developed is generally expressed as a function of the external stresses imposed on soil in terms of some parameters. These parameters are known as *pore water pressure parameters*. The sections to follow discuss the development of pore water pressure in saturated soils due to undrained loading for the three types of loading explained earlier.

8.1 ONE-DIMENSIONAL COMPRESSION

Figure 8.1 represents the nature of loading for this condition. This type of loading is same as the loading in Cases 1, 2, 3 and 4 discussed under one-dimensional consolidation in Ch. 7 (Fig. 7.14 to 7.16, 7.19 to 7.21).

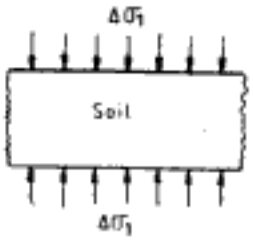

Fig. 8.1 One-dimensional compression loading

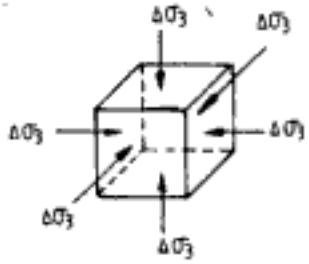

Fig. 8.2 Isotropic loading

The excess pore water pressure Δu developed because of external stress $\Delta\sigma_1$ is given by

$$\Delta u = \Delta\sigma_1 \tag{8.1}$$

That is, the pore water pressure increases by the same amount as the increase in the external stress. This is what has been considered in the one-dimensional consolidation cases also.

8.2 THREE-DIMENSIONAL UNIFORM LOADING OR ISOTROPIC LOADING

Figure 8.2 shows a soil element under isotropic loading conditions. The external stress increases by the same amount ($\Delta\sigma_3$) in all directions. Such a situation is obtained typically in a triaxial experiment where a cylindrical soil sample is subjected to confining pressure. The increase in pore water pressure is given as,

$$\Delta u = B\Delta\sigma_3 \tag{8.2}$$

where B = a pore water pressure parameter or coefficient. It is also referred to as B-factor. B is dependent on degree of saturation S, of the soil. Figure 8.3 shows the variation of B with S. For saturated soils $B = 1$. Thus,

$$\Delta u = \Delta\sigma_3, \qquad \text{when } S = 1 \tag{8.3}$$

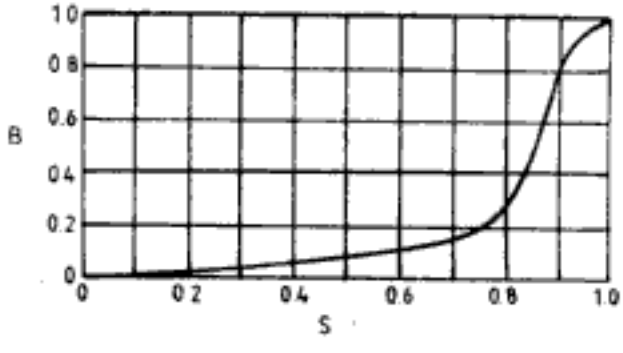

Fig. 8.3 Relationship between pore water pressure parameter B and degree of saturation S

8.3 THREE-DIMENSIONAL UNIFORM LOADING FOLLOWED BY ONE-DIMENSIONAL LOADING OR ISOTROPIC LOADING FOLLOWED BY DEVIATORIC LOADING

Figure 8.4 presents the details of loading for this case. The soil element is first subjected to an isotropic stress increase $\Delta\sigma_3$. Following this, the vertical axial stress is increased by $(\Delta\sigma_1 - \Delta\sigma_3)$. This is a typical loading of soil samples in triaxial testing where the confining pressure is first applied. The deviatoric stress is applied following this. The pore water pressure developed by such loading is given by,

$$\Delta u = B\{\Delta\sigma_3 + A\,(\Delta\sigma_1 - \Delta\sigma_3)\} \tag{8.4}$$

where A = a pore water pressure parameter or coefficient often called as A-factor.

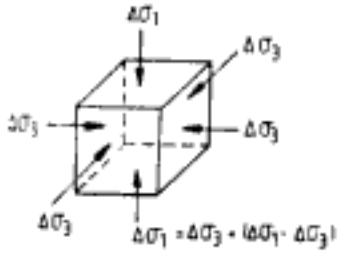

Fig. 8.4 Isotropic loading followed by deviatoric loading

Value of A depends on strain levels in soils and also on overconsolidation ratio. At high strain levels, namely at failure conditions of soils A-factor is designated as A_f. Tables 8.1 and 8.2 give typical values of A_f which are useful in the determination of shear strength parameters of soils. Figure 8.5 gives the variation of A_f with OCR. Table 8.3 gives the values of A-factor at low strain levels, such as that prevail in the determination of foundation settlements.

Table 8.1 Values of A at Failure Conditions (A_f)

Type of soil (S=1)	A_f
Highly sensitive clay	0.75 to 1.5
Normally consolidated clay	0.5 to 1.0
Compacted sandy clay	0.25 to 0.75
Lightly overconsolidated clay	0 to 0.5
Compacted clay gravel	−0.25 to 0.25
Heavily overconsolidated clay	−0.5 to 0

(After Skempton, 1954. By permission of The Institution of Civil Engineers, London)

Table 8.2 Values of A at Failure Conditions (A_f)

Type of soil ($S = 1$)	A_f
Very loose fine sand	2 to 3
Sensitive clay	1.5 to 2.5
Normally consolidated clay	0.7 to 1.3
Lightly overconsolidated clay	0.3 to 0.7
Heavily overconsolidated clay	−0.5 to 0

(After Bjerrum)

Table 8.3 Values of A at Low Strains (for Foundation Settlement)

Type of soil ($S = 1$)	A
Very sensitive soft clay	> 1
Normally consolidated clay	0.5 to 1
Overconsolidated clay	0.25 to 0.5
Heavily overconsolidated sandy clay	0 to 0.25

(After Skempton and Bjerrum, 1957. By permission of The Institution of Civil Engineers, London)

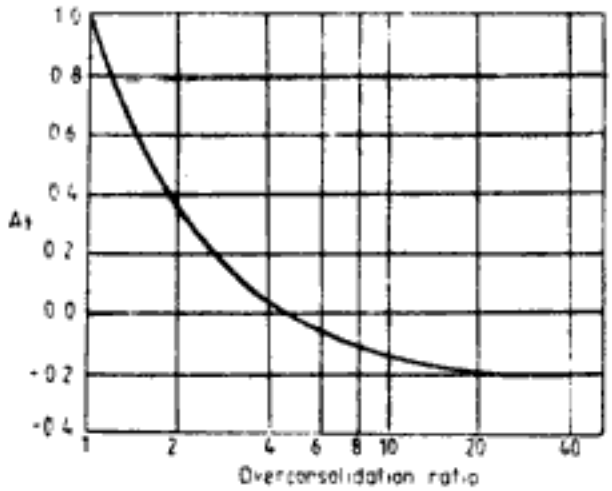

Fig. 8.5 Variation of A-factor at failure with overconsolidation ratio

Pore water pressure parameters A and B were first suggested by Skempton (1954). Hence, they are also known as Skempton's parameters. The discussions on pore water pressure development due to different types of loading are summarised in Table 8.4.

Q 8.1: A saturated, normally consolidated soil sample in a triaxial test is first subjected to a confining pressure of 2 kg/cm² and then tested under undrained conditions. At failure the vertical axial stress on the sample is 2.9 kg/cm². Determine the pore water pressure in the soil sample at failure.

Table 8.4

Type of loading		Increase in pore water pressure, Δu	Typical examples of loading
One dimensional compression	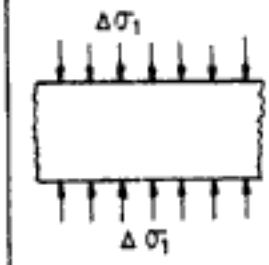	$\Delta u = \Delta\sigma_1$	Construction of areal fill ; Thickness of soil small compared to dimensions of foundation
Three dimensional uniform loading	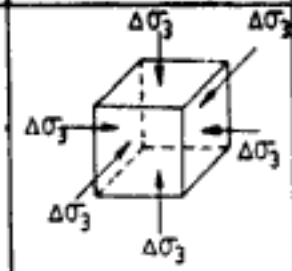	$\Delta u = B\,\Delta\sigma_3$	Soil sample in triaxial testing subjected to increase in confining pressure
Three dimensional uniform loading followed by one dimensional loading	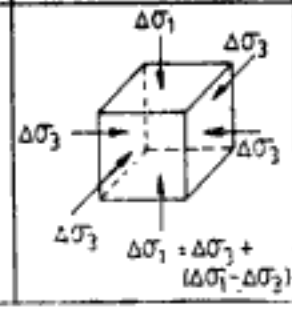	$\Delta u = B[\Delta\sigma_3 + A(\Delta\sigma_1 - \Delta\sigma_3)]$	Construction of embankments on deep soil deposits ; Thickness of soil large compared to dimension of foundations

'A' and 'B' are called pore water pressure parameters. B = 1 for saturated soil 'A' depends on strain levels and overconsolidation ratio. All loadings are undrained loading.

Ans: This test is an example of three-dimensional uniform loading followed by one-dimensional loading.

$$\Delta\sigma_3 = 2 \text{ kg/cm}^2$$
$$\Delta\sigma_1 = 2.9 \text{ kg/cm}^2$$
$$\Delta\sigma_1 - \Delta\sigma_3 = 2.9 - 2 = 0.9 \text{ kg/cm}^2$$

To determine Δu Eq. 8.4 must be used. For saturated soil $B = 1$. From Tables 8.1 and 8.2 and Fig. 8.5 value of A_f for normally consolidated soil (OCR = 1) can be taken as 0.9. Therefore, pore water pressure developed at failure is,

$$\Delta u = 1 \times \{2 + 0.9 \times 0.9\} = 2.81 \text{ kg/cm}^2$$

9

SHEAR STRENGTH OF SATURATED SOILS

To analyse a number of problems in soil engineering like the bearing capacity of foundations, stability of slopes, earth pressures on retaining walls, a good knowledge of shear strength and shear strength parameters of soil is required. Consider a soil element as shown in Fig. 9.1. The element is subjected to vertical and horizontal principal stresses σ_1 and σ_3 respectively. On any plane within the element there will act a normal stress and a shear stress, σ and τ respectively. At failure conditions of the soil element there will be one particular plane called *failure plane* along which the shear stress reaches its failure value. This failure value of shear stress, τ_f along failure plane is known as *shear strength* of soil. τ_f is a function of the normal stress on the failure plane and is given by the relationship,

$$\tau_f = c + \sigma \tan \phi \tag{9.1}$$

where c = cohesion intercept

ϕ = angle of shearing resistance

c and ϕ are called *shear strength parameters* of soil. Equation 9.1 represents the failure criterion in soils and is popularly known as *Mohr-Coulomb failure criterion*. Figure 9.2 gives a graphical representation of this criterion. The figure shows a failure envelope which means that for soil to be stable the combination of normal and shear stresses along any plane must lie below this envelope. If the combination lies above the envelope the mass is unstable. Figure 9.2 also shows a set of semi-circles, called Mohr's circles. These represent the different combinations of principal stresses σ_1 and σ_3 (plotted on the diameter) shown in Fig. 9.1 for which τ_f is reached along the failure plane. The failure envelope is tangential to these set of Mohr's circles.

Equation 9.1 is given in terms of total stress σ on the failure plane. The equation can be rewritten in the form of effective stress as follows,

$$\tau_f = \bar{c} + (\sigma - u) \tan \bar{\phi} = \bar{c} + \bar{\sigma} \tan \bar{\phi} \tag{9.2}$$

where $\bar{c}$ and $\bar{\phi}$ are called *effective stress parameters*, c and ϕ are known as *total stress parameters*. Figure 9.3 represents failure criterion expressed in Eq. 9.2. The failure envelope is

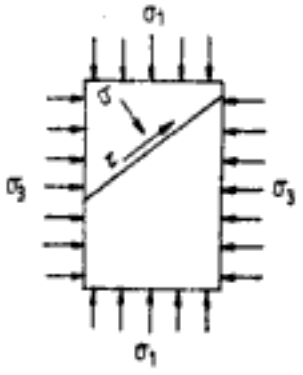

Fig. 9.1 Stresses on a soil element and along a plane

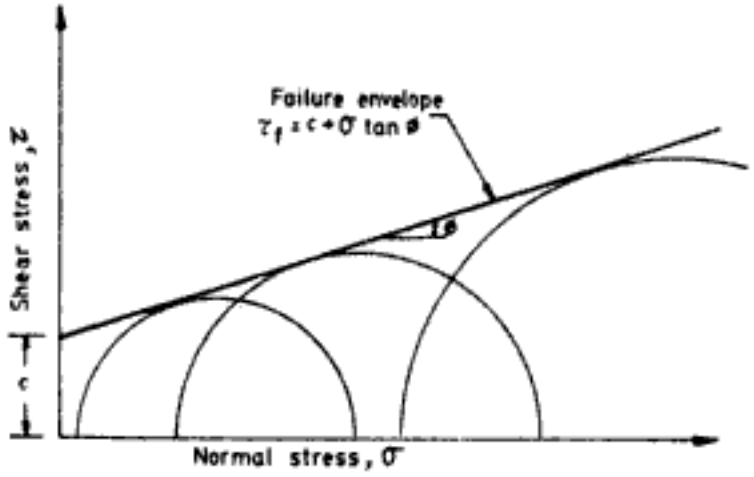

Fig. 9.2 Mohr-Coulomb failure criterion in soils in terms of total stress and the total stress parameters

tangential to Mohr's circles drawn in terms of principal effective stresses, i.e., $\bar{\sigma}_1 = \sigma_1 - u$ and $\bar{\sigma}_3 = \sigma_3 - u$, plotted along the diameter.

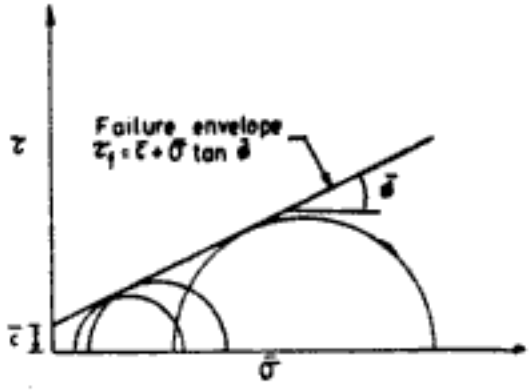

Fig. 9.3 Mohr-Coulomb failure criterion for soils in terms of effective stress and the effective stress parameters

Total stress and effective stress parameters are not constant quantities for a soil. Their numerical values depend on factors like drainage, stress history, etc.

Shear strength and shear strength parameters are determined by carrying out some tests on soils. In the laboratory the tests are carried out on soil samples. Most common laboratory tests are (i) triaxial shear test, and (ii) direct shear test. For soft and sensitive soils vane shear test is carried out in the field.

9.1 TRIAXIAL SHEAR TEST

Nowadays triaxial shear test is the most preferred form of shear test on soils. A variety of loading patterns can be simulated in triaxial shear test. A close control over pore water pressure and its measurement is also possible.

9.1.1 Triaxial Shear Test Set-up

A triaxial shear test set-up consists of four main parts. These are:

1. Triaxial cell
2. Load frame
3. Constant cell pressure system
4. Pore water pressure measuring system

There have been continuous technological developments in the design of each part of the system. A highly sophisticated system may incorporate microprocessors and electronic transducers. Only a brief description of the basic system which may be found in most of the laboratories and universities is presented here.

1. *Triaxial cell*

The triaxial cell is a chamber for housing the soil sample and it facilitates application of confining pressure and axial stress on the soil sample. Figure 9.4 shows a typical cell with a soil sample. The cell is in two parts, namely, (i) a perspex body and (ii) a metal base.

The perspex body contains the loading ram and air release valve.

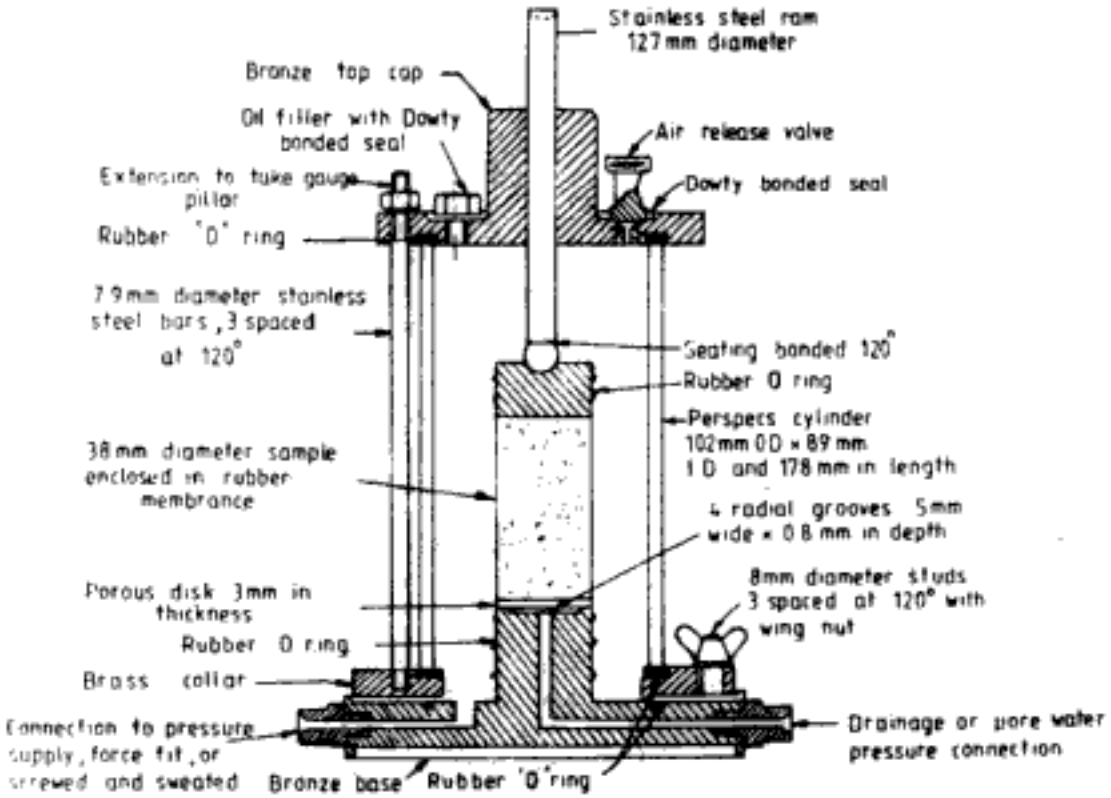

Fig. 9.4 Cross-section of a typical triaxial cell (After Bishop and Henkel, 1962. Reprinted by permission of Edward Arnold (Publishers) Ltd, London)

Figure 9.5 gives a schematic diagram of the details of the metal base. There is a pedestal on the base on which the soil sample is mounted. There are two openings in the pedestal. These openings facilitate,

(a) drainage of water from the sample—for example in the case of consolidation of soil sample;

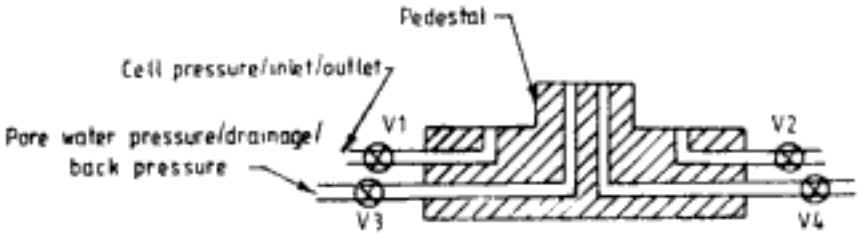

Fig. 9.5 Details of metallic base

(b) application of back pressure—as may be required to saturate the soil sample or to measure negative pore water pressure;
(c) the measurement of pore water pressure—when effective stress is required to be computed in undrained test.

These two openings in the pedestal are connected to valves V3 and V4 on the base. There are two more openings which are located on the base itself. These two openings facilitate,

(a) letting water inside the cell;
(b) draining water from the cell;
(c) application of cell/confining pressure on soil sample.

The openings on the base are connected to valves V_1 and V_2 in Fig. 9.5. Triaxial cells are available in different sizes. The most commonly used are the cells to test cylindrical samples of dimensions 38 mm diameter $\times$ 76 mm height. Cells are also specified in terms of maximum confining pressure which they can safely withstand.

2. *Load frame*

Load frame is a device to (i) support the triaxial cell, and (ii) to apply and measure deviatoric load on soil sample.

The load frame has a gear box assembly. By a judicious combination of gears the sample can be deformed at the desired constant rate of deformation. The triaxial tests are therefore known as *strain controlled tests*. The sample is strained against a reaction frame. The load required to deform the sample is read off from a calibrated proving ring attached to the load frame. The deformation of the soil sample is measured using a dial gauge attached to the proving ring.

3. *Constant cell pressure system*

Cell pressure is required to be applied on the soil sample in most of the experiments either to consolidate the soil sample or while shearing the soil sample. This pressure must be maintained constant during these stages. The pressure is usually applied through de-aired water filled around the soil sample in the cell. The soil sample is protected from contact with water by means of enclosing it in a rubber membrane.

There are many ways of developing cell pressure and maintaining it at the desired constant level. But perhaps the simplest and economical device is the self-compensating mercury pot system developed by Bishop. Figure 9.6 shows a line diagram of this system.

The system consists of a movable top pot usually of perspex. It is partly filled with mercury and is hung from a calibrated spring. The pot and spring together can be physically moved up or down. The mercury surface in top pot is open to atmosphere. A nylon tubing is

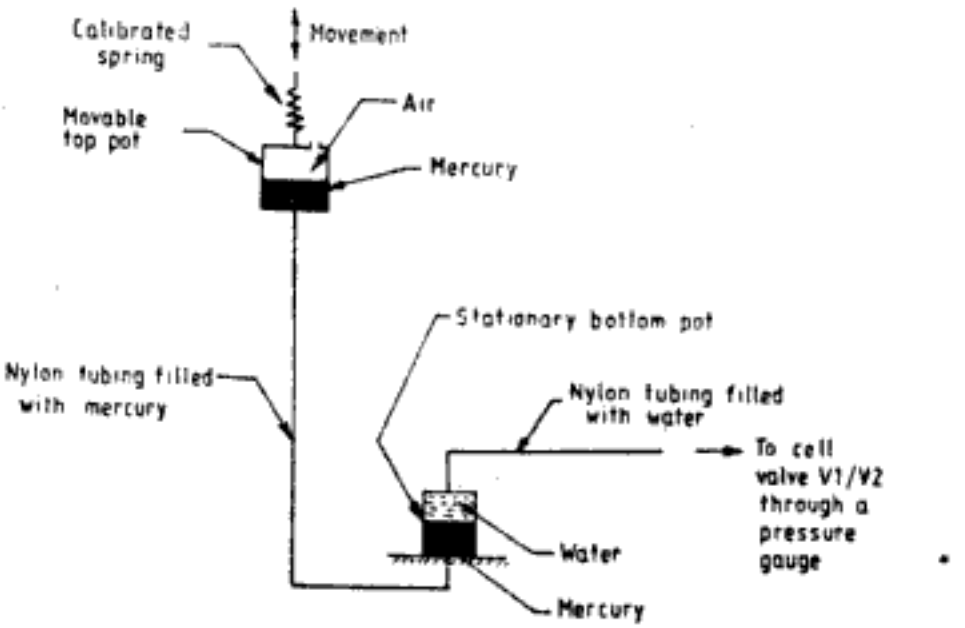

Fig. 9.6 Self compensating mercury pot constant pressure system

attached to the bottom of the movable top pot. The other end of the tubing is connected to the bottom of a stationary pot (also of perspex). This pot is partly filled with mercury and the rest with water. Mercury is present continuously in the nylon tubing connecting the top and bottom pots. To the top of the stationary bottom pot another nylon tubing is attached which is full of water and the other end of this tubing is connected to triaxial cell through a pressure gauge, using leak-proof connections.

The cell pressure is developed by the standing column of mercury in the nylon tubing and in the movable top pot. Therefore, in order to develop a desired cell pressure the movable pot has to be raised to the required level. The pressure is read off from the pressure gauge.

The system maintains the built-up pressure automatically. Consider there is some minor leakage in the triaxial cell. Same quantity of water will migrate from the nylon tubing into the cell. As a result, the level of mercury in the bottom pot will rise slightly and that at the top pot will come down slightly. This drop in level of mercury reduces the weight of the movable pot. The spring is so calibrated that because of the loss in weight it compresses and pulls the pot up by a distance so as to compensate for the loss in pressure. That is why the system is called a self-compensating system.

4. *Pore water pressure measuring system*

A common method of measuring pore water pressure in soil sample uses the null indicator system which was developed by Bishop. The null indicator system is schematically shown in Fig. 9.7.

To operate the null indicator system the mercury in null indicator is initially set up at a particular level. If additional pore water pressure is developed in the soil sample it is transmitted through water in the metal tubing to the top of mercury in null indicator. The excess pressure pushes the level of mercury down from its original level. This action is countered by operating the piston and the mercury level is pushed up to the same initial level thus maintaining undrained conditions in the soil sample. The pressure required to do this is equal to the pore water pressure in the soil sample and is registered in the pressure gauge.

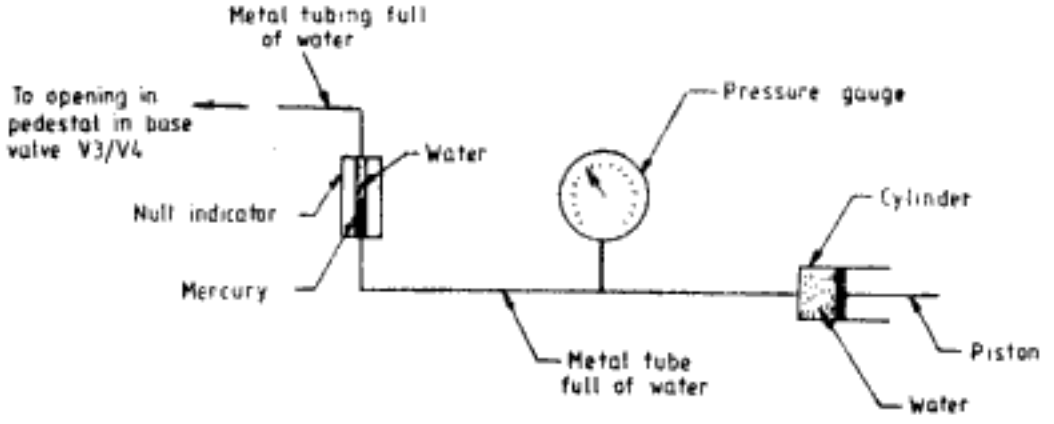

Fig. 9.7 Null indicator system

Figure 9.8 shows a line diagram of the linkages between the four parts of the triaxial shear test set-up.

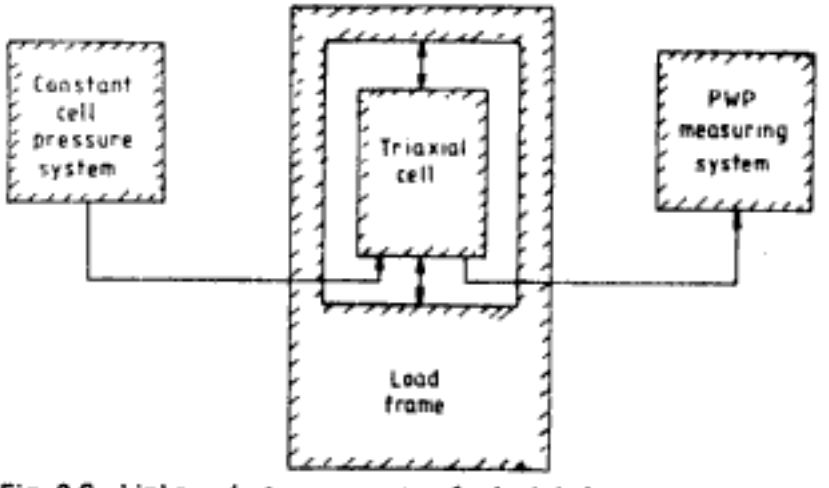

Fig. 9.8 Linkage between parts of triaxial shear test set-up

9.1.2 Types of Triaxial Compression Tests

A wide variety of tests are possible in triaxial shear testing. But for most engineering purposes the following tests are adequate.

1. Unconfined compression test (UC)
2. Unconsolidated undrained test (UU)
3. Consolidated undrained test (CU)
4. Consolidated drained test or drained test (CD or D)

Generally there are three different and successive stages in a triaxial shear test. These three stages are:

Stage I: Preparation of soil sample
Stage II: Application of cell pressure
Stage III: Application of additional axial stress at constant cell pressure

The dissipation of pore water pressure or drainage during Stage II and Stage III of testing depends upon the type of test. Table 9.1 gives the drainage conditions during these stages

for the four types of test. Often pore water pressure is measured in consolidated undrained test to evaluate effective stress parameters. Such a test is designated as $\overline{CU}$ test.

Table 9.1 Types of Triaxial Compression Tests and Drainage Conditions

Type of test	Drainage conditions during stages II and III of triaxial shear test	
	Stage II: Application of cell pressure only	Stage III: Application of additional axial stress at constant cell pressure
Unconfined compression test—UC	(No cell pressure)	Drainage not allowed
Unconsolidated undrained test—UU	Drainage not allowed (hence unconsolidated)	Drainage not allowed (hence undrained)
Consolidated undrained test—CU	Drainage allowed (hence consolidated)	Drainage not allowed (hence undrained)
Consolidated drained or drained test—CD or D	Drainage allowed (hence consolidated)	Drainage allowed (hence drained)

$\overline{CU}$ Test indicates consolidated undrained test with pore water pressure measurements during the third stage of the test.

9.2 CHANGES IN TOTAL STRESS, PORE WATER PRESSURE AND EFFECTIVE STRESS IN TRIAXIAL COMPRESSION TESTS

In the triaxial compression tests total stress, pore water pressure, and effective stress in soil samples change during the three stages of testing explained in Sec. 9.1.2. Tables 9.2, 9.3, and 9.4 give these changes for unconsolidated undrained test, consolidated undrained test, and consolidated drained test respectively. The changes in total stress are the physically induced stresses during triaxial testing. The changes in pore water pressure and effective stress develop as a consequence to total stress changes. The changes in pore water pressure can be obtained from principles explained in Ch. 8. The effective stress can then be computed by Eq. 6.5.

For all the experiments indicated in Tables 9.2, 9.3 and 9.4 the pore water pressure during sample preparation is given as a residual pressure, u_r. This is the pore water pressure due to capillary action of water in soil and is a negative pressure. Hence, the effective stress at this stage is a positive quantity. Upon application of cell pressure and deviatoric stress this residual pressure is neutralised and pore water pressure becomes positive.

9.3 SHEAR STRENGTH PARAMETERS FROM TRIAXIAL COMPRESSION TESTS

The triaxial test data can be used to plot the Mohr's circles and the failure envelope shown in Figs 9.2 and 9.3 from which the shear strength parameters can be determined.

9.3.1 Normally Consolidated Soils

1. *Unconfined compression test*

In unconfined compression test confining pressure σ_3 is zero. The axial stress at failure is σ_{1f} The Mohr's circle and failure envelope for UC test are shown in Fig. 9.9.

Table 9.2

Stages of testing	Total stress	Pore water pressure	Effective stress
STAGE I Preparation of soil sample	$\sigma_1 = 0$ $\sigma_3 = 0$	u $u = -u_r$	$\bar{\sigma}_1 = u_r$ $\bar{\sigma}_3 = u_r$
STAGE II Application of cell pressure, σ_c, without drainage	$\sigma_1 = \sigma_c$ $\sigma_3 = \sigma_c$	u $u = -u_r + B\,\sigma_c$	$\bar{\sigma}_1 = u_r + (1-B)\,\sigma_c$ $\bar{\sigma}_3 = u_r + (1-B)\,\sigma_c$
STAGE III Increase in axial stress $\Delta\sigma_a$, without drainage	$\sigma_1 = \sigma_c + \Delta\sigma_a$ $\sigma_3 = \sigma_c$	u $u = -u_r + B[\sigma_c + A\,\Delta\sigma_a]$	$\bar{\sigma}_1 = u_r + (1-B)\sigma_c + (1-BA)\,\Delta\sigma_a$ $\bar{\sigma}_3 = u_r + (1-B)\sigma_c - BA\,\Delta\sigma_a$

u_r = Residual pore water pressure in the soil sample

σ_1, σ_3 = Major and minor total principal stresses respectively

$\bar{\sigma}_1, \bar{\sigma}_3$ = Major and minor effective principal stresses respectively

A, B = Pore water pressure parameters

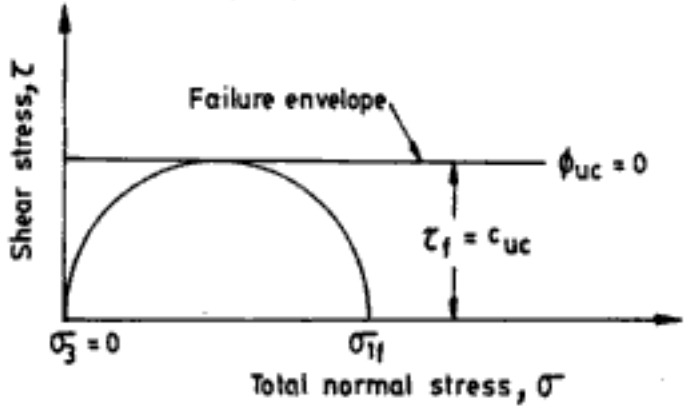

Fig. 9.9 Failure envelope for *UC* test

Table 9.3

Stages of testing	Total stress	Pore water pressure	Effective stress
STAGE I Preparation of soil sample	$\sigma_1 = 0$ $\sigma_3 = 0$	u $u = -u_r$	$\bar{\sigma}_1 = u_r$ $\bar{\sigma}_3 = u_r$
STAGE II Application of cell pressure, σ_c , with drainage	$\sigma_1 = \sigma_c$ $\sigma_3 = \sigma_c$	u $u = 0$	$\bar{\sigma}_1 = \sigma_c$ $\bar{\sigma}_3 = \sigma_c$
STAGE III Increase in axial stress, $\Delta\sigma_a$, without drainage	$\sigma_1 = \sigma_c + \Delta\sigma_a$ $\sigma_3 = \sigma_c$	u $u = BA\Delta\sigma_a$	$\bar{\sigma}_1 = \sigma_c + (1-BA)\Delta\sigma_a$ $\bar{\sigma}_3 = \sigma_c - BA\,\Delta\sigma_a$

u_r = Residual pore water pressure in the soil sample

σ_1, σ_3 = Major and minor total principal stresses respectively

$\bar{\sigma}_1$, $\bar{\sigma}_3$ = Major and minor effective principal stresses respectively

A = Pore water pressure parameter

The failure envelope is horizontal in this case. Hence, the angle of shearing resistance is zero, i.e.,

$$\phi_{UC} = 0 \tag{9.3}$$

The subscript UC for ϕ in Eq. 9.3 denotes that the sample has been tested in unconfined compression. Also the Mohr's circles are drawn with total stresses of σ_{1f} and σ_3. Hence the parameters obtained are also total stress parameters. The other shear strength parameter, cohesion intercept, in UC test is given by,

$$c_{UC} = \frac{\sigma_{1f}}{2} \tag{9.4}$$

Table 9.4

Stages of testing	Total stress	Pore water pressure	Effective stress
STAGE I Preparation of soil sample	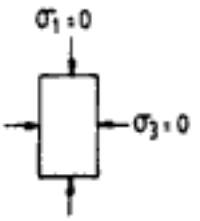	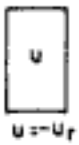	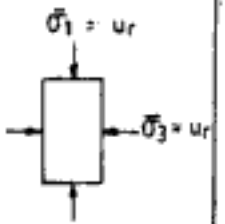
STAGE II Application of cell pressure, σ_c, with drainage	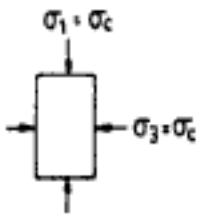		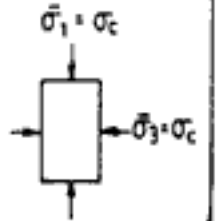
STAGE III Increase in axial stress, $\Delta\sigma_a$, with drainage	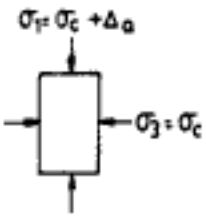		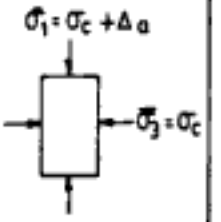

u_r = Residual pore water pressure in the soil sample

σ_1, σ_3 = Major and minor total principal stresses respectively

$\bar{\sigma}_1, \bar{\sigma}_3$ = Major and minor effective principal stresses respectively

Subscript UC in Eq. 9.4 stands for c being obtained from UC test. The shear strength of soil sample is then given by

$$\tau_f = c_{UC} \tag{9.5}$$

Unconfined compressive strength, q_u, is the axial stress σ_1 at failure.

$$q_u = \sigma_{1f} = 2c_{UC} \tag{9.6}$$

Terzaghi and Peck (1948) give a general relationship between the consistency of clays and unconfined compressive strength. This is given in Table 9.5.

Table 9.5 Relationship between Unconfined Compressive Strength (q_u) and Consistency of Clays

Soil consistency	Very soft	Soft	Medium	Stiff	Very stiff	Hard
q_u kg/cm²	0-0.25	0.25-0.5	0.5-1.0	1.0-2.0	2.0-4.0	> 4.0

2. *Unconsolidated undrained test*

In this test a minimum of three soil samples are subjected to different confining pressures σ_3 and then loaded to failure. The resulting Mohr's envelope will be as shown in Fig. 9.10. The figure is drawn with total stresses and hence, defines total stress parameters. The failure envelope is horizontal and shear strength is given by,

$$\tau_f = c_{UU} \tag{9.7}$$

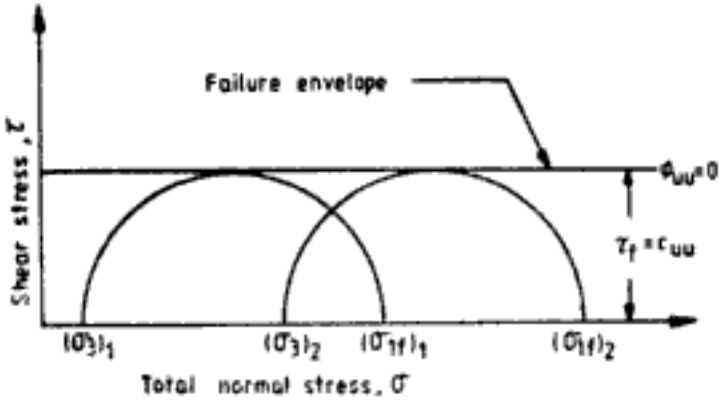

Fig. 9.10 Failure envelope for *UU* test

where c_{UU} = cohesion intercept in unconsolidated undrained test. Angle of shearing resistance ϕ_{UU} is zero. Theoretically,

$$c_{UC} = c_{UU} = c_u \tag{9.8}$$

where c_u is referred to as *undrained cohesion*. But generally some differences could be observed between the values of c_{UC} and c_{UU}. Similarly,

$$\phi_{UC} = \phi_{UU} = \phi_u = 0 \tag{9.9}$$

3. *Consolidated undrained test*

In this test soil sample is initially consolidated under confining pressure. This pressure is known as initial *effective confining pressure* ($\bar{\sigma}_c$). After consolidation, the confining pressure and pore water pressure may be increased by the same amount thus keeping the effective stress still constant at $\bar{\sigma}_c$. This operation is called application of *back pressure*, u_B. Back pressure is applied in order to saturate the soil sample and to facilitate measurement of negative pore water pressure during application of deviatoric stress in the case of overconsolidated clays. The soil sample is sheared under this elevated cell pressure σ_3 and it fails at a vertical axial stress of σ_{1f}. Mohr's circles for determination of total stress parameters are drawn with $(\sigma_{1f} - u_B)$, and $\{(\sigma_3 - u_B) = \bar{\sigma}_c\}$ as major and minor total principal stresses at failure, respectively. The resulting failure envelope in shown is Fig. 9.11. Shear strength of soil can be expressed as,

$$\tau_f = c_{CU} + \sigma \tan \phi_{CU} \tag{9.10}$$

where c_{CU} and ϕ_{CU} are total stress parameters from consolidated undrained test.

Consolidated undrained test can be carried out with measurement of pore water pressure while shearing the soil sample. Knowing the pore water pressure it is possible to determine the effective stresses in soil at any stage. For determination of effective stress parameters

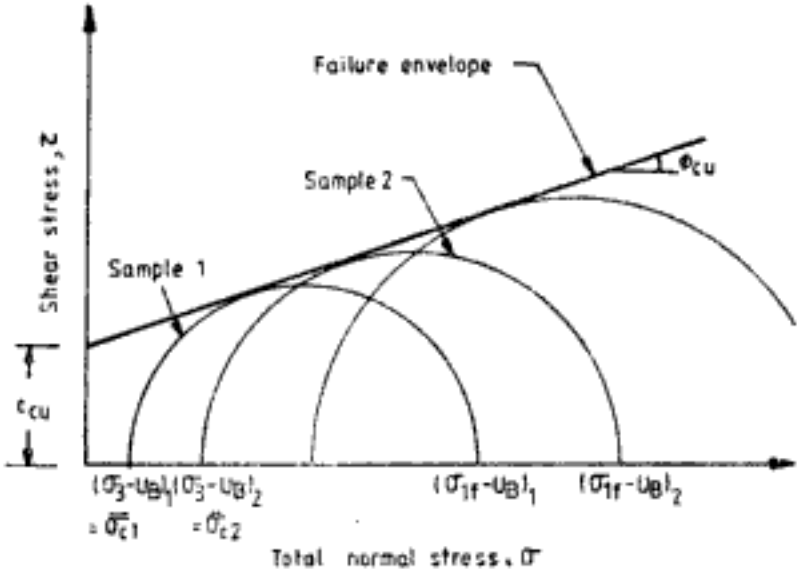

Fig. 9.11 Total stress failure envelope for $\overline{CU}$ test

Mohr's circles can be drawn with $(\sigma_{1f} - u_f)$ and $(\sigma_3 - u_f)$ as major and minor effective principal stresses at failure respectively. u_f is the pore water pressure at failure. The failure envelope with effective stresses is shown in Fig. 9.12. The shear strength is given by,

$$\tau_f = \bar{c}_{CU} + \bar{\sigma} \tan \bar{\phi}_{CU} \tag{9.11}$$

where $\bar{c}_{CU}$ and $\bar{\phi}_{CU}$ are effective stress parameters from consolidated undrained test. For normally consolidated soils $\bar{c}_{CU}$ is zero or almost negligible.

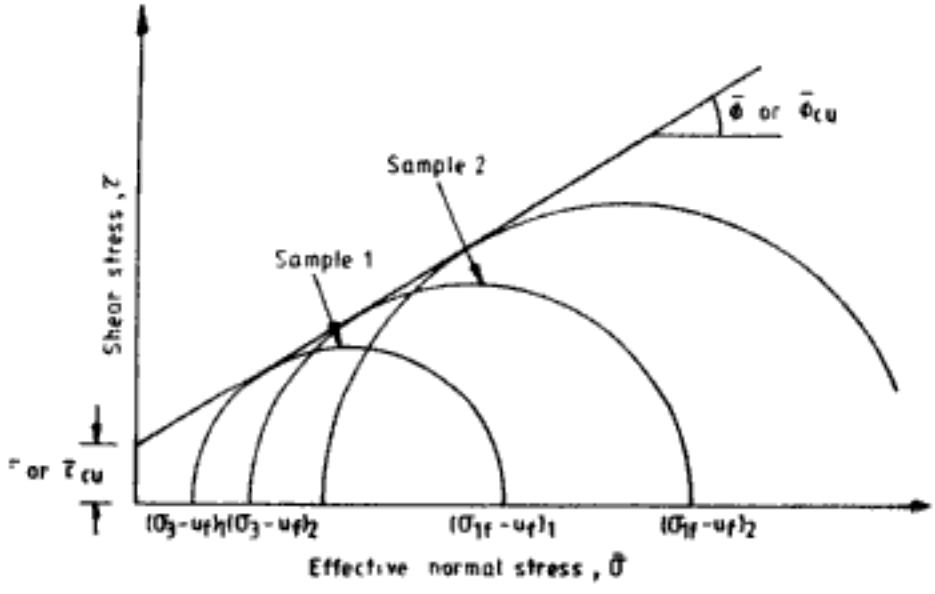

Fig. 9.12 Effective stress failure envelope for *CD* test

4. *Consolidated drained test or drained test*

In consolidated drained test the sample is first consolidated under confining pressure. Then the sample is sheared under the same confining pressure. Thus is this test $\sigma_3 = \bar{\sigma}_c$. Drainage

is permitted during shearing of sample. Hence, the pore water pressure at all stages of test is zero and always effective stress prevails. Mohr's circles in terms of effective major and minor principal stresses at failure $\bar{\sigma}_{1f}$ and $\bar{\sigma}_{3f} = \bar{\sigma}_c$, respectively, can be drawn to get effective stress parameters. The failure envelope for the test is shown in Fig. 9.13. Shear strength is expressed as,

$$\tau_f = \bar{c}_{CD} + \bar{\sigma} \tan \bar{\phi}_{CD} = \bar{c}_D + \bar{\sigma} \tan \bar{\phi}_D \tag{9.12}$$

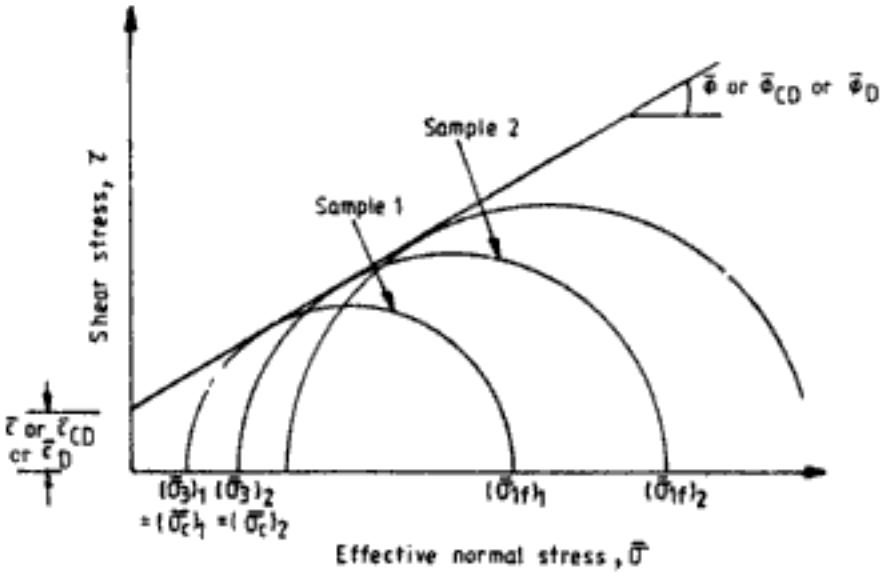

Fig. 9.13 Effective stress failure envelope for CD test

where, $\bar{c}_{CD}(=\bar{c}_D)$ and $\bar{\phi}_{CD}(=\bar{\phi}_D)$ are effective stress parameters from consolidated drained (or drained) test. For normally consolidated soils $\bar{c}_{CD}$ (or $\bar{c}_D$) is zero or insignificant. Theoretically, for normally consolidated soils,

$$\bar{c}_{CU} = \bar{c}_{CD} \text{ (or } \bar{c}_D) \tag{9.13}$$

and is commonly designated as $\bar{c}$. Also,

$$\bar{\phi}_{CU} = \bar{\phi}_{CD} \text{ (or } \bar{\phi}_D) \tag{9.14}$$

and is commonly represented as $\bar{\phi}$. This means that effective stress parameters $\bar{c}$ and $\bar{\phi}$ are uniquely defined for normally consolidated soils and do not depend upon the manner of testing. Whereas total stress parameters c (like c_{UC}, c_{UU}, c_{CU}) and ϕ (like ϕ_{UC}, ϕ_{UU}, ϕ_{CU}) depend upon the manner of testing and are not uniquely defined for normally consolidated soils.

In laboratory testing, however, there may be slight differences in effective stress parameters determined from consolidated undrained test and drained test. Value of $\bar{c}$ for normally consolidated soils is zero or insignificant.

9.3.2 Overconsolidated Soils

The effective stress failure envelope for overconsolidated soil is curved as shown in Fig. 9.14. At low effective stress levels the envelope is curved. At high effective stress the envelopes for normally and overconsolidated soils tend to merge. The effective stress parameters $\bar{c}$ and $\bar{\phi}$

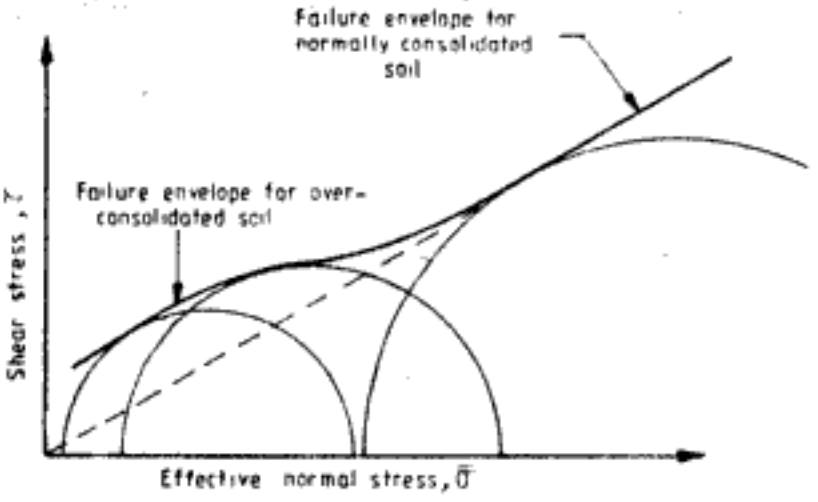

Fig. 9.14 Failure envelope for overconsolidated soil

are to be determined by making linear approximation for curved failure envelope of overconsolidated soil. τ_f, $\bar{c}$ and $\bar{\phi}$ are also to be defined over stress ranges. Figure 9.15 shows the linear approximation for the curved failure envelope. The expressions for shear strength from this approximation are as follows:

$$\tau_f = \bar{c}_1 + \bar{\sigma} \tan \bar{\phi}_1 \quad \text{for effective stress ranges between } \bar{\sigma}_A \text{ and } \bar{\sigma}_B \tag{9.15}$$

$$\tau_f = \bar{c}_2 + \bar{\sigma} \tan \bar{\phi}_2 \quad \text{for effective stress ranges between } \bar{\sigma}_C \text{ and } \bar{\sigma}_D \tag{9.16}$$

$$\tau_f = \bar{\sigma} \tan \bar{\phi} \quad \text{for effective stress ranges above } \bar{\sigma}_E\text{—the normally consolidated range} \tag{9.17}$$

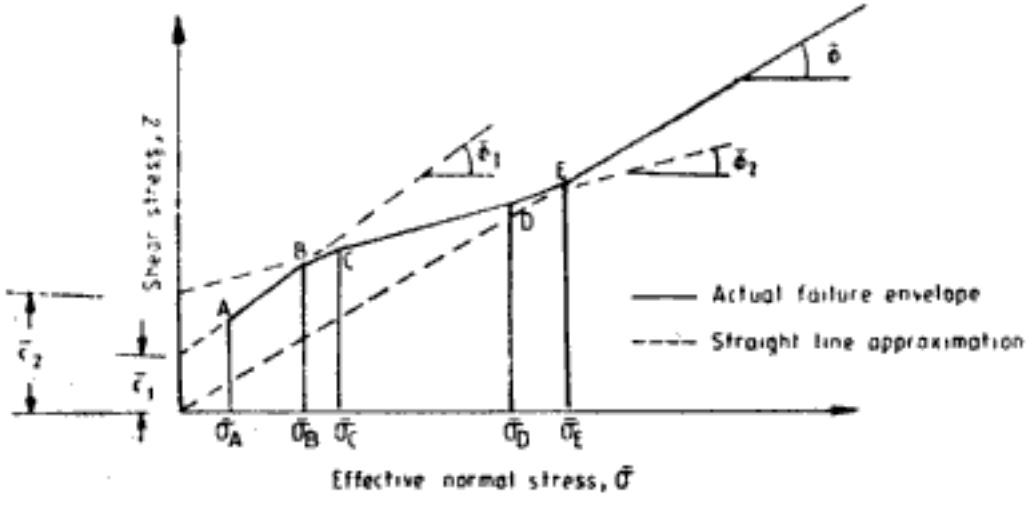

Fig. 9.15 Linear approximation for failure envelope of overconsolidated soil

$\bar{c}_1$ and $\bar{\phi}_1$ are effective stress parameters in stress range from $\bar{\sigma}_A$ to $\bar{\sigma}_B$. $\bar{c}_2$ and $\bar{\phi}_2$ are effective stress parameters in stress range from $\bar{\sigma}_C$ to $\bar{\sigma}_D$. Above $\bar{\sigma}_E$, $\bar{\phi}$ is the effective stress parameter. Following are some of the points to note about $\bar{c}$ and $\bar{\phi}$ for overconsolidated soils.

1. **The magnitude of $\bar{c}$ and $\bar{\phi}$ for an overconsolidated clay depends on the amount and duration of the preconsolidation pressure (or the OCR).**

2. The $\bar{c}$ and $\bar{\phi}$ values also depend on the effective stress range over which a straight line fit is made to the curved envelope.
3. When effective stress is very small compared to preconsolidation pressure (stress range $\bar{\sigma}_A$ to $\bar{\sigma}_B$ in Fig. 9.15)—i.e., when OCR is high—$\bar{c}$ will be relatively small and $\bar{\phi}$ will depend on the magnitude of preconsolidation pressure (void ratio).
4. When effective stress is a large fraction of preconsolidation pressure (stress range $\bar{\sigma}_C$ to $\bar{\sigma}_D$ in Fig. 9.15)—i.e., when OCR is low—$\bar{\phi}$ will be slightly less than the value for normally consolidated clay, while $\bar{c}$ will depend on the magnitude of preconsolidation pressure (void ratio).
5. Generally, the $\bar{\phi}$ for overconsolidated clay is about equal to that for normally consolidated clay.
6. $\bar{c}$ values are often assumed to vary from 0.05 kg/cm^2 to 0.25 kg/cm^2 in preliminary design.

9.4 PEAK AND RESIDUAL OR ULTIMATE SHEAR STRENGTH

9.4.1 Fine Grained Soils

Assume that failure is induced along the failure plane by keeping the effective normal stress on the failure plane at a constant value. Figure 9.16 shows the variation of shear stress mobilised with shear displacement along the plane, for overconsolidated and normally consolidated soils of the same soil type. The curves exhibit peak values of shear stress known as *peak shear strength*. After reaching the peak value both the curves show a decrease in shear stress

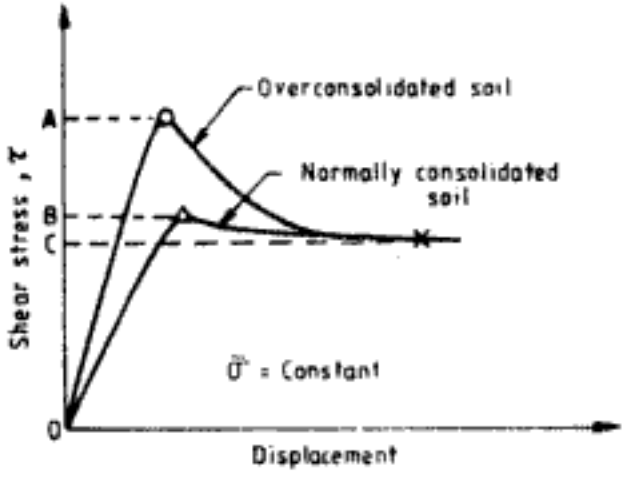

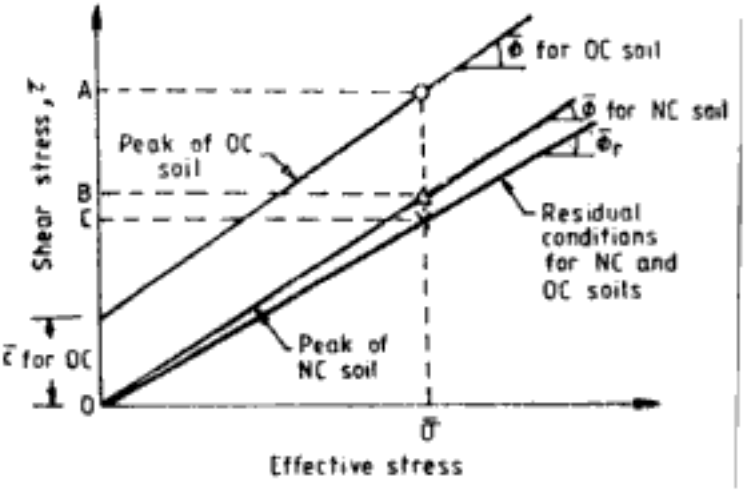

OA - Peak shear strength of OC soil

OB - Peak shear strength of NC soil

OC - Residual or ultimate shear strength

Fig. 9.16 Peak and residual (ultimate) shear strength for normally consolidated and overconsolidated soils

Fig. 9.17 Failure envelopes for peak and residual conditions for normally consolidated and overconsolidated soils

and reach the same constant ultimate shear stress. This is known as *residual or ultimate shear strength*. Failure envelope can be drawn with respect to both peak strength and ultimate strength. Figure 9.17 shows these envelopes. $\bar{c}$ and $\bar{\phi}$ are effective stress parameters corresponding to peak shear strength of soil. Residual effective angle of shearing resistance, $\bar{\phi}_r$ is the parameter corresponding to residual shear strength of soil. Residual strength of a soil is independent of the past stress history and is given by the equation,

$$\tau_{f\text{-residual}} = \bar{\sigma} \tan \bar{\phi}_r \tag{9.18}$$

Following are some more features of peak and residual shear strength of fine grained soils:

1. The difference in the peak and residual shear strength is pronounced as the degree of overconsolidation increases. However, it is also noticeable in normally consolidated clays.
2. The residual shear strength of remoulded and undisturbed soil samples are nearly the same.
3. The failure envelope for residual strength is generally a straight line through origin and slightly less steep than the failure envelope for the peak strength of normally consolidated clay.
4. The value of residual angle of shearing resistance, $\bar{\phi}_r$, depends on the amount of clay content. For clay contents approaching 100% the $\bar{\phi}_r$ values are nearly the same as ϕ_μ (ϕ_μ is the mineral-to-mineral friction angle) for sheet minerals. For very low clay contents $\bar{\phi}_r$ is the same magnitude as ϕ_μ between quartz particles.

Table 9.6 gives typical values of $\bar{\phi}$ for some fine grained soils. It also gives some other characteristics of the soils.

Table 9.6 Typical Values of $\bar{\phi}$ for Fine-grained Soils

Type of soil	Liquid limit	Plasticity index	% clay size	Activity	$\bar{\phi}$ (degrees)
Sodium bentonite	570	530	87	6.1	12
Sodium illite	85	50	—	—	19.6
Kaolinite	63	25	78	0.32	21.5
Remoulded Boston clay	48	23	54	0.43	31
Remoulded London clay	74	49	50	0.98	20.5
Bombay marine clay	115	70	48	1.46	24
Calcutta clay	80	40	—	—	26
Farakka clay	79	48	34	1.41	26

It is found that $\bar{\phi}$ decreases with increasing plasticity index of soil. This trend is evident from Table 9.6. Kenney (1959) gives the variation of $\bar{\phi}$ with plasticity index for normally consolidated soils. This is shown in Fig. 9.18. It is difficult to determine $\bar{\phi}$ for extremely plastic clay such as montmorillonite, because of the long time required for dissipation of pore water pressure in triaxial shear test. In such soils the magnitude of $\bar{\phi}$ is uncertain.

Figure 9.19 indicates the variation of $\bar{\phi}_r$ with clay content. For highly plastic sodium mont morillonites value of $\bar{\phi}_r$ can be as small as 3° to 4°. Figure 9.20 gives the correlation for $\bar{\phi}$, and $\bar{\phi}_r$ with I_p for normally consolidated clays according to Bowles (1982).

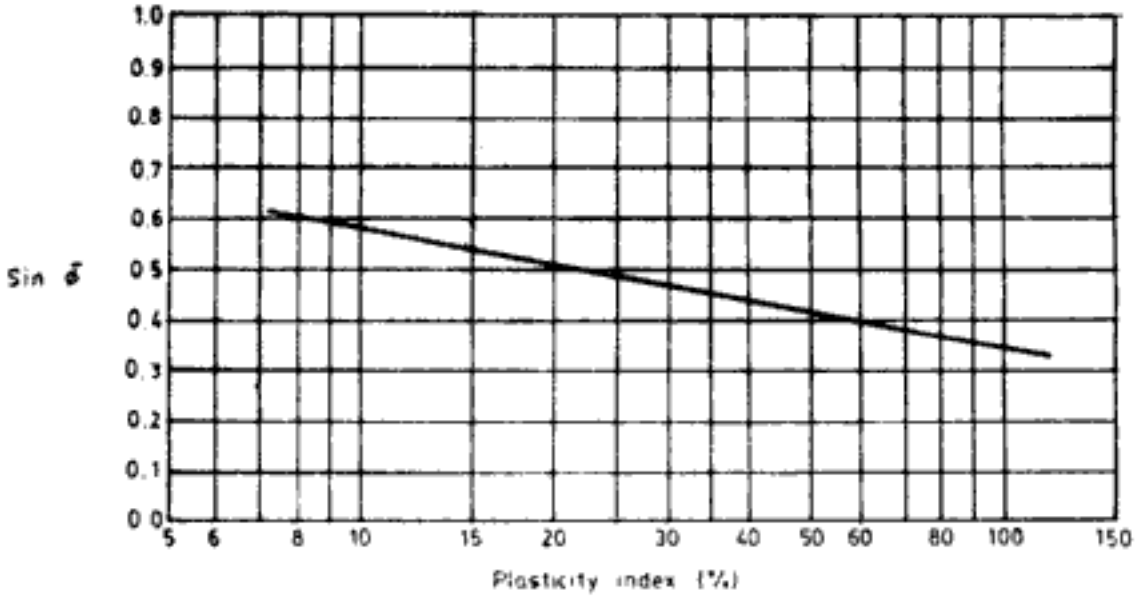

Fig. 9.18 Relationship between sin $\bar{\phi}$ and plasticity index for normally consolidated soils (After Kenney, 1959. By permission of American Society of Civil Engineers, New York)

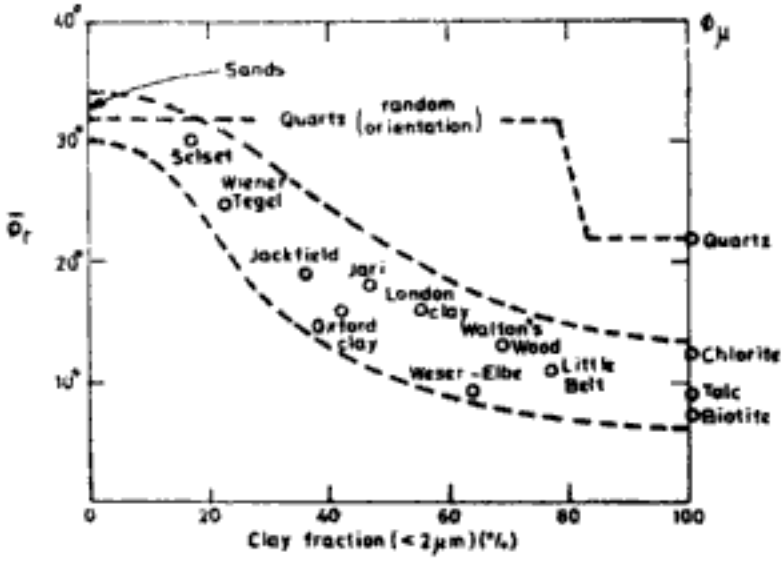

Fig. 9.19 Relationship between $\bar{\phi}_r$ and clay content (After Skempton, 1964. Reprinted by permission of the Institution of Civil Engineers, London)

9.4.2 Coarse Grained Soils

The shear stress–shear displacement behaviour in case of coarse grained soils is represented in Fig. 9.21. Sand in dense or medium dense conditions reaches a peak shear strength which with further shear displacement decreases to reach same constant ultimate shear strength. The sand in loose condition also tends to reach the same ultimate shear strength. This ultimate shear strength is frequently referred to as residual shear strength or *shear strength at*

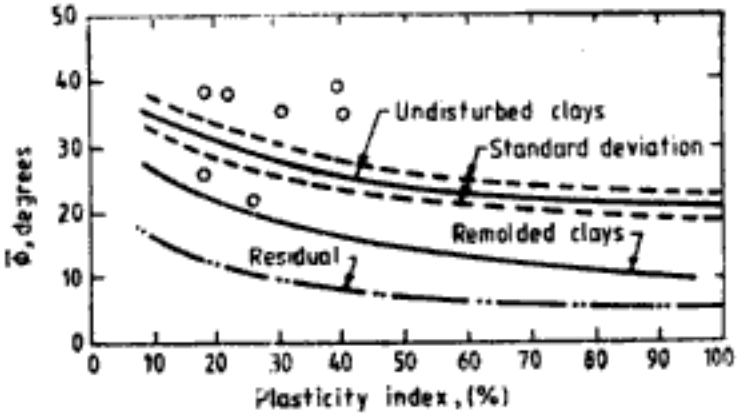

Fig. 9.20 Correlation between $\bar{\phi}$ and plasticity index (After Bowles, 1982. Reprinted by permission of McGraw-Hill Book Company, New York)

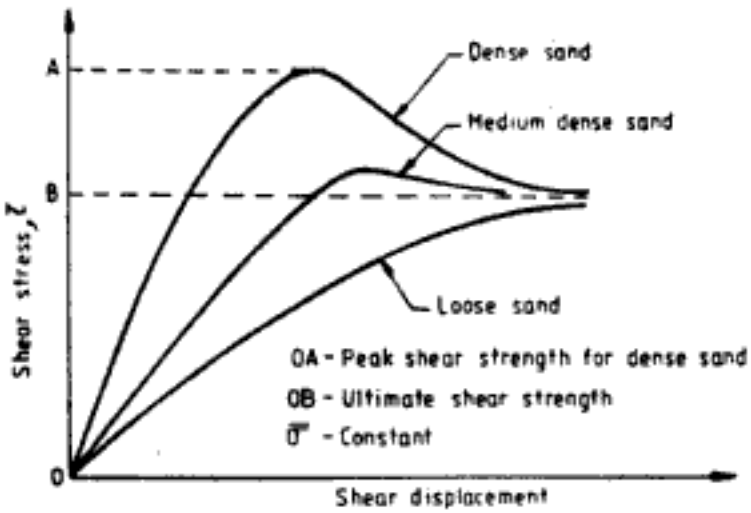

Fig. 9.21 Shear stress—displacement relationships for sand

constant volume. Figure 9.22 shows the failure envelopes for peak shear strength and residual shear strength. Peak shear strength is given by equation,

$$\tau_{f\text{-peak}} = \bar{\sigma} \tan \bar{\phi} \tag{9.19}$$

Residual shear strength is given by,

$$\tau_{f\text{-residual}} = \bar{\sigma} \tan \bar{\phi}_r \tag{9.20}$$

$\bar{\phi}$ and $\bar{\phi}_r$ are effective stress parameters for peak shear strength and residual shear strength, respectively.

Lambe and Whitman (1969) provide guidelines for selection of $\bar{\phi}$ and $\bar{\phi}_r$ for use in engineering problems. These are given in Table 9.7.

Typical values of angle of shearing resistance for coarse grained soils according to Hough (1957) are given in Table 9.8. Table 9.9 gives the effect of angularity and grading on the peak angle of shearing resistance of coarse grained soils.

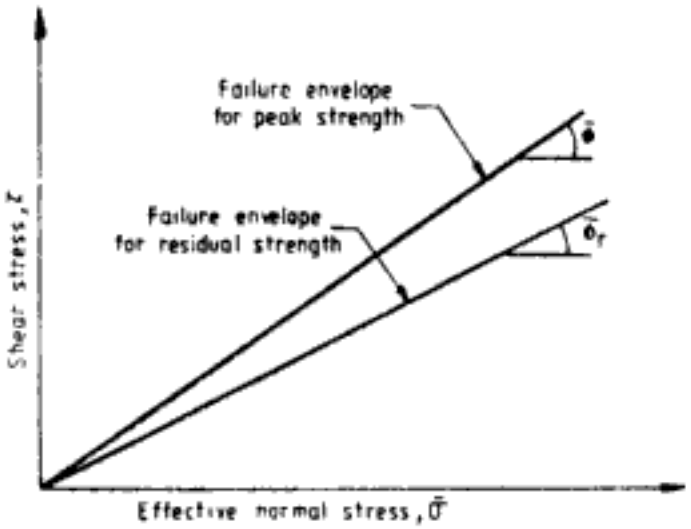

Fig. 9.22 Failure envelopes for coarse grained soils

Table 9.7 Criteria for Selection of Angle of Shearing Resistance in Sand for Use in Various Engineering Problems

Problem	Angle of shearing resistance	Angle of shearing resistance depends on
Internal strength of sand at small strains	$\bar{\phi}$	composition of soil; initial void ratio and confining stress
Internal strength of sand at very large strains	$\bar{\phi}_r$	composition of soil and void ratio at ultimate conditions
Sliding of sand on smooth surface (e.g., against smooth retaining wall)	ϕ_μ—the particle-to-particle friction angle	nature of soil mineral and surface
Sliding of sand on rough surface (e.g., against rough retaining wall)	$\bar{\phi}_r$	composition of soil; void ratio at ultimate conditions

For quartz sand the friction angle ϕ_μ is generally in the range of 26° to 30°.
(After Lambe and Whitman, 1969. Reprinted by permission of John Wiley & Sons, Inc., New York)

Q 9.1: A UU test is carried out on a saturated normally consolidated clay sample at a confining pressure of 3 kg/cm². The deviatoric stress at failure is 1 kg/cm². (a) Determine the shear strength of soil and its shear strength parameters. (b) If the sample is tested at a confining pressure of 4 kg/cm² what will be the vertical axial stress (σ_1) at failure?

Ans: (a) $(\sigma_1 - \sigma_3)$ is the deviatoric stress. At failure $\sigma_1 - \sigma_3 = 1$ kg/cm². This is the diameter of the Mohr's circle (Fig. 9.10).

$$\tau_f = \frac{\sigma_1 - \sigma_3}{2} = 0.5 \text{ kg/cm}^2$$

$$c_u = \tau_f = 0.5 \text{ kg/cm}^2 \quad \text{(Eqs 9.7 and 9.8)}$$

$$\phi_u = 0° \quad \text{(Eq. 9.9, Fig. 9.10)}$$

(b) In UU test at all confining pressures $(\sigma_1 - \sigma_3)$ is same (Fig. 9.10).

$$\sigma_3 = 4 \text{ kg/cm}^2$$

Table 9.8 Values of $\bar{\phi}$ and $\bar{\phi}_r$ for Cohesionless Soils

Soil type	Slope/angle of repose		$\bar{\phi}_r$ (degrees)	$\bar{\phi}$ (degrees)	
	i (degrees)	Slope (vertical to horizontal)		Medium dense	Dense
Silt (non-plastic)	26 to 30	1 on 2 to 1 on 1.75	26 to 30	28 to 32	30 to 34
Uniform fine to medium sand	26 to 30	1 on 2 to 1 on 1.75	26 to 30	30 to 34	32 to 36
Well graded sand	30 to 34	1 on 1.75 to 1 on 1.50	30 to 34	34 to 40	38 to 46
Sand and gravel	32 to 36	1 on 1.60 to 1 on 1.40	32 to 36	36 to 42	40 to 48

Note: 1. Within each range assign lower values if particles are well rounded or if there is significant soft shale or mica content, higher values for hard, angular particles. Use lower values for high normal pressures than for moderate normal pressure.
2. The maximum slope at which a loosely dumped material is stable is known as *angle of repose*.
(After Hough, 1975. Reprinted by permission of John Wiley & Sons, Inc., New York)

Table 9.9 Effect of Angularity and Grading on $\bar{\phi}$ of Cohesionless Soils

Shape and grading	$\bar{\phi}$ (degrees)	
	Loose	Dense
Rounded, uniform	30	37
Rounded, well graded	34	40
Angular, uniform	35	43
Angular, well graded	39	45

$$\sigma_1 - \sigma_3 = 1 \text{ kg/cm}^2$$

$$\therefore \quad \sigma_1 = 4 + 1 = 5 \text{ kg/cm}^2$$

Q 9.2: Data on $\overline{CU}$ test carried out on two saturated soil samples are given below. Determine the total and effective stress shear strength parameters.

	Sample 1	*Sample 2*
Consolidation pressure ($\bar{\sigma}_c$)	2.75 kg/cm²	4.25 kg/cm²
Back pressure (u_B)	2 kg/cm²	2 kg/cm²
Confining pressure (σ_3)	4.75 kg/cm²	6.25 kg/cm²
Axial stress at failure (σ_{1f})	6.75 kg/cm²	9.25 kg/cm²
Pore water pressure at failure (u_f)	3.75 kg/cm²	4.75 kg/cm²

Ans: *Total stress parameters*

For sample 1:

$$\text{Minor principal stress at failure} = \sigma_3 - u_B = \bar{\sigma}_c = 2.75 \text{ kg/cm}^2$$

$$\text{Major principal stress at failure} = \sigma_{1f} - u_B = 6.75 - 2 = 4.75 \text{ kg/cm}^2$$

For sample 2:

Minor principal stress at failure = 4.25 kg/cm²

Major principal stress at failure = 9.25 − 2 = 7.25 kg/cm²

Figure 9.23 shows the Mohr's circles for samples 1 and 2 and the failure envelope, from which,

$$c_{CU} = 0.06 \text{ kg/cm}^2$$

$$\phi_{CU} = \phi = 14.4°$$

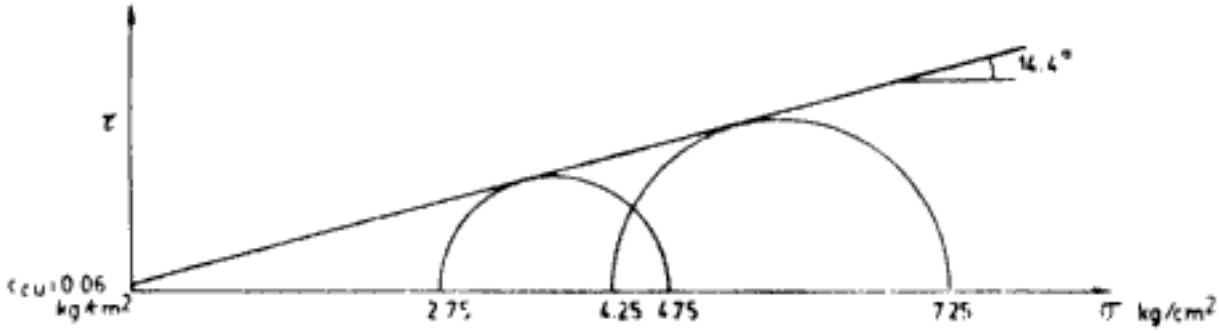

Fig. 9.23 Q 9.2

Effective stress parameters

For sample 1:

$$\bar{\sigma}_3 = \sigma_3 - u_f = 4.75 - 3.75 = 1 \text{ kg/cm}^2$$

$$\bar{\sigma}_1 = \sigma_{1f} - u_f = 6.75 - 3.75 = 3 \text{ kg/cm}^2$$

For sample 2:

$$\bar{\sigma}_3 = 6.25 - 4.75 = 1.5 \text{ kg/cm}^2$$

$$\bar{\sigma}_1 = 9.25 - 4.75 = 4.5 \text{ kg/cm}^2$$

Failure envelope is shown in Fig. 9.24.

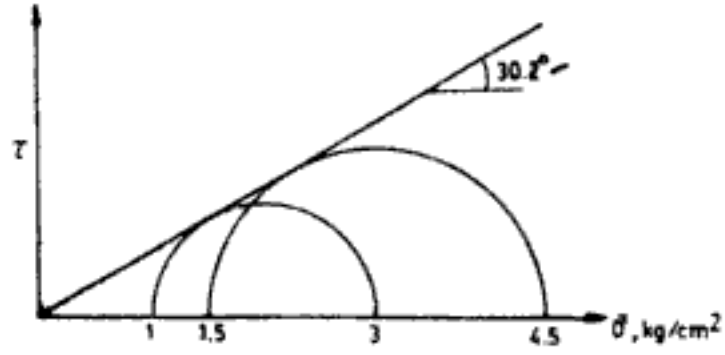

Fig. 9.24 Q 9.2

From Fig. 9.24

$$\bar{c}_{CU} = 0$$

$$\bar{\phi}_{CU} = \bar{\phi} = 30.2°$$

Q 9.3: A sand sample is consolidated at a confining pressure of 1 kg/cm² and later sheared allowing free drainage. Axial stress at failure is 3.5 kg/cm². Determine shear strength parameters.

Ans: This is a CD test and all stresses are effective stresses.

$$\bar{\sigma}_3 = 1 \text{ kg/cm}^2$$
$$\bar{\sigma}_1 = 3.5 \text{ kg/cm}^2$$

Mohr's circle can be drawn. Since there is no cohesion intercept in sand under drained conditions (Fig. 9.22) failure envelope can be drawn as shown in Fig. 9.25.
From Fig. 9.25,

$$\bar{c} = 0,$$
$$\phi_{CD} = \bar{\phi} = 33.7°$$

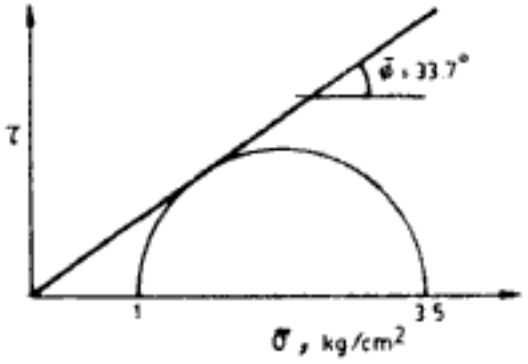

Fig. 9.25 Q 9.3

9.5 UNDRAINED AND DRAINED SHEAR STRENGTH

Consider two identical soil samples. The two samples will have same effective stress parameters $\bar{c}$ and $\bar{\phi}$. Let both samples be consolidated under the same confining pressure of $\bar{\sigma}_c$. This confining pressure is called initial effective consolidation pressure. After this let one of the samples be tested under UU condition (where σ_3 can be greater than $\bar{\sigma}_c$). Let the other sample be tested under drained condition with $\sigma_3 = \bar{\sigma}_c$ or at undrained conditions with measurement of pore water pressure (where σ_3 can be greater than $\bar{\sigma}_c$ and equal to $\bar{\sigma}_c + u_B$). The results of UU test on the first soil sample are shown in Fig. 9.26 and the results of CD test or CU test on second sample are shown in terms of effective stress in Fig. 9.27.

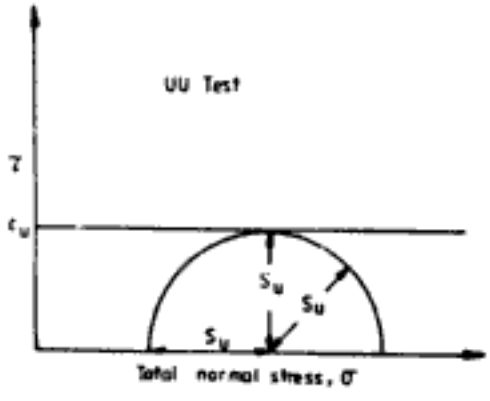

Fig. 9.26 Undrained strength

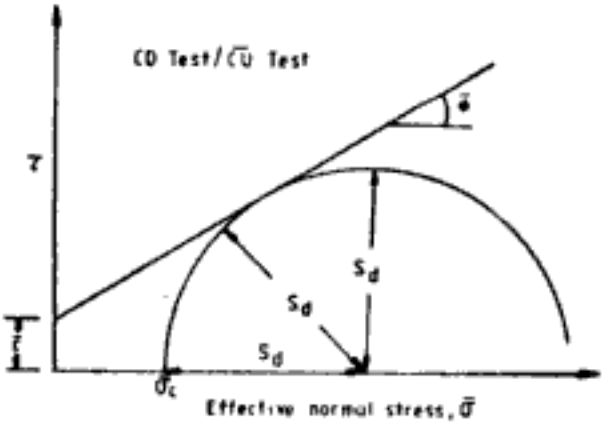

Fig. 9.27 Drained strength

9.5.1 Undrained Strength

As shown in Fig. 9.26 the radius of the Mohr's circle obtained from UU test is defined as *undrained strength*, S_u. Since this is the same as cohesion intercept it is also referred to as *undrained cohesion*, c_u.

Then, $$S_u = c_u = \frac{\sigma_1 - \sigma_3}{2} \text{ in UU condition} \tag{9.21}$$

If we measure pore water pressure in UU test also, Mohr's circle can be drawn in terms of effective stress. The failure envelope will then give the effective stress parameters $\bar{c}$ and $\bar{\phi}$. It is possible to express S_u in terms of $\bar{c}$ and $\bar{\phi}$ as below,

$$S_u = (\bar{\sigma}_c + \bar{c} \cot \bar{\phi}) \left\{ \frac{\sin \bar{\phi}}{1 - (1 - 2A_f) \sin \bar{\phi}} \right\} \tag{9.22}$$

where A_f = A-factor at failure. For normally consolidated soils $\bar{c} = 0$, therefore

$$S_u = \bar{\sigma}_c \left\{ \frac{\sin \bar{\phi}}{1 - (1 - 2A_f) \sin \bar{\phi}} \right\} \tag{9.23}$$

Equations 9.22 and 9.23 are for isotropic consolidation under $\bar{\sigma}_c$. In the field, however, the vertical and horizontal effective stresses on an element are different (refer to Ch. 13). Let the vertical and horizontal effective stresses be $\bar{\sigma}_v$ and $K_0\bar{\sigma}_v$ respectively as shown in Fig. 9.28. K_0 is the coefficient at rest earth pressure. If the soil sample is initially consolidated under conditions simulating this state of stress, then,

S_u of soil is given by the relationship,

$$S_u = (\bar{\sigma}_v + \bar{c} \cot \bar{\phi}) \left\{ \frac{\sin \bar{\phi}[K_0 + A_f(1 - K_0)]}{1 - (1 - 2A_f) \sin \bar{\phi}} \right\} \tag{9.24}$$

For normally consolidated clays $\bar{c} = 0$, hence

$$\frac{S_u}{\bar{\sigma}_v} = \frac{\sin \bar{\phi}[K_0 + A_f(1 - K_0)]}{1 - (1 - 2A_f) \sin \bar{\phi}} \tag{9.25}$$

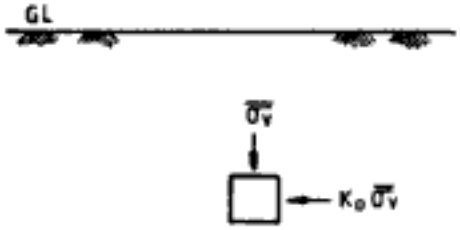

Fig. 9.28 Effective stresses on a soil element

1. *Empirical correlations for undrained strength*

Skempton (1957) gives the following correlations for normally consolidated natural deposits,

$$\frac{S_u}{\bar{\sigma}_v} = 0.11 + 0.0037 I_p \tag{9.26}$$

where I_p is the plasticity index of soil in per cent.

Another relationship between $S_u/\bar{\sigma}_v$ and I_p given by Osterman (1959) is shown in Fig. 9.29. This gives the variation for normally consolidated clays and marine clays. In terms of liquid limit Karlsson and Viberg (1967) give the following relationship for normally consolidated clays,

$$\frac{S_u}{\bar{\sigma}_v} = 0.005 w_L \quad \text{for } w_L > 30\% \tag{9.27}$$

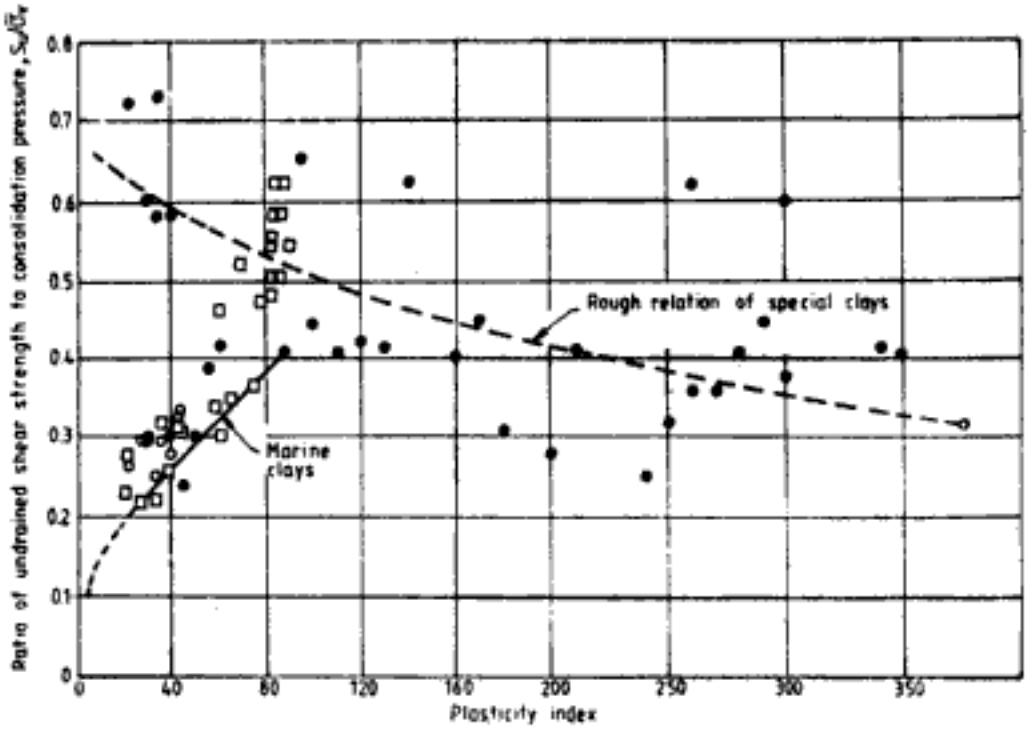

Fig. 9.29 $S_u/\bar{\sigma}_v$ **ratio as a function of plasticity index** (After Osterman, 1959)

Bjerrum and Simons (1960) give the following relationships for normally consolidated clays,

$$\frac{S_u}{\bar{\sigma}_v} = 0.045(I_p)^{0.5} \quad \text{for } I_p > 5\% \tag{9.28}$$

$$\frac{S_u}{\bar{\sigma}_v} = 0.18(I_L)^{-0.5} \quad \text{for } I_L > 0.5 \tag{9.29}$$

where I_L is the liquidity index.
For remoulded clays,

$$\frac{S_u}{\bar{\sigma}_v} = 0.3 \pm 0.1 \tag{9.30}$$

For overconsolidated clays Ladd and Foot (1974) define a nondimensional quantity β as follows,

$$\beta = \frac{(S_u/\bar{\sigma}_v)_{\text{overconsolidated}}}{(S_u/\bar{\sigma}_v)_{\text{normally consolidated}}} \tag{9.31}$$

Variation of β with overconsolidation ratio is given in Fig. 9.30.

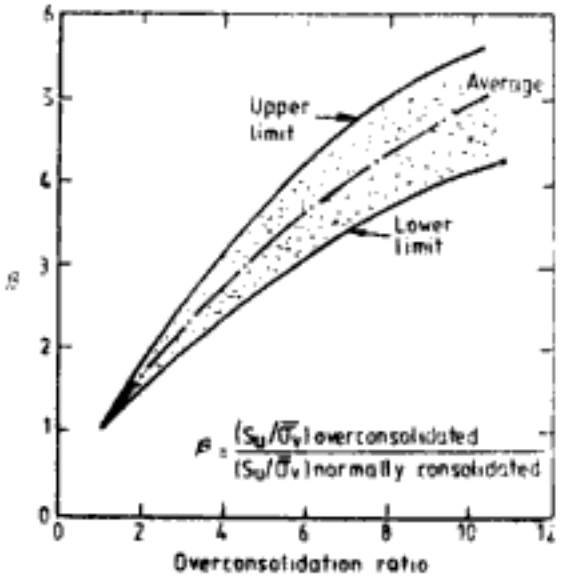

Fig. 9.30 Variation of β with overconsolidation ratio (After Das, 1983. Reprinted by permission of Hemisphere Publishing Corporation, New York)

The analytical and empirical relationships can be used to estimate the undrained strength of soil and to know whether the soil is normally- or overconsolidated.

In order to use Fig. 9.30 undisturbed soil sample must be obtained from the field. From consolidation test preconsolidation pressure $\bar{p}_c$ is obtained (see Ch. 14 for procedure). A remoulded soil sample is prepared and consolidated under K_0 times the present $\bar{\sigma}_v$ and its S_u is determined. This is the S_u for normally consolidated sample. OCR can be computed as $\bar{p}_c/\bar{\sigma}_v$. β can be obtained from Fig. 9.30 and the $S_u/\bar{\sigma}_v$ of overconsolidated clay can be computed using Eq. 9.31. Table 9.10 gives empirical relationship between standard penetration number, N (explained in Ch. 19), undrained cohesion and consistency of soil. Similarly the correlation between static cone penetration resistance (Ch. 19) and undrained cohesion is given in Table 9.11.

Table 9.10 Empirical Relationship between Standard Penetration Resistance Values and Undrained Cohesion of Clays

Consistency of soil	Very soft	Soft	Medium	Stiff	Very stiff	Hard
Standard penetration number, N	0–2	2–4	4–8	8–16	16–32	> 32
Undrained cohesion, c_u kg/cm²	0–0.125	0.125–0.25	0.25–0.50	0.50–1.00	1.00–2.00	> 2.00

The empirical correlation between standard penetration resistance value (N) and undrained cohesion (c_u) of cohesive soils is very unreliable. Unless the project is very small, proper soil testing should be done to determine the shear strength parameters. The standard penetration test should be always used only as a guide.

Table 9.11 Empirical Correlation between Static Cone Point Resistance (q_c) and Undrained Cohesion of Cohesive Soils

Soil type	Static cone point resistance value, q_c (kg/cm²)	Range of undrained cohesion, c_u (kg/cm²)
Normally consolidated clays	$q_c < 20$	$(q_c/18)$ to $(q_c/15)$
Overconsolidated clays	$q_c > 20$	$(q_c/26)$ to $(q_c/22)$

Q 9.4 The liquid limit and plastic limit of a saturated normally consolidated clay deposit are 63% and 38% respectively. The saturated density of soil is 1.9 T/m³. Determine the undrained strength of the soil sample at 15 m below ground level.

Ans: I_p of soil $= 63 - 38 = 25$

$\bar{\sigma}_v$ at 15 m below ground level $= 1.9 \times 15 = 28.5$ T/m²

Using Eq. 9.26 $$\frac{S_u}{\bar{\sigma}_v} = 0.11 + (0.0037 \times 25) = 0.2025$$

Using Eq. 9.28 $$\frac{S_u}{\bar{\sigma}_v} = 0.045 \times (25)^{0.5} = 0.225$$

From Eq. 9.27 $$\frac{S_u}{\bar{\sigma}_v} = 0.005 \times 63 = 0.315$$

If we assume $\bar{\phi} = 30°$, $K_0 = 1/3$ and $A_f = 0.9$,

From Eq. 9.25 $$\frac{S_u}{\bar{\sigma}_v} = \frac{\sin 30°\{(1/3) + 0.9(1 - 1/3)\}}{1 - \{(1 - 2 \times 0.9) \times \frac{1}{2}\}}$$

$$= 0.333$$

From all these calculations an average value of $S_u/\bar{\sigma}_v$ can be assumed as 0.25

$\therefore$ undrained strength of soil sample at 15 m depth $= 0.25 \times 28.5 = 7.125$ T/m²

Q 9.5: If the deposit in Q 9.4 is overconsolidated and the preconsolidation pressure at a depth of 15 m is 112 T/m² determine the undrained strength of the soil sample.

Ans: Overconsolidation ratio $= 112/28.5 = 3.93$

$(S_u/\bar{\sigma}_v)_{\text{normally consolidated}} = 0.25$, from Q 9.4

From Fig. 9.30 $\beta = 2.7$

From Eq. 9.31

$(S_u/\bar{\sigma}_v)_{\text{overconsolidated}} = 2.7 \times 0.25 = 0.675$

$$S_u = 0.675 \times 28.5 = 19.24 \text{ T/m}^2$$

9.5.2 Drained Strength

The radius of the Mohr's circle obtained from CD or $\overline{CU}$ test in Fig. 9.27 is defined as *drained strength, S_d.*

Then,
$$S_d = \frac{\bar{\sigma}_1 - \bar{\sigma}_c}{2} \tag{9.32}$$

From geometry of the figure, S_d can be expressed in terms of $\bar{c}$ and $\bar{\phi}$ as

$$S_d = (\bar{\sigma}_c + \bar{c} \cot \bar{\phi}) \frac{\sin \bar{\phi}}{(1 - \sin \bar{\phi})} \tag{9.33}$$

For normally consolidated soils $\bar{c} = 0$, therefore

$$S_d = \frac{\bar{\sigma}_c \sin \bar{\phi}}{(1 - \sin \bar{\phi})} \tag{9.34}$$

The relationship between S_u and S_d is described in Table 9.12.

Table 9.12 Relative Magnitude of Drained and Undrained Shear Strength for Specimens with the Same Initial Effective Consolidation Stress

Triaxial shear test	Normally consolidated clay	Heavily over-consolidated clay
Compression loading (σ_1 increasing with σ_3 remaining constant)	$S_d > S_u$	$S_u \cong S_d$
Compression unloading (σ_3 decreasing with σ_1 remaining constant)	$S_u \cong S_d$	$S_u \gg S_d$

9.6 SENSITIVITY

Some soils in their undisturbed state show a high shear strength. However, upon remoulding they lose shear strength considerably. Such soils are said to be sensitive. The stress-strain behaviour of sensitive soils will be as shown in Fig. 9.31. Sensitivity is defined as,

$$\text{Sensitivity} = \frac{S_{u\text{-undisturbed soil}}}{S_{u\text{-remoulded soil}}} \tag{9.35}$$

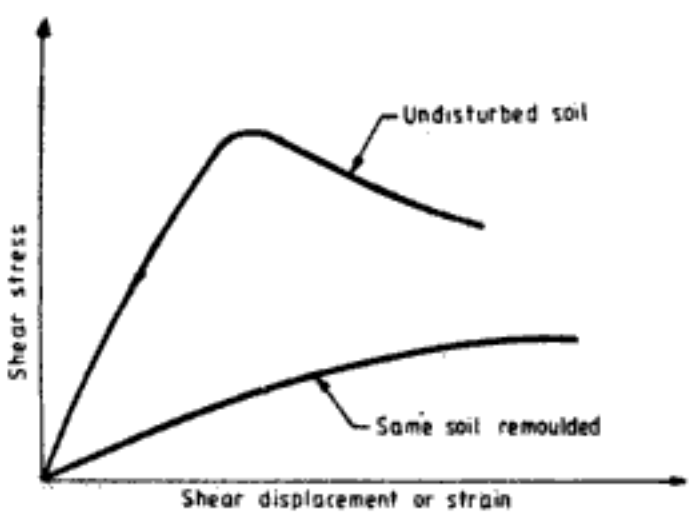

Fig. 9.31 Stress-strain relationships for sensitive soils

Table 9.13 indicates the categories of sensitive soils based upon the value of sensitivity.

Table 9.13 Categories of Sensitive Soils

Soil	Sensitivity
Insensitive clays	1
Low sensitivity clays	1-2
Medium sensitivity clays	2-4
Sensitive clays	4-8
Extra-sensitive clays	> 8
Quick clays	> 16

Some important points on sensitive clays are given below:

1. Sensitivity is related to liquidity index since the greatest loss of strength should occur in a highly flocculated soil whose water content is very large compared to its liquid limit.
2. Quick clays present special problems in the selection of shear strength parameters. Large axial strains are required to develop the peak shear resistance during drained loading of normally consolidated clays, and quick and sensitive clays. Because of this, it is usually considered that the angle of shearing resistance for quick clay is quite small, even less than the residual angle of shearing resistance.
3. Use of $\bar{c}$ and $\bar{\phi}$ corresponding to peak resistance will lead to a great overestimate of the stability of slopes in quick clay.

9.7 STRESS PATH

Stress path gives a continuous representation of successive states of stress that a soil sample passes through during shear test. Stress path is obtained by plotting the experimental data on p-q coordinates defined as

$$p = \frac{\sigma_1 + \sigma_3}{2} \tag{9.36}$$

$$q = \frac{\sigma_1 - \sigma_3}{2} \tag{9.37}$$

Stress path coordinates with respect to effective stresses are,

$$\bar{p} = \frac{\bar{\sigma}_1 + \bar{\sigma}_3}{2} = \frac{(\sigma_1 - u) + (\sigma_3 - u)}{2} = p - u \tag{9.38}$$

$$\bar{q} = \frac{\bar{\sigma}_1 - \bar{\sigma}_3}{2} = \frac{(\sigma_1 - u) - (\sigma_3 - u)}{2} = q \tag{9.39}$$

Stress path for a consolidated drained test is shown in Fig. 9.32. The sample is initially consolidated at a confining pressure corresponding to point A in the diagram. After this the axial stress is increased at the same confining pressure. Figure shows the Mohr's circles at different stages of loading. The $\bar{p}$, $\bar{q}$ coordinates at the various stages are joined together

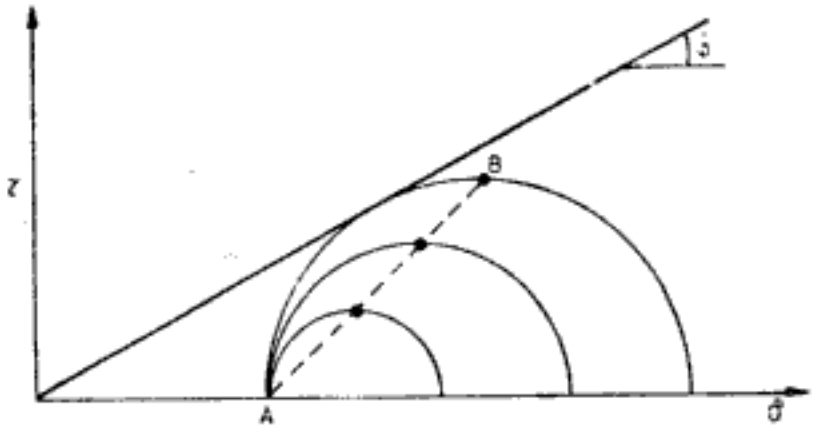

Fig. 9.32 Stress path for CD test

by line AB which forms the stress path for the experiment. The stress path need not be a straight line. It can be curved for a CU test as shown in Fig. 9.33 where AB is the stress path. The locus of $\bar{p} - \bar{q}$ coordinates corresponding to Mohr's circles at failure such as point B in Figs 9.32 and 9.33 of identical soil samples is a straight line. This is referred to as

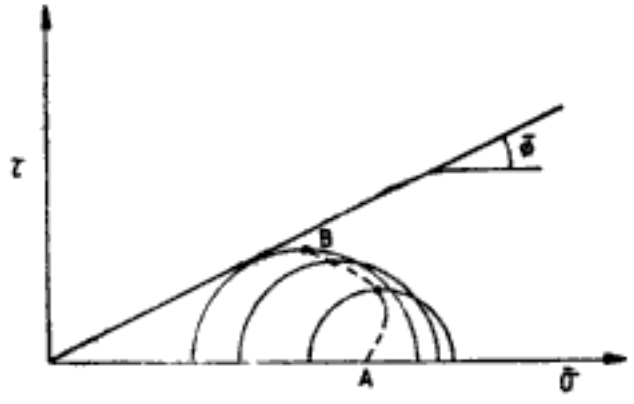

Fig. 9.33 Stress path for $\overline{CU}$ test

K_f line as shown in Figs 9.34 and 9.35. K_f line passes through origin if soil has no cohesion intercept $\bar{c}$, but makes an intercept with ordinate if soil has cohesion intercept.

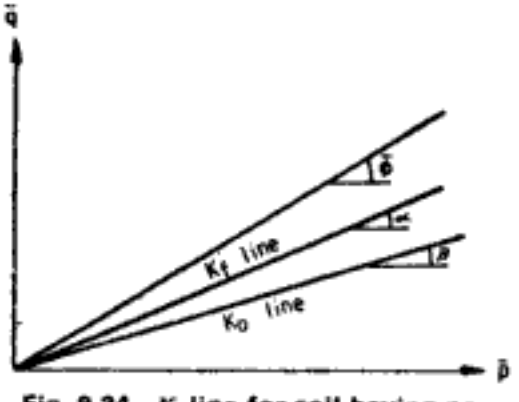

Fig. 9.34 K_f line for soil having no cohesion intercept $\bar{c}$

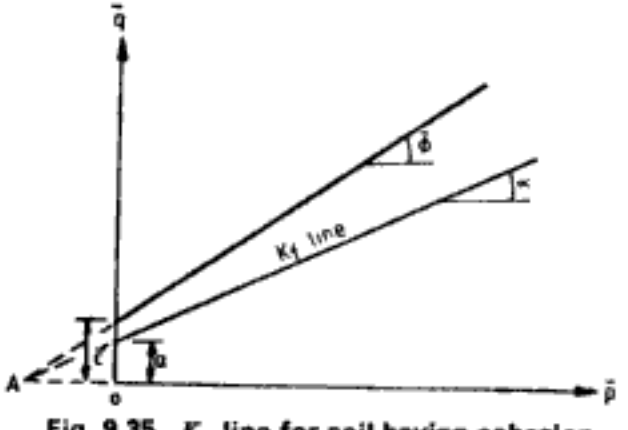

Fig. 9.35 K_f line for soil having cohesion intercept c

Figures 9.34 and 9.35 also show the inclination α of K_f line in relation to inclination $\bar{\phi}$ of failure envelope. From geometrical relationships the following equations can be obtained.

$$\tan \alpha = \sin \bar{\phi} \tag{9.40}$$

$$\bar{c} = \frac{a}{\cos \bar{\phi}} \tag{9.41}$$

The state of stresses on a soil element in field is represented by the Mohr's circle in Fig. 9.36. The locus of $\bar{p}$, $\bar{q}$ coordinates of Mohr's circles representing *in situ* stresses is a straight line and is referred to as K_0 *line*. Inclination of K_0 line in relation to failure envelope and K_f line is shown in Fig. 9.34. Slope β of K_0 line can be obtained from

$$\tan \beta = \left(\frac{1 - K_0}{1 + K_0}\right)$$

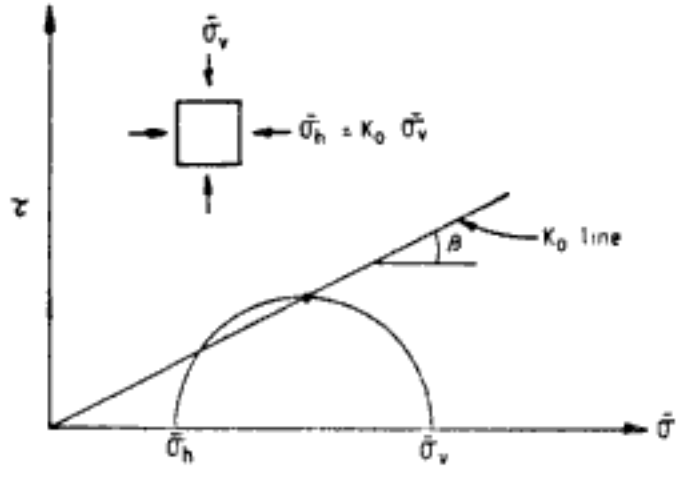

Fig. 9.36 K_0 line

Relationships for K_0 are explained in Ch. 16. For any given point on a stress path the corresponding principal stresses can be determined by drawing straight lines at 45° as shown in Fig. 9.37. The figure shows determination of principal stresses for a point C on stress

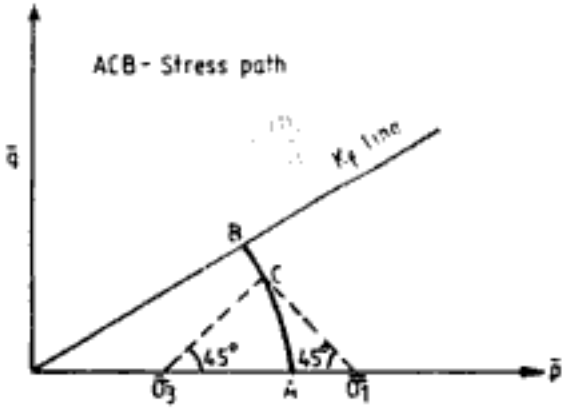

Fig. 9.37 Determination of principal stresses for a point on stress path ($\bar{\sigma}_1$,$\bar{\sigma}_3$—major and minor principal stress, respectively, for point C)

path AB. The stress paths for a normally consolidated soil are geometrically similar. The contours of equal axial strain, $\epsilon_1 = \Delta L/L$, on different stress paths of a soil are nearly straight lines. These are shown in Fig. 9.38.

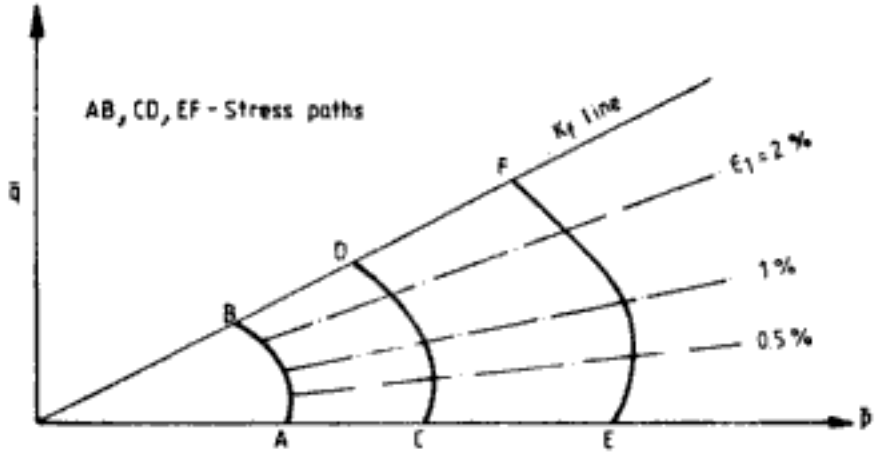

Fig. 9.38 Stress paths with axial strain contours

Q 9.6: From Fig. 9.35 derive relationships between principal stresses at failure and shear strength parameters.

Ans: From Eq. 9.40 $\tan \alpha = \sin \bar{\phi}$

In Fig. 9.35 $AO = \dfrac{\bar{c}}{\tan \bar{\phi}}$

$$\tan \alpha = \frac{(\bar{\sigma}_1 - \bar{\sigma}_3)/2}{\left(\dfrac{\bar{c}}{\tan \bar{\phi}}\right) + \left(\dfrac{\bar{\sigma}_1 + \bar{\sigma}_3}{2}\right)} = \sin \bar{\phi} \tag{9.42}$$

where, $\bar{\sigma}_1$ and $\bar{\sigma}_3$ are principal stresses at failure. For normally consolidated soils and cohesionless soils $\bar{c} = 0$. Therefore,

$$\sin \bar{\phi} = \frac{(\bar{\sigma}_1 - \bar{\sigma}_3)}{(\bar{\sigma}_1 + \bar{\sigma}_3)} \tag{9.43}$$

For total stresses,

$$\sin \phi = \frac{(\sigma_1 - \sigma_3)}{(\sigma_1 + \sigma_3)} \tag{9.44}$$

For soils with $\bar{c}$ values, Eq. 9.42, can be rearranged to give

$$\bar{\sigma}_1 = 2\bar{c} \frac{\cos \bar{\phi}}{(1 - \sin \bar{\phi})} + \bar{\sigma}_3 \frac{(1 + \sin \bar{\phi})}{(1 - \sin \bar{\phi})}$$

or
$$\bar{\sigma}_1 = 2\bar{c} \tan \left(45 + \frac{\bar{\phi}}{2}\right) + \bar{\sigma}_3 \tan^2 \left(45 + \frac{\bar{\phi}}{2}\right) \tag{9.45}$$

Similarly,
$$\bar{\sigma}_3 = \bar{\sigma}_1 \tan^2 \left(45 - \frac{\bar{\phi}}{2}\right) - 2\bar{c} \tan \left(45 - \frac{\bar{\phi}}{2}\right) \tag{9.46}$$

For total stresses σ_1 and σ_3 relationships are same as Eqs 9.45 and 9.46 but are in terms of total stress parameters c and ϕ.

Q 9.7: Redo Q 9.2 using the relationships developed in Q 9.6.

Ans: *Total stress parameters*

Let $$\tan (45 + \phi/2) = m$$

For sample 1, from Eq. 9.45, but in terms of total stress,

$$4.75 = 2c\,m + 2.75m^2 \qquad \text{(a)}$$

Similarly for sample 2

$$7.25 = 2c\,m + 4.25m^2 \qquad \text{(b)}$$

Solving Eqs (a) and (b)

$$c = 0.06 \text{ kg/cm}^2$$
$$\phi = 14.48^\circ$$

Note that in Eqs (a) and (b) failure values of σ_1 and σ_3 are used after correcting for back pressure.

Effective stress parameters

Let $$\tan (45 + \bar{\phi}/2) = M$$

For sample 1, from Eq. 9.45

$$3 = 2\bar{c}M + M^2 \qquad \text{(c)}$$

For sample 2

$$4.5 = 2\bar{c}M + 1.5M^2 \qquad \text{(d)}$$

Solving (c) and (d)

$$\bar{c} = 0$$
$$\bar{\phi} = 30^\circ$$

Q 9.8: Redo Q 9.3 using relationships developed in Q 9.6.

Ans: Since sand is cohesionless, Eq. 9.43 can be used.

$$\sin \bar{\phi} = \frac{3.5 - 1}{3.5 + 1} = \frac{2.5}{4.5} = 0.556$$
$$\bar{\phi} = 33.75^\circ$$

9.8 ELASTIC PROPERTIES OF SOIL FROM TRIAXIAL COMPRESSION TESTS

The elastic properties often used in analysis of soil engineering problems are modulus of elasticity (E), Poisson's ratio (μ), and shear modulus (G).

9.8.1 Modulus of Elasticity

Modulus of elasticity is obtained from deviator stress versus axial strain curve. Modulus obtained from undrained conditions is known as *undrained modulus* (E_u) and that obtained from drained conditions is the *drained modulus* (E_d). A typical stress-strain curve from triaxial shear test is shown in Fig. 9.39. It is evident that the curve is non-linear for most of

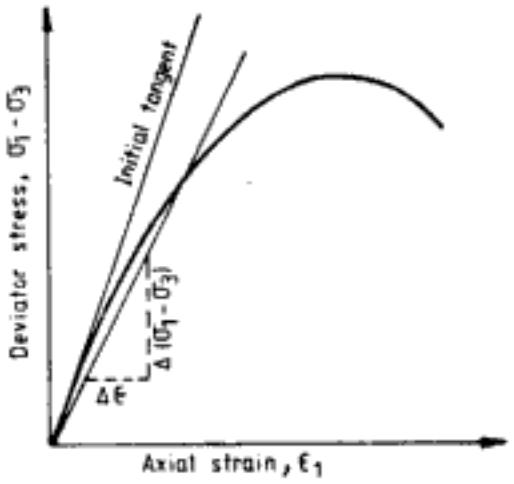

Fig. 9.39 Elastic modulus of soil from stress-strain curve

its part. Two types of modulus can be defined for such a curve, namely, *tangent modulus* and *secant modulus*. Tangent modulus is the slope of the stress-strain curve which varies from point to point.

$$\text{Tangent modulus} = \frac{d(\sigma_1 - \sigma_3)}{d\epsilon_1} \tag{9.47}$$

Secant modulus is defined as the ratio of difference in deviator stress to the corresponding axial strain.

$$\text{Secant modulus} = \frac{\Delta(\sigma_1 - \sigma_3)}{\Delta\epsilon_1} \tag{9.48}$$

Thus tangent modulus and secant modulus are not constant for a soil and will have to be specified over stress ranges. There are many different recommendations regarding determination and selection of modulus of soil for engineering applications.

Bowles (1982) recommends the use of initial tangent modulus, which is the slope of the initial straight line portion of the stress-strain curve. The reasons given in support of this are (i) soil is elastic and there is less divergence between different curves in this region, and (ii) the tangent modulus gives higher values for elastic modulus than the secant modulus. Lambe and Whitman say that elastic modulus for soil is usually the secant modulus from zero deviator stress to a deviator stress equal to 1/2 or 1/3 of peak deviator stress, since a safety factor of 2 or 3 is commonly used in soil engineering practice.

Kondner (1963) proposes a semi-empirical relationship to determine modulus of soils. According to him the stress-strain curve can be represented by the following hyperbolic equation,

$$\sigma_1 - \sigma_3 = \frac{\epsilon_1}{a + b\epsilon_1} \tag{9.49}$$

which can be rewritten as

$$\frac{\epsilon_1}{\sigma_1 - \sigma_3} = a + b\epsilon_1 \tag{9.50}$$

A plot of $\epsilon_1/(\sigma_1 - \sigma_3)$ vs. ϵ_1 will be a straight line with slope b and making an intercept of a with ordinate (Fig. 9.40). Modulus of soil is then,

$$E = \frac{1}{a} \tag{9.51}$$

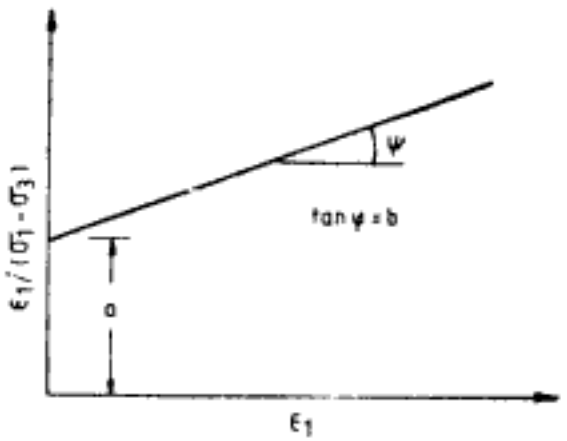

Fig. 9.40 Determination of soil modulus by Kondner's procedure

For undrained modulus is clayey soils the following correlations between E_u and undrained strength S_u will be useful.

For normally consolidated sensitive clay,

$$E_u = (200 \text{ to } 500)S_u \tag{9.52}$$

For normally consolidated insensitive clay and lightly overconsolidated clay,

$$E_u = (750 \text{ to } 1200)S_u \tag{9.53}$$

For heavily overconsolidated clay,

$$E_u = (1500 \text{ to } 2000)S_u \tag{9.54}$$

Table 9.14 gives some typical values of elastic modulus of different types of soils.

9.8.2 Poisson's Ratio

Poisson's ratio is defined as ratio of lateral strain ϵ_3 to axial strain ϵ_1 in triaxial compression tests.

$$\mu = \frac{\epsilon_3}{\epsilon_1} \tag{9.55}$$

Poisson's ratio is also not constant for soils but depends on stress and strain levels. But the value of μ does not greatly influence results in soil engineering problems.

Value of μ for soils ranges from 0 to 0.5. For saturated soils it tends to 0.5 and for dry soils to 0. Table 9.15 gives typical values of μ for different soil types.

9.8.3 Shear Modulus

Shear modulus G can be determined from the following relationship,

$$G = \frac{E}{2(1 + \mu)} \tag{9.56}$$

Table 9.14 Typical Range of Values for the Static Stress-Strain Modulus E for Selected Soils (Field Values Depend on Stress History, Water Content, Density, etc.)

Soil	E kg/cm²
Clay:	
Very soft	20–150
Soft	50–250
Medium	150–500
Hard	500–1000
Sandy	250–2500
Glacial till:	
Loose	100–1600
Dense	1500–7250
Very dense	4800–15000
Loess	150–600
Sand:	
Silty	75–250
Loose	100–250
Dense	500–850
Sand and gravel:	
Loose	500–1500
Dense	1000–2000
Shale	1500–150000
Silt	20–200

Table 9.15 Typical Range of Values for Poisson's Ratio, μ

Type of soil	μ
Clay, saturated	0.4–0.5
Clay, unsaturated	0.1–0.3
Sandy clay	0.2–0.3
Silt	0.3–0.35
Sand (dense)	0.2–0.4
Coarse (void ratio = 0.4–0.7)	0.15
Fine-grained (void ratio = 0.4–0.7)	0.25
Rock	0.1–0.4 (depends somewhat on type of rock)
Loess	0.1–0.3
Ice	0.36
Concrete	0.15

The above discussions on elastic properties are for static conditions. For dynamic conditions, the elastic properties are evaluated from cyclic load tests and other special tests.

9.9 OTHER FORMS OF SHEAR STRENGTH TESTS

9.9.1 Direct Shear Test

Direct shear test is the earliest among the different procedures currently being used to determine shear strength of soil. A schematic representation of the test is shown in Fig. 9.41.

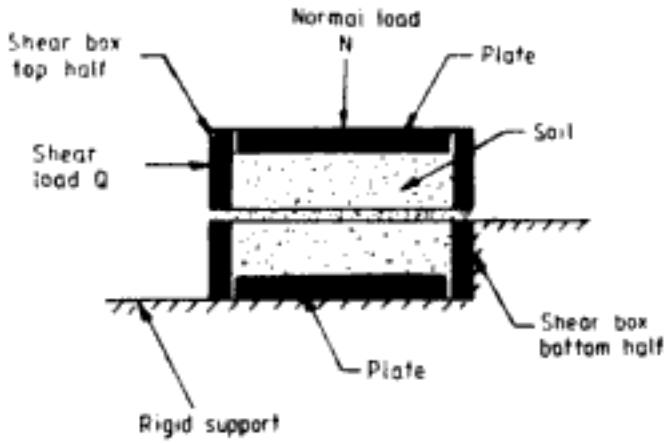

Fig. 9.41 Direct shear box assembly

The test is carried out as follows.

The soil sample is contained in a shear box which is in two halves. The sample is subjected to a normal load N. One half of the shear box is held firmly. The other half is slid horizontally over the portion which is held firmly. The soil sample thus gets sheared along the plane separating the two halves of the shear box. The shear displacement and shear load can be continuously recorded. The shear strength of soil is,

$$\tau_f = \frac{Q_f}{A}, \text{ at a normal stress of } \sigma = \frac{N}{A} \tag{9.57}$$

where Q_f = shear load at failure

A = area of plane of failure.

By repeating the test for different values of σ the failure envelope can be obtained in $\tau - \sigma$ plot. Though direct shear test is easy and inexpensive to perform, it has some limitations. The following are a few of them.

1. The failure plane is not the weakest but is predetermined.
2. There is no control over dissipation of pore water pressure nor it can be measured.
3. Shear stress distribution is not uniform over the plane of shear. It is more at edge than at centre. This leads to progressive failure.

ϕ determined from direct shear tests is generally more than ϕ obtained from triaxial shear tests, by about 2°, especially for dense sands.

9.9.2 Vane Shear Test

This is a test carried out in field to determine the *in situ* undrained strength of clay soils and is useful in soft soils where it is difficult to obtain a soil sample and also in sensitive soils where the sampling operations considerably reduce the shear strength of natural soils. The vane consists of four thin steel plates welded to a steel torque rod at right angles to each other (Fig. 9.42).

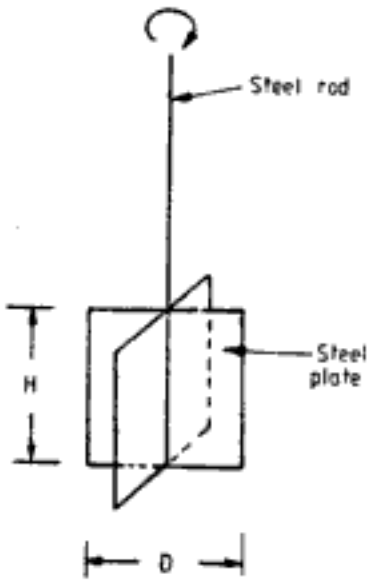

Fig. 9.42 Details of vane

The vane is inserted into the soil and then rotated by applying torque through the torque rod. The vane shears a soil cylinder the dimensions of which are equal to the diameter and height of the vane. The torque required to fail the soil cylinder can be recorded. The undrained shear strength can be calculated from

$$S_u = \frac{T}{\pi\left(\frac{D^2H}{2} + \frac{D^3}{6}\right)} \tag{9.58}$$

where T = failure torque
D = diameter of vane
H = height of vane

Equation 9.58 is applicable when the soil is sheared along the height and at both ends of the cylinder. However, if the vane is not inserted sufficiently deep into the soil, shear resistance will be mobilised only along the height and at one end (bottom) of the cylinder. In this case,

$$S_u = \frac{T}{\pi\left(\frac{D^2H}{2} + \frac{D^3}{12}\right)} \tag{9.59}$$

It has been found that field vane shear test overestimates the undrained shear strength of soils. For design purpose S_u is then determined as

$$S_u = \lambda S_{u\text{-vane}} \tag{9.60}$$

where λ = a correction factor

$S_{u\text{-vane}}$ = undrained strength by vane shear test

Correlation of λ with plasticity index suggested by Bjerrum (1972) is shown in Fig. 9.43.

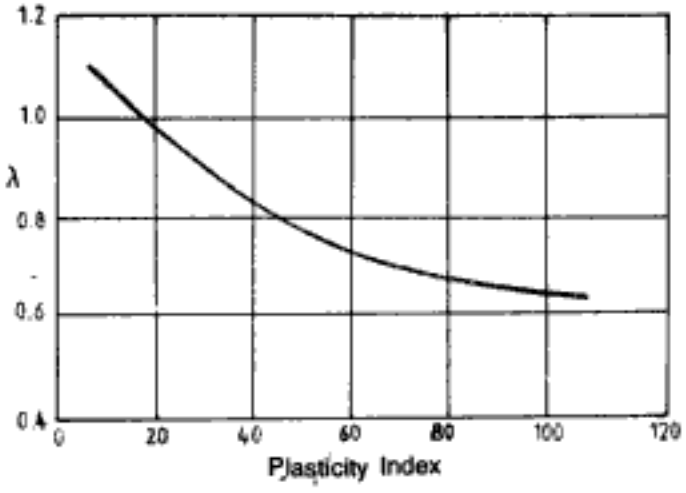

Fig. 9.43 Correlation factor for vane shear test (after Bjerrum, 1972)

9.10 SHEAR STRENGTH FOR PLANE STRAIN CONDITIONS

The shear strength parameters are generally determined from triaxial shear tests. However, many times the field conditions differ from triaxial shear test conditions and approach plane strain conditions. Soil below strip footings, embankments, retaining wall are some examples of plane strain conditions. For these conditions the value of ϕ determined from triaxial shear tests will be modified. In order to calculate bearing capacity of strip foundations, ϕ can be modified as,

$$\phi = 1.1\phi_t \tag{9.61}$$

where, $\phi_t = \phi$ determined from triaxial shear tests. For rectangular foundations Meyerhof (1963) suggests,

$$\phi = \left(1.1 - 0.1\,\frac{B}{L}\right)\phi_t \tag{9.62}$$

where L and B are length and width of foundation, respectively ($L > B$).

10
FOUNDATION LOADS

Proper selection of the type of foundation, its analysis and design requires the knowledge of the loads which the foundation will have to transmit to the soil. From an analysis of the superstructure the loads and moments at foundation level can be determined. To a foundation designer a layout of the structure with the location and magnitude of forces at foundation level are generally provided.

Table 10.1 gives a summary of the loads to be considered in the design of foundations. Figure 10.1 portrays some of these loads for a footing. Specifications for live load, wind load and earthquake forces are usually given in building codes. In analysis of any structure

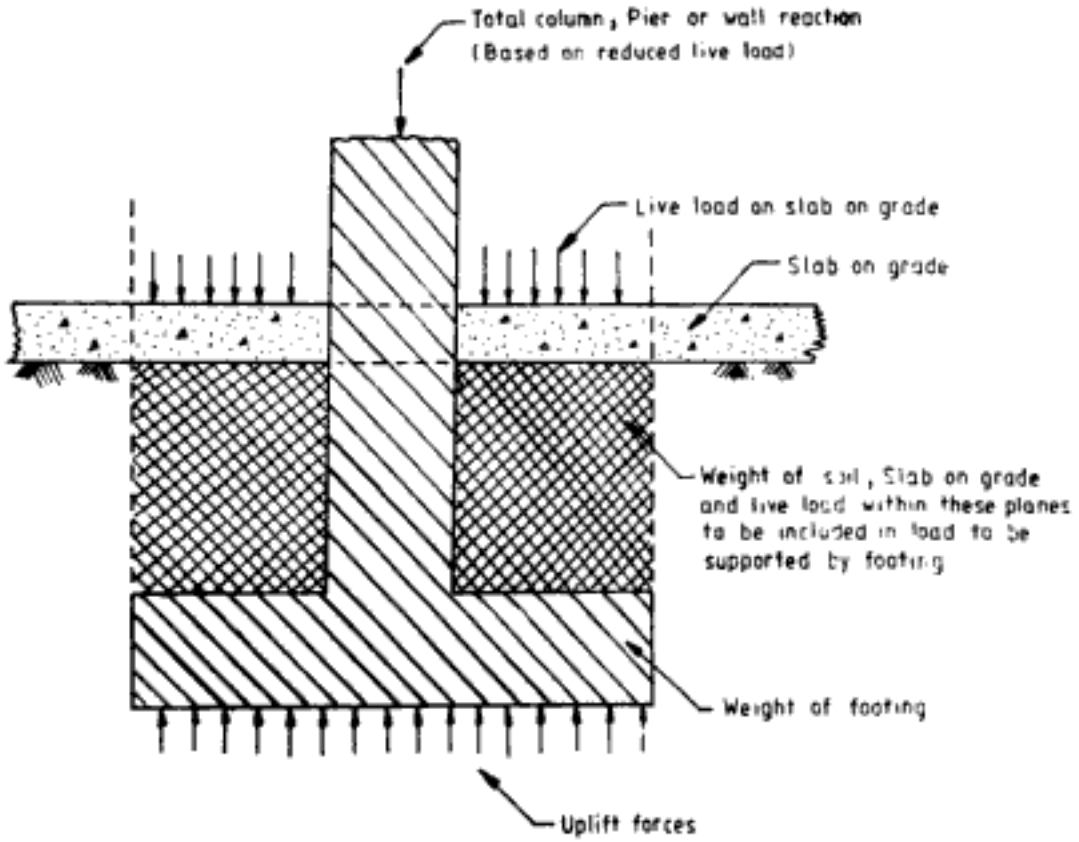

Fig. 10.1 Some basic foundation loads

Table 10.1 Summary of Loads to be Considered in the Design of Foundation Elements
(From Johnson and Kavanagh, 1968. Reprinted by permission of McGraw-Hill Book Company, New York)

I. VERTICAL LOADS
1. *Dead load:*
(a) Column reactions due to self weight of superstructure
(b) Weight of walls, footings, piers and pile caps
(c) Weight of slabs on grade
(d) Weight of overlying soil
2. *Live load:*
(a) Loads due to occupancy
(b) Surcharge including live load on ground floor slabs
3. *Buoyancy and uplift*
4. *Downdrag or negative skin friction:*
(a) Due to remoulding of soil
(b) Due to general settlement of soil at the site
5. *Heave:*
(a) Expansive soils
(b) Freezing of ground
II. LATERAL LOADS
1. *Wind forces*
2. *Earthquake forces*
3. *Lateral earth pressure*
4. *Fluid pressures*
III. IMPACT LOADS
1. Impact equivalents related to moving and dynamic loads

the loading scheme marks the first stage. Part of the loads (dead load, live load, wind forces, earthquake equivalent forces, impact, etc.) are worked out by the structural engineer largely on the basis of codal recommendations. The other part (earth pressure, uplift, downdrag, etc.) are provided by the foundation engineer. Portions only which are of relevance to foundation engineering practice will be reviewed in this chapter for a general overview.

10.1 REDUCTION IN LIVE LOAD

Live loads are generally treated as equivalent distributed or concentrated loads. The probability of live loads occurring simultaneously over large areas of a building is less than the probability of their occurrence over limited areas. For this reason reduced live loads are considered in determining design loads for foundation elements. Following are some excerpts from provisions in National Building Code of India (NBC), 1983 about reduction in live loads.

"*3.1.2 Reduction in Floor Live Loads*

3.1.2.1. Except as provided for in 3.1.2.2 and 3.1.2.3 the reductions given in the table

(Table 10.2) in assumed total live loads on floors may be made in designing columns, walls, piers, their supports and foundations.

Table 10.2 Reduction in Live Load

Number of floors carried by member under consideration	% reduction of total live load on all floors above the member under consideration
1	0
2	10
3	20
4	30
5 or more	40

(After National Building Code of India, 1983)

3.1.2.2 No reduction shall be made in the case of warehouses, garages and other buildings used for storage purposes and for factories and workshops designed for 500 kg/sq. m. However, for buildings such as factories and workshops designed for a live load of more than 500 kg/sq. m., the reduction given under 3.1.2.1 may be made, provided that the loading assumed for any column, wall, etc., is not less than that which would have been if all floors had been designed for 500 kg/sq. m. with no reduction."

10.2 PROVISIONS FOR LATERAL FORCES

10.2.1 Wind Load

According to NBC, wind pressures are expressed in terms of a basic pressure p which is an equivalent static pressure in the direction of flow of wind. The wind pressure map of India is given in two separate figures. The first figure gives the basic maximum wind pressure map of India including winds of short duration, and the second figure gives the basic maximum wind pressure map of India excluding winds of short duration.

The NBC states:

"In view of the wind phenomena and the nature of the wind and the relatively short period over which it acts, it may not be necessary to treat it in the same manner as live loads. In the case of working stress designs higher stresses than those normally permissible in the case of live loads, and in the case of ultimate load designs lower load factors than those normally adopted for live loads, could be permitted when wind loads are taken into consideration."

In the absence of specific recommendations:

"The permissible stresses and load factors shall be as in Table 10.3 for different values of K, where

$$K = \frac{\text{Wind pressure for a given location as obtained from the figure which includes winds of short duration}}{\text{Wind pressure for the same location as obtained from the figure which excludes winds of short duration}} \qquad (10.1)$$

Values of K for some major cities of India are given in the table (Table 10.4). The NBC further states:

"The permissible soil pressure when wind load is considered shall be taken as the normal allowable bearing pressure on the soil multiplied by the same factors as those for permissible stresses given in the table (Table 10.3)."

Table 10.3 Load Factors and Permissible Stresses

K	Permissible stress not more than		Load factor not less than	
1.0	1.0 times the increased stress, for wind load in combination with other loads		1.0 times the load factor, for wind load in combination with other loads	
1.5	1.04	—do—	0.96	—do—
1.67	1.06	—do—	0.95	—do—
2.00	1.08	—do—	0.91	—do—
2.50	1.13	—do—	0.88	—do—

(After National Building Code of India, 1983)

Table 10.4 Values of K in Eq. 10.1 for Some Major Indian Cities

City	K	City	K
Ahmedabad	1.67	Jaipur	2.50
Bangalore	1.67	Kanpur	2.50
Bhopal	2.50	Lucknow	2.50
Bhubaneshwar	1.00	Madras	1.00
Bombay	1.00	Madurai	1.67
Calcutta	1.00	Patna	2.50
Chandigarh	2.50	Simla	1.67
Delhi	2.50	Srinagar	2.50
Guwahati	2.50	Trivandrum	1.00
Hyderabad	1.67	Visakhapatnam	1.00

Note: Values are based on wind pressure up to a height of 30 m above the mean retarding surface.

Under the heading "Foundations" NBC says,

"Where the bearing pressure due to wind is less than 25% of that due to dead and live loads, it may be neglected in design. Where this exceeds 25% foundations may be so proportioned that the pressure due to combined dead, live and wind loads does not exceed the allowable bearing pressure by more than 25%."

10.2.2 Seismic Load

According to NBC:

"When earthquake forces are included, the permissible increase in the allowable bearing pressure of soil shall be as given in the table (Table 10.5) depending on the type of foundation of the structure."

Table 10.5 Permissible Increase in Allowable Bearing Pressure or Resistance of Soils

Type of soil mainly constituting the foundation	Permissible increase in allowable bearing pressure, %					
	Piles passing through any soil but resting on soil type 1	Piles not covered under col (2)	Raft foundation	Combined or isolated RCC footing with tie beams	Isolated RCC footing without tie beams or unreinforced strip foundations	Well foundations
(1)	(2)	(3)	(4)	(5)	(6)	(7)
Type I Rock or Hard Soils—Well graded gravels and sand-gravel mixtures with or without clay binder, and clayey sands poorly graded or sand-clay mixtures (GB, CW, SB, SW and SC) having N above 30, where N is the standard penetration value	50	—	50	50	50	50
Type II Medium Soils—All soils with N between 10 and 30 and poorly graded sands or gravelly sands with little or no fines (SP) with $N > 15$	50	25	50	25	25	25
Type III Soft Soils—All soils other than SP with $N < 10$	50	25	50	25	—	25

(After National Building Code of India, 1983. Reprinted by permission of Indian Standards Institution, New Delhi)

Note 1: The allowable bearing pressure shall be determined in accordance with [V1-2(5)].

Note 2: If any increase in bearing pressure has already been permitted for forces other than seismic forces the total increase in allowable bearing pressure when seismic force is also included shall not exceed the limits specified above.

Note 3: In the case of submerged loose sands and soils falling under classification SP with standard penetration values less than the values specified in Note 5 below, the vibrations caused by earthquake may cause liquefaction or excessive total and differential settlements. In important projects, this aspect of the problem need be investigated and appropriate methods of compaction or stabilization adopted to achieve suitable N. Alternatively, deep pile foundation may be provided and taken to depths well into the layers which are not likely to liquefy.

Note 4: The piles should be designed for lateral loads neglecting lateral resistance of soil layers liable to liquefy.

Note 5: Desirable field values of N are as follows:

Zones III, IV and V	15	*See* Part VI Structural Design Section I Loads
Zones I and II	10	

10.3 LOAD COMBINATIONS

A judicious combination of the working loads keeping in view the probability of their acting together and their disposition in relation to other loads is required. In the absence of design recommendation the following may be taken as a general guidance (NBC 1983):

1. Dead load alone
2. Dead load + partial or full live load whichever causes the most critical condition in the structure.
3. Dead load + wind or seismic load.
4. Dead load + such part or whole of the specified live load whichever is most likely to occur in combination with the specified wind or seismic loads + wind or seismic loads.
5. Dead load + such parts of the live load as would be imposed on the structure during the period of erection + wind or seismic load + erection loads.

For design purposes, wind load and seismic forces shall be assumed not to act simultaneously. Both forces shall, however, be investigated separately and adequately provided for.

11

LOCATION AND DEPTH OF FOUNDATIONS

Foundations may be broadly classified into two categories,

1. Shallow foundations,
2. Deep foundations.

Strip footings, spread footings—both isolated and combined—raft or mat foundations are examples of shallow foundations. As a rough measure the ratio of depth of embedment to width of foundations does not exceed 1 for shallow foundations. Piles and caissons are deep foundations.

Shallow and deep foundations differ in the following ways:

1. *Geometry*

Figures 11.1 and 11.2 show a footing and pile respectively.

For shallow foundations

$$\frac{D}{B} \leq 1 \tag{11.1}$$

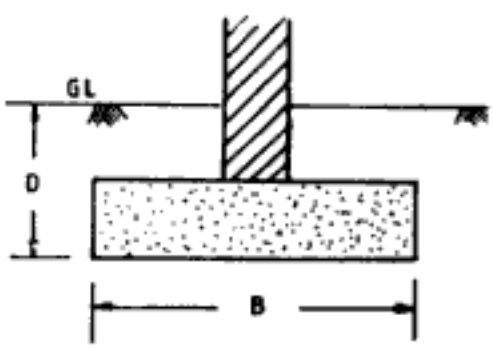

Fig. 11.1 Footing

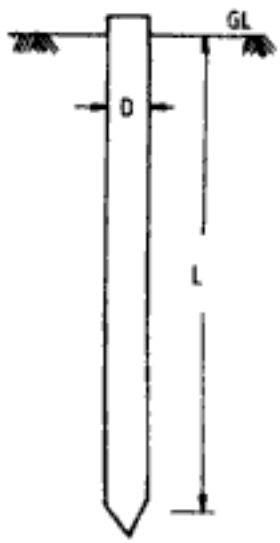

Fig. 11.2 Pile

where D and B are depth of embedment and width of foundation respectively. Foundations with D/B ratio > 1 but < 15 are moderately deep. For deep foundations D/B ratio > 15. In pile foundations the width is usually designated as D (the pile diameter or width) and length as L as shown in Fig. 11.2. Hence, $L/D > 15$ for deep foundations.

2. *Mechanism of load transfer*

In shallow foundations the load is transmitted to the soil which lies immediately below the foundation (Fig. 11.3). Whereas in deep foundations the load is transferred partly by skin friction or shear stresses along the mantle and the rest by point load or vertical stresses at the toe of the foundation (Fig. 11.4).

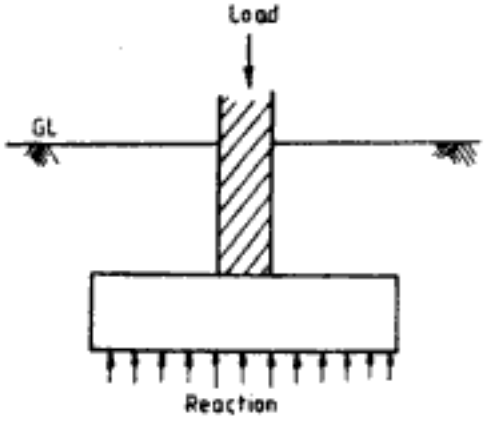

Fig. 11.3 Load transfer in shallow foundations

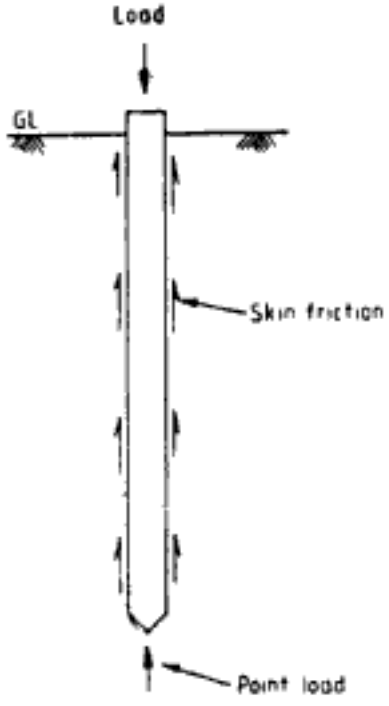

Fig. 11.4 Load transfer in deep foundations

3. *Changes induced in soil during installation*

The methods of construction of shallow and deep foundation are not only different but they induce distinctly different changes in soil. Shallow foundations are constructed in open excavations in a visible manner. Whereas deep foundations are installed in the interior of earth unaided by visible inspection. As shown in Fig. 11.5 the extent of disturbance of soil is limited to a very small zone during the construction of shallow foundations. But in deep foundations irrespective of the method of construction a larger zone of soil is affected extending over the entire length of deep foundation (Fig. 11.6).

11.1 MINIMUM DIMENSIONS OF SHALLOW FOUNDATIONS

From structural considerations codes and handbooks specify minimum dimensions for foundations. Some such useful specifications are given in Tables 11.1 and 11.2.

Table 11.1 Minimum Foundation Dimensions

Nomenclature :–

B = Width or breadth of footing

w = Width of supported wall or column

D = Depth of footing

d = Thickness of footing

d_e = Edge thickness of tapered footing

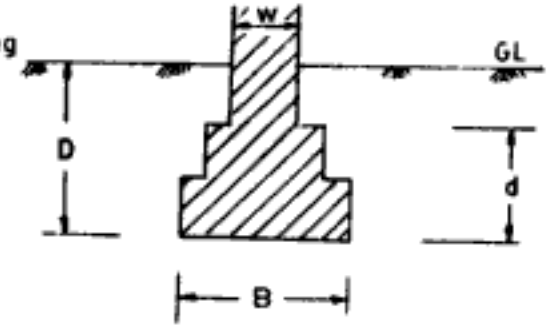

Minimum width of footing

$B \geq 2w + 30\,cm$

B and w in cm

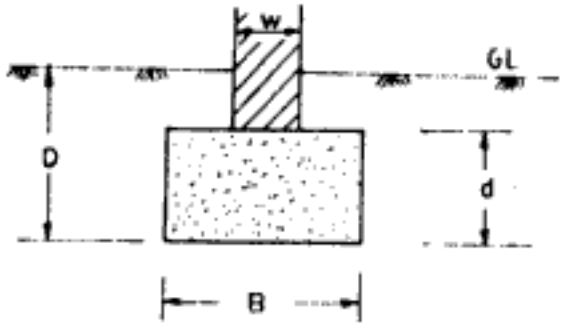

Maximum width from considerations of load transfer :

$B \leq w + d$ for brickwork and stone masonry

$B \leq w + \frac{4}{3}d$ for lime concrete

$B \leq w + 2d$ for cement concrete

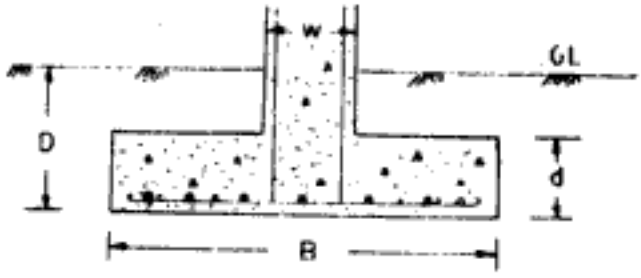

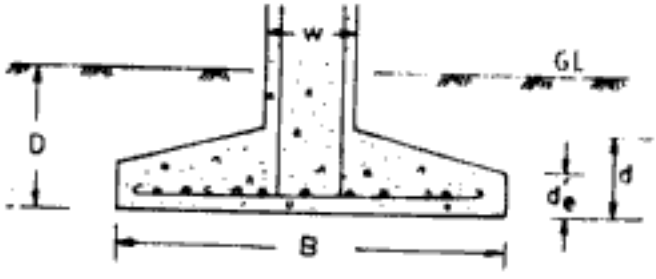

Table 11.2 Minimum Foundation Dimensions

Minimum thickness at the edge of reinforced or plain concrete footing = 15 cm
Minimum depth of foundation = 50 cm (except on rock or other weather resistant ground)
For shallow foundation: $D \leqslant B$
For deep foundation : $D > 2B$

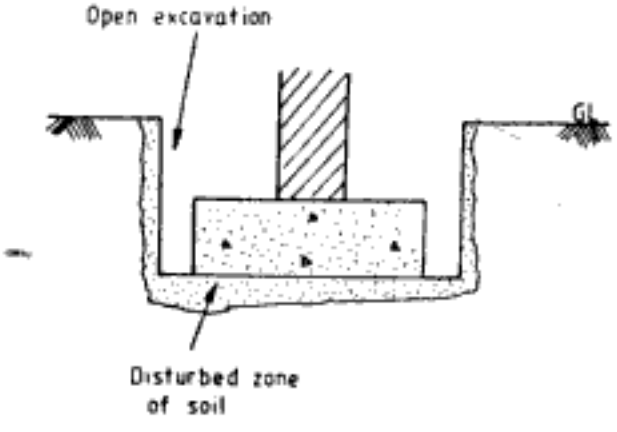

Fig. 11.5 Disturbance of soil during construction of shallow foundation

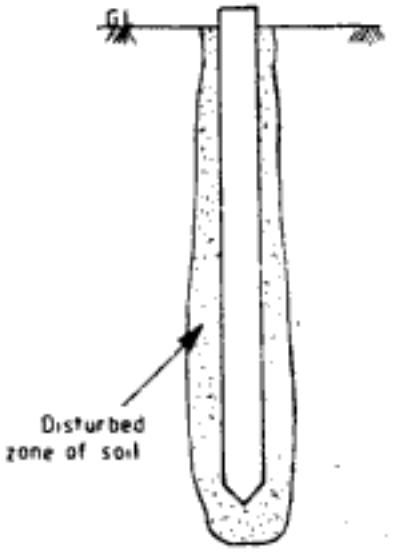

Fig. 11.6 Disturbance of soil during installation of deep foundation

11.2 REQUIREMENTS OF SATISFACTORY FOUNDATION

A properly designed foundation must satisfy the following three design criteria:

1. Location and depth criterion
2. Stability criterion or bearing capacity criterion
3. Settlement criterion

Criterion 1: A foundation must be properly located in the available area and must be founded at the correct depth.

Criterion 2: While in service the foundation must be safe from failure. Failures are of two kinds, structural and by rupture of soil. The structural design must ensure the safety of the foundation against structural failure. Because the consequences due to structural failure are disastrous and the remedial work for inadequate design is prohibitively expensive, a higher safety factor or load factor than for superstructure design is used in the structural design of foundations. But in soil mechanics parlance foundation failure is synonymous with soil rupture failure. The foundation is considered to be structurally sound. Geotechnical engineers are primarily concerned with ensuring a good safety margin against failure of foundations by soil rupture.

Criterion 3: Even if the foundation is safe against failure, during its lifetime it should not undergo excessive settlement which will cause damage to the building or will impair its utility. Stability criterion of foundations is akin to considerations for moment of resistance in the design of beams. And settlement criterion of foundations is analogous to considerations for deflection of beams.

Location and depth criterion will be discussed in more detail in this chapter. Chapter 12 discusses stability criterion and Ch. 14 the settlement criterion.

11.3 DETERMINANTS OF FOUNDATION LOCATION AND DEPTH

11.3.1 Depth of Volume Change

The depth of foundation should be such as to place the foundation below the zone of volume change. The zone of volume change varies from 1.2 to 3.5 m in the case of black cotton soils. Table 11.3 provides guidelines to assess the susceptibility of soils for volume change.

Table 11.3 Identification of Susceptibility of Soils for Volume Change

Likelihood of volume change with changes in moisture	Plasticity index		Shrinkage limit
	Arid regions	Humid regions	
Little	0–15	0–30	12 or more
Little to moderate	15–30	30–50	10–12
Moderate to severe	30 or more	50 or more	10 and less

(After Sowers 1962)

High plastic clay may undergo little or no swelling if it has a liquidity index of 0.2 or more. But it is susceptible to shrinkage on drying.

Following are some guidelines for minimum foundation depth where volume change is expected:

(a) Minimum depth 1.5 m. However, maximum depth of volume change is limited to ground water level.

(b) Below strata susceptible to high volume change but within the limits of (a) above.

(c) Below large root systems.

(d) Below any level of artificially increased temperature.

11.3.2 Depth of Scour

For river structures and structures adjoining rivers the following two types of scour must be considered in the determination of the location of foundations.

1. *Normal scour* is the lowering of the bed of a stream during periods of high flood flow.
2. *Accelerated scour* is localised, intensified scour caused by some obstruction such as a bridge pier.

Total scour is the sum of normal scour and accelerated scour. For safety, the depth of bridge piers and similar foundations must be at a level well below the total of normal and accelerated scour depths.

Total scour by Lacey's formulae

In India Lacey's formulae are generally used to determine normal scour depth. These empirical formulae are given below:

$$D_{\text{Lacey}} = D_L = 0.47\left(\frac{Q}{f}\right)^{1/3} \tag{11.2}$$

$$d_{\text{Lacey}} = d_L = 1.338\left(\frac{q^2}{f}\right)^{1/3} \tag{11.3}$$

where D_L = maximum depth of flow or regime depth of flow or depth of normal scour below high flood level—in terms of total discharge—given in metres

d_L = as above for D_L but in terms of local or concentrated discharge—given in metres (For large rivers in alluvium $D_L = d_L$)

Q = total discharge in cumecs

q = concentrated discharge in cumecs per metre run of waterway

f = silt factor = $1.76\sqrt{m}$ where m is the weighted mean diameter of particles in mm(f varies from 0.5 for fine silt to 9.0 for coarse gravel)

Recommendations have been made to determine total scour depth based on normal scour obtained from Lacey's formula for D_L. Tables 11.4 and 11.5 give some of these correlations for Indian river conditions.

Table 11.4 Khosla Committee's Recommendations for Total Scour (Incorporated in IRS Bridge Structure Code)

Classification	Description	Total scour depth below high flood level
Class A	Straight reach	1.25 D_L
Class B	Moderate bend	1.50 D_L
Class C	Severe bend	1.75 D_L
Class D	Right-angled bend	2.00 D_L
Class E	Severe swirls	2.50 D_L

Scours classified under classes D and E are likely to occur at the nose of piers and guide banks respectively

Table 11.5 Sethi's Recommendations for Total Scour

Location of scour	Total scour depth below high flood level
Maximum scour around piers	2.00 D_L
Maximum scour at nose of curved head of guide bank-upstream	2.75 D_L
Scour along straight shanks of guide bank and tail	1.75 D_L
Portions of shank opposite pier	2.00 D_L
Scour at nose of spurs	2–2.50 D_L

(After Sethi, 1960)

Total scour by Laursen and Toch's curves

Based on laboratory experiments Laursen and Toch (1956) recommend design curves for determination of total scour below stream bed level.

Figure 11.7 shows the curve using which total scour for a rectangular pier which is aligned parallel to the direction of flow can be determined. For piers having other nose forms they propose shape coefficient K_s with which the total scour obtained for rectangular pier must be multiplied. Table 11.6 gives the shape coefficients.

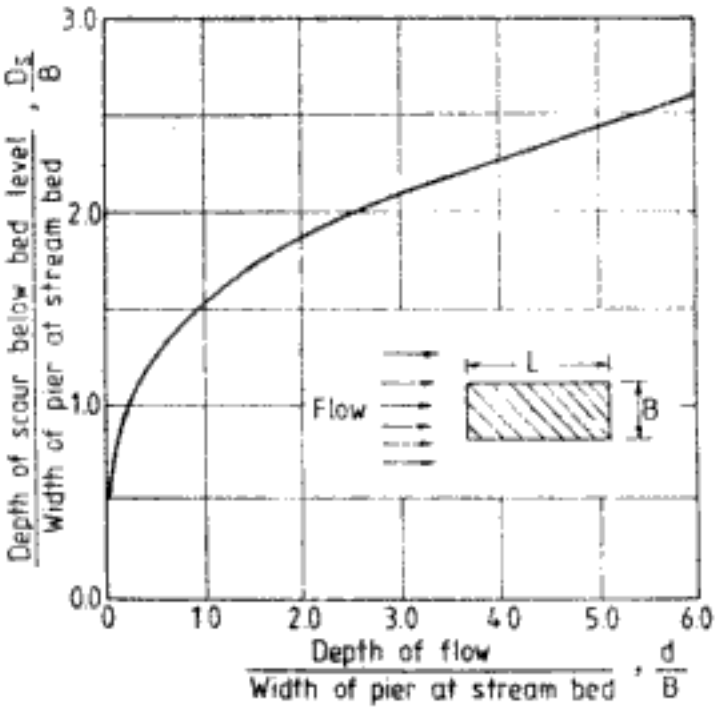

Fig. 11.7 Basic design curve for depth of total scour for a rectangular pier aligned with the flow (After Laursen and Toch, 1956)

Table 11.6 Shape Coefficients for Correcting Depth of Scour for Piers Aligned with Flow

Nose form	Length-width ratio	Shape coefficient, K_s
Rectangular	—	1.00
Semi-circular	—	0.90
Elliptic	2 : 1	0.80
Elliptic	3 : 1	0.75
Lenticular	2 : 1	0.80
Lenticular	3 : 1	0.70

(After Laursen and Toch, 1956)

For rectangular piers inclined to direction of flow Laursen and Toch recommend correction factors shown in Fig. 11.8. For inclined piers having other than rectangular nose forms in addition to correction factors for pier alignment shape coefficient given in Table 11.6 must also be applied. Q 11.1 illustrates the use of Laursen and Toch's procedure.

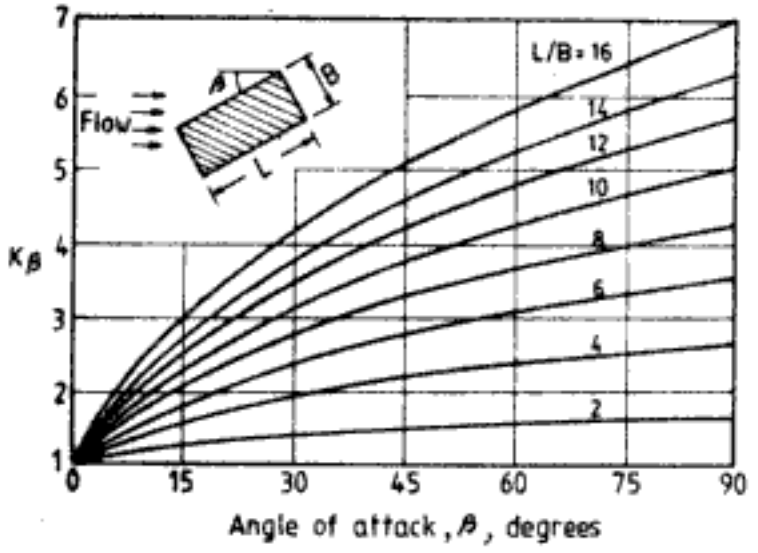

Fig. 11.8 Correction factors for depth of scour for rectangular piers inclined to the direction of flow
(After Laursen and Toch, 1956)

Q 11.1 Determine the total scour by Laursen and Toch's method given the following data:
Length of pier = 7.74 m = L
Breadth of pier = 2.81 m = B
Normal bed level below water level = 4.30 m = d
Nose form—semi-circular
$\beta = 10°$

Ans: $\dfrac{L}{B} = \dfrac{7.74}{2.81} = 2.75$

From Table 11.6, shape coefficient for semi-circular nose form, $K_s = 0.9$
From Fig. 11.8 correction factor, $K_\beta = 1.3$

$$\frac{d}{B} = \frac{4.3}{2.81} = 1.53$$

From Fig. 11.7 $\dfrac{D_s}{B} = 1.76$

Total depth of scour below normal bed level,

$$D_s = \frac{D_s}{B} B K_s K_\beta \qquad (11.4)$$

$$= 1.76 \times 2.81 \times 0.9 \times 1.3$$

$\therefore$ $D_s = 5.79$ m

11.3.3 Groundwater Level

Ordinarily shallow foundations are placed above groundwater level in order to avoid construction difficulties and to prevent uplift forces acting on foundations. Water proofing requirements can also be avoided.

11.3.4 Adjoining Structures

The foundation must lie within the boundary of the site and should not extend into adjacent property line to avoid legal disputes.

If there is a structure already in the adjacent site the foundation for the new structure can be located by the guideline explained in Fig. 11.9.

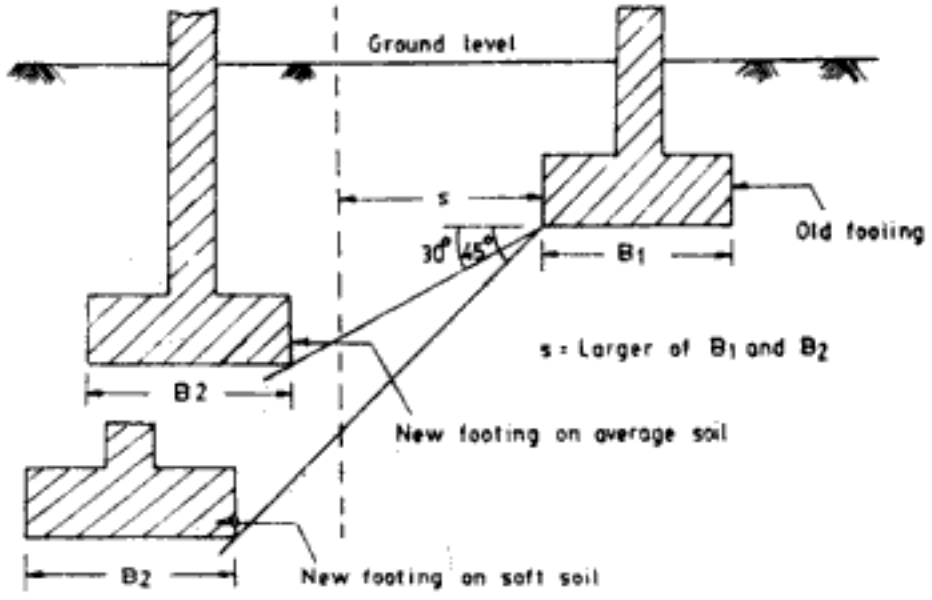

Fig. 11.9 Locating new footing adjacent to existing structure

The edge of new footing must be at a distance of minimum s away from the old footing, where s is the larger of the two footing widths. Also the depth of new footing must be such that its bottom edge should not intersect the line drawn downwards at 45° from the bottom edge of old footing in case of soft soil or the line drawn at 30° in the case of average soil. This method of location of new footing will avoid damages occurring to the existing structure.

While determining the depth and location of foundation possible construction activities in the adjacent area must also be considered. For example, if deep excavations are anticipated for a proposed adjacent high-rise construction, the foundation could be placed at a safe depth taking this into account.

For depth of footings where footings are adjacent to sloping ground or where the bottom of the footings of a structure are at different levels or at levels different from the levels of footings of adjoining structures, Indian Standard Code IS: 1904-1978 makes the following recommendations:

1. When the ground surface slopes downward adjacent to a footing, the sloping surface should not encroach upon a frustum of bearing material under the footing having sides which make an angle (θ) with the horizontal of 60° for rock and 30° for soil and the horizontal distance from the lower edge of the footing to the sloping surface (t) should be at least 60 cm for rock and 90 cm for soil.

Figure 11.10 shows this particular condition.

2. In case of footings in granular soil, a line drawn between the lower adjacent edges of adjacent footings should not have a slope steeper than two horizontal to one vertical.

Figure 11.11 explains this condition.

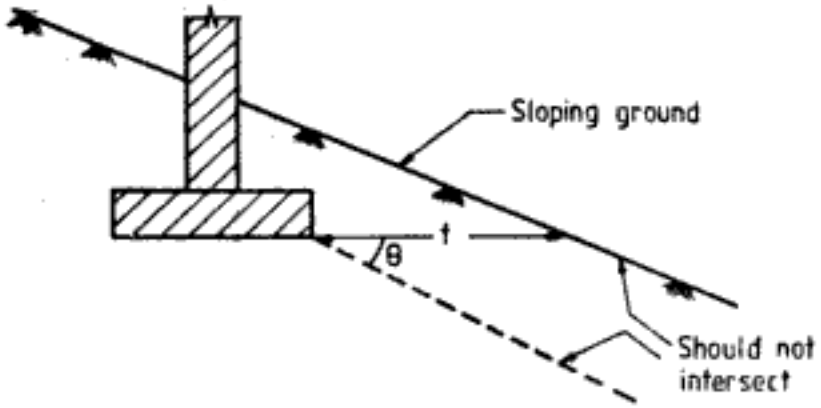

Fig. 11.10 Footing in sloping ground

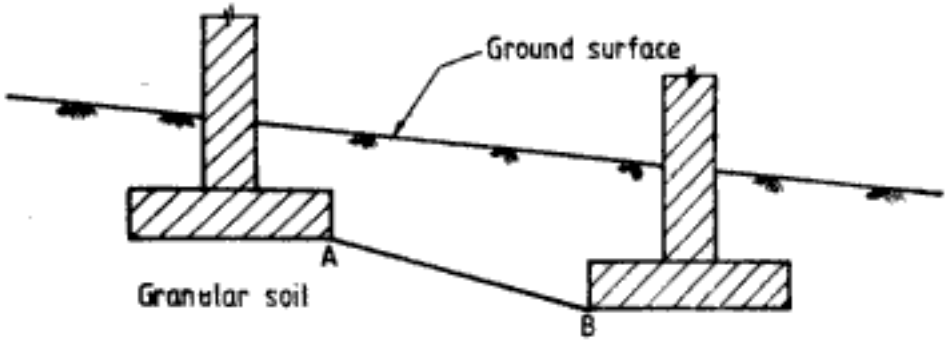

Fig. 11.11 Footings at different levels in granular soil

3. In clayey soils where the concrete or the masonry of the footings is deposited directly against the vertical sides of the excavation, a line drawn between the lower adjacent edge of the upper footing and the upper adjacent edge of the lower footing should not have a slope steeper than two horizontal to one vertical.

11.3.5 Underground Utilities and Defects

While planning the location and depth of foundation the utilities like water supply lines, sewerage lines, etc., present below ground level must be taken into account. Local municipal regulations will have stipulations regarding construction activities above these utilities. The presence of underground defects such as cavities, abandoned mines, quarries filled with earth and refuse must also be carefully considered.

12

BEARING CAPACITY OF SHALLOW FOUNDATIONS

The first of the three criteria which a properly designed foundation should satisfy is explained in Ch. 11. The second is stability criterion. That is, the foundation must be safe against soil rupture or shear failure of soil. This is also referred to as bearing capacity criterion in the sense that the foundation must have sufficient factor of safety against ultimate load bearing capacity of soil. This chapter deals with the manner of satisfying the bearing capacity criterion.

Before dealing with the procedures of obtaining ultimate bearing capacity of soils it is necessary to understand the different types of failure mechanism and the conditions which favour the occurrence of a particular type of failure mechanism. There are three types of failure mechanism. These are,

1. General shear failure
2. Punching shear failure
3. Local shear failure

The important characteristics of these patterns of failure are explained below.

12.1 TYPES OF BEARING CAPACITY FAILURE

12.1.1 General Shear Failure

The failure pattern in general shear failure for a footing at the surface of ground is shown in Fig. 12.1. Some of the important characteristics of general shear failure are:

(a) It has a well defined failure pattern.
(b) Failure is sudden and catastrophic.
(c) Failure is accompanied by tilting of foundation.
(d) There is a tendency for the soil adjacent to foundation to bulge.

Figure 12.2 shows the typical load vs. settlement diagram when general shear failure takes place. Ultimate or failure load of foundation is clearly evident.

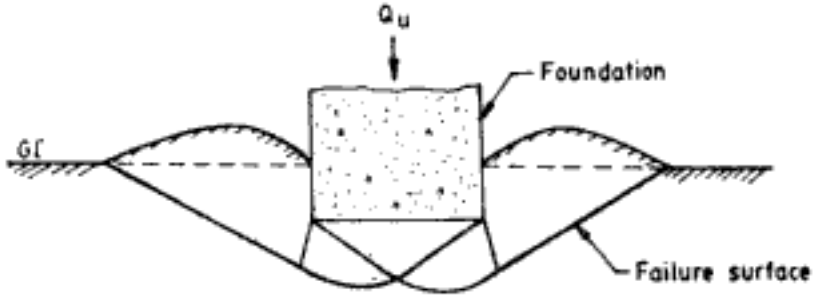

Fig. 12.1 Failure mechanism for general shear failure

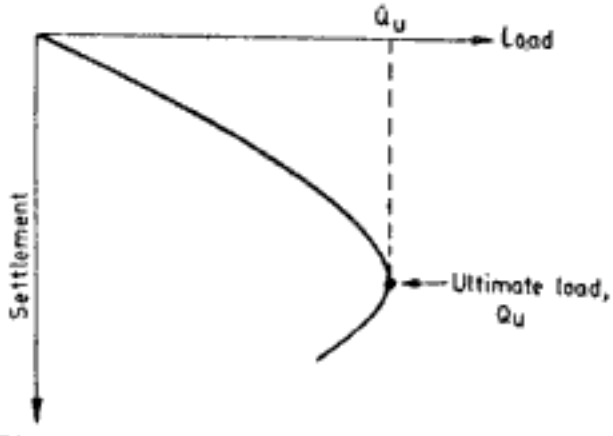

Fig. 12.2 Load-settlement diagram for general shear failure

12.1.2 Punching Shear Failure

Figure 12.3 shows the failure mechanism for punching shear failure and Fig. 12.4 shows the corresponding load-settlement curve.

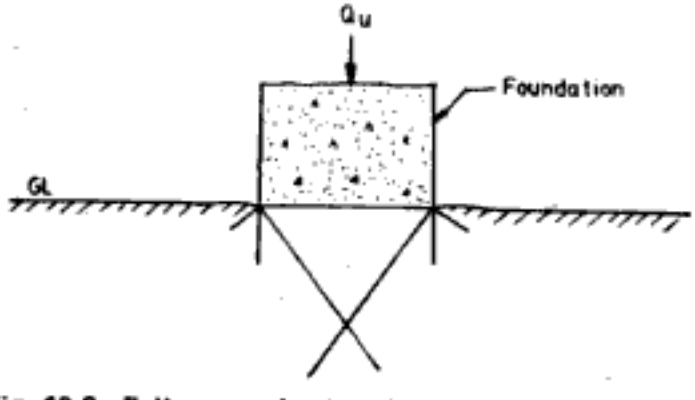

Fig. 12.3 Failure mechanism for punching shear failure

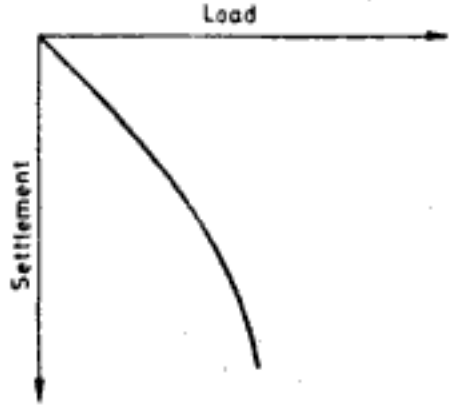

Fig. 12.4 Load-settlement diagram for punching shear failure

Characteristics of punching shear failure are as follows:

(a) Failure pattern is not easy to observe.
(b) Soil outside the loaded area is not affected.

(c) Horizontal and vertical equilibrium of footing are maintained.
(d) There is a continuous increase in vertical load with the vertical movement of footing. This means that ultimate load is not clearly discernible, as can be observed from Fig. 12.4.

12.1.3 Local Shear Failure

Figures 12.5 and 12.6 show failure mechanism and load-settlement curve respectively for local shear failure.

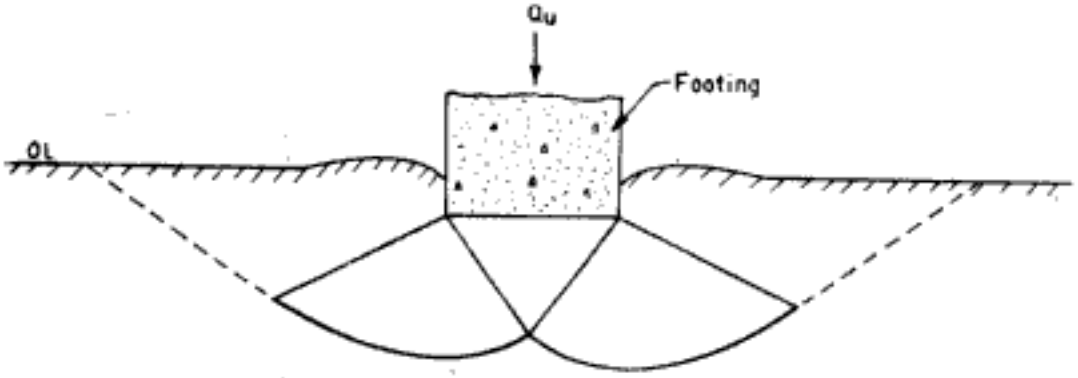

Fig. 12.5 Failure mechanism for local shear failure

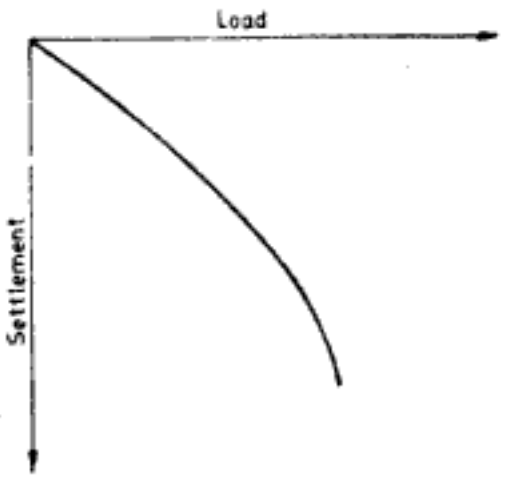

Fig. 12.6 Load-settlement diagram for local shear failure

Characteristics of local shear failure are:

(a) Failure pattern is clearly defined only immediately below the foundation.
(b) There is visible soil bulging on the sides of footing.
(c) There is no catastrophic collapse or tilting of foundation.
(d) Ultimate load is not clearly distinguishable.
(e) It is a transitional mode of failure retaining the characteristics of both general shear failure and punching shear failure.

Table 12.1 gives the conditions under which the different modes of failure can be expected to occur. Figure 12.7 (De Beer, 1970) shows the dependence of failure mechanism in sand

Table 12.1 Conditions for Modes of Failure

Under these conditions	Expect this type of shear failure
Footings on the surface or at shallow depths in very dense sand	General shear failure
Footings on saturated, normally consolidated clay under undrained loading	General shear failure
Very deep footings in dense sand	Punching shear failure
Footings on the surface or at shallow depths in loose sand	Punching shear failure
Footings on very dense sand loaded by transient dynamic loads	Punching shear failure
Footings on very dense sand underlain by loose sand or soft clay	Punching shear failure
Footings on saturated, normally consolidated clay under drained loading	Punching/local shear failure

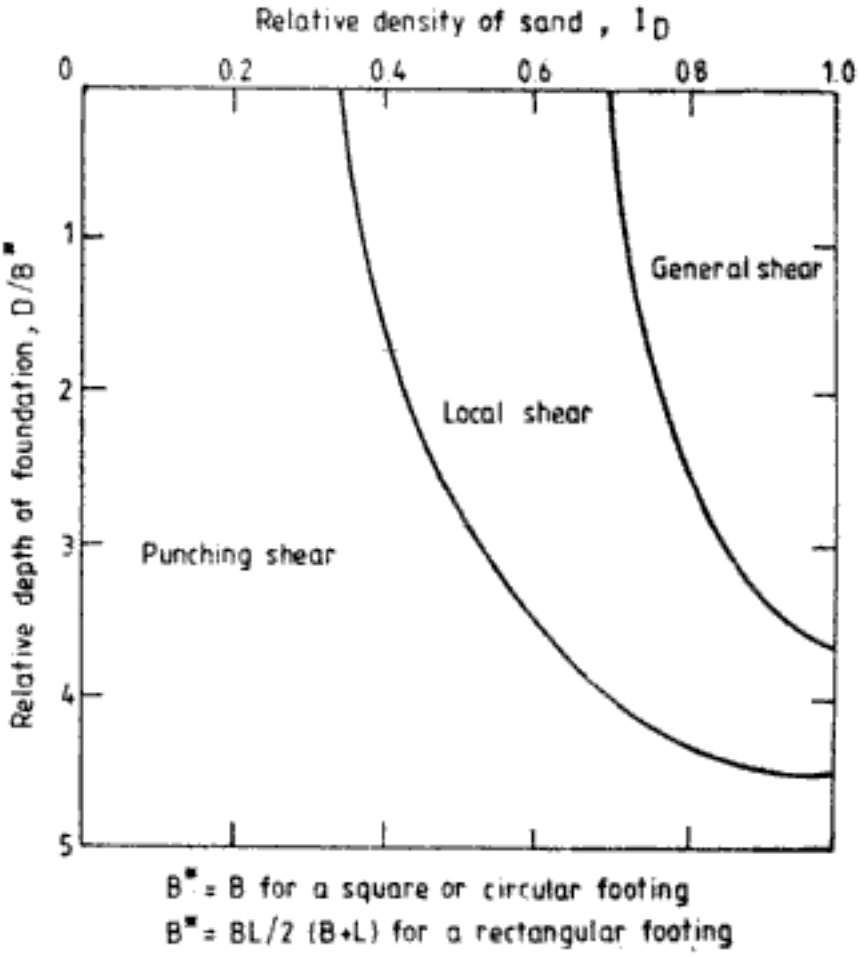

Fig. 12.7 Expected modes of failure of footings in sand (After De Beer, 1970; reprinted with permission of Institution of Civil Engineers, London)

on relative density. From this it appears that shallow foundations in very dense sand fail by general shear failure. Shallow foundations in loose sand and deep foundations irrespective of the density of sand will fail by punching shear failure. Table 12.2 gives the recommendation for expected mode of failure in cohesionless soils according to Indian Standard Code IS: 6403-1981.

Table 12.2 Mode of Failure for Cohesionless Soils

Relative density I_D	Void ratio e	Condition	Mode of failure
Greater than 70%	Less than 0.55	Dense	General shear
Less than 20%	Greater than 0.75	Loose	Local shear (as well as punching shear)
20% to 70%	0.55 to 0.75	Medium	Interpolate between dense and loose conditions

After IS: 6403-1981. Reprinted by permission of Indian Standards Institution, New Delhi

12.2 ULTIMATE BEARING CAPACITY OF SHALLOW FOUNDATIONS

Most of the procedures currently used in foundation engineering practice for the determination of ultimate bearing capacity of shallow foundations are based on *limiting equilibrium method*. In this method a feasible failure pattern in soil such as the one shown in Fig. 12.8 is assumed. The load intensity at failure called ultimate bearing capacity, q_{ult}, is then evaluated from considerations of static equilibrium of forces acting on the wedge immediately below the foundation. In this approach the following other points may also be noted.

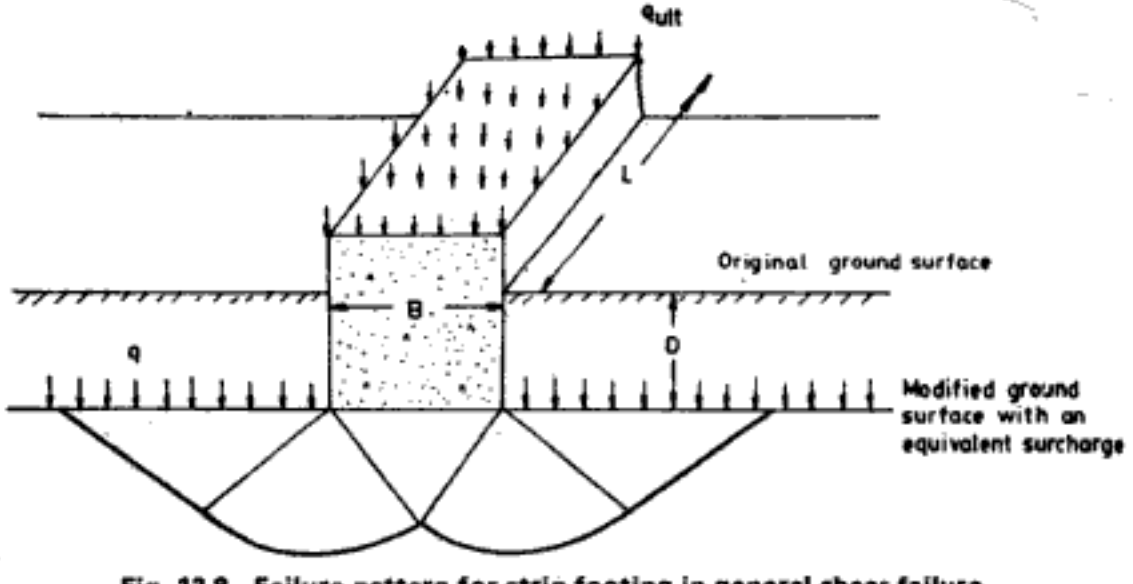

Fig. 12.8 Failure pattern for strip footing in general shear failure

1. The basic solution for ultimate bearing capacity is obtained for a strip footing under the following assumptions. The footing rests on the surface of a deep homogeneous $c - \phi$ soil. The load on the footing is vertical and concentric. The ground surface is horizontal. The footing fails in general shear failure.
2. In the basic solution for strip footing correction factors are introduced to account for deviations from assumed conditions, like shape of foundation, eccentric loading, inclined loading, nonhomogeneity of soil, slope of ground surface, presence of water table, depth of embedment, different modes of failure, etc.

Two other approaches to ultimate bearing capacity analysis are (i) *limit equilibrium method*, and (ii) *limit analysis method*. An excellent description and comparison of all the three methods is given by Chen (1975). It must be also pointed out here that analyses for ultimate bearing capacity are not perfect analyses. Very simple to immensely complex solutions are available. The analyses presented in this book, it is considered, are adequate for most of the situations encountered in practice.

12.2.1 Ultimate Bearing Capacity of Strip Footings ($L > 5B$) in General Shear Failure

Figure 12.8 shows a strip footing subjected to concentric vertical loading, at the instant of failure. The footing is embedded at depth D. To simplify analysis D is replaced by an equivalent surcharge q, where,

$$q = \text{density of soil} \times D \tag{12.1}$$

Thus the footing can be considered as a surface footing with a surcharge q, acting on the soil. The failure pattern is also shown in Fig. 12.8. The analysis for strip footing will be valid when L/B ratio is greater than 5.

Equation for ultimate bearing capacity of strip footing can be expressed as,

$$q_{ult} = cN_c + qN_q + 0.5\gamma B N_\gamma \tag{12.2}$$

where q_{ult} = ultimate bearing capacity

c = cohesion (c = cohesion intercept, $\bar{c}$ for drained condition and c = undrained shear strength, S_u for undrained conditions)

q = overburden stress at base level of foundation

γ = density of soil below the base of footing

B = width of footing

L = length of footing ($> 5B$)

N_c, N_q, N_γ = bearing capacity factors, which depend on ϕ.

A number of investigators have proposed expressions for bearing capacity factors of which a few are selectively presented here. Terzaghi (1943) gives the following equations for bearing capacity factors.

$$N_c = \cot\phi \left\{ \frac{a^2}{2\cos^2\left(\frac{\pi}{4} + \frac{\phi}{2}\right)} - 1 \right\} = (N_q - 1)\cot\phi \tag{12.3}$$

$$N_q = \frac{a^2}{2\cos^2\left(\frac{\pi}{4} + \frac{\phi}{2}\right)} \tag{12.4}$$

$$N_\gamma = \tfrac{1}{2} \tan \phi \left(\frac{K_p}{\cos^2 \phi} - 1 \right) \tag{12.5}$$

where $$a = \exp \left\{ \left(\frac{3}{4}\pi - \frac{\phi}{2} \right) \tan \phi \right\}$$

K_p = dimensionless quantity dependent on ϕ

Terzaghi's bearing capacity factors are given in Table 12.3. These factors which were once very popular are not used now due to the incorrect failure mechanism assumed for obtaining the solutions. Indian Standard Code of Practice (IS: 6403-1981) also recommends the use of bearing capacity factors which are different from those given in Table 12.3.

Table 12.3 Terzaghi's Bearing Capacity Factors

$\phi°$	N_c	N_q	N_γ	$\phi°$	N_c	N_q	N_γ
0	5.7	1.0	0.0	30	37.2	22.5	19.7
5	7.3	1.6	0.5	34	52.6	36.5	35.0
10	9.6	2.7	1.2	35	57.8	41.4	42.4
15	12.9	4.4	2.5	40	95.7	81.3	100.4
20	17.7	7.4	5.0	45	172.3	173.3	297.5
25	25.1	12.7	9.7	48	258.3	287.9	780.1

Meyerhof (1951, 1963) makes the following recommendations for bearing capacity factors:

$$N_c = (N_q - 1) \cot \phi \tag{12.6}$$

$$N_q = \exp (\pi \tan \phi) \tan^2 (45 + \phi/2) \tag{12.7}$$

$$N_\gamma = (N_q - 1) \tan (1.4\phi) \tag{12.8}$$

} *P-R-M* factors

According to Hansen (1957, 1970) the bearing capacity factors can be expressed as,

$$N_c = (N_q - 1) \cot \phi \tag{12.6}$$

$$N_q = \exp (\pi \tan \phi) \tan^2 (45 + \phi/2) \tag{12.7}$$

$$N_\gamma = 1.5(N_q - 1) \tan \phi \tag{12.9}$$

} *P-R-H* factors

According to Vesic's (1974) recommendations bearing capacity factors can be written as

$$N_c = (N_q - 1) \cot \phi \tag{12.6}$$

$$N_q = \exp (\pi \tan \phi) \tan^2 (45 + \phi/2) \tag{12.7}$$

$$N_\gamma = 2(N_q + 1) \tan \phi \tag{12.10}$$

} *P-R-C-K-V* factors

Meyerhof, Hansen and Vesic make identical recommendations for N_c and N_q. The expression for N_c is due to Prandtl (1920) and that for N_q is due to Reissner (1924). The expressions for N_γ in Eq. 12.10 are conservative simplifications of the formula due to Caquot-Kerisel. Hence Meyerhof's recommendations are herein referred to as P-R-M factors, Hansen's recommendations are referred to as P-R-H factors and those of Vesic's as P-R-C-K-V factors. The numerical values of the bearing capacity factors are tabulated in

Table 12.4. It may be noted that IS Code (IS: 6403-1981) incorporates P-R-C-K-V factors.

Table 12.4 Values of Bearing Capacity Factors in Meyerhof's, Hansen's and Vesic's Recommendations

ϕ (degrees)	N_c (Eq. 12.6)	N_q (Eq. 12.7)	N_γ in		
			Eq. 12.8	Eq. 12.9	Eq. 12.10
0	5.14	1.0	0.0	0.0	0.0
5	6.5	1.6	0.1	0.1	0.4
10	8.3	2.5	0.4	0.4	1.2
15	11.0	3.9	1.1	1.2	2.6
20	14.8	6.4	2.9	2.9	5.4
25	20.7	10.7	6.8	6.8	10.9
26	22.2	11.9	8.0	7.9	12.6
28	25.8	14.7	11.2	10.9	16.7
30	30.1	18.4	15.7	15.1	22.4
32	35.5	23.2	22.0	20.8	30.2
34	42.2	29.4	31.1	28.8	41.0
36	50.6	37.8	44.5	40.1	56.4
38	61.4	48.9	64.0	56.2	78.0
40	75.3	64.2	93.7	79.5	109.4
45	133.9	134.9	262.8	200.8	270.0
50	266.9	319.1	874.0	563.6	763.0

12.2.2 Correction for Depth of Water Table

According to Vesic if the highest level of water table is permanently below the base of the footing such that $z_w \geqslant B$ (Fig. 12.9), the value of γ in the bearing capacity equation (Eq. 12.2) should be taken as $\gamma = \gamma_m$, where γ_m is the moist density of soil corresponding to the minimum moisture content of the soil above the water table.

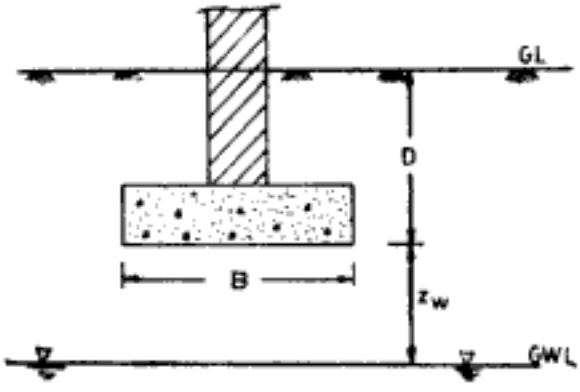

Fig. 12.9 Effect of water table on bearing capacity

If the highest groundwater level is always below the base of the footing such that $z_w \leqslant B$, then

$$\gamma = \gamma_b + \left\{\left(\frac{z_w}{B}\right)(\gamma_m - \gamma_b)\right\} \tag{12.11}$$

where, γ_b is the submerged or buoyant density of soil.

For water table at or above the level of foundation base $\gamma = \gamma_b$.

Q 12.1: To find the ultimate bearing capacity of a 2 m wide strip footing, embedded 1 m in dry dense sand. Density of dry sand, $\gamma_d = 1.8$ T/cu.m; $\bar{\phi} = 40°$; $\bar{c} = 0$.

Ans: Since the footing is in dry sand effective stress parameters $\bar{c}$ and $\bar{\phi}$ are used in the bearing capacity equation.

$$q_{ult} = qN_q + 0.5\gamma BN_\gamma \qquad (\text{since } \bar{c} = 0)$$
$$q = \gamma_d D = 1.8 \times 1 = 1.8 \text{ T/sq.m}$$

For γ in the equation use $\gamma_d (= 1.8$ T/cu.m) since the soil is dry.
Choosing appropriate N_q and N_γ values for the different solutions:

$q_{ult} = 1.8 \times 81.3 + 0.5 \times 1.8 \times 2 \times 100.4 = 327$ T/sq.m (according to Terzaghi)
$q_{ult} = 1.8 \times 64.2 + 0.5 \times 1.8 \times 2 \times 93.7 = 284$ T/sq.m (according to P-R-M)
$q_{ult} = 1.8 \times 64.2 + 0.5 \times 1.8 \times 2 \times 79.5 = 259$ T/sq.m (according to P-R-H)
$q_{ult} = 1.8 \times 64.2 + 0.5 \times 1.8 \times 2 \times 109.4 = 312$ T/sq.m (according to P-R-C-K-V)

Q 12.2: To find the ultimate bearing capacity of the footing in Q 12.1 when the groundwater level is present at 0.5 m below the ground surface. Saturated density of sand = 2 T/cu.m.

Ans: Since the drainage occurs very fast in sand, effective stress parameters $\bar{c}$ and $\bar{\phi}$ are used in the bearing capacity equation ($\bar{c} = 0$).

In the calculation of q, $D = 1$ m will be considered in two parts. Top 0.5 m is above groundwater level (assumed dry) with a density of 1.8 T/cu.m. The lower 0.5 m is submerged and has a buoyant density of 1 T/cu.m.

$$q = 0.5 \times 1.8 + 0.5 \times 1 = 1.4 \text{ T/sq. m}$$

For γ in the bearing capacity equation (Eq. 12.2), use $\gamma_b (= 1$ T/cu.m) since the groundwater level is above the base of the footing.

Using appropriate N_q and N_γ values:

$q_{ult} = 1.4 \times 81.3 + 0.5 \times 1 \times 2 \times 100.4 = 214$ T/sq.m (according to Terzaghi)
$q_{ult} = 1.4 \times 64.2 + 0.5 \times 1 \times 2 \times 93.7 = 184$ T/sq.m (according to P-R-M)
$q_{ult} = 1.4 \times 64.2 + 0.5 \times 1 \times 2 \times 79.5 = 169$ T/sq.m (according to P-R-H)
$q_{ult} = 1.4 \times 64.2 + 0.5 \times 1 \times 2 \times 109.4 = 199$ T/sq.m (according to P-R-C-K-V)

Note: The above solutions (to Qs 12.1 and 12.2) using Meyerhof's and Hansen's recommendations are not exact. When the footing is embedded in the ground they recommend to include depth factors. The same examples are solved in Q 12.4 using these depth factors.

Q 12.3: To find the ultimate bearing capacity of a 1.5 m wide strip footing, embedded 1 m in saturated clay under four different conditions given below.

$$S_u = 8 \text{ T/sq. m}, \quad \bar{c} = 1 \text{ T/sq. m}, \quad \bar{\phi} = 25°$$
$$\gamma_{sat} = 1.8 \text{ T/cu.m}$$

(a) q_{ult} under undrained conditions of loading and when groundwater table is very deep below the base of the footing.
(b) q_{ult} under drained conditions of loading and groundwater table is located very deep below footing.
(c) q_{ult} under undrained conditions of loading and groundwater is at 0.5 m below ground surface.
(d) q_{ult} under drained conditions of loading and groundwater is at 0.5 m below ground surface.

Ans: (a) Under undrained conditions of loading $\phi = 0$. The equation for bearing capacity (Eq. 12.2) reduces to

$$q_{ult} = cN_c + q \qquad \because \quad N_\gamma = 0 \text{ and } N_q = 1 \text{ in all solutions}$$
$$q = \gamma D = 1.8 \times 1 = 1.8 \text{ T/sq.m}$$
$$c = S_u = 8 \text{ T/sq.m}$$

Using appropriate bearing capacity factors

$q_{ult} = 8 \times 5.7 + 1.8 = 47$ T/sq.m (according to Terzaghi)
$q_{ult} = 8 \times 5.14 + 1.8 = 43$ T/sq.m (according to P-R-M, P-R-H, and P-R-C-K-V)

(b) Under drained conditions of loading effective stress parameters $\bar{c}$ and $\bar{\phi}$ are used.

$$q_{ult} = \bar{c}\, N_c + qN_q + 0.5\gamma BN_\gamma$$

N_c, N_q, and N_γ are chosen for $\bar{\phi} = 25°$

$$\gamma = \gamma_{sat}$$
$q_{ult} = 1 \times 25.1 + 1.8 \times 1 \times 12.7 + 0.5 \times 1.8 \times 1.5 \times 9.7$
$= 61$ T/sq.m (according to Terzaghi)
$q_{ult} = 1 \times 20.7 + 1.8 \times 1 \times 10.7 + 0.5 \times 1.8 \times 1.5 \times 6.8$
$= 49$ T/sq.m (according to P-R-M and P-R-H)
$q_{ult} = 1 \times 20.7 + 1.8 \times 1 \times 10.7 + 0.5 \times 1.8 \times 1.5 \times 10.9$
$= 55$ T/sq.m (according to P-R-C-K-V)

(c) Same as (a) but to account for groundwater level

$$\phi = 0$$
$q_{ult} = cN_c + q \qquad c = S_u = 8$ T/sq.m
$q = 1.8 \times 0.5 + 0.8 \times 0.5 = 1.3$ T/sq.m
$q_{ult} = 8 \times 5.7 + 1.3 = 47$ T/sq.m (according to Terzaghi)
$q_{ult} = 8 \times 5.14 + 1.3 = 42$ T/sq.m (according to P-R-M, P-R-H and P-R-C-K-V)

(d) Same as (b) but to account for groundwater level

$$q_{ult} = \bar{c}N_c + qN_q + 0.5\gamma BN_\gamma$$
$q = 1.3$ T/sq.m; $\gamma = \gamma_b = 0.8$ T/cu.m
$q_{ult} = 1 \times 25.1 + 1.3 \times 12.7 + 0.5 \times 0.8 \times 1.5 \times 9.7$
$= 47$ T/sq.m (according to Terzaghi)
$q_{ult} = 1 \times 20.7 + 1.3 \times 10.7 + 0.5 \times 0.8 \times 1.5 \times 6.8$
$= 39$ T/sq.m (according to P-R-M, and P-R-H)

$$q_{ult} = 1 \times 20.7 + 1.3 \times 10.7 + 0.5 \times 0.8 \times 1.5 \times 10.9$$
$$= 41 \text{ T/sq.m} \quad \text{(according to P-R-C-K-V)}$$

Note: The depth factors recommended by Meyerhof, and Hansen have not been used in P-R-M, P-R-H solutions.

12.2.3 Correction for Eccentricity of Load

When the load on the footing is acting eccentrically, to compute the ultimate bearing capacity the footing dimensions are modified such that the load is concentric to the modified dimensions of footing. The modified dimensions are taken as effective dimensions in the calculation of bearing capacity.

Strip footings: The eccentricity, e_B, is in the direction of the width of the footing (Fig. 12.10). Modified effective width of footing $= B' = B - 2e_B$.

Rectangular footings: In rectangular footing there can be eccentricity only along width (e_B) or only in the direction of length (e_L) or in the direction of both width and length (e_B and e_L), as shown in Fig. 12.11.

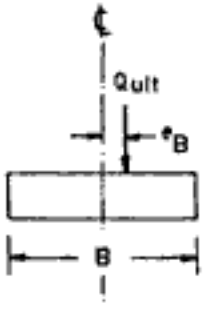

Fig. 12.10 Eccentric load on strip footing

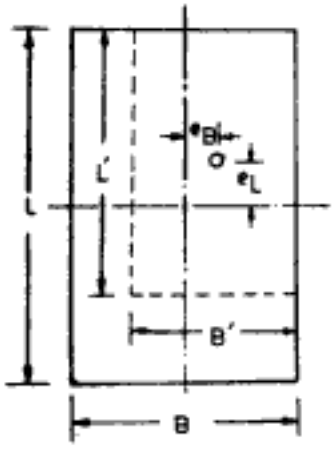

Fig. 12.11 Eccentric load on rectangular footing

Modified effective dimensions are:

$$L' = L - 2e_L; \qquad B' = B - 2e_B$$

When there is no eccentricity

$$L' = L; \qquad B' = B$$

12.2.4 Correction Factors for Shape of Footings, Depth of Embedment and Load Inclination

The expression for bearing capacity of strip footing is now modified as follows:

$$q_{ult} = cN_c S_c d_c i_c + qN_q S_q d_q i_q + 0.5\gamma B N_\gamma S_\gamma d_\gamma i_\gamma \qquad (12.12)$$

The above equation is applicable for all values of ϕ according to Meyerhof, and Vesic, but only for $\phi > 0$ according to Hansen. For $\phi = 0$, Hansen gives,

$$q_{ult} = cN_c(1 + S_c + d_c - i_c) + q \qquad \text{(for } \phi = 0, \text{ according to Hansen)} \qquad (12.13)$$

In Eqs 12.12 and 12.13

S_c, S_q, S_γ = shape factors

d_c, d_q, d_γ = depth of embedment factors

i_c, i_q, i_γ = inclination factors

The correction factors recommended by Meyerhof, Hansen, and Vesic are given in Tables 12.5, 12.6 and 12.7 respectively. Vesic's factors are much more comprehensive and exhaustive. Hence Vesic's factors are recommended for use in the solution of problems. The correction factors of Meyerhof, Hansen and Vesic must be used with their respective recommendations for bearing capacity factors, namely with P-R-M, P-R-H, and P-R-C-K-V factors respectively.

Q. 12.4: To solve Q 12.1 to Q 12.3 by Meyerhof's, and Hansen's methods using depth factors.

Ans: Q. 12.1 In this case $q_{ult} = qd_qN_q + 0.5\gamma BN_\gamma d_\gamma$

According to Meyerhof (Table 12.5) : $d_q = 1.11$ $d_\gamma = 1$

According to Hansen (Table 12.6): $d_q = 1.07$ $d_\gamma = 1$

Using these correction factors,

$q_{ult} = 297$ T/sq.m (according to Meyerhof) against the figure of 284 T/sq.m in Q 12.1 without depth correction factors

$q_{ult} = 267$ T/sq.m (according to Hansen) against the value of 259 T/sq.m in Q 12.1 without depth correction factors

Q 12.2

$q_{ult} = qN_qd_q + 0.5\gamma BN_\gamma d_\gamma$

$d_q = 1.11$ $d_\gamma = 1$ according to Meyerhof

$d_q = 1.07$ $d_\gamma = 1$ according to Hansen

Table 12.5 Meyerhof's Correction Factors

Factor	Value or expression	
S_c	$1 + 0.2 \tan^2(45 + \phi/2)\frac{B'}{L'}$	
S_q, S_γ	$1 + 0.1 \tan^2(45 + \phi/2)\frac{B'}{L'}$	for $\phi > 10°$
	1 for $\phi = 0°$	
d_c	$1 + 0.2 \tan(45 + \phi/2)\frac{D}{B'}$	
d_q, d_γ	$1 + 0.1 \tan(45 + \phi/2)\frac{D}{B'}$	for $\phi > 10°$ and $D \leqslant B$
	1 for $\phi = 0°$ and $D \leqslant B$	
i_c, i_q	$\left(1 - \frac{\alpha}{90^2}\right)^2$ α in degrees	
	$\alpha = \tan^{-1}(H/V)$	
i_γ	$\left(1 - \frac{\alpha}{\phi}\right)^2$	

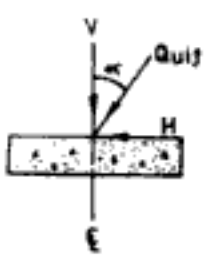

Table 12.6 Hansen's Correction Factor

Factor	Value or expression
S_c	$0.2i_c \frac{B'}{L'}$ for $\phi = 0$
	$0.2(1 - 2i_c)(B'/L')$ for $\phi > 0$
S_q	$1 + i_q(B'/L') \sin \phi$
S_γ	$1 - 0.4i_\gamma(B'/L')$
d_c	$0.4(D/B)$ for $D \leqslant B$ and $\phi = 0$
	$0.4 \tan^{-1}(D/B)$ for $D > B$ and $\phi = 0$
	$1 + 0.4(D/B)$ for $D \leqslant B$ and $\phi > 0$
	$1 + 0.4 \tan^{-1}(D/B)$ for $D > B$ and $\phi > 0$
d_q	$1 + 2 \tan \phi(1 - 2 \sin \phi)^2(D/B)$ for $D \leqslant B$
	$1 + 2 \tan \phi(1 - \sin \phi)^2 \tan^{-1}(D/B)$ for $D > B$
d_γ	1
i_c	$1 - \{H/(2B'L'c)\}$ for $\phi = 0$ — For V and H see figure in Table 12.5
	$0.5\{1 + [(1 - H)/(B'L'S_u)]^{1/2}\}$ for $\phi = 0$
i_q	$\{1 - [0.5H/(V + B'L'c \cot \phi)]\}^5$
i_γ	$\{1 - [0.7H/(V + B'L'c \cot \phi)]\}^5$

Table 12.7 Vesic's Correction Factors

Factor	Value or expression	
S_c	$1 + (B/L)(N_q/N_c)$ for rectangle	
	$1 + (N_q/N_c)$ for circle, square	
S_q	$1 + (B/L) \tan \phi$ for rectangle	
	$1 + \tan \phi$ for circle, square	
S_γ	$1 - 0.4\,(B/L)$ for rectangle	
	0.6 for circle, square	
d_c, d_q, d_γ	1	
i_c	$i_q - [(1 - i_q)/N_c \tan \phi]$ for $\phi > 0$	$m = m_B = \dfrac{2 + (B/L)}{1 + (B/L)}$
	$1 - [mH/(B'L' S_u N_c)]$ for $\phi = 0$	for inclination in direction of B
i_q	$\{1 - [H/(V + B'L' c \cot \phi)]\}^m$	$m = m_L = \dfrac{2 + (L/B)}{1 + (L/B)}$
i_γ	$\{1 - [H/(V + B'L' c \cot \phi)]\}^{m+1}$	for inclination in direction of L.
	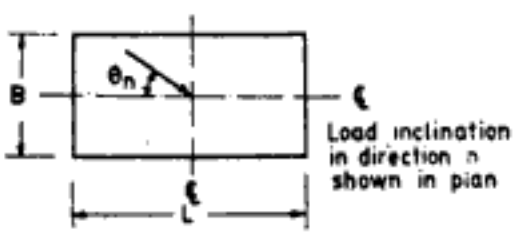 Load inclination in direction n shown in plan	For load inclination in direction n, making angle θ_n with the direction of L: $m = m_n = m_L \cos^2\theta_n + m_B \sin^2 \theta_n$

For V and H see figure in Table 12.5

Using these correction factors,

$q_{ult} = 287$ T/sq.m (according to Meyerhof) against the value of 277 T/sq.m in Q 12.2

$q_{ult} = 255$ T/sq.m (according to Hansen) against the value of 249 T/sq.m in Q 12.2

Q 12.3 (a) $q_{ult} = cN_c d_c + qN_q d_q$ according to Meyerhof

$d_c = 1.133 \quad d_q = 1$

Using these values,

$q_{ult} = 48$ T/sq.m according to Meyerhof against 43 T/sq. m in Q 12.3a

$q_{ult} = cN_c(1 + d_c) + q$ (for $\phi = 0$ according to Hansen, Eq. 12.13)

$d_c = 0.27$

$\therefore\ q_{ult} = 54$ T/sq.m according to Hansen, against the value of 43 T/sq.m in Q 12.3a.

(b) $q_{ult} = cN_c d_c + qN_q d_q + 0.5\gamma BN_\gamma d_\gamma$

$d_c = 1.157 \quad d_q = 1.078 \quad d_\gamma = 1$ according to Meyerhof

$d_c = 1.27 \quad d_q = 1.01 \quad d_\gamma = 1$ according to Hansen

Using the above values,

$q_{ult} = 54$ T/sq.m according to Meyerhof, against the figure of 49 T/sq.m in Q 12.3b

$q_{ult} = 60$ T/sq.m according to Hansen, against the value of 49 T/sq.m in Q 12.3b

(c) $q_{ult} = cN_c d_c + qN_q d_q$ according to Meyerhof

$d_c = 1.133 \quad d_q = 1$

$\therefore\ q_{ult} = 48$ T/sq.m against the value of 42 T/sq.m in Q 12.3c

$q_{ult} = cN_c(1 + d_c) + q$ according to Hansen

$d_c = 0.27$

$\therefore\ q_{ult} = 53$ T/sq.m against the value of 42 T/sq.m in Q 12.3c

(d) $q_{ult} = cN_c d_c + qN_q d_q + 0.5\gamma BN_\gamma d_\gamma$

$d_c = 1.157 \quad d_q = 1.078 \quad d_\gamma = 1$ according to Meyerhof

$d_c = 1.27 \quad d_q = 1.01 \quad d_\gamma = 1$ according to Hansen

Using these values of depth factors

$q_{ult} = 43$ T/sq.m according to Meyerhof, against the value of 39 T/sq.m in Q 12.3d

$q_{ult} = 44$ T/sq.m according to Hansen, against the value of 39 T/sq.m in Q 12.3d

Q 12.5: To find the ultimate bearing capacity of a rectangular footing ($L \times B = 3$ m $\times 1.5$ m) embedded 1 m in saturated clay. The loading is drained vertical loading and $\bar{c} = 1$ T/sq.m, $\bar{\phi} = 25°$. The saturated density of soil is 1.8 g/cc. The groundwater is at 0.5 m below ground surface. (Same as Q 12.3d, but rectangular footing.)

Ans: According to Vesic, from Eq. 12.12 and Table 12.7

$$q_{ult} = cN_c S_c + qN_q S_q + 0.5\gamma BN_\gamma S_\gamma$$

$$S_c = 1 + \left(\frac{1.5}{3}\right)\left(\frac{10.7}{20.7}\right) = 1.26$$

$$S_q = 1 + \left(\frac{1.5}{3}\right)\tan 25° = 1.233$$

$$S_\gamma = 1 - 0.4\left(\frac{1.5}{3}\right) = 0.8$$

Using these shape factors

$$q_{ult} = 1\times 20.7\times 1.26 + 1.3\times 10.7\times 1.233 + 0.5\times 0.8\times 1.5\times 10.9\times 0.8$$
$$= 48 \text{ T/sq.m}$$

Q. 12.6: To compute the ultimate bearing capacity of a rectangular footing of sides 1.75 m × 3.5 m when a load inclined at an angle of 10° to vertical acts on the footing. The footing is embedded 1 m below ground level and the groundwater is very deep below the footing. The soil is saturated and has a density of $\gamma_{sat} = 1.8$ g/cc. The rate of loading is very slow and drained conditions prevail. $\bar{c} = 1$ T/sq.m; $\bar{\phi} = 25°$. To compute the ultimate bearing capacity when,

(a) the load is eccentric in the direction of B by 10 cm and is inclined away from the centre in the direction of B;
(b) the load is eccentric in the direction of L by 15 cm and is inclined away from the centre in the direction of B;
(c) the load is eccentric in the direction of B by 10 cm, in the direction of L by 15 cm and is inclined towards the nearest corner of the footing.

Ans: Vesic's method is used in the solution. Correction factors are adopted from Table 12.7. Ultimate bearing capacity, q_{ult} is (Eq. 12.12)

$$q_{ult} = cN_cS_ci_cd_c + qN_qS_qi_qd_q + 0.5\gamma B'N_\gamma S_\gamma i_\gamma d_\gamma$$
$$c = \bar{c} = 1 \text{ T/sq.m} \qquad \text{Effective stress parameters are used}$$
$$\phi = \bar{\phi} = 25° \qquad \text{since drained conditions prevail}$$

From Table 12.4

$$N_c = 20.7; \qquad N_q = 10.7; \qquad N_\gamma = 10.9$$
$$q = 1.8 \text{ T/sq.m}; \quad \gamma = \gamma_{sat} = 1.8 \text{ T/cu. m}$$

From Table 12.7

$$S_c = 1 + \left(\frac{1.75}{3.5}\right)\left(\frac{10.7}{20.7}\right) = 1.26$$

$$S_q = 1 + \left(\frac{1.75}{3.5}\right)\tan 25° = 1.233$$

$$S_\gamma = 1 - 0.4\left(\frac{1.75}{3.5}\right) = 0.8$$

$$d_c = d_q = d_\gamma = 1$$

$$\therefore \qquad q_{ult} = 26.08i_c + 23.75i_q + 7.85B'i_\gamma$$

(a) *Inclination in the direction of B (Fig. 12.12)*

$$e_B = 10 \text{ cm (Fig. 12.11)}$$
$$B' = 1.75 - 0.2 = 1.55 \text{ m}$$
$$q_{ult} = 26.08i_c + 23.75i_q + 12.16i_\gamma$$

Area of foundation, $A_f = B' \times L'$
$$= 1.55\times 3.5 = 5.425 \text{ sq.m}$$

The inclination factors i_c, i_q, i_γ are functions of vertical and horizontal loads (V and H respectively) which in turn depend on q_{ult}. Hence q_{ult} is solved by trial and error.

$$V = q_{ult} \times A_f$$

$$H = V \tan \alpha$$

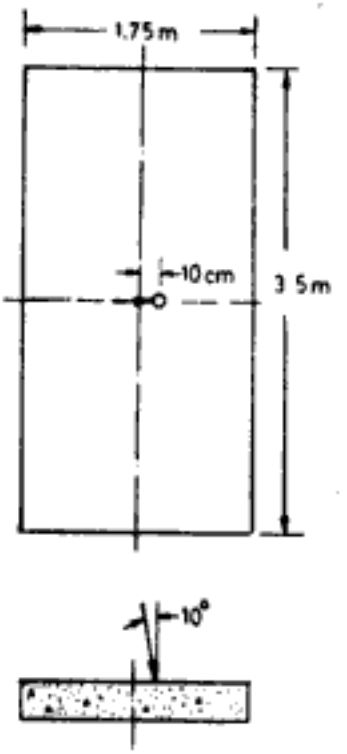

Fig. 12.12 Load inclination in the direction of B

But the maximum value of H is limited to $(cA_f + V \tan \phi)$.
Thus when $\alpha < \phi$, $V \tan \alpha$ is always less than $(cA_f + V \tan \phi)$.

I Trial: Assume $i_c = i_q = i_\gamma = 1$ (i.e., assuming no inclination)

$$\therefore \qquad q_{ult} = 26.08 + 23.75 + 12.16 = 62 \text{ T/sq.m}$$

i_c, i_q, and i_γ can now be evaluated using this value of q_{ult} to find V and H. By reiteration q_{ult} value can be obtained. As it is evident that the value of all the inclination factors are less than 1, for faster convergence of results even to begin with a value of q_{ult} less than 62 T/sq.m can be assumed.

$$q_{ult} = 50 \text{ T/sq.m, say}$$

$$\therefore \qquad V = 50 \times 5.425 = 271.25 \text{ T}$$

$$H = 271.25 \tan 10° = 48 \text{ T}$$

$$m = m_B = \frac{2 + (1.75/3.5)}{1 + (1.75/3.5)} = 1.67$$

$$i_q = \left(1 - \frac{48}{271.25 + 5.425 \times 1 \times \cot 25°}\right)^{1.67} = 0.733$$

$$i_c = 0.733 - \frac{1 - 0.733}{20.7 \tan 25°} = 0.70$$

$$i_\gamma = \left(1 - \frac{48}{271.25 + 5.425 \times 1 \times \cot 25°}\right)^{2.67} = 0.61$$

Substituting these values of inclination factors

$$q_{ult} = 26.08 \times 0.70 + 23.75 \times 0.733 + 12.16 \times 0.61 = 43 \text{ T/sq.m}$$

II Trial: Assuming $q_{ult} = 43$ T/sq.m

$$V = 43 \times 5.425 = 233 \text{ T}$$

$$H = 233 \tan 10° = 41 \text{ T}$$

Using these values of V and H in the expressions for inclination factors,

$$i_c = 0.709; \quad i_q = 0.736; \quad i_\gamma = 0.61$$

Using these factors in the bearing capacity equation,

$q_{ult} = 43$ T/sq.m (same as the assumed value in II Trial)

Hence $q_{ult} = 43$ T/sq.m

Ultimate value of inclined load $= \dfrac{V}{\cos \alpha}$

$$= \frac{43 \times 5.425}{\cos 10°}$$

$$= 237 \text{ T}$$

(b) *Inclination in the direction of L (Fig. 12.13):* The solution is similar to solution for Q 12.6a but with inclination in the direction of L.

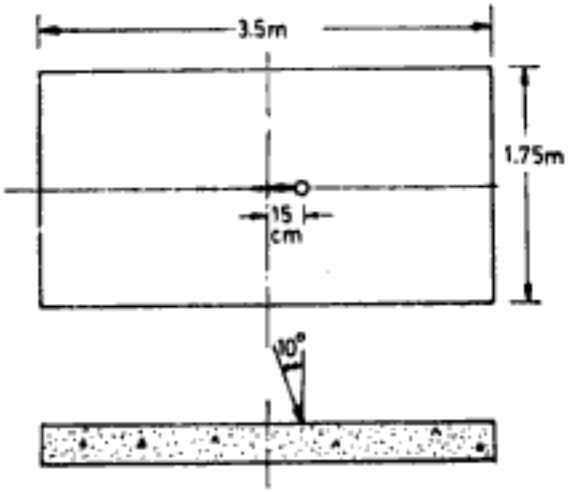

Fig. 12.13 Load inclination in the direction of L

$$e_L = 15 \text{ cm (Fig. 12.11)}$$

$$L' = 3.5 - 0.3 = 3.2 \text{ m}$$

$$A_f = 1.75 \times 3.2 = 5.6 \text{ sq.m}$$

$$B' = B = 1.75 \text{ m}$$

Using correction factors from Table 12.7 in Eq. 12.12,

$$q_{ult} = 26.08 i_c + 23.75 i_q + 13.734 i_\gamma$$

I Trial

Assuming $i_c = i_q = i_\gamma = 1$

$$q_{ult} = 26.08 + 23.75 + 13.734$$

$$= 63.56 \text{ T/sq.m}$$

Assuming $q_{ult} = 50$ T/sq.m since inclination factors are actually less than 1,

$$V = 50 \times 5.6 = 280 \text{ T}$$

$$H = 280 \tan 10^\circ = 49 \text{ T}$$

$$m = m_L = \frac{2 + (3.5/1.75)}{1 + (3.5/1.75)} = 1.33$$

Using these values in the equations for inclination factors,

$$i_c = 0.76;\ i_q = 0.783;\ i_\gamma = 0.652$$

$$\therefore \quad q_{ult} = 26.08 \times 0.76 + 23.75 \times 0.783 + 13.734 \times 0.652$$

$$= 47 \text{ T/sq.m}$$

II Trial

Assuming $q_{ult} = 47$ T/sq.m

$$V = 47 \times 5.6 = 263.2 \text{ T}$$

$$H = 263.2 \tan 10^\circ = 46 \text{ T}$$

The new values of inclination factors are:

$$i_c = 0.762;\ i_q = 0.784;\ i_\gamma = 0.653$$

Using these inclination factors,

$q_{ult} = 47$ T/sq.m (same value as assumed in II trial)

Ultimate value of inclined load $= 47 \times 5.6/\cos 10^\circ = 267$ T

(c) *Inclination towards a corner of the footing (Fig. 12.14)*: The solution is similar to solution for Q 12.6a but with inclination towards nearest corner of footing.

$$e_B = 0.1 \text{ m}; \qquad B' = 1.75 - 0.2 = 1.55 \text{ m}$$

$$e_L = 0.15 \text{ m}; \qquad L' = 3.5 - 0.3 = 3.2 \text{ m}$$

$$A_f = 3.2 \times 1.55 = 4.96 \text{ sq. m}$$

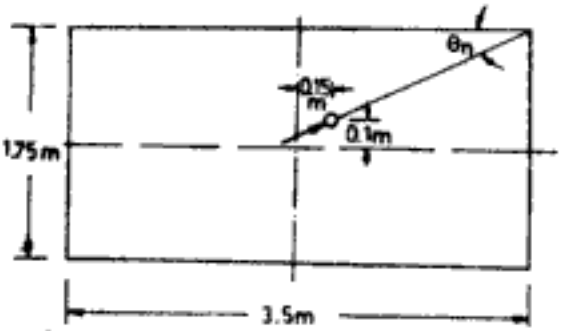

Fig. 12.14 Load inclination towards corner

Using correction factors from Table 12.7 in Eq. 12.12

$$q_{ult} = 26.08 i_c + 23.75 i_q + 12.16 i_\gamma$$

I Trial

Assuming $i_c = i_q = i_\gamma = 1$

$$q_{ult} = 26.08 + 23.75 + 12.16 = 62 \text{ T/sq.m}$$

Now assume $q_{ult} = 50$ T/sq.m

$$V = 50 \times 4.96 = 248 \text{ T}$$

$$H = 248 \tan 10^\circ = 44 \text{ T}$$

The exponent m in the evaluation of inclination factors is worked out as follows:

The value of angle θ_n which the load makes with the direction of the length of the footing is as shown in Fig. 12.14 (the load is inclined towards the nearest corner).

Thus $$\theta_n = \tan^{-1}\frac{1.55}{3.2} = 26.84^\circ$$

$$m_L = 1.33; \quad m_B = 1.67$$

Hence, $$m = m_n = 1.33\cos^2 26.84^\circ + 1.67\sin^2 26.84^\circ = 1.4$$

Using these values in the calculations for inclination factors,

$$i_c = 0.765;\ i_q = 0.77;\ i_\gamma = 0.64$$

Hence, $$q_{ult} = 26.08\times0.765 + 23.75\times0.77 + 12.16\times0.64 = 46 \text{ T/sq.m}$$

II Trial

Assuming $q_{ult} = 46$ T/sq.m

$$V = 46\times4.96 = 228 \text{ T}$$

$$H = 228\tan 10^\circ = 40 \text{ T}$$

The new values of inclination factors are,

$$i_c = 0.765;\ i_q = 0.77,\ i_\gamma = 0.64$$

Hence $q_{ult} = 46$ T/sq.m (same value as assumed in II trial)

Ultimate value of inclined load $= 46\times4.96/\cos 10^\circ = 232$ T

12.2.5 Correction Factors for Base Tilt and Ground Surface Slope

Foundation bases may be kept inclined to transmit large horizontal loads. By placing the base perpendicular to the inclined load the bearing capacity can be increased. Also cases of sloping ground surfaces are quite common. Correction factors (b_c, b_q, b_γ) for base tilt and (g_c, g_q, g_γ) for ground slope are introduced in the equation for ultimate bearing capacity.

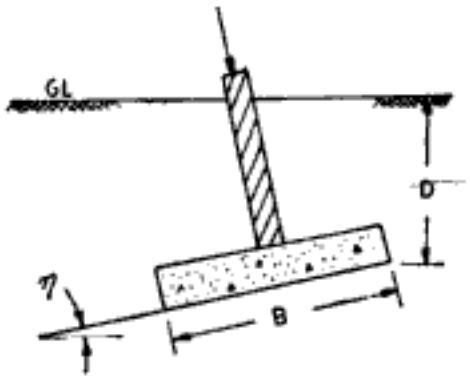

Fig. 12.15 Base tilt (η)

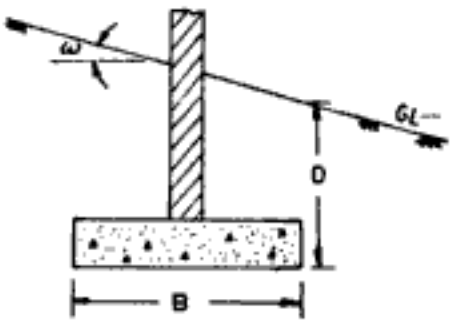

Fig. 12.16 Sloping ground surface (ω)

The resulting equation is as follows:

According to Vesic:

$$q_{ult} = cN_cS_ci_cb_cg_c + q\cos\omega N_qS_qi_qb_qg_q + 0.5\gamma BN_\gamma S_\gamma i_\gamma b_\gamma g_\gamma \qquad (12.14)$$

When $\omega > 0$ and $\phi = 0$; $N_\gamma \neq 0$ but $N_\gamma = -2\sin\omega$

Therefore, $$q_{ult} = cN_cS_ci_cb_cg_c + q\cos\omega N_qi_qb_qg_q - \gamma B\sin\omega S_\gamma i_\gamma b_\gamma g_\gamma \qquad (12.15)$$

for $\omega > 0, \phi = 0$

According to Hansen:

$$q_{ult} = cN_cS_cd_ci_cb_cg_c + qN_qS_qd_qi_qb_qg_q + 0.5\gamma BN_\gamma S_\gamma d_\gamma i_\gamma b_\gamma g_\gamma \qquad (12.16)$$

And under undrained conditions,

$$q_{ult} = cN_c(1 + S_c + d_c - i_c - b_c - g_c) + q \qquad \text{for } \phi = 0 \qquad (12.17)$$

Tilt and ground slope factors are given in Table 12.8.

Table 12.8 Expressions for Base Tilt and Ground Slope Factors

Factors	Vesic	Hansen
b_c	$b_q - [(1 - b_q)/N_c \tan \phi]$ for $\phi > 0°$ $1 - [2\eta/(\pi + 2)]$ for $\phi = 0°$ η in radians	$1 - (\eta°/147°)$ for $\phi > 0°$ $\eta°/147°$ for $\phi = 0°$
b_q	$(1 - \eta \tan \phi)^2$ η in radians	$\exp(-2\eta \tan \phi)$
b_γ	$(1 - \eta \tan \phi)^2$	$\exp(-2.7\,\eta \tan \phi)$
g_c	$g_q - [(1 - g_q)/N_c \tan \phi]$ for $\phi > 0°$ $1 - [2\omega/(\pi + 2)]$ for $\phi = 0°$ ω in radians	$1 - (\omega°/147°)$ for $\phi > 0°$ $\omega°/147°$ for $\phi = 0°$
g_q, g_γ	$(1 - \tan \omega°)^2$	$(1 - 0.5 \tan \omega°)^5$
Limits for using the factors	$\eta < 45°$; $\omega < 45°$ $\omega < \phi$ The ground slope factors may be used for $0 < \omega < \phi/2$. For $\omega > \phi/2$ an analysis of slope stability is also to be performed	$\omega \leqslant \phi$ $\eta + \omega \leqslant 90°$

Q 12.7 To compute the ultimate bearing capacity of the footing in Q 12.6 but with the footing having a base tilt of 10° to the horizontal such that the inclined load acts perpendicularly on the footing.

Ans: The equation for ultimate bearing capacity is

$$q_{ult} = cN_cS_cb_c + qN_qS_qb_q + 0.5\gamma BN_\gamma S_\gamma b_\gamma$$

since $i_c = i_q = i_\gamma = 1$ as the load is now acting normally on the footing. From Table 12.8 the base tilt factors according to Vesic are:

$$b_q = b_\gamma = (1 - \eta \tan \phi)^2 = 0.844$$

$$b_c = b_q - \left\{\frac{(1 - b_q)}{N_c \tan \phi}\right\} = 0.823$$

Using the other factors (due to Vesic) as computed in Q 12.6,

(a) $B' = 1.55$ m; $q_{ult} = 52$ T/sq.m, against the value of 43 T/sq.m computed in Q 12.6, an increase of 21% in q_{ult}.
Ultimate inclined load = 282 T (previous value 237 T)

(b) $B' = 1.75$ m; $q_{ult} = 53$ T/sq.m, against the value of 47 T/sq.m computed in Q 12.6, an increase of 13% in q_{ult}.
Ultimate inclined load = 297 T (previous value 267 T).

(c) $B' = 1.55$ m; $q_{ult} = 52$ T/sq.m, against the value of 46 T/sq.m in Q 12.6, an increase of 13% in q_{ult}.
Ultimate inclined load = 258 T (previous value 232 T)

Q 12.8. To compute the ultimate bearing capacity of the footing shown in Fig. 12.17. The other data are as below:

$$L \times B = 2 \text{ m} \times 3 \text{ m}; \qquad D = 1 \text{ m}$$
$$\bar{c} = 0.5 \text{ T/m}^2; \qquad \bar{\phi} = 30°$$
$$\gamma_{sat} = 1.9 \text{ g/cc}$$

Ground slope, $\omega = 10°$

The soil is saturated and the loading corresponds to drained conditions. The watertable is very deep below the ground surface.

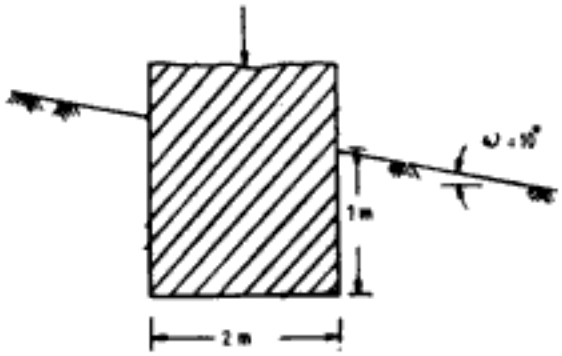

Fig. 12.17 Q 12.8

Ans: Vesic's factors from Tables 12.4, 12.7 and 12.8 are used in the solution. The equation for ultimate bearing capacity in this case is,

$$q_{ult} = cN_cS_cg_c + qN_qS_qg_q + 0.5\gamma BN_\gamma S_\gamma g_\gamma$$

for $\phi = 30°$; $N_c = 30.1$, $N_q = 18.4$, $N_\gamma = 22.4$

$$S_c = 1 + \left(\frac{2}{3}\right)\left(\frac{18.4}{30.1}\right) = 1.408$$

$$S_q = 1 + \left(\frac{2}{3}\right) \tan 30° = 1.385$$

$$S_\gamma = 1 - 0.4\left(\frac{2}{3}\right) = 0.733$$

$$g_q = g_\gamma = (1 - \tan 10°)^2 = 0.678$$

$$g_c = 0.678 - \frac{1 - 0.678}{30.1 \tan 30°} = 0.66$$

$$q = 1 \times 1.9 = 1.9 \text{ T/m}^2$$

Using these values in the equation for bearing capacity

$$q_{ult} = 68 \text{ T/m}^2$$

Q 12.9: To compute the ultimate bearing capacity of the footing in Q 12.8 when it has a tilt of 5° as shown in Fig. 12.18.

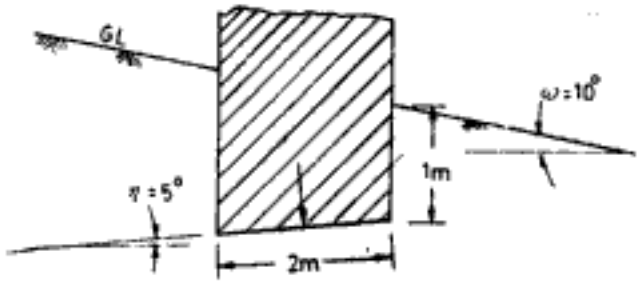

Fig. 12.18. Q 12.9

Ans: The equation for ultimate bearing capacity in this case is,

$$q_{ult} = cN_cS_cg_cb_c + qN_qS_qg_qb_q + 0.5\gamma BN_\gamma S_\gamma g_\gamma b_\gamma$$

From Table 12.8 the values for base tilt factors according to Vesic are,

$$b_q = b_\gamma = \left(1 - 5\frac{\pi}{180}\tan 30°\right)^2 = 0.902$$

$$b_c = 0.902 - \frac{1 - 0.902}{30.1\tan 30°} = 0.896$$

Using these and other values computed in Q 12.8 the ultimate bearing capacity is

$$q_{ult} = 75\ \text{T/m}^2$$

12.2.6 Indian Standard Code Recommendations for Ultimate Bearing Capacity of Shallow Foundations

As per IS: 6403-1981 the equation for ultimate bearing capacity of shallow foundations in general shear failure is:

$$q_{ult} = cN_cS_cd_ci_c + qN_qS_qi_qd_q + 0.5\gamma B'N_\gamma S_\gamma d_\gamma i_\gamma W' \qquad (12.18)$$

where W' = factor which takes into account the influence of watertable as explained below

$W' = 1$, if the watertable is likely to remain permanently at or below a depth of $(D + B)$ beneath the ground level surrounding the footing (i.e., $z_w \geqslant B$ in Fig. 12.19)

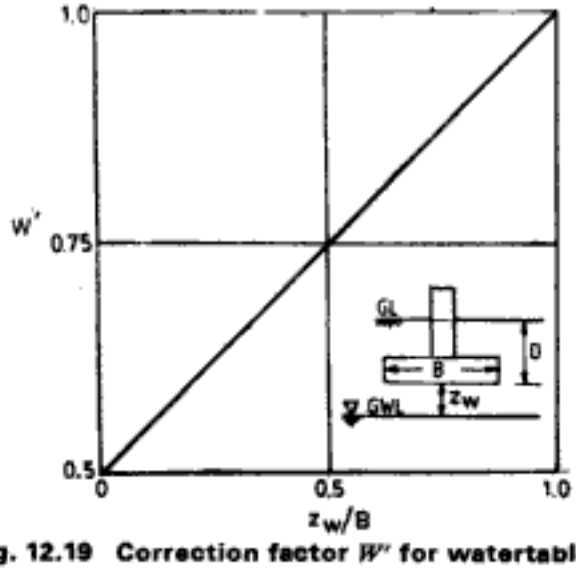

Fig. 12.19 Correction factor W' for watertable

W' = 0.5, if the watertable is located at a depth D or likely to rise to the base of the footing or above

W' = to be linearly interpolated between 0.5 and 1, if the watertable is likely to be permanently located at a depth greater than D but less than $(D + B)$ (i.e., $0 < z_w < B$ in Fig. 12.19)

N_c, N_q, N_γ = bearing capacity factors—the same as P-R-C-K-V factors, namely Eqs 12.6, 12.7 and 12.10.

The recommendations for shape factors (S_c, S_q, S_γ), depth factors (d_c, d_q, d_γ), and inclination factors (i_c, i_q, i_γ) are given in Table 12.9.

Table 12.9 Correction Factors as per IS: 6403-1981

Factors	Value or expression	
S_c	$1 + 0.2B/L$ for rectangle 1.3 for square and circle	
S_q	$1 + 0.2B/L$ for rectangle 1.2 for square and circle	
S_γ	$1 - 0.4B/L$ for rectangle 0.8 for square 0.6 for circle	
d_c	$1 + 0.2(D/B) \tan(45 + \phi/2)$	The depth correction factors are to be applied only when backfilling is done with proper compaction
d_q, d_γ	$1 + 0.1(D/B) \tan(45 + \phi/2)$ for $\phi > 10°$ 1 for $\phi < 10°$	
i_c, i_q	$(1 - \alpha°/90)^2$	
i_γ	$(1 - \alpha/\phi)^2$	For α see figure in Table 12.5

Q 12.10: Redo the problem in Q 12.6 with IS Code recommendations.

Ans: As per IS Code recommendations from Table 12.9

$$S_c = S_q = 1 + 0.2\left(\frac{1.75}{3.5}\right) = 1.1$$

$$S_\gamma = 1 - 0.4\left(\frac{1.75}{3.5}\right) = 0.8$$

$$d_c = 1 + 0.2\left(\frac{1.75}{3.5}\right)\tan\left(45 + \frac{25}{2}\right) = 1.18$$

$$d_q = d_\gamma = 1 + 0.1\left(\frac{1.75}{3.5}\right)\tan\left(45 + \frac{25}{2}\right) = 1.09$$

$$i_c = i_q = \left(1 - \frac{10}{90}\right)^2 = 0.79$$

$$i_\gamma = \left(1 - \frac{10}{25}\right)^2 = 0.36$$

$$W' = 1$$

Using depth factors d_c, d_q, d_γ:

(a) $B' = 1.55$ m; $q_{ult} = 44$ T/m²—against 43 T/m² obtained using Vesic's correction factors

(b) $B' = 1.75$ m; $q_{ult} = 45$ T/m²—against 47 T/m² obtained using Vesic's correction factors

(c) $B' = 1.55$ m; $q_{ult} = 44$ T/m²—against 46 T/m² worked out using Vesic's correction factors

Without using depth factors d_c, d_q, d_γ (if backfill is not properly compacted)

(a) $B' = 1.55$ m; $q_{ult} = 39$ T/m²

(b) $B' = 1.75$ m; $q_{ult} = 39$ T/m²

(c) $B' = 1.55$ m; $q_{ult} = 39$ T/m²

12.3 ULTIMATE BEARING CAPACITY OF FOOTINGS ON OR ADJACENT TO SLOPES

For gentle slopes the ground slope factors explained in Sec. 12.2.5 can be used to get the ultimate bearing capacity of footings. For steep slopes the analyses presented here can be used.

12.3.1 Bowles' Analysis

The two general cases of footings on slopes are shown in Fig. 12.20. According to Bowles (1982) the equation for ultimate bearing capacity is given as

$$q_{ult} = c\bar{N}_c S_c i_c + q\bar{N}_q S_q i_q + 0.5\gamma B N_\gamma S_\gamma d_\gamma i_\gamma \qquad (12.19)$$

where $\bar{N}_c$, $\bar{N}_q$ = Bowles' bearing capacity factors dependent on ϕ, ω, D/B and b/B

N_γ = bearing capacity factor (dependent on ϕ only) as given by Hansen in Table 12.4

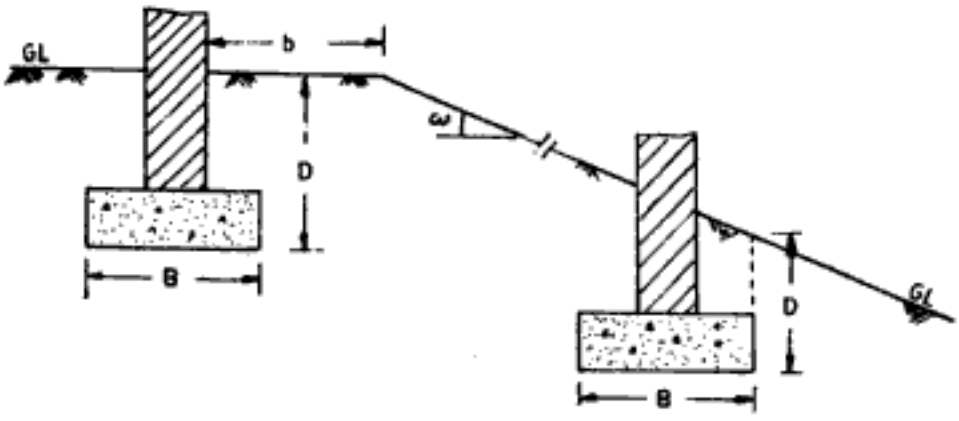

Fig. 12.20 Footings on slopes

The bearing capacity factors and correction factors for shape, depth and load inclination are given in Tables 12.10 and 12.11 respectively.

Q 12.11: To compute the ultimate bearing capacity of the footing in Q 12.8 using Bowles' factors

Ans: According to Bowles (Table 12.11)

$$S_c = 1 + \frac{2}{3}\left(\frac{18.4}{30.1}\right) = 1.408$$

$$S_q = 1.385; \quad S_\gamma = 1.267; \quad d_\gamma = 1$$

From Table 12.10 for $\omega = 10°$; $D/B = 1/2 = 0.5$; $b/B = 0/2 = 0$; $\phi = 30°$

$$\overline{N}_c = 30.14; \quad \overline{N}_q = 10.15 \quad \text{and} \quad \overline{N}_\gamma = 15.1$$

Using these values in the bearing capacity equation (Eq. 12.19)

$$q_{ult} = 0.5 \times 30.14 \times 1.408 + 1.9 \times 10.15 \times 1.385 + 0.5 \times 1.9 \times 2 \times 15.1 \times 1.267 \times 1$$

$q_{ult} = 84$ T/m^2—against 83 T/m^2 calculated using Vesic's ground slope factors in Q 12.8.

Q 12.12: To compute the q_{ult} of the footing in Q 12.8 when $b = 2$ m (Fig. 12.20) using Bowles' factors.

Ans: The only change from solution for Q 12.11 is in the values of bearing capacity factors. For $b/B = 2/2 = 1$; $\omega = 10°$, $D/B = 0.5$, and $\phi = 30°$: $\overline{N}_c = 30.14$, $\overline{N}_q = 13.94$, $\overline{N}_\gamma = 15.1$. Using these values, and values of depth and shape factors as in Q 12.11

$$q_{ult} = 94 \text{ T/m}^2$$

12.3.2 Meyerhof's Solution for Strip Footings

1. *Foundations on the face of slope (Fig. 12.21)*

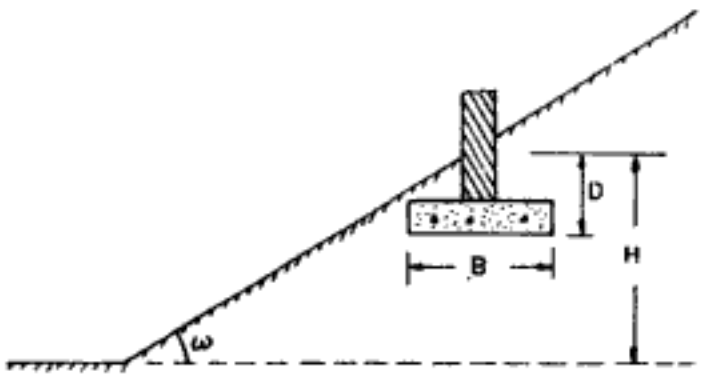

Fig. 12.21 Footing on face of slope

(a) For undrained loading or purely cohesive soil (i.e., $\phi = 0$) the equation for ultimate bearing capacity of footing is given by Meyerhof (1957) as

$$q_{ult} = cN_{cq} \tag{12.20}$$

where N_{cq} is bearing capacity factor and

$$N_{cq} = f(N_S, D/B, \omega)$$

and N_S = stability factor defined as

$$N_S = \gamma H/c \quad (\gamma \text{ the density, } c \text{ the undrained cohesion of soil})$$

Figure 12.22 gives bearing capacity factor N_{cq}.

Table 12.10 Bowles' Bearing Capacity Factors $\bar{N}_c$, $\bar{N}_q$

		$b/B = 0$					$b/B = 0.5$				
	$\phi°$ / $\omega°$	0	10	20	30	40	0	10	20	30	40
$D/B = 0$	0	5.14 1.03	8.34 2.47	14.83 6.40	30.14 18.40	75.31 64.20	5.14 1.03	8.34 2.47	14.83 6.40	30.14 18.40	75.31 64.20
	10	4.89 1.03	7.80 2.47	13.57 6.40	26.80 18.40	64.42 64.20	5.14 1.03	8.15 2.47	14.06 6.40	27.62 18.40	65.87 64.20
	20	4.63 1.03	7.28 2.47	12.39 6.40	23.78 18.40	55.01 64.20	5.12 1.03	7.96 2.47	13.40 6.40	25.39 18.40	57.87 64.20
	30	4.38 1.03	6.77 2.47	11.28 6.40	21.05 18.40	46.88 64.20	5.10 1.03	7.77 2.47	12.75 6.40	23.40 18.40	51.07 64.20
	60	3.62 1.03	5.33 2.47	8.33 6.40	14.34 18.40	28.56 64.20	4.86 1.03	7.07 2.47	10.89 6.40	18.40 18.40	35.81 64.20
$D/B = 0.5$	0	5.14 1.03	8.34 2.47	14.83 6.40	30.14 18.40	75.31 64.20	5.14 1.03	8.34 2.47	14.83 6.40	30.14 18.40	75.31 64.20
	10	5.14 0.79	8.34 1.70	14.8 3.94	330.14 10.15	72.67 31.61	5.14 0.94	8.34 2.03	14.83 4.73	30.14 12.17	74.12 37.80
	20	5.14 0.79	8.34 1.62	14.83 3.58	28.19 8.79	62.88 25.88	5.14 1.03	8.34 2.33	14.83 5.19	29.79 12.66	65.74 36.91
	30	5.14 0.72	8.34 1.43	13.83 3.03	25.11 7.09	54.13 14.79	5.14 1.03	8.34 2.47	14.83 5.36	27.46 12.40	50.32 34.02
	60	4.34 0.28	6.33 0.50	9.81 0.95	16.68 1.98	32.75 4.78	5.14 1.03	8.07 2.13	12.37 3.92	20.74 7.83	40.00 18.04
$D/B = 0.75$	0	5.14 1.03	8.34 2.47	14.83 6.40	30.14 18.40	75.31 64.20	5.14 1.03	8.34 2.47	14.83 6.40	30.14 18.40	75.31 64.20
	10	5.14 0.92	8.34 1.95	14.83 4.43	30.14 11.16	75.31 33.94	—	—	—	—	—
	20	5.14 0.94	8.34 1.90	14.83 4.11	30.14 9.84	66.81 28.21	—	—	—	—	—
	30	5.14 0.88	8.34 1.71	14.83 3.54	27.14 8.08	57.76 21.91	—	—	—	—	—
	60	4.70 0.37	8.34 0.63	10.55 1.17	17.85 2.36	34.84 5.52	—	—	—	—	—

for Footings on or Adjacent to a Slope

$b/B = 0.75$					$b/B = 1.0$					$b/B = 1.5$				
0	10	20	30	40	0	10	20	30	40	0	10	20	30	40
5.14	8.34	14.83	30.14	75.31	5.14	8.34	14.83	30.14	75.31	5.14	8.34	14.83	30.14	75.31
1.03	2.47	6.40	18.40	64.20	1.03	2.47	6.40	18 40	64.20	1.03	2.47	6.40	18.40	64.20
5.14	8.33	14.34	28.02	66.60	5.14	8.34	14.60	28.43	67.33	5.14	8.34	14.83	29.24	68.78
1.03	2.47	6.40	18.40	64.20	1.03	2.47	6.40	18.40	64.20	1.03	2.47	6.40	18.40	64.20
5.14	8.31	13.90	26.19	59.31	5.14	8.34	14.41	26.99	60.74	5.14	8.34	14.83	28.59	63.60
1.03	2.47	6.40	18.40	64.20	1.03	2.47	6.40	18.40	64.20	1.03	2.47	6.40	18.40	64.20
5.14	8.27	13.49	24.57	53.16	5.14	8.34	14.23	25.74	55.26	5.14	8.34	14.83	28.09	59.44
1.03	2.47	6.40	18.40	64.20	1.03	2.47	6.40	18.40	64.20	1.03	2.47	6.40	18.40	64.20
5.14	7.94	12.17	20.43	39.44	5.14	8.34	13.45	22.44	43.06	5.14	8.34	14.83	26.52	50.32
1.03	2.47	6.40	18.40	64.20	1.03	2.47	6.40	18.40	64.20	1.03	2.47	6.40	18.40	64.20
—	—	—	—	—	5.14	8.34	14.83	30.14	75.31	—	—	—	—	—
					1.03	2.47	6.40	18.40	64.20					
—	—	—	—	—	5.14	8.34	14.83	30.14	75.31	—	—	—	—	—
					1.01	2.26	5.35	13.94	43.57					
—	—	—	—	—	5.14	8.34	14.83	30.14	68.61	—	—	—	—	—
					1.03	2.47	6.40	16.29	47.76					
—	—	—	—	—	5.14	8.34	14.83	29.80	62.51	—	—	—	—	—
					1.03	2.47	6.40	17.81	48.90					
—	—	—	—	—	5.14	8.34	14.83	24.80	47.25	—	—	—	—	—
					1.03	2.47	6.40	15.66	35.82					
5.14	8.34	14.83	30.14	75.31	5.14	8.34	14.83	30.14	75.31	5.14	8.34	14.83	30.14	75.31
1.03	2.47	6.40	18.40	64.20	1.03	2.47	6.40	18.40	64.20	1.03	2.47	6.40	18.40	64.20
5.14	8.34	14 83	30.14	75.31	—	—	—	—	—	5.14	8.34	14.83	30.14	75.31
1.03	2.34	5.34	13.47	40.83						1.03	2.47	6.01	15.39	47.09
5.14	8.34	14.83	30.14	71.11	—	—	—	—	—	5.14	8.34	14.83	30.14	75.31
1.03	2.47	6.04	14.39	40.88						1.03	2.47	6.40	18.40	53.21
5.14	8.34	14.83	30.14	64.04	—	—	—	—	—	5.14	8.34	14.83	30.14	70.32
1.03	2.47	6.40	14.52	38.72						1.03	2.47	6.40	18.40	56.41
5.14	8.34	14.38	23.94	45.72	—	—	—	—	—	5.14	8.34	14.83	30.03	56.60
1.03	2.47	5.14	10.05	22.56						1.03	2.47	6.40	18.40	46.18

(Contd.)

	ω° \ φ°	0	10	20	30	40	0	10	20	30	40
$D/B = 1.0$	0	5.14 1.03	8.34 2.47	14.83 6.40	30.1 18.40	475.31 64.20	5.14 1.03	8.34 2.47	14.83 6.40	30.14 18.40	75.31 64.20
	10	5.14 1.03	8.34 2.19	14.83 4.91	30.14 12.16	75.31 30.24	5.14 1.03	8.34 2.44	14.83 5.47	30.14 13.52	75.31 40.14
	20	5.14 1.03	8.34 2.17	14.83 4.63	30.14 10.88	70.75 30.54	5.14 1.03	8.34 2.47	14.83 5.80	30.14 13.56	73.61 37.73
	30	5.14 1.03	8.34 1.98	14.83 4.04	29.17 9.05	61.39 24.03	5.14 1.03	8.34 2.47	14.83 5.77	30.14 12.81	65.57 33.55
	60	5.06 0.45	7.33 0.77	11.29 1.39	19.03 2.76	36.93 6.27	5.14 1.03	8.34 2.04	13.84 3.66	23.09 7.01	44.19 15.55
$D/B = 1.5$	0	5.14 1.03	8.34 2.47	14.83 6.40	30.14 18.40	75.31 64.20	5.14 1.03	8.34 2.47	14.83 6.40	30.14 18.40	75.31 64.20
	10	5.14 1.03	8.34 2.47	14.83 5.85	30.14 14.13	75.31 42.81	5.14 1.03	8.34 2.47	14.83 6.33	30.14 15.26	75.31 43.94
	20	5.14 1.03	8.34 2.47	14.83 5.65	30.14 12.93	75.31 35.14	5.14 1.03	8.34 2.47	14.83 6.40	30.14 15.20	75.31 41.04
	30	5.14 1.03	8.34 2.47	14.83 5.04	30.14 10.99	68.64 28.23	5.14 1.03	8.34 2.47	14.83 6.40	30.14 14.23	72.83 36.18
	60	5.14 0.62	8.34 1.04	12.76 1.83	21.37 3.52	41.12 7.80	5.14 1.03	8.34 2.19	14.83 3.85	25.43 7.28	48.37 15.77

$b/B = 0.75$					$b/B = 1.0$					$b/B = 1.5$				
0	10	20	30	40	0	10	20	30	40	0	10	20	30	40
5.14	8.34	14.83	30.14	75.31	5.14	8.34	14.83	30.14	75.31	5.14	8.34	14.83	30.14	75.31
1.03	2.47	6.40	18.40	64.20	1.03	2.47	6.40	18.40	64.20	1.03	2.47	6.40	18.40	64.20
—	—	—	—	—	5.14	8.34	14.83	30.14	75.31	—	—	—	—	—
					1.03	2.47	5.95	14.75	43.83					
—	—	—	—	—	5.14	8.34	14.83	30.14	75.31	—	—	—	—	—
					1.03	2.47	6.40	16.11	44.80					
—	—	—	—	—	5.14	8.34	14.83	30.14	69.76	—	—	—	—	—
					1.03	2.47	6.40	16.61	43.38					
—	—	—	—	—	5.14	8.34	14.83	27.14	51.44	—	—	—	—	—
					1.03	2.47	6.36	12.28	27.10					
5.14	8.34	14.83	30.14	75.31	5.14	8.34	14.83	30.14	75.31	5.14	8.34	14.13	30.14	75.31
1.03	2.47	6.40	18.40	64.20	1.03	2.47	6.40	18.40	64.20	1.03	2.47	6.40	18.40	64.20
5.14	8.34	14.83	30.14	75.31	5.14	8.34	14.83	30.14	75.31	5.14	8.34	14.83	30.14	75.31
1.03	2.47	6.40	15.79	45.45	1.03	2.47	6.40	16.30	46.93	1.03	2.47	6.40	17.26	49.77
5.14	8.34	14 83	30.14	75.31	5.14	8.34	14.83	30.14	75.31	5.14	8.34	14.83	30.14	75.31
1.03	2.47	6.40	16.31	43.96	1.03	2.47	6.40	17.39	46.85	1.03	2.47	6.40	18.40	52.58
5.14	8.34	14.83	30.14	74.92	5.14	8.34	14.83	30.14	75.31	5.14	8.34	14.83	30.14	75.31
1.03	2.47	6.40	15.85	40.23	1.03	2.47	6.40	17.48	44.32	1.03	2.47	6.40	18.40	52.63
5.14	8.34	14.83	27.46	52.00	5.14	8.34	14.83	29.49	55.63	5.14	8.34	14.83	30.14	62.98
1.03	2.47	4.97	9.41	20.33	1.03	2.47	6.17	11.69	25.26	1.03	2.47	6.40	16.72	36.17

Notes: 1. The value at top is $\overline{N}_c$ and the value at bottom is $\overline{N}_q$

2. For variable identification refer to Fig. 12.20

3. Base values for $\omega = 0°$ may be used when $b/B > 1.5$ to 2.

After Bowles, 1982. Reprinted by permission of McGraw-Hill Book Company, New York.

(Contd.)

Table 12.11 Correction Factors Recommended by Bowles

Factors	Expression or value
S_c	$0.2B/L$ for $\phi = 0°$ $1 + (N_q/N_c)(B/L)$ for $\phi > 0°$
S_q	$1 + (B/L) \tan \phi$
S_γ	$1 - 0.4(B/L)$
d_c	$0.4(D/B)$ for $\phi = 0°$ and $D \leqslant B$ $0.4 \arctan (D/B)$—for $\phi = 0°$ and $D > B$ $1 + 0.4(D/B)$ for $\phi > 0°$ and $D \leqslant B$ $1 + 0.4 \arctan (D/B)$—for $\phi > 0°$ and $D > B$
d_q	$1 + 2 \tan \phi(1 - \sin \phi)^2 (D/B)$ for $D \leqslant B$ $1 + 2 \tan \phi(1 - \sin \phi)^2 \arctan (D/B)$ for $D > B$
d_γ	1
i_c	$0.5 - 0.5 [1 - H/cB'L']^{0.5}$ for $\phi = 0°$ $i_q - [(1 - i_q)/(N_q - 1)]$ for $\phi > 0°$
i_q	$[1 - 0.5H/(V + c \cot \phi B'L')]^5$
i_γ	$[1 - 0.7H/(V + c \cot \phi B'L')]^5$ for $\omega = 0°$ $[1 - [(0.7 + \omega°/450°)H/(V + c \cot \phi B'L')]]^5$ for $\omega > 0°$

After Bowles, 1982. Reprinted by permission of McGraw-Hill Book Company, New York.

(b) Purely frictional soil (i.e., $c = 0$):

In this case $$q_{ult} = 0.5\gamma B N_{\gamma q} \tag{12.21}$$

The bearing capacity factor $N_{\gamma q}$ as shown in Fig. 12.23 is dependent on ϕ, D/B and ω.

2. *Foundations on top of slope (Fig. 12.24)*

(a) Undrained loading condition or purely cohesive soil (i.e., $\phi = 0$):
Here again, $$q_{ult} = cN_{cq} \tag{12.20}$$
and the variation of N_{cq} with ω, D/B and N_s is shown in Fig. 12.25.

(b) Purely frictional soil (i.e., $c = 0$):
The ultimate bearing capacity is given by,

$$q_{ult} = 0.5\gamma B N_{\gamma q} \tag{12.21}$$

The variation of $N_{\gamma q}$ with ϕ, D/B and ω is shown in Fig. 12.26.

Q 12.13: To determine the ultimate bearing capacity of a strip footing on the face of a slope under undrained conditions of loading given the following data for Fig. 12.21.

$c_u = 20$ T/m²; $\gamma = 2$ T/m²;
$\phi = 0°$; $D = 0$ m; $B = 1.5$ m;
$\omega = 20°$; $H = 10$ m

Ans:

$$N_s = 2 \times \frac{10}{20} = 1$$

From Fig. 12.22 $N_{cq} = 3.8$

$$q_{ult} = 20 \times 3.8 = 76 \text{ T/m}^2$$

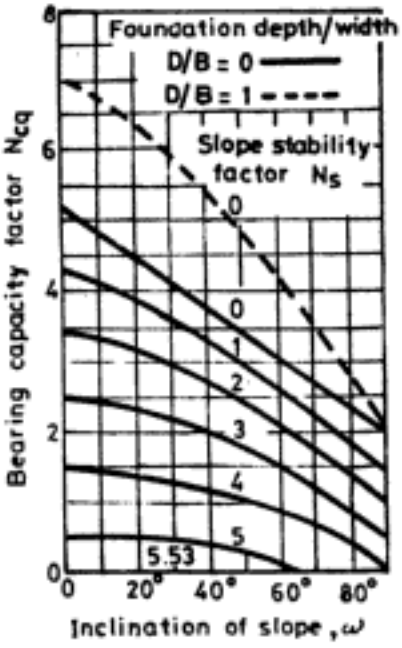

Fig. 12.22 Bearing capacity factors for strip foundation on face of slope of purely cohesive material (After Meyerhof, 1957; reprinted with permission of Butterworth Scientific, Surrey, UK)

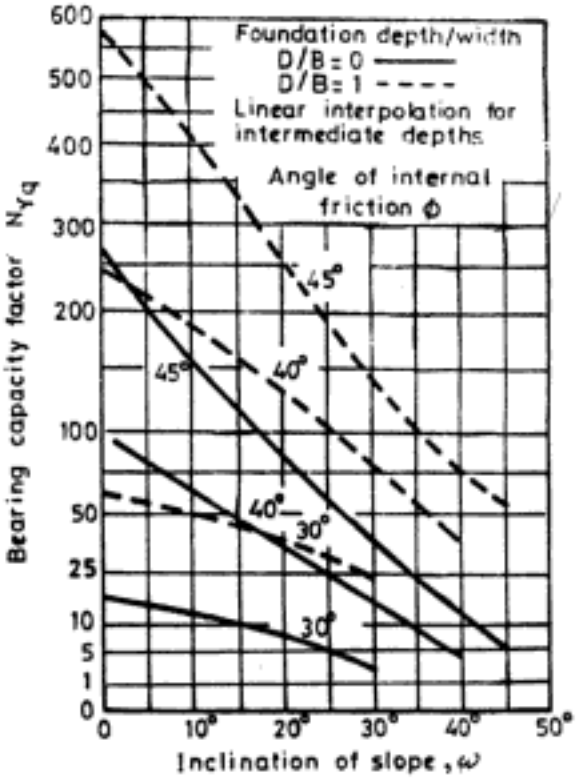

Fig. 12.23 Bearing capacity factors for strip foundation on face of slope of cohesionless soil (After Meyerhof, 1957; reprinted with permission of Butterworth Scientific, Surrey, UK)

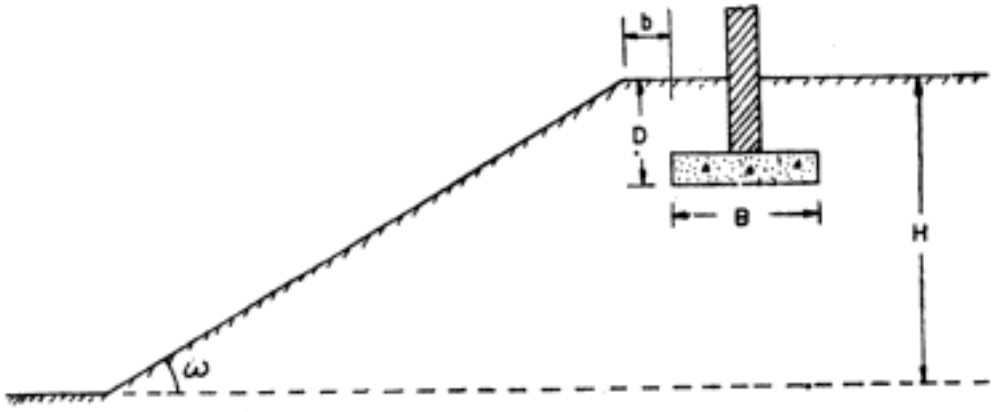

Fig. 12.24 Footing on top of slope

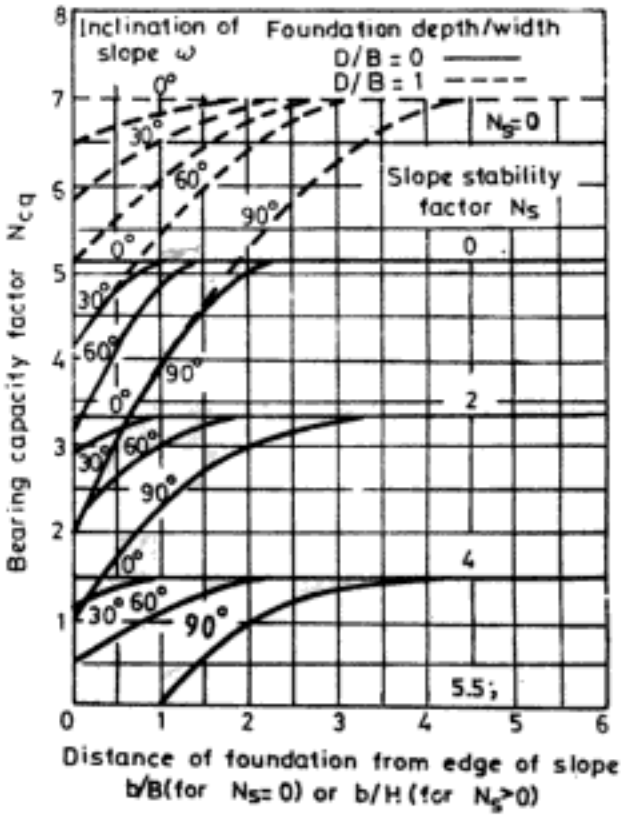

Fig 12.25 Bearing capacity factors for strip foundation on top of slope of purely cohesive soil (After Meyerhof, 1957; reprinted with permission of Butterworth Scientific, Surrey, UK)

Q 12.14: To determine the ultimate bearing capacity of a strip footing on the face of a slope (Fig. 12.21) of sand, given the following data:

$$c = 0 \text{ T/m}^2; \quad \phi = 40°; \quad \gamma = 1.9 \text{ T/cu. m};$$
$$B = 1.5 \text{ m}; \quad D = 1.5 \text{ m}; \quad \omega = 20°$$

Ans: From Fig. 12.23 $N_{\gamma q} = 130$ for $\omega = 20°$; $\dfrac{D}{B} = 1$ and $\phi = 40°$

Hence, $$q_{ult} = 0.5 \times 1.9 \times 1.5 \times 130 = 185 \text{ T/m}^2$$

Q 12.15: To determine the ultimate bearing capacity of a strip footing on the top of a clay slope under undrained loading conditions, given the following data for Fig. 12.24.

$$c_u = 20 \text{ T/m}^2; \quad \phi = 0°; \quad \gamma = 2 \text{ T/m}^3; \quad b = 3 \text{ m};$$
$$B = 1.5 \text{ m}; \quad D = 0 \text{ m}; \quad H = 20 \text{ m}; \quad \omega = 30°$$

Ans: $N_s = 2 \times 20/20 = 2$; since $N_s > 0$, b/H is computed.

$$b/H = 3/20 = 0.15$$

From Fig. 12.25 $N_{cq} \simeq 3$

Hence, $$q_{ult} = 20 \times 3 = 60 \text{ T/m}^2$$

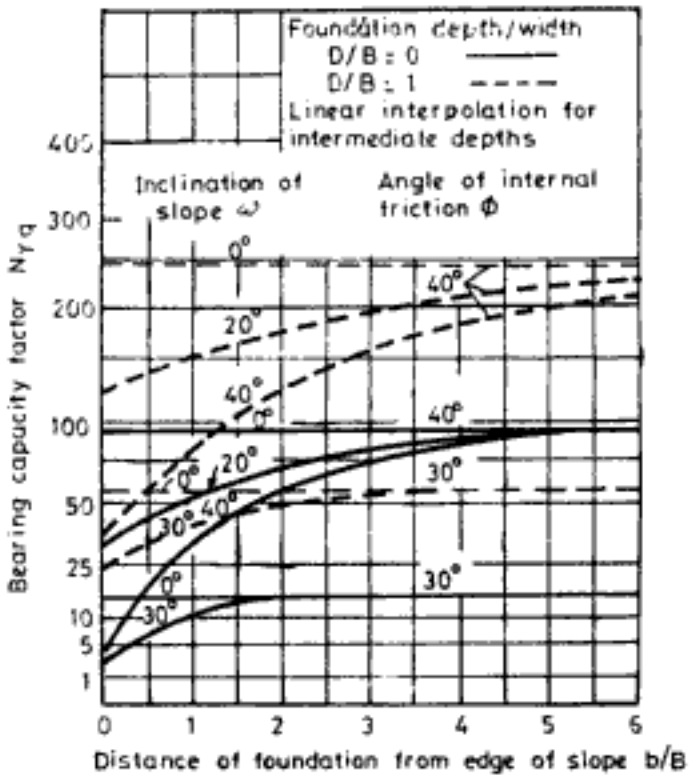

Fig. 12.26 Bearing capacity factors for strip foundation on top of slope of cohesionless soil (After Meyerhof, 1957; reprinted with permission of Buttorworth Scientific; Surrey, UK)

(Using Bowles' analysis for $b/B = 2$, the ultimate bearing capacity of the footing on top of infinite slope can be computed as 107 T/m²)

Q 12.16: To compute the ultimate bearing capacity of a strip footing on the top of a slope of sand, given the following data.

$$c = 0 \text{ T/m}^2; \quad \phi = 40°; \quad \gamma = 1.9 \text{ T/m}^3;$$
$$b = 3 \text{ m}; \quad B = 1.5 \text{ m}; \quad D = 1.5 \text{ m}; \quad \omega = 20°$$

Ans:

$$b/B = 3/1.5 = 2; \quad D/B = 1.5/1.5 = 1$$

From Fig. 12.26 $\quad N_{\gamma q} = 180$

$$\therefore \quad q_{ult} = 0.5 \times 1.9 \times 1.5 \times 180 = 256 \text{ T/m}^2$$

(Using Bowles' analysis the ultimate bearing capacity of footing on top of infinite slope can be computed as 261 T/m².)

Meyerhof also makes the following recommendations or modifications to his solutions: The bearing capacity of a foundation on completely submerged material below a stationary watertable is given with γ replaced by γ_b (= buoyant density) of the soil. If the water percolates through the soil, a flownet analysis is required. The bearing capacity after rapid draw-

down of the watertable of a completely submerged foundation can be estimated using a reduced angle of shear resistance, ϕ_{re}, instead of ϕ where

$$\phi_{re} = \tan^{-1}\left(\frac{\gamma_b}{\gamma}\tan\phi\right) \tag{12.22}$$

The effect of tension crack on the bearing capacity of foundations on top of a slope of purely cohesive material can be estimated with good approximation using a reduced cohesion c_{re}, instead of c, where,

$$c_{re} = \left(1 - \frac{0.8\omega^{\circ} z_c}{90^{\circ} H}\right) c \tag{12.23}$$

where z_c = depth of tension crack completely filled with water

For a given height and inclination of the slope the bearing capacity factor increases with greater foundation distance from the edge of the slope, and beyond a distance of about 2 to 4 times the height of the slope the bearing capacity is independent of the slope angle. The bearing capacity of foundations on slopes of purely cohesive soil is governed by foundation failure for small slope height (N_s approaches zero) and by overall slope stability for greater heights. Figures 12.22 and 12.25 incorporate both these possibilities.

It must be noted that while Meyerhof's analysis considers both slope stability and foundation failure, Bowles' analysis considers only the foundation failure.

However, Shields, *et al.* (1977) conclude from experimental investigations that the bearing capacity of spread footings adjacent to a slope in granular soil is highly overestimated by Meyerhof's theory. At shallow depths close to the crest of the slope the theory gives nearly the correct values.

12.4 ULTIMATE BEARING CAPACITY OF FOUNDATIONS UNDER NON-HOMOGENEOUS SOIL CONDITIONS

12.4.1 Button's Solutions

Button (1953) gives solution for the case of a two-layer cohesive soil system ($c_1 > 0; c_2 > 0$). The footing is loaded under undrained loading conditions ($\phi_1 = \phi_2 = 0$). For strip footings on the surface of top layer (i.e., $D = 0$), according to Button,

$$q_{ult} = c_1 N_c + q \tag{12.24}$$

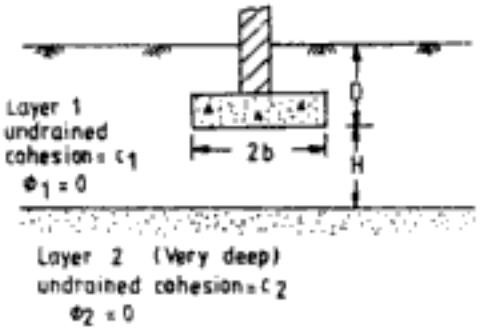

Fig. 12.27 Footing in layered soil

The value of bearing capacity factor, N_c, is dependent on c_1/c_2 and H/b. N_c is to be determined from the chart shown in Fig. 12.28.

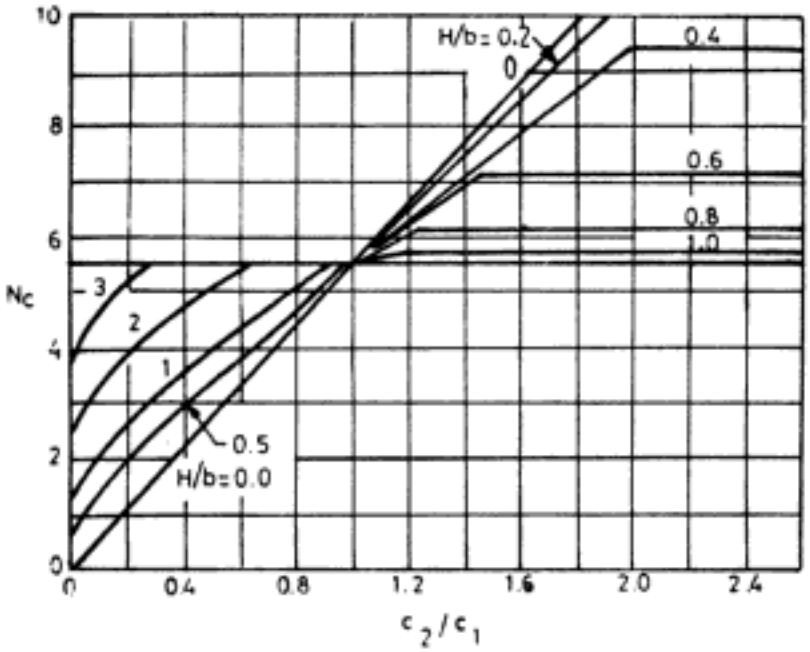

Fig. 12.28 Bearing capacity factor N_c for strip foundation in layered soil (After Button, 1953)

For other shapes of footings and under embedded conditions, according to Bowles,

$$q_{ult} = c_1 N_c (1 + S_c + d_c) + q \tag{12.25}$$

Shape factors and depth factors as recommended by Bowles are to be used.

Q 12 17: To compute the ultimate bearing capacity of the strip footing shown in Fig. 12.29, using Button's analysis.

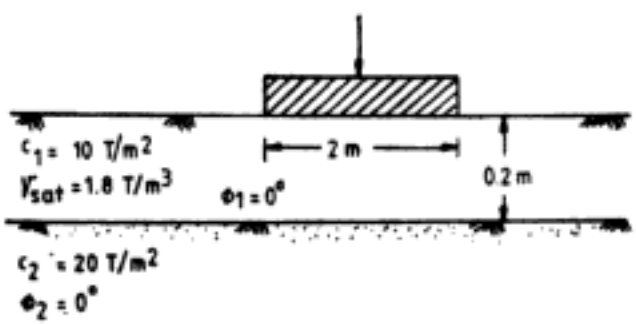

Fig. 12.29 Q 12.17

Ans:

$$\frac{c_2}{c_1} = \frac{20}{10} = 2$$

$$B = 2b = 2 \text{ m}$$

$$\frac{H}{b} = \frac{0.2}{1} = 0.2$$

From Fig. 12.28, $N_c = 10.5$

$\therefore$ $q_{ult} = 10 \times 10.5 = 105$ T/m² against the value of 55 T/m² when $c_2/c_1 = 1$, i.e., homogeneous soil conditions. The result indicates the increase in the bearing capacity due to the presence of lower stiff soil deposit.

Q 12.18: To compute the ultimate bearing capacity of the strip footing shown in Fig. 12.30 using Button's analysis.

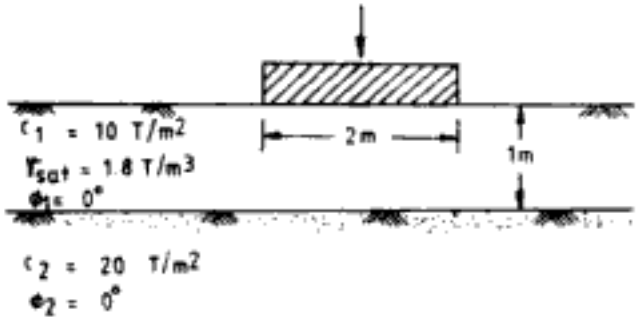

Fig. 12.30 Q 12.18

Ans:

$$\frac{c_2}{c_1} = \frac{20}{10} = 2$$

$$B = 2b = 2\,\text{m}$$

$$\frac{H}{b} = \frac{1}{1} = 1$$

From Fig. 12.28, $N_c = 5.72$

$q_{ult} = 10 \times 5.72 = 57.2$ T/m²—against 55 T/m² when $c_1 = c_2$. Comparing the value of q_{ult} to that obtained in Q 12.17 one can infer the reduction in the influence of the bottom stiff deposit due to the increase in the thickness of soil layer 1 below the base of the footing —thickness of the top soft soil layer increases from 0.2 m to 1 m, which reduces the q_{ult} value from 105 T/m² to 57 T/m².

Q12.19: To compute the ultimate bearing capacity of the strip footing shown in Fig. 12.31 using Button's analysis.

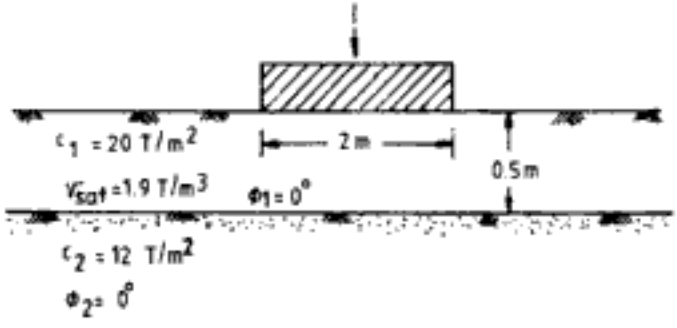

Fig. 12.31 Q 12.19

Ans:

$$\frac{c_2}{c_1} = \frac{12}{20} = 0.6$$

$$\frac{H}{b} = \frac{0.5}{1} = 0.5$$

From Fig. 12.28, $N_c = 3.8$

$q_{ult} = 20 \times 3.8 = 76$ T/m² —against a value of 110 T/m² for the case of $c_1 = c_2 = 20$ T/m². The result indicates the adverse influence of the bottom soft layer on the ultimate bearing capacity of the footing.

Q 12.20: To compute the ultimate bearing capacity of the strip footing shown in Fig. 12.32 using Button's analysis.

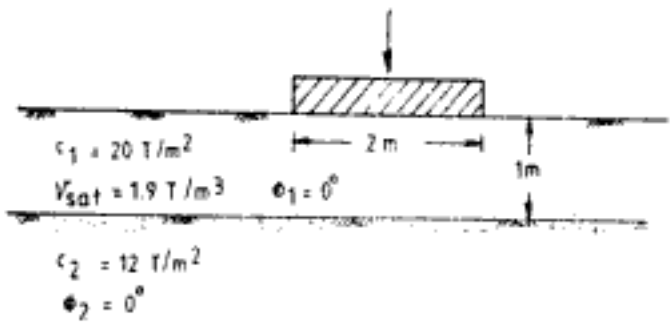

Fig. 12.32 Q 12.20

Ans:

$$\frac{c_2}{c_1} = \frac{12}{20} = 0.6$$

$$\frac{H}{b} = \frac{1}{1} = 1$$

From Fig. 12.28, $N_c = 4.3$

$q_{ult} = 20 \times 4.3 = 86$ T/m²—against a value of 110 T/m² for the case of $c_1 = c_2 = 20$ T/m². The comparison of the q_{ult} values in Q 12.20 and in Q 12.19 indicates the decreasing influence of the bottom soft deposit due to the increase in the thickness of the top soil layer below the base of the footing.

Q 12.21: To compute the ultimate bearing capacity of the square footing shown in Fig. 12.33 using Button's analysis.

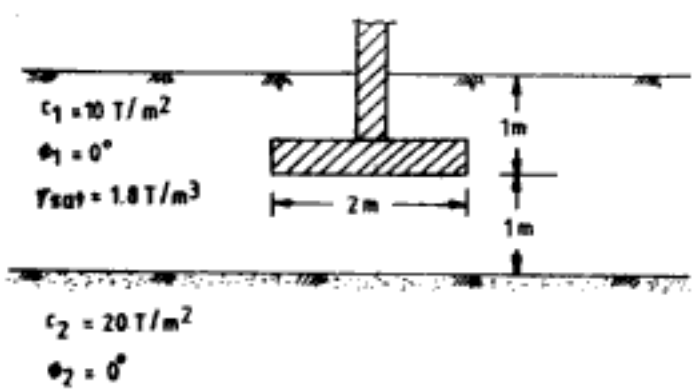

Fig. 12.33 Q 12.21

Ans:

$$\frac{c_2}{c_1} = \frac{20}{10} = 2$$

$$\frac{H}{b} = \frac{1}{1} = 1$$

From Fig. 12.28, $N_c = 5.72$

According to Bowles, from Table 12.11

$$S_c = 0.2 \times 1 = 0.2$$

$$d_c = 0.4 \times \frac{1}{2} = 0.2; \quad q = 1.8 \times 1 = 1.8 \text{ T/m}^2$$

$q_{ult} = [10 \times 5.72 \times (1 + 0.2 + 0.2)] + 1.8 = 82 \text{ T/m}^2$

The problem is same as the one solved in Q 12.18 but for the shape and depth of embedment of footing. The corrections for these indicate the increase in the bearing capacity of the footing.

Q 12.22: To compute the ultimate bearing capacity of the square footing shown in Fig. 12.34 using Button's analysis.

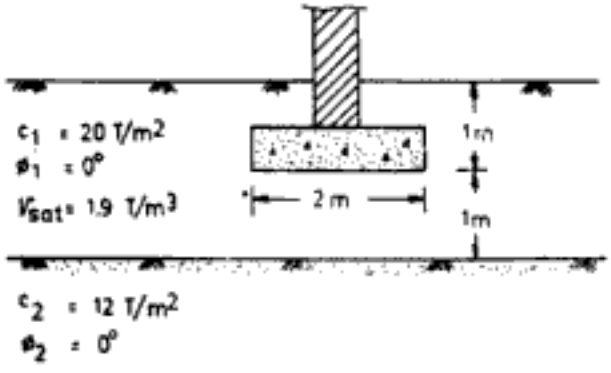

Fig. 12.34 Q 12.22

Ans:

$$\frac{c_2}{c_1} = \frac{12}{20} = 0.6$$

$$\frac{H}{b} = \frac{1}{1} = 1$$

From Fig. 12.28, $N_c = 4.3$. The shape and depth factors are same as in Q 12.21.

$q_{ult} = 20 \times 4.3 \times 1.4 + 1.9 = 122 \text{ T/m}^2$

The problem is same as the one solved in Q 12.20 except for the shape and depth of embedment of footing. The corrections for these show the increase in the bearing capacity of the footing.

Reddy and Srinivasan (1967) extend Button's solutions to anisotropic soils. The anisotropy of soil is identified by parameter K defined as,

$$K = \frac{\text{vertical shear strength}}{\text{horizontal shear strength}} \tag{12.26}$$

$K = 1$ for isotropic conditions. K is < 1 for overconsolidated soils and is > 1 for normally consolidated soils. Solutions in this case are also expressed in the form of Eqs 12.24 and 12.25. The charts for N_c for three values of K are shown in Fig. 12.35. $K = 1$ in these charts corresponds to Button's solutions.

Meyerhof and Brown (1967) suggest that in case of anisotropic conditions analysed by Reddy and Srinivasan, q_{ult} can be obtained with sufficient accuracy using Button's solutions but

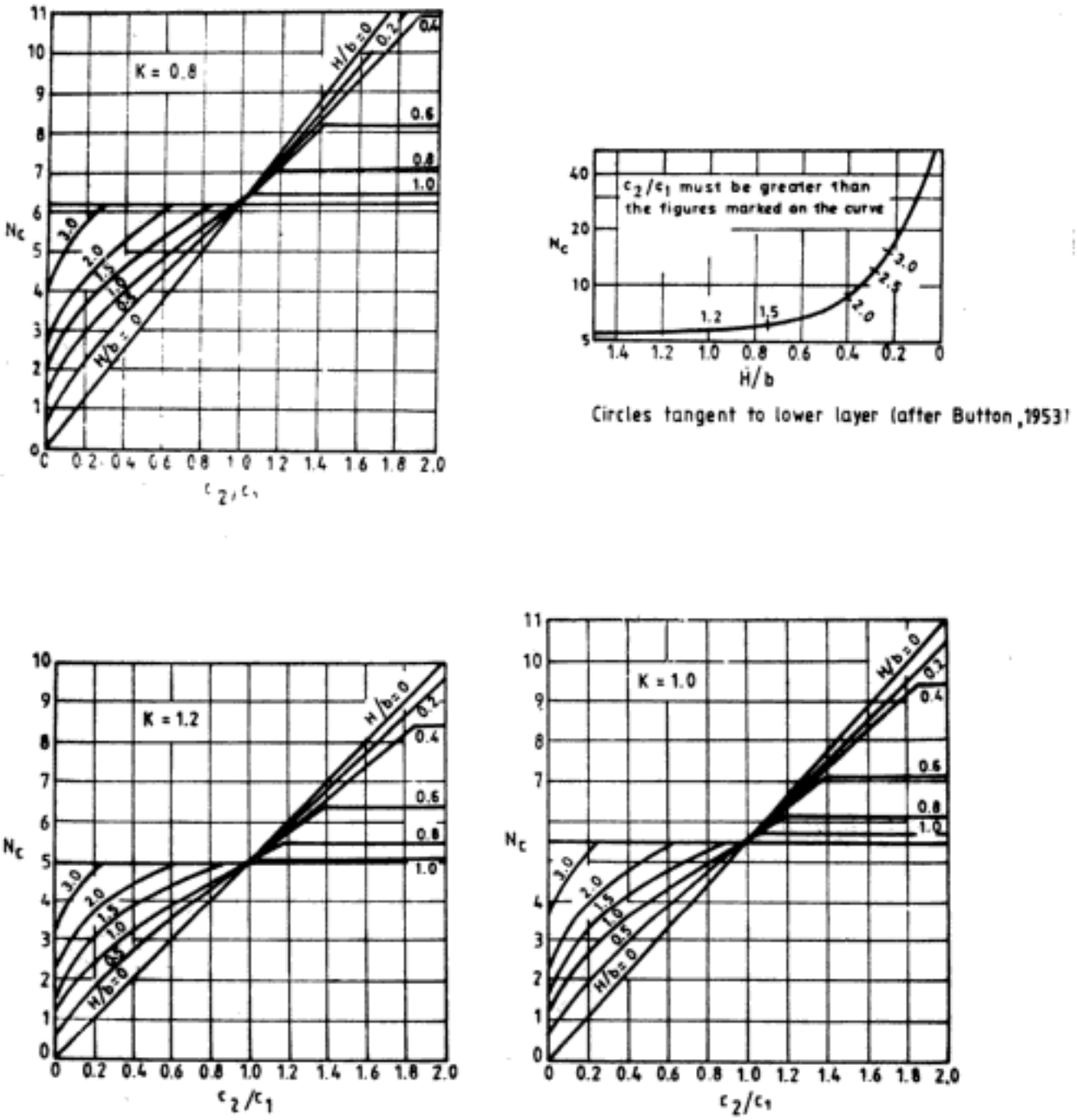

Fig. 12.35 Bearing capacity factor N_c for strip foundation in anisotropic and layered soil (After Reddy and Srinivasan, 1967; reprinted by permission of American Society of Civil Engineers, New York)

employing average cohesion for soil layers as (vertical shear strength + horizontal shear strength)/2.

12.4.2 Vesic's Recommendations

1. *Case a*: Top layer and bottom layer are clay, saturated, and undrained loading condition prevails (i.e., $\phi_1 = \phi_2 = 0°$)

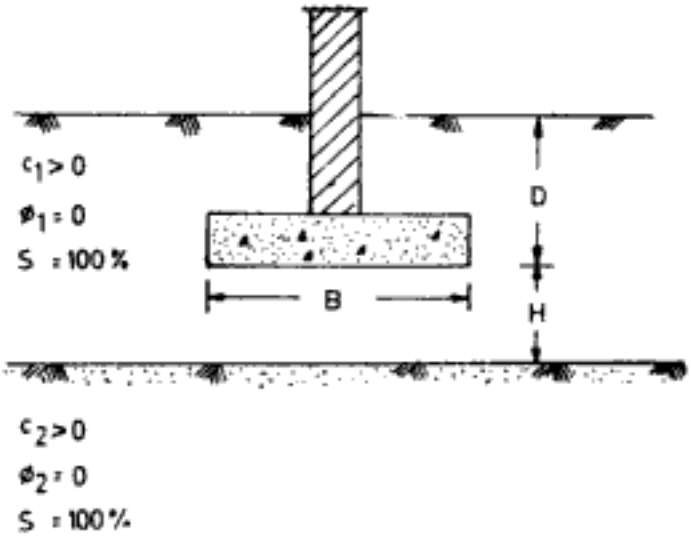

Fig. 12.36 Footing in purely cohesive ($\phi = 0$) layered soil

Situation I: $c_1 < c_2$ (soft layer overlying stiff deposit). The equation for ultimate bearing capacity is given as,

$$q_{ult} = c_1 N_m + q \tag{12.27}$$

where N_m = modified bearing capacity factor dependent upon c_2/c_1, H/B and L/B

$$N_m = \frac{KN_c^*(N_c^* + \beta - 1)[(K+1)(N_c^*)^2 + (1 + K\beta)N_c^* + \beta - 1]}{[K(K+1)N_c^* + K + \beta - 1][(N_c^* + \beta)N_c^* + \beta - 1] - (KN_c^* + \beta - 1)(N_c^* + 1)} \tag{12.28}$$

where $K = c_2/c_1$

$\beta = BL/[2(B + L)H]$

$N_c^* = S_c N_c$

e.g., for circular and square foundations: $\beta = B/4H$; $N_c^* = 6.14$ for strip footings: $\beta = B/2H$; $N_c^* = 5.14$.

The values of N_m for the case of $c_1 < c_2$ for strip footings, and square/circular footings are given in Tables 12.12 and 12.13 respectively.

Q 12.23: To compute the ultimate bearing capacity of footing in Q 12.17 using Vesic's recommendations.
Ans:

$$\frac{B}{H} = \frac{2}{0.2} = 10$$

$$\frac{c_2}{c_1} = \frac{20}{10} = 2$$

Table 12.12 N_m Values ($\phi_1 = 0$, $c_1 < c_2$, $\phi_2 = 0$) Strip and Long Rectangular Footing ($L/B \geqslant 5$)

c_2/c_1 \ B/H	2	4	6	8	10	20
1	5.14	5.14	5.14	5.14	5.14	5.14
1.5	5.14	5.31	5.45	5.59	5.70	6.14
2	5.14	5.43	5.69	5.92	6.13	6.95
3	5.14	5.59	6.00	6.38	6.74	8.16
4	5.14	5.69	6.21	6.69	7.14	9.02
5	5.14	5.76	6.35	6.90	7.42	9.66
10	5.14	5.93	6.69	7.43	8.14	11.40
∞	5.14	6.14	7.14	8.14	9.14	14.14

For $B/H < 2$; $N_m = 5.14$
After Vesic, 1974.

Table 12.13 Values of N_m($\phi_1 = \phi_2 = 0$; $c_1 < c_2$) Square or Circular Footing ($L/B = 1$)

c_2/c_1 \ B/H	4	8	12	16	20	40
1	6.14	6.14	6.14	6.14	6.14	6.14
1.5	6.14	6.34	6.49	6.63	6.76	7.25
2	6.14	6.46	6.73	6.98	7.20	8.10
3	6.14	6.63	7.05	7.45	7.82	9.36
4	6.14	6.73	7.26	7.75	8.23	10.24
5	6.14	6.80	7.40	7.97	8.51	10.58
10	6.14	6.96	7.74	8.49	9.22	12.58
∞	6.14	7.17	8.17	9.17	10.17	15.17

For $B/H < 4$; $N_m = 6.14$
After Vesic, 1974.

From Table 12.12 $N_m = 6.13$

$\therefore q_{ult} = 10 \times 6.13 = 61$ T/m². Compare this against the value of 105 T/m² calculated in Q 12.17 using Button's analysis. Vesic's method indicates lesser influence on bearing capacity due to the presence of bottom stiff deposit than Button's analysis.

Q 12.24: To compute the ultimate bearing capacity of footing in Q 12.18 using Vesic's recommendations.
Ans:

$$\frac{B}{H} = \frac{2}{1} = 2$$

$$\frac{c_2}{c_1} = \frac{20}{10} = 2$$

From Table 12.12, $N_m = 5.14$.

$\therefore$ $q_{ult} = 10 \times 5.14 = 51$ T/m²

Compare this with the value of 57 T/m² obtained in Q 12.18 using Button's analysis. While Button's analysis indicates still a very minor influence on bearing capacity by stiff lower deposit at $B/H = 2$, Vesic's recommendations indicate no influence at all due to the lower stiff deposit. For,

$$N_m = 5.14 = N_c \quad \text{at } \phi = 0^\circ$$

Q 12.25: To compute the ultimate bearing capacity of footing in Q 12.21 using Vesic's recommendations.
Ans:

$$\frac{B}{H} = \frac{2}{1} = 2$$

$$\frac{L}{B} = \frac{2}{2} = 1$$

$$\frac{c_2}{c_1} = \frac{20}{10} = 2$$

$$q = 1.8 \text{ T/m}^2$$

From Table 12.13, $N_m = 6.14$, i.e. up to $B/H = 4$ the bottom stiff deposit has no influence on the bearing capacity of footing.

$\therefore$ $q_{ult} = 10 \times 6.14 + 1.8 = 63$ T/m²—against a value of 82 T/m² computed using Button's analysis in Q 12.21.

Situation II: $c_2 < c_1$ (stiff layer overlying soft deposit). The equation for ultimate bearing capacity is given as,

$$q_{ult} = c_1 \bar{N}_m + q \tag{12.29}$$

where $\bar{N}_m$ = modified bearing capacity factor dependent on c_2/c_1, B/H and L/B

$$\bar{N}_m = \frac{1}{\beta} + KS_cN_c \leqslant S_cN_c \tag{12.30}$$

where $K = \dfrac{c_2}{c_1}$

$$\beta = \frac{BL}{2(B + L)H}$$

Values of $\bar{N}_m$ for strip, and square or circular foundations are given in Tables 12.14 and 12.15 respectively.

Q 12.26: To compute the q_{ult} of footing in Q 12.19 using Vesic's recommendations.

Ans: $\dfrac{c_2}{c_1} = 0.6$; $\dfrac{B}{H} = 2/0.5 = 4$

From Table 12.14 $\bar{N}_m = 4.08$

$q_{ult} = 20 \times 4.08 = 82$ T/m²—against the value of 76 T/m² calculated from Button's analysis. Vesic's recommendations indicate a lesser influence of underlying soft deposit than Button's analysis.

Q 12.27: To compute the q_{ult} of footing in Q 12.20 using Vesic's recommendations.

Ans: $\dfrac{c_2}{c_1} = 0.6$; $\dfrac{B}{H} = 2/1 = 2$; $\bar{N}_m = 5.08$ (From Table 12.14)

Table 12.14 Values of $\bar{N}_m$ for Strip Footings for the Case of $c_2 < c_1$; $\phi_1 = \phi_2 = 0°$

c_2/c_1 \ B/H	1	2	4	6	8	10	20
1	5.14	5.14	5.14	5.14	5.14	5.14	5.14
0.8	5.14	5.14	5.11	4.78	4.61	4.51	4.31
0.6	5.14	5.08	4.08	3.75	3.58	3.48	3.28
0.4	5.14	4.06	3.06	2.72	2.56	2.46	2.26
0.2	5.03	3.03	2.03	1.69	1.53	1.43	1.23
0.1	4.51	2.51	1.51	1.18	1.01	0.91	0.71

Table 12.15 Values of $\bar{N}_m$ for Square or Circular Footings for the Case of $c_2 < c_1$; $\phi_1 = \phi_2 = 0°$

c_2/c_1 \ B/H	1	2	4	6	8	10	20
1	6.14	6.14	6.14	6.14	6.14	6.14	6.14
0.8	6.14	6.14	5.91	5.58	5.41	5.31	5.11
0.6	6.14	5.68	4.68	4.35	4.18	4.08	3.88
0.4	6.14	4.46	3.46	3.12	2.96	2.86	2.66
0.2	5.23	3.23	2.23	1.89	1.73	1.63	1.43
0.1	4.61	2.61	1.61	1.28	1.11	1.01	0.81

$\therefore$ $q_{ult} = 20 \times 5.08 = 102$ T/m²—against the value of 86 T/m² by Button's procedure.

Q 12.28: To compute the q_{ult} of footing in Q 12.22 using Vesic's recommendations.

Ans: $\frac{c_2}{c_1} = 0.6$; $\frac{B}{H} = 2/1 = 2$; $\frac{L}{B} = 1$

Using Table 12.15 $\bar{N}_m = 5.68$

$q_{ult} = 20 \times 5.68 = 144$ T/m²—against the value of 122 T/m² calculated using Button's procedure

The influence of lower deposit on bearing capacity is greater in Button's analysis than in the recommendations due to Vesic. As a result, in

Situation I ($c_1 < c_2$; $\phi_1 = \phi_2 = 0$) $q_{ult-Button} > q_{ult-Vesic}$

Situation II ($c_2 < c_1$; $\phi_1 = \phi_2 = 0$) $q_{ult-Button} < q_{ult-Vesic}$

2. *Case b*: Stiff stratum underlain by soft stratum and drained conditions of loading

Situation I: Top and bottom strata are $c - \phi$ soils. The equation for ultimate bearing capacity is,

$$q_{ult} = [q''_u + (1 + \bar{K})\, c_1 \cot \phi_1] \exp\left[2\bar{K} \tan \phi_1 (H/B)\left(1 + \frac{B}{L}\right)\right] - \frac{1}{\bar{K}} c_1 \cot \phi_1 \leqslant q'_u \tag{12.31}$$

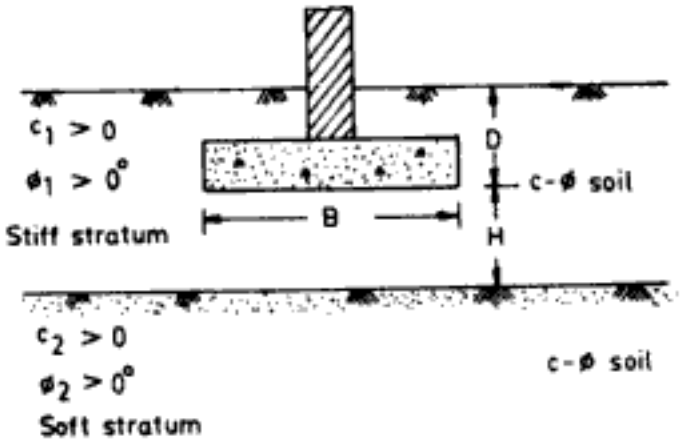

Fig. 12.37 Footing in c-ϕ layered soil

where $K = \dfrac{1 - \sin^2 \phi_1}{1 + \sin^2 \phi_1}$

q_u'' = the ultimate bearing capacity of a fictitious footing of the same size and shape as the actual footing, but resting on top of the bottom soft deposit

$q_u' = q_{ult}$ of the footing in the upper layer considered as homogeneous soil mass

Situation II: The upper layer is cohesionless ($c_1 = 0$) and the bottom in a $c - \phi$ soil

In this case,

$$q_{ult} = q_u'' \exp\left[0.67\left(1 + \frac{B}{L}\right)\frac{H}{B}\right] \qquad \text{for } 25° \leqslant \phi_1 \leqslant 50° \tag{12.32}$$

In Situation II the critical depth beyond which the lower soft layer has no influence on ultimate bearing capacity can be determined from the relationship:

$$\left(\frac{H}{B}\right)_{crit} = 3 \ln \frac{q_u'/q_u''}{2[1+B/L]} \tag{12.33}$$

Q 12.29: To compute the ultimate bearing capacity of the rectangular footing ($L \times B = 4$ m $\times 2$ m) shown in Fig. 12.38.

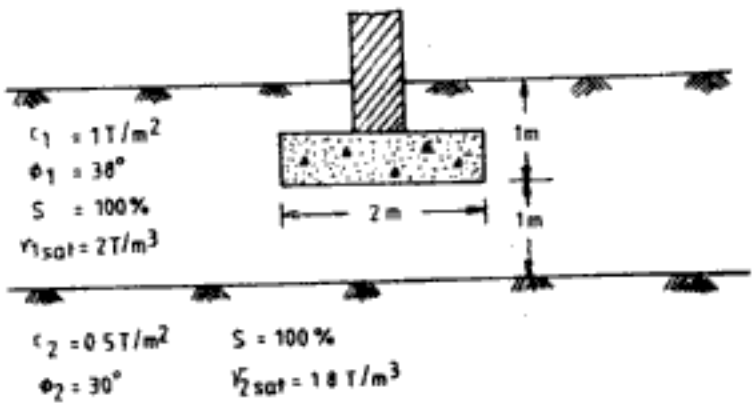

Fig. 12.38 Q 12.29

Ans: Using Vesic's solution,

q_u'' = q_{ult} of the given footing when it rests on top of the bottom soft deposit, i.e depth of embedment for the footing (D) = 2 m, in this case

$$\therefore \quad q_u'' = c_2 N_c S_c + q N_q S_q + 0.5\gamma_2 B N_\gamma S_\gamma$$

where N_c, N_q, N_γ and shape factors are determined using value of ϕ_2

From Table 12.4 for $\phi_2 = 30°$: $N_c = 30.1$; $N_q = 18.4$; $N_\gamma = 22.4$

$$S_c = 1 + \left(\frac{2}{4}\right)\left(\frac{18.4}{30.1}\right) = 1.31$$

$$S_q = 1 + \left(\frac{2}{4}\right) \tan 30° = 1.29$$

$$S_\gamma = 1 - 0.4\left(\frac{2}{4}\right) = 0.8$$

$$\therefore \quad q_u'' = 0.5 \times 30.1 \times 1.31 + 2 \times 2 \times 18.4 \times 1.29 + 0.5 \times 1.8 \times 2 \times 22.4 \times 0.8$$
$$= 147 \text{ T/m}^2$$

q_u' = q_{ult} of the given footing when the top stiff stratum is a homogeneous mass

$$\therefore \quad q_u' = c_1 N_c S_c + q N_q S_q + 0.5\gamma_1 B N_\gamma S_\gamma$$

here the bearing capacity factors and the shape factors are determined using ϕ_1

For $\phi_1 = 38°$: $N_c = 61.4$; $N_q = 48.9$; $N_\gamma = 78$

$$S_c = 1 + \left(\frac{2}{4}\right)\left(\frac{48.9}{61.4}\right) = 1.40$$

$$S_q = 1 + \left(\frac{2}{4}\right) \tan 38° = 1.39$$

$$S_\gamma = 1 - 0.4\left(\frac{2}{4}\right) = 0.8$$

$$\therefore \quad q_u' = 1 \times 61.4 \times 1.40 + 2 \times 1 \times 48.9 \times 1.39 + 0.5 \times 2 \times 2 \times 78 \times 0.8$$
$$= 347 \text{ T/m}^2$$

In Eq. 12.31

$$K = \frac{1 - \sin^2 38°}{1 + \sin^2 38°} = 0.45$$

Now $$q_{ult} = [147 + (1 + 0.45) \times 1 \times \cot 38°] \exp\left[2 \times 0.45 \times \tan 38° \times \frac{1}{2} \times \left(1 + \frac{2}{4}\right)\right] - \left[\left(\frac{1}{0.6}\right) \times 1 \times \cot 38°\right] = 249 \text{ T/m}^2 < 347 \text{ T/m}^2$$ when the lower soft deposit does not influence the bearing capacity

Q 12.30: To compute the ultimate bearing capacity of the rectangular footing ($L \times B$ = 4 m × 2 m) shown in Fig. 12.39.

Ans: $q_u'' = 147$ T/m² For determination of the value of q_u'' refer to Q 12.29.

$$q_u' = qN_qS_q + 0.5\gamma_1 BN_\gamma S_\gamma$$

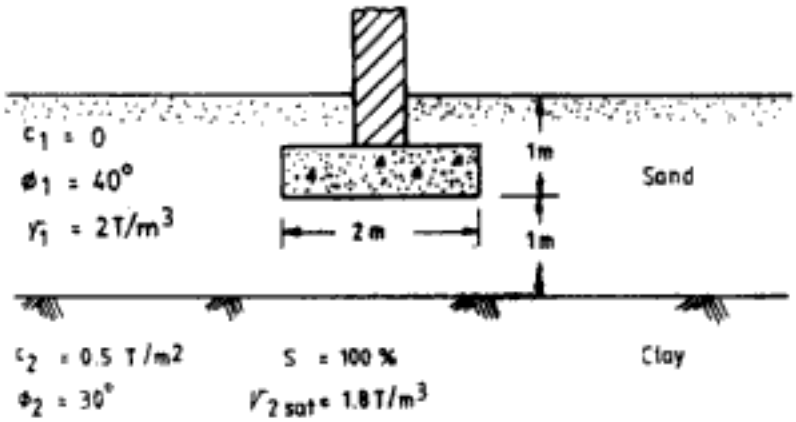

Fig. 12.39 Q 12.30

For $\phi = 40°$: $N_q = 64.2$; $N_\gamma = 109.4$

$$S_q = 1 + \left(\frac{2}{4}\right) \tan 40° = 1.42$$

$$S_\gamma = 1 - 0.4\left(\frac{2}{4}\right) = 0.8$$

$$q'_u = 2 \times 1 \times 64.2 \times 1.42 + 0.5 \times 2 \times 2 \times 109.4 \times 0.8$$
$$= 357 \text{ T/m}^2$$

From Eq. 12.33, $\left(\frac{H}{B}\right)_{crit} = \frac{3 \times \ln (357/147)}{2(1 + 2/4)} = 0.887$

$$\left(\frac{H}{B}\right)_{actual} = \frac{1}{2} = 0.5 < \left(\frac{H}{B}\right)_{critical}$$

Since the value of $(H/B)_{actual}$ is less than $(H/B)_{critical}$ the bottom soft layer will influence the bearing capacity of the footing.

From Eq. 12.32, $q_{ult} = 147 \exp\left[0.67\left(1 + \frac{2}{4}\right)\frac{1}{2}\right]$

$= 243 \text{ T/m}^2 < 357 \text{ T/m}^2$, when the bottom soft deposit does not influence the bearing capacity

3. *Case c*: Soil layer underlain by infinitely stiff deposit or rigid stratum—drained and undrained conditions of loading

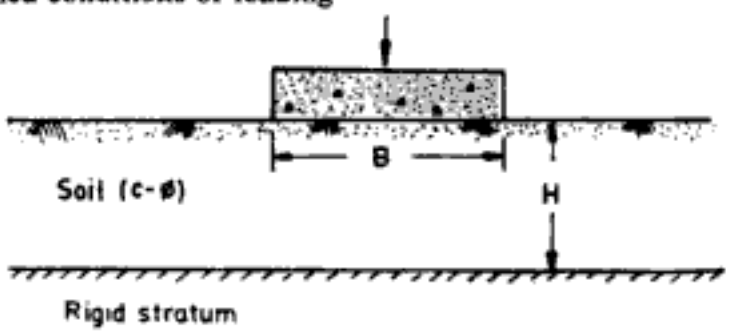

Fig. 12.40 Footing in c-ϕ soil layer underlain by rigid stratum

The equation for ultimate bearing capacity of a strip footing in this case is given as,

$$q_{ult} = cN_c r_c + qN_q r_q + 0.5\gamma BN_\gamma r_\gamma \quad (12.34)$$

where r_c, r_q, r_γ are correction factors for the presence of rigid stratum at a depth H below the footing, and r_c, r_q, r_γ values are dependent on B/H and the value of ϕ of the soil.

Also, $r_c \geq 1$, $r_q \geq 1$, $r_\gamma \geq 1$ since the rigid stratum tends to increase the bearing capacity of the footing.

The influence of the rigid stratum on the bearing capacity of the footing increases as,

(a) the value of B/H increases (i.e., as B increases or as H decreases), and as
(b) the value of ϕ increases

The values of r_c, r_q, r_γ are given in Tables 12.16, 12.17 and 12.18 respectively.

Table 12.16 Values of Correction Factor, r_c

ϕ° \ B/H	1	2	3	4	5	6	8	10	Remarks
0	1.00	1.02	1.11	1.21	1.30	1.40	1.59	1.78	$r_c = 1$ for $B/H < 1.41$
10	1.00	1.11	1.35	1.62	1.95	2.33	3.34	4.77	$r_c = 1$ for $B/H < 1.12$
20	1.01	1.39	2.12	3.29	5.17	8.29	22.00	61.50	$r_c = 1$ for $B/H < 0.86$
30	1.13	2.50	6.36	17.40	50.20	150	1444	14800	$r_c = 1$ for $B/H < 0.63$

Adapted from Vesic, 1974.

Table 12.17 Values of Correction Factor, r_q

ϕ° \ B/H	1	2	3	4	5	6	8	10	Remarks
0	1.00	1.00	1.00	1.00	1.00	1.00	1.00	1.00	$r_q = 1$ for all B/H
10	1.00	1.07	1.21	1.37	1.56	1.79	2.39	3.25	$r_q = 1$ for $B/H < 1.12$
20	1.01	1.33	1.95	2.93	4.52	7.14	18.70	51.90	$r_q = 1$ for $B/H < 0.86$
30	1.12	2.42	6.07	16.50	47.50	142	1370	14000	$r_q = 1$ for $B/H < 0.63$

Adapted from Vesic, 1974.

Q 12.31: To compute the ultimate bearing capacity of the strip footing shown in Fig. 12.41: (a) under undrained loading conditions and (b) under drained loading conditions.

***Ans*: (a) under undrained loading conditions:**

$$c = c_u = 6\ \text{T/m}^2 \quad \text{and} \quad \phi = 0^\circ$$

$$\frac{B}{H} = \frac{2}{1} = 2$$

Table 12.18 Values of Correction Factor, r_γ

$\phi°$ \ B/H	2	3	4	5	6	8	10	Remarks
0	1.00	1.00	1.00	1.00	1.00	1.00	1.00	$r_\gamma = 1$ for all B/H
10	1.00	1.00	1.00	1.01	1.04	1.12	1.36	$r_\gamma = 1$ for $B/H < 4.07$
20	1.00	1.07	1.28	1.63	2.20	4.41	9.82	$r_\gamma = 1$ for $B/H < 2.14$
30	1.20	2.07	4.23	9.90	24.80	178	1450	$r_\gamma = 1$ for $B/H < 1.3$

Adapted from Vesic, 1974.

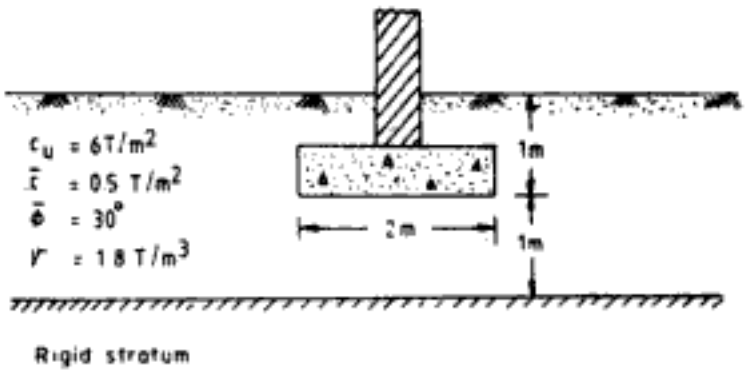

Fig. 12.41 Q 12.31

From Tables 12.16 and 12.17 for $\phi = 0°$ and $B/H = 2$: $r_c = 1.02$, $r_q = 1.00$

$$\therefore \quad q_{ult} = 6 \times 5.14 \times 1.02 + 1.8 \times 1 \times 1 \times 1$$
$$= 33 \text{ T/m}^2$$

(b) under drained loading conditions:

$$c = \bar{c} = 0.5 \text{ T/m}^2 \quad \text{and} \quad \phi = \bar{\phi} = 30°$$

For $\phi = 30°$ and $B/H = 2$: $r_c = 2.5$, $r_q = 2.42$, $r_\gamma = 1.2$

$$\therefore \quad q_{ult} = 0.5 \times 30.1 \times 2.5 + 1.8 \times 1 \times 18.4 \times 2.42 + 0.5 \times 1.8 \times 2 \times 22.4 \times 1.2$$
$$= 166 \text{ T/m}^2$$

12.4.3 Footing on Multilayer Deposit

When footing rests on a multilayer deposit as shown in Fig. 12.42, Bowles (1982) recommends that the ultimate bearing capacity of the footing be determined using average values of cohesion, c_{av} and angle of shearing resistance, ϕ_{av}. The average values are computed over a depth H below the base of the footing, where

$$H = \sum_{j=1}^{n} h_j = 0.5\, B \tan\left(45 + \frac{\phi_{av}}{2}\right) \qquad (12.35)$$

c_{av} and ϕ_{av} are given by,

$$c_{av} = \frac{\sum_{j=1}^{n} c_j h_j}{\sum_{j=1}^{n} h_j} \tag{12.36}$$

$$\tan \phi_{av} = \frac{\sum_{j=1}^{n} h_j \tan \phi_j}{\sum_{j=1}^{n} h_j} \tag{12.37}$$

If necessary any value of h_j may be multiplied by a suitable weighting factor. The average parameters should be determined by trial and error since the term H used in the equations is itself dependent on ϕ_{av}.

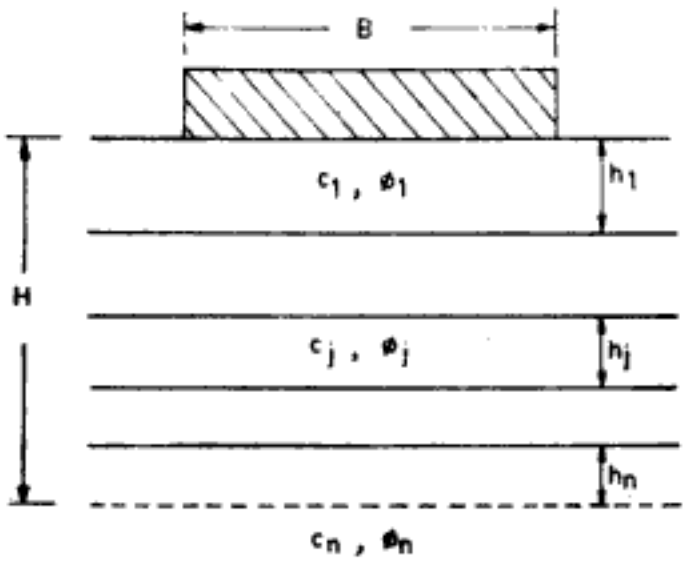

Fig. 12.42 Footing on multilayered soil deposit

12.5 CORRECTIONS FOR DIFFERENT MODES OF FAILURE

The determination of the ultimate bearing capacity of shallow foundations explained heretofore is for the case of general shear failure. For the other modes of failure the procedures require corrections or modifications.

12.5.1 For Local Shear Failure

Terzaghi recommends the c and ϕ values to be modified as follows:

$$c^* = 0.67c \tag{12.38}$$

$$\phi^* = \tan^{-1}(0.67 \tan \phi) \tag{12.39}$$

Now, the ultimate bearing capacity is determined with these values of c^* and ϕ^*—using them in the procedures explained for general shear failure (e.g., bearing capacity factors and correction factors are reckoned for ϕ^*).

IS Code (IS: 6403-1981) gives the same recommendations due to Terzaghi, however, with respect to different bearing capacity factors—i.e., with respect to bearing capacity factors recommended by Vesic or the P-R-C-K-V factors.

Vesic suggests the following modification for ϕ in the case of sands,

$$\phi^* = \tan^{-1}[(0.67 + I_D - 0.75\, I_D^2) \tan \phi] \qquad (12.40)$$

in the range of $0 \leqslant I_D \leqslant 0.67$ (I_D = relative density)

For $I_D \geqslant 0.67$: $\phi^* = \phi$ i.e., general shear failure occurs.

Experiments on small size model foundations carried out by Ismael and Vesic (1981) show that for shallow foundations Terzaghi's recommendation to use reduced shear strength parameters is conservative.

Vesic suggests compressibility factors to take into account scale effects and other modes of failure. Ismael and Vesic's test results show these to be satisfactory for shallow foundations. However, the validity or applicability of these compressibility factors for prototype foundations is yet to be confirmed. The procedure also requires elaborate laboratory testing of soils to determine their rigidity modulus. For these reasons, Vesic's compressibility factors are not discussed here.

Q 12.32: To compute the ultimate bearing capacity of the square footing shown in Fig. 12.43.

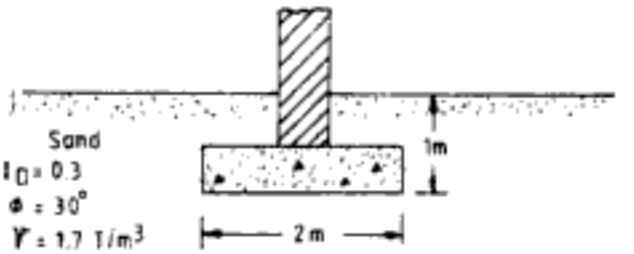

Fig. 12.43 Q 12.32

Ans: The ultimate bearing capacity will be computed using IS Code Method and Vesic's recommendations.

(a) IS Code procedure:

$$\phi^* = \tan^{-1}\left(\frac{2}{3}\tan 30^\circ\right) = 21.05^\circ$$

For $\phi = 21.05^\circ$ (by linear interpolation):

$$N_q = 7.29,\ N_\gamma = 6.49$$

$$q_{ult} = qN_qS_qd_q + 0.5\gamma BN_\gamma S_\gamma d_\gamma$$

$$S_q = 1.2,\ S_\gamma = 0.8,\ d_q = d_\gamma = 1.07$$

$$\therefore \quad q_{ult-\phi^*} = 25\ \text{T/m}^2$$

According to IS recommendations (Table 12.2) for I_D between 0.2 and 0.7 q_{ult} is to be interpolated between local shear failure and general shear failure. For general shear failure: $\phi = 30^\circ$, $d_q = d_\gamma = 1.087$

$$q_{ult-\phi} = 74\ \text{T/m}^2$$

By linear interpolation;

$$q_{ult} = 25 + (74 - 25) \times \frac{10}{50}$$

$$= 35 \text{ T/m}^2$$

(b) Vesic's procedure:

$$\phi^* = \tan^{-1} [(0.67 + 0.3 - 0.75 \times 0.3^2) \tan 30^\circ]$$

$$= 27.52^\circ$$

By linear interpolation: $N_q = 14.53$, $N_\gamma = 16.64$

$$S_q = 1 + \left(\frac{2}{2}\right) \tan 27.52^\circ = 1.52$$

$$S_\gamma = 0.6$$

$$\therefore \quad q_{ult} = qN_qS_q + 0.5\gamma BN_\gamma S_\gamma$$

$$= 1.7 \times 1 \times 14.53 \times 1.52 + 0.5 \times 1.7 \times 2 \times 16.64 \times 0.6$$

$$= 54 \text{ T/m}^2$$

(Recall that according to Vesic, Terzaghi's recommendations are conservative.) It may be, however, noted that rarely will be footings placed on cohesionless soil with relative density less than 0.5.

Peck, Hanson and Thornburn (1953) give bearing capacity factors which automatically incorporate adjustments for local shear failure. These are meant for use in cohesionless soils. The curves are obtained on the following principles:

For $\phi \geq 38^\circ$ the curves are same as for general shear failure

For $\phi \leq 28^\circ$ the N_γ and N_q are equal to the values at $\phi^* = \tan^{-1}$ (0.67 tan ϕ) i.e., Terzaghi's suggestion. Thus, for $\phi = 28^\circ$, the N_γ value is that corresponding to $\phi = 19.6^\circ$.

For $28^\circ < \phi < 38^\circ$ smooth transition curves are drawn.

Peck, Hanson and Thornburn have given the curves from Terzaghi's bearing capacity factors. The author has adopted the above concept of Peck, Hanson and Thornburn for P-R-C-K-V bearing capacity factors. These factors which automatically incorporate the adjustments for mode of failure are shown in Fig. 12.44. These curves are recommended for calculation of ultimate bearing capacity of foundations in cohesionless soils.

12.6 ULTIMATE NET BEARING CAPACITY ($q_{ult-net}$)

The ultimate net bearing capacity is the net intensity of loading at the base of the foundation which would cause shear failure of soil. This is obtained as the difference of ultimate bearing capacity (q_{ult}) and the effective surcharge intensity (q) at the base level of foundations.

$$q_{ult-net} = q_{ult} - q \tag{12.41}$$

Hence, the equation for ultimate net bearing capacity for a strip footing for the case of general shear failure will read as,

$$q_{ult-net} = cN_c + q(N_q - 1) + 0.5\gamma BN_\gamma \tag{12.42}$$

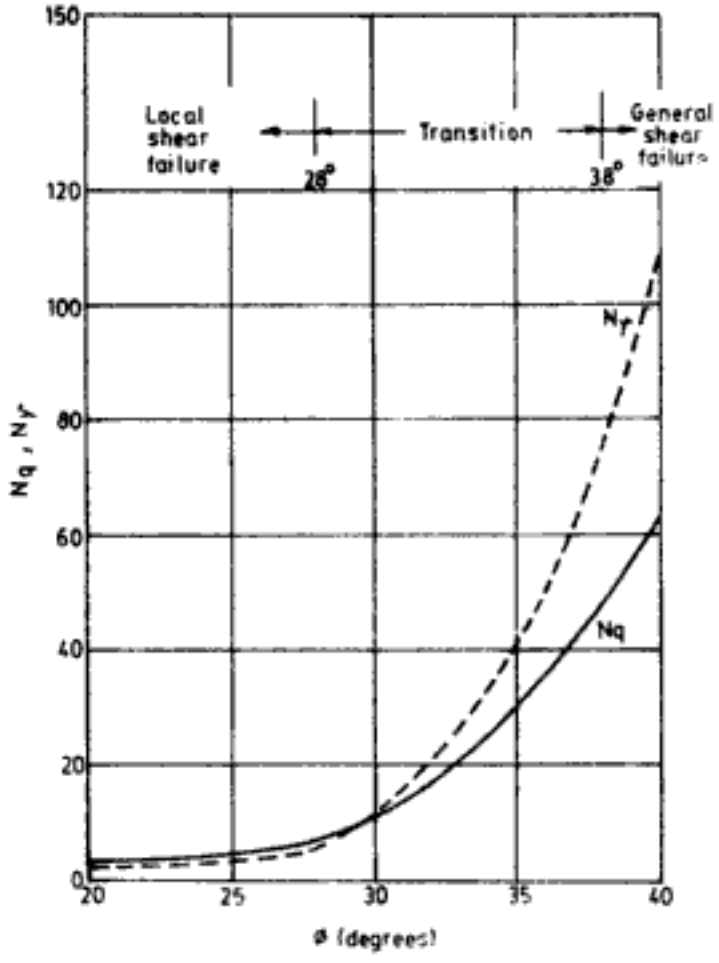

Fig. 12.44 Bearing capacity factors (P-R-C-K-V) modified to account for mode of failure

For other effects the correction factors could be applied to the above equation as explained for ultimate bearing capacity.

Q 12.33: To determine the ultimate net bearing capacity of the footing in Q 12.5.

Ans: The equation for ultimate net bearing capacity in this case is:

$$q_{ult-net} = cN_cS_c + q(N_q - 1)S_q + 0.5\gamma BN_\gamma S_\gamma$$

Substituting the values as indicated in Q 12.5

$$q_{ult-net} = 1\times 20.7\times 1.26 + 1.3\times(10.7 - 1)\times 1.233 + 0.5\times 0.8\times 1.5\times 10.9\times 0.8$$
$$= 47 \text{ T/m}^2$$

12.7 SAFE NET BEARING CAPACITY ($q_{safe-net}$)

Safe net bearing capacity is the maximum net intensity of loading that the foundation will safely carry without the risk of shear failure of soil irrespective of any amount of settlement that may occur. It is obtained by dividing the ultimate net bearing capacity by a suitable factor of safety (FS).

$$q_{safe-net} = \frac{q_{ult-net}}{FS} \qquad (12.43)$$

12.7.1 Selection of Factor of Safety

1. *IS Code recommendations*

As per National Building Code of India—1983, ". . . the bearing capacity shall be calculated from stability consideration of shear; factor of safety of 2.5 shall be adopted for safe bearing capacity."

2. *Recommendations by Bowles*

Against shear failure Bowles recommends the following safety factors:

Spread footings—2 to 3
Mat foundations—1.7 to 2.5
Footings subjected to uplift force—1.7 to 2.5

A factor of safety of 3 may be used for the following combination of design loads:

Design load = $R_D \times$(dead load) + $R_L \times$(live load) + $R_S \times$(snow load) + hydrostatic pressure

Wind and earthquake loads may be considered transitory, and one may use FS = 2.0 for the following combination of loads:

Design load = $R_D \times$(dead load) + $R_L \times$(live load) + $R_W \times$(wind load) + hydrostatic pressure

Design load = $R_D \times$(dead load) + $R_L \times$(live load) + $R_E \times$(earthquake load) + $R_S \times$(slow load)

The factors R_i are code reduction or amplification factors for both load condition and load combination.

3. *Teng's recommendation*

According to Teng (1962), "A factor of safety of 3 is usually used under normal loading conditions and a factor of safety of 2 under combined maximum load."

4. *Vesic's recommendations*

Vesic in his recommendation of safety factors recognises that the choice of safety factors should depend on the character and expected life of the structure as well as on the consequences of failure. "The selection of safety factors for design cannot be made properly without assessing the degree of reliability of all other parameters that enter into design, such as design loads, strength and deformation characteristics of the soil mass, etc. In view of this each case is to be considered separately by the designer." His recommendations (Table 12.19) may be used as a guide for permanent structures in reasonably homogeneous soil conditions.

5. *Hansen's partial safety factors*

In this approach the uncertainties involved with different variables such as foundation loads or soil strength are introduced separately as "partial safety factors". In a nominal state of failure the acting loads are multiplied by certain partial factors, while the strength parameters c and ϕ are reduced by other partial factors. See Table 12.20 for Hansen's partial safety factors.

Q 12.34: To determine the safe net bearing capacity of the footing in Q 12.5.

Ans: The safe net bearing capacity will be determined by traditional approach and using partial safety factors.

Table 12.19 Vesic's Minimum Safety Factors for Design of Shallow Foundations

Category	Typical structure	Characteristics of the category	Soil exploration	
			Thorough, complete	Limited
A	Railway bridges, warehouses, blast furnaces, retaining walls, silos	Maximum design load likely to occur often; consequences of failure disastrous	3.0	4.0
B	Highway bridges, light industrial and public buildings	Maximum design load may occur occasionally; consequences of failure serious	2.5	3.5
C	Apartment and office buildings	Maximum design load unlikely to occur	2.0	3.0

Remarks:

1. For temporary structures these factors can be reduced to 75 per cent of the above values. However, in no case should the safety factors lower than 2.0 be used.
2. For exceptionally tall buildings, such as chimneys and towers, or generally whenever progressive bearing capacity failure may be feared, these factors should be increased by 20 to 50 per cent.
3. The possibility of flooding of foundation soil and/or removal of existing overburden by scour or excavation should be given adequate consideration.
4. It is advisable to check both the short term (end-of-construction) and long-term stability, unless one of the two conditions is clearly less favourable.
5. It is understood that all foundations will be analysed also with respect to maximum tolerable total and differential settlement. If settlement governs the design, higher safety factors must be used.

After Vesic, 1974.

Table 12.20 Hansen's Partial Safety Factors for Design of Shallow Foundations

Load factors		
Dead load	1.00	
Steady water pressure	1.00	
Fluctuating water pressure	1.20	(1.10)
Live loads (general)	1.50	(1.25)
Wind loads	1.50	(1.25)
Earth pressure or grain pressure in silos	1.20	(1.10)
Strength factors		
Cohesion, c	2.00	(1.80)
Angle of shearing resistance, tan ϕ	1.20	(1.10)

Remark: The numbers in the parentheses refer to temporary structures of to extraordinary combinations of loading such as (dead load + most unfavourable live load + most unfavourable wind load) After Vesic, 1974.

(a) *Traditional approach*

$q_{ult-net} = 47$ T/m^2 as determined in Q 12.33

Using a factor of safety of 3,

$q_{safe-net} = 47/3 = 16$ T/m^2

(b) *Partial safety factors approach*

Let us assume that the loading is normal (which justifies using FS = 3 in the traditional approach) and the loading is 65% due to live load and 35% due to dead load. Using strength factors: $c = 1/2 = 0.5$ T/m²

$\tan \phi = \tan 25°/1.2 \quad \therefore \quad \phi = 21.24°$

For $\phi = 21.24°$: $N_c = 16.3$, $N_q = 7.47$, $N_\gamma = 6.76$

$S_c = 1 + (1.5/3)(7.47/16.3) = 1.229$

$S_q = 1 + (1.5/3) \tan 21.24° = 1.194$

$S_\gamma = 1 - 0.4(1.5/3) = 0.8$

The ultimate net bearing capacity of the footing is,

$q_{ult-net} = 0.5 \times 16.3 \times 1.229 + 1.3 \times (7.47 - 1) \times 1.194 + 0.5 \times 0.8 \times 1.5 \times 6.76 \times 0.8$

$= 24$ T/m²

Average load factor (ALF) is computed as,

$$ALF = \frac{[(\% \text{ live load} \times \text{load factor for live load}) + (\% \text{ dead load} \times \text{load factor for dead load})]}{100}$$

$= (65 \times 1.5 + 35 \times 1)/100$

$ALF = 1.325$

Now, $q_{safe-net} = q_{ult-net}/ALF$

$= 24/1.325$

$= 18$ T/m²

12.8 SAFE BEARING PRESSURE ($q_{safe-pr}$)

Safe bearing pressure is the maximum net intensity of loading that soil by the foundation without the settlement exceeding the p mined for each type of structure and type of soil. (Detail Settlement of Shallow Foundations.)

12.9 ALLOWABLE BEARING PRESSURE (q

Allowable bearing pressure is the minimur from considerations of shear failure) and tions of permissible settlement).

When wind and seismic forces are consi suitably modified. Provisions in National 10.

12.10 ACTUAL BEARING PRESSURE ($q_{act-net}$)

Actual bearing pressure is the net intensity of loading that the foundation actually transfers to the soil. It is evident that,

$$q_{act-net} \leqslant q_{all-net}$$

12.11 BEARING CAPACITY BASED ON STANDARD PENETRATION TEST

In case of cohesionless soils the standard penetration test results can be used to determine the ultimate bearing capacity of footings. The determination of standard penetration resistance value (N) is explained in Ch. 19.

The standard penetration resistance is determined at a number of selected points at intervals of 75 cm in the vertical direction or at change of strata if it occurs earlier. The average value of N (corrected) between the level of the base of the footing and a depth equal to 1.5 to 2 times the width of the foundation below the base is determined. In computing the average any individual value more than 50 per cent of the average should be neglected. But the values for all loose seams should be included.

12.11.1 Correlation Between Standard Penetration Number, N, and Angle of Shearing Resistance, ϕ

The empirical correlation given in Fig. 12.45 between ϕ and N can be used to know approximately the value of ϕ in the analysis for bearing capacity (Peck, Hanson, and Thornburn, 3).

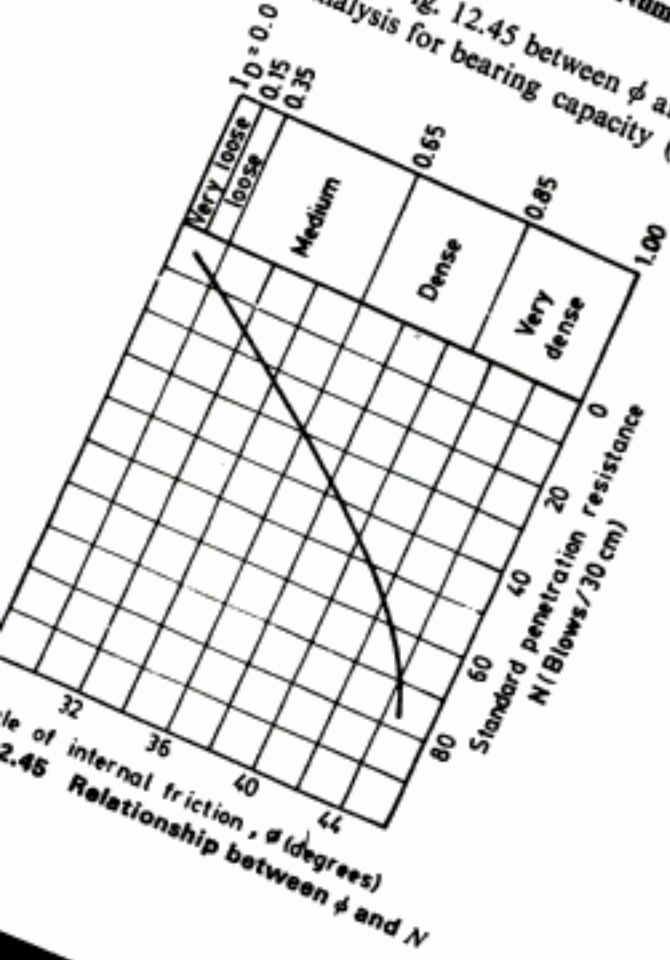

2.45 Relationship between ϕ and N

12.10 ACTUAL BEARING PRESSURE ($q_{act-net}$)

Actual bearing pressure is the net intensity of loading that the foundation actually transfers to the soil. It is evident that,

$$q_{act-net} \leqslant q_{all-net}$$

12.11 BEARING CAPACITY BASED ON STANDARD PENETRATION TEST

In case of cohesionless soils the standard penetration test results can be used to determine the ultimate bearing capacity of footings. The determination of standard penetration resistance value (N) is explained in Ch. 19.

The standard penetration resistance is determined at a number of selected points at intervals of 75 cm in the vertical direction or at change of strata if it occurs earlier. The average value of N (corrected) between the level of the base of the footing and a depth equal to 1.5 to 2 times the width of the foundation below the base is determined. In computing the average any individual value more than 50 per cent of the average should be neglected. But the values for all loose seams should be included.

12.11.1 Correlation Between Standard Penetration Number, N, and Angle of Shearing Resistance, ϕ

The empirical correlation given in Fig. 12.45 between ϕ and N can be used to know approximately the value of ϕ in the analysis for bearing capacity (Peck, Hanson, and Thornburn, 1953).

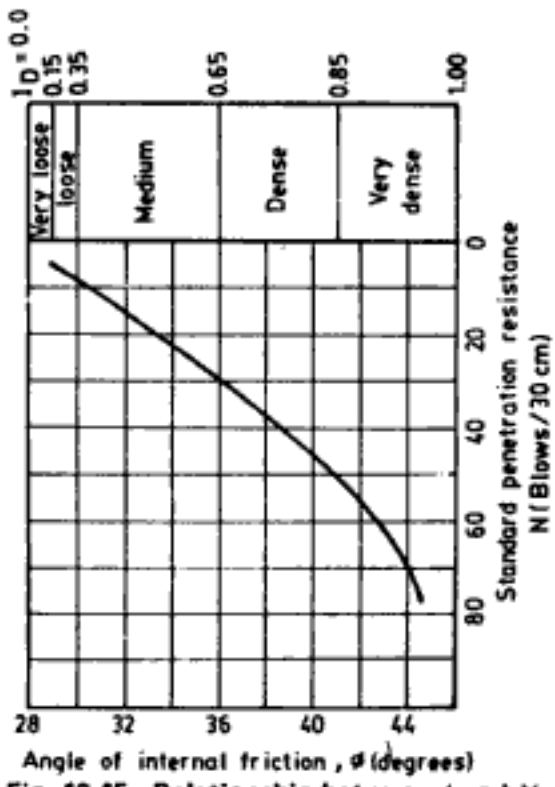

Fig. 12.45 Relationship between ϕ and N

(b) *Partial safety factors approach*

Let us assume that the loading is normal (which justifies using FS = 3 in the traditional approach) and the loading is 65% due to live load and 35% due to dead load. Using strength factors: $c = 1/2 = 0.5$ T/m²

$$\tan \phi = \tan 25°/1.2 \qquad \therefore \quad \phi = 21.24°$$

For $\phi = 21.24°$: $N_c = 16.3$, $N_q = 7.47$, $N_\gamma = 6.76$

$$S_c = 1 + (1.5/3)(7.47/16.3) = 1.229$$

$$S_q = 1 + (1.5/3) \tan 21.24° = 1.194$$

$$S_\gamma = 1 - 0.4(1.5/3) = 0.8$$

The ultimate net bearing capacity of the footing is,

$$q_{ult-net} = 0.5 \times 16.3 \times 1.229 + 1.3 \times (7.47 - 1) \times 1.194 + 0.5 \times 0.8 \times 1.5 \times 6.76 \times 0.8$$

$$= 24 \text{ T/m}^2$$

Average load factor (ALF) is computed as,

$$\text{ALF} = \frac{[(\%\text{ live load} \times \text{load factor for live load}) + (\%\text{ dead load} \times \text{load factor for dead load})]}{100}$$

$$= (65 \times 1.5 + 35 \times 1)/100$$

$$\text{ALF} = 1.325$$

Now, $q_{safe-net} = q_{ult-net}/\text{ALF}$

$$= 24/1.325$$

$$= 18 \text{ T/m}^2$$

12.8 SAFE BEARING PRESSURE ($q_{safe-pr}$)

Safe bearing pressure is the maximum net intensity of loading that can be imposed on the soil by the foundation without the settlement exceeding the permissible value—to be determined for each type of structure and type of soil. (Details are described in Chapter 14: Settlement of Shallow Foundations.)

12.9 ALLOWABLE BEARING PRESSURE ($q_{all-net}$)

Allowable bearing pressure is the minimum of the safe net bearing capacity (determined from considerations of shear failure) and safe bearing pressure (determined from considerations of permissible settlement).

When wind and seismic forces are considered in design the allowable bearing pressure is suitably modified. Provisions in National Building Code of India (1983) are discussed in Ch. 10.

Q 12.35: To determine the ultimate bearing capacity of the rectangular footing shown in Fig. 12.46. Length of footing is 3 m and the breadth is 2 m. The average density of the soil near the surface is 1.7 T/m³ and the average density below the base of the footing is 1.8 T/m³.

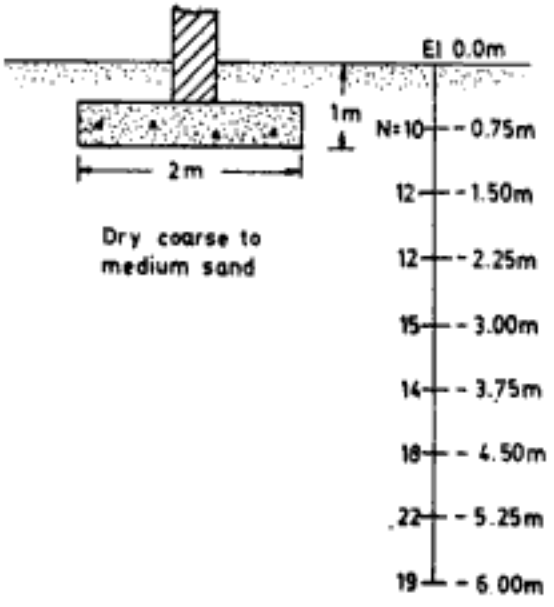

Fig. 12.46 Q 12.35

Ans: The SPT values between elevation El. −1.00 m and El −5.00 m will be considered in design (since $2B = 4$ m). There are 5 values for N in this zone of depth. The average of these 5 values is

$$N_{av} = (12 + 12 + 15 + 14 + 18)/5 = 14$$

From Fig. 12.45, for $N = 14$, $\phi = 31°$

From Fig. 12.44, $N_q = 14.5$ $N_\gamma = 17$

According to Vesic, shape factors are,

$$S_q = 1 + (2/3)\tan 31° = 1.4$$

$$S_\gamma = 1 - 0.4(2/3) = 0.733$$

Ultimate net bearing capacity is

$$q_{ult-net} = 1.7 \times 1 \times (14.5 - 1) \times 1.4 + 0.5 \times 1.8 \times 2 \times 17 \times 0.733$$

$$= 55 \text{ T/m}^2$$

$$q_{safe-net} = 55/3 = 18 \text{ T/m}^2$$

Note: No correction for measured N values has been used in the solution. This has been done to show the conservatism of the solution and to keep the historic perspective. The current practice is, however, to correct the measured N values for overburden pressure and dilatancy wherever appropriate before using them in the solution. This is demonstrated in Question 12.37 to 12.46.

12.11.2 Terzaghi and Peck's Correlation Between Safe Bearing Pressure ($q_{safe-pr}$) and Standard Penetration Resistance Value in Cohesionless Soils

The empirical correlation (for dry cohesionless soils) between SPT values (N) and $q_{safe-pr}$ for surface footings proposed by Terzaghi and Peck (1948) is shown in Fig. 12.47. The safe

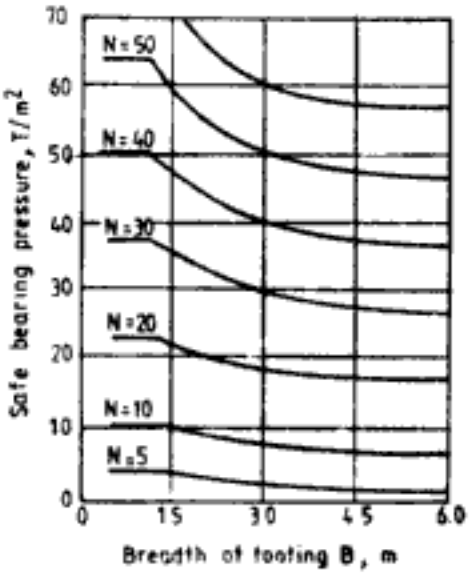

Fig. 12.47 Correlation between $q_{safe-net}$ and N

bearing pressure is for a permissible settlement of 2.5 cm. For any other value of permissible settlement the safe bearing pressure can be linearly extrapolated. Say, for any value of permissible settlement S_p, the safe bearing pressure ($q_{safe-pr,\ Sp}$) is given by the relationship:

$$q_{safe-pr,\ Sp} = \frac{q_{safe-pr}}{2.5} S_p C_W C_D \tag{12.44}$$

where, $q_{safe-pr}$ is obtained from Fig. 12.47. The average value of *measured* N within a zone of $2B$ below the base of the footing should be used. The correlations shown in Figs 12.45 and 12.47 when originally proposed made use of measured values of N. There is considerable evidence to show that such a procedure leads to over-conservative results (D'Appolonia et al., 1968, Sutherland 1975, Foot and Koutsoftas 1984). The current practice is to correct the measured values of N before using them in the correlations. The corrections applied are:

1. Overburden correction
2. Dilatancy correction for saturated fine sands, silty sands and silts

A number of procedures have been suggested for correction. Some of these are discussed in this chapter and some more in Chaps 14 and 19.
In Eq. 12.44.

C_W = correction factor for the effect of water table, Fig. 12.48 (z_w, is the depth of water table below the base of the footing)

C_D = correction factor for the effect of depth of embedment of footing, Fig. 12.48

Q 12.36: To determine the allowable net bearing pressure for the footing in Q 12.35, if the permissible settlement is 4 cm. Use Terzaghi and Peck's correlations.

Ans: Based on measured values of N, the average value as determined in Q 12.35 is 14. From Fig. 12.47, for surface footings on dry sand,

$$q_{safe-pr} = 10 \text{ T/m}^2$$

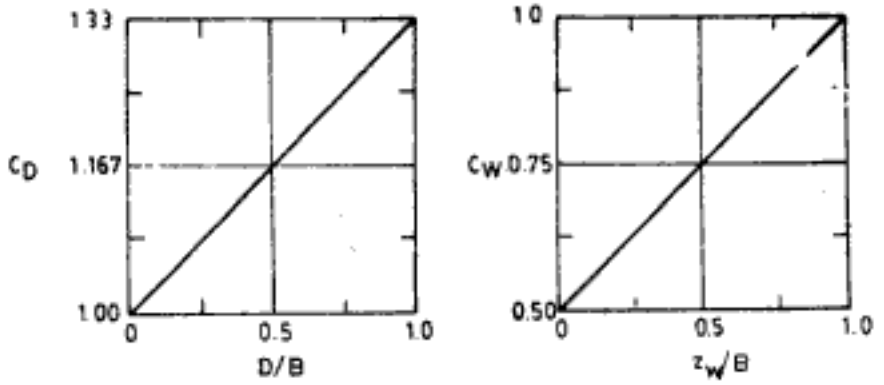

Fig. 12.48 Correction factors C_D and C_W

From Fig. 12.48, for $z_w/B = 0$, $C_w = 1$

for $D/B = \frac{1}{2}$, $C_D = 1.167$

$S_p = 4$ cm

$$q_{safe-pr} = 10 \times \frac{4}{2.5} \times 1 \times 1.167 = 19 \text{ T/m}^2$$

From Q12.35 $q_{safe-net} = 18$ T/m²

Therefore, $q_{all-net} = 18$ T/m²—almost both bearing capacity and settlement criteria govern design

Note: Terzaghi and Peck correlations are not recommended for use in design. Also see note to Q 12.35.

Q 12.37: To determine the allowable net bearing pressure for the footing in Q 12.35, when the water table is at 1 m below the base of the footing. $S_p = 4$ cm. Use Terzaghi and Peck's correlations.

Ans: The ultimate net bearing capacity calculated in Q 12.35 is modified to,

$$q_{ult-net} = 1.7 \times 1 \times (14.5 - 1) \times 1.4 + 0.5 \times 1.8 \times 2 \times 17 \times 0.733 \times 0.75$$

$= 50$ T/m², i.e., a correction factor of 0.75 is introduced in the N_γ term, since $z_w/B = 0.5$, see Fig. 12.19 and Eq. 12.18

$$q_{safe-net} = 50/3 = 17 \text{ T/m}^2$$

From Fig. 12.48, for $z_w/B = \frac{1}{2}$, $C_W = 0.75$

for $D/B = \frac{1}{2}$, $C_D = 1.167$

$\therefore$ $$q_{safe-pr} = 10 \times \frac{4}{2.5} \times 0.75 \times 1.167 = 14 \text{ T/m}^2$$

$q_{all-net} = 14$ T/m²—settlement criterion governs design

Note: See note under Q 12.35 and Q 12.36

12.11.3 Meyerhof's Correlation Between N and $q_{safe-pr}$

Meyerhof (1956, 1974) recommends the following relationships,

$$q_{safe-pr} = 1.22 N K_{D1} \quad \text{for } B \leq 1.2 \text{ m} \qquad (12.45)$$

and $$q_{safe-pr} = 0.81 N K_{D2}\left(\frac{B+0.3}{B}\right)^2 \quad \text{for } B > 1.2 \text{ m} \tag{12.46}$$

In the above expressions,

$q_{safe-pr}$ is obtained in T/m²

B is in metres and the depth correction factors are

$$K_{D1} = 1 + 0.2\left(\frac{D}{B}\right) \leqslant 1.2$$

$$K_{D2} = 1 + 0.33\left(\frac{D}{B}\right) \leqslant 1.33$$

Meyerhof suggests no correction for effect of water table, for the reason that it will be already reflected in the value of N. Meyerhof's recommendations are also for a permissible settlement of 2.5 cm and for other permissible values, the safe bearing pressure can be linearly extrapolated.

12.11.4 Bowles' Correlation Between N and $q_{safe-pr}$

Bowles (1982) recommends a 50% increase in the values obtained from Meyerhof's relationships. Accordingly,

$$q_{safe-pr} = 2K_{D2}N \quad \text{for } B \leqslant 1.2 \text{ m} \tag{12.47}$$

and $$q_{safe-pr} = 1.25 N K_{D2}\left(\frac{B+0.3}{B}\right)^2 \quad \text{for } B > 1.2 \text{ m} \tag{12.48}$$

Figure 12.49 shows the empirical relationships as per equations recommended by Bowles. In order to obtain values due to Meyerhof's equations, the values obtained from Fig. 12.49 will have to be divided by 1.5. In using Bowles' correlations the measured N values must be corrected for overburden pressure using Bazarra's equations described in Ch. 19 (Eqs 19.6 and 19.7). Bowles, however, recommends that the corrected N value should not exceed twice the measured N value nor should it be much less than the measured N value. Further when the N value indicates relative density less than 0.5 (Fig. 12.45) Bazarra's corrections should not be used.

Q 12.38: To determine the allowable net bearing pressure for the footing in Q 12.35 using Bowles' recommendations. $S_e = 4$ cm.

Ans: The values of N in Fig. 12.46 should be corrected using Bazarra's procedure.

El, m	$\bar{p}_o$, kg/cm²	C_N (Eq. 19.6)	N_{meas}	N_{corr}
−1.50	0.21	2.17(=2)	12	24
−2.25	0.27	1.92	12	23
−3.00	0.33	1.72	15	26
−3.75	0.39	1.56	14	22
−4.50	0.45	1.43	18	26

Av. value of $N_{corr} = (24 + 23 + 26 + 22 + 26)/5 = 24$

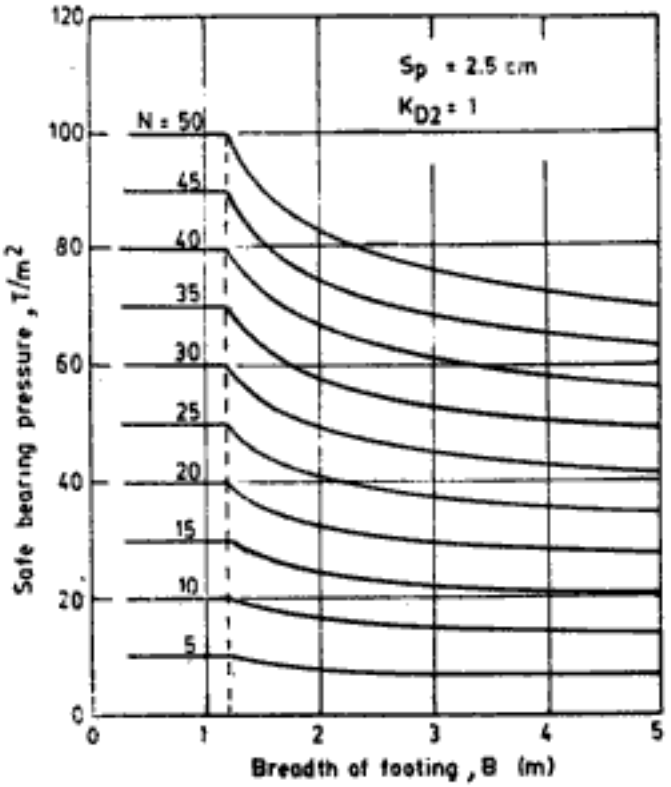

Fig. 12.49 Bowles' correlation between $q_{safe-pr}$ and N with N corrected according to Bazarra's procedure

From Fig. 12.49, for $N = 24$ and $B = 2$ m:

$$q_{safe-pr} = 39 \text{ T/m}^2$$

$$K_{D2} = 1 + 0.33\left(\frac{1}{2}\right) = 1.165$$

$$S_p = 4 \text{ cm}$$

From Eq. 12.48 $q_{safe-pr} = 1.25 \times 24 \times 1.165 \times \left(\frac{2 + 0.3}{2}\right)^2 = 46.22 \text{ T/m}^2$ for $S_p = 2.5$ cm

$$q_{safe-pr} = 46.22 \times \frac{4}{2.5} = 74 \text{ T/m}^2 \quad \text{for } S_p = 4 \text{ cm}$$

(According to Meyerhof's recommendations, $q_{safe-pr} = 74/1.5 = 49 \text{ T/m}^2$). From Fig. 12.45 $\phi = 34°$. Proceeding in the same manner as explained in Q 12.35

$$q_{safe-net} = 36 \text{ T/m}^2$$

$\therefore$ allowable net bearing pressure $q_{all-net} = 36 \text{ T/m}^2$ i.e., shear failure is the governing criterion

Q 12.39: To determine allowable net bearing pressure for footing in Q 12.35 using Meyerhof's recommendation when ground water table is 1 m below base of footing. $S_p = 4$ cm.

Ans: According to Bowles (Meyerhof) no reduction in $q_{safe-pr}$ is necessary for presence of water table. Therefore $q_{safe-pr}$ will be same as worked out in Q 12.39.

$$q_{safe-pr} = 74 \text{ T/m}^2$$

But in the ultimate bearing capacity calculations the N_γ term will be multiplied by a correction factor of 0.75 (Eq. 12.18).

$$\therefore \qquad q_{\text{safe-net}} = 32 \text{ T/m}^2.$$

$$\therefore \qquad q_{\text{all-net}} = 32 \text{ T/m}^2\text{—bearing capacity criterion governs design}$$

12.11.5 Peck, Hanson and Thornburn's (1974) Correlation Between N and $q_{\text{all-net}}$

The original recommendations of Terzaghi and Peck have been revised and the modified recommendations are presented in Fig. 12.50. The pressure obtained from the figure is allowable bearing pressure since the charts take into consideration both bearing capacity criterion and settlement criterion. The sloping linear portion of the curves define the limiting pressure when bearing capacity considerations govern the allowable pressure. To obtain this part of curve safe bearing capacity is calculated using Terzaghi's bearing capacity factors and a factor of safety of 2. The horizontal line portion of the curves define the limiting pressure when settlement considerations govern the design. The value corresponding to this horizontal portion is given by,

$$q_{\text{all-net}} = 1.1N \text{ T/m}^2 \tag{12.49}$$

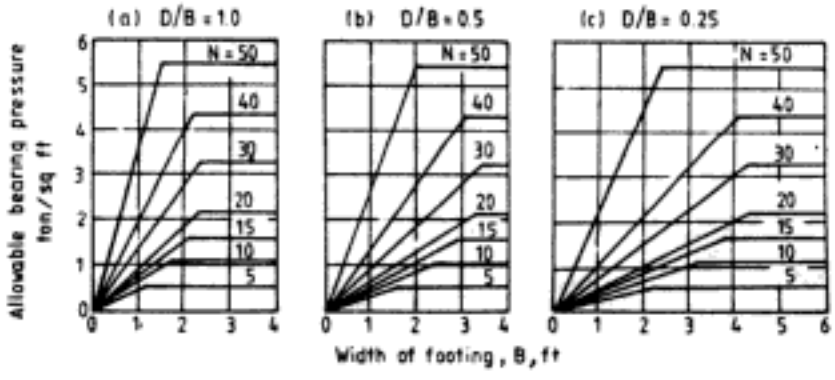

Fig. 12.50 Peck, Hanson, and Thornburn's correlations between allowable bearing pressure and N (After Peck, Hanson and Thorburn, 1974; reprinted by permission of John Wiley and Sons, New York)

The measured N values are to be corrected for overburden pressure according to procedure suggested by Peck, Hanson and Thornburn described in Ch. 19. The allowable net bearing pressures in the figure are for a permissible total settlement of 2.5 cm. The correction factor for water table position is given as,

$$C_W = 0.5 + \frac{z_w}{D + B} \leqslant 1 \tag{12.50}$$

and is shown in Fig. 12.51. According to this recommendation for C_W, the effect of the ground water table on settlement is less than what is originally proposed by Terzaghi and Peck for cases other than a surface foundation with the ground water table at ground surface.

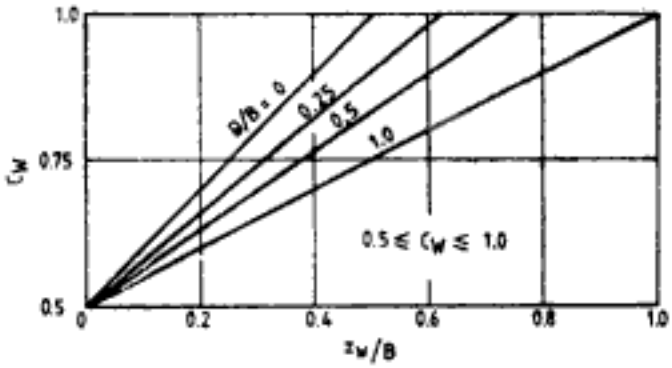

Fig. 12.51 Peck, Hanson and Thornburn's correction factor C_W for water table

Q 12.40: To determine allowable net bearing pressure for the footing in Q 12.35 using Peck, Hanson and Thornburn's correlations $S_p = 4$ cm.

Ans: The N values are corrected using Eq. 19.5 and Fig. 19.8.

El, m	C_N	N_{meas}	N_{corr}
−1.50	1.51	12	18
−2.25	1.44	12	17
−3.00	1.37	15	21
−3.75	1.32	14	18
−4.50	1.27	18	23

Av. $N_{corr} = (18 + 17 + 21 + 18 + 23)/5 = 19$

Since sand is coarse to medium no correction for dilatancy is required.

From Fig. 12.50, for $D/B = 0.5$, $N = 19$, and $B = 2$ m the allowable bearing pressure is obtained on the horizontal portion of the curve. Therefore, settlement criterion governs the design.

$$q_{all-net} = 20.9 \text{ T/m}^2 \qquad \text{for } S_p = 2.5 \text{ cm}$$

$$\text{For } S_p = 4 \text{ cm}, \qquad q_{all-net} = \frac{4}{2.5} \times 20.9 = 33 \text{ T/m}^2$$

It must be noted here that Peck, Hanson and Thornburn's correlations use a factor of safety of only two on ultimate bearing capacity against the ordinarily used value of 3. Let the q_{ult} be computed as follows:

From Fig. 12.45 for $N = 19$, $\phi = 32.5°$

From Fig. 12.44 $N_q = 19.5$, $N_\gamma = 25$

According to Vesic the shape factors are,

$$S_q = 1 + \left(\frac{2}{3}\right) \tan 32.5° = 1.425$$

$$S_\gamma = 1 - 0.4 \left(\frac{2}{3}\right) = 0.733$$

$$q_{ult-net} = 1.7 \times 1 \times (19.5 - 1) \times 1.425 + 0.5 \times 1.8 \times 2 \times 25 \times 0.733$$

$$= 78 \text{ T/m}^2$$

$$q_{safe-net} = 78/3 = 26 \text{ T/m}^2$$

Therefore if a factor of safety of 3 against shear failure is desired, $q_{all-net} = 26$ T/m², with bearing capacity criterion governing the design.

Q 12.41: To determine the allowable net bearing pressure for footing in Q 12.35 using Peck, Hanson and Thornburn's correlation when the ground water table is at 1 m below the base of the footing. $S_p = 4$ cm.

Ans:

$$z_w = 1 \text{ m}$$

$$C_W = 0.5 + \frac{1}{(1+2)} = 0.833$$

For a settlement of 4 cm,

$$q_{safe-pr} = 0.833 \times 33 = 27 \text{ T/m}^2$$

The safe net bearing capacity with a factor of safety of 3 is 23 T/m² with a correction factor of 0.75 for N_γ term in Q 12.40. Therefore,

$q_{all-net} = 23$ T/m²—bearing capacity criterion governs the design

12.11.6 Teng's Correlations Between Standard Penetration Resistance (N), Ultimate Net Bearing Capacity and Safe Bearing Pressure

According to Teng (1962), the empirical correlations between N and $q_{ult-net}$ are as given below:

From bearing capacity considerations,

for very long and strip footings:

$$q_{ult-net} = \frac{1}{62}\left[3N^2BR'_w + 5(100 + N^2)DR_w\right] \tag{12.51}$$

for square and circular footings:

$$q_{ult-net} = \frac{1}{31}\left[N^2BR'_w + 3(100 + N^2)DR_w\right] \tag{12.52}$$

From settlement considerations the equations for safe bearing pressure are as follows:

$$q_{safe-pr} = 3.5(N-3)\left(\frac{B+0.3}{2B}\right)^2 R'_w C_D \quad \text{for } S_p = 2.5 \text{ cm} \tag{12.53}$$

$$= 1.4(N-3)\left(\frac{B+0.3}{2B}\right)^2 R'_w C_D S_p \tag{12.54}$$

for a specified permissible settlement of S_p in cm

In Eqs 12.51 to 12.54,

$q_{ult-net}$ and $q_{safe-pr}$ are in T/m²

B and D are in metres

N = corrected SPT values as explained below

$N_{corr} = C_N N_{meas}$

$$C_N = \frac{1.15}{\bar{p}_o + 0.7} \qquad \text{for } 0 < \bar{p}_o < 1.05 \tag{12.55}$$

$$= \frac{3.5}{\bar{p}_o + 0.7} \qquad \text{for } 1.05 \leqslant \bar{p}_o < 2.8 \tag{12.56}$$

$$= 1 \qquad \text{for } \bar{p}_o \geqslant 2.8 \tag{12.57}$$

$\bar{p}_0$ values are in kg/cm²

R_w, R'_w = correction factors for water table level (see Fig. 12.52)

C_D = correction factor for depth of embedment

$= 1 + (D/B), \leqslant 2$

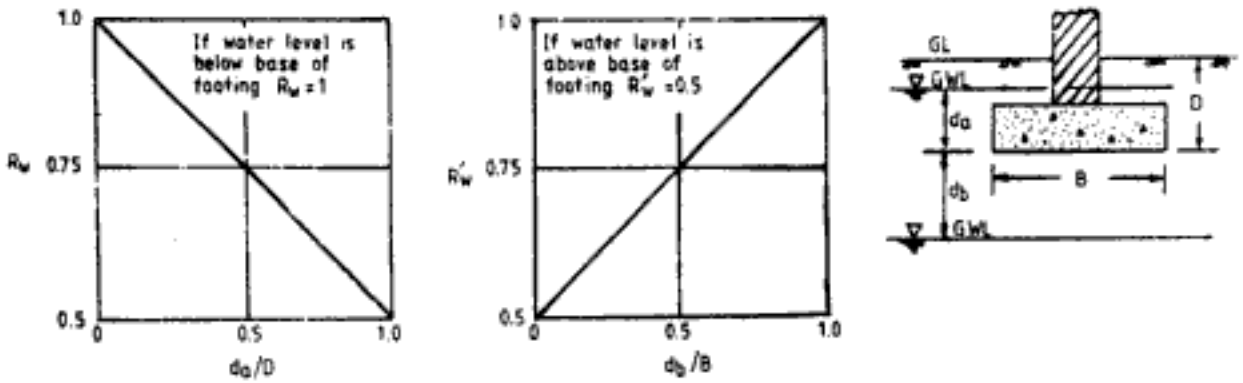

Fig. 12.52 Correction factors R_w and R'_w for water table

Q 12.42: To determine allowable net bearing pressure for the footing in Q 12.35 using Teng's correlations. $S_e = 4$ cm.

Ans: The observed N values are corrected using Eq. 12.55 as $\bar{p}_o$ values are less than 1.05 kg/cm² (see Q 12.38).

El, m	C_N	N_{meas}	N_{corr}
−1.50	1.92	12	23
−2.25	1.80	20	22
−3.00	1.70	26	26
−3.75	1.61	30	23
−4.50	1.52	40	27

Av. $N_{corr} = (23 + 22 + 26 + 23 + 27)/5 = 24$

Since the sand is dry, $R_w = R'_w = 1$

Substituting in Eq. 12.52

$$q_{ult-net} = \frac{1}{31}[24^2 \times 2 \times 1 + 3 \times (100 + 24^2) \times 1 \times 1]$$

$$= 102 \text{ T/m}^2$$

$$q_{safe-net} = 102/3 = 34 \text{ T/m}^2$$

Also from Eq. 12.54

$$q_{safe-pr} = 1.4 \times (24 - 3) \times \left(\frac{2 + 0.3}{4}\right)^2 \times 1 \times \left(1 + \frac{1}{2}\right) \times 4$$

$$= 58 \text{ T/m}^2$$

The allowable net bearing pressure is

$q_{all-net} = 34 \text{ T/m}^2$ — bearing capacity criterion governs design

Q 12.43: To determine allowable net bearing pressure for the footing in Q 12.35 using Teng's correlations when the ground water table is 1 m below the base of footing. $S_s = 4$ cm.

Ans: $d_b = 1$ m; $d_b/B = 1/2$

From Fig. 12.52 $R'_w = 0.75$ and $R_w = 1$

Substituting values in Eq. 12.52 (see also Q 12.42)

$$q_{ult-net} = 93 \text{ T/m}^2$$

$$q_{safe-net} = 93/3 = 31 \text{ T/m}^2$$

From Eq. 12.54

$$q_{safe-pr} = 43 \text{ T/m}^2$$

$\therefore$ allowable net bearing pressure = 31 T/m^2 —bearing capacity criterion governs design

Q 12.44: To determine allowable net bearing pressure for the footing in Q 12.35 using Teng's correlations when the ground water table is 0.5 m above the base of the footing. $S_s = 4$ cm.

Ans: $d_a = 0.5$ m, $d_a/D = 0.5/1 = 0.5$

From Fig. 12.52 $R'_w = 0.75$. Since water level is above base of the footing $R'_w = 0.5$. Substituting in Eq. 12.52 (see also Q 12.42)

$$q_{ult-net} = 68 \text{ T/m}^2$$

$$q_{safe-net} = 68/3 = 23 \text{ T/m}^2$$

From Eq. 12.54

$$q_{safe-pr} = 29 \text{ T/m}^2$$

Allowable net bearing pressure = 23 T/m^2 —bearing capacity criterion governs design

12.11.7 Indian Standard Code Recommendation

IS: 6403–1981 gives the same correlation between N and ϕ shown in Fig. 12.45. The measured N values are to be corrected by the procedure recommended by Peck, Hanson and Thornburn (1974) (IS: 2131–1981) for overburden pressure and also for dilatancy in case of saturated fine sand, silty sand and silt. Since the code recommends P–R–C–K–V factors, the bearing capacity factors can be determined from Fig. 12.44 which incorporates correction for mode of failure. The correction factors from Table 12.9 are used in Eq. 12.18 to determine the ultimate bearing capacity.

The safe bearing pressure can be determined from Fig. 14.29 for any specified amount of settlement. Knowing q_{ult} and $q_{safe-pr}$ the allowable net bearing pressure on soil can be determined.

Q 12.45: To determine allowable net bearing pressure for the footing in Q 12.35 using IS Code recommendations.

Ans: The corrections for N have been already carried out in Q 12.40.

$$\text{Av. } N_{corr} = 19$$

Using Figs 12.45, 12.44, Table 12.9, and Eq. 12.18

$$q_{ult-net} = 69 \text{ T/m}^2$$

$$q_{safe-net} = 69/3 = 23 \text{ T/m}^2$$

From Fig. 14.29 for $N = 19$ and $B = 2$ m the settlement for a pressure of 10 T/m² is 1.5 cm

For $$S_p = 4 \text{ cm}, \quad q_{safe-pr} = \frac{10}{1.5} \times 4 = 27 \text{ T/m}^2$$

The allowable net bearing pressure = 23 T/m², i.e., bearing capacity criterion governs design

Q 12.46: To determine allowable net bearing pressure for the footing in Q 12.35 using IS Code recommendations when the ground water table is 1 m below the base of footing.

Ans: Proceeding in the same manner as in Q 12.45 but incorporating appropriate corrections for presence of water below footing,

$$q_{safe-net} = 20 \text{ T/m}^2$$

$$q_{safe-pr} = 20 \text{ T/m}^2$$

$$\therefore \quad q_{all-net} = 20 \text{ T/m}^2$$

—i.e., both bearing capacity and settlement considerations govern design

Comparison of Different Empirical Correlations

Table 12.21 presents the results of the solutions for Q 12.36 to Q 12.46 in which allowable bearing pressure for the same footing at two different conditions has been determined using different empirical procedures.

Table 12.21 Allowable Net Bearing Pressure Using Different Correlations

Method	Dry sand		Ground water 1 m below base of footing	
	$q_{all-net}$ T/m²	governing criterion	$q_{all-net}$ T/m²	governing criterion
Terzaghi and Peck	18	bearing capacity and settlement	14	settlement
Bowles	36	bearing capacity	32	bearing capacity
Peck, Hanson and Thornburn	26	bearing capacity (FS = 3)	23	bearing capacity (FS = 3)
Teng	34	bearing capacity	31	bearing capacity
Indian Standard Code	23	bearing capacity	20	bearing capacity

The following points may be noted from the comparison of results.

1. Terzaghi and Peck correlations are conservative and are not used in design.
2. Bowles' and Teng's procedures tend to give the same results. Similarly Peck, Hanson and Thornburn's and Indian Standard Code procedures give nearly same results. The former procedures predict significantly higher values than the latter procedures. In

Indian Institute of Technology, Delhi, for more than 100 field designs so far Teng's procedure has been used. The soil conditions are silty sand, sandy silt and fine sand. Hence, dilatancy correction is also applied below water table. However, the allowable bearing pressure is usually specified for 2.5 cm total settlement, with the provision that for other permissible limits the values may be linearly extrapolated.

3. Because of the medium dense nature of the deposit bearing capacity is the governing criterion both in the presence and absence of ground water. But with increase in the denseness of the deposit settlement will govern the design particularly when water table is present. However, this depends on the breadth of footing also.
4. The presence of water table is generally believed to lower the allowable net bearing pressure. Hence, in sand $q_{all-net}$ must be computed with the shallowest possible water table, even if it may be a temporary one, because in sand the settlement occurs very rapidly.

12.11.8 Empirical Correlations Between Standard Penetration Resistance Number (N) and Safe Bearing Pressure for Mat Foundations

The correlations explained in Sections 12.11.2 to 12.11.7 are for spread footings. A structure on a mat of dimensions 6 m × 6 m or larger, can withstand greater settlement than if it were supported on spread footing. Mat foundation tends to bridge over irregularities or heterogeneity of the soil and hence the average settlement of a mat foundation does not approach the extreme values for spread footings. From the viewpoint of permissible settlement, thus a higher value of safe bearing pressure is permissible. However, because of scale effects the ultimate bearing capacity of mat foundation from considerations of shear failure will tend to be lower than that for spread footing.

Terzaghi and Peck's correlation

For mat foundations on granular soils, Terzaghi and Peck recommend an increase of 100% in the safe bearing pressure. Thus the value obtained from Fig. 12.47 is doubled in the case of mat foundations.

Meyerhof's correlation

According to Meyerhof,

$$q_{safe-pr} = 0.81NK_D \quad \text{in T/m}^2 \qquad \text{for } S_p = 2.5 \text{ cm} \tag{12.58}$$

and $$K_D = 1 + 0.33(D/B) \leqslant 1.33$$

No correction for water table is required.

Bowles' correlation

As in the case of spread footings Bowles recommend a 50% increase over Meyerhof's correlation. Thus, according to Bowles

$$q_{safe-pr} = 1.22NK_D \text{ in T/m}^2 \qquad \text{for } S_p = 2.5 \text{ cm} \tag{12.59}$$

A comparison of Meyerhof's and Bowles' correlations with their respective correlations for spread footings (for $B > 1.2$ m) reveals that as the size of the foundation increases the correlations for spread footings will automatically converge to the correlations given for mat foundations, because the term $[(B + 0.3)/B]^2$ approaches unity.

Teng's correlations:
From considerations of shear failure, Teng (1962) gives

$$q_{ult-net} = \frac{1}{31}\left[\frac{2}{3}N^2BR'_w + 2(100 + N^2)DR_w\right] \tag{12.60}$$

and from settlement considerations,

$$q_{safe-pr} = 1.75(N - 3)R'_wC_D \qquad \text{for } S_p = 2.5 \text{ cm} \tag{12.61}$$

$$= 0.7(N - 3)R'_wC_DS_p \qquad \text{for a specified permissible settlement of } S_p \text{ in cm} \tag{12.62}$$

In Eqs. 12.60 to 12.62,

$q_{ult-net}$ and $q_{safe-pr}$ are in T/m²
B and D are in metres
N = corrected SPT values as explained in Sec. 12.11.6
R_w, R'_w = correction factors for level of water-table (see Fig. 12.52)
C_D = correction factor for depth of embedment
$= 1 + (D/B) \leqslant 2$

A comparison of Teng's correlations for spread footings and mat foundations shows the following. From considerations of shear failure, the correlation given for ultimate net bearing capacity of foundation is equal to the correlation given for spread footings multiplied by 2/3. This to some extent may incorporate the scale effects due to the differences in the sizes of footings and mats. The safe bearing pressure from considerations of permissible settlement has been doubled for the mat foundations. Because as value of B increases the term $[(B + 0.3)/2B]^2$ in the expression for spread footings tends to a value of $\frac{1}{4}$.

Peck, Hanson and Thornburn's Correlation:
Stating that bearing capacity requirement is generally satisfied in mat foundation because of their large size and it is usually the settlement criterion which governs design, Peck, Hanson and Thornburn give the following correlation,

$$q_{all-net} = 2.2\,N \text{ T/m}^2 \qquad \text{for } 5 \leqslant N \leqslant 50 \tag{12.63}$$

Corrections for N and groundwater table are to be carried out as explained in Sec. 12.11.5. For $N > 50$, Eq. 12.63 becomes conservative. For $N < 5$, sand is very loose and requires compaction or the raft may have to be supported on piles. The allowable net bearing pressure may be increased somewhat if bedrock lies at a depth of one half the width of raft below the base of raft. It may be noted that Eq. 12.63 is a 100 per cent increase in the safe bearing pressure suggested for spread footings by the same authors (Eq. 12.50).

12.12 EMPIRICAL CORRELATIONS BETWEEN STATIC CONE RESISTANCE (q_c) AND BEARING CAPACITY OF FOUNDATIONS

Static cone resistance obtained in cohesionless soils (described in Ch. 19) can be used to determine ultimate bearing capacity and safe bearing pressure using empirical correlations.

12.12.1 Schemertmann's Correlation Between q_c and q_{ult}

The bearing capacity factor N_γ can be evaluated using the following correlation, (Schemertmann, 1975)

$$N_\gamma = \frac{q_c}{0.8} \tag{12.64}$$

where q_c = static cone point resistance in kg/cm²
From N_γ, the value of ϕ can be determined and hence N_q can be obtained for use in the calculation of ultimate bearing capacity.

12.12.2 Indian Standard Code (IS: 6403-1981) Recommendations

The static cone point resistance q_c with depth is determined at a number of selected points. The observed value is corrected for the dead weight of sounding rods. Then the average value of q_c at each location is determined between the level of the base of the footing and the depth equal to $1\frac{1}{2}$ to 2 times the width of the footing below the base of the footing. The average of the q_c values is determined for each location and the minimum of the average values is used in the design.

The ultimate net bearing capacity of shallow strip footings in cohesionless soil deposits is obtained from Fig. 12.53.

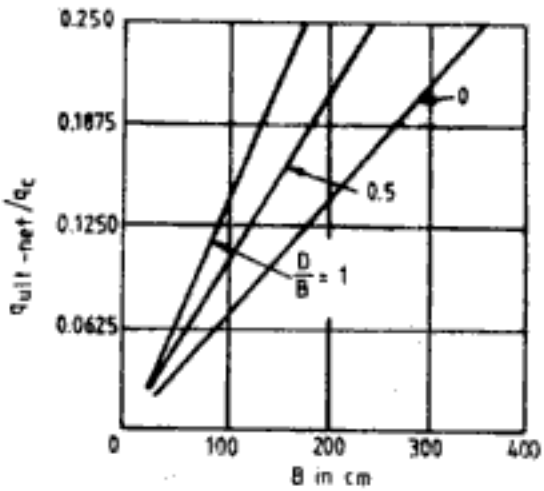

Fig. 12.53 Correlation between $q_{ult-net}$ and q_c (After IS: 6403-1981; reprinted by permission of Indian Standards Institution, New Delhi)

12.12.3 Meyerhof's Correlation Between q_c and $q_{safe-pr}$

Meyerhof's (1956, 1965) recommendations are applicable to square or strip foundations on dry sands. For a permissible settlement (S_p) of 2.5 cm,

$$q_{safe-pr} = 0.667 q_c \qquad \text{for } B \leq 1.2 \text{ m} \tag{12.65}$$

$$q_{safe-pr} = 0.392 q_c \left(\frac{B + 0.3}{B}\right)^2 \qquad \text{for } B > 1.2 \text{ m} \tag{12.66}$$

where $q_{safe-pr}$ is in T/m², q_c is in kg/cm², and B is in m.

An approximate formula to cover all foundations irrespective of width is,

$$q_{ssafe-pr} = 0.50 q_c \quad (q_c \text{ in kg/cm}^2) \tag{12.67}$$

The correction for depth of embedment should be carried out as explained in Sec. 12.11.3. There is no correction for groundwater the influence of which is considered to be reflected in the value of q_c. For permissible settlements other than 2.5 cm the safe bearing pressure can be linearly extrapolated.

It should be noted that these formulae are based on the approximate rule that the N-value is one-quarter of the static cone resistance when the value of static cone resistance is in ksf (N value is one-half of the static cone resistance when expressed in kg/cm^2).

Q 12.47: To determine the allowable net bearing pressure of a strip footing of width 1.5 m embedded 1 m in dry sand. The results of static cone penetration test is given in Fig. 12.54. Dry density of sand near footing level = 1.7 T/cu.m. Permissible settlement = 4 cm.

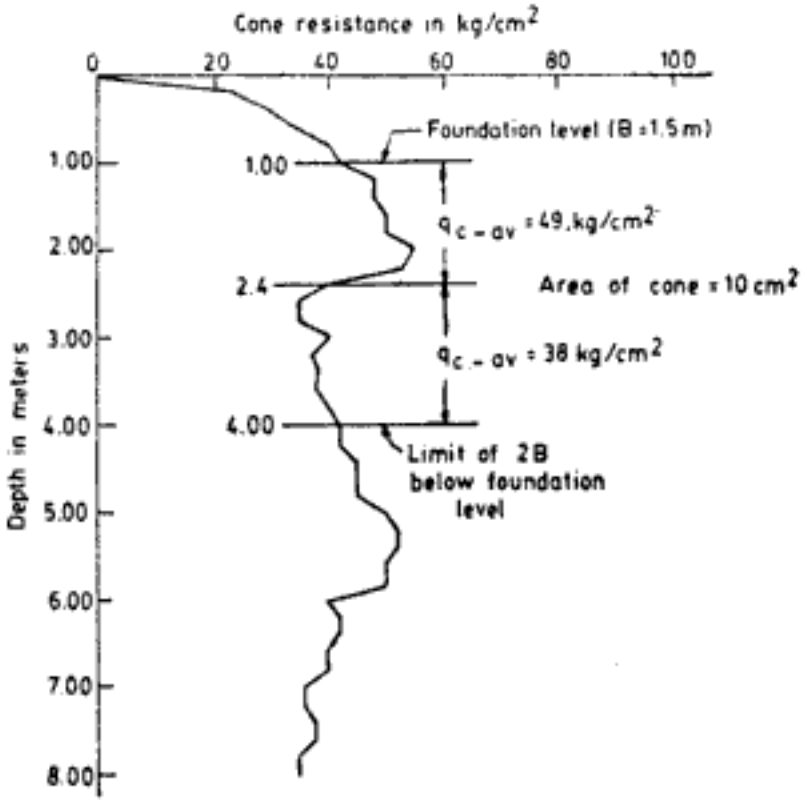

Fig. 12.54 Q.12.47

Ans: First, the average value for q_c between the level of footing and the depth equal to $2B$ below the footing should be determined, i.e., in this problem the average value of q_c should be known from depth 1 to 4 m.

As shown in Fig. 12.54 between depth 1 m and 2.4 m the average value of q_c may be taken as 49 kg/cm^2 and between depth 2.4 m and 4 m as 38 kg/cm^2. Using weighted average,

$$q_{c-av} = \frac{(2.4 - 1) \times 49 + (4 - 2.4) \times 38}{(4 - 1)}$$

$$= 43.13 \text{ kg/cm}^2$$

(depending upon the shape of the cone penetration diagram, it can be split into a number of zones, each having nearly a constant value of q_c).

Using Schemertmann's procedure:

$$N_\gamma = 43.13/0.8 = 53.9$$

From Table 12.4 and corresponding to Vesic's recommendation (Eq. 12.10)

$$\phi = 35.7°$$

$$\therefore \quad N_q = 36.5$$

Hence, ultimate bearing capacity is,

$$q_{ult} = 1.7\times1\times36.5 + 0.5\times1.7\times1.5\times53.9 = 131 \text{ T/m}^2$$

Also, $$q_{ult-net} = 1.7\times1\times(36.5 - 1) + 0.5\times1.7\times1.5\times53.9 = 129 \text{ T/m}^2$$

Hence, safe net bearing capacity, for FS = 3 is

$$q_{safe-net} = 129/3 = 43 \text{ T/m}^2$$

Using IS code recommendation (for $q_{safe-net}$):

$$D/B = 1/1.5 = 0.67$$

Using Fig. 12.53 and interpolating between curves $D/B = 0.5$ and 1.0, for $B = 150$ cm,

$$\frac{q_{ult-net}}{q_c} \simeq 0.175$$

$$\therefore \quad q_{ult-net} = 0.175\times43.13 = 7.5 \text{ kg/cm}^2 = 75 \text{ T/m}^2$$

Using FS = 3, $$q_{safe-net} = 25 \text{ T/m}^2$$

Using Meyerhof's relationships (for $q_{safe-pr}$):
Since $B > 1.2$ m, from Eq. 12.66

$$q_{safe-pr} = 0.392\, q_c \left(\frac{B + 0.3}{B}\right)^2 \left(1 + 0.33\frac{D}{B}\right)\left(\frac{S_p}{2.5}\right) \quad \text{T/m}^2$$

q_c in kg/cm²; B in m; $(1 + 0.33D/B) \leqslant 1.33$; S_p in cm
Substituting the values

$$q_{safe-pr} = 30 \text{ T/m}^2$$

Allowable net bearing pressure:
If we consider Schemertmann's approach and Meyerhof's approach:

$q_{all-net} = 30$ T/m² i.e., settlement considerations govern the design

If we consider IS code recommendations and Meyerhof's approach:

$q_{all-net} = 25$ T/m², i.e., shear failure governs the design

12.13 BEARING CAPACITY AND BEARING PRESSURE FROM PLATE LOAD TEST

The results obtained from a plate load test, carried out as explained in Ch. 19 can be used to determine the ultimate bearing capacity and allowable bearing pressure of foundations.

The typical pressure intensity vs. settlement of plate diagram is as shown in Fig. 12.55. Compare the curves with the load-settlement curves for different modes of failure in Figs 12.2, 12.4 and 12.6.

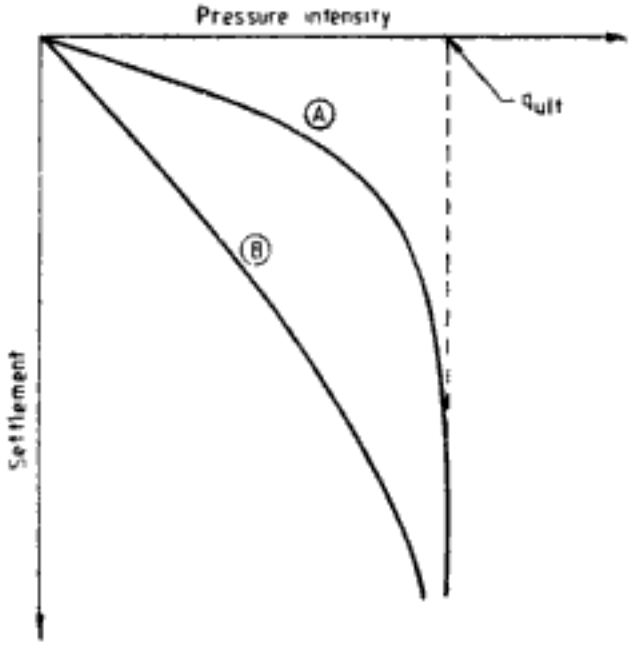

Fig. 12.55 Plate load test data

Where the curve shows a distinct peak or failure (curve A) the ultimate bearing capacity can be easily identified and q_{ult} corresponds to this peak intensity.

Where the failure is not clearly visible (curve *B*), the following empirical correlation can be used to determine the safe bearing pressure in the case of cohesionless soils:

$$\frac{S_f}{S_{pl}} = \left[\frac{B_f(B_{pl} + 30)}{B_{pl}(B_f + 30)}\right]^2 \tag{12.68}$$

where S_f = the total permissible deformation of a footing of width B_f (B_f in cm)

B_{pl} = width of test plate in cm

S_{pl} = settlement of test plate, in same units as of S_f

Knowing S_f, B_f, and B_{pl}, the value of S_{pl} can be worked out from the above relationship. From the pressure intensity-settlement curve the pressure intensity corresponding to S_{pl} can be read off—which is the allowable bearing pressure on the foundation. This recommendation for cohesionless soils is very approximate. For more details refer to Ch. 14.

12.14 PRESUMPTIVE SAFE BEARING CAPACITY

For the design of foundations of lightly loaded structures and for a preliminary design of any structure the presumptive bearing capacity may be used. National Building Code of India recommends presumptive safe bearing capacities for various types of soil which are given in Table 12.22.

Table 12.22 Safe Bearing Capacity

Sl. No.	Type of rocks/soils	Safe bearing capacity kN/m²	Remarks
	(a) *Rocks*		
1.	Rocks (hard) without lamination and defects, for example, granite, trap and diorite	3 240	—
2.	Laminated rocks, for example, stone and limestone in sound condition	1 620	—
3.	Residual deposits of shattered and broken bed rock and hard shale, cemented material	880	—
4.	Soft rock	440	—
	(b) *Non-cohesive soils*		
5.	Gravel, sand and gravel, compact and offering high resistance to penetration when excavated by tools	440	*See* Note 2
6.	Coarse sand, compact and dry	440	Dry means that the groundwater level is at a depth not less than the width of the foundation below the base of the foundation
7.	Medium sand, compact and dry	245	—
8.	Fine sand, silt (dry lumps easily pulverized by the fingers)	150	—
9.	Loose gravel or sand-gravel mixture, loose coarse to medium sand, dry	245	*See* Note 2
10.	Fine sand, loose and dry	100	—
	(c) *Cohesive soils*		
11.	Soft shale, hard or stiff clay in deep bed, dry	440	This group is susceptible to long term consolidation settlement
12.	Medium clay, readily indented with a thumb nail	245	—
13.	Moist clay and sand-clay mixture which can be indented with strong thumb pressure	150	—
14.	Soft clay indented with moderate thumb pressure	100	—
15.	Very soft clay which can be penetrated several centimetres with the thumb	50	—
16.	Black cotton soil or other shrinkable or expansive clay in dry condition (50 per cent saturation)	—	*See* Note 3. To be determined after investigation
	(d) *Peat*		
17.	Peat	—	*See* Notes 3 and 4. To be determined after investigation
	(e) *Made-up ground*		
18.	Fills or made-up ground	—	*See* Notes 2 and 4. To be determined after investigation

NOTE 1: Values listed in the table are from shear consideration only.

NOTE 2: Values are very much rough for the following reasons:

(a) Effect of characteristics of foundations (that is, effect of depth, width, shape, roughness, etc.) has not been considered.

(b) Effect of range of soil properties (that is, angle of frictional resistance, cohesion, water-table, density, etc.) has not been considered.

(c) Effect of eccentricity and indication of loads has not been considered.

NOTE 3: For non-cohesive soils, the values listed in the table shall be reduced by 50 per cent if the water-table is above or near the base of footing.

NOTE 4: Compactness of non-cohesive soils may be determined by driving a cone of 65 mm dia and 60° apex angle by a hammer of 65 kg falling from 75 cm. If corrected number of blows (N) for 30 cm penetration is less than 10, the soil is called loose; if N lies between 10 and 30, it is medium, and if more than 30, the soil is called dense.

13

ELASTIC SOLUTIONS FOR VERTICAL STRESSES AND DISPLACEMENTS IN SOILS

13.1 DEFINITIONS AND SIGN CONVENTIONS

In soil mechanics compressive stresses are considered as positive. The normal stresses and shear stresses acting on an element of soil are shown in Fig. 13.1. The stresses are positive in sign.

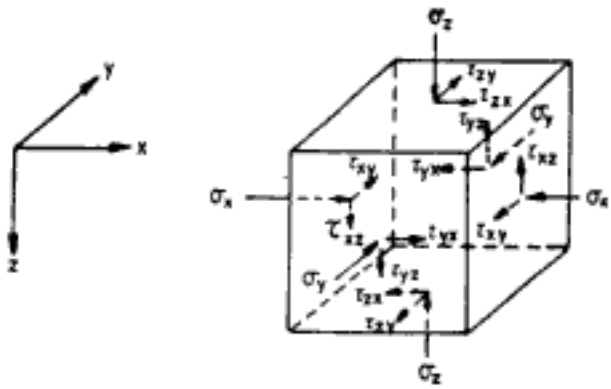

Fig. 13.1 Stresses on a soil element

The normal stresses σ_x, σ_y, σ_z are positive when directed into the surface. τ_{ij} is the shear stress acting in the j-direction on a plane normal to the i-axis. The shear stress is positive when directed in a negative cartesian direction while acting on a plane the outward normal of which points in a positive direction, or when directed in a positive cartesian direction while acting on a plane whose outward normal points in a negative cartesian direction.

For static equilibrium,

$$\tau_{xy} = \tau_{yx}; \qquad \tau_{yz} = \tau_{zy}; \qquad \tau_{zx} = \tau_{xz}$$

For different types of loading and material properties solutions are available in literature defining the complete state of stress, strain or displacement at a point. But conventionally in most of the applications in soil mechanics, computations are based only on vertical stress

and vertical displacement. Hence, solutions for only these two components of stresses and displacements are presented in this chapter. For other stresses and displacements readers may refer to Poulos and Davis (1974).

13.2 POINT LOADS

13.2.1 Boussinesq's Solution

Boussinesq's solution for stresses and displacements due to a point load is based on the following assumptions.

1. The load acts as a vertical concentrated load.
2. The elastic medium has properties of Young's modulus E and Poisson's ratio μ.
3. Load acts on the surface of semi-infinite body.
4. The medium is linearly elastic, homogeneous and isotropic.

The equation for vertical stress at a point as shown in Fig. 13.2 is,

$$\sigma_z = \frac{P}{z^2} K \tag{13.1}$$

where $$K = \frac{3}{2\pi} \frac{1}{(1 + r^2/z^2)^{5/2}}, \text{ a dimensionless factor} \tag{13.2}$$

Values of K are given in Table 13.1.

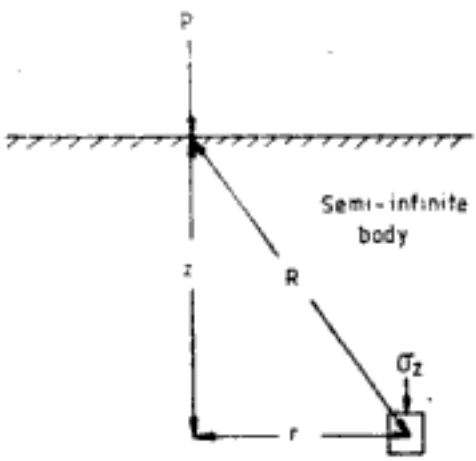

Fig. 13.2 Point load on the surface of semi-infinite medium

Table 13.1 Values of K (Eq. 3.12)

r/z	K	r/z	K
0	0.4775	0.6	0.2214
0.1	0.4657	0.7	0.1762
0.2	0.4329	0.8	0.1386
0.3	0.3849	0.9	0.1083
0.4	0.3294	1.0	0.0844
0.5	0.2773	2.0	0.0085

The equation for vertical displacement ρ_z is,

$$\rho_z = \frac{P}{Ez} \bar{K} \tag{13.3}$$

where $\bar{K}$ is a dimensionless factor given by,

$$\bar{K} = \frac{(1 + \mu)}{2\pi (1 + r^2/z^2)^{1/2}} \left[2(1 - \mu) + \frac{1}{(1 + r^2/z^2)} \right] \tag{13.4}$$

Values of $\bar{K}$ are given in Table 13.2.

Table 13.2 Values of $\bar{K}$ (Eq. 13.4)

r/z	$\mu = 0$	$\mu = 0.3$	$\mu = 0.5$
0	0.4775	0.4966	0.4775
0.1	0.4735	0.4921	0.4727
0.2	0.4622	0.4791	0.4592
0.3	0.4447	0.4592	0.4384
0.4	0.4229	0.4346	0.4127
0.5	0.3986	0.4071	0.3844
0.6	0.3733	0.3788	0.3552
0.7	0 3483	0.3511	0.3268
0.8	0.3243	0.3247	0.3001
0.9	0.3020	0.3003	0.2755
1.0	0.2813	0.2780	0.2532
2.0	0.1566	0.1480	0.1281

13.2.2 Point Load on Finite Layer

Burmister (1943, 1945) studied this problem. The expression for vertical stress at a point as shown in Fig. 13.3 is as follows,

$$\sigma_z = \frac{P}{2\pi h^2} I_{\sigma z} \tag{13.5}$$

where, $I_{\sigma z}$ = a dimensionless factor.

The expression for vertical displacement at a point on the surface (i.e., $z = 0$) is,

$$\rho_0 = \frac{P}{2\pi h E} I_{\rho 0} \tag{13.6}$$

where $I_{\rho 0}$ is a dimensionless factor.

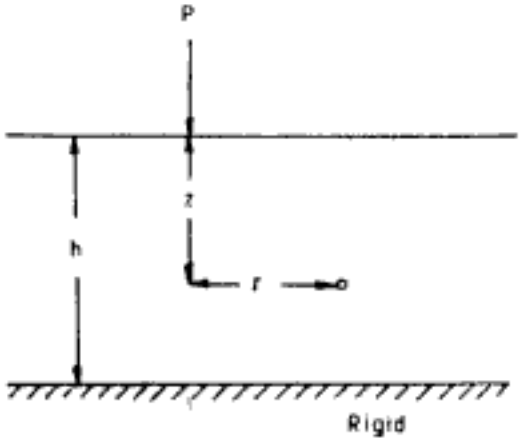

Fig. 13.3 Point load on the surface of finite layer

Numerical values of $I_{\sigma z}$ and $I_{\rho 0}$ (Poulos and Davis, 1974) are given in Tables 13.3 and 13.4, respectively. Other important solutions for point loads are summarised in Table 13.5.

Table 13.3 Values of Influence Factor $I_{\sigma z}$ for Vertical Stress σ_z (Vertical Point Load on Finite Layer)

$$\sigma_z = I_{\sigma z} P/2\pi h^2$$

r/h \ z/h	$I_{\sigma z}$ for Poisson's Ratio $\mu = 0.0$									
	1.0	0.9	0.8	0.7	0.6	0.5	0.4	0.3	0.2	0.1
0.0	4.422	4.993	5.779	7.005	9.017	12.50	19.10	33.55	75.11	300.0
0.1	4.308	4.844	5.571	6.680	8.448	11.37	16.45	25.82	43.04	53.07
0.2	3.989	4.431	5.005	5.826	7.022	8.738	11.05	13.49	13.36	5.400
0.3	3.523	3.842	4.225	4.713	5.316	5.970	6.426	6.067	4.028	0.980
0.4	2.982	3.178	3.386	3.601	3.782	3.827	3.554	2.741	1.419	0.280
0.5	2.432	2.528	2.606	2.642	2.595	2.397	1.977	1.323	0.594	0.112
0.6	1.923	1.947	1.943	1.886	1.747	1.499	1.132	0.690	0.288	0.057
0.7	1.481	1.460	1.412	1.319	1.165	0.944	0.669	0.384	0.155	0.035
0.8	1.114	1.070	1.006	0.910	0.770	0.597	0.404	0.223	0.089	0.023
0.9	0.821	0.768	0.702	0.615	0.504	0.376	0.245	0.131	0.052	0.015
1.0	0.593	0.541	0.481	0.408	0.324	0.233	0.146	0.075	0.029	0.010
1.25	0.238	0.201	0.164	0.127	0.090	0.056	0.028	0.010	0.001	−0.001
1.5	0.074	0.055	0.036	0.020	0.006	−0.006	−0.012	−0.013	−0.010	−0.007
1.75	0.007	−0.003	−0.011	−0.018	−0.021	−0.023	−0.022	−0.018	−0.014	−0.010
2.0	−0.017	−0.020	−0.023	−0.025	−0.025	−0.023	−0.020	−0.017	−0.013	−0.010
2.5	−0.019	−0.018	−0.018	−0.016	−0.015	−0.013	−0.011	−0.009	−0.007	−0.006
3.0	−0.010	−0.009	−0.008	−0.007	−0.006	−0.005	−0.004	−0.003	−0.002	−0.001
3.5	−0.004	−0.003	−0.002	−0.002	−0.001	−0.000	0.000	0.001	0.001	0.001
4.0	−0.000	0.000	0.000	0.001	0.001	0.001	0.002	0.002	0.002	0.002
6.0	0.001	0.001	0.001	0.001	0.001	0.001	0.001	0.001	0.001	0.001
8.0	0.000	0.000	0.000	0.000	0.000	0.000	0.000	0.000	0.000	0.000
10.0	0.000	0.000	0.000	0.000	0.000	0.000	0.000	0.000	0.000	0.000

r/h \ z/h	$I_{\sigma z}$ for Poisson's Ratio $\mu = 0.2$									
	1.0	0.9	0.8	0.7	0.6	0.5	0.4	0.3	0.2	0.1
0.0	4.358	5.028	5.853	7.089	9.098	12.57	19.15	33.59	75.13	300.0
0.1	4.243	4.874	5.640	6.761	8.525	11.44	16.51	25.86	43.06	53.08
0.2	3.919	4.448	5.060	5.894	7.089	8.797	11.10	13.52	13.38	5.415
0.3	3.447	3.840	4.259	4.763	5.369	6.018	6.466	6.098	4.050	0.994
0.4	2.902	3.157	3.399	3.630	3.817	3.862	3.585	2.766	1.437	0.293
0.5	2.352	2.490	2.597	2.651	2.613	2.418	1.998	1.341	0.669	0.124
0.6	1.844	1.898	1.918	1.878	1.750	1.507	1.143	0.701	0.298	0.067
0.7	1.407	1.405	1.376	1.298	1.155	0.941	0.671	0.389	0.161	0.041
0.8	1.048	1.015	0.964	0.879	0.752	0.586	0.399	0.222	0.091	0.026
0.9	0.764	0.716	0.659	0.581	0.480	0.360	0.235	0.126	0.051	0.016
1.0	0.545	0.494	0.439	0.374	0.297	0.214	0.133	0.068	0.025	0.008
1.25	0.213	0.172	0.135	0.099	0.066	0.036	0.013	−0.001	−0.007	−0.006
1.5	0.067	0.042	0.021	0.004	−0.010	−0.018	−0.022	−0.021	−0.017	−0.012
1.75	0.010	−0.003	−0.014	−0.022	−0.026	−0.028	−0.026	−0.022	−0.017	−0.012
2.0	−0.008	−0.014	−0.019	−0.022	−0.024	−0.023	−0.020	−0.017	−0.013	−0.010
2.5	−0.008	−0.009	−0.009	−0.010	−0.009	−0.009	−0.007	−0.006	−0.005	−0.004
3.0	−0.002	−0.002	−0.002	−0.001	−0.001	−0.001	−0.001	−0.000	0.000	0.001
3.5	0.001	0.001	0.001	0.002	0.002	0.002	0.002	0.002	0.002	0.002
4.0	0.002	0.002	0.002	0.002	0.002	0.002	0.002	0.002	0.002	0.002
6.0	0.000	0.000	0.000	0.000	0.000	0.000	0.000	0.000	0.000	0.000
8.0	−0.000	−0.000	−0.000	−0.000	−0.000	−0.000	−0.000	−0.000	−0.000	−0.000
10.0	−0.000	−0.000	−0.000	−0.000	−0.000	−0.000	−0.000	−0.000	−0.000	−0.000

(Contd.)

Table 13.3 *(Contd.)*

r/h \ z/h	$I_{\sigma z}$ for Poisson's Ratio $\mu = 0.4$									
	1.0	0.9	0.8	0.7	0.6	0.5	0.4	0.3	0.2	0.1
0.0	4.454	5.259	6.113	7.330	9.297	12.73	19.25	33.64	75.15	300.0
0.1	4.329	5.091	5.887	6.990	8.717	11.58	16.60	25.92	43.08	53.07
0.2	3.980	4.626	5.270	6.093	7.257	8.926	11.18	13.57	13.40	5.404
0.3	3.472	3.963	4.416	4.917	5.502	6.121	6.536	6.135	4.058	0.981
0.4	2.890	3.221	3.496	3.734	3.910	3.936	3.634	2.791	1.440	0.279
0.5	2.306	2.500	2.639	2.705	2.665	2.461	2.026	1.353	0.605	0.108
0.6	1.775	1.865	1.912	1.888	1.767	1.523	1.153	0.702	0.290	0.051
0.7	1.323	1.343	1.336	1.276	1.143	0.935	0.666	0.381	0.150	0.027
0.8	0.959	0.936	0.902	0.833	0.720	0.563	0.382	0.209	0.079	0.014
0.9	0.671	0.632	0.587	0.523	0.436	0.327	0.212	0.109	0.039	0.007
1.0	0.466	0.412	0.365	0.312	0.248	0.177	0.107	0.050	0.015	0.002
1.25	0.163	0.116	0.080	0.050	0.025	0.007	−0.007	−0.012	−0.010	−0.003
1.5	0.045	0.016	−0.007	−0.022	−0.031	−0.004	−0.031	−0.023	−0.013	−0.004
1.75	0.009	−0.007	−0.020	−0.028	−0.031	−0.030	−0.025	−0.017	−0.009	−0.002
2.0	0.003	−0.006	−0.013	−0.017	−0.018	−0.017	−0.014	−0.009	−0.005	0.001
2.5	0.007	0.005	0.003	0.001	0.001	−0.000	0.000	0.001	0.001	0.002
3.0	0.008	0.007	0.006	0.005	0.005	0.004	0.003	0.003	0.003	0.002
3.5	0.006	0.006	0.005	0.004	0.004	0.003	0.003	0.002	0.002	0.002
4.0	0.004	0.003	0.003	0.003	0.002	0.002	0.001	0.001	0.001	0.001
6.0	0.000	0.000	0.000	0.000	0.000	−0.000	−0.000	−0.000	−0.000	−0.000
8.0	−0.000	−0.000	−0.000	−0.000	−0.000	−0.000	−0.000	−0.000	−0.000	−0.000
10.0	−0.000	−0.000	−0.000	−0 000	−0.000	−0.000	−0.000	−0.000	−0.000	−0.000

r/h \ z/h	$I_{\sigma z}$ for Poisson's Ratio $\mu = 0.5$									
	1.0	0.9	0.8	0.7	0.6	0.5	0.4	0.3	0.2	0.1
0.0	4.695	5.603	6.457	7.631	9.542	12.91	19.39	33.75	75.26	300.0
0.1	4.556	5.417	6.215	7.279	8.951	11.76	16.73	26.01	43.17	53.17
0.2	4.171	4.905	5.554	6.345	7.463	9.080	11.29	13.64	13.44	5.438
0.3	3.612	4.175	4.638	5.118	5.666	6.241	6.610	6.167	4.053	0.947
0.4	2.974	3.359	3.649	3.876	4.027	4.019	3.679	2.795	1.403	0.205
0.5	2.341	2.571	2.726	2.791	2.738	2.512	2.049	1.344	0.561	0.032
0.6	1.770	1.882	1.945	1.927	1.803	1.549	1.162	0.692	0.257	−0.001
0.7	1.291	1.321	1.329	1.279	1.152	0.943	0.669	0.378	0.139	0.010
0.8	0.911	0.891	0.869	0.813	0.710	0.561	0.385	0.215	0.089	0.029
0.9	0.623	0.576	0.540	0.490	0.415	0.319	0.216	0.124	0.064	0.042
1.0	0.412	0.355	0.314	0.272	0.223	0.166	0.111	0.069	0.047	0.046
1.25	0.123	0.072	0.037	0.015	0.000	−0.007	0.007	0.000	0.014	0.029
1.5	0.023	−0.011	−0.034	−0.048	−0.052	−0.048	−0.039	−0.025	−0.010	0.003
1.75	−0.003	−0.023	−0.037	−0.046	−0.048	−0.046	−0.039	−0.030	−0.021	−0.013
2.0	−0.005	−0.016	−0.024	−0.030	−0.032	−0.033	−0.030	−0.026	−0.021	−0.018
2.5	0.004	−0.012	−0.002	−0.005	−0.007	−0.008	−0.009	−0.010	−0.010	−0.011
3.0	0.008	0.007	0.005	−0.003	0.002	0.001	−0.001	−0.002	−0.003	−0.003
3.5	0.008	0.007	0.006	0.005	0.004	0.003	0.002	0.001	0.001	0.000
4.0	0.006	0.006	0.005	0.004	0.003	0.003	0.002	0.002	0.002	0.002
6.0	0.002	0.002	0.001	0.001	0.001	0.001	0.001	0.001	0.001	0.001
8.0	0.000	0.000	0.000	0.000	0.000	0.000	0.000	0.000	0.000	0.000
10.0	−0.000	−0.000	−0.000	−0.000	−0.000	−0.000	−0.000	−0.000	−0.000	−0.000

After Poulos and Davis, 1974.

Table 13.4 Influence Values I_{ρ_0} for Surface Displacements due to Point Load on Finite Layer

r/h \ μ	0	0.2	0.4	0.5
0.05	37.580	35.921	31.052	27.351
0.1	17.586	16.728	14.260	13.360
0.2	7.624	7.162	5.897	4.914
0.3	4.327	4.016	3.154	2.480
0.4	2.720	2.478	1.827	1.320
0.5	1.792	1.599	1.092	0.699
0.6	1.212	1.048	0.635	0.290
0.7	0.823	0.690	0.352	0.051
0.8	0.560	0.450	0.168	−0.079
0.9	0.373	0.286	0.053	−0.160
1.0	0.250	0.182	−0.011	−0.183
1.25	0.080	0.031	−0.085	−0.194
1.5	0.013	−0.002	−0.077	−0.156
1.75	−0.007	−0.007	−0.048	−0.123
2.0	−0.012	−0.011	−0.039	−0.083
2.5	−0.004	−0.017	−0.025	−0.036
3.0	−0.003	0.001	−0.008	−0.025
3.5	−0.003	0.000	−0.004	−0.018
4.0	−0.001	0.000	−0.003	−0.012
6.0	−0.000	−0.000	−0.001	−0.002
8.0	−0.000	−0.000	−0.000	−0.000
10.0	−0.000	−0.000	−0.000	−0.000

After Poulos and Davis, 1974.

Table 13.5 Solutions for Point Load

Solution	Type of point load
Kelvin's solution	Vertical point load acting within an infinite elastic mass
Cerutti's solution	Horizontal point load acting on the surface of a semi-infinite elastic mass
Mindlin's solution I	Vertical point load acting beneath the surface of a semi-infinite elastic mass
Mindlin's solution II	Horizontal point load acting beneath the surface of a semi-infinite elastic mass

13.3 DISTRIBUTED LOADING ON THE SURFACE OF SEMI-INFINITE MASS

13.3.1 Uniform Vertical Strip Loading

The expression for vertical stress at point (x, z) shown in Fig. 13.4 is,

$$\sigma_z = qI_{\sigma z} \tag{13.7}$$

where

$$I_{\sigma z} = \frac{1}{\pi}[\alpha + \sin\alpha \cos(\alpha + 2\delta)] \tag{13.8}$$

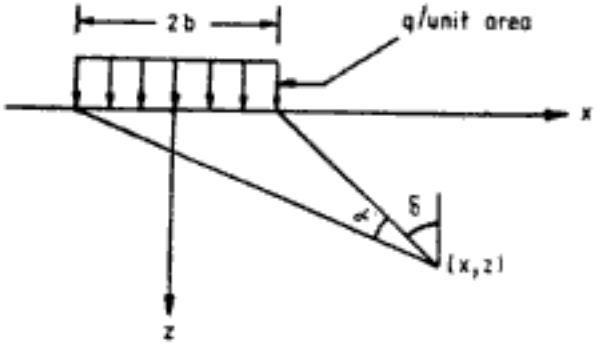

Fig. 13.4 Uniform vertical strip loading on the surface of semi-infinite medium

Values of I_{oz} are given in Table 13.6.

Table 13.6 Values of I_{oz} (Eq. 13.8)

z/b \ $\lvert x/b \rvert$	0	0.5	1.0	1.5	2.0	2.5	3.0
0	1.0000	1.0000	1.0000	1.0000	1.0000	1.0000	1.0000
0.25	—	0.9787	0.4996	0.0177	0.0027	—	—
0.5	0.9594	0.9028	0.4969	0.0892	0.0194	0.0068	0.0026
1.0	0.8183	0.7352	0.4797	0.2488	0.0776	0.0357	0.0171
1.5	0.6678	0.6078	0.4480	0.2704	0.1458	0.0771	0.0427
2.0	0.5508	0.5107	0.4095	0.2876	0.1847	0.1139	0.0705
2.5	0.4617	0.4372	0.3701	0.2851	0.2045	0.1409	0.0952
3.0	0.3954	—	—	—	—	—	0.1139
3.5	0.3457	—	—	—	—	—	—
4.0	0.3050	—	—	—	—	—	—

After Jurgenson, 1934.

Displacements due to strip loading on a semi-infinite mass are meaningful only when evaluated as displacement of one point to another, neither being located at infinity. The vertical displacement at the surface, relative to the centre of the strip is given by,

$$\rho_z(x, 0) - \rho_z(0, 0) = \frac{2q(1-\mu^2)}{\pi E}[(x-b)\ln|x-b| - (x+b)\ln|x+b| + 2b\ln b] \tag{13.9}$$

13.3.2 Vertical Strip Loading Increasing Linearly

The equation for vertical stress, σ_z, at point (x, z) (Fig. 13.5) is given by,

$$\sigma_z = qI_{oz} \tag{13.7}$$

where the dimensionless factor I_{oz} is given by,

$$I_{oz} = \frac{1}{2\pi}\left(\frac{x}{b}\alpha - \sin 2\delta\right) \tag{13.10}$$

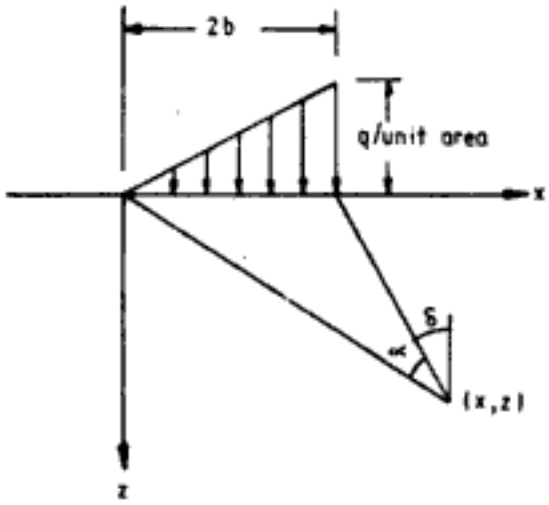

Fig. 13.5 Linearly increasing vertical strip load on the surface of semi-infinite medium

Numerical values of I_{oz} are given in Table 13.7.

The vertical displacement of a point on the surface, relative to the value at $x = 0$, is given by,

$$\rho_z(x, 0) - \rho_z(0, 0) = \frac{q(1 - \mu^2)}{\pi bE}\left[2b^2 \ln 2b - \frac{x^2}{2} \ln x + \left(\frac{x^2}{2} - 2b^2\right) \ln | 2b - x | + bx\right] \quad (13.11)$$

Table 13.7 Values of I_{oz} Eq. (13.10)

z/b \ x/b	−3	−2	−1	0	1	2	3	5
0.0	0.00	0.00	0.00	0.00	0.50	0.50	0.00	0.00
0.5	0.00	0.00	0.00	0.08	0.48	0.42	0.02	0.00
1.0	0.00	0.00	0.02	0.13	0.41	0.35	0.06	0.00
2.0	0.01	0.03	0.06	0.16	0.28	0.25	0.13	0.01
3.0	0.02	0.05	0.10	0.15	0.20	0.19	0.12	0.04
4.0	0.03	0.06	0.09	0.13	0.16	0.15	0.11	0.05

After Scott, 1963.

13.3.3 Asymmetrical Vertical Triangular Strip Loading

The equation for vertical stress at a point (x, z) (Fig. 13.6) is given by (Gray, 1936),

$$\sigma_z = qI_{oz} \quad (13.7)$$

where $$I_{oz} = \frac{1}{\pi}\left(\frac{x}{a}\alpha + \frac{a + b - x}{b}\beta\right) \quad (13.12)$$

13.3.4 Symmetric Vertical Triangular Strip Loading

The equation for vertical stress at (x, z) (Fig. 13.7) is given by (Gray, 1936),

$$\sigma_z = qI_{oz} \quad (13.7)$$

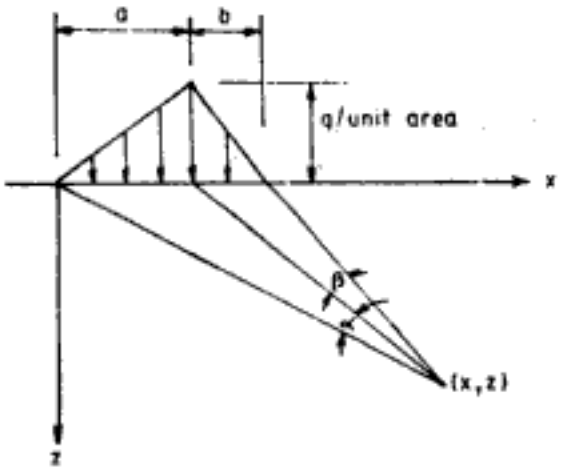

Fig. 13.6 Assymmetrical vertical strip loading on the surface of semi-infinite medium.

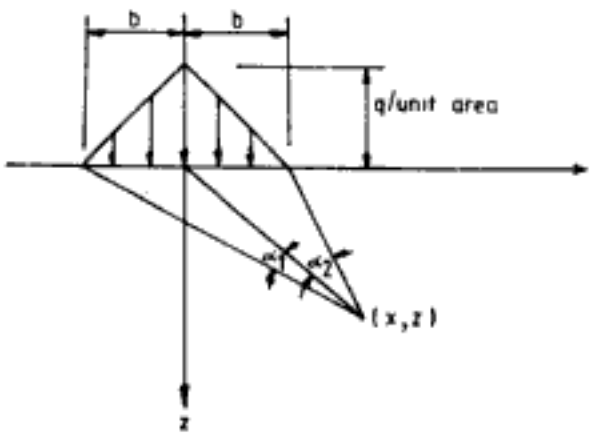

Fig. 13.7 Symmetrical vertical triangular strip loading on the surface of semi-infinite medium

where
$$I_{oz} = \frac{1}{\pi}\left[(\alpha_1 + \alpha_2) + \frac{x}{b}(\alpha_1 - \alpha_2)\right] \tag{13.13}$$

Table 13.8 gives numerical values of I_{oz}.

Table 13.8 Values of I_{oz} for Symmetric Vertical Triangular Loading (Eq. 13.13)

z/b \ $\lvert x/b \rvert$	0	0.25	0.5	0.75	1.0	1.25	1.5	2.0
0	1.0000	0.7500	0.5000	0.2500	0.0000	0.0000	0.0000	0.0000
0.25	0.8440	0.7196	0.4949	0.2620	0.0766	0.0155	0.0046	—
0.50	0.7048	0.6344	0.4714	0.2875	0.1393	0.0580	0.0250	0.0064
0.75	0.5904	0.5462	0.4350	0.3000	0.1813	0.1002	0.0545	—
1.00	0.5000	0.4711	0.3955	0.2980	0.2048	0.1319	0.0824	0.0332
1.25	0.4296	0.4101	0.3577	0.2869	0.2148	0.1526	0.1049	—
1.50	0.3744	—	0.3238	—	0.2159	—	0.1211	0.0636
1.75	0.3305	—	—	—	0.2048	—	—	—
2.00	0.2952	—	0.2682	—	—	—	0.1375	0.0862
2.50	0.2422	—	0.2266	—	0.1874	—	0.1403	0.0985

After Jurgenson, 1934.

3.3.5 Embankment Type Vertical Strip Loading

Gray (1936) gives the following solution for vertical stress at a point (x, z) as shown in in Fig. 13.8,

$$\sigma_z = qI_{oz} \tag{13.7}$$

where
$$I_{oz} = \left[\beta + \frac{x\alpha}{a} - \frac{z}{R^2}(x - b)\right] \tag{13.14}$$

or
$$I_{oz} = \frac{1}{\pi}\left\{\beta + \frac{x\alpha}{a} - \left[\frac{z}{b}\left(\frac{x}{b} - 1\right)\right] \Big/ \left[\frac{z^2}{b^2} + \left(1 - \frac{x}{b}\right)^2\right]\right\} \tag{13.15}$$

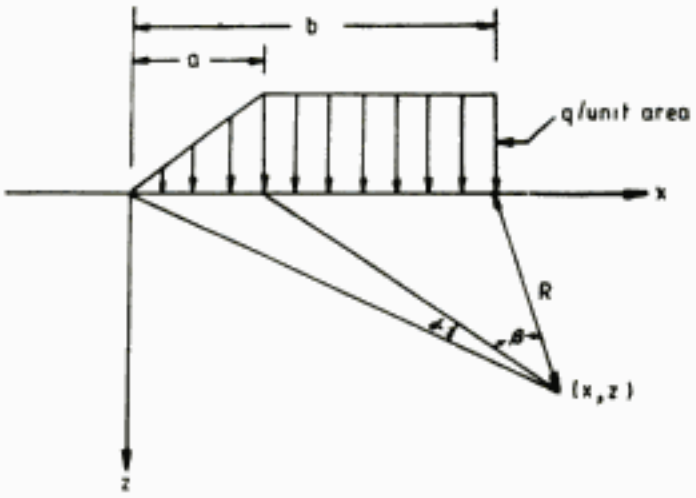

Fig. 13.8 Embankment-type vertical strip loading on the surface of the semi-infinite medium

Osterberg (1957) gives the influence chart (Fig. 13.9) for σ_z beneath the edge of the embankment. For this case,

$$\sigma_z = qI_{oz} \tag{13.7}$$

where

$$I_{oz} = \frac{1}{\pi}\left[\alpha\left(1 + \frac{b}{a}\right) + \beta\right] \tag{13.16}$$

Figure 13.9 gives the values for I_{oz}. Note that 'b' used in Osterberg's solution and Gray's solution are different (inset in Fig. 13.9 and Fig. 13.8).

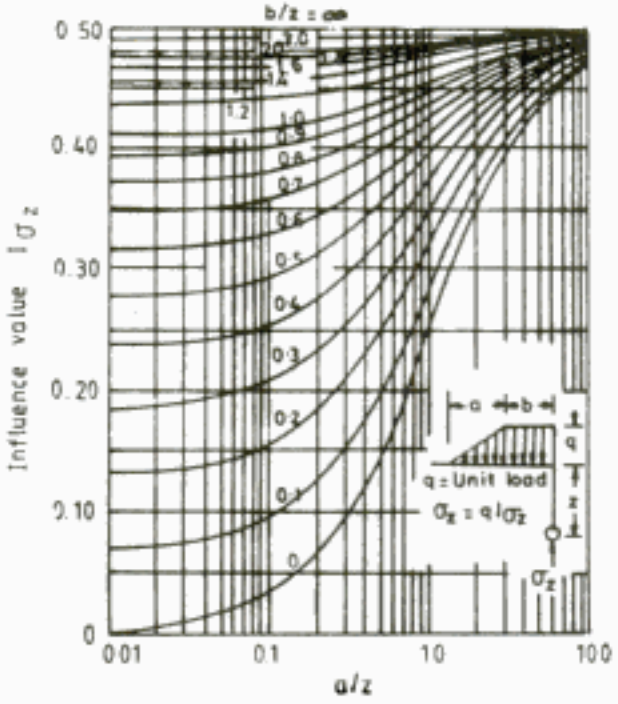

Fig. 13.9 Influence chart for vertical stress beneath the edge of embankment (After Osterberg, 1957; reprinted by permission of Butterworth Scientific, Surrey, UK)

Q 13.1: To determine the vertical stress at point P below an earth fill (strip) as shown in Fig. 13.10. The density of soil in earth fill is 2 T/cu.m.

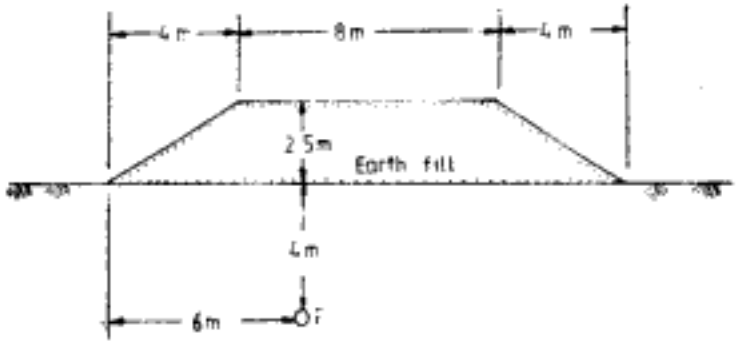

Fig. 13.10 Q 13.1

Ans: The vertical stress at point P due to the earth fill can be determined using the solutions explained so far, using the principle of superposition. Alternative superpositions are possible, four of which are explained below:

Alternative I:

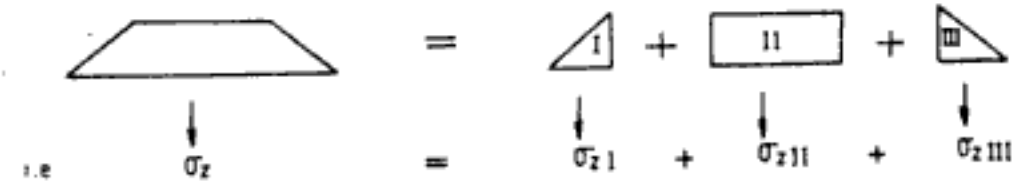

σ_{zI} = vertical stress at P due to I

σ_{zII} = vertical stress at P due to II

σ_{zIII} = vertical stress at P due to III

For σ_{zI} :

$$\frac{x}{b} = \frac{6}{2} = 3$$

$$\frac{z}{b} = \frac{4}{2} = 2$$

From Table 13.7 $I_{\sigma zI} = 0.13$

For σ_{zII} :

$$\left|\frac{x}{b}\right| = \frac{2}{4} = 0.5$$

$$\frac{z}{b} = \frac{4}{4} = 1$$

From Table 13.6 $I_{\sigma zII} = 0.7352$

For $\sigma_{\sigma zIII}$:

$$\frac{x}{b} = \frac{10}{2} = 5$$

$$\frac{z}{b} = \frac{4}{2} = 2$$

From Table 13.7 $I_{\sigma z III} = 0.01$

The value of q for all cases $= 2 \times 2.5 = 5$ T/m²

Since q is same,

$$\sigma_z = (I_{\sigma z I} + I_{\sigma z II} + I_{\sigma z III})q$$
$$= (0.13 + 0.7352 + 0.01) \times 5$$
$$= 4.376 \text{ T/m}^2$$

Alternative II:

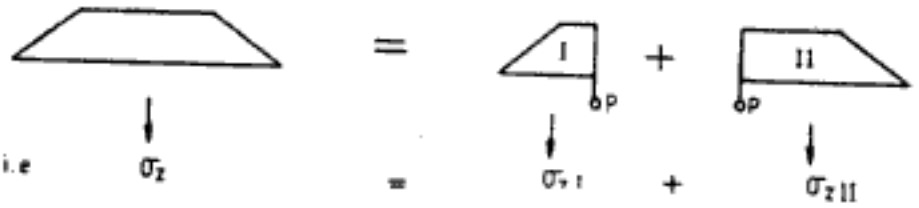

For σ_{zI}: $\frac{b}{z} = \frac{2}{4} = 0.5$

$$\frac{a}{z} = \frac{4}{4} = 1$$

From Fig. 13.9 $I_{\sigma z I} = 0.395$

For σ_{zII}: $\frac{b}{z} = \frac{6}{4} = 1.5$

$$\frac{a}{z} = \frac{4}{4} = 1$$

From Fig. 13.9 $I_{\sigma z II} = 0.475$

Value of q is 5 T/m² for I and II. Hence,

$$\sigma_z = (0.395 + 0.475) \times 5 = 4.35 \text{ T/m}^2$$

Alternative III:

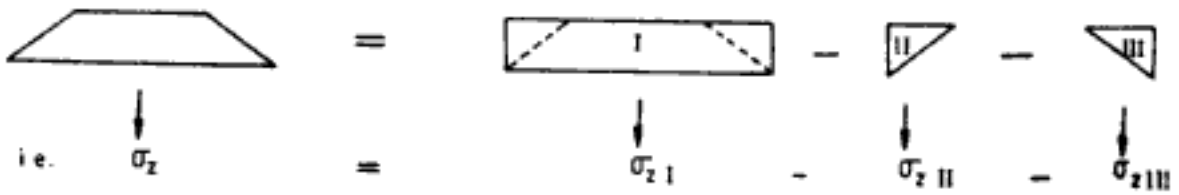

For σ_{z1}:

$$\left|\frac{x}{b}\right| = \frac{2}{8} = 0.25$$

$$\frac{z}{b} = \frac{4}{8} = 0.5$$

From Table 13.6, $I_{oz1} = (0.9594 + 0.9028)/2 = 0.9311$, by linear interpolation.

For σ_{zII}:

$$\frac{x}{b} = -\frac{2}{2} = -1$$

$$\frac{z}{b} = \frac{4}{2} = 2$$

From Table 13.7 $I_{ozII} = 0.06$

For σ_{zIII}:

$$\frac{x}{b} = -\frac{6}{2} = -3$$

$$\frac{z}{b} = \frac{4}{2} = 2$$

From Table 13.7, $I_{ozIII} = 0.01$.

Since $q = 5$ T/m² for I, II and III,

$$\sigma_z = 5 \times (0.9311 - 0.06 - 0.01) = 4.3055 \text{ T/m}^2$$

Alternative IV:

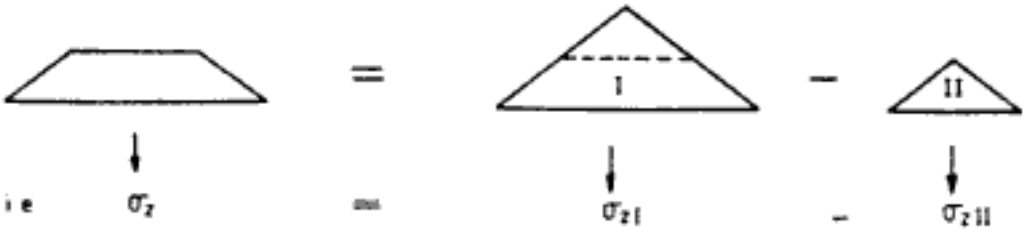

For σ_{z1}:

$$\left|\frac{x}{b}\right| = \frac{2}{8} = 0.25$$

$$\frac{z}{b} = \frac{4}{8} = 0.5$$

From Table 13.8, $I_{oz1} = 0.6344$.

For σ_{zII}:

$$\left|\frac{x}{b}\right| = \frac{2}{4} = 0.5$$

$$\frac{z}{b} = \frac{4}{4} = 1$$

From Table 13.8, $I_{ozII} = 0.3955$.

For I, $q = 10\ \text{T/m}^2$ (i.e., 5×2) and for II, $q = 5\ \text{T/m}^2$

$$\therefore \qquad \sigma_z = (10 \times 0.6344) - (5 \times 0.3955) = 4.3665\ \text{T/m}^2$$

Note: The small differences in the value of σ_z from the various alternatives are due to rounding off error, errors in interpolation, etc. However, all give solutions accurate enough for practical purposes.

13.3.6 Distributed Load Covering Half the Infinite Plane

1. *Uniformly distributed load*:

Gray (1936) gives the solution for load distribution as shown in Fig. 13.11. The equation for vertical stress at a point is given by the equation,

$$\sigma_z = qI_{oz} \tag{13.7}$$

where

$$I_{oz} = \frac{1}{\pi}\left(\beta + \frac{xz}{R^2}\right) \tag{13.17}$$

Table 13.9 gives numerical values of I_{oz}.

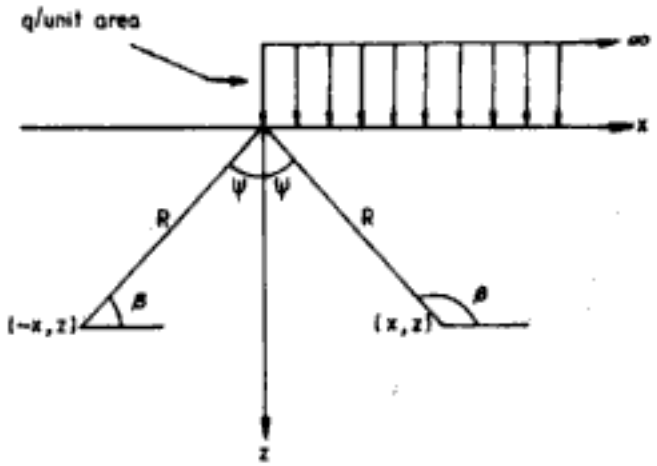

Fig. 13.11 Uniformly distributed vertical load over half the infinite plane

Table 13.9 Values of I_{oz} (Eq. 13.17)

x/z	I_{oz}	x/z	I_{oz}
−10	0.0002	0	0.5000
−5	0.0016	0.1	0.5632
−2	0.0202	0.25	0.6529
−1	0.0908	0.5	0.7749
−0.5	0.2251	1	0.9092
−0.25	0.3471	2	0.9797
−0.1	0.4368	5	0.9984
		10	0.9998

2. *Linearly increasing vertical loading*

The equation for vertical stress at a point, as shown in Fig. 13.12 (Gray 1936), is,

$$\sigma_z = \frac{q_0}{\pi a}(x\beta + z) \tag{13.18}$$

If a is taken as $|x|$, then

$$q_0 = q_x$$

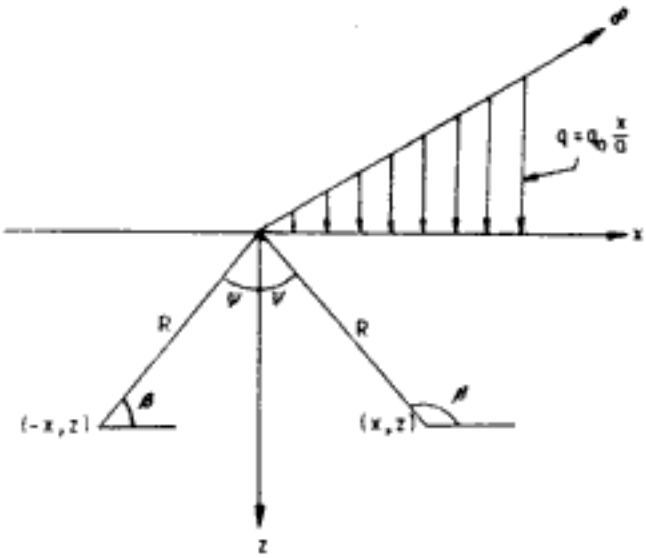

Fig. 13.12 Linearly increasing vertical load on half plane

where q_x is the vertical load intensity at $x = |x|$. Then the expression for σ_z can be rewritten as,

$$\sigma_z = q_x I_{oz} \tag{13.19}$$

where

$$I_{oz} = \frac{1}{\pi |x|}(x\beta + z) \tag{13.20}$$

Numerical values of I_{oz} are given in Table 13.10. The influence factor according to Eq. 13.20 cannot be used to evaluate the stresses along the z-axis, for when $x \to 0$, $q_x \to 0$.

Table 13.10 Values of I_{oz} (Eq. 13.20)

x/z	I_{oz}	x/z	I_{oz}
−10	0.0001	0.1	3.7148
−5	0.0008	0.25	1.8512
−2	0.0116	0.5	1.2842
−1	0.0683	1.0	1.0683
−0.5	0.2842	2.0	1.0116
−0.25	0.8512	5.0	1.0008
−0.1	2.7148	10.0	1.0001

3. *Vertical embankment loading*
The vertical stress at a point in this case (Fig. 13.13) is given by (Gray, 1936)

$$\sigma_z = qI_{oz} \tag{13.7}$$

where

$$I_{oz} = \frac{1}{\pi}\left(\beta + \frac{x}{a}\alpha\right) \tag{13.21}$$

Numerical values of I_{oz} are given in Table 13.11.

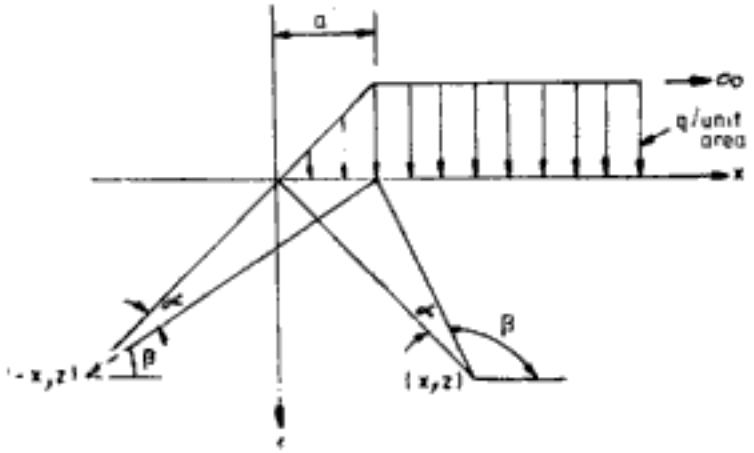

Fig. 13.13 Vertical embankment type loading on half plane

Table 13.11 Values of I_{oz} (Eq. 13.21)

z/a / x/a	0	0.25	0.5	0.75	1.0	1.25	1.5	2.0	2.5
−1.0	0.0000	—	0.0083	—	0.0452	—	0.0967	0.1475	0.1915
−0.75	0.0000	0.0023	0.0147	—	—	—	—	—	—
−0.5	0.0000	0.0051	0.0286	0.0650	0.1045	0.1422	0.1762	0.2317	0.2734
−0.25	0.0000	0.0161	0.0633	0.1156	0.1630	0.2032	—	—	—
0.0	0.0000	0.0780	0.1476	0.2048	0.2500	0.2852	0.3129	0.3524	0.3789
0.25	0.2500	0.2643	0.3023	0.3381	0.3659	0.3867	—	—	—
0.5	0.5000	0.5000	0.5000	0.5000	0.5000	0.5000	0.5000	0.5000	0.5000
0.75	0.7500	0.7357	0.6978	0.6619	0.6341	0.6133	—	—	—
1.0	1.0000	0.9220	0.8524	0.7951	0.7500	0.7148	0.6871	0.6476	0.6211
1.25	1.0000	0.9803	0.9367	0.8844	0.8370	—	0.7632	0.7123	0.6765
1.50	1.0000	0.9949	0.9714	0.9350	0.8955	—	0.8238	0.7682	0.7266
2.0	1.0000	0.9989	0.9916	—	0.9548	—	0.9032	0.8524	0.8085

After Jurgenson, 1934.

4. *Embankment type vertical loading with canal opening*
The loading is shown in Fig. 13.14.

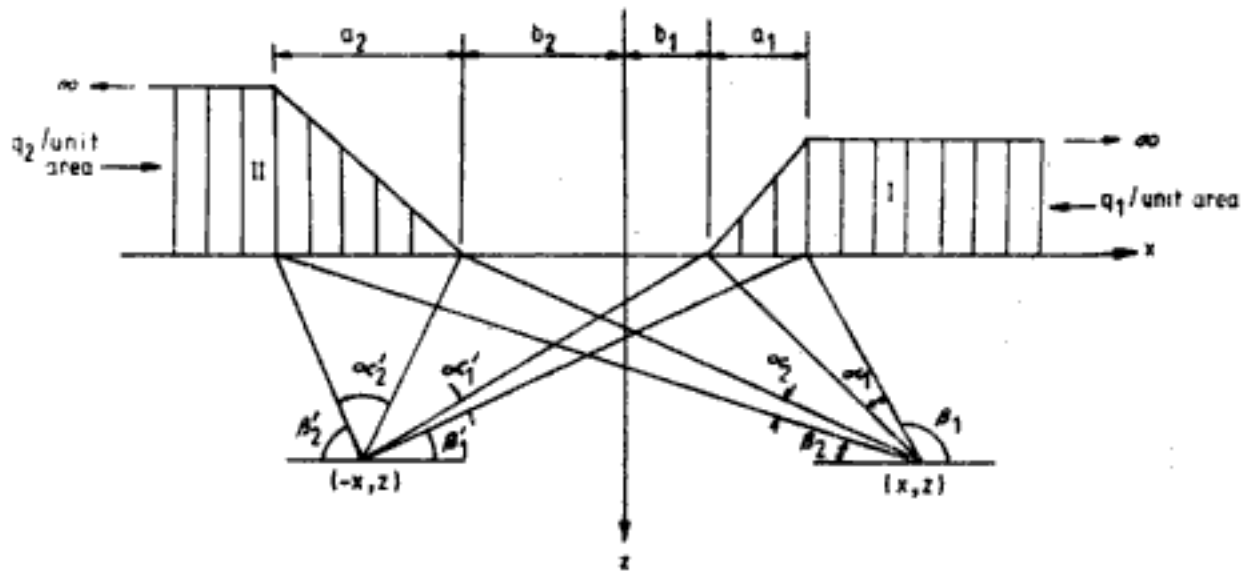

Fig. 13.14 Embankment type loading with canal opening

By principle of superposition, using Eq. 13.21, the vertical stress at a point is given by,

$$\sigma_z = \sigma_{zI} + \sigma_{zII}$$

where σ_{zI} = vertical stress due to embankment I, and
σ_{zII} = vertical stress due to embankment II

$$\left.\begin{aligned} \sigma_{zI} &= \frac{q_1}{\pi}\left[\beta_1 + \frac{(x - b_1)}{a_1}\alpha_1\right] \\ \sigma_{zII} &= \frac{q_2}{\pi}\left[\beta_2 - \frac{(x + b_2)}{a_2}\alpha_2\right] \end{aligned}\right\} \text{ for point } (x, z)$$

and

$$\left.\begin{aligned} \sigma_{zI} &= \frac{q_1}{\pi}\left[\beta_1' - \frac{(x + b_1)}{a_1}\alpha_1'\right] \\ \sigma_{zII} &= \frac{q_2}{\pi}\left[\beta_2' + \frac{(x - b_2)}{a_2}\alpha_2'\right] \end{aligned}\right\} \text{ for point } (-x, z)$$

Use $x = |x|$ in the above equations for σ_{zI} and σ_{zII}. For the case when

$$a_1 = a_2 = a; \quad b_1 = b_2 = b; \quad q_1 = q_2 = q$$

the vertical stress at any point is given by,

$$\sigma_z = \frac{q}{\pi}\left[(\beta_1 + \beta_2) + \left|\frac{x}{a}\right|(\alpha_1 - \alpha_2) - \frac{b}{a}(\alpha_1 + \alpha_2)\right]$$

13.3.7 Uniform Vertical Loading on a Circular Area

The diameter of the circle is $2a$ (Fig. 13.15). The vertical stress at point (r, z) is given by

$$\sigma_z = qI_{\sigma z} \tag{13.7}$$

where

$$I_{\sigma z} = A + B \tag{13.22}$$

Numerical values of A and B are given in Tables 13.12 and 13.13 respectively. Variation of $I_{\sigma z}$ with r/a and z/a is shown in Fig. 13.16.

Table 13.12

z/a \ r/a	0	0.2	0.4	0.6	0.8	1	1.2	1.5
0	1.0	1.0	1.0	1.0	1.0	.5	0	0
0.1	.90050	.89748	.88679	.86126	.78797	.43015	.09645	.02787
0.2	.80388	.79824	.77884	.73483	.63014	.38269	.15433	.05251
0.3	.71265	.70518	.68316	.62690	.52081	.34375	.17964	.07199
0.4	.62861	.62015	.59241	.53767	.44329	.31048	.18709	.08593
0.5	.55279	.54403	.51622	.46448	.38390	.28156	.18556	.09499
0.6	.48550	.47691	.45078	.40427	.33676	.25588	.17952	.10010
0.7	.42654	.41874	.39491	.35428	.29833	.21727	.17124	.10228
0.8	.37531	.36832	.34729	.31243	.26581	.21297	.16206	.10236
0.9	.33104	.32492	.30669	.27707	.23832	.19488	.15253	.10094
1	.29289	.28763	.27005	.24697	.21468	.17868	.14329	.09849
1.2	.23178	.22795	.21662	.19890	.17626	.15101	.12570	.09192
1.5	.16795	.16552	.15877	.14804	.13436	.11892	.10296	.08048
2	.10557	.10453	.10140	.09647	.09011	.08269	.07471	.06275
2.5	.07152	.07098	.06947	.06698	.06373	.05974	.05555	.04880
3	.05132	.05101	.05022	.04886	.04707	.04487	.04241	.03839
4	.02986	.02976	.02907	.02802	.02832	.02749	.02651	.02490
5	.01942	.01938				.01835		
6	.01361					.01307		
7	.01005					.00976		
8	.00772					.00755		
9	.00612					.00600		
10								.00477

Function *A*

2	3	4	5	6	7	8	10	12	14
0	0	0	0	0	0	0	0	0	
.00856	.00211	.00084	.00042						
.01680	.00419	.00167	.00083	.00048	.00030	.00020			
.02440	.00622	.00250							
.03118									
.03701	.01013	.00407	.00209	.00118	.00071	.00053	.00025	.00014	.00009
.04558									
.05185	.01742	.00761	.00393	.00226	.00143	.00097	.00050	.00029	.00018
.05260	.01935	.00871	.00459	.00269	.00171	.00115			
.05116	.02142	.01013	.00548	.00325	.00210	.00141	.00073	.00043	.00027
.04496	.02221	.01160	.00659	.00399	.00264	.00180	.00094	.00056	.00036
.03787	.02143	.01221	.00732	.00463	.00308	.00214	.00115	.00068	.00043
.03150	.01980	.01220	.00770	.00505	.00346	.00242	.00132	.00079	.00051
.02193	.01592	.01109	.00768	.00536	.00384	.00282	.00160	.00099	.00065
.01573	.01249	.00949	.00708	.00527	.00394	.00298	.00179	.00113	.00075
.01168	.00983	.00795	.00628	.00492	.00384	.00299	.00188	.00124	.00084
.00894	.00784	.00661	.00548	.00445	.00360	.00291	.00193	.00130	.00091
.00703	.00635	.00554	.00472	.00398	.00332	.00276	.00189	.00134	.00094
.00566	.00520	.00466	.00409	.00353	.00301	.00256	.00184	.00133	.00096
.00465	.00438	.00397	.00352	.00326	.00273	.00241			

After Ahlvin and Ulery, 1962. By permission of Transportation Research Board, National Research Council, Washington, D.C.

Table 13.13

z/a \ r/a	0	0.2	0.4	0.6	0.8	1	1.2	1.5
0	0	0	0	0	0	0	0	0
0.1	.09852	.10140	.11138	.13424	.18796	.05388	−.07899	−.02672
0.2	.18857	.19306	.20772	.23524	.25983	.08513	−.07759	−.04448
0.3	.26362	.26787	.28018	.29483	.27257	.10757	−.04316	−.04999
0.4	.32016	.32259	.32748	.32273	.26925	.12404	−.00766	−.04535
0.5	.35777	.35752	.35323	.33106	.26236	.13591	.02165	−.03455
0.6	.37831	.37531	.36308	.32822	.25411	.14440	.04457	−.02101
0.7	.38487	.37962	.36072	.31929	.24638	.14986	.06209	−.00702
0.8	.38091	.37408	.35133	.30699	.23779	.15292	.07530	.00614
0.9	.36962	.36275	.33734	.29299	.22891	.15404	.08507	.01795
1	.35355	.34553	.32075	.27819	.21978	.15355	.09210	.02814
1.2	.31485	.30730	.28481	.24836	.20113	.14915	.10002	.04378
1.5	.25602	.25025	.23338	.20694	.17368	.13732	.10193	.05745
2	.17889	.18144	.16644	.15198	.13375	.11331	.09254	.06371
2.5	.12807	.12633	.12126	.11327	.10298	.09130	.07869	.06022
3	.09487	.09394	.09099	.08635	.08033	.07325	.06551	.05354
4	.05707	.05666	.05562	.05383	.05145	.04773	.04532	.03995
5	.03772	.03760				.03384		
6	.02666					.02468		
7	.01980					.01868		
8	.01526					.01459		
9	.01212					.01170		
10								.00924

Function *B*

2	3	4	5	6	7	8	10	12	14
0	0	0	0	0	0				
−.00845	−.00210	.00084	.00042						
−.01593	−.00412	−.00166	−.00083	−.00024	−.00015	−.00010			
−.02166	−.00599	.00245							
−.02522									
−.02651	−.00991	−.00388	−.00199	−.00116	−.00073	−.00049	−.00025	−.00014	−.00009
−.02329									
−.01005	−.01115	−.00608	−.00344	−.00210	−.00135	−.00092	−.00048	−.00028	−.00018
.00023	−.00995	−.00632	−.00378	−.00236	−.00156	−.00107			
.01385	−.00669	−.00600	−.00401	−.00265	−.00181	−.00126	−.00068	−.00040	−.00026
.02836	.00028	−.00410	−.00371	−.00278	−.00202	−.00148	−.00084	−.00050	−.00033
.03429	.00661	−.00130	−.00271	−.00250	−.00201	−.00156	−.00094	−.00059	−.00039
.03511	.01112	.00157	−.00134	−.00192	−.00179	−.00151	−.00099	−.00065	−.00046
.03066	.01515	.00595	.00155	−.00029	−.00094	−.00109	−.00094	−.00068	−.00050
.02474	.01522	.00810	.00371	.00132	.00013	−.00043	−.00070	−.00061	−.00049
.01968	.01380	.00867	.00496	.00254	.00110	.00028	−.00037	−.00047	−.00045
.01577	.01204	.08042	.00547	.00332	.00185	.00093	−.00002	−.00029	−.00037
.01279	.01034	.00779	.00554	.00372	.00236	.00141	.00035	−.00008	−.00025
.01054	.00888	.00705	.00533	.00386	.00265	.00178	.00066	.00012	−.00012
.00879	.00764	.00631	.00501	.00382	.00281	.00199			

After Ahlvin and Ulery, 1962. By permission of Transportation Research Board, National Research Council, Washington, D.C.

Table 13.14

z/a \ r/a	0	0.2	0.4	0.6	0.8	1	1.2	1.5
0	2.0	1.97987	1.91751	1.80575	1.62553	1.27319	.93676	.71185
0.1	1.80998	1.79018	1.72886	1.61961	1.44711	1.18107	.92670	.70888
0.2	1.63961	1.62068	1.56242	1.46001	1.30614	1.09996	.90098	.70074
0.3	1.48806	1.47044	1.40979	1.32442	1.19210	1.02740	.86726	.68823
0.4	1.35407	1.33802	1.28963	1.20822	1.09555	.96202	.83042	.67238
0.5	1.23607	1.22176	1.17894	1.10830	1.01312	.90298	.79308	.65429
0.6	1.13238	1.11998	1.08350	1.02154	.94120	.84917	.75653	.63469
0.7	1.04131	1.03037	.99794	.91049	.87742	.80030	.72143	.61442
0.8	.96125	.95175	.92386	.87928	.82136	.75571	.68809	.59398
0.9	.89072	.88251	.85856	.82616	.77950	.71495	.65677	.57361
1	.82843	.85005	.80465	.76809	.72587	.67769	.62701	.55364
1.2	.72410	.71882	.70370	.67937	.64814	.61187	.57329	.51552
1.5	.60555	.60233	.57246	.57633	.55559	.53138	.50496	.46379
2	.47214	.47022	.44512	.45656	.44502	.43202	.41702	.39242
2.5	.38518	.38403	.38098	.37608	.36940	.36155	.35243	.33698
3	.32457	.32403	.32184	.31887	.31464	.30969	.30381	.29364
4	.24620	.24588	.24820	.25128	.24168	.23932	.23668	.23164
5	.19805	.19785				.19455		
6	.16554					.16326		
7	.14217					.14077		
8	.12448					.12352		
9	.11079					.10989		
10								.09900

Function H

2	3	4	5	6	7	8	10	12	14
.51671	.33815	.25200	.20045	16626	.14315	.12576	.09918	.08346	.07023
.51627	.33794	.25184	.20081						
.51382	.33726	.25162	.20072	.16688	.14288	.12512			
.50966	.33638	.25124							
.50412									
.49728	.33293	.24996	.19982	.16668	.14273	.12493	.09996	.08295	.07123
.48061									
.45122	.31877	.24386	.19673	.16516	.14182	.12394	.09952	.08292	.07104
.43013	.31162	.24070	.19520	.16369	.14099	.12350			
.39872	.29945	.23495	.19053	.16199	.14058	.12281	.09876	.08270	.07064
.35054	.27740	.22418	.18618	.15846	.13762	.12124	.09792	.08196	.07026
.30913	.25550	.21208	.17898	.15395	.13463	.11928	.09700	.08115	.06980
.27453	.23487	.19977	.17154	.14919	.13119	.11694	.09558	.08061	.06897
.22188	.19908	.17640	.15596	.13864	.12396	.11172	.09300	.07864	.06848
.18450	.17080	.15575	.14130	.12785	.11615	.10585	.08915	.07675	.06695
.15750	.14868	.13842	.12792	.11778	.10836	.09990	.08562	.07452	.06522
.13699	.13097	.12404	.11620	.10843	.10101	.09387	.08197	.07210	.06377
.12112	.11680	.11176	.10600	.09976	.09400	.08848	.07800	.06928	.06200
.10854	.10548	.10161	.09702	.09234	.08784	.08298	.07407	.06678	.05976
.09820	.09510	.09290	.08980	.08300	.08180	.07710			

After Ahlvin and Ulery, 1962. By permission of Transportation Research Board, National Research Council, Washington, D.C.

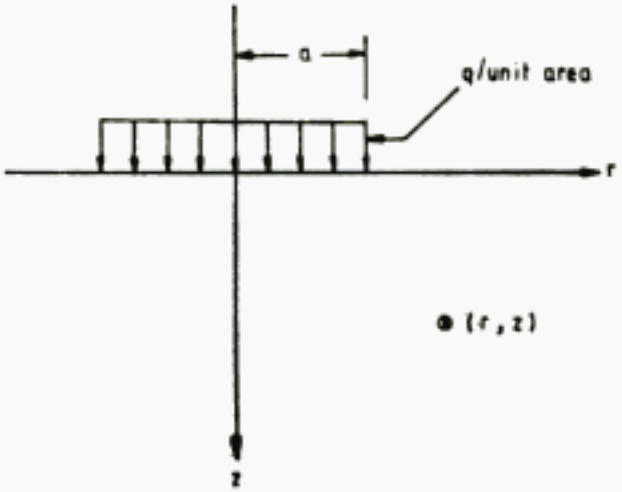

Fig. 13.15 Uniform vertical loading on circular area

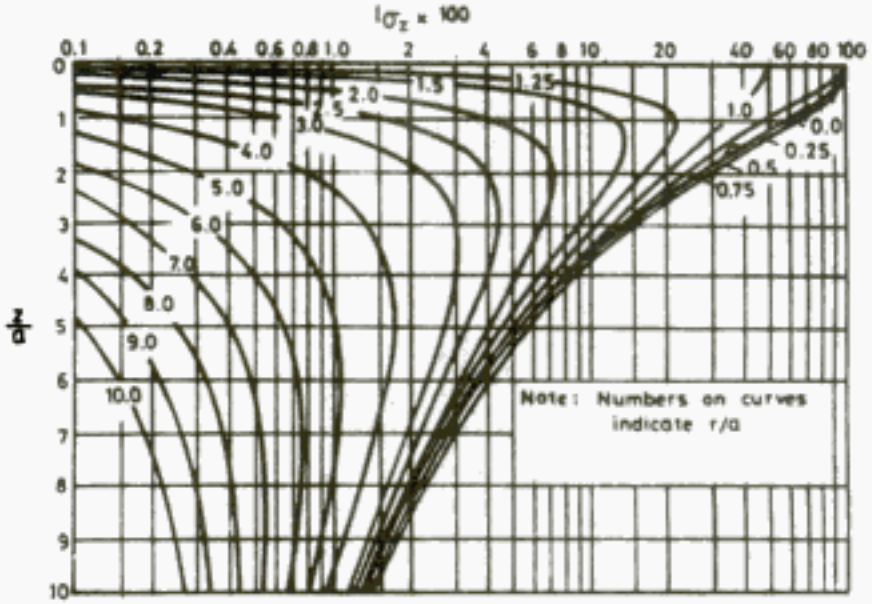

Fig. 13.16 Vertical stress influence factor for stress beneath circular loaded area (After Foster and Ahlvin, 1954; by permission of Transportation Research Board, National Research Council, Washington D.C.)

The vertical deflection at (r, z) is given by,

$$\rho_z = \frac{qa}{E} I_{\rho z} \tag{13.23}$$

where $I_{\rho z}$ = deflection factor $= (1 + \mu)\left[\frac{z}{a}A + (1 - \mu)H\right]$ (13.24)

Values of A and H are given in Tables 13.12 and 13.14, respectively. Variation of deflection factor with z/a and r/a for Poisson's ratio value $\mu = 0.5$ is shown in Fig. 13.17. For the particular case of stresses and displacements along the z-axis (i.e., $r = 0$):

$$\sigma_z = q\left\{1 - \left[\frac{1}{1 + (a/z)^2}\right]^{3/2}\right\} \tag{13.25}$$

and $$\sigma_z = \frac{2qa}{E}(1 - \mu^2)\left[\sqrt{1 + \left(\frac{z}{a}\right)^2} - \frac{z}{a}\right]\left[1 + \frac{z/a}{2(1 - \mu)\sqrt{1 + (z/a)^2}}\right] \tag{13.26}$$

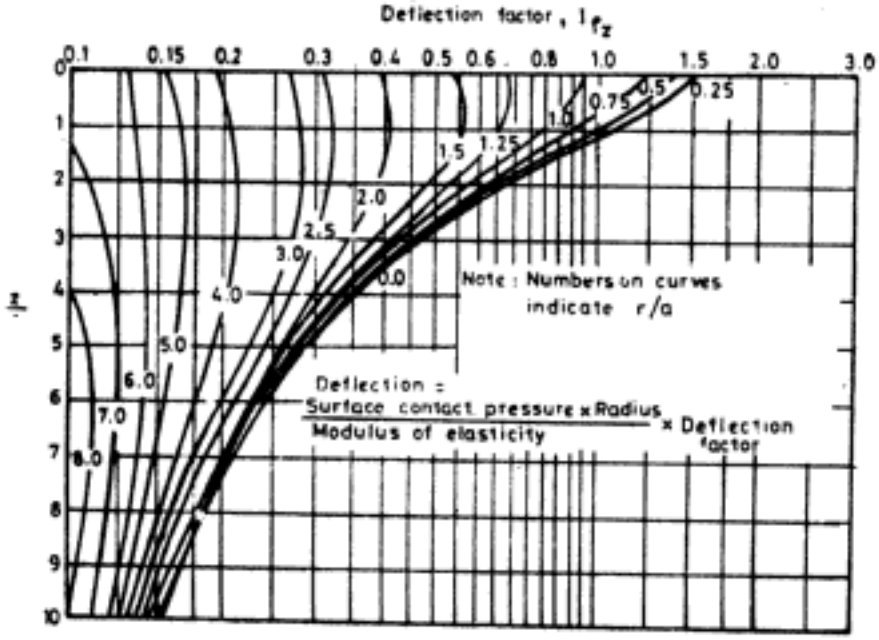

Fig. 13.17 Deflection factor for vertical deflection beneath uniformly loaded circular area (After Foster and Ahlvin, 1954; by permission of Transportation Research Board, National Research Council, Washington D.C.)

13.3.8 Uniform Vertical Loading on Annulus

Figure 13.19 gives the variation of vertical stress at a point below the centre of the annulus [i.e., $r = (R_1 + R_2)/2$] with depth.

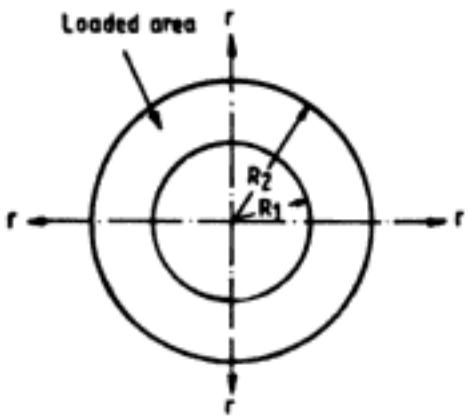

Fig. 13.18 Loading on annulus

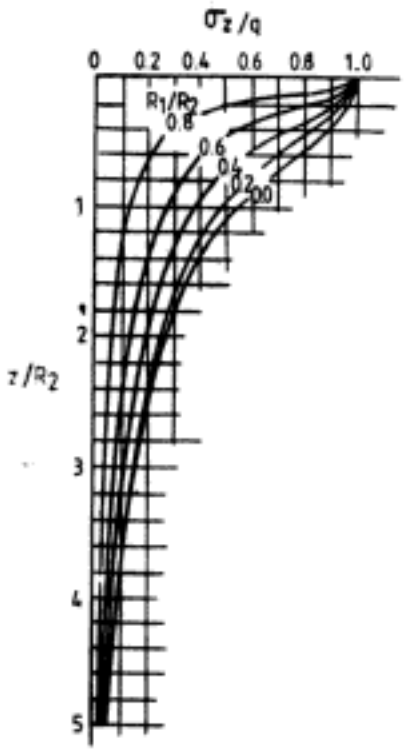

Fig. 13.19 Vertical stress below the centre of uniformly loaded annulus (After Szechy and Verga, 1978; reprinted by permission of Akademiari Kidao, Budapest)

The vertical surface displacement of a point on the annulus can be expressed as follows,

$$\rho_z = \frac{qR_2(1-\mu^2)}{E} I_{\rho z} \tag{13.27}$$

The values of $I_{\rho z}$ for the internal circumference ($r = R_1$), the centre line ($r = (R_1 + R_2)/2$) and the external circumference ($r = R_2$) are given in Table 13.15. The average or mean displacement of the annulus is also given by Eq. 13.27. Values of $I_{\rho z}$ for the mean displacement are also given in Table 13.15.

Table 13.15 Values of $I_{\rho z}$ (Eq. 13.27)

$I_{\rho z}$ for \ R_1/R_2	0.0	0.1	0.2	0.3	0.4	0.5	0.6	0.7	0.8	0.9	1.0
Internal circumference	2.000	1.868	1.725	1.572	1.408	1.232	1.042	0.837	0.613	0.367	0.000
Centre line	2.000	1.800	1.600	1.400	1.200	1.000	0.800	0.600	0.400	0.200	0.000
External circumference	1.273	1.263	1.233	1.182	1.110	1.014	0.894	0.746	0.566	0.346	0.000
Mean displacement	1.698	1.688	1.628	1.538	1.418	1.274	1.104	0.910	0.712	0.444	0.000

3.9 Distributed Load on Rectangular Area

Uniform vertical loading

Figure 13.20 shows the loading in which length of rectangle is l, and breadth or width of rectangle is b ($l \geqslant b$).

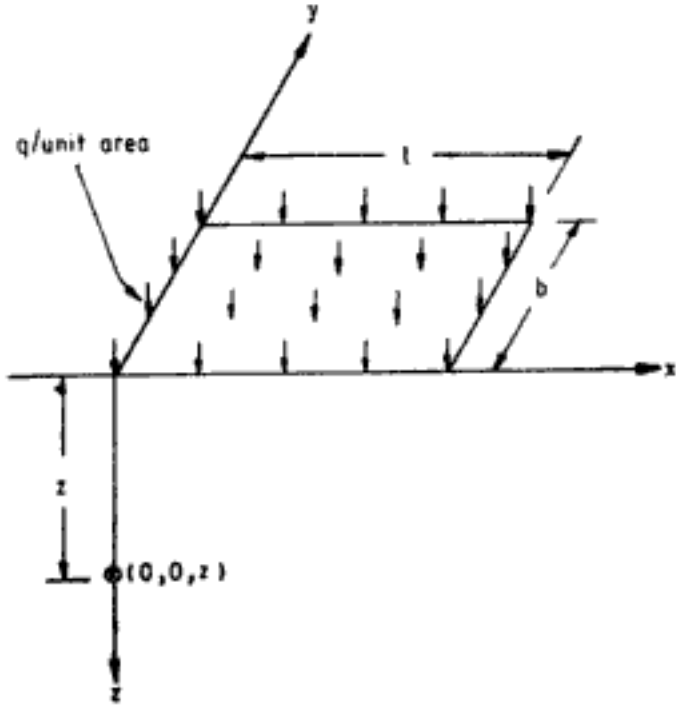

Fig. 13.20 Uniform vertical loading on rectangular area

The equation for vertical stress at a point beneath the corner of the rectangular loaded area is given by,

$$\sigma_z = qI_{oz} \tag{13.7}$$

where the influence factor I_{oz} is given by Steinbrenner (1936) as,

$$I_{oz} = \frac{1}{2\pi}\left[\frac{mn}{\sqrt{1+m^2+n^2}}\,\frac{1+m^2+2n^2}{(1+n^2)(m^2+n^2)} + \sin^{-1}\frac{m}{\sqrt{m^2+n^2}\sqrt{1+n^2}}\right] \tag{13.28}$$

where $m = l/b\ (\geqslant 1)$

$n = z/b$

The variation of I_{oz} with m and n is shown in Fig. 13.21 and in Table 13.16. In this figure m and n are *not* interchangeable.

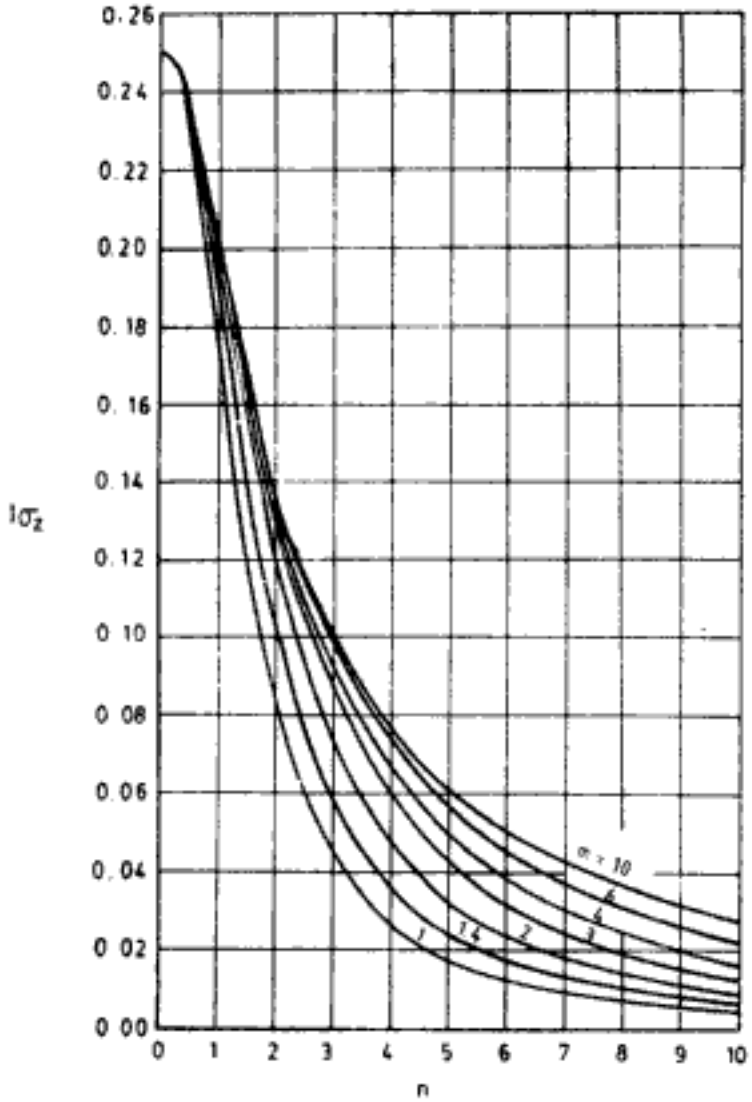

Fig. 13.21 Influence factor for vertical stress beneath the corner of uniformly loaded rectangular area (Eq. 13.28) (After Steinbrenner, 1936)

Table 13.16 Values of $I_{\sigma z}$ (Eq. 13.28) for Stress Increase Directly Below the Corner of Uniformly Loaded Rectangular Areas Using Boussinesq's Equation

n \ m	1	2	3	5	10
0.1	0.2498	0.2499	0.2499	0.2499	0.2499
0.2	0.2485	0.2491	0.2492	0.2492	0.2492
0.3	0.2457	0.2472	0.2474	0.2474	0.2474
0.4	0.2401	0.2439	0.2442	0.2443	0.2443
0.5	0.2325	0.2391	0.2397	0.2398	0.2399
0.6	0.2229	0.2293	0.2339	0.2342	0.2342
0.7	0.2118	0.2257	0.2271	0.2275	0.2276
0.8	0.1999	0.2176	0.2196	0.2202	0.2202
0.9	0.1876	0.2089	0.2116	0.2124	0.2125
1.0	0.1755	0.1999	0.2034	0.2044	0.2046
2	0.0840	0.1202	0.1314	0.1363	0.1374
3	0.0447	0.0732	0.0870	0.0959	0.0987
5	0.0179	0.0328	0.0435	0.0547	0.0610
10	0.0047	0.0092	0.0132	0.0198	0.0279

Fadum (1948) gives the expression for $I_{\sigma z}$ as a function of l/z $(= m_1)$ and b/z $(= n_1)$. Fadum's influence factors are shown in Fig. 13.22. In this figure m_1 and n_1 are interchange-

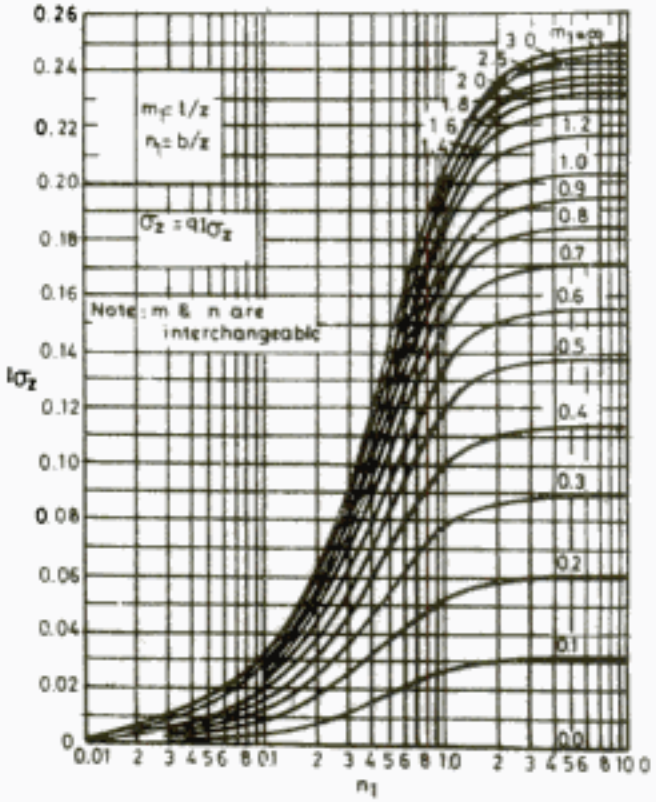

Fig. 13.22 Fadum's influence factors for vertical stress beneath corner of uniformly loaded rectangle (After Fadum, 1948)

able. For vertical displacement beneath the corner of a rectangle at point (0, 0, z) in Fig. 13.20 Steinbrenner (1934) gives,

$$\rho_z = \frac{qb}{E} I_{\rho z} \tag{13.29}$$

where deflection factor $I_{\rho z}$ is given by

$$I_{\rho z} = \frac{(1-\mu^2)}{2}\left(A_1 - \frac{1-2\mu}{1-\mu}B_1\right) \tag{13.30}$$

$$A_1 = \frac{1}{\pi}\left(\ln \frac{\sqrt{1+m^2+n^2}+m}{\sqrt{1+m^2+n^2}-m} + m \ln \frac{\sqrt{1+m^2+n^2}+1}{\sqrt{1+m^2+n^2}-1}\right)$$

$$B_1 = \frac{n}{\pi} \tan^{-1} \frac{m}{n\sqrt{1+m^2+n^2}}$$

$$m = l/b;$$

$$n = z/b$$

Numerical values of A_1 and B_1 (Harr, 1966) are given in Table 13.17. Giroud (1968) gives the expressions and influence factors for the vertical displacement at the surface ($z = 0$) for four points on the rectangle, namely, corner, centre, midpoint of length and midpoint of breadth. For all points the equation for vertical displacement is given by,

$$\rho = \frac{q(1-\mu^2)b}{E} I_{\rho i} \tag{13.31}$$

where $I_{\rho i} = I_{\rho L}$ for mid-point of length
$I_{\rho i} = I_{\rho B}$ for mid-point of breadth
$I_{\rho i} = I_{\rho c}$ for corner
$I_{\rho i} = I_{\rho 0}$ for centre

For mean displacement of rectangle $I_{\rho i} = I_{\rho m}$.
The numerical values of the influence factors are shown in Fig. 13.23 and in Table 13.18.

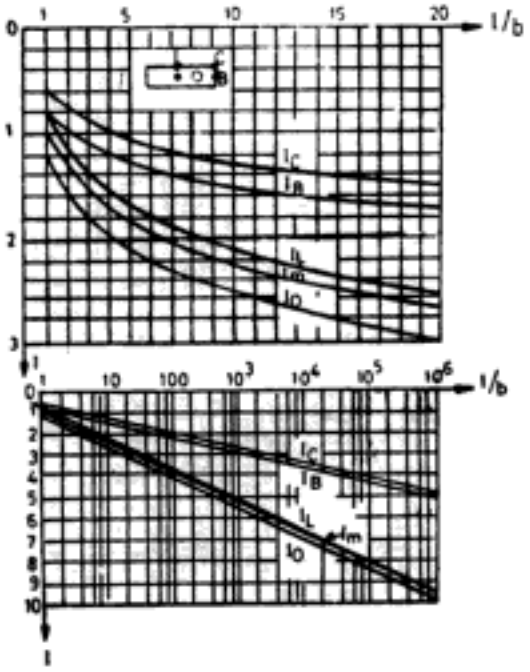

Fig. 13.23 Influence factors for vertical surface displacement beneath uniformly loaded rectangle (After Giroud, 1968; with permission of American Society of Civil Engineers, New York)

Table 13.17 Values of A_1 and B_1 for Eq. 13.30, $m=l/b$, $n=z/b$

n		$m=1$	$m=1.5$	$m=2$	$m=3$	$m=5$	$m=7$	$m=10$	$m=15$	$m=20$	$m=30$	$m=50$	$m=100$
0.0	A_1	1.122	1.358	1.532	1.783	2.105	2.318	2.544	2.802	2.985	3.243	3.568	4.010
	B_1	0.000	0.000	0.000	0.000	0.000	0.000	0.000	0.000	0.000	0.000	0.000	0.000
0.2	A_1	1.105	1.343	1.518	1.770	2.092	2.305	2.532	2.790	2.973	3.231	3.556	3.997
	B_1	0.082	0.085	0.086	0.087	0.087	0.087	0.087	0.087	0.087	0.087	0.087	0.087
0.4	A_1	1.057	1.301	1.479	1.733	2.056	2.270	2.497	2.755	2.938	3.196	3.521	3.962
	B_1	0.132	0.142	0.146	0.149	0.151	0.151	0.151	0.151	0.151	0.152	0.152	0.152
0.6	A_1	0.989	1.240	1.422	1.679	2.004	2.219	2.446	2.704	2.887	3.145	3.470	3.912
	B_1	0.158	0.176	0.184	0.191	0.195	0.196	0.196	0.197	0.197	0.197	0.197	0.197
0.8	A_1	0.914	1.169	1.354	1.615	1.943	2.158	2.386	2.644	2.827	3.086	3.411	3.852
	B_1	0.167	0.194	0.207	0.218	0.224	0.226	0.227	0.228	0.228	0.228	0.228	0.228
1.0	A_1	0.838	1.094	1.282	1.547	1.878	2.094	2.322	2.581	2.764	3.022	3.348	3.789
	B_1	0.167	0.200	0.218	0.234	0.244	0.247	0.248	0.249	0.250	0.250	0.250	0.250
1.2	A_1	0.768	1.020	1.209	1.478	1.812	2.029	2.258	2.517	2.701	2.959	3.284	3.726
	B_1	0.161	0.200	0.222	0.243	0.257	0.261	0.263	0.264	0.265	0.265	0.265	0.265
1.4	A_1	0.704	0.950	1.139	1.411	1.748	1.966	2.196	2.455	2.639	2.897	3.223	3.664
	B_1	0.154	0.196	0.221	0.247	0.265	0.270	0.273	0.275	0.276	0.276	0.276	0.276
1.6	A_1	0.647	0.886	1.073	1.346	1.686	1.906	2.136	2.396	2.580	2.839	3.164	3.605
	B_1	0.145	0.189	0.217	0.248	0.269	0.277	0.281	0.283	0.283	0.284	0.284	0.284
1.8	A_1	0.596	0.826	1.011	1.284	1.627	1.848	2.080	2.340	2.524	2.783	3.108	3.550
	B_1	0.136	0.181	0.212	0.246	0.272	0.281	0.286	0.288	0.289	0.290	0.290	0.290
2.0	A_1	0.552	0.773	0.954	1.226	1.571	1.794	2.026	2.287	2.471	2.730	3.056	3.497
	B_1	0.128	0.173	0.205	0.243	0.273	0.283	0.289	0.292	0.294	0.294	0.295	0.295
2.5	A_1	0.463	0.660	0.829	1.095	1.444	1.670	1.904	2.167	2.352	2.612	2.937	3.379
	B_1	0.110	0.153	0.186	0.230	0.269	0.284	0.293	0.298	0.300	0.302	0.302	0.303
3.0	A_1	0.396	0.572	0.728	0.984	1.332	1.561	1.798	2.063	2.249	2.509	2.835	3.277
	B_1	0.096	0.136	0.168	0.215	0.262	0.282	0.294	0.301	0.304	0.306	0.307	0.307
3.5	A_1	0.346	0.503	0.647	0.890	1.234	1.465	1.705	1.971	2.158	2.419	2.745	3.187
	B_1	0.084	0.121	0.152	0.200	0.253	0.277	0.292	0.302	0.305	0.308	0.309	0.310
4.0	A_1	0.306	0.448	0.580	0.809	1.147	1.379	1.621	1.890	2.077	2.339	2.666	3.108
	B_1	0.075	0.109	0.138	0.186	0.243	0.270	0.289	0.301	0.306	0.309	0.311	0.312

4.5 A_1	0.274	0.404	0.525	0.741	1.070	1.301	1.545	1.816	2.005	2.267	2.594	3.036
B_1	0.067	0.098	0.126	0.173	0.222	0.263	0.285	0.300	0.305	0.310	0.312	0.313
5.0 A_1	0.248	0.367	0.479	0.682	1.001	1.231	1.477	1.749	1.939	2.202	2.530	2.972
B_1	0.061	0.090	0.116	0.161	0.221	0.255	0.281	0.298	0.305	0.310	0.313	0.314
6.0 A_1	0.208	0.309	0.406	0.586	0.884	1.109	1.355	1.631	1.823	2.088	2.417	2.860
B_1	0.052	0.076	0.099	0.141	0.201	0.239	0.270	0.293	0.302	0.309	0.313	0.315
7.0 A_1	0.179	0.267	0.352	0.513	0.788	1.006	1.251	1.529	1.723	1.990	2.320	2.764
B_1	0.045	0.066	0.087	0.124	0.183	0.223	0.259	0.286	0.298	0.308	0.313	0.315
8.0 A_1	0.158	0.235	0.310	0.455	0.710	0.918	1.160	1.440	1.635	1.904	2.236	2.680
B_1	0.039	0.058	0.077	0.111	0.168	0.208	0.247	0.279	0.294	0.306	0.313	0.316
9.0 A_1	0.140	0.209	0.277	0.408	0.644	0.843	1.080	1.360	1.556	1.828	2.161	2.606
B_1	0.035	0.052	0.069	0.100	0.154	0.194	0.235	0.272	0.289	0.304	0.312	0.316
10.0 A_1	0.126	0.189	0.251	0.370	0.589	0.778	1.009	1.287	1.485	1.759	2.093	2.539
B_1	0.032	0.047	0.062	0.091	0.142	0.182	0.224	0.264	0.284	0.301	0.311	0.316
12.0 A_1	0.106	0.158	0.210	0.311	0.502	0.672	0.889	1.162	1.361	1.638	1.976	2.423
B_1	0.026	0.039	0.052	0.077	0.122	0.160	0.203	0.248	0.272	0.295	0.309	0.315
14.0 A_1	0.091	0.136	0.180	0.268	0.436	0.590	0.792	1.057	1.255	1.534	1.875	2.325
B_1	0.023	0.034	0.045	0.067	0.107	0.142	0.185	0.232	0.260	0.288	0.306	0.315
16.0 A_1	0.079	0.119	0.158	0.236	0.385	0.525	0.712	0.967	1.163	1.443	1.787	2.239
B_1	0.020	0.030	0.039	0.059	0.095	0.127	0.168	0.217	0.248	0.280	0.303	0.314
18.0 A_1	0.071	0.106	0.141	0.210	0.345	0.472	0.646	0.890	1.082	1.362	1.709	2.164
B_1	0.018	0.026	0.035	0.052	0.085	0.115	0.154	0.204	0.236	0.273	0.299	0.313
20.0 A_1	0.064	0.095	0.127	0.189	0.312	0.428	0.591	0.823	1.011	1.290	1.639	2.096
B_1	0.016	0.024	0.032	0.047	0.077	0.105	0.142	0.191	0.225	0.265	0.295	0.312
30.0 A_1	0.042	0.064	0.085	0.127	0.210	0.292	0.410	0.591	0.751	1.011	1.363	1.831
B_1	0.011	0.016	0.021	0.032	0.052	0.072	0.101	0.142	0.176	0.225	0.273	0.305
40.0 A_1	0.032	0.048	0.064	0.095	0.158	0.221	0.312	0.457	0.591	0.823	1.164	1.640
B_1	0.008	0.012	0.016	0.024	0.039	0.055	0.077	0.112	0.142	0.191	0.249	0.295
50.0 A_1	0.025	0.038	0.051	0.076	0.127	0.177	0.251	0.371	0.485	0.690	1.011	1.488
B_1	0.006	0.010	0.013	0.019	0.032	0.044	0.062	0.091	0.118	0.164	0.225	0.285
60.0 A_1	0.021	0.032	0.042	0.064	0.106	0.148	0.210	0.312	0.410	0.591	0.890	1.363
B_1	0.005	0.008	0.011	0.016	0.026	0.037	0.052	0.077	0.101	0.142	0.204	0.273

(Contd)

Table 13.17 (*Contd.*)

n		$m=1$	$m=1.5$	$m=2$	$m=3$	$m=5$	$m=7$	$m=10$	$m=15$	$m=20$	$m=30$	$m=50$	$m=100$
70.0	A_1	0.018	0.027	0.036	0.055	0.091	0.127	0.181	0.269	0.354	0.516	0.793	1.256
	B_1	0.005	0.007	0.009	0.014	0.023	0.032	0.045	0.067	0.087	0.125	0.185	0.261
80.0	A_1	0.016	0.024	0.032	0.048	0.079	0.111	0.158	0.236	0.312	0.457	0.713	1.164
	B_1	0.004	0.006	0.008	0.012	0.020	0.028	0.039	0.059	0.077	0.112	0.169	0.249
90.0	A_1	0.014	0.021	0.028	0.042	0.071	0.099	0.141	0.210	0.278	0.410	0.647	1.083
	B_1	0.004	0.005	0.007	0.011	0.018	0.025	0.035	0.052	0.069	0.101	0.155	0.237
100.0	A_1	0.013	0.019	0.025	0.038	0.064	0.089	0.127	0.190	0.251	0.371	0.591	1.011
	B_1	0.003	0.005	0.006	0.010	0.016	0.022	0.032	0.047	0.062	0.091	0.142	0.225

After Harr, 1966. Reprinted by permission of McGraw-Hill Book Company, New York.

Table 13.18 Influence Factors for Vertical Surface Displacement Beneath Rectangle

$\alpha = l/b$	$I_{\rho C}$	$I_{\rho L}$	$I_{\rho B}$	$I_{\rho 0}$	$I_{\rho m}$	$\alpha = l/b$	$I_{\rho C}$	$I_{\rho L}$	$I_{\rho B}$	$I_{\rho 0}$	$I_{\rho m}$
1	0.561	0.766	0.766	1.122	0.946	15	1.401	2.362	1.621	2.802	2.498
1.1	0.588	0.810	0.795	1.176	0.992	20	1.493	2.544	1.713	2.985	2.677
1.2	0.613	0.852	0.822	1.226	1.035	25	1.564	2.686	1.784	3.127	2.817
1.3	0.636	0.892	0.847	1.273	1.075	30	1.622	2.802	1.842	3.243	2.932
1.4	0.658	0.930	0.870	1.317	1.112	40	1.713	2.985	1.934	3.426	3.113
1.5	0.679	0.966	0.892	1.358	1.148	50	1.784	3.127	2.005	3.568	3.254
1.6	0.698	1.000	0.912	1.396	1.181	60	1.842	3.243	2.063	3.684	3.370
1.7	0.716	1.033	0.931	1.433	1.213	70	1.891	3.341	2.112	3.783	3.467
1.8	0.734	1.064	0.949	1.467	1.244	80	1.934	3.426	2.154	3.868	3.552
1.9	0.750	1.094	0.966	1.500	1.273	90	1.971	3.501	2.192	3.943	3.627
2	0.766	1.122	0.982	1.532	1.300	100	2.005	3.568	2.225	4.010	3.693
2.2	0.795	1.176	1.012	1.590	1.353	200	2.225	4.010	2.446	4.451	4.134
2.4	0.822	1.226	1.039	1.644	1.401	300	2.355	4.268	2.575	4.709	4.391
2.5	0.835	1.250	1.052	1.669	1.424	400	2.446	4.451	2.667	4.892	4.574
3	0.892	1.358	1.110	1.783	1.527	500	2.517	4.593	2.738	5.034	4.717
3.5	0.940	1.450	1.159	1.880	1.616	600	2.575	4.709	2.796	5.150	4.833
4	0.982	1.532	1.201	1.964	1.694	700	2.624	4.807	2.845	5.248	4.931
4.5	1.019	1.604	1.239	2.038	1.763	800	2.667	4.892	2.887	5.333	5.015
5	1.052	1.669	1.272	2.105	1.826	900	2.704	4.967	2.925	5.408	5.092
6	1.110	1.783	1.330	2.220	1.935	10^3	2.738	5.034	2.958	5.476	5.158
7	1.159	1.880	1.379	2.318	2.028	10^4	3.471	6.500	3.691	6.941	6.623
8	1.201	1.964	1.422	2.403	2.110	10^5	4.204	7.966	4.424	8.407	8.089
9	1.239	2.038	1.459	2.477	2.182	10^6	4.937	9.432	5.157	9.874	9.555
10	1.272	2.105	1.493	2.544	2.246	∞	∞	∞	∞	∞	∞
						circle	0.640	0.640	0.640	1.000	0.850

After Giroud, 1968. By permission of American Society of Civil Engineers, New York.

For vertical stress and vertical displacement at points other than points below the corner of the rectangle, the principle of superposition can be used. The principle is explained in Qs 13.2, 13.3 and 13.4.

Q. 13.2: The rectangle *ABCD* shown in Fig. 13.24 is subjected to an uniform load of 12 T/m². To determine (a) the vertical stress at a depth of 5 m below the point *x*, and (b) the vertical elastic displacement at the surface at point *x*. For soil, $\mu = 0.25$ and $E = 500$ kg/cm².

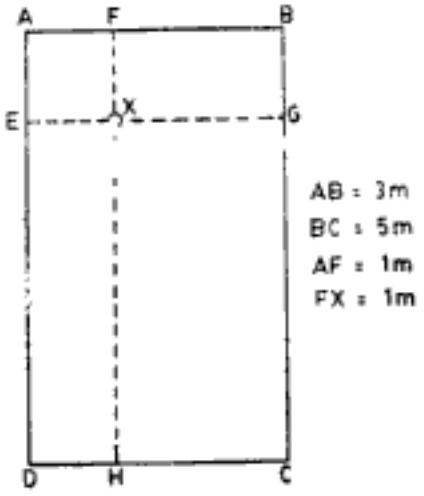

Fig. 13.24 Q 13.2

Ans: (a) The point *x* is below the corner of 4 rectangles as constructed in Fig. 13.24. The vertical stress below *x* is the sum of vertical stresses below the corner of each rectangle.

i.e., $\sigma_{z(ABCD)} = \sigma_{z(FAEX)} + \sigma_{z(FBGX)} + \sigma_{z(GCHX)} + \sigma_{z(HDEX)}$

$\sigma_{z(FAEX)}$: for $FAEX$, $l = b = 1$ m

$\therefore$ $l/b = m = 1$; $z/b = n = 5/1 = 5$

From Fig. 13.21 $I_{oz} = 0.018$

$$\sigma_{z(FAEX)} = 12 \times 0.018 = 0.216 \text{ T/m}^2$$

$\sigma_{z(FBGX)}$: For $FBGX$, $l = 2$ m; $b = 1$ m

$\therefore$ $m = l/b = 2/1 = 2$; $n = z/b = 5/1 = 5$

From Fig. 13.21 $I_{oz} = 0.032$

$$\sigma_{z(FBGX)} = 12 \times 0.032 = 0.384 \text{ T/m}^2$$

$\sigma_{z(GCHX)}$: For $GCHX$, $l = 4$ m; $b = 2$ m

$m = l/b = 4/2 = 2$; $n = z/b = 5/2 = 2.5$

From Fig. 13.21 $I_{oz} = 0.093$

$$\sigma_{z(GCHX)} = 12 \times 0.093 = 1.116 \text{ T/m}^2$$

$\sigma_{z(HDEX)}$: For $HDEX$, $l = 4$ m; $b = 1$ m

$m = 4/1 = 4$; $n = 5/1 = 5$

From Fig. 13.21 $I_{\sigma z} = 0.05$

$$\sigma_{z(HDEX)} = 12 \times 0.05 = 0.6 \text{ T/m}^2$$

$$\therefore \quad \sigma_{z(ABCD)} = 0.216 + 0.384 + 1.116 + 0.6 = 2.316 \text{ T/m}^2$$

at 5 m below point x.

In the same manner as for vertical stress, the surface deflection at x can be computed as,

$$\rho_{(ABCD)} = \rho_{(FAEX)} + \rho_{(FBGX)} + \rho_{(GCHX)} + \rho_{(HDEX)}$$

The surface deflection factors for rectangles can be determined using Table 13.18 from which the values for $I_{\rho c}$ can be selected.

For $FAEX$, $I_{\rho c} = 0.561$
For $FBGX$, $I_{\rho c} = 0.766$
For $GCHX$, $I_{\rho c} = 0.766$
For $HDEX$, $I_{\rho c} = 0.982$

$$\therefore \quad \rho_{(ABCD)} = \frac{12(1 - 0.25^2)}{5000} [(1 \times 0.561) + (1 \times 0.766) + (2 \times 0.766) + (1 \times 0.982)]$$

$$= 0.00864 \text{ m} = 0.864 \text{ cm at surface at point } x$$

Q 13.3: To determine the vertical stress at 5 m below point x in Fig. 13.25 and the surface deflection at x due to uniformly distributed load on rectangle $ABCD$.

$AB = 3$ m
$BC = 5$ m
$EX = EA = 1$ m

The soil and load data are as in Q 13.2.

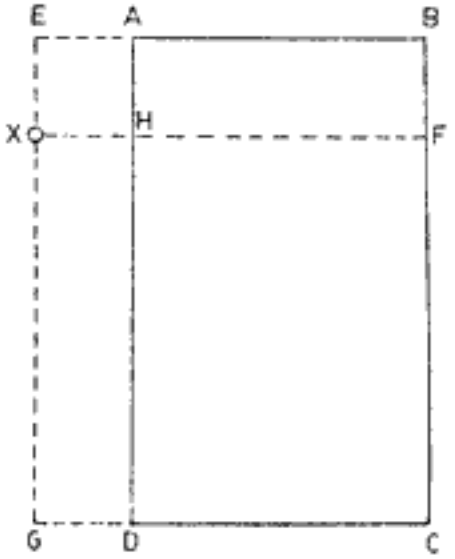

Fig. 13.25 Q 13.3

Ans: Construction in Fig. 13.25 shows the point x to be below the corner of a set of rectangles. The vertical stress below point x is expressed as,

$$\sigma_{z(ABCD)} = \sigma_{z(EBFX)} + \sigma_{z(FCGX)} - \sigma_{z(EAHX)} - \sigma_{z(HDGX)}$$

and the surface displacement at x is given by

$$\rho_{(ABCD)} = \rho_{(EBFX)} + \rho_{(FCGX)} - \rho_{(EAHX)} - \rho_{(HDGX)}$$

Proceeding as in Q 13.2

For $EBFX$, $I_{\sigma z} = 0.049$ and $I_{\rho c} = 0.982$

For $FCGX$, $I_{\sigma z} = 0.149$ and $I_{\rho c} = 0.561$

For $EAHX$, $I_{\sigma z} = 0.018$ and $I_{\rho c} = 0.561$

For $HDGX$, $I_{\sigma z} = 0.049$ and $I_{\rho c} = 0.982$

Hence, $\sigma_{z(ABCD)} = 12(0.049 + 0.149 - 0.018 - 0.049)$

$= 1.572$ T/m^2, 5 m below point x

$$\rho_{(ABCD)} = \frac{12(1 - 0.25^2)}{5000}(1\times0.982 + 4\times0.561 - 1\times0.561 - 1\times0.982)$$

$= 0.00379$ m $= 0.379$ cm, at surface at point x

Q 13.4: To determine the vertical stress at 4 m below point x shown in Fig. 13.26 and the surface deflection at point x, due to uniform loading on rectangle $ABCD$.

$AB = 3$ m

$BC = 5$ m

$FB = BG = 1$ m

The loading and soil data are as given in Q. 13.2.

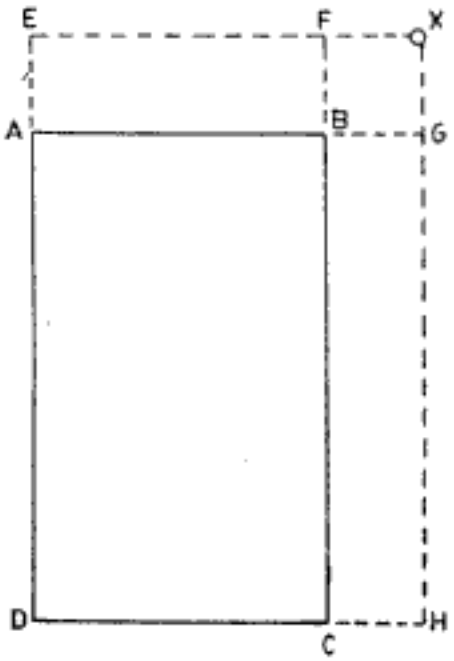

Fig. 13.26 Q 13.4

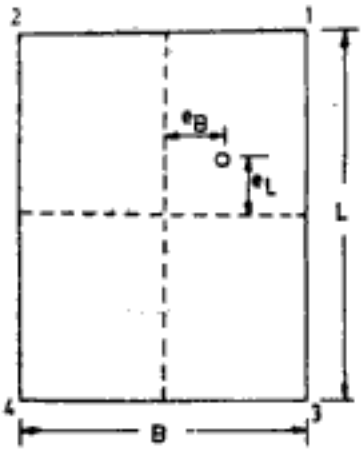

Fig. 13.27 Vertical eccentric load on rectangle

Ans: The point x is shown to lie at the corner of a set of rectangles as constructed in Fig. 13.26. Now, by principle of superposition,

$$\sigma_{z(ABCD)} = \sigma_{z(EDHX)} - \sigma_{z(EAGX)} - \sigma_{z(FCHX)} + \sigma_{z(FBGX)}$$

and,
$$\rho_{(ABCD)} = \rho_{(EDHX)} - \rho_{(EAGX)} - \rho_{(FCHX)} + \rho_{(FBGX)}$$

Proceeding as in Q 13.2

For $EDHX$, $I_{\sigma z} = 0.193$; $I_{\rho c} = 0.679$
For $EAGX$, $I_{\sigma z} = 0.067$; $I_{\rho c} = 0.982$
For $FCHX$, $I_{\sigma z} = 0.074$; $I_{\rho c} = 1.110$
For $FBGX$, $I_{\sigma z} = 0.027$; $I_{\rho c} = 0.561$

Hence, $\sigma_{z(ABCD)} = 12(0.193 - 0.067 - 0.074 + 0.027)$
$= 0.948$ T/m^2, at 4 m below x

$$\rho_{(ABCD)} = \frac{12\,(1 - 0.25^2)}{5000}\,(4\times0.679 - 1\times0.982 - 1\times1.11 + 1\times0.561)$$

$= 0.00267$ m $= 0.267$ cm, at surface at point x

2. *Rectangle with eccentric vertical load*

For computing the stresses and displacements below the rectangle the following approximate method can be used.

The contact pressure distribution is assumed to be linear and the following values under the four corners (Fig. 13.27) are calculated first.

$$\text{Under corner 1, } q_1 = \frac{6Q}{LB}\left(\frac{1}{6} + \frac{e_L}{L} + \frac{e_B}{B}\right) \tag{13.32}$$

$$\text{Under corner 2, } q_2 = \frac{6Q}{LB}\left(\frac{1}{6} + \frac{e_L}{L} - \frac{e_B}{B}\right) \tag{13.33}$$

$$\text{Under corner 3, } q_3 = \frac{6Q}{LB}\left(\frac{1}{6} - \frac{e_L}{L} + \frac{e_B}{B}\right) \tag{13.34}$$

$$\text{Under corner 4, } q_4 = \frac{6Q}{LB}\left(\frac{1}{6} - \frac{e_L}{L} - \frac{e_B}{B}\right) \tag{13.35}$$

where Q = total vertical load.

The contact pressure body can be cut into three parts, each of which can be handled independently in computations.

The first part is a uniform contact pressure of magnitude q_4 (Eq. 13.35).

The second part is a linearly increasing contact pressure along the side L, with zero along the edge 3–4 and a constant value of q_B along the edge 1–2. q_B is given by,

$$q_B = q_1 - q_3 = \frac{12Q}{LB}\,\frac{e_L}{L} \tag{13.36}$$

The third part is a contact pressure which increases linearly along side B, from zero along edge 2–4 to a constant value of q_A along the edge 1–3. q_A is given by

$$q_A = q_1 - q_2 = \frac{12Q}{LB}\,\frac{e_B}{B} \tag{13.37}$$

The total stress and displacement at a point is equal to the sum of the stress and displacement calculated for each part separately.

Stamatopoulos (1959) expresses the displacement of the corners (Fig. 13.28) for linearly changing contact pressure as,

$$\rho_z = \frac{qL(1-\mu^2)}{E} I_{\rho z} \tag{13.38}$$

Values of $I_{\rho z}$ are shown in Fig. 13.28. Equation 13.38 and Fig. 13.28 can be suitably adapted when the contact pressure changes linearly along side B. The method is demonstrated in Q 13.5.

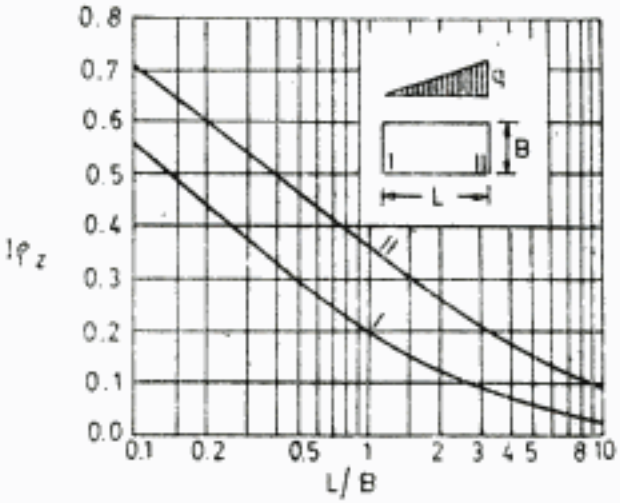

Fig. 13.28 Influence values for settlement of a corner of a rectangular area due to linearly changing contact pressure (After Stamatopoulos, 1959; by permission of American Society of Civil Engineers, New York)

Q 13.5: To determine the vertical surface displacement at the corners of a rectangle 4 m×2 m. Total load on the rectangle is 60 T acting eccentrically. $e_L = 0.2$ m, $e_B = 0.1$ m. The elastic constants of semi-infinite mass are $E = 200$ kg/cm², $\mu = 0.5$.

Ans: Referring to Fig. 13.27 the contact pressure intensities at the four corners of the rectangle are (From Eqs 13.32 to 13.35),

$$q_1 = 12 \text{ T/m}^2$$
$$q_2 = q_3 = 7.5 \text{ T/m}^2$$
$$q_4 = 3 \text{ T/m}^2$$

Displacement due to uniform pressure of q_4 $(= \rho_{z-I})$

$$q = 3 \text{ T/m}^2$$

For $L/B = 2$, from Table 13.18 $I_{\rho z}(= I_{\rho c}) = 0.766$ for corners. Substituting in Eq. 13.31 the vertical displacement of all corners is,

$$\rho_{z-I(1,2,3,4)} = \frac{3\times(1-0.5^2)\times 2}{2000}\times 0.766 = 1.72\times 10^{-3} \text{ m}$$
$$= 1.72 \text{ mm}$$

Displacement due to linearly increasing pressure along side L varying from zero to q_B ($= \rho_{z-II}$)

From Eq. 13.36 $q_B = 12 - 7.5 = 4.5$ T/m²

$L/B = 4/2 = 2$

$I_{\rho z}$ for corners 1 and 2 in Fig. 13.27 using curve II in Fig. 13.28,

$$I_{\rho z(1,2)} \simeq 0.265$$

$I_{\rho z}$ for corners 3 and 4, using curve I in Fig. 13.28 $\simeq 0.12$

Substituting in Eq. 13.38, the vertical displacement at corners 1 and 2 is,

$$\rho_{z-II(1)} = \rho_{z-II(2)} = \frac{4.5 \times 4 \times (1 - 0.5^2)}{2000} \times 0.265$$

$$= 1.79 \times 10^{-3} \text{ m} = 1.79 \text{ mm}$$

Similarly for corners 3 and 4

$$\rho_{z-II(3)} = \rho_{z-II(4)} = 0.81 \times 10^{-3} \text{ m} = 0.81 \text{ mm}$$

Displacement due to linearly increasing pressure along side B varying from zero to q_A ($= \rho_{z-III}$)

From Eq. 13.37 $q_A = 12 - 7.5 = 4.5$ T/m²

$L/B = 2/4 = 0.5$ (Note that in Fig. 13.28 the side along which the pressure increases is not the length or largest dimension of the rectangle)

For corners 1 and 3 from curve II of Fig. 13.28

$$I_{\rho z(1,3)} \simeq 0.47$$

For corners 2 and 4 from curve I of Fig. 13.28

$$I_{\rho z(2,4)} \simeq 0.3$$

Substituting in Eq. 13.38, the vertical displacement at corners 1 and 3 is,

$$\rho_{z-III(1)} = \rho_{z-III(3)} = \frac{4.5 \times 2 \times (1 - 0.5^2)}{2000} \times 0.47$$

$$= 1.58 \times 10^{-3} \text{ m} = 1.58 \text{ mm}$$

Similarly for corners 2 and 4

$$\rho_{z-III(2)} = \rho_{z-III(4)} = 1.01 \times 10^{-3} \text{ m} = 1.01 \text{ mm}$$

The total vertical displacement at a corner $= \rho_{z-I} + \rho_{z-II} + \rho_{z-III}$

At corner 1, $\rho_z = 1.72 + 1.79 + 1.58 = 5.09$ mm

At corner 2, $\rho_z = 1.72 + 1.79 + 1.01 = 4.52$ mm

At corner 3, $\rho_z = 1.72 + 0.81 + 1.58 = 4.11$ mm

At corner 4, $\rho_z = 1.72 + 0.81 + 1.01 = 3.54$ mm

13.3.10 Loading on Irregularly Shaped Areas

1. *Newmark's method*

This is a graphical procedure which involves the use of influence chart. Newmark's influence charts for vertical stresses and displacements are shown in Figs 13.29 to 13.32. The following steps explain the procedure of using these charts.

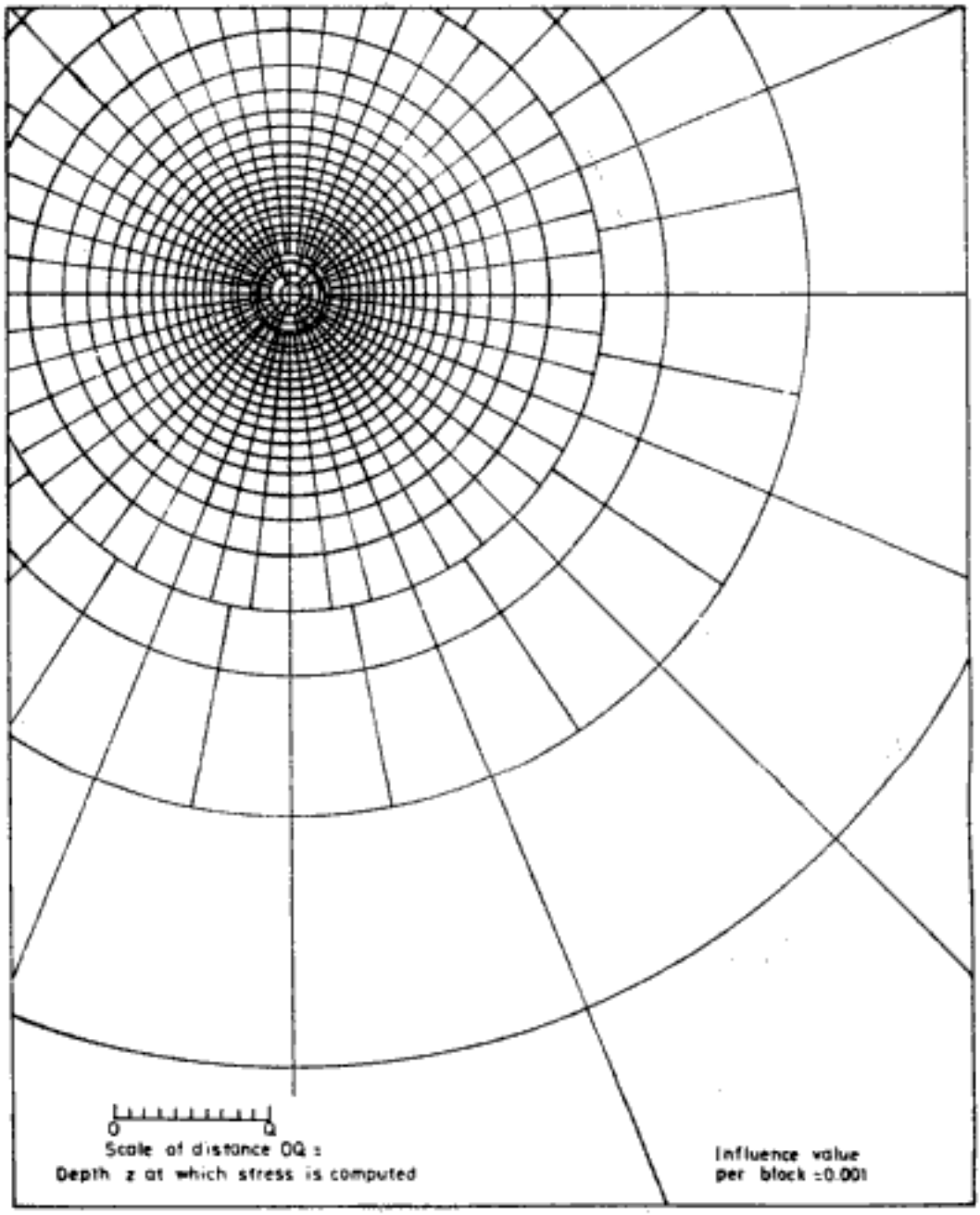

Fig. 13.29 Influence chart for vertical stress σ_z for all values of μ, $\sigma_z = 0.001\ Nq$; where N = number of influence blocks (After Newmark, 1942; drawn after Poulos and Davis, 1974)

Step 1: A plan of the loaded area is drawn on a tracing paper to the scale marked on the chart. The point below which the stress or displacement is required is located on the plan.

Step 2: This drawing is placed on the chart in such a way that the origin of the chart coincides with the point beneath which stress or displacement is required.

Step 3: The number of influence blocks covered by the drawing on the chart is counted. Parts or fractions of blocks may be estimated with sufficient accuracy. The number of blocks covered will be the same irrespective of the orientation of the drawing on the chart.

Step 4: To get the vertical stress the number of blocks is multiplied by the appropriate influence value shown on the chart and the loading intensity.

To obtain surface displacement the formula shown in Fig. 13.30 is used.

Figure 13.31 and the formula in the figure can be used for displacement at a depth z below a point when value of Poisson's ratio is 0.5. For values of Poisson's ratio other than 0.5 chart shown in Fig. 13.32 will have to be used for correcting the vertical displacement obtained from Fig. 13.31.

2, Sector method

For irregular shape loaded areas Poulos (1967a) describes a procedure called sector method for determination of stresses and displacements at a point inside or outside the loaded area.

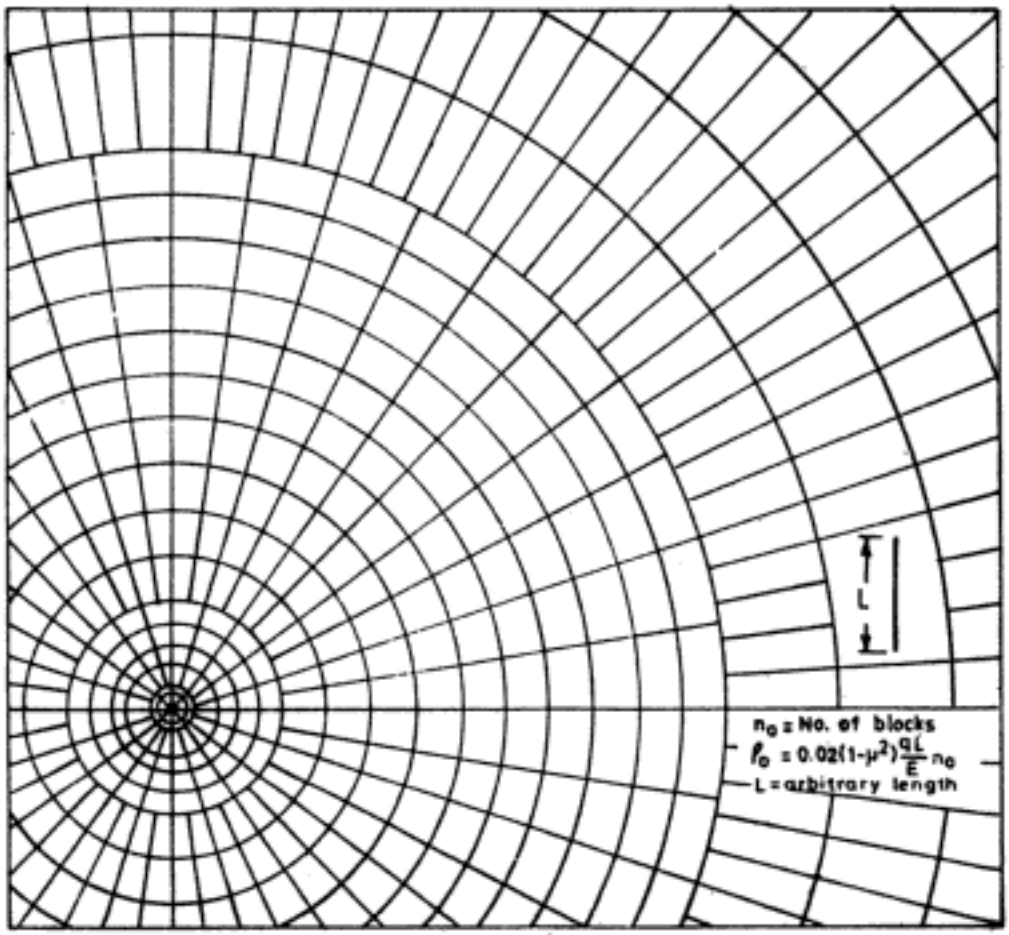

Fig. 13.30 Influence chart for vertical displacement at surface

$$\rho_o = 0.02\ (1 - \mu^2)\ \frac{qL}{E}\ n_o$$

n_o = number of influence blocks

L = any convenient arbitrary length

(After Newmark 1947; drawn after Poulos and Davis, 1974)

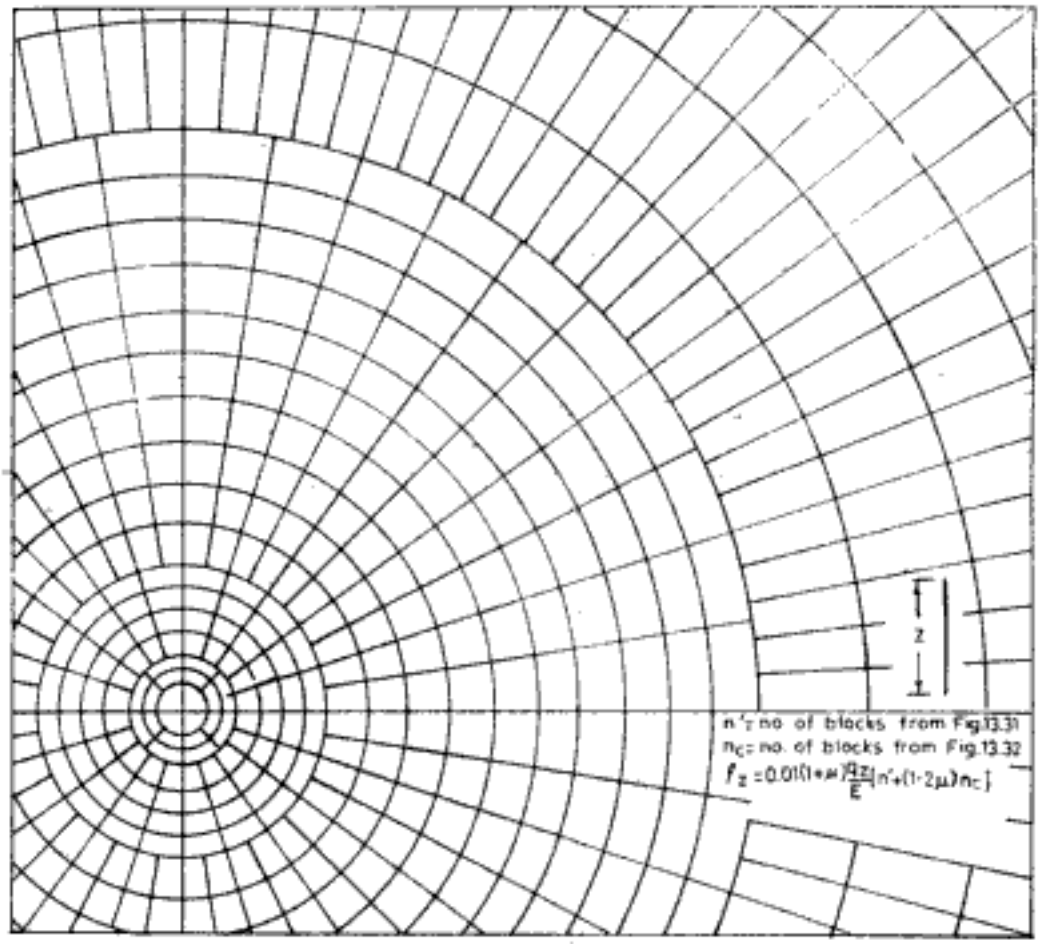

Z = depth at which displacement is computed

Fig. 13.31 Influence chart for vertical displacement at depth z below surface for $\mu = 0.5$

$$\rho_z = 0.01\,(1 + \mu)\,\frac{qz}{E}\,[n' + (1 - 2\mu)\,n_c]$$

n' = **number of blocks from Fig. 13.31**

n_c = **number of blocks from Fig. 13.32**

z = **depth at which displacement is computed**

(After Newmark, 1947; drawn after Poulos and Davis, 1974)

Procedure for a point (O_E) lying outside the loaded area:

Step 1: The loaded area is drawn to a convenient scale.

Step 2: The surface origin, O_E of the point is located. The surface origin is that point on the surface of the elastic solid through which the vertical line passing through the point at which stress or displacement is required emanates.

Step 3: Draw a small angled ($\delta\theta$) sector to cut the loaded area. For example AO_EB is the sector in Fig. 13.33 in which $ABCD$ is the part in the loaded area.

Step 4: Determine the two mean sector radii. $r_s = r_1$ and $r_s = r_2$ are the two mean sector radii.

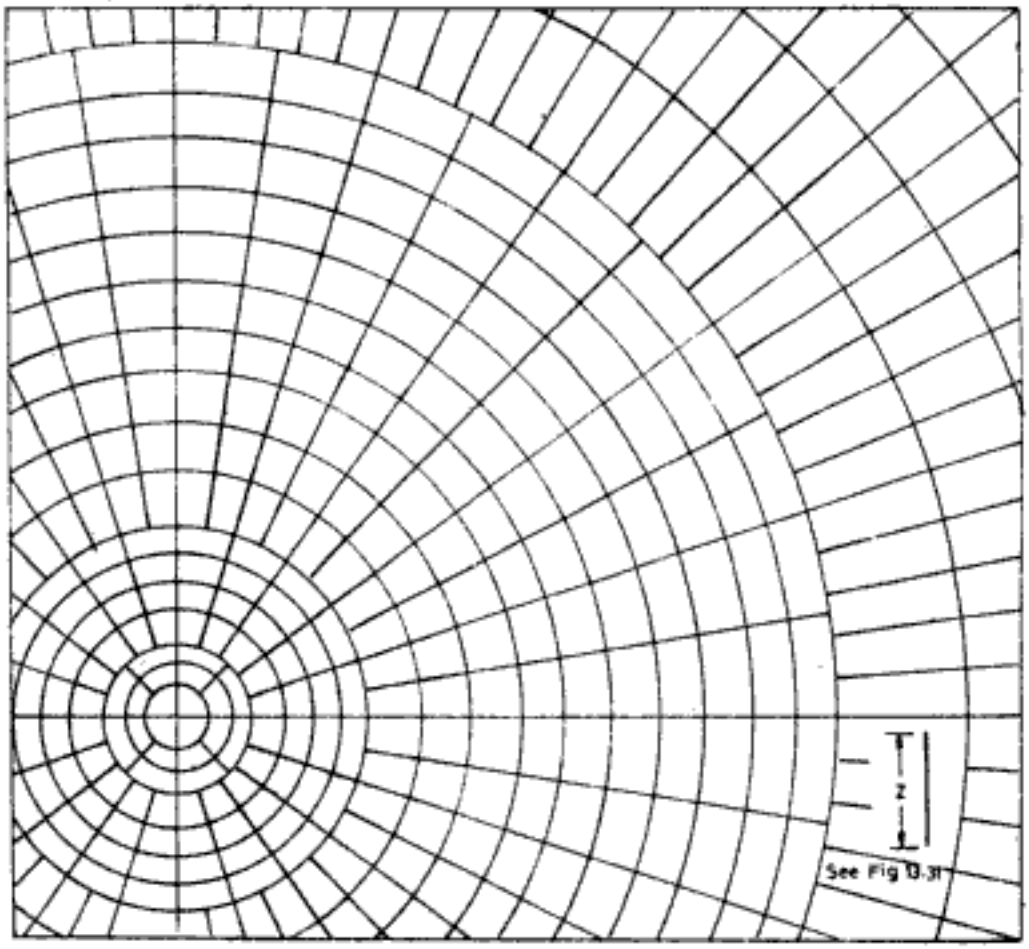

z = depth at which displacement is computed

Fig. 13.32 Influence chart for Poisson's ratio correction for vertical displacement at depth z below surface. z = depth at which displacement is computed (After Newmark, 1947; drawn after Poulos and Davis, 1974)

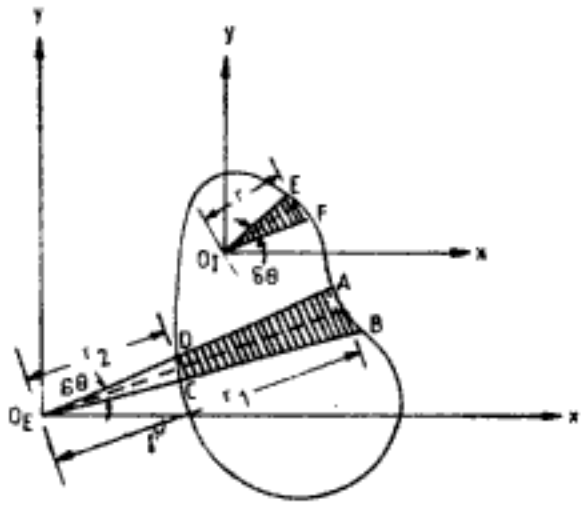

Fig. 13.33 Sector method

For vertical stress

Step 5: From Fig. 13.34 obtain the sector influence values, say I_{S1} and I_{S2}, corresponding to r_1 (i.e., $r_s/z = r_1/z$) and r_2 (i.e., $r_s/z = r_2/z$).

Step 6: The vertical stress at the required point due to loaded area of the sector $ABCD$ is computed as

$$\sigma_{z(ABCD)} = q\,\delta\theta\,(I_{S1} - I_{S2}) \tag{13.39}$$

Step 7: Repeat steps 3 to 6 until the loaded area has been fully covered by a number of small angled sectors and the required vertical stress is $\sigma_z = \Sigma\sigma_{Z(ABCD)}$.

For surface displacement:

First complete steps 1 to 4 described above.

Step 5: Obtain the vertical displacement at the required point due to load over $ABCD$, as

$$\rho_{o(ABCD)} = \frac{q}{\pi}\,\delta\theta\,\frac{(1-\mu^2)}{E}\,(r_1 - r_2) \tag{13.40}$$

Step 6: Repeat steps 3 to 5 until the loaded area has been fully covered by a number of small angled sectors and $\rho_o = \Sigma\,\rho_{o(ABCD)}$.

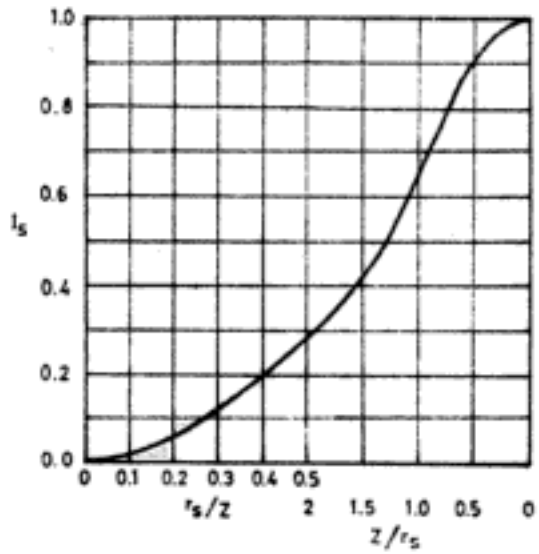

Fig. 13.34 Sector influence values for σ_z (After Poulos, 1974; reprinted with permission of John Wiley and Sons, Inc., New York)

Procedure for a point O_f lying inside the loaded area

Step 1: The loaded area is drawn to a convenient scale.

Step 2: The surface origin O_f of the point is located.

Step 3: Draw a small angled sector ($\delta\theta$) to cut the loaded area. For example EO_fF is the sector in Fig. 13.33.

Step 4: Determine the mean sector radius, $r_s = r$ is the mean radius.

For vertical stress

Step 5: From Fig. 13.34 obtain the sector influence value, say I_s corresponding to r (i.e., $r_s/z = r/z$).

Step 6: The vertical stress at the required point due to the loaded area of the sector EO_1F is computed as

$$\sigma_{z(EO_1F)} = q\,\delta\theta\,I_s \tag{13.41}$$

Step 7: Repeat steps 3 to 6 until the loaded area has been fully covered by a number of small angled sectors and the required vertical stress is $\sigma_z = \Sigma\sigma_z(EO_1F)$.

For vertical surface displacement

First complete steps 1 to 4 described above.

Step 5: Obtain the vertical displacement at the required point due to load over EO_1F, as

$$\rho_{0(EO_1F)} = \frac{q}{\pi}\,\delta\theta\,\frac{(1-\mu^2)}{E}\,r \tag{13.42}$$

Step 6: Repeat steps 3 to 5 until the loaded area has been fully covered by a number of small angled sectors and the required vertical surface displacement is,

$$\rho_o = \Sigma\rho_o(EO_1F)$$

13.4 LOADED AREAS EMBEDDED IN SEMI-INFINITE MASS

13.4.1 Circular Area (Fig. 13.35)

Radius of circle = a

Depth of embedment = h

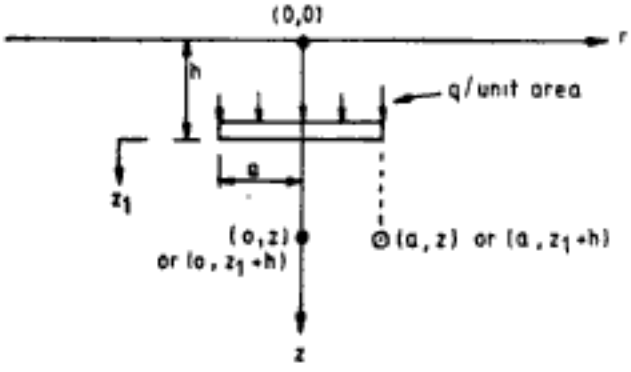

Fig. 13.35 Uniformly loaded embedded circular area

Nishida (1966) gives the expressions for vertical stress below the centre and edge of the loaded area in the form,

$$\sigma_z = qI_{oz} \tag{13.7}$$

where I_{oz} is the appropriate dimensionless influence factor.

Table 13.19 gives the numerical values of I_{oz} for centre and edge for different values of μ, z_1/a, and h/a. Note that z is reckoned from the surface of semi-infinite mass whereas z_1 is reckoned from the level of the loaded area. Thus $z = z_1 + h$.

Table 13.19 Vertical Stress σ_z Beneath Circular Area

		I_{σ_z} (centre)					I_{σ_z} (edge)				
μ	z_1/a \ μ_1/a	0	1	2	3	∞	0	1	2	3	∞
0.00	0	1.00	0.70	0.56	0.54	0.50	0.50	0.33	0.30	0.28	0.25
	1	0.64	0.35	0.30	0.27	0.25	0.34	0.21	0.18	0.17	0.13
	2	0.28	0.17	0.13	0.12	0.10	0.20	0.12	0.10	0.09	0.07
	4	0.09	0.06	0.05	0.04	0.03	0.12	0.05	0.04	0.03	0.01
0.25	0	1.00	0.71	0.57	0.53	0.50	0.50	0.38	0.31	0.28	0.25
	1	0.64	0.46	0.39	0.29	0.26	0.34	0.24	0.18	0.15	0.13
	2	0.28	0.18	0.15	0.13	0.11	0.20	0.13	0.11	0.09	0.08
	4	0.09	0.07	0.06	0.04	0.03	0.12	0.06	0.05	0.03	0.02
0.50	0	1.00	0.75	0.58	0.54	0.50	0.50	0.40	0.32	0.28	0.25
	1	0.64	0.45	0.38	0.35	0.34	0.34	0.29	0.21	0.19	0.16
	2	0.28	0.22	0.18	0.15	0.14	0.20	0.17	0.13	0.11	0.10
	4	0.09	0.08	0.07	0.04	0.04	0.12	0.07	0.06	0.05	0.04

After Nishida, 1966. By permission of Laboratorio Nacional de Engenharia Civil, Lisboa, Portugal.

Nishida (1966) also gives the expressions for vertical displacement ρ_z. The expression for surface displacement below the centre or edge of the footing is given as

$$\rho_o = \frac{qa}{E} I_{\rho i} \tag{13.43}$$

where $I_{\rho i}$ = appropriate deflection factor
$I_{\rho i} = I_{\rho c}$ for centre of loaded area
$I_{\rho i} = I_{\rho e}$ for the edge

Table 13.20 gives numerical values of $I_{\rho c}$ and $I_{\rho e}$. Yet another method (Poulos, 1967a) of determining surface displacement is to determine the surface displacement first by using Fig. 13.17 and then to multiply this value by a reduction factor R_F obtained from Fig. 13.36 to account for depth of embedment of the loaded area.

Table 13.20 Influence Factors for Vertical Displacement of Embedded Circle

	I_{ρ_c} (centre)			I_{ρ_e} (edge)		
h/a \ μ	0.50	0.25	0.00	0.50	0.25	0.00
0.00	1.500	1.875	2.000	0.955	1.194	1.273
3.50	0.908	0.995	0.909			
5.00	0.862	0.947	0.862	0.586	0.640	0.585
100	0.750	0.833	0.750	0.478	0.530	0.478
1000	0.750	0.833	0.750	0.478	0.530	0.478

After Nishida, 1966. By permission of Laboratorio Nacional de Engenharia Civil, Lisboa, Portugal.

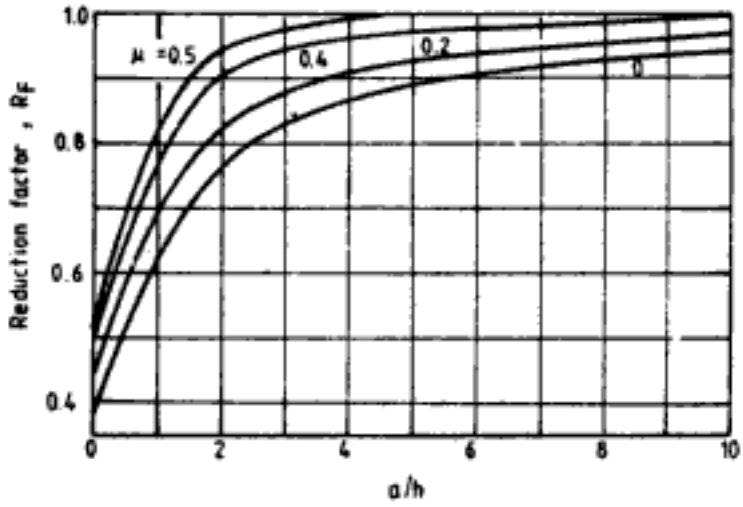

Fig. 13.36 Reduction factor R_F for surface displacement to account for depth of embedment
(After Poulos and Davis, 1967a)

13.4.2 Uniform Vertical Load on a Rectangular Area

Skopek (1961) obtained the solution for vertical stress beneath the corner of a uniformly loaded embedded rectangular area shown in Fig. 13.37.

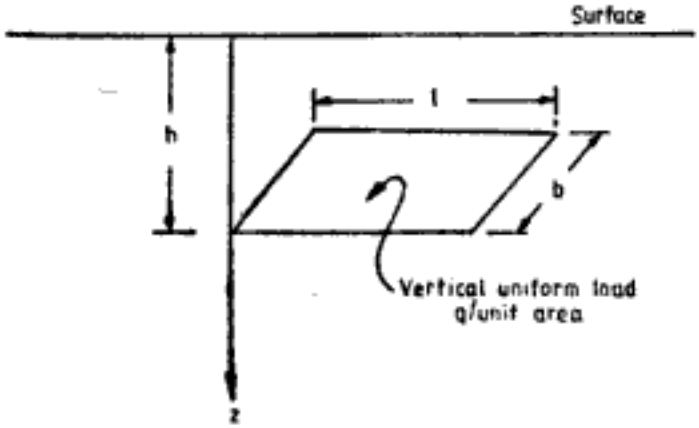

Fig. 13.37 Embedded rectangular area

The equation for vertical stress is given by

$$\sigma_z = \frac{q}{4\pi(1-\mu)}\left\{(1-\mu)\left[\arctan\frac{lb}{(z-h)R_1} + \arctan\frac{lb}{(z+h)R_2}\right]\right.$$
$$+\frac{(z-h)bR_1}{2lr_1^2} - \frac{b(z-h)^3}{2lr_3^2R_1} + \frac{[(3-4\mu)z(z+h) - h(5z-h)]bR_2}{2(z+h)lr_2^2}$$
$$-\frac{[(3-4\mu)z(z+h)^2 - h(z+h)(5z-h)]b}{2lr_4^2R_2} + \frac{2hz(z+h)bR_2^3}{l^3r_2^4}$$
$$\left.+\frac{3hzbR_2r_3^2}{(z+h)l^3r_2^2} - \frac{hz(z+h)^3b}{lr_4^4R_2}\left[\frac{2l^2-(z+h)^2}{l^2} - \frac{b^2}{R_2^2}\right]\right\} \qquad (13.44)$$

where
$$R_1^2 = l^2 + b^2 + (z - h)^2$$
$$R_2^2 = l^2 + b^2 + (z + h)^2$$
$$r_1^2 = b^2 + (z - h)^2$$
$$r_2^2 = b^2 + (z + h)^2$$
$$r_3^2 = l^2 + (z - h)^2$$
$$r_4^2 = l^2 + (z + h)^2$$
$$r_5^2 = l^2 - (z + h)^2$$

Note that z is reckoned from the surface.

Groth and Chapman (1969) give the expression for vertical displacement of corner of the rectangle as,

$$\rho_{z\text{-corner}} = \frac{qb}{E} I_{\rho\text{-corner}} \tag{13.45}$$

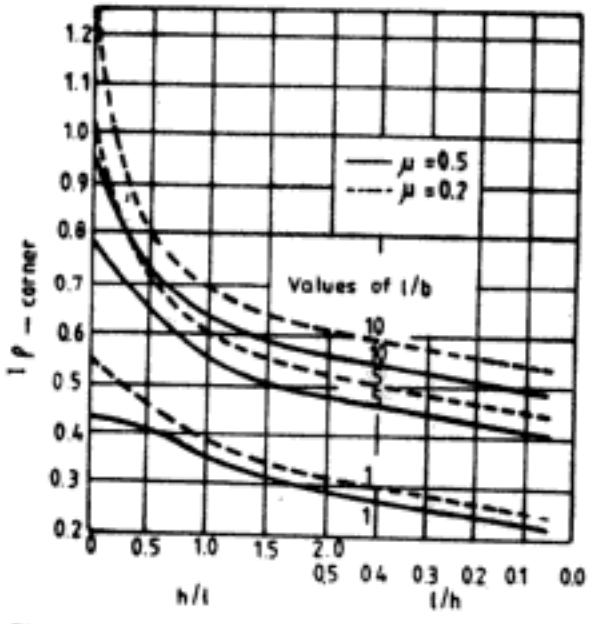

Fig. 13.38 Vertical displacement factor for corner of embedded rectangle (Eq. 13.45) (After Groth and Chapman, 1969)

Values of $I_{\rho\text{-corner}}$ in Eq. 13.45 can be obtained from Fig. 13.38. According to Fox (1948b), the *mean* elastic vertical displacement of a uniformly loaded rectangle of $2b \times 2l$ embedded at a depth h below the surface is given by

$$\rho_m = \frac{q(1 + \mu)}{4\pi E(1 - \mu)} \sum_{s=1}^{5} \beta_s W_s \tag{13.46}$$

where
$$\beta_1 = 3 - 4\mu$$
$$\beta_2 = 5 - 12\mu + 8\mu^2$$
$$\beta_3 = -4\mu(1 - 2\mu)$$
$$\beta_4 = -1 + 4\mu - 8\mu^2$$

$$\beta_5 = -4(1 - 2\mu)^2$$

$$W_1 = 2b \ln \frac{r_4 + 2l}{2b} + 2l \ln \frac{r_4 + 2b}{2l} - \frac{r_4^3 - 8b^3 - 8l^3}{12bl}$$

$$W_2 = 2b \ln \frac{r_3 + 2l}{r_1} + 2l \ln \frac{r_3 + 2b}{r_2} - \frac{r_3^3 - r_2^3 - r_1^3 + r^3}{12bl}$$

$$W_3 = \frac{r^2}{2b} \ln \frac{(2l + r_2)r_1}{(2l + r_3)r} + \frac{r^2}{2l} \ln \frac{(2b + r_1)r_2}{(2b + r_3)r}$$

$$W_4 = \frac{r^2(r_1 + r_2 - r_3 - r)}{4bl}$$

$$W_5 = r \arctan\left(\frac{4bl}{rr_3}\right)$$

$$r = 2h \qquad r_1^2 = 4b^2 + r^2 \qquad r_2^2 = 4l^2 + r^2$$

$$r_3^2 = 4b^2 + 4l^2 + r^2 \qquad r_4^2 = 4b^2 + 4l^2$$

Fox also obtained the relationship between the mean displacement of an embedded footing and the mean displacement of the same footing at the surface. Thus the ratio $\rho_{m\text{-embedded}}/\rho_{m\text{-surface}}$ is a correction factor or reduction factor that should be applied to the mean displacement of the hypothetical footing at the surface. Figure 13.39 shows the variation of this factor for $\mu = 0.5$. For other values of μ Fig. 13.40 gives the values of the correction factor (Bowles, 1982). The average or mean displacement of a uniformly loaded rectangle on the surface of the semi-infinite mass with $\mu = 0.5$ is expressed as,

$$\rho_{z\text{-mean}} = \frac{3q\sqrt{LB}}{4E} I_{pz} \tag{13.47}$$

Values of I_{pz} are given in Fig. 13.41.

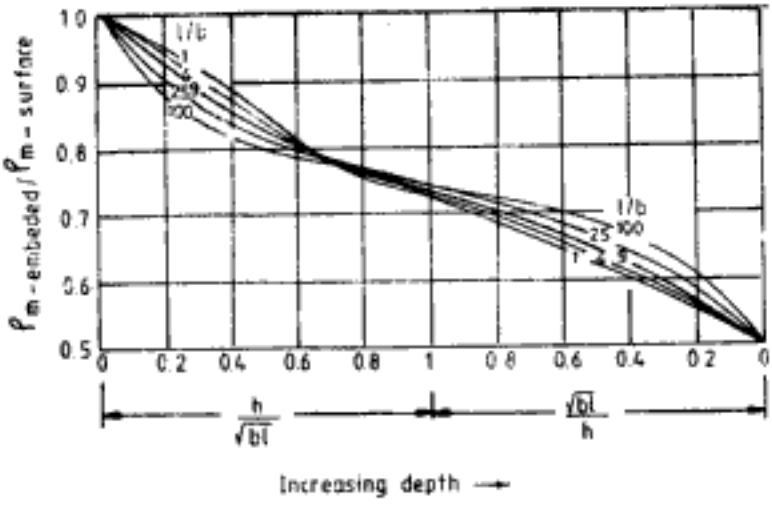

Fig. 13.39 Ratio of mean displacement of rectangle at depth h to that of rectangle at surface. $\mu = 0.5$. l b and h are as in Fig. 13.37 (After Fox, 1948b)

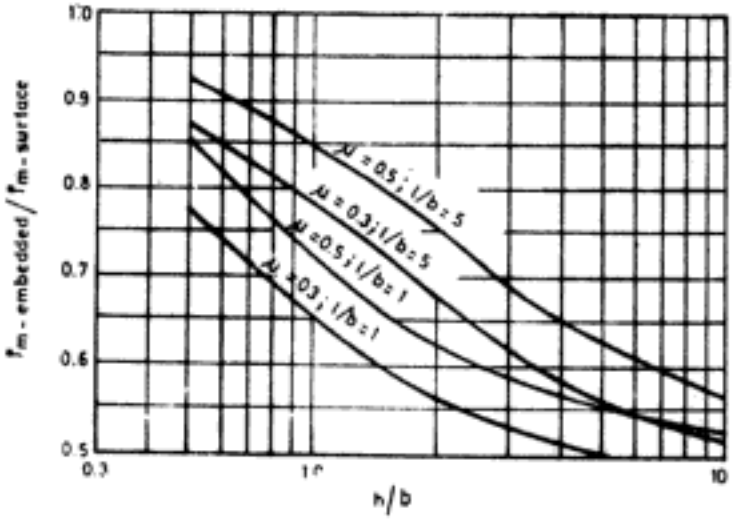

Fig. 13.40 **Ratio of mean displacement of rectangle (Fig. 13.37) at depth h to that of rectangle at surface** (After Bowles, 1982; reprinted with permission of McGraw-Hill Book Company, New York)

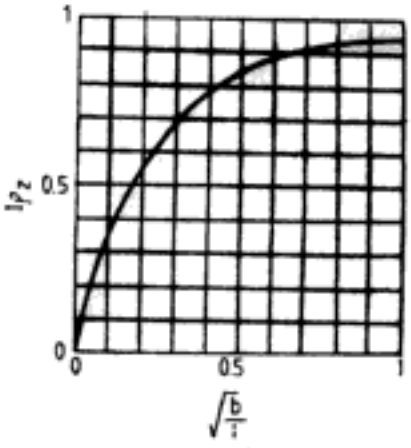

Fig. 13.41 **Influence factor for average vertical displacement of uniformly loaded rectangular area**

13.4.3 Irregularly Shaped Embedded Areas

For vertical displacement of the loaded area the sector method explained for loaded area on the surface can be used incorporating a correction factor or reduction factor for the displacement of each sector considered. For every sector the vertical displacement is multiplied by a reduction factor obtained from Fig. 13.36. In this case in Fig. 13.36 the x-axis must be taken as (r_s/h).

For vertical stress no influence charts are available.

13.5 LOADED AREAS ON THE SURFACE OF A FINITE LAYER

A rigid base underlies a finite layer of elastic medium as shown in Fig. 13.42. Solutions are available for stresses and displacements for conditions of rough rigid base (adhesive interface) and smooth rigid base (smooth interface). Solutions of rough rigid base condition are mainly presented here which is more close to soil engineering situations.

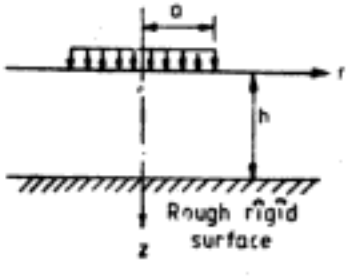

Fig. 13.42 **Rigid base below finite thickness elastic layer**

13.5.1 Uniform Vertical Loading on a Circular Area

Milovic (1970) gives the equation for vertical stress at a point below the centre of the circle (Fig. 13.42) as,

$$\sigma_{z\text{-centre}} = qI_{\sigma z\text{-centre}} \tag{13.48}$$

Figure 13.43 gives the values of $I_{\sigma z\text{-centre}}$. The vertical stress at a point below the edge of the circle is given by,

$$\sigma_{z\text{-edge}} = qI_{\sigma z\text{-edge}} \tag{13.49}$$

Figure 13.44 gives the values for influence factor $I_{\sigma z\text{-edge}}$. For various points within the loaded area, Milovic (1970) obtained solutions for the vertical surface displacement. The equation for vertical displacement is given by,

$$\rho_z = \frac{2qa}{E} I_{\rho z} \tag{13.50}$$

Numerical values of $I_{\rho z}$ are given in Table 13.21.

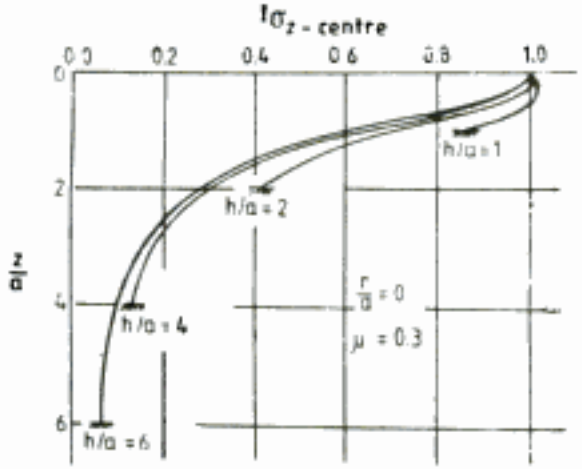

Fig. 13.43 Influence factor for vertical stress beneath centre (After Milovic, 1970)

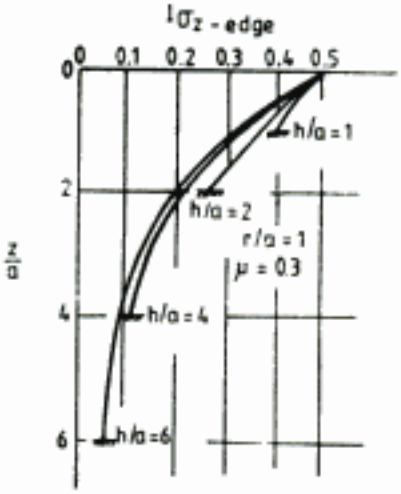

Fig. 13.44 Influence factor for vertical stress beneath edge (After Milovic, 1970)

13.5.2 Uniform Vertical Loading on a Rectangular Area

Burmister (1956) gives the solutions for vertical stress for points beneath the corner of a rectangular loaded area shown in Fig. 13.45. The vertical stress is expressed as

$$\sigma_z = qI_{\sigma z} \tag{13.7}$$

The values of $I_{\sigma z}$ for $z = 0.2h$, $0.4h$, $0.6h$, $0.8h$, and h, for $\mu = 0.4$ are shown in Figs 13.46 to 13.50.

Ueshita and Meyerhof (1968) give the following expression for the surface displacement of the corner of the rectangle,

$$\rho_z = \frac{qB}{E} I_{\rho z} \tag{13.51}$$

Table 13.21 Influence Factors I_{pz} for Vertical Surface Displacement within Circular Area (Eq. 13.50)

(Rough Rigid Base)

μ	h/a \ r/a	0	0.2	0.4	0.6	0.8	1.0
0.15	1	0.464	0.458	0.441	0.408	0.348	0.208
	2	0.684	0.674	0.645	0.593	0.509	0.348
	4	0.811	0.800	0.768	0.710	0.619	0.463
	6	0.839	0.827	0.794	0.736	0.646	0.501
0.30	1	0.397	0.392	0.379	0.351	0.301	0.173
	2	0.613	0.604	0.578	0.531	0.456	0.305
	4	0.740	0.732	0.703	0.651	0.568	0.420
	6	0.770	0.762	0.733	0.681	0.597	0.458
0.45	1	0.278	0.276	0.267	0.250	0.213	0.109
	2	0.489	0.482	0.461	0.422	0.361	0.229
	4	0.612	0.608	0.585	0.541	0.472	0.340
	6	0.637	0.635	0.612	0.568	0.499	0.374

After Milovic, 1970.

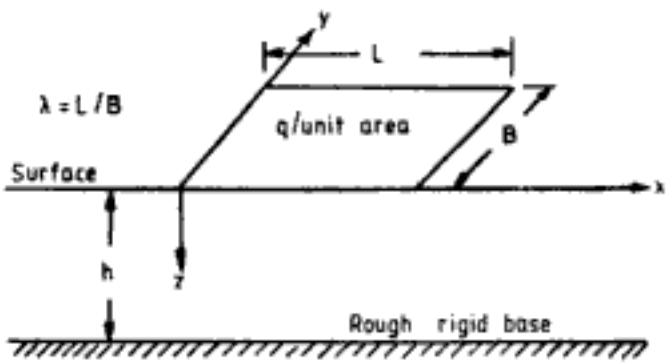

Fig. 13.45 Rectangle on a finite thickness layer

Figures 13.51 to 13.56 give the values of I_{pz} for six different values of μ. In these figures the curves on the left for different values of λ are for $h/B \leqslant 1$ and those on the right are for $h/B \geqslant 1$. Also shown in these figures are the influence factor values when the medium is semi-infinite (Boussinesq's case). Milovic and Tournier (1971) give the following equation for vertical stress at points beneath the centre and corner of the rectangle;

$$\sigma_z = qI_{\sigma z} \tag{13.7}$$

The values of $I_{\sigma z}$ for centre and corner are given in Tables 13.22 and 13.23 respectively.

Milovic and Tournier give the expression for the vertical surface displacement of the centre and corner of the rectangle as

$$\rho_{z\text{-surface}} = \frac{qB}{E} I_{pz} \tag{13.52}$$

The values of the deflection factor I_{pz} for the centre and corner of the rectangle are given in Table 13.24.

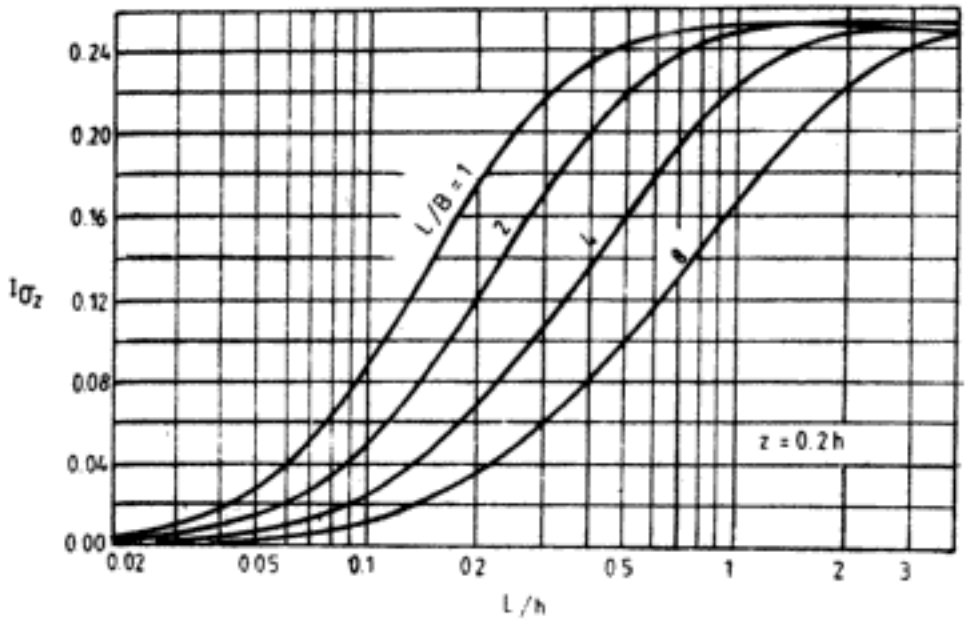

Fig. 13.46 **Influence factor for vertical stress beneath the corner of rectangle from Burmister layer theory, $\mu = 0.4$, $z = 0.2h$** (After Burmister, 1956;with permission of Transportation Research Board, National Research Council, Washington, DC)

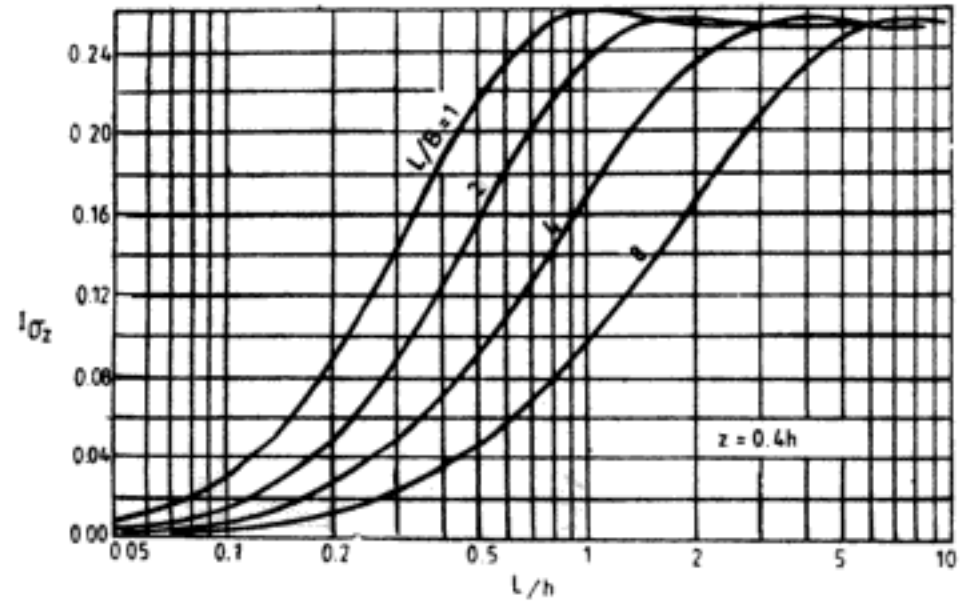

Fig. 13.47 **Influence factor for vertical stress beneath the corner of rectangle from Burmister layer theory, $\mu = 0.4$, $z = 0.4h$** (After Burmister 1956; with permission of Transportation Research Board, National Research Council, Washington, DC)

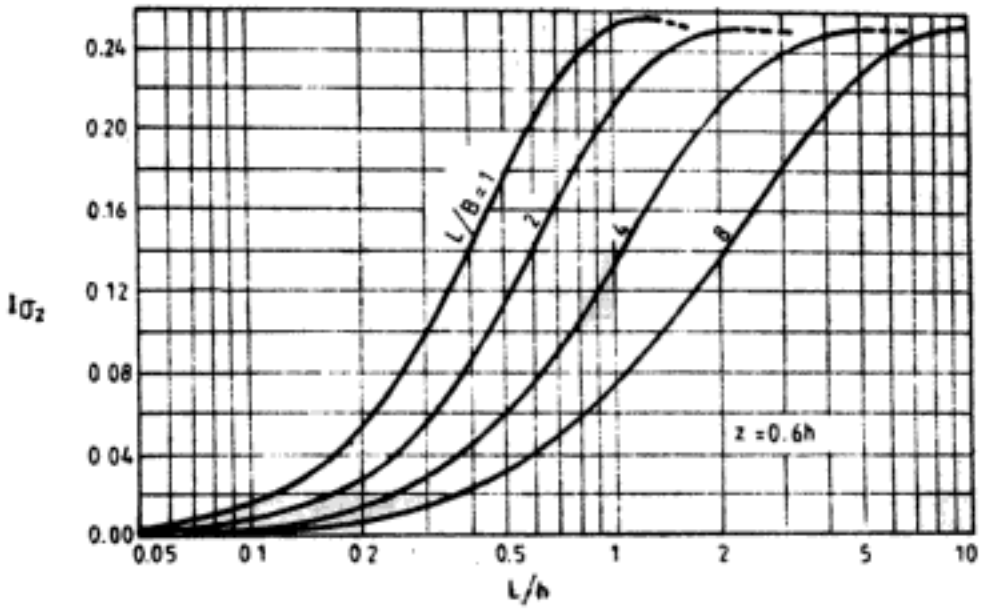

Fig. 13.48 **Influence factor for vertical stress beneath the corner of rectangle from Burmister layer theory, $\mu = 0.4$, $z = 0.6h$**
(After Burmister, 1956; with permission of Transportation Research Board, National Research Council, Washington, DC)

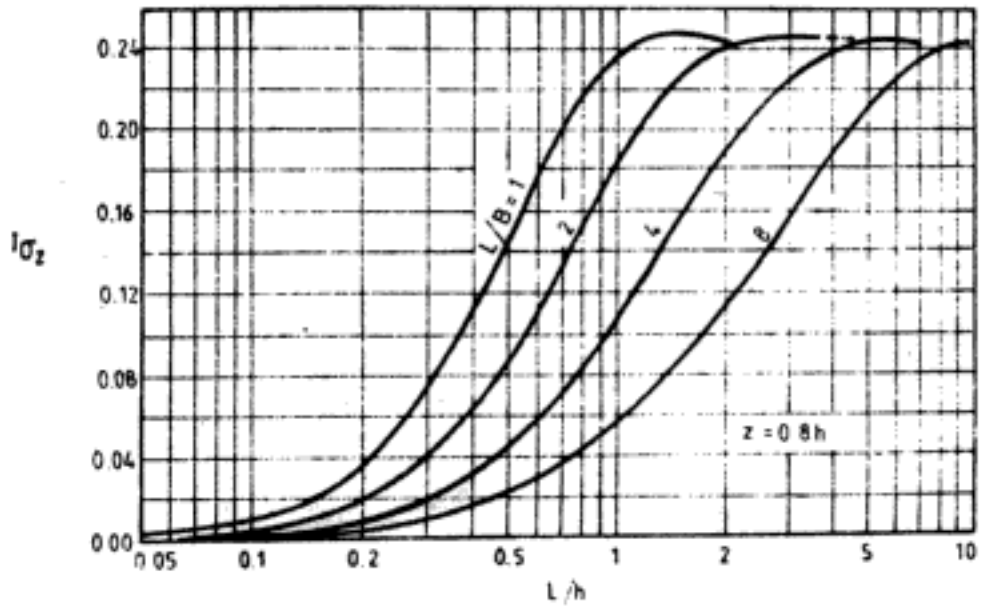

Fig. 13.49 **Influence factor for vertical stress beneath the corner of rectangle from Burmister layer theory, $\mu = 0.4$, $z = 0.8h$**
(After Burmister, 1956; with permission of Transportation Research Board, National Research Council, Washington, DC)

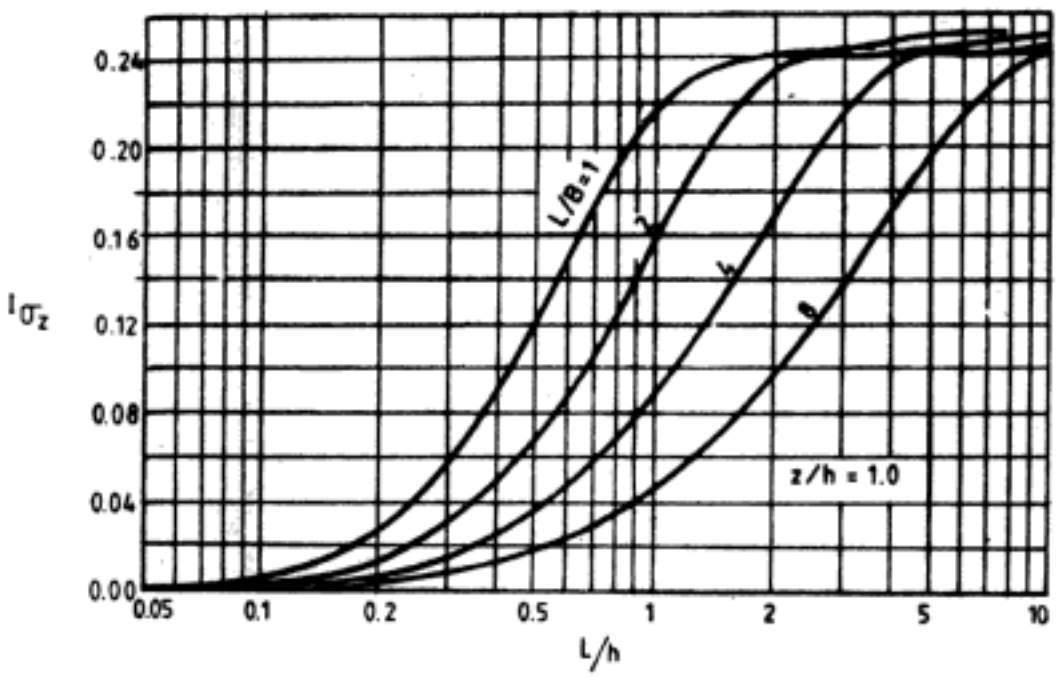

Fig. 13.50 Influence factor for vertical stress beneath the corner of rectangle from Burmister layer theory, $\mu = 0.4$, $z = h$
(After Burmister, 1956; with permission of Transportation Research Board, National Research Council, Washington, DC)

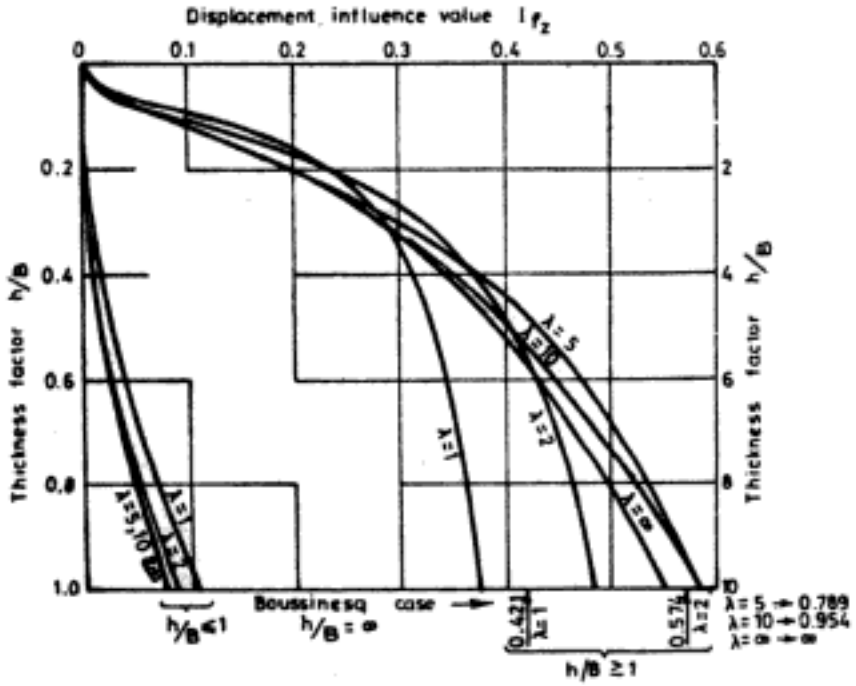

Fig. 13.51 Displacement factor for corner of rectangle, $\mu = 0.5$, (Eq. 13.51) (After Ueshita and Meyerhof, 1968; by permission of Transportation Research Board, National Research Council, Washington, DC)

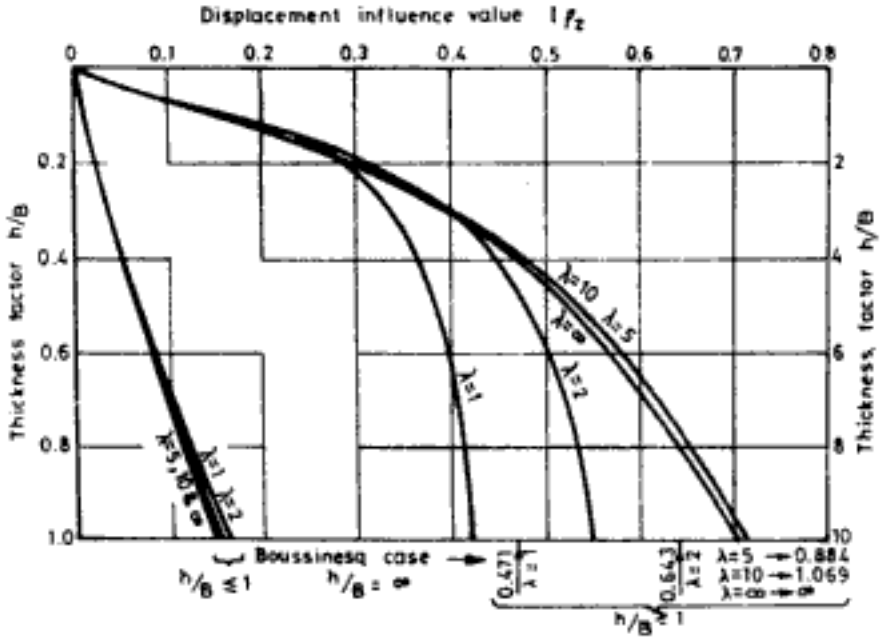

Fig. 13.52 Displacement factor for corner of rectangle, $\mu = 0.4$, Eq. (13.51) (After Ueshita and Meyerhof, 1968; by permission of Transportation Research Board, National Research Council, Washington, DC)

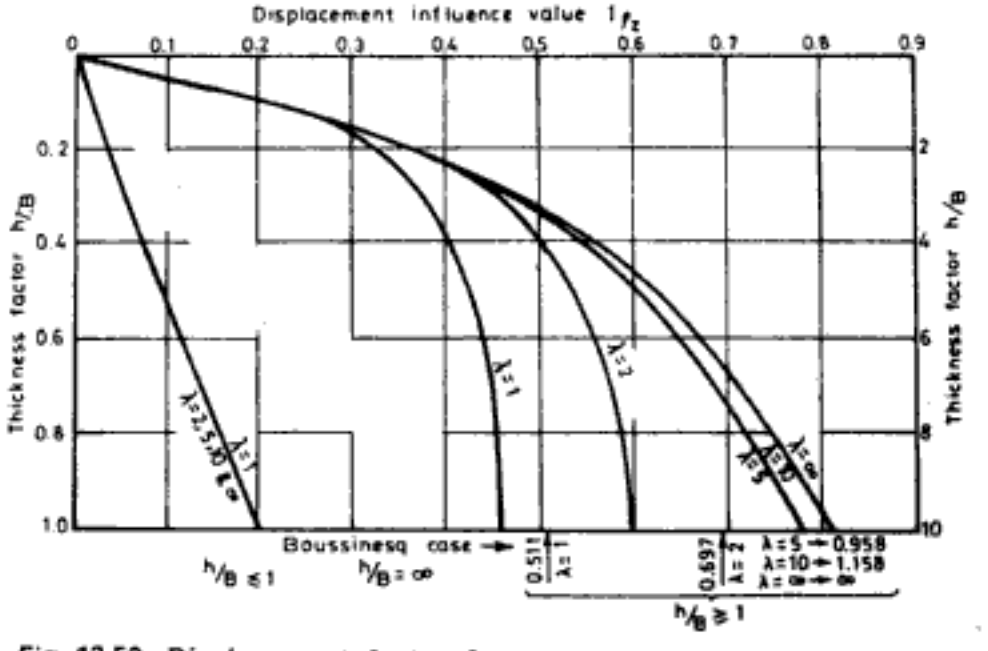

Fig. 13.53 Displacement factor for corner of rectangle, $\mu = 0.3$, (Eq. 13.51) (After Ueshita and Meyerhof, 1968; by permission of Transportation Research Board, National Research Council, Washington, DC)

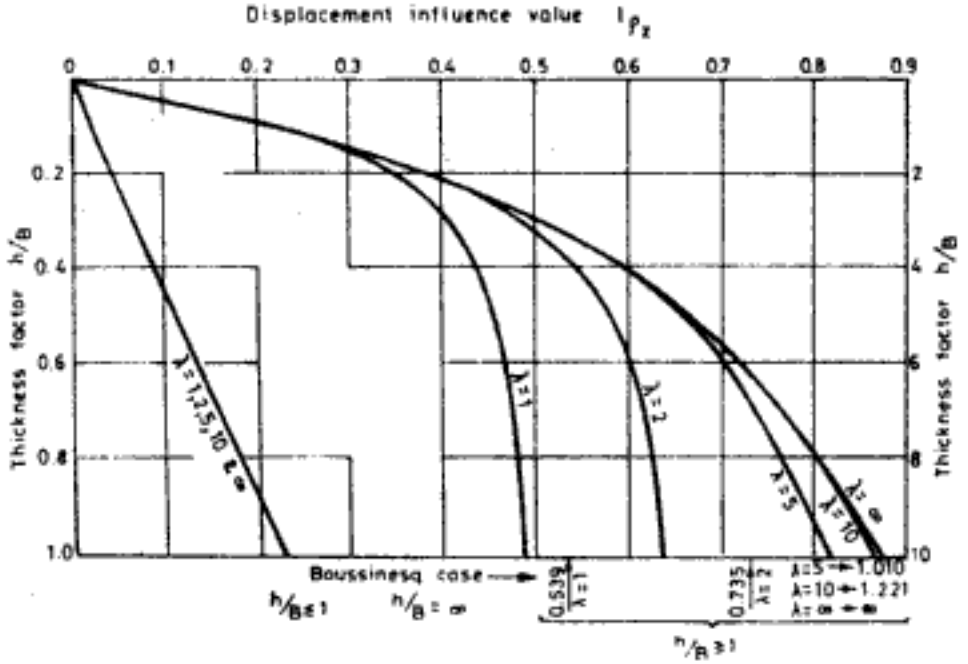

Fig. 13.54 Displacement factor for corner of rectangle, $\mu = 0.2$, (Eq. 13.51) (After Ueshita and Meyerhof, 1968; by permission of Transportation Research Board, National Research Council Washington, DC)

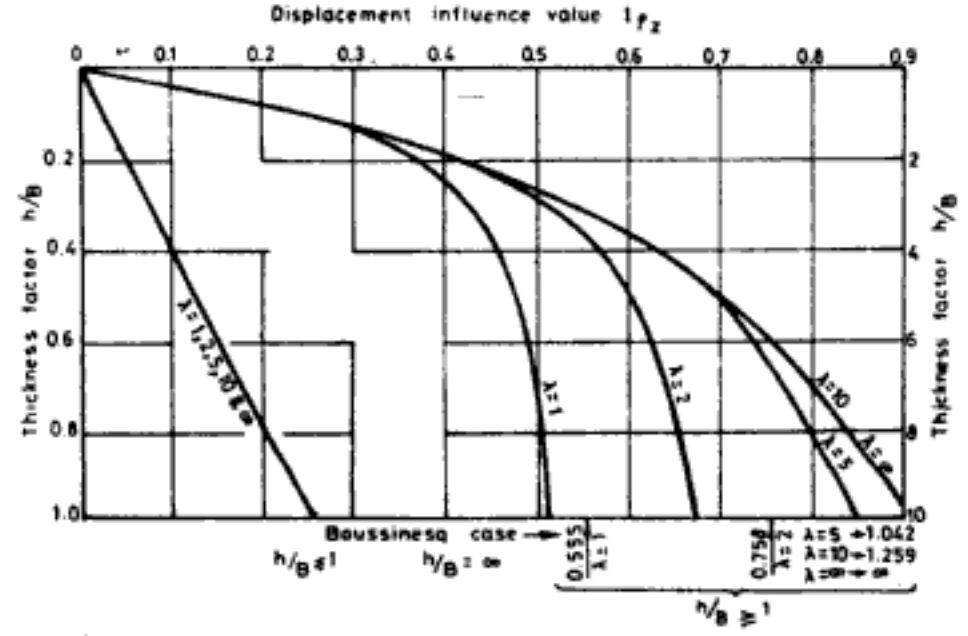

Fig. 13.55 Displacement factor for corner of rectangle, $\mu = 0.1$, (Eq. 13.51) (After Ueshita and Meyerhof, 1968; by permission of Transportation Research Board, National Research Council, Washington, DC)

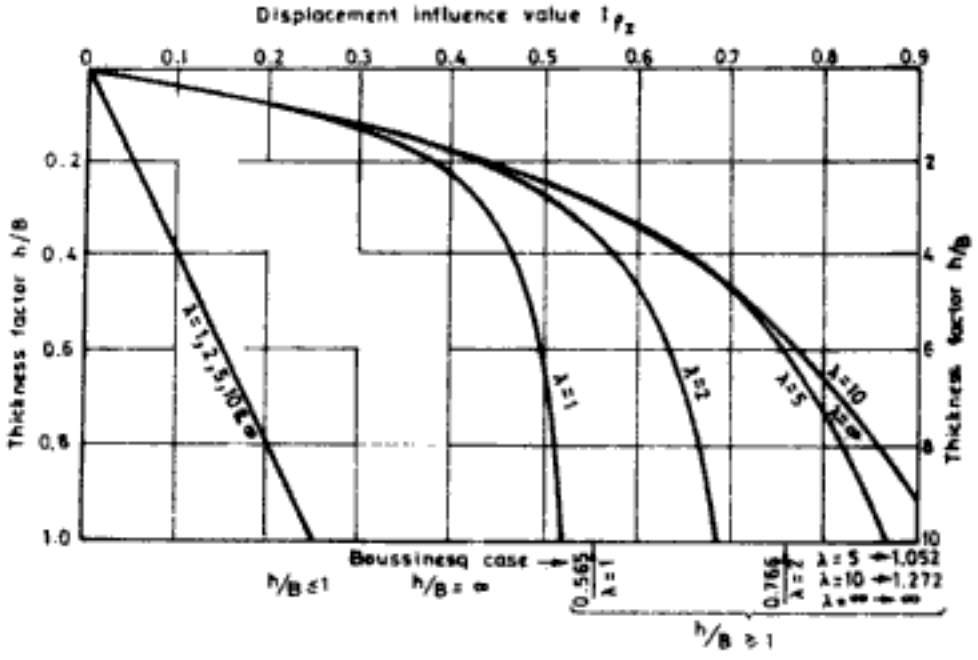

Fig. 13.56 Displacement factor for corner of rectangle, $\mu = 0$, (Eq. 13.51) (After Ueshita and Meyerhof, 1968; by permission of Transportation Research Board, National Research Council, Washington, DC)

13.5.3 Vertical Loading on Irregularly Shaped Areas

The sector method as explained in the case of semi-infinite body Sec. (13.3.10) can be used. The vertical stress $\Delta\sigma_z$ due to a sector is given by

$$\Delta\sigma_z = \frac{q\delta\theta}{2\pi} I_{s\sigma} \tag{13.53}$$

and the vertical displacement is,

$$\Delta\rho_z = \frac{qh\delta\theta}{2\pi E} I_{sp} \tag{13.54}$$

Figure 13.57 gives the values of I_{sp} and Figs 13.58 to 13.61 give the values of $I_{s\sigma}$ for four different values of Poisson's ratio (Poulos, 1967b).

13.6 LOADED AREAS EMBEDDED IN A FINITE LAYER

13.6.1 Uniform Vertical Loading on Rectangle

The rectangular area ($L \times B$) is embedded at a depth D from the surface and the thickness of the layer is H below the loaded area (inset in Fig. 13.62). Janbu, Bjerrum and Kjaernsli (1956) give the expression for the *mean* (or average) vertical displacement of the rectangle as follows,

$$\rho_{z\text{-mean}} = \frac{qB\mu_0\mu_1}{E} \tag{13.55}$$

Table 13.22 Values of I_{oz} for Points Below the Centre of Rectangle

h/B	z/B	$L/B = 1$			$L/B = 2$			$L/B = 5$		
		$\mu=0.15$	$\mu=0.30$	$\mu=0.45$	$\mu=0.15$	$\mu=0.30$	$\mu=0.45$	$\mu=0.15$	$\mu=0.30$	$\mu=0.45$
1.0	0.00	1.000	1.000	1.000	1.000	1.000	1.000	1.000	1.000	1.000
	0.10	0.974	0.974	0.974	0.992	0.992	0.992	0.996	0.996	0.996
	0.20	0.941	0.943	0.947	0.976	0.977	0.981	0.980	0.981	0.983
	0.40	0.837	0.842	0.855	0.919	0.924	0.936	0.920	0.922	0.930
	0.60	0.682	0.690	0.712	0.821	0.827	0.847	0.830	0.832	0.843
	0.80	0.563	0.570	0.595	0.732	0.734	0.754	0.753	0.751	0.760
	1.00	0.473	0.468	0.478	0.651	0.638	0.639	0.688	0.672	0.665
2.0	0.00	1.000	1.000	1.000	1.000	1.000	1.000	1.000	1.000	1.000
	0.10	0.970	0.970	0.970	0.985	0.985	0.985	0.990	0.990	0.990
	0.20	0.931	0.931	0.931	0.963	0.963	0.964	0.971	0.971	0.972
	0.40	0.802	0.802	0.804	0.877	0.878	0.880	0.889	0.890	0.893
	0.80	0.462	0.464	0.469	0.615	0.619	0.627	0.667	0.670	0.677
	1.20	0.282	0.286	0.294	0.436	0.441	0.455	0.524	0.528	0.539
	1.60	0.200	0.204	0.215	0.334	0.340	0.356	0.441	0.443	0.455
	2.00	0.157	0.155	0.161	0.271	0.269	0.277	0.385	0.377	0.379
3.0	0.00	1.000	1.000	1.000	1.000	1.000	1.000	1.000	1.000	1.000
	0.10	0.970	0.970	0.970	0.982	0.982	0.982	0.990	0.990	0.990
	0.20	0.930	0.930	0.930	0.961	0.962	0.962	0.969	0.969	0.970
	0.40	0.799	0.799	0.799	0.872	0.872	0.873	0.884	0.884	0.885
	0.80	0.452	0.453	0.454	0.598	0.599	0.602	0.649	0.650	0.653
	1.20	0.263	0.264	0.266	0.403	0.405	0.409	0.489	0.492	0.498
	1.60	0.170	0.172	0.175	0.286	0.289	0.295	0.391	0.395	0.404
	2.00	0.122	0.124	0.129	0.217	0.220	0.229	0.329	0.333	0.344
	2.50	0.091	0.093	0.099	0.168	0.171	0.180	0.278	0.281	0.292
	3.00	0.073	0.073	0.076	0.137	0.137	0.142	0.241	0.238	0.242
5.0	0.00	1.000	1.000	1.000	1.000	1.000	1.000	1.000	1.000	1.000
	0.10	0.970	0.970	0.970	0.981	0.981	0.981	0.990	0.990	0.990
	0.20	0.930	0.930	0.930	0.961	0.961	0.961	0.969	0.969	0.969
	0.40	0.798	0.798	0.798	0.870	0.870	0.870	0.881	0.881	0.882
	0.80	0.450	0.450	0.450	0.594	0.594	0.594	0.641	0.641	0.642
	1.20	0.258	0.258	0.258	0.393	0.394	0.395	0.474	0.475	0.476
	1.60	0.162	0.162	0.163	0.270	0.271	0.272	0.367	0.368	0.370
	2.00	0.110	0.111	0.112	0.195	0.195	0.197	0.294	0.296	0.299
	2.50	0.075	0.075	0.077	0.138	0.139	0.141	0.233	0.235	0.239
	3.00	0.055	0.056	0.057	0.104	0.105	0.108	0.191	0.193	0.199
	3.50	0.043	0.044	0.046	0.083	0.085	0.088	0.162	0.165	0.172
	4.00	0.036	0.037	0.039	0.070	0.071	0.075	0.141	0.144	0.152
	4.50	0.031	0.032	0.034	0.060	0.062	0.065	0.126	0.128	0.135
	5.00	0.027	0.027	0.029	0.053	0.053	0.056	0.113	0.113	0.117

After Milovic and Tournier, 1971.

Table 13.23 Values of Influence Factor $I_{\sigma z}$ for Vertical Stress Below the Corner

h/B	z/B	$L/B = 1$			$L/B = 2$			$L/B = 5$		
		$\mu = 0.15$	$\mu = 0.30$	$\mu = 0.45$	$\mu = 0.15$	$\mu = 0.30$	$\mu = 0.45$	$\mu = 0.15$	$\mu = 0.30$	$\mu = 0.45$
1.0	0.00	0.250	0.250	0.250	0.250	0.250	0.250	0.250	0.250	0.250
	0.20	0.250	0.250	0.250	0.250	0.250	0.250	0.250	0.250	0.250
	0.40	0.250	0.250	0.250	0.250	0.250	0.250	0.250	0.250	0.250
	0.60	0.250	0.250	0.250	0.250	0.250	0.250	0.250	0.250	0.250
	0.80	0.241	0.238	0.239	0.248	0.244	0.240	0.247	0.244	0.242
	1.00	0.227	0.220	0.215	0.241	0.232	0.223	0.239	0.233	0.226
2.0	0.00	0.250	0.250	0.250	0.250	0.250	0.250	0.250	0.250	0.250
	0.20	0.250	0.250	0.250	0.250	0.250	0.250	0.250	0.250	0.250
	0.40	0.243	0.244	0.245	0.248	0.249	0.250	0.247	0.247	0.248
	0.80	0.210	0.211	0.214	0.230	0.231	0.234	0.230	0.230	0.232
	1.20	0.170	0.172	0.178	0.205	0.207	0.212	0.207	0.208	0.211
	1.60	0.141	0.142	0.149	0.183	0.183	0.188	0.188	0.188	0.190
	2.00	0.118	0.117	0.120	0.163	0.160	0.160	0.172	0.168	0.166
3.0	0.00	0.250	0.250	0.250	0.250	0.250	0.250	0.250	0.250	0.250
	0.20	0.249	0.249	0.249	0.250	0.250	0.250	0.249	0.249	0.249
	0.40	0.241	0.241	0.242	0.246	0.246	0.246	0.245	0.246	0.246
	0.80	0.203	0.203	0.204	0.222	0.222	0.224	0.224	0.225	0.223
	1.20	0.157	0.158	0.160	0.190	0.191	0.194	0.197	0.197	0.199
	1.60	0.121	0.122	0.125	0.162	0.163	0.167	0.173	0.174	0.176
	2.00	0.096	0.098	0.102	0.139	0.141	0.146	0.155	0.156	0.159
	2.50	0.077	0.078	0.083	0.119	0.120	0.125	0.139	0.138	0.141
	3.00	0.064	0.064	0.066	0.103	0.102	0.104	0.126	0.123	0.123
5.0	0.00	0.250	0.250	0.250	0.250	0.250	0.250	0.250	0.250	0.250
	0.20	0.249	0.249	0.249	0.250	0.250	0.250	0.249	0.249	0.249
	0.40	0.241	0.241	0.240	0.245	0.245	0.245	0.245	0.245	0.245
	0.80	0.200	0.200	0.201	0.218	0.219	0.219	0.221	0.221	0.222
	1.20	0.152	0.153	0.153	0.183	0.184	0.184	0.191	0.191	0.192
	1.60	0.114	0.114	0.115	0.151	0.151	0.152	0.164	0.164	0.166
	2.00	0.086	0.087	0.087	0.124	0.125	0.126	0.142	0.143	0.145
	2.50	0.063	0.064	0.065	0.099	0.100	0.102	0.122	0.123	0.125
	3.00	0.049	0.050	0.051	0.081	0.082	0.085	0.107	0.108	0.111
	3.50	0.040	0.040	0.042	0.068	0.069	0.073	0.096	0.097	0.101
	4.00	0.034	0.034	0.036	0.059	0.060	0.064	0.088	0.089	0.092
	4.50	0.029	0.030	0.032	0.053	0.053	0.057	0.081	0.082	0.085
	5.00	0.026	0.026	0.027	0.047	0.047	0.049	0.075	0.075	0.076

After Milovic and Tournier, 1971.

Table 13.24 Values of $I_{\rho z}$ for Surface Displacement (Eq. 13.52)

h/B	$L/B = 1$			$L/B = 2$			$L/B = 5$		
	$\mu=0.15$	$\mu=0.30$	$\mu=0.45$	$\mu=0.15$	$\mu=0.30$	$\mu=0.45$	$\mu=0.15$	$\mu=0.30$	$\mu=0.45$
				Centre of Rectangle					
0.50	0.45	0.38	0.25	0.46	0.38	0.23	0.47	0.38	0.22
1.00	0.71	0.63	0.50	0.81	0.71	0.53	0.82	0.70	0.49
2.00	0.88	0.81	0.68	1.11	1.00	0.82	1.23	1.09	0.84
3.00	0.95	0.87	0.74	1.23	1.12	0.94	1.45	1.31	1.06
5.00	1.00	0.92	0.80	1.33	1.23	1.05	1.67	1.52	1.27
				Corner of Rectangle					
0.50	0.12	0.10	0.05	0.12	0.10	0.03	0.12	0.09	0.04
1.00	0.23	0.20	0.13	0.24	0.20	0.05	0.24	0.19	0.11
2.00	0.36	0.32	0.26	0.41	0.36	0.09	0.41	0.35	0.25
3.00	0.42	0.38	0.31	0.51	0.45	0.11	0.53	0.46	0.35
5.00	0.47	0.43	0.36	0.60	0.54	0.13	0.68	0.61	0.48

After Milovic and Tournier, 1971.

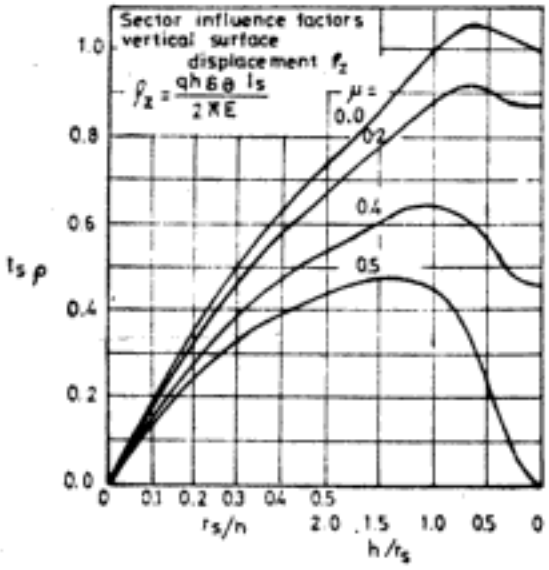

Fig. 13.57 Sector curves for vertical surface displacement (After Poulos, 1967b; with permission of The Institution of Civil Engineers, London)

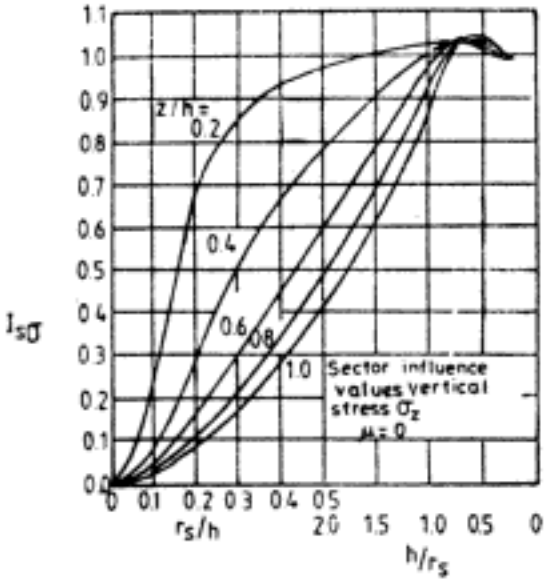

Fig. 13.58 Sector curves for vertical stress $\mu = 0$ (After Poulos, 1967b; with permission of The Institution of Civil Engineers, London)

where μ_0 = a factor dependent on L/B and D/B and thus takes into account effect of depth of embedment

μ_1 = a factor dependent on L/B and H/B and thus takes into account the effect of thickness of the layer

Values of μ_0 and μ_1 are shown in Fig. 13.62 for Poisson's ratio (μ) equal to 0.5. Christian and Carrier (1978) modified the charts for μ_0 and μ_1 after a critical evaluation. These are given in Fig. 13.63.

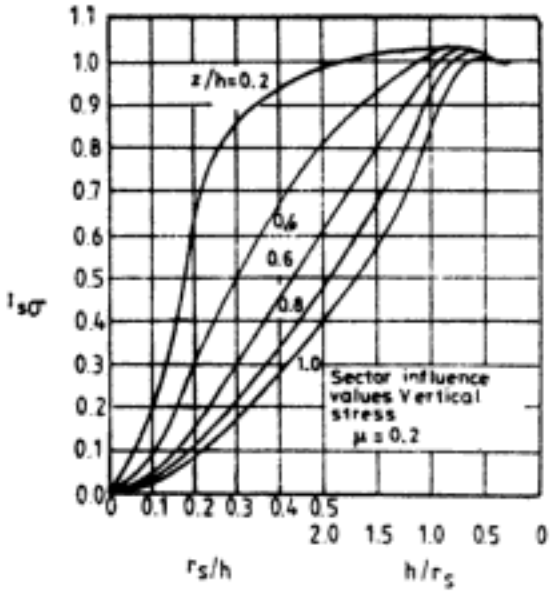

Fig. 13.59 Sector curves for vertical stress, $\mu = 0.2$ (After Poulos, 1967b; with permission of The Institution of Civil Engineers, London)

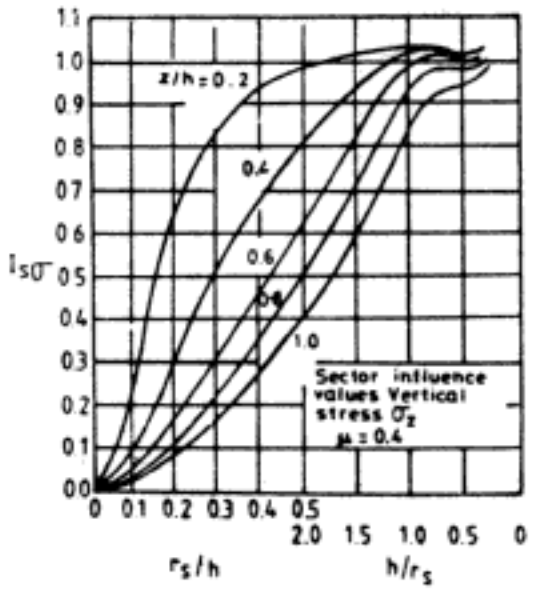

Fig. 13.60 Sector curves for vertical stress, $\mu = 0.4$ (After Poulos, 1967b; with permission of The Institution of Civil Engineers, London)

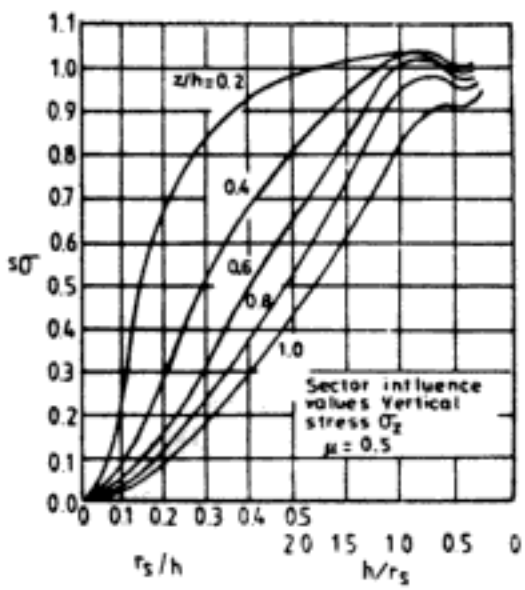

Fig. 13.61 Sector curves for vertical stress, $\mu = 0.5$ (After Poulos, 1967b; with permission of The Institution of Civil Engineers, London)

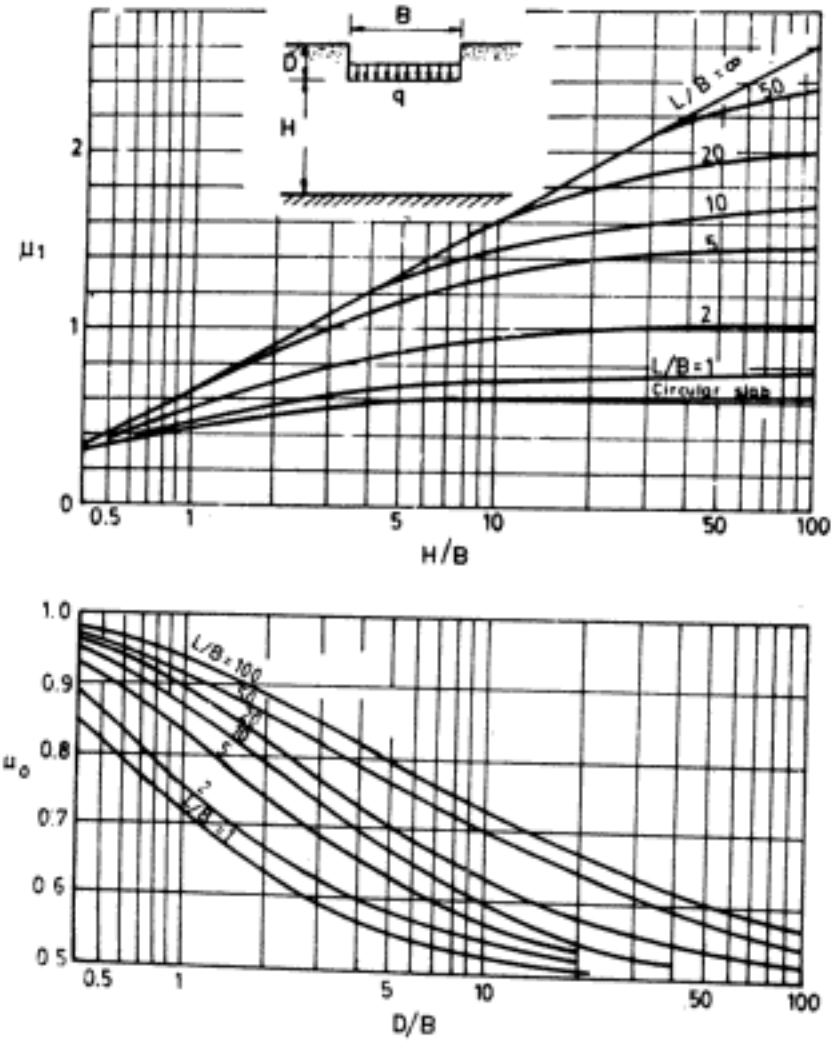

Fig. 13.62 Factors for calculation of vertical displacement of rectangles and strips embedded in finite layer
(After Janbu, *et al.*, 1956; with permission of Norwegian Geotechnical Institute, Oslo)

13.7 LOADED AREAS ON THE SURFACE OF MULTI-LAYER SYSTEMS

13.7.1 Two-layer Systems

1. *Unifom vertical loading on circular area*

Figure 13.64 shows the two-layer system. The thickness of top layer is h. The top layer has properties E_1, μ_1 and the bottom layer E_2, μ_2.

Figure 13.65 shows the variation of the vertical stress at the interface of the two layers beneath the centre of the footing. The figure shows the influence of ratios E_1/E_2 and h/a on the vertical stress.

The variation of vertical stress along the interface for a particular value of $h/a = 1$ is shown in Fig. 13.66.

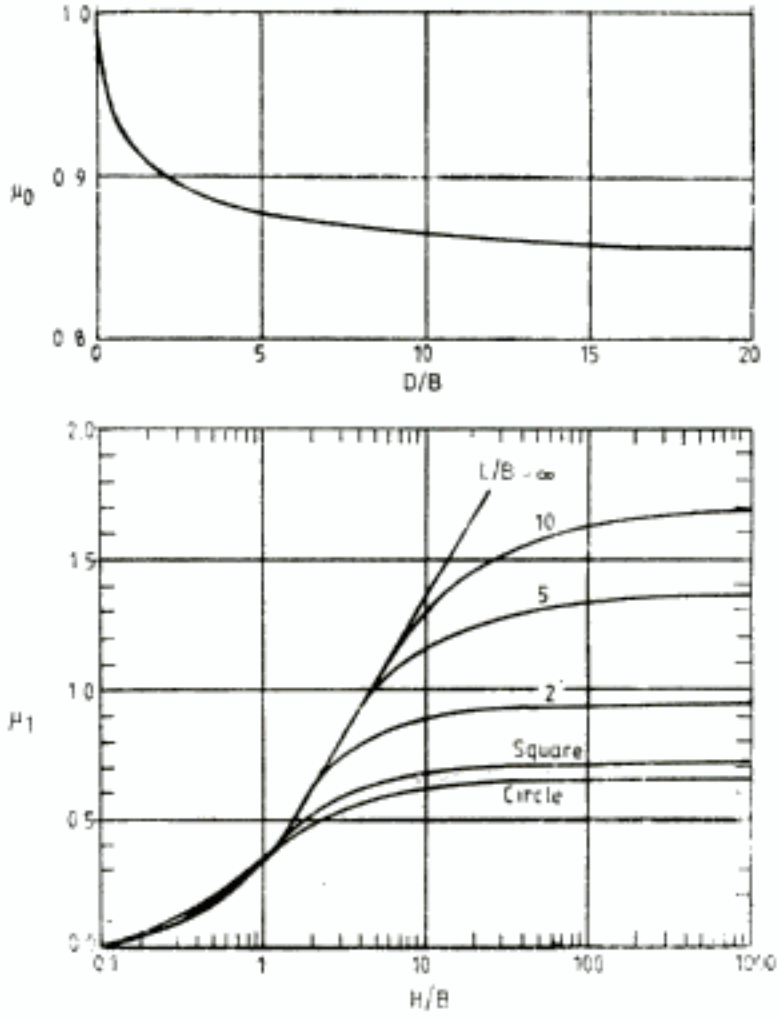

Fig. 13.63 Modified values of μ_0 and μ_1 in Eq. 13.55 (After Christian and Carrier, 1978; with permission of National Research Council, Canada)

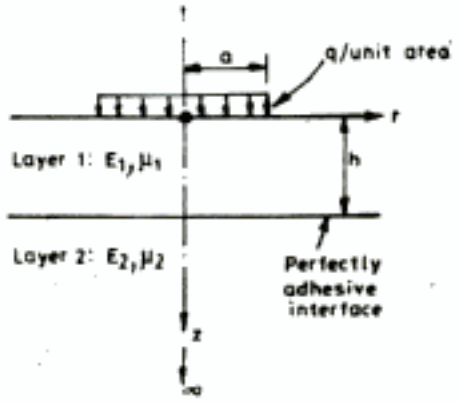

Fig. 13.64 Uniform vertical loading on a circle on a two-layer system

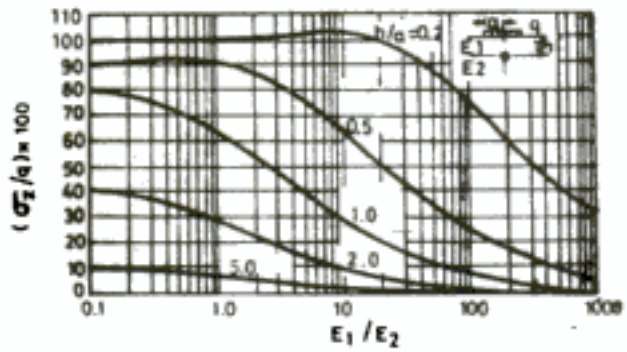

Fig. 13.65 Vertical stress at the interface of layers along the axis ($\mu_1 = \mu_2 = 0.5$). (After Fox, 1948a)

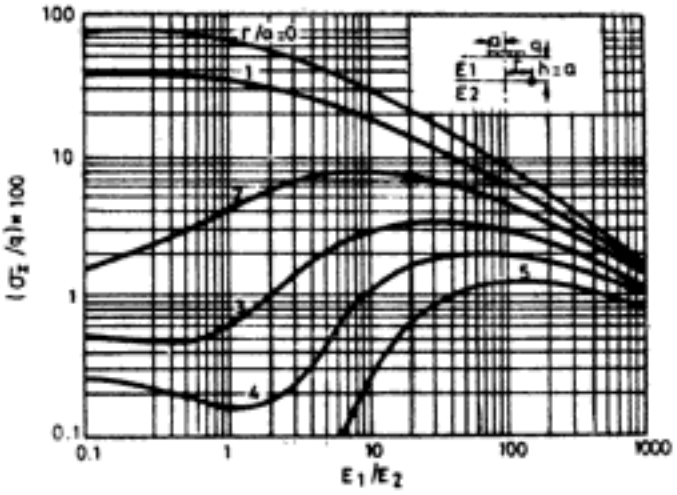

Fig. 13.66 Vertical stress along the interface of the layers for h/a = 1 ($\mu_1 = \mu_2 = 0.5$) (After Fox, 1948a)

Values of σ_z as percentage of applied loading q, in the lower layer along the axis of the footing is given in Table 13.25.

Table 13.25 Axial Stress σ_z as Percentage of Applied Loading in the Lower Layer of Two-layer System, $\mu_1 = \mu_2 = 0.5$

Depth below interface	E_1/E_2			
	1	10	100	1000
		$a/h = \frac{1}{2}$		
0	28.4	10.1	2.38	0.51
h	8.7	4.70	1.58	0.42
2h	4.03	2.78	1.17	0.35
3h	2.30	1.84	0.91	0.31
4h	1.48	1.29	0.74	0.28
		$a/h = 1$		
0	64.6	29.2	8.1	1.85
h	28.4	16.8	6.0	1.62
2h	14.5	10.5	4.6	1.43
3h	8.7	7.0	3.6	1.24
4h	5.7	5.0	2.9	1.10
		$a/h = 2$		
0	91.1	64.4	24.6	7.10
h	64.6	48.0	20.5	6.06
2h	42.4	34.0	16.5	5.42
3h	28.4	24.4	13.3	4.80
4h	20.0	18.1	10.8	4.28

After Fox, 1948a.

Deflection factors for vertical surface displacement at the centre of the circle are shown in Fig. 13.67 for the case of $\mu_1 = 0.2$, $\mu_2 = 0.4$, in Fig. 13.68 for the case of $\mu_1 = \mu_2 = 0.5$ and in Fig. 13.69 for the case of $\mu_1 = \mu_2 = 0.35$. The corresponding expressions for vertical settlement at the centre are also given in these figures. Burmister (1965) describes the surface displacement at the centre of a uniformly loaded circle on an elastic layer in terms of the surface displacement of a homogeneous system.

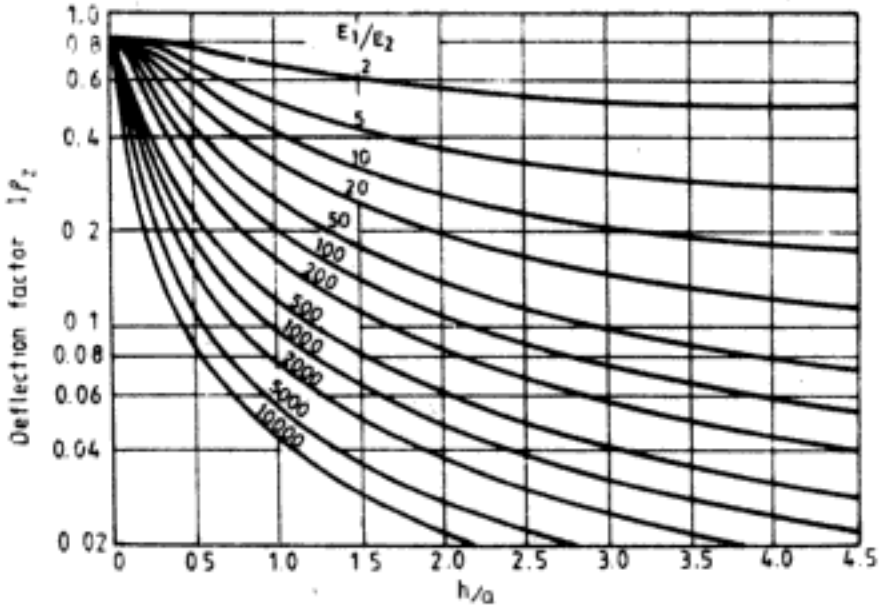

Fig. 13.67 Displacement factors for vertical displacement at the centre of circle from Burmister's layered system theory. $\mu_1 = 0.2$, $\mu_2 = 0.4$

$\rho_z = \frac{2aq}{E_2} I\rho_z$ (After Burmister, 1962)

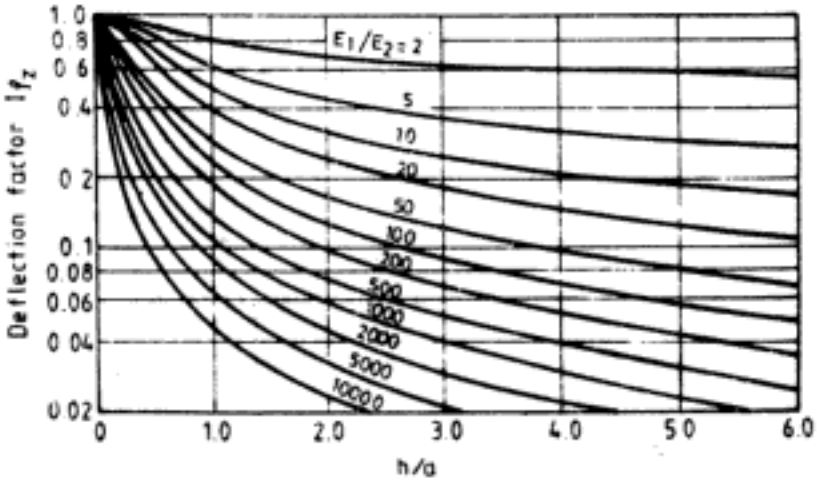

Fig. 13.68 Displacement factors for vertical displacement at the centre of the circle, $\mu_1 = \mu_2 = 0.5$

$\rho_z = \frac{1.5aq}{E_2} I\rho_z$ (After Burmister, 1945)

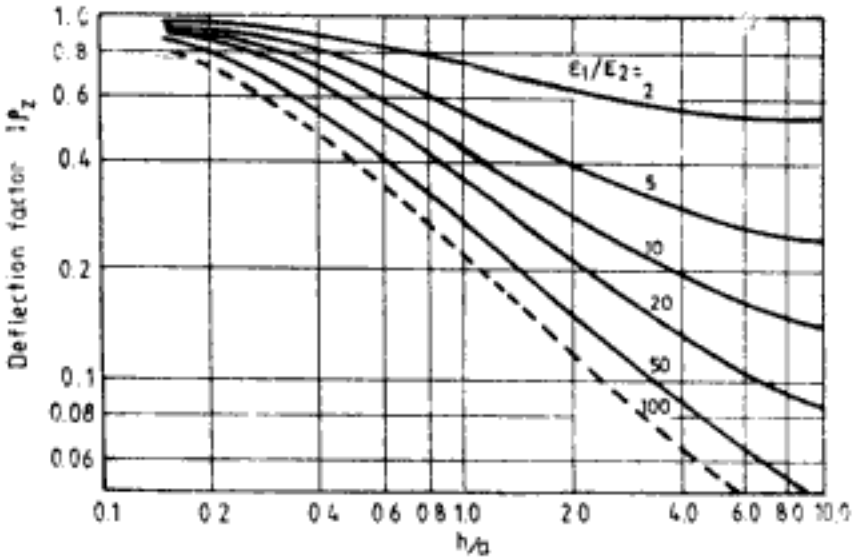

Fig. 13.69 Displacement factors for vertical displacement at the centre of the circle, $\mu_1 = \mu_2 = 0.35$

$\rho_z = \dfrac{1.755aq}{E_2} I\rho_z$ (After Thenn de Barros, 1966; with permission of Transportation Research Board, National Research Council, Washington, DC)

Thus,

$$\rho_{z(\text{layer})} = \alpha \rho_{z(\text{semi-infinite mass})} \tag{13.56}$$

In Eq. 13.56

$\rho_{z(\text{layer})}$ = the required displacement at the centre of the circle at the surface of the layer with elastic parameters E_1 and μ_1 and thickness h underlain by an infinite depth of material with elastic parameters E_2 and μ_2

$\rho_{z(\text{semi-infinite mass})}$ = displacement at the centre of the circle resting on the surface of a homogeneous half-space with elastic parameters E_2 and μ_2

α = correction factor relating $\rho_{z(\text{layer})}$ and $\rho_{z(\text{semi-infinite mass})}$

Values of α for $\mu_1 = \mu_2 = 0.4$ are given in Table 13.26. Ueshita and Meyerhof (1967) propose that the two-layer system can be converted into an equivalent homogeneous semi-

Table 13.26 Correction Factor α at the Centre of a Uniformly Loaded Circular Area on an Elastic Layer E_1 Underlain by a Less Stiff Elastic Material E_2 of Infinite Depth ($\mu_1 = \mu_2 = 0.4$)

$\frac{h}{a}$	E_1/E_2			
	2	5	10	100
0.2	0.972	0.943	0.923	0.76
0.5	0.885	0.779	0.699	0.431
1.0	0.747	0.566	0.463	0.228
2.0	0.627	0.399	0.287	0.121
5.0	0.550	0.274	0.175	0.058
10.0	0.525	0.238	0.136	0.036

After Burmister, 1965.

infinite mass having a constant equivalent Young's modulus, E_{eq}. This equivalent modulus can be now used with the deflection factors for uniform loading on circular area on a semi-infinite mass (e.g., Fig. 13.17). The variation of E_{eq}/E_2 with h/a and E_1/E_2 is shown in Fig. 13.70.

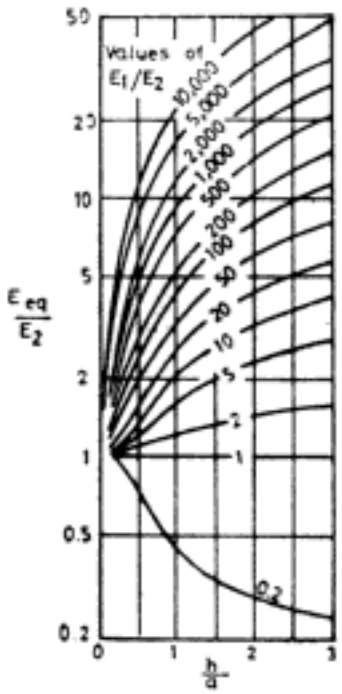

Fig. 13.70 Equivalent modulus E_{eq} of two-layer system: $\mu_1 = \mu_2 = 0.5$ (After Ueshita and Meyerhof, 1967)

Q 13.6: To determine the surface displacement at the centre of an uniformly loaded circular area resting on the top of the surface layer of a two-layer system. Given the following data:

$E_1 = 400$ kg/cm² $\quad E_2 = 200$ kg/cm²

$\mu_1 = \mu_2 = 0.4$

$a = 1.5$ m $\quad h = 3$ m $\quad q = 10$ T/m²

Ans: Burmister's solution given in Eq. 13.56 will be used to solve the problem.

$$E_1/E_2 = 400/200 = 2 \qquad h/a = 3/1.5 = 2$$

From Table 13.26 $\quad \alpha = 0.627$

In Eq. 13.56, $\rho_{z(\text{semi-infinite mass})}$ is given by Eq. 13.23.

i.e., $$\rho_{z(\text{semi-infinite mass})} = \frac{qa}{E_2} I_{\rho z}$$

where $$I_{\rho z} = (1 - \mu_2^2)H \qquad \because \; z/a = 0$$

From Table 13.14 for $r/a = 0$ and $z/a = 0$; $H = 2.0$

$$I_{\rho z} = (1 - 0.16) \times 2 = 1.68$$

$$\therefore \qquad \rho_{z(\text{semi-infinite mass})} = \frac{10 \times 1.5}{2000} \times 1.68 = 0.0126 \text{ m} = 12.6 \text{ mm}$$

From Eq. 13.56,

$$\rho_{z(\text{layer})} = 0.627 \times 12.6 = 7.9 \text{ mm}$$

which is the surface displacement at the centre of the circle.

Q 13.7: To determine the surface displacement at the centre of a uniformly loaded circle resting on the top of surface layer of a two-layer system. Given the following data:

$E_1 = 400 \text{ kg/cm}^2$ $\quad E_2 = 200 \text{ kg/cm}^2$
$\mu_1 = \mu_2 = 0.5$ $\quad a = 1 \text{ m}$
$h = 3 \text{ m}$ $\quad q = 10 \text{ T/m}^2$

Ans: *Procedure 1*: The problem will be first solved using Burmister's solution given in Fig. 13.68.

$$E_1/E_2 = 400/200 = 2 \qquad h/a = 3/1 = 3$$

From Fig. 13.68 $\qquad I_{\rho z} = 0.62$

The surface displacement at centre of circle is,

$$\rho_z = \frac{1.5 \times 1 \times 10}{2000} \times 0.62 = 4.65 \times 10^{-3} \text{ m} = 4.65 \text{ mm}$$

Procedure 2: Ueshita and Meyerhof's equivalent modulus will be used to solve the problem.

From Fig. 13.70 $\qquad E_{eq}/E_2 = 1.67$ (for $h/a = 3$ and $E_1/E_2 = 2$)

$$E_{eq} = 1.67 \times 200 = 334 \text{ kg/cm}^2$$

From Fig. 13.17 the surface displacement at the centre of the circle on the equivalent homogeneous system is,

$$\rho_z = \frac{10 \times 1 \times 1.5}{3340} = 4.49 \times 10^{-3} \text{ m} = 4.49 \text{ mm}$$

13.7.2 Three-layer Systems

Jones (1962) gives an extensive tabulation of stresses at the layer interfaces, on the axis of the circle shown in Fig. 13.71. Tables 13.27 to 13.33 present the values of vertical stresses at the interfaces. In these tables,

$a_1 = a/h_2$; $\quad H = h_1/h_2$

$k_1 = E_1/E_2$; $\quad k_2 = E_2/E_3$

$\mu_1 = \mu_2 = \mu_3 = 0.5$

σ_{z1} = vertical stress below the centre of circle and at the interface of layers 1 and 2

σ_{z2} = vertical stress below the centre of circle and at the interface of layers 2 and 3

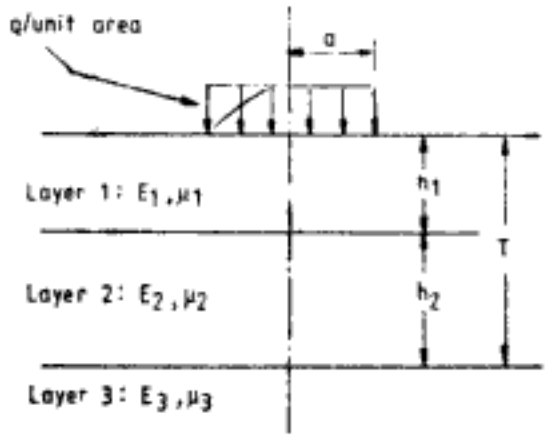

Fig. 13.71 Circular footing on three-layer system

Table 13.27 Values of σ_{z1} for $H = 0.125$

		σ_{z1}/q			
	a_1	$k_1 = 0.2$	$k_1 = 2$	$k_1 = 20$	$k_1 = 200$
$k_2 = 0.2$	0.1	0.66045	0.43055	0.14648	0.03694
	0.2	0.90249	0.78688	0.39260	0.12327
	0.4	0.95295	0.98760	0.80302	0.36329
	0.8	0.99520	1.01028	1.06594	0.82050
	1.6	1.00064	1.00647	1.02942	1.12440
	3.2	0.99970	0.99822	0.99817	0.99506
$k_2 = 2.0$	0.1	0.66048	0.42950	0.14529	0.03481
	0.2	0.90157	0.78424	0.38799	0.11491
	0.4	0.95120	0.98044	0.78651	0.33218
	0.8	0.99235	0.99434	1.02218	0.72695
	1.6	0.99918	0.99364	0.99060	1.00203
	3.2	1.00032	0.99922	0.99893	1.00828
$k_2 = 20.0$	0.1	0.66235	0.43022	0.14447	0.03336
	0.2	0.90415	0.78414	0.38469	0.10928
	0.4	0.95135	0.97493	0.77394	0.31094
	0.8	0.98778	0.97806	0.98610	0.65934
	1.6	0.99407	0.96921	0.93712	0.87931
	3.2	0.99821	0.98591	0.96330	0.93309
$k_2 = 200.0$	0.1	0.66266	0.42925	0.14422	0.03307
	0.2	0.90370	0.78267	0.38388	0.10810
	0.4	0.94719	0.97369	0.77131	0.30639
	0.8	0.99105	0.97295	0.97701	0.64383
	1.6	0.99146	0.95546	0.91645	0.84110
	3.2	0.99332	0.96377	0.92662	0.86807

After Jones, 1962. By permission of Transportation Research Board, National Research Council, Washington, DC.

Table 13.28 Values of σ_{z1}

		σ_{z1}/q							
		$H = 0.25$				$H = 0.5$			
	a_1	$k_1 = 0.2$	$k_1 = 2$	$k_1 = 20$	$k_1 = 200$	$k_1 = 0.2$	$k_1 = 2$	$k_1 = 20$	$k_1 = 200$
$k_2 = 0.2$	0.1	0.27115	0.15577	0.04596	0.01139	0.07943	0.04496	0.01351	0.00363
	0.2	0.66109	0.43310	0.15126	0.04180	0.27189	0.15978	0.05079	0.01414
	0.4	0.90404	0.79551	0.41030	0.14196	0.66375	0.44523	0.16972	0.05256
	0.8	0.95659	1.00871	0.85464	0.42603	0.91143	0.83298	0.47191	0.18107
	1.6	0.99703	1.02425	1.12013	0.94520	0.96334	1.05462	0.97452	0.53465
	3.2	0.99927	0.99617	0.99676	1.10738	0.99310	0.99967	1.09911	1.04537
$k_2 = 2.0$	0.1	0.27103	0.15524	0.04381	0.00909	0.07906	0.04330	0.01122	0.00215
	0.2	0.66010	0.42809	0.14282	0.03269	0.27046	0.15325	0.04172	0.00826
	0.4	0.90120	0.77939	0.37882	0.10684	0.65847	0.42077	0.13480	0.02946
	0.8	0.94928	0.96703	0.75904	0.30477	0.89579	0.75683	0.35175	0.09508
	1.6	0.99029	0.98156	0.98743	0.66786	0.94217	0.93447	0.70221	0.27135
	3.2	1.00000	0.99840	1.00064	0.98447	0.99189	0.98801	0.97420	0.62399
$k_2 = 20.0$	0.1	0.26945	0.15436	0.04236	0.00776	0.07862	0.04193	0.00990	0.00149
	0.2	0.66161	0.42462	0.13708	0.02741	0.26873	0.14808	0.03648	0.00564
	0.4	0.90102	0.76647	0.35716	0.08634	0.65188	0.40086	0.11448	0.01911
	0.8	0.94012	0.92757	0.68947	0.23137	0.87401	0.69098	0.27934	0.05574
	1.6	0.97277	0.91393	0.85490	0.46835	0.89568	0.79338	0.50790	0.13946
	3.2	0.99075	0.95243	0.90325	0.71083	0.95392	0.85940	0.70903	0.30247
$k_2 = 200.0$	0.1	0.27072	0.15414	0.04204	0.00744	0.07820	0.04160	0.00960	0.00133
	0.2	0.65909	0.42365	0.13584	0.02616	0.26803	0.14676	0.03526	0.00498
	0.4	0.89724	0.76296	0.35237	0.08141	0.64904	0.39570	0.10970	0.01649
	0.8	0.93596	0.91600	0.67286	0.21293	0.86406	0.67257	0.26149	0.04553
	1.6	0.96370	0.88406	0.81223	0.40876	0.86677	0.74106	0.45078	0.10209
	3.2	0.97335	0.89712	0.82390	0.56613	0.89703	0.75176	0.57074	0.18358

After Jones, 1962. By permission of Transportation Research Board, National Research Council, Washington, DC.

Table 13.29 Values of σ_{z1}

		σ_{z1}/q							
		$H = 1.0$				$H = 2.0$			
	a_1	$k_1=0.2$	$k_1=2.0$	$k_1=20$	$k_1=200$	$k_1=0.2$	$k_1=2.0$	$k_1=20$	$k_1=200$
$k_2 = 0.2$	0.1	0.02090	0.01241	0.00417	0.00117	0.00540	0.00356	0.00134	0.00036
	0.2	0.08023	0.04816	0.01641	0.00464	0.02138	0.01415	0.00533	0.00144
	0.4	0.27493	0.17203	0.06210	0.01814	0.08209	0.05493	0.02100	0.00572
	0.8	0.67330	0.48612	0.21057	0.06766	0.28150	0.19661	0.07950	0.02231
	1.6	0.92595	0.91312	0.58218	0.22994	0.68908	0.55306	0.26613	0.08215
	3.2	0.95852	1.04671	1.06296	0.62710	0.93103	0.96647	0.67882	0.26576
$k_2 = 2.0$	0.1	0.02045	0.01083	0.00263	0.00049	0.00502	0.00250	0.00059	0.00011
	0.2	0.07845	0.04176	0.01029	0.00195	0.01986	0.00991	0.00235	0.00045
	0.4	0.26816	0.14665	0.03810	0.00746	0.07630	0.03832	0.00922	0.00179
	0.8	0.65090	0.39942	0.12173	0.02647	0.26196	0.13516	0.03412	0.00685
	1.6	0.88171	0.71032	0.31575	0.08556	0.63535	0.36644	0.10918	0.02441
	3.2	0.94153	0.92112	0.66041	0.25186	0.87025	0.67384	0.29183	0.08061
$k_2 = 20.0$	0.1	0.01981	0.00963	0.00193	0.00027	0.00444	0.00181	0.00033	0.00005
	0.2	0.07587	0.03697	0.00751	0.00104	0.01756	0.00716	0.00130	0.00018
	0.4	0.25817	0.12805	0.02713	0.00384	0.06706	0.02746	0.00503	0.00071
	0.8	0.61544	0.33263	0.08027	0.01236	0.22561	0.09396	0.01782	0.00261
	1.6	0.78884	0.52721	0.17961	0.03379	0.51929	0.23065	0.05012	0.00819
	3.2	0.82936	0.65530	0.34355	0.08859	0.65700	0.37001	0.11331	0.02341
$k_2 = 200.0$	0.1	0.01952	0.00925	0.00176	0.00021	0.00414	0.00164	0.00027	0.00003
	0.2	0.07473	0.03561	0.00683	0.00082	0.01635	0.00647	0.00106	0.00012
	0.4	0.25368	0.12348	0.02443	0.00298	0.06231	0.02470	0.00406	0.00047
	0.8	0.59853	0.31422	0.06983	0.00893	0.20757	0.08326	0.01397	0.00165
	1.6	0.73387	0.46897	0.14191	0.02065	0.45550	0.19224	0.03538	0.00445
	3.2	0.70248	0.51161	0.22655	0.04154	0.48642	0.25526	0.06182	0.00929

After Jones, 1962. By permission of Transportation Research Board, National Research Council, Washington, DC.

Table 13.30 Values of σ_{z1}

		σ_{z1}/q							
		$H = 4.0$				$H = 8.0$			
	a_1	$k_1 = 0.2$	$k_1 = 2$	$k_1 = 20$	$k_1 = 200$	$k_1 = 0.2$	$k_1 = 2$	$k_1 = 20$	$k_1 = 200$
$k_2 = 0.2$	0.1	0.00139	0.00103	0.00042	0.00010	0.00035	0.00028	0.00012	0.00003
	0.2	0.00555	0.00411	0.00166	0.00042	0.00142	0.00113	0.00047	0.00011
	0.4	0.02198	0.01631	0.00663	0.00167	0.00566	0.00451	0.00190	0.00046
	0.8	0.08435	0.06319	0.02603	0.00663	0.02240	0.01786	0.00754	0.00182
	1.6	0.28870	0.22413	0.09718	0.02562	0.08589	0.06895	0.02947	0.00720
	3.2	0.70074	0.60654	0.31040	0.09166	0.29318	0.24127	0.10817	0.02751
$k_2 = 2.0$	0.1	0.00123	0.00057	0.00013	0.00003	0.00030	0.00013	0.00003	0.00001
	0.2	0.00491	0.00228	0.00054	0.00011	0.00120	0.00053	0.00013	0.00003
	0.4	0.01942	0.00905	0.00214	0.00042	0.00479	0.00213	0.00050	0.00010
	0.8	0.07447	0.03500	0.00837	0.00168	0.01894	0.00844	0.00200	0.00041
	1.6	0.25449	0.12354	0.03109	0.00646	0.07271	0.03269	0.00786	0.00162
	3.2	0.62074	0.34121	0.10140	0.02332	0.24933	0.11640	0.02944	0.00625
$k_2 = 20.0$	0.1	0.00087	0.00030	0.00005	0.00001	0.00016	0.00005	0.00001	0.00000
	0.2	0.00346	0.00119	0.00021	0.00003	0.00065	0.00019	0.00004	0.00001
	0.4	0.01367	0.00469	0.00083	0.00013	0.00260	0.00076	0.00014	0.00002
	0.8	0.05207	0.01790	0.00321	0.00050	0.01026	0.00300	0.00056	0.00010
	1.6	0.17367	0.06045	0.01130	0.00186	0.03926	0.01154	0.00217	0.00039
	3.2	0.39955	0.14979	0.03258	0.00612	0.13335	0.04003	0.00791	0.00149
$k_2 = 200.0$	0.1	0.00069	0.00023	0.00003	0.00000	0.00009	0.00003	0.00000	0.00000
	0.2	0.00274	0.00091	0.00014	0.00002	0.00036	0.00011	0.00002	0.00000
	0.4	0.01079	0.00360	0.00054	0.00007	0.00145	0.00042	0.00006	0.00001
	0.8	0.04074	0.01360	0.00206	0.00025	0.00573	0.00167	0.00025	0.00003
	1.6	0.13117	0.04409	0.00683	0.00086	0.02160	0.00629	0.00096	0.00013
	3.2	0.26403	0.09323	0.01590	0.00225	0.06938	0.02020	0.00319	0.00047

After Jones, 1962. By permission of Transportation Research Board, National Research Council, Washington, DC.

Table 13.31 Values of σ_{z2}

		σ_{z2}/q											
		$H = 0.125$				$H = 0.25$				$H = 0.5$			
	a_1	$k_1 = 0.2$	$k_1 = 2.0$	$k_1 = 20$	$k_1 = 200$	$k_1 = 0.2$	$k_1 = 2.0$	$k_1 = 20$	$k_1 = 200$	$k_1 = 0.2$	$k_1 = 2.0$	$k_1 = 20$	$k_1 = 200$
$k_2 = 0.2$	0.1	0.01557	0.01682	0.01645	0.01137	0.01259	0.01348	0.01107	0.00589	0.00914	0.00903	0.00596	0.00256
	0.2	0.06027	0.06511	0.06407	0.04473	0.04892	0.05259	0.04357	0.02334	0.03577	0.03551	0.02361	0.01021
	0.4	0.21282	0.23005	0.23135	0.16785	0.17538	0.19094	0.16337	0.09024	0.13135	0.13314	0.09110	0.04014
	0.8	0.56395	0.60886	0.64741	0.53144	0.48699	0.54570	0.51644	0.31785	0.38994	0.42199	0.31904	0.15048
	1.6	0.86258	0.90959	1.00911	1.03707	0.81249	0.90563	1.01061	0.83371	0.72106	0.85529	0.82609	0.48201
	3.2	0.94143	0.94322	0.97317	1.00400	0.92951	0.93918	0.99168	1.10259	0.89599	0.94506	1.08304	1.00671
$k_2 = 2.0$	0.1	0.00892	0.00896	0.00810	0.00549	0.00739	0.00710	0.00530	0.00259	0.00557	0.00465	0.00259	0.00094
	0.2	0.03480	0.03493	0.03170	0.02167	0.02893	0.02783	0.02091	0.01027	0.02190	0.01836	0.01028	0.00373
	0.4	0.12656	0.12667	0.11650	0.08229	0.10664	0.10306	0.07933	0.04000	0.08222	0.06974	0.03998	0.01474
	0.8	0.37307	0.36932	0.34941	0.27307	0.32617	0.31771	0.26278	0.14513	0.26429	0.23256	0.14419	0.05622
	1.6	0.74038	0.72113	0.69014	0.63916	0.69047	0.66753	0.61673	0.42940	0.60357	0.56298	0.42106	0.19358
	3.2	0.97137	0.96148	0.93487	0.92560	0.95608	0.93798	0.91258	0.84545	0.91215	0.88655	0.82256	0.52912
$k_2 = 20.0$	0.1	0.00256	0.00228	0.00182	0.00128	0.00222	0.00179	0.00123	0.00065	0.00175	0.00117	0.00063	0.00023
	0.2	0.01011	0.00899	0.00716	0.00509	0.00877	0.00706	0.00488	0.00257	0.00692	0.00464	0.00251	0.00094
	0.4	0.03838	0.03392	0.02710	0.01972	0.03354	0.02697	0.01888	0.01014	0.02676	0.01799	0.00988	0.00372
	0.8	0.13049	0.11350	0.09061	0.07045	0.11658	0.09285	0.06741	0.03844	0.09552	0.06476	0.03731	0.01453
	1.6	0.36442	0.31263	0.24528	0.20963	0.33692	0.26454	0.20115	0.13148	0.28721	0.19803	0.12654	0.05399
	3.2	0.76669	0.68433	0.55490	0.49938	0.73532	0.60754	0.48647	0.37342	0.66445	0.49238	0.35807	0.18091
$k_2 = 200.0$	0.1	0.00057	0.00046	0.00033	0.00025	0.00051	0.00036	0.00024	0.00014	0.00041	0.00024	0.00013	0.00005
	0.2	0.00226	0.00183	0.00131	0.00098	0.00202	0.00143	0.00095	0.00056	0.00163	0.00095	0.00054	0.00022
	0.4	0.00881	0.00711	0.00505	0.00386	0.00791	0.00557	0.00372	0.00224	0.00643	0.00374	0.00214	0.00086
	0.8	0.03259	0.02597	0.01830	0.01455	0.02961	0.02064	0.01399	0.00871	0.02436	0.01416	0.00831	0.00340
	1.6	0.11034	0.08700	0.06007	0.05011	0.10193	0.07014	0.04830	0.03234	0.08540	0.04972	0.03070	0.01315
	3.2	0.32659	0.26292	0.18395	0.15719	0.30707	0.21692	0.15278	0.11049	0.26467	0.15960	0.10470	0.04854

After Jones, 1962. By permission of Transportation Research Board, National Research Council, Washington, DC.

Table 13.32 Values of σ_{z2}

		σ_{z2}/q							
		$H = 1.0$				$H = 2.0$			
	σ_1	$k_1 = 0.2$	$k_1 = 2.0$	$k_1 = 20$	$k_1 = 200$	$k_1 = 0.2$	$k_1 = 2.0$	$k_1 = 20$	$k_1 = 200$
$k_2 = 0.2$	0.1	0.00541	0.00490	0.00271	0.00097	0.00242	0.00216	0.00108	0.00033
	0.2	0.02138	0.01943	0.01080	0.00388	0.00964	0.00861	0.00429	0.00130
	0.4	0.08125	0.07496	0.04241	0.01538	0.03770	0.03386	0.01702	0.00518
	0.8	0.26887	0.26193	0.15808	0.05952	0.13832	0.12702	0.06576	0.02038
	1.6	0.60229	0.67611	0.49705	0.21214	0.40830	0.40376	0.23186	0.07675
	3.2	0.82194	0.95985	1.00217	0.60056	0.73496	0.83197	0.63006	0.25484
$k_2 = 2.0$	0.1	0.00356	0.00241	0.00100	0.00029	0.00180	0.00100	0.00033	0.00008
	0.2	0.01410	0.00958	0.00397	0.00116	0.00716	0.00397	0.00130	0.00033
	0.4	0.05427	0.03724	0.01565	0.00460	0.02815	0.01569	0.00518	0.00131
	0.8	0.18842	0.13401	0.05938	0.01797	0.10523	0.05974	0.02023	0.00520
	1.6	0.48957	0.38690	0.20098	0.06671	0.33075	0.20145	0.07444	0.02003
	3.2	0.81663	0.75805	0.53398	0.22047	0.68388	0.51156	0.23852	0.07248
$k_2 = 20.0$	0.1	0.00118	0.00061	0.00024	0.00007	0.00065	0.00025	0.00008	0.00002
	0.2	0.00471	0.00241	0.00098	0.00028	0.00260	0.00099	0.00031	0.00007
	0.4	0.01846	0.00950	0.00387	0.00110	0.01030	0.00394	0.00123	0.00030
	0.8	0.06839	0.03578	0.01507	0.00436	0.03956	0.01535	0.00485	0.00119
	1.6	0.21770	0.12007	0.05549	0.01683	0.13743	0.05599	0.01862	0.00467
	3.2	0.53612	0.33669	0.18344	0.06167	0.37409	0.17843	0.06728	0.01784
$k_2 = 200.0$	0.1	0.00028	0.00013	0.00006	0.00002	0.00015	0.00005	0.00002	0.00000
	0.2	0.00110	0.00051	0.00022	0.00006	0.00058	0.00021	0.00007	0.00002
	0.4	0.00436	0.00202	0.00088	0.00025	0.00231	0.00085	0.00028	0.00007
	0.8	0.01679	0.00783	0.00348	0.00100	0.00905	0.00335	0.00110	0.00026
	1.6	0.06020	0.02874	0.01339	0.00392	0.03363	0.01283	0.00431	0.00104
	3.2	0.19189	0.09751	0.04911	0.01505	0.11105	0.04612	0.01644	0.00409

After Jones, 1962. By permission of Transportation Research Board, National Research Council, Washington DC.

Table 13.33 Values of σ_{z2}

		σ_{z2}/q							
		$H = 4.0$				$H = 8.0$			
	a_1	$k_1 = 0.2$	$k_1 = 2.0$	$k_1 = 20$	$k_1 = 200$	$k_1 = 0.2$	$k_1 = 2.0$	$k_1 = 20$	$k_1 = 200$
$k_2 = 0.2$	0.1	0.00086	0.00078	0.00037	0.00010	0.00027	0.00024	0.00011	0.00003
	0.2	0.00345	0.00312	0.00148	0.00039	0.00108	0.00096	0.00044	0.00011
	0.4	0.01371	0.01241	0.00588	0.00157	0.00432	0.00384	0.00176	0.00044
	0.8	0.05323	0.04842	0.02319	0.00625	0.01711	0.01522	0.00701	0.00175
	1.6	0.19003	0.17617	0.08758	0.02427	0.06610	0.05900	0.02746	0.00693
	3.2	0.51882	0.50917	0.28747	0.08799	0.23182	0.20949	0.10145	0.02656
$k_2 = 2.0$	0.1	0.00071	0.00034	0.00010	0.00002	0.00023	0.00010	0.00003	0.00001
	0.2	0.00283	0.00137	0.00039	0.00009	0.00091	0.00041	0.00011	0.00002
	0.4	0.01126	0.00544	0.00154	0.00036	0.00364	0.00164	0.00043	0.00009
	0.8	0.04388	0.02135	0.00610	0.00142	0.01446	0.00653	0.00170	0.00038
	1.6	0.15904	0.07972	0.02358	0.00560	0.05601	0.02556	0.00673	0.00149
	3.2	0.45455	0.25441	0.08444	0.02126	0.19828	0.09405	0.02579	0.00584
$k_2 = 20.0$	0.1	0.00028	0.00008	0.00002	0.00000	0.00009	0.00002	0.00001	0.00000
	0.2	0.00111	0.00034	0.00009	0.00002	0.00037	0.00010	0.00002	0.00001
	0.4	0.00443	0.00134	0.00035	0.00008	0.00149	0.00040	0.00009	0.00002
	0.8	0.01741	0.00532	0.00138	0.00031	0.00594	0.00159	0.00037	0.00008
	1.6	0.06525	0.02049	0.00542	0.00124	0.02320	0.00630	0.00147	0.00032
	3.2	0.20965	0.07294	0.02061	0.00483	0.08510	0.02409	0.00576	0.00127
$k_2 = 200.0$	0.1	0.00006	0.00002	0.00000	0.00000	0.00002	0.00001	0.00000	0.00000
	0.2	0.00024	0.00007	0.00002	0.00000	0.00008	0.00002	0.00000	0.00000
	0.4	0.00095	0.00029	0.00008	0.00002	0.00032	0.00008	0.00002	0.00000
	0.8	0.00378	0.00115	0.00030	0.00007	0.00127	0.00034	0.00008	0.00002
	1.6	0.01456	0.00451	0.00120	0.00027	0.00503	0.00135	0.00032	0.00007
	3.2	0.05161	0.01705	0.00468	0.00107	0.01912	0.00527	0.00125	0.00027

After Jones, 1962. By permission of Transportation Research Board, National Research Council, Washington, DC.

Ueshita and Meyerhof (1967) give solutions for vertical surface displacement of a uniformly loaded circle on a three-layer system. The vertical surface displacements at the centre and edge are given by the equation,

$$\rho_z = \frac{1.5qa}{E_3} I_{pz} \tag{13.57}$$

where I_{pz} is the appropriate deflection factor. Figure 13.72 gives the values of deflection factors. In Eq. 13.57 and Fig. 13.72, $\mu_1 = \mu_2 = \mu_3 = 0.5$.

For the case of $\mu_1 = \mu_2 = \mu_3 = 0.35$, Thenn de Barros (1966) gives the equation for the vertical displacement at the centre of the circle as,

$$\rho_z = \frac{1.755qa}{E_3} I_{pz} \tag{13.58}$$

The values of I_{pz} in Eq. 13.58 are given in Tables 13.34 to 13.38. In these tables,

$$k_1 = E_1/E_2 \quad \text{and} \quad k_2 = E_2/E_3$$

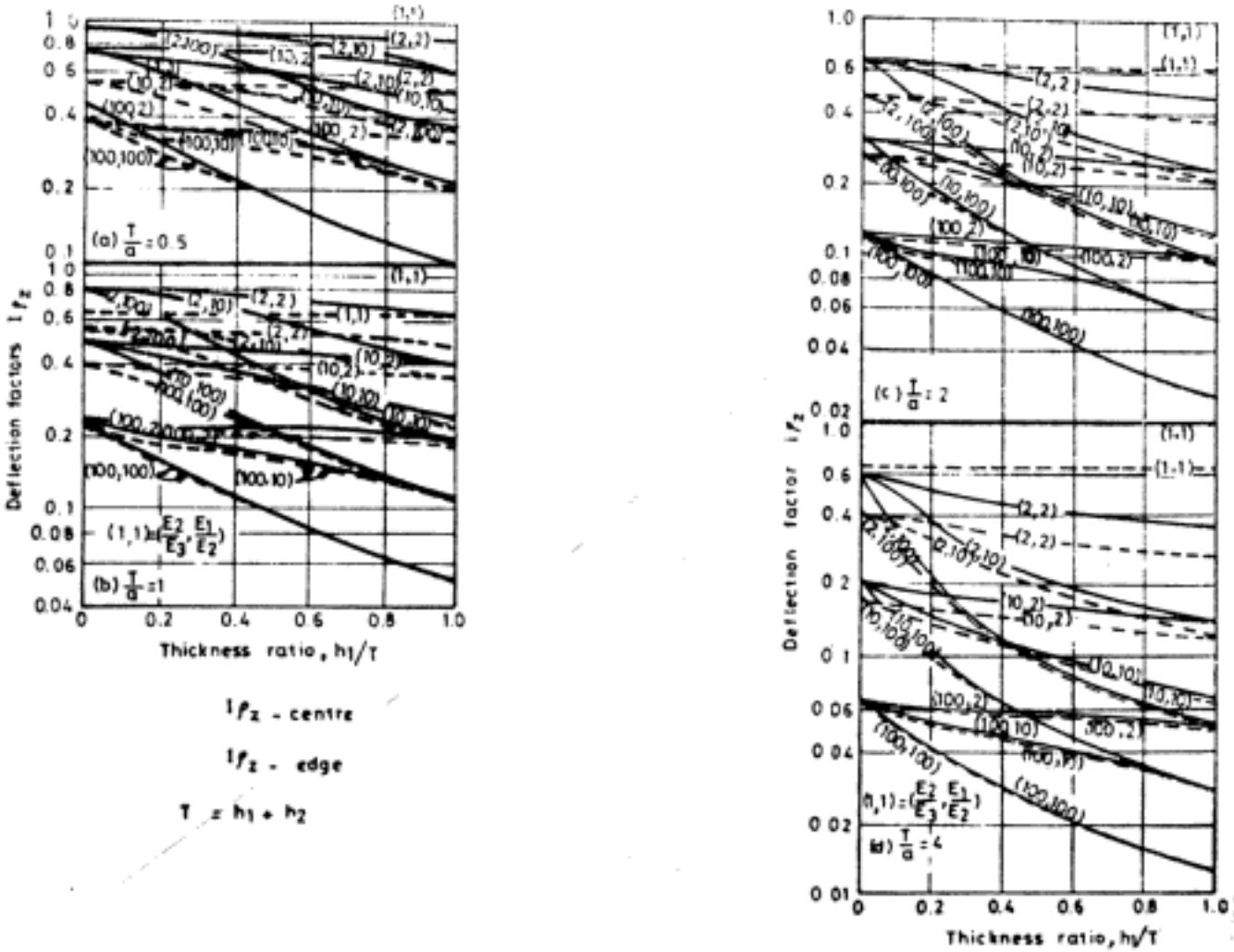

Fig. 13.72 Deflection factors for vertical displacement of uniformly loaded circle on a three-layer system (After Ueshita and Meyerhof, 1967)

Table 13.34 Displacement Factors I_{pz}

$k_1 = 2$

		h_1/a					
k_2	h_2/a	0.156	0.312	0.625	1.25	2.5	5
2	0.312	0.858	0.789	0.662	0.510	0.394	—
	0.625	0.772	0.717	0.616	0.489	0.387	0.323
	1.25	0.669	0.633	0.560	0.460	0.375	0.319
	2.5	—	0.564	0.508	0.428	0.360	0.314
	5	—	—	0.470	0.400	0.343	0.306
5	0.312	0.747	0.651	0.505	0.352	0.240	—
	0.625	0.601	0.537	0.438	0.324	0.231	0.171
	1.25	0.449	0.416	0.359	0.284	0.215	0.166
	2.5	—	0.320	0.287	0.240	0.194	0.158
	5	—	—	0.235	0.202	0.172	0.148
10	0.312	0.664	0.559	0.415	0.274	0.174	—
	0.625	0.500	0.436	0.346	0.246	0.165	0.112
	1.25	0.344	0.315	0.267	0.207	0.150	0.108
	2.5	—	0.221	0.198	0.165	0.130	0.100
	5	—	—	0.149	0.128	0.108	0.0903

After Thenn de Barros, 1966. By permission of Transportation Research Board, National Research Council, Washington, DC.

Table 13.35 Displacement Factors I_{pz}

$k_1 = 5$

		h_1/a					
k_2	h_2/a	0.156	0.312	0.625	1.25	2.5	5
2	0.312	0.830	0.733	0.556	0.372	0.246	—
	0.625	0.745	0.669	0.522	0.359	0.242	0.174
	1.25	0.648	0.593	0.476	0.339	0.235	0.172
	2.5	—	0.528	0.430	0.313	0.224	0.168
	5	—	—	0.394	0.289	0.211	0.163
5	0.312	0.713	0.598	0.427	0.268	0.162	—
	0.625	0.572	0.497	0.378	0.250	0.157	0.101
	1.25	0.429	0.387	0.312	0.223	0.148	0.0989
	2.5	—	0.299	0.249	0.188	0.134	0.0944
	5	—	—	0.202	0.155	0.116	0.0871
10	0.312	0.626	0.508	0.350	0.211	0.122	—
	0.625	0.469	0.401	0.301	0.195	0.118	0.0712
	1.25	0.325	0.291	0.236	0.168	0.109	0.0691
	2.5	—	0.206	0.174	0.134	0.0954	0.0649
	5	—	—	0.130	0.102	0.0779	0.0579

After Thenn de Barros, 1966. By permission of Transportation Research Board, National Research Council, Washington, DC.

Table 13.36 Displacement Factors I_{pz}

$k_1 = 10$

k_2	h_2/a	h_1/a = 0.156	0.312	0.625	1.25	2.5	5
2	0.312	0.811	0.687	0.483	0.298	0.181	—
	0.625	0.729	0.630	0.457	0.290	0.178	0.116
	1.25	0.634	0.561	0.420	0.275	0.174	0.115
	2.5	—	0.499	0.379	0.255	0.166	0.112
	5	—	—	0.346	0.234	0.156	0.109
5	0.312	0.689	0.553	0.369	0.217	0.123	—
	0.625	0.553	0.467	0.334	0.207	0.121	0.0720
	1.25	0.416	0.367	0.281	0.187	0.115	0.0706
	2.5	—	0.284	0.225	0.160	0.105	0.0679
	5	—	—	0.181	0.130	0.0912	0.0629
10	0.312	0.601	0.467	0.302	0.172	0.0946	—
	0.625	0.405	0.376	0.267	0.163	0.0924	0.0525
	1.25	0.312	0.275	0.214	0.144	0.0876	0.0514
	2.5	—	0.195	0.159	0.117	0.0782	0.0489
	5	—	—	0.117	0.0885	0.0642	0.0442

After Thenn de Barros, 1966. By permission of Transportation Research Board, National Research Council, Washington, DC.

Table 13.37 Displacement Factors I_{pz}

$k_1 = 20$

k_2	h_2/a	$h_1 = 20$ 0.156	0.312	0.625	1.25	2.5	5
2	0.312	0.789	0.629	0.411	0.239	0.136	—
	0.625	0.711	0.583	0.394	0.234	0.135	0.0809
	1.25	0.621	0.523	0.365	0.224	0.132	0.0802
	2.5	—	0.465	0.331	0.209	0.127	0.0788
	5	—	—	0.300	0.191	0.120	0.0764
5	0.312	0.662	0.501	0.313	0.175	0.0953	—
	0.625	0 535	0.433	0.290	0.169	0.0939	0.0528
	1.25	0.404	0.345	0.250	0.157	0.0909	0.0521
	2.5	—	0.267	0.202	0.136	0.0846	0.0506
	5	—	—	0.161	0.112	0.0742	0.0475
10	0.312	0.573	0.419	0.254	0.139	0.0740	—
	0.625	0.434	0.349	0.232	0.134	0.0729	0.0396
	1.25	0 301	0.260	0.193	0.123	0.0703	0.0390
	2.5	—	0.184	0.145	0.102	0.0645	0.0377
	5	—	—	0.106	0.0779	0.0542	0.0348

After Thenn de Barros, 1966. By permission of Transportation Research Board, National Research Council, Washington, DC.

Table 13.38 Displacement Factors $I_{\rho z}$

$k_1 = 50$

k_2	h_2/a	h_1/a 0.156	0.312	0.625	1.25	2.5	5
2	0.312	0.744	0.538	0.324	0.178	0.0960	—
	0.625	0.677	0.508	0.314	0.175	0.0953	0.0532
	1.25	0.594	0.461	0.297	0.170	0.0940	0.0528
	2.5	—	0.411	0.271	0.161	0.0915	0.0522
	5	—	—	0.245	0.148	0.0868	0.0509
5	0.312	0.612	0.421	0.244	0.131	0.0687	—
	0.625	0.507	0.378	0.233	0.128	0.0681	0.0364
	1.25	0.387	0.311	0.209	0.122	0.0667	0.0361
	2.5	—	0.241	0.173	0.110	0.0637	0.0354
	5	—	—	0.137	0.0915	0.0575	0.0338
10	0.312	0.524	0.348	0.197	0.104	0.0539	—
	0.625	0.410	0.305	0.187	0.102	0.0534	0.0280
	1.25	0.288	0.237	0.164	0.0966	0.0523	0.0277
	2.5	—	0.169	0.128	0.0847	0.0496	0.0272
	5	—	—	0.0926	0.0664	0.0436	0.0258

After Thenn de Barros, 1966. By permission of Transportation Research Board, National Research Council, Washington, DC.

13.7.3 Approximate Solutions to Layered Systems

1. *Steinbrenner's method*

For the case of an elastic layer underlain by a rough rigid base the surface displacement at the corner of a rectangular loaded area (Fig. 13.45) is approximately given by (Steinbrenner, 1934),

$$\rho_z = \frac{qB}{E} I_{\rho z} \tag{13.59}$$

where $I_{\rho z} = (1 - \mu^2)F_1 + (1 - \mu - 2\mu^2)F_2$

The values of F_1 and F_2 are shown in Fig. 13.73. Steinbrenner's method for a single layer can be extended to any number of layers as explained below. The vertical surface displacement at the corner of an uniformly loaded rectangle on the top of n layers is (Fig. 13.74),

$$\rho_z = qB\left[\sum_{i=1}^{n-1} \frac{\{I_{\rho z(i+1)} - I_{\rho zi}\}}{E_i} + \frac{I_{\rho zn}}{E_n}\right] \tag{13.60}$$

where, E_i and μ_i are the elastic parameters of layer i. $I_{\rho zi}$ is the vertical displacement factor (Eq. 13.59 and Fig. 13.73) corresponding to a depth factor and H_i/B (Fig. 13.74), where H_i is the depth below the ground surface to the top of the layer i.

Steinbrenner's approximate method is most satisfactory for layered systems in which modulus (E) increases rather than decreases with depth.

2. *Palmer and Barber's method*

In a general two-layer system Palmer and Barber (1940) replace the upper layer of thickness

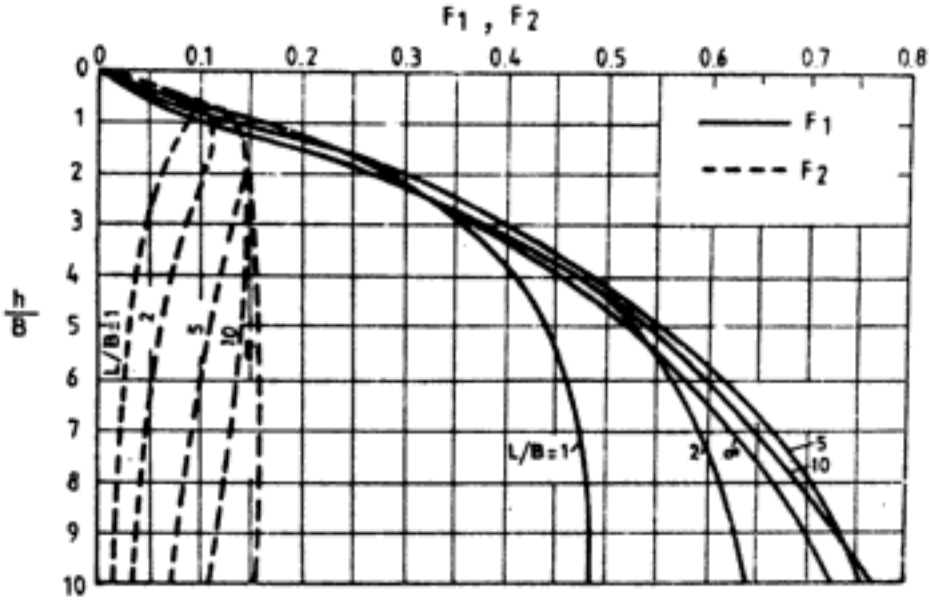

Fig. 13.73 Factors F_1 and F_2 for calculating vertical displacement of rectangle (After Steinbrenner, 1934)

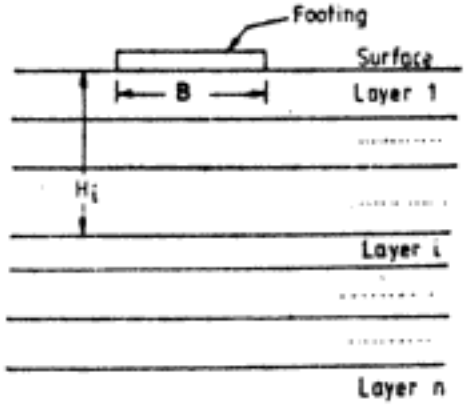

Fig. 13.74 Surface footing on a multi-layer system

h having elastic parameters E_1, μ_1 by an equivalent thickness h_{eq} having elastic parameters of the lower layer material, i.e., E_2, μ_2. The value of h_{eq} is given by,

$$h_{eq} = \left[\frac{E_1(1 - \mu_2^2)}{E_2(1 - \mu_1^2)}\right]^{1/3} \tag{13.61}$$

The vertical surface displacement is then obtained by adding the vertical displacement of the equivalent layer between $z = 0$ and $z = h_{eq}$ to the vertical displacement at a depth h_{eq} in a semi-infinite mass.

For example, for a uniformly loaded circle of radius a on the surface of a two-layer system having $\mu_1 = \mu_2 = 0.5$, the vertical displacement at centre at depth h_{eq} in a semi-infinite mass is,

$$\rho_1 = \frac{1.5qa^2}{E_2[a^2 + h_{eq}^2\{E_1/E_2\}^{2/3}]^{1/2}} \tag{13.62}$$

The displacement within the equivalent layer, ρ_2, is

$$\rho_2 = \frac{E_2}{E_1}\left[\frac{1.5qa}{E_2} - \rho_1\right] \tag{13.63}$$

The vertical surface displacement, $\rho_z = \rho_1 + \rho_2$

$$\rho_z = \frac{1.5qa}{E_2}\left[\frac{a}{\{a^2 + h_{eq}^2(E_1/E_2)^{2/3}\}^{1/2}}(1 - E_2/E_1) + E_2/E_1\right] \tag{13.64}$$

Palmer and Barber's method can be extended to multi-layer systems by repeated replacement of overlying layers by equivalent thicknesses of the lowermost material.

3. *Odemark's method*

Odemark's method (1949) can be used to estimate the vertical displacement in a three-layer elastic system with $\mu_1 = \mu_2 = \mu_3 = 0.5$. The vertical surface displacement at the centre of a uniformly loaded circle (Fig. 13.71) is given by,

$$\rho_z = \frac{2(1 - \mu_3^2)}{E_3} qaI_{\rho z} \tag{13.65}$$

where $I_{\rho z} = I_{\rho z1} + I_{\rho z2} + I_{\rho z3}$

$$I_{\rho z1} = \frac{E_3}{E_1}\left[1 - \frac{1}{\{1 + N_1^2(T/a)^2\}^{1/2}}\right]$$

$$I_{\rho z2} = \frac{E_3}{E_2}\left[\frac{1}{\{1 + N_2^2(T/a)^2\}^{1/2}} - \frac{1}{\{1 + \overline{N}_2^2(T/a)^2\}^{1/2}}\right]$$

$$I_{\rho z3} = \frac{1}{\{1 + N_3^2(T/a)^2\}^{1/2}}$$

$$N_1 = 0.9\left(\frac{h_1}{T}\right)$$

$$\overline{N}_1 = 0.9\left(\frac{h_2}{T}\right)$$

$$N_2 = N_1\left(\frac{E_1}{E_3}\frac{E_3}{E_m}\right)^{1/3}$$

$$\overline{N}_2 = N_2 + \overline{N}_1$$

$$N_3 = N_2 + \overline{N}_1(E_2/E_3)^{1/3}$$

$$\frac{E_3}{E_m} = \left\{\frac{1 + N_2^2(T/a)^2}{1 + N_3^2(T/a)^2}\right\}^{1/2} + \frac{E_3}{E_2}\left[1 - \left\{\frac{1 + N_2^2(T/a)^2}{1 + \overline{N}_2^2(T/a)^2}\right\}^{1/2}\right]$$

E_m = equivalent modulus of elasticity of the composite underlayer

The value of (E_3/E_m) is determined by solving the equation for E_3/E_m iteratively. $I_{\rho z}$ can then be determined.

Odemark's method gives satisfactory results when E decreases with depth.

4. *Vesic's method*

Vesic (1963) gives the following equation for the vertical surface displacement of the centre of a uniformly loaded circular area.

$$\rho_z = 2qa \sum_{i=1}^{n} \frac{(1-\mu_i)^2}{E_i}(I_i - I_{i-1}) \tag{13.66}$$

where μ_i = Poisson's ratio of the ith layer
I_i = displacement factor of the ith layer, corresponding to z_i/a
z_i = depth from surface to base of layer i (see inset in Fig. 13.75)
when $i = n$, i.e., for the lowermost layer $I_i = I_n = 1$

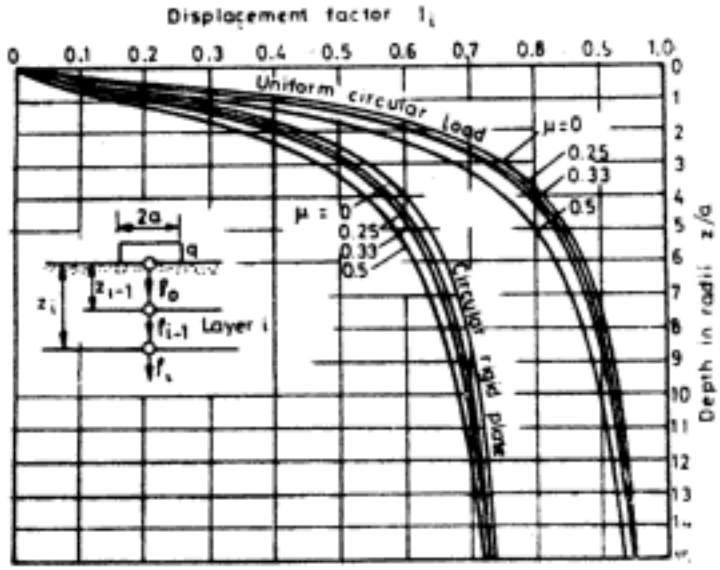

Fig. 13.75 Approximate displacement factors for vertical displacement of circle on a multi-layer system
[After Vesic, 1963]

5. *Approximations for equivalent modulus of upper layers*

Ueshita and Meyerhof's recommendations in the case of two-layer systems are explained in Sec. 13.7.1.

Thenn de Barros (1966) makes the following recommendation in the case of three-layer systems. The upper two layers of thickness h_1 and h_2 are replaced by a single layer of thickness $h_1 + h_2$ having an equivalent modulus,

$$E_{eq} = \left[\frac{h_1\sqrt[3]{E_1} + h_2\sqrt[3]{E_2}}{h_1 + h_2}\right]^3 \tag{13.67}$$

The three-layer system is thus reduced to a two-layer system and the displacement can be determined using procedures explained for two-layer systems or the approximate methods.

Q 13.8: To determine the surface displacement at the corner of a square on the surface of an elastic layer underlain by rough rigid base (Fig. 13.76).

Ans: 1. *Ueshita-Meyerhof's method*

$$L/B = 3/3 = 1; \quad h/B = 3/3 = 1$$

From Fig. 13.51, $I_{\rho z} = 0.105$

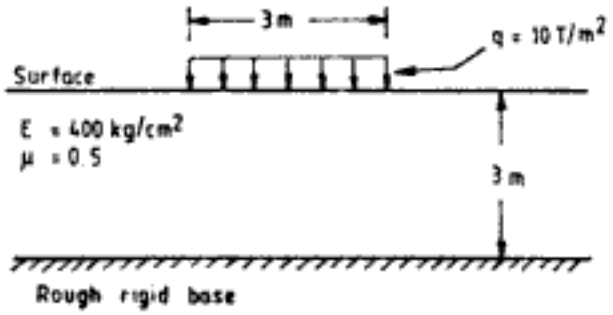

Fig. 13.76 Q 13.8

Substituting in Eq. 13.51 the displacement at corner is,

$$\rho_z = \frac{10 \times 3}{4000} \times 0.105$$
$$= 0.79 \times 10^{-3} \text{ m} = 0.79 \text{ mm}$$

2. *Steinbrenner's approximate method*

$$L/B = 1; \quad h/B = 3/3 = 1$$

From Fig. 13.73, $F_1 = 0.15$, $F_2 = 0.085$

In Eq. 13.59 $I_{\rho z} = (1 - 0.5)^2 \times 0.15 + (1 - 0.5 - 2 \times 0.5^2) \times 0.085$
$= 0.1125$

Substituting in Eq. 13.59,

$$\rho_z = \frac{10 \times 3}{4000} \times 0.1125 = 0.84 \times 10^{-3} \text{ m} = 0.84 \text{ mm}$$

Q 13.9: To determine the surface displacement at the corner of a square on the surface of a two-layer elastic system (Fig. 13.77).

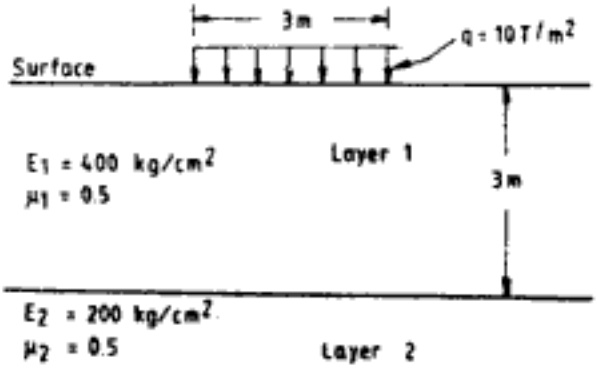

Fig. 13.77 Q 13.9

Ans: 1. *Ueshita-Meyerhof's equivalent modulus*

Figure 13.70 will be used to obtain the equivalent modulus. In order to use this figure, the equivalent radius of the square is obtained from,

$$a = \sqrt{\frac{LB}{\pi}} = \sqrt{\frac{3 \times 3}{\pi}} = 1.692 \text{ (i.e., by equating area of the circle and the square)}$$

$$h/a = 3/1.692 = 1.77$$

$$E_1/E_2 = 400/200 = 2$$

From Fig. 13.70, $E_{eq}/E_2 \simeq 1.46$ i.e., $E_{eq} = 292$ kg/cm². From Ueshita-Meyerhof's curves in Fig. 13.51, $I_{pz} = 0.421$ as $h/B \to \infty$. Substituting in Eq. 13.51, the displacement at the corner of the square is,

$$\rho_z = \frac{10 \times 3}{2920} \times 0.421$$

$$= 4.33 \times 10^{-3} \text{ m} = 4.33 \text{ mm}$$

2. *Steinbrenner's method*

Steinbrenner's equation (Eq. 13.60) for vertical displacement becomes, when $n = 2$,

$$\rho_z = qB \left[\frac{I_{pz2} - I_{pz1}}{E_1} + \frac{I_{pz2}}{E_2} \right] \tag{13.68}$$

I_{pz1} and I_{pz2} are determined using Fig. 13.73.

For I_{pz1}: $H_1 = 0$, hence $F_1 = F_2 = 0$ and $I_{pz1} = 0$

For I_{pz2}: $H_2 = 3$ m, $H_2/B = 3/3 = 1$, $L/B = 1$

$$F_1 = 0.15 \quad \text{and} \quad F_2 = 0.085$$

$$I_{pz2} = 0.1125 \text{ (see Q 13.8)}$$

From Eq. 13.68

$$\rho_z = 10 \times 3 \times \left[\frac{0.1125}{4000} + \frac{0.1125}{2000} \right]$$

$$= 2.53 \times 10^{-3} \text{ m} = 2.53 \text{ mm}$$

The method gives unsatisfactory results because modulus decreases with depth.

Q 13.10: To determine the vertical surface displacement at the centre of a uniformly loaded circle on the surface of a three-layer elastic system (Fig. 13.78).

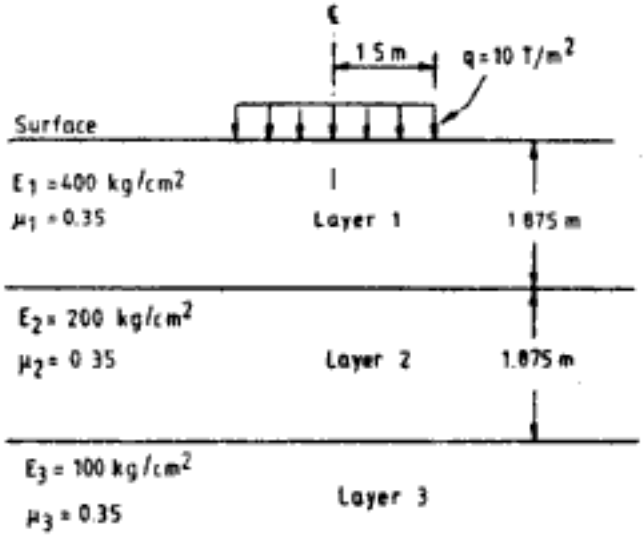

Fig. 13.78 Q 13.10

Ans: 1. *Thenn de Barros method*

$$k_1 = E_1/E_2 = 400/200 = 2$$
$$k_2 = E_2/E_3 = 200/100 = 2$$
$$h_1/a = h_2/a = 1.875/1.5 = 1.25$$

From Table 13.34 $I_{\rho z} = 0.46$

Substituting in Eq. 13.58

$$\rho_z = \frac{1.755 \times 10 \times 1.5}{1000} \times 0.46$$
$$= 12.11 \times 10^{-3} \text{ m} = 12.11 \text{ mm}$$

2. *Vesic's approximate method*

Vesic's Eq. 13.66 is written as follows for a three-layer system,

$$\rho_z = 2aq \sum_{i=1}^{3} \frac{(1 - \mu_i^2)}{E_i}(I_i - I_{i-1})$$

In the above equation, values of I_i are obtained from Fig. 13.75.

For I_0, $z_0/a = 0$, $I_0 = 0$
For I_1, $z_1/a = 1.875/1.5 = 1.25$, $I_1 = 0.45$
For I_2, $z_2/a = 3.75/1.5 = 2.5$, $I_2 = 0.68$
For I_3, $z/a \to \infty$, $I_3 = 1$

Substituting for ρ_z,

$$\rho_z = 2 \times 1.5 \times 10 \times \left[\frac{(1 - 0.35^2)}{4000} \times (0.45 - 0) + \frac{(1 - 0.35^2)}{2000} \times (0.68 - 0.45) + \frac{(1 - 0.35^2)}{1000} \times (1 - 0.68)\right]$$
$$= 14.41 \times 10^{-3} \text{ m} = 14.41 \text{ mm}$$

3. *Thenn de Barros' approximate method*

The three-layer system will be converted into an equivalent two-layer system. The equivalent modulus of the top layer is computed using Eq. 13.67.

$$E_{eq} = \left(\frac{1.875\sqrt[3]{400} + 1.875\sqrt[3]{200}}{3.75}\right)^3$$
$$= 288.55 \text{ kg/cm}^2$$

The equivalent two-layer system is shown in Fig. 13.79. Using Thenn de Barros' curves in Fig. 13.69,

$$E_{eq}/E_3 = 2.88 \quad h/a = 3.75/1.5 = 2.5$$
$$I_{\rho z} \simeq 0.55$$

$\therefore$
$$\rho_z = \frac{1755 \times 10 \times 1.5}{1000} \times 0.55$$
$$= 14.48 \times 10^{-3} \text{ m} = 14.48 \text{ mm}$$

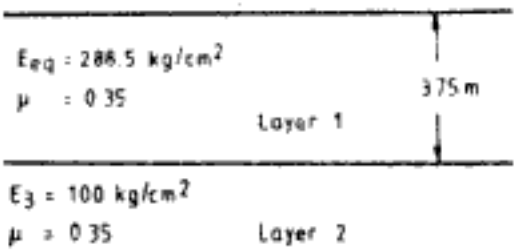

Fig. 13.79 Equivalent two-layer system for the three-layer system in Fig. 13.78

Q 13.11: To determine the vertical surface displacement at the centre of a uniformly loaded circle on the surface of a three-layer elastic system shown in Fig. 13.80.

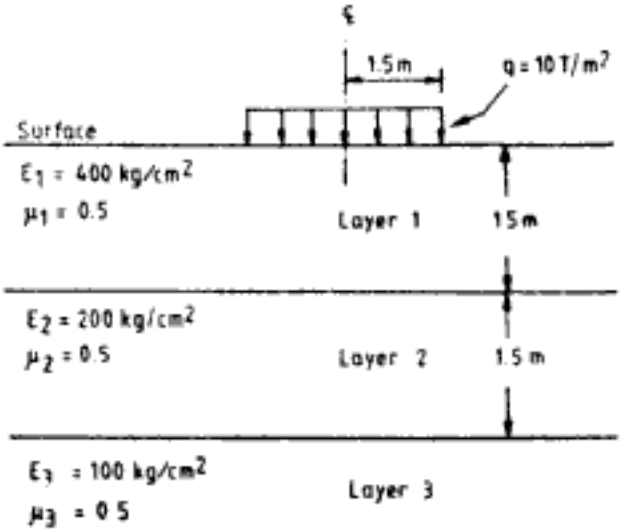

Fig. 13.80 Q 13.11

Ans: 1. *Ueshita-Meyerhof's method*

Equation 13.57 and Fig. 13.72 will be used to obtain the solution.

$$T = 1.5 + 1.5 = 3 \text{ m}$$
$$T/a = 3/1.5 = 2$$
$$h_1/T = h_2/T = 1.5/3 = 0.5$$
$$E_2/E_3 = 200/100 = 2$$
$$E_1/E_2 = 400/200 = 2$$

From Fig. 13.72,

$$I_{\rho z} \simeq 0.56$$

Substituting in Eq. 13.57, the displacement at centre is,

$$\rho_z = \frac{1.5 \times 10 \times 1.5}{1000} \times 0.56$$
$$= 12.6 \times 10^{-3} \text{ m} = 12.6 \text{ mm}$$

1. *Odemark's approximate method*

To use Eq. 13.65 of this method first E_3/E_m has to be solved for. Letting $E_3/E_m = x$,

$$N_1 = \overline{N}_1 = 0.9 \times 0.5 = 0.45$$

$$E_1/E_3 = 4;\ E_2/E_3 = 2$$

$$E_3/E_1 = 0.25;\ E_3/E_2 = 0.5$$

$$N_2 = 0.45(4x)^{1/3};\ N_2^2 = 0.2025(4x)^{2/3}$$

$$\overline{N}_2 = 0.45[(4x)^{1/3} + 1];\ \overline{N}_2^2 = 0.2025[(4x)^{1/3} + 1]^2$$

$$N_3 = 0.45(4x)^{1/3} + 0.45(2)^{1/3} = 0.45[(4x)^{1/3} + 1.26]$$

$$T/a = 2;\ (T/a)^2 = 4;\ N_3^2 = 0.2025[(4x)^{1/3} + 1.26]^2$$

$$x = \left\{\frac{1 + 0.2025(4x)^{2/3} \times 4}{1 + 0.2025[(4x)^{1/3} + 1.26]^2 \times 4}\right\}^{1/2} + 0.5 \times \left[1 - \left\{\frac{1 + 0.2025(4x)^{2/3} \times 4}{1 + 0.2025[(4x)^{1/3} + 1]^2 \times 4}\right\}^{1/2}\right]$$

Value of x (i.e., E_3/E_m) can be solved iteratively. Substituting $x = 1$ in the RHS of the above equation, $x = 0.79$

Substituting $x = 0.85$ in the RHS of the equation, $x = 0.786$

Substituting $x = 0.8$ in the RHS of the equation, $x = 0.785$

$\therefore$ $$x = E_3/E_m = 0.785$$

Using this value of x

$$N_1 = \overline{N}_1 = 0.45$$

$$N_2 = 0.659$$

$$\overline{N}_2 = 1.109$$

$$N_3 = 1.226$$

$$I_{pz1} = \frac{100}{400}\left[1 - \frac{1}{(1 + 0.45^2 \times 4)^{1/2}}\right] = 0.0642$$

$$I_{pz2} = \frac{100}{200}\left[\frac{1}{(1 + 0.659^2 \times 4)^{1/2}} - \frac{1}{(1 + 1.109^2 \times 4)^{1/2}}\right] = 0.0967$$

$$I_{pz3} = \frac{1}{(1 + 1.226^2 \times 4)^{1/2}} = 0.378$$

$$I_{pz} = 0.0642 + 0.0967 + 0.378 = 0.5389$$

Substituting in Eq. 13.65

$$\rho_z = \frac{2 \times (1 - 0.5)^2}{1000} \times 10 \times 1.5 \times 0.5389$$

$$= 12.13 \times 10^{-3}\ \text{m} = 12.13\ \text{mm}$$

3. *Vesic's approximate method*

The application of this method for three-layer system is already explained in Q 13.10.

For I_0, $z_0/a = 0$, $I_0 = 0$

For I_1, $z_1/a = 1$, $I_1 = 0.28$

For I_2, $z_2/a = 2$, $I_2 = 0.55$

For I_3, $z/a \to \infty$, $I_3 = 1.0$

Substituting for ρ_z,

$$\rho_z = 2 \times 1.5 \times 10 \times \left[\frac{(1 - 0.5^2)}{4000} \times (0.28 - 0) + \frac{(1 - 0.5^2)}{2000} \times (0.55 - 0.28) + \frac{(1 - 0.5^2)}{1000} \times (1 - 0.55)\right]$$

$$= 14.74 \times 10^{-3} \text{ m} = 14.74 \text{ mm}$$

13.8 RIGID LOADED AREAS

13.8.1 Loaded Areas on Semi-Infinite Mass

1. *Symmetrical vertical loading on a rigid circle* (Fig. 13.81)

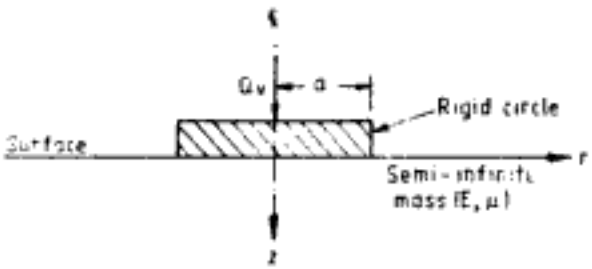

Fig. 13.81 Rigid circle on half-space

Vertical contact pressure distribution at the interface is given by,

$$\sigma_z = \frac{q_{av}}{\left[2\left(1 - \frac{r^2}{a^2}\right)\right]^{1/2}} \tag{13.69}$$

where r = radial distance from centre ($\leqslant a$)
a = radius of circle
q_{av} = average applied pressure
$= Q_v/\pi a^2$
Q_v = total vertical load

The vertical stress distribution beneath the circle obtained by Muki (1961) is shown in Fig. 13.82. The vertical stress distribution along the axis of the circle is given by Schiffman and Aggarwala (1961) as,

$$\sigma_z = q_{av} I_{oz} \tag{13.70}$$

where $I_{oz} = \dfrac{1 + 3(z^2/a^2)}{2[1 + (z^2/a^2)]^2}$

Values of I_{oz} are given in Table 13.39.

The uniform vertical displacement of the rigid circle is given by,

$$\rho_z = \frac{q_{av} a}{E} \frac{\pi}{2}(1 - \mu^2) \tag{13.71}$$

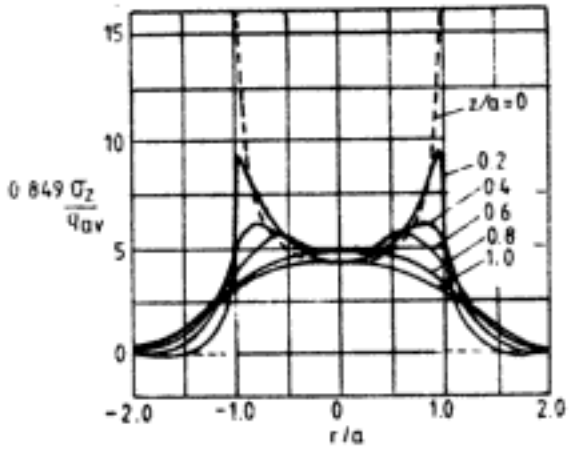

Fig.13.82 Vertical stress distribution beneath rigid circle on half-space (After Muki, 1961; with permission of North-Holland Publishing Company, Amsterdam)

Table 13.39 Values of $I_{\sigma z}$ (Eqs 13.70 and 13.73)

z/a	$I_{\sigma z}$	z/a	$I_{\sigma z}$
0.00	0.500	2.00	0.260
0.20	0.518	3.00	0.140
0.40	0.550	4.00	0.085
0.60	0.562	5.00	0.056
0.80	0.543	7.00	0.030
1.00	0.500	10.00	0.015

2. *Moment loading of a circle* (Fig. 13.83)

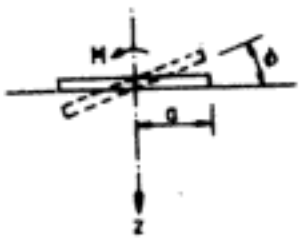

Fig. 13.83 Moment loading on rigid circle

According to Sneddon (1946), the expression for vertical stress at a point in the semi-infinite mass due to a moment M acting on the rigid circle is,

$$\sigma_z = \frac{3M}{4a^3\pi}\left[R^{-1/2}\sin\frac{\psi}{2} + \frac{z}{a}R^{-3/2}\left\{\frac{z}{a}\sin\left(\frac{3}{2}\psi\right) - \cos\left(\frac{3}{2}\psi\right)\right\}\right] \tag{13.72}$$

where $$R^2 = \left\{\left(\frac{r}{a}\right)^2 + \left(\frac{z}{a}\right)^2 - 1\right\}^2 + 4\left(\frac{z}{a}\right)^2$$

$$\psi = \tan^{-1}\left\{\frac{2(z/a)}{(r/a)^2 + (z/a)^2 - 1}\right\}$$

For the case of vertical stress along the axis of the circle,

$$\sigma_z = \frac{3M}{2a^3\pi} I_{\sigma z} \tag{13.73}$$

where $$I_{\sigma z} = \frac{1 + 3(z/a)^2}{2\{1 + (z/a)^2\}^2}$$

Numerical values of $I_{\sigma z}$ are given in Table 13.39. Vertical contact pressure at the interface is given by,

$$\sigma_z = \frac{3M}{4a^3\pi}\frac{1}{\sqrt{1 - (r/a)^2}} \qquad 0 \leqslant \frac{r}{a} \leqslant 1 \tag{13.74}$$

Rotation, ϕ, of the rigid circle is given by (Borowica, 1943),

$$\tan \phi = \frac{3M(1 - \mu^2)}{4Ea^3} \tag{13.75}$$

3. *Torsion loading of a circle* (Fig. 13.84)
Reissner and Sagoci (1944) give the expression for angular rotation θ of a circle due to torque T as,

$$\theta = \frac{3T(1 + \mu)}{8Ea^3} \tag{13.76}$$

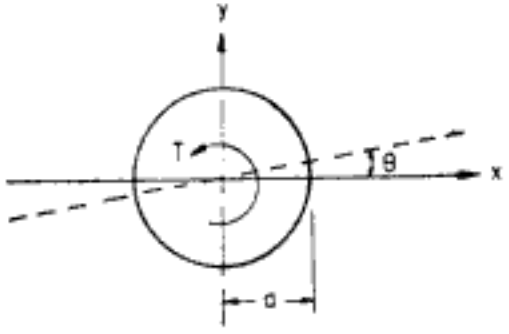

Fig. 13.84 Torsional loading of rigid circle

4. *Horizontal loading on circle* (Fig. 13.85)
The uniform horizontal displacement, ρ_x, of the circle in the direction of total horizontal load Q_h is given by (Bycroft, 1956),

$$\rho_x = \frac{(7 - 8\mu)(1 + \mu)Q_h\pi a}{16(1 - \mu)E} \tag{13.77}$$

5. *Symmetrical vertical loading on rigid circular ring* (Fig. 13.86)

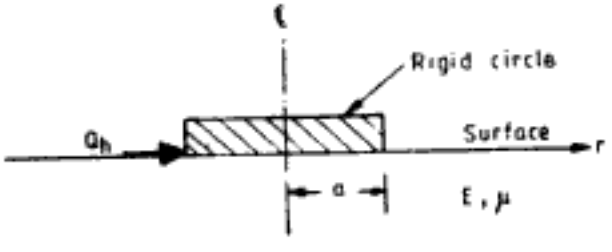

Fig. 13.85 Shear load on rigid circle

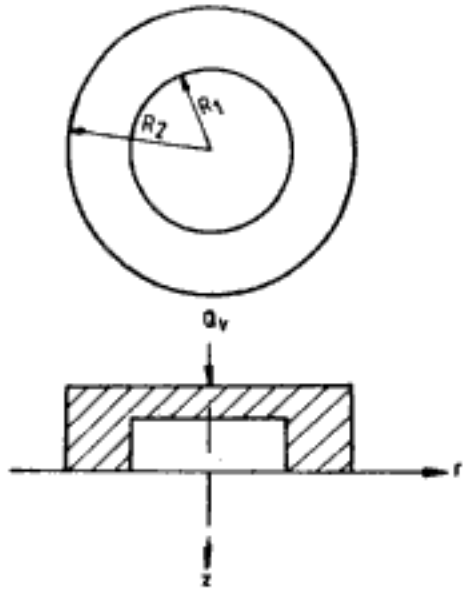

Fig. 13.86 Vertical load on rigid ring

The uniform vertical displacement of the ring is given by (Egorov, 1965),

$$\rho_z = \frac{Q_r(1-\mu^2)}{ER_2} I_{\rho z} \tag{13.78}$$

Table 13.40 gives the values of $I_{\rho z}$. In Table 13.40 $n = R_1/R_2$.

Table 13.40 Values of $I_{\rho z}$ for Rigid Ring (Eq. 13.78)

n	0	0.2	0.4	0.6	0.8	0.9	0.95
$I_{\rho z}$	0.50	0.50	0.51	0.52	0.57	0.60	0.65

After Egorov, 1965.

6. *Symmetrical vertical loading on rigid rectangle*
Whitman and Richart (1967) give the approximate value of vertical displacement of the rectangle by the equation,

$$\rho_z = \frac{Q_r(1-\mu^2)}{\beta_z E\sqrt{BL}} \tag{13.79}$$

Variation of β_z with L/B ratio is shown in Fig. 13.87.

7. *Rectangle with vertical eccentric load* (Fig. 13.27)
The rotation or angular deflection of the rectangular rigid area due to the eccentric load Q is given by Gorbunov-Posadov (1949).

The angle ϕ_L that side L makes with horizontal is given by,

$$\tan\phi_L = \frac{8Qe_L(1-\mu^2)}{L^3E} K_1 \tag{13.80}$$

and the angle ϕ_B that side B makes with horizontal is given by,

$$\tan\phi_B = \frac{8Qe_B(1-\mu^2)}{B^3E} K_2 \tag{13.81}$$

The resultant rotation ϕ of the rectangle is obtained as,

$$\tan\phi = (\tan^2\phi_L + \tan^2\phi_B)^{1/2} \tag{13.82}$$

Values of K_1 and K_2 in Eqs. 13.80 and 13.81 are shown in Fig. 13.88.

Q13.12: To determine the angular deflection of a rectangle 4 m×2 m resting on the surface of a semi-infinite mass with $E = 200$ kg/cm² and $\mu = 0.5$. The vertical eccentric load = 60 T, $e_L = 0.2$ m, $e_B = 0.1$ m.

Ans: From Fig. 13.88 for $L/B = 2$, $K_1 \simeq 0.85$, $K_2 \simeq 0.3$.
Using Eq. 13.80,

$$\tan\phi_L = \frac{8\times60\times0.2\times(1-0.5^2)}{4^3\times2000}\times0.85 = 0.478\times10^{-3}$$

i.e., $\phi_L = 0.0274$ degrees

Using Eq. 13.81,

$$\tan\phi_B = \frac{8\times60\times0.1\times(1-0.5^2)}{2^3\times2000}\times0.3 = 0.675\times10^{-3}$$

i.e. $\phi_B = 0.0387$ degrees

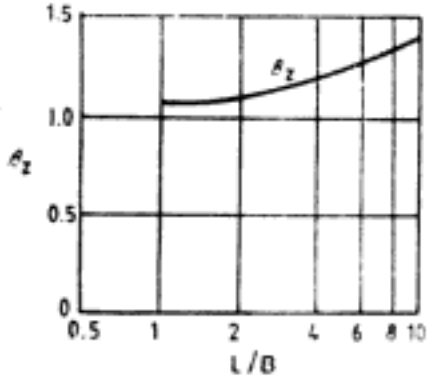

Fig. 13.87 **Coefficient β_z for rigid rectangle** (After Whitman and Richart, 1967, with permission of American Society of Civil Engineers, New York)

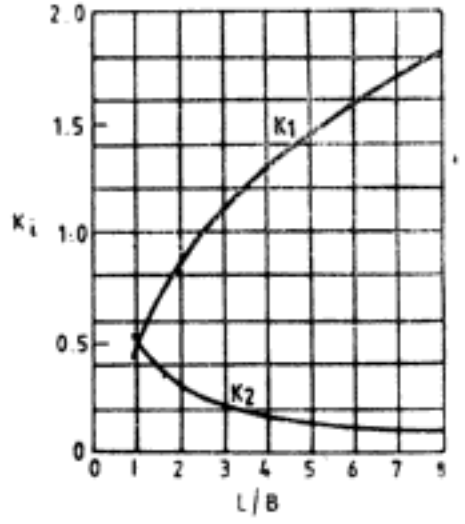

Fig. 13.88 **Coefficients K_1 and K_2 for calculating the tilt of rigid rectangle** (After Gorbunov-Posadov, 1949)

Using Eq. 13.82

$$\tan \phi = 8.272 \times 10^{-4}$$

i.e., $$\phi = 0.0474 \text{ degrees}$$

8. *Horizontal loading on rectangle*

Barkan (1962) gives the approximate expression for uniform horizontal displacement ρ_h, due to a load Q_h acting in the direction of B as,

$$\rho_h = \frac{Q_h(1 - \mu^2)}{\beta_x E \sqrt{BL}} \tag{13.83}$$

Values of β_x are shown in Table 13.41. It must be noted that in Eq. 13.83 and Table 13.41 B is the dimension of the footing along the direction of Q_h and *not* the smallest dimension.

Table 13.41 Values of β_x

μ	L/B						
	0.5	1	1.5	2	3	5	10
0.1	1.040	1.000	1.010	1.020	1.050	1.150	1.250
0.2	0.990	0.938	0.942	0.945	0.975	1.050	1.160
0.3	0.926	0.868	0.864	0.870	0.906	0.950	1.040
0.4	0.844	0.792	0.770	0.784	0.806	0.850	0.940
0.5	0.770	0.704	0.692	0.686	0.700	0.732	0.840

After Barkan, 1962.

9. *Moment loading on a rectangle*

The approximate solution for the rotation of the base of the rectangle (Fig. 13.89) due to moment M applied in the direction of L is (Lee, 1962)

$$\phi = \frac{M(1 - \mu^2)}{L^2 B E} I_\phi \tag{13.84}$$

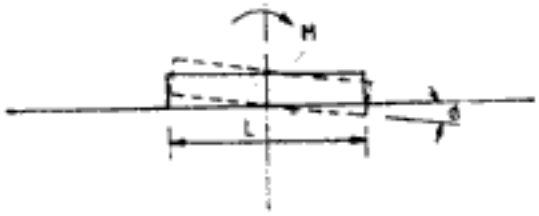

Fig. 13.89 Moment loading on rigid rectangle

Values of I_ϕ are given in Table 13.42. It must be noted that in Eq. 13.84 and Table 13.42, L is the dimension of the rectangle in the direction of M and *no* the largest dimension.

Table 13.42 Values of I_ϕ

L/B	0.1	0.2	0.5	1.0	1.5	2	5	10	100	∞
I_ϕ	1.59	2.29	3.33	3.70	4.12	4.38	4.82	4.93	5.06	5.10

After Lee, 1962; Whitman and Richart, 1967.

13.8.2 Loaded Areas on Finite Layer

1. *Symmetric vertical loading on circle* (Fig. 13.90)
Figure 13.91 gives the comparison of the variation of the vertical stress along the z-axis for rigid and flexible loaded circles.

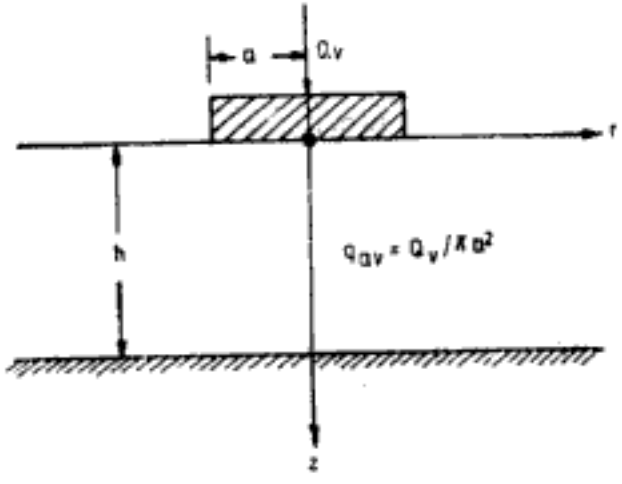

Fig. 13.90 Vertical load on rigid circle on finite layer

The uniform vertical displacement of the rigid circle is given by (Poulos, 1968),

$$\rho_z = \frac{q_{av} a}{E} I_{\rho z} \tag{13.85}$$

Figure 13.92 gives the values of deflection factors $I_{\rho z}$.

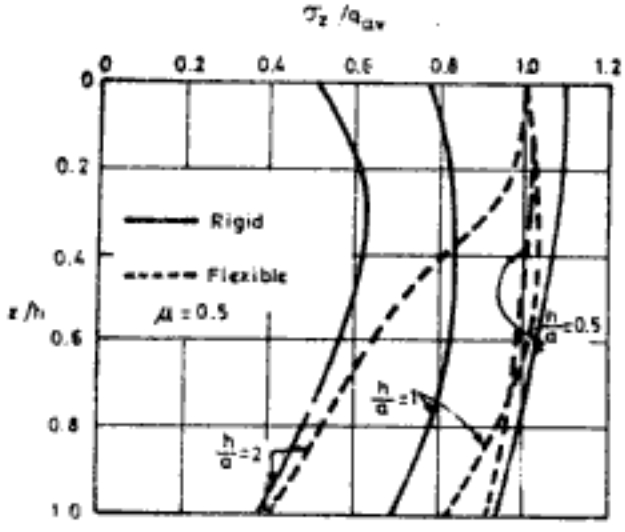

Fig. 13.91 Vertical stress along axis of rigid circle on finite layer

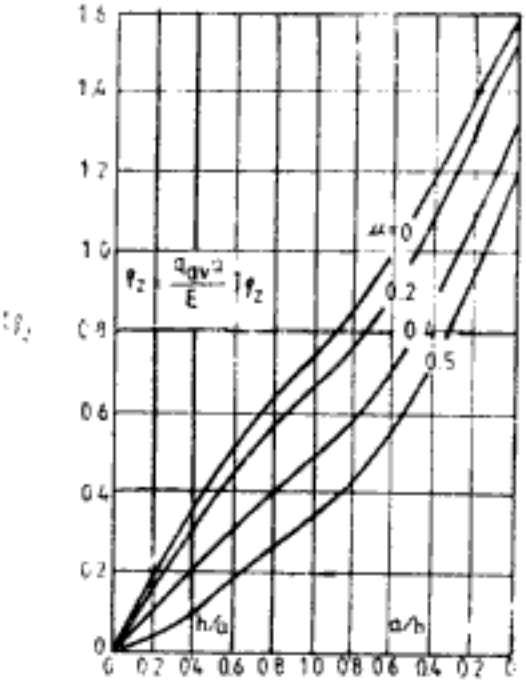

Fig. 13.92 **Deflection factor for vertical displacement of rigid circle on finite layer** (After Poulos, 1968; with permission)

2. *Moment loading on circle* (Fig. 13.93)

Yegorov and Nichiporovich (1961) give the approximate solution for rotation ϕ of the circle as,

$$\phi = \frac{(1-\mu^2)M}{4a^3Ex} \tag{13.86}$$

where $x = (1/3)a_1 + (1/5)a_3$. Values of a_1 and a_3 are tabulated in Table 13.43.

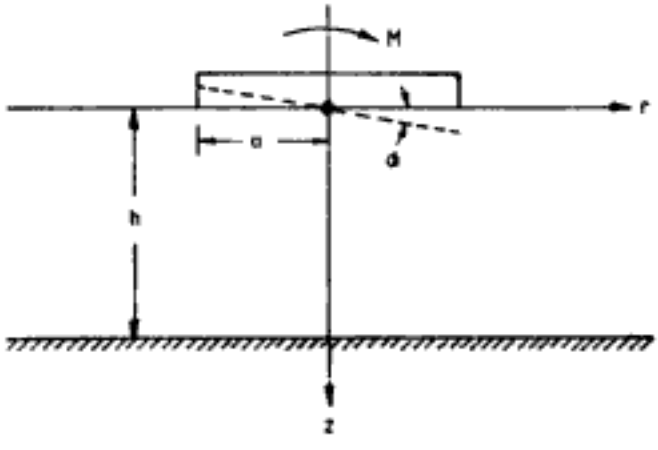

Fig. 13.93 **Moment loading on rigid circle on finite layer**

Table 13.43 Factors for Rigid Circle Subjected to Moment

h/a	a_1	a_2
0.25	4.23	−2.33
0.5	2.14	−0.70
1.0	1.25	−0.10
1.5	1.10	−0.03
2.0	1.04	0
3.0	1.01	0
⩾5.0	1.00	0

After Yegorov and Nichiporovich, 1961.

3. *Rectangle on finite layer and subjected to vertical loading*
Sovinc (1969) gives the expression for vertical displacement of the rectangle as,

$$\rho_z = \frac{q_{av}L}{E} I_{\rho z} \qquad L > B \tag{13.87}$$

The values of $I_{\rho z}$ are shown in Fig. 13.94 for $\mu = 0.5$.

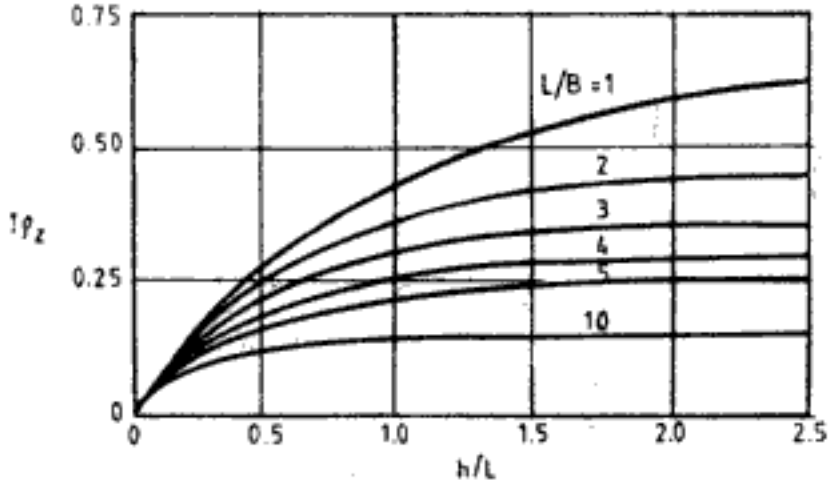

Fig. 13.94 Displacement factor for vertical displacement of rigid rectangle on finite layer (After Sovinc, 1969)

4. *Moment loading on rigid rectangle*
Sovinc gives the equations for rotation ϕ of the rectangle when the moment is acting in the direction of L (L is not the largest dimension of rectangle) as,

$$\phi = \frac{8M}{L^3 E} I_\phi \tag{13.88}$$

Figure 13.95 gives the values of I_ϕ for $\mu = 0.5$.

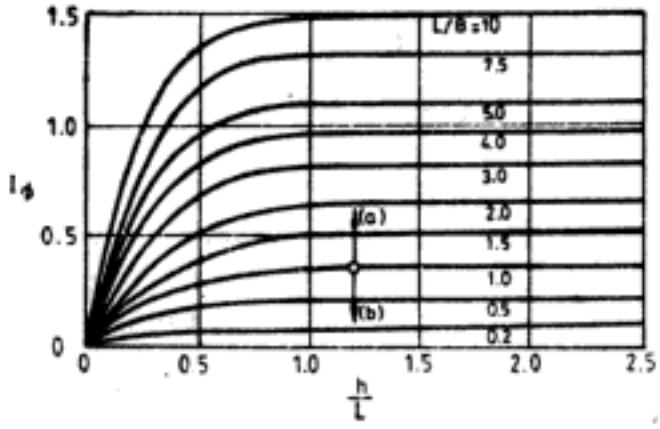

Fig. 13.95 Factor for rotation of rigid rectangle on finite layer (a) Moment acting in the direction of length (b) Moment acting in the direction of breadth (After Sovinc, 1969)

13.8.3 Rigid Loaded Areas Embedded within a Semi-infinite Mass

1. *Vertical loading on circle*

Butterfield and Banerjee (1971) present solutions for a rigid circle of radius a and embedded at depth h below the surface of a semi-infinite mass. Figure 13.96 gives the variation of vertical stress with depth. In this figure z is the distance below the circle. σ_z is not greatly affected by values of μ, it decreases slightly as μ decreases.

Solutions for vertical displacement of the circle are shown in Fig. 13.97.

2. *Vertical loading on rectangle*

The variation of vertical stress beneath the loaded area (rectangle $L \times B$, embedded at depth h below surface) is shown for two particular cases in Figs. 13.98 and 13.99 (Butterfield and Banerjee, 1971).

Solutions for vertical displacement are shown in Fig. 13.100. The vertical displacement can also be determined by the procedure suggested by Fox (Eq. 13.46, Fig. 13.38) for the displacement of a rectangle embedded below the surface.

13.8.4 Approximations for Vertical Displacement of Rigid Loaded Areas

According to Fox (1948b) the vertical displacement of a rigid loaded area may be approximated by the mean vertical displacement of the uniformly loaded flexible area of the same shape and dimensions.

According to Schleicher (1926), the vertical displacement of rigid footings is about 7 per cent smaller than the mean displacement of flexible footings.

Davis and Taylor (1962) make the following recommendations for the vertical displacement of rigid loaded areas:

For circle and strip:

$$\rho_{z\text{-rigid}} \simeq \frac{1}{2}[\rho_{z\text{-centre}} + \rho_{z\text{-edge}}]_{\text{flexible}} \tag{13.89}$$

For rectangle:

$$\rho_{z\text{-rigid}} \simeq \frac{1}{3}[2\rho_{z\text{-centre}} + \rho_{z\text{-corner}}]_{\text{flexible}} \tag{13.90}$$

Hidden page

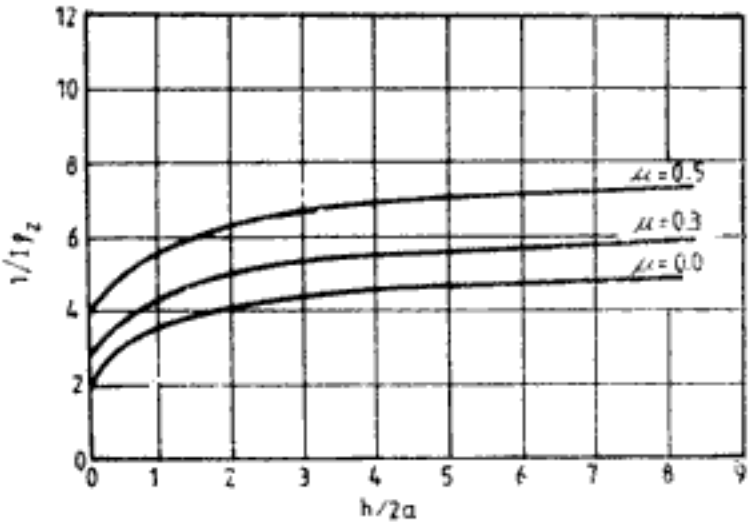

Fig. 13.97 Displacement factor for vertical displacement of embedded rigid circle

$$\rho_z = \frac{Q_v\,(1+\mu)}{Ea} I_{\rho z}$$

(After Butterfield and Banerjee, 1971; with permission of Southeast Asian Geotechnical Society, Bangkok)

1. *Concept of characteristic point*

For flexible loaded areas, the vertical displacement under uniform vertical loading, is maximum at the centre and is minimum at the corner in rectangles or at the edge in circles. Rigid loaded areas undergo uniform displacement. The displacement at a particular point on a flexible loaded area tends to be the same as the uniform displacement of a rigid loaded area, both having the same area and shape and bearing the same total load. This point is called the characteristic point. The characteristic points for rectangles and circles are shown in Fig. 13.101. (Grasshoff, 1955—vide Szechy and Varga, 1978). Table 13.44 gives the values of σ_z/q for points below the characteristic point in case of rectangles (Kany, 1959).

Q 13.13: To determine the displacement of a rigid rectangle resting on the surface of a semi-infinite elastic mass with parameters $E = 200$ kg/cm² and $\mu = 0.5$. Dimensions of rectangle are 4 m × 2 m. Total vertical load on the rectangle is 60 T.

Ans: $L/B = 4/2 = 2$

From Fig. 13.87 $\beta_z = 1.09$

Substituting in Eq. 13.79 the vertical displacement is,

$$\rho_z = \frac{60\times(1-0.5^2)}{1.09\times 2000\times\sqrt{2\times 4}} = 7.3\times 10^{-3}\ \text{m} = 7.3\ \text{mm}$$

Approximate methods

Method 1. For a flexible loaded area of same dimensions,

$$q = 60/(4\times 2) = 7.5\ \text{T/m}^2$$

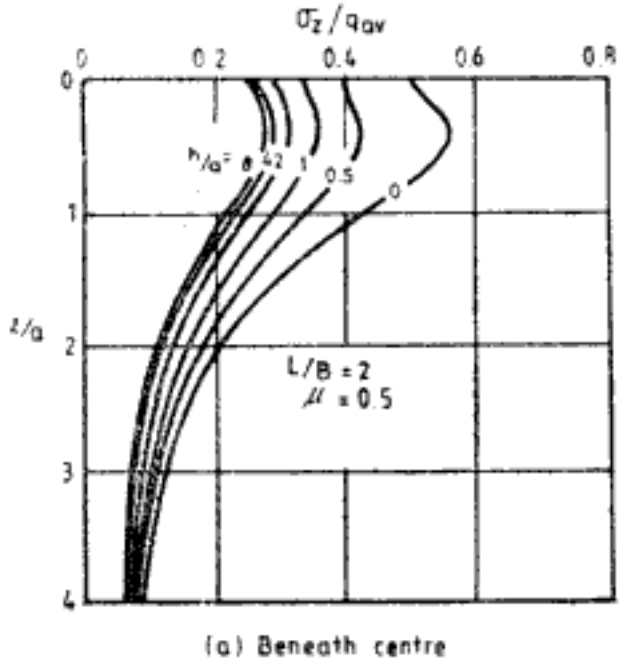

(a) Beneath centre

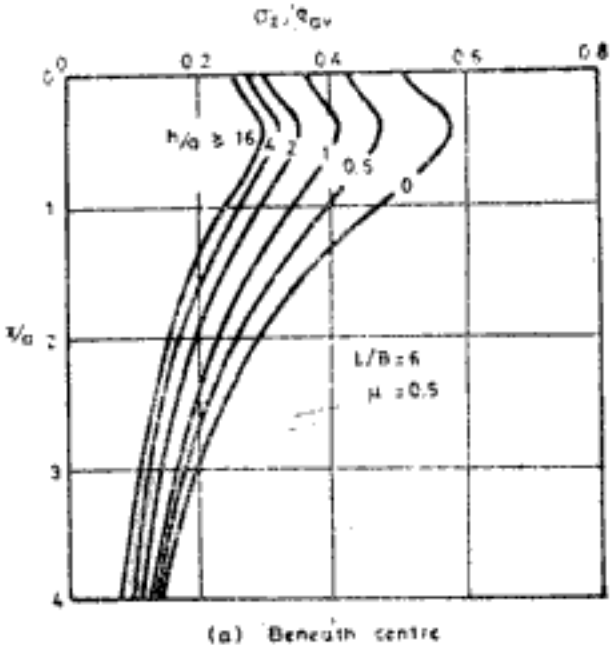

(a) Beneath centre

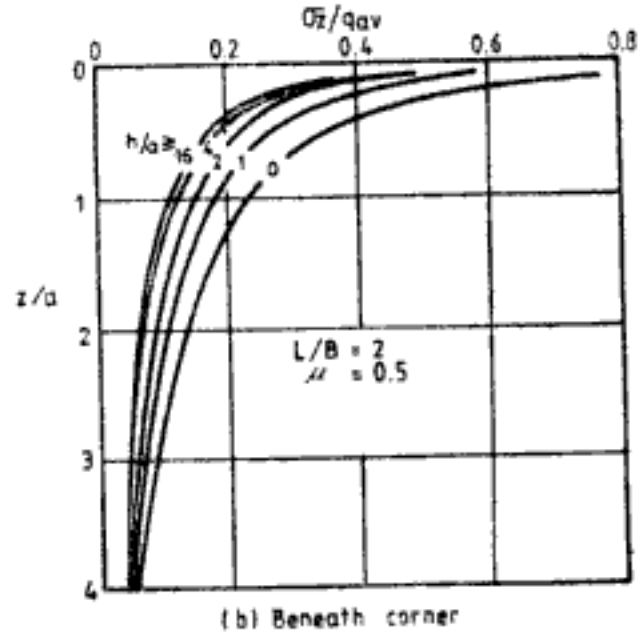

(b) Beneath corner

Fig. 13.98 Vertical stress beneath embedded rigid rectangle (After Butterfield and Banerjee 1971; with permission of Southeast Asian Geotechnical Society, Bangkok)

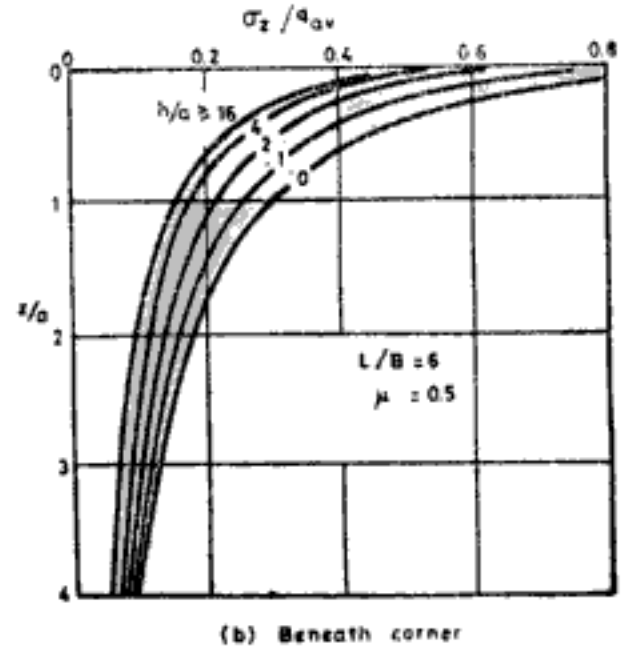

(b) Beneath corner

Fig. 13.99 Vertical stress beneath embedded rigid rectangle (After Butterfield and Banerjee, 1971; with permission of Southeast Asian Geotechnical Society, Bangkok)

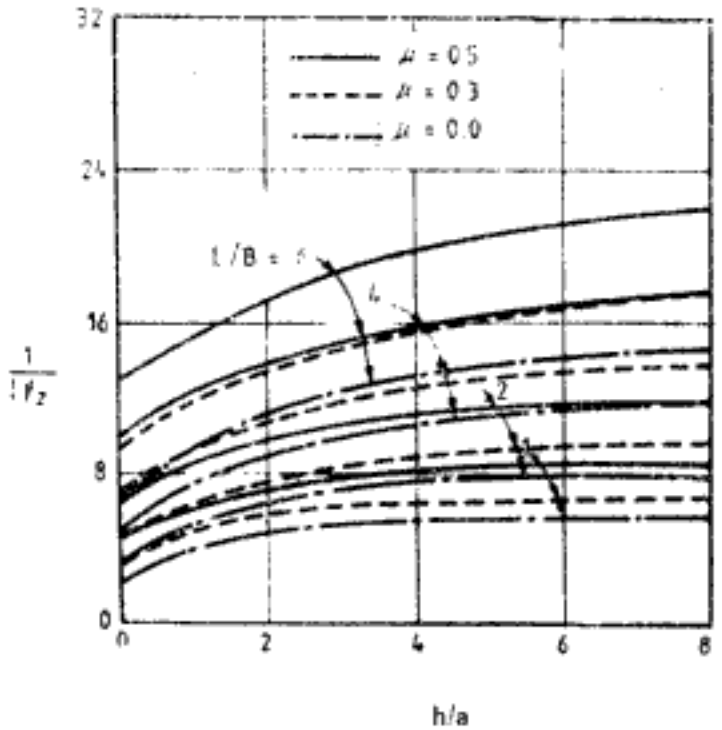

Fig. 13.100 Displacement factor for vertical displacement of embedded rigid rectangle

$$\rho_z = \frac{2Q_v(1+\mu)}{Ea} I_{\rho z}$$

(After Butterfield and Banerjee, 1971; with permission of Southeast Asian Geotechnical Society, Bangkok)

Table 13.44 Vertical Stresses σ_z/q Under the Characteristic Point of Rectangles

z/B \ L/B	1	1.5	2	3	5	10	∞
0.05	0.98	0.98	0.99	0.99	0.99	0.99	0.99
0.10	0.90	0.93	0.94	0.94	0.94	0.94	0.94
0.15	0.79	0.84	0.86	0.88	0.88	0.88	0.88
0.2	0.69	0.76	0.79	0.81	0.82	0.83	0.83
0.3	0.56	0.62	0.66	0.71	0.73	0.74	0.74
0.5	0.41	0.46	0.50	0.56	0.60	0.63	0.63
0.7	0.32	0.37	0.40	0.45	0.51	0.55	0.56
1	0.23	0.28	0.31	0.35	0.40	0.45	0.47
1.5	0.14	0.18	0.21	0.24	0.28	0.33	0.36
2	0.09	0.13	0.15	0.17	0.21	0.25	0.29
3	0.05	0.07	0.08	0.10	0.13	0.16	0.20
5	0.02	0.03	0.03	0.05	0.06	0.08	0.13
7	0.01	0.01	0.02	0.03	0.04	0.05	0.09
10	~0	0.01	0.01	0.01	0.02	0.03	0.06
20		~0	~0	~0	0.01	0.01	0.03

After Kany, 1959.

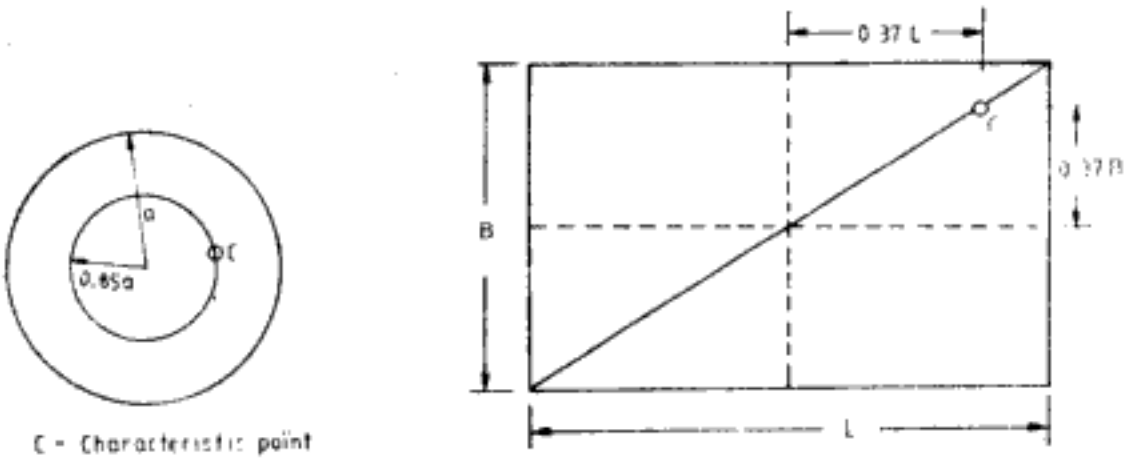

C = Characteristic point
(Any point on the inner circle shown is a characteristic point)

(There are three more such characteristic points towards each corner)

Fig. 13.101 Characteristic points for circle and rectangle

For vertical displacement at the centre of loaded area (Fig. 13.20),

$$l = 2 \text{ m}, \quad b = 1 \text{ m}, \quad l/b = 2 = \text{m}, \quad n = 0$$

From Table 13.17 $A_1 = 1.532, \quad B_1 = 0$

Substituting in Eq. 13.30

$$I_{\rho z} = \frac{(1 - 0.5^2)}{2} \times 1.532 = 0.5745$$

Substituting in Eq. 13.29 and multiplying by 4

$$\rho_{z(\text{centre})} = 4 \times \frac{7.5 \times 1}{2000} \times 0.5745 = 8.62 \times 10^{-3} \text{ m} = 8.62 \text{ mm}$$

For vertical displacement at the corner of loaded area,

$$b = 2 \text{ m}, \quad l = 4 \text{ m}, \quad \text{i.e.,} \quad m = 2, \quad n = 0 \quad \text{and} \quad I_{\rho z} = 0.5745$$

From Eq. 13.29

$$\rho_{z(\text{corner})} = \frac{7.5 \times 2}{2000} \times 0.5745 = 4.31 \times 10^{-3} \text{ m} = 4.31 \text{ mm}$$

From Eq. 13.90 the approximate value of the vertical displacement of a rigid loaded area is,

$$\rho_z = \frac{1}{3}(2 \times 8.62 + 4.31)$$

$$= 7.18 \text{ mm}$$

The same result could be obtained using Giroud's equation (Eq. 13.31) and deflection factors (Table 13.18).

Method 2. The mean displacement of flexible loaded area can also be computed from Fox's results.

$$\sqrt{B/L} = \sqrt{2/4} = \sqrt{0.5} = 0.707$$

From Fig. 13.41, $I_{\rho z} \simeq 0.915$

Hidden page

13.9 LOADED AREAS ON WESTERGAARD MATERIAL

Westergaard material is a semi-infinite mass which cannot deform in the lateral direction but is free to deform in the vertical direction. The Westergaard solutions are applicable in cases of soil mass reinforced by numerous thin rigid layers of cemented material and in over-consolidated clays (where $E_h > E_v$) within the overconsolidation range.

13.9.1 Point Load on Surface of Semi-infinite Mass (Fig. 13.2)

The vertical stress at a point within the half-space is given by,

$$\sigma_z = \frac{P}{z^2} K_W \tag{13.91}$$

where $K_W = \frac{1}{2\pi\eta^2}\left[\left(\frac{r}{\eta z}\right)^2 + 1\right]^{-3/2}$

$$\eta = \sqrt{\frac{(1-2\mu)}{2(1-\mu)}}$$

μ = Poisson's ratio of soil between rigid sheets.

Table 13.45 gives the values of K_W. It can be noted that unlike Boussinesq's solution (for homogeneous semi-infinite mass) the stresses are dependent on elastic parameter μ.

Table 13.45 Values of K_W (Eq. 13.91)

r/z	K		
	$\mu = 0$	$\mu = 0.3$	$\mu = 0.45$
0.00	0.3183	0.5570	1.7567
0.10	0.3090	0.5290	1.4970
0.25	0.2668	0.4140	0.7986
0.50	0.1733	0.2170	0.2411
0.75	0.1028	0.1089	0.0908
1.00	0.0612	0.0584	0.0421
2.00	0.0118	0.0096	0.0058
3.00	0.0038	0.0030	0.0018
4.00	0.0017	0.0013	0.0007
5.00	0.0009	0.0007	0.0004
10.00	0.0001	—	—

13.9.2 Uniformly Loaded Circular Area (Fig. 13.15)

The vertical stress along the axis of the circle of radius a is given by

$$\sigma_z = q\left[1 - \left\{1 + \left(\frac{a}{z}\right)^2\right\}^{-3/4}\right] = qI_{oz} \tag{13.92}$$

Values of I_{oz} are given in Table 13.46.

13.9.3 Uniform Vertical Loading on Rectangle (Fig. 13.20)

The vertical stress at a point z below the corner of the rectangle is given by the equation,

$$\sigma_z = qI_{oz} \tag{13.7}$$

Hidden page

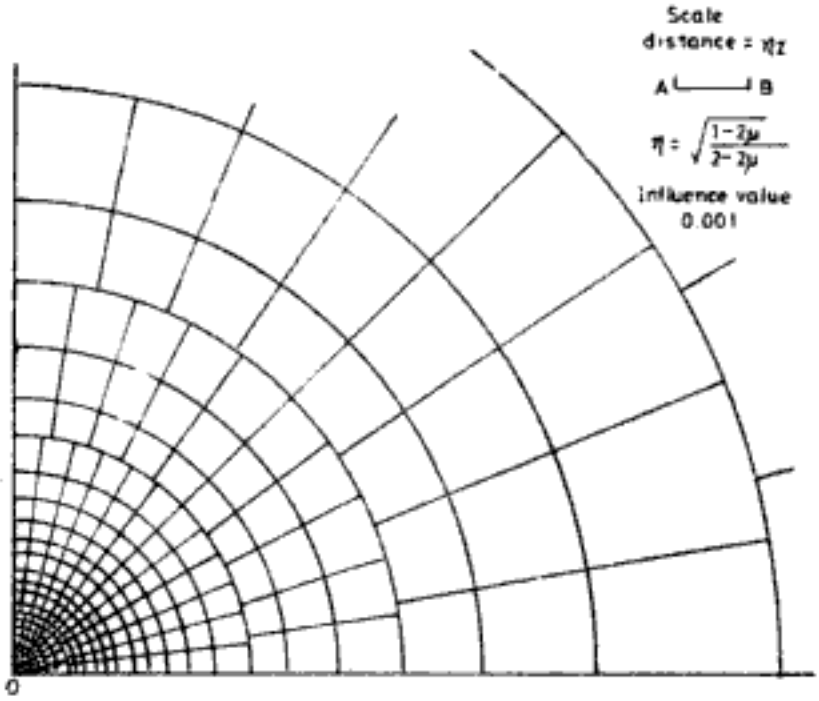

Fig. 13.103 Influence chart for vertical stress in Westergaard material (After Fenske, 1900)

13.10 LOADED AREAS BENEATH THE SURFACE IN WESTERGAARD MATERIAL

13.10.1 Vertical Point Load (Fig. 13.104)

The vertical stress at a radial distance r and at depth z below the surface due to a point load Q acting at depth h ($h < z$) below the surface is given by (Westergaard, 1938)

$$\sigma_z = \frac{Q}{4\pi}\left[\frac{\eta(z-h)}{\{r^2+\eta^2(z-h)^2\}^{3/2}} + \frac{\eta(z+h)}{\{r^2+\eta^2(z+h)^2\}^{3/2}}\right] \tag{13.93}$$

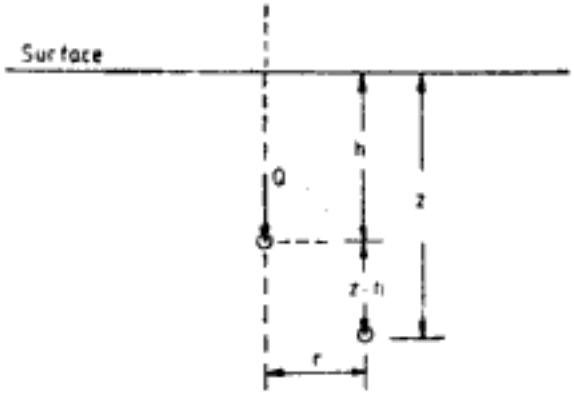

Fig. 13.104 Vertical load beneath the surface in Westergaard medium

13.10.2 Uniform Vertical Loading on Circle (Fig. 13.35)

The vertical stress along the axis of the circle can be obtained from the following equation (Babu Shanker, 1977),

$$\sigma_z = qI_{oz} \tag{13.7}$$

where $$I_{oz} = 1 - \frac{1}{2}\left[\frac{\eta(m-1)}{\{n^2+\eta^2(m-1)^2\}^{1/2}} + \frac{\eta(m+1)}{\{n^2+\eta^2(m+1)^2\}^{1/2}}\right]$$

$m = z/h \quad n = a/h$

13.10.3 Uniform Vertical Loading on Rectangle (Fig. 13.37)

The vertical stress at a point below the corner of the rectangle, z from the surface is given by,

$$\sigma_z = qI_{oz} \tag{13.7}$$

where $$I_{oz} = \frac{1}{4\pi}\left[\sin^{-1}\left\{\frac{m^2n^2}{m^2n^2 + K_1^2m^2 + K_1^2n^2 + K_1^4}\right\}^{1/2} + \sin^{-1}\left\{\frac{m^2n^2}{m^2n^2 + K_2^2m^2 + K_2^2n^2 + K_2^4}\right\}^{1/2}\right]$$

$K_1 = \eta(1 - h/z) \quad K_2 = \eta(1 + h/z)$

$m = l/z \quad n = b/z \quad m$ and n are interchangeable.

Stresses at other points can be determined by the principle of superposition.

13.11 LOADED AREAS ON NON-HOMOGENEOUS ELASTIC BODY

13.11.1 Semi-infinite Mass with Linear Increase in Modulus with Depth

1. *Uniform vertical loading or strip* (Fig. 13.105)

Gibson (1967) considers the case of an elastic half space with constant Poisson's ratio but the shear modulus G increasing linearly with depth according to the relationship,

$$G(z) = G(0) + mz \tag{13.94}$$

For the case of a linear increase in G with depth starting from zero at the surface (i.e., $G(0) = 0$; $\beta = 0$), the vertical displacement when $\mu = 0.5$ is given by,

$$\rho_z = \frac{q}{2\pi m}\left[\tan^{-1}\left(\frac{b+x}{z}\right) + \tan^{-1}\left(\frac{b-x}{z}\right)\right] \tag{13.95}$$

The vertical displacement profile at different depths within the medium is shown in Fig. 13.106.

It may be noted that the stresses are identical in cases of homogeneous elastic half space and non-homogeneous medium with modulus increasing linearly with depth beginning from zero at the surface, when $\mu = 0.5$ in both the cases. This conclusion regarding the two media are valid for all cases of surface loading (i.e., square, circular, etc.). Further when $\beta = 0$ and $\mu = 0.5$ the surface displacement of loaded area is uniform (See in Fig. 13.106 the curve for $z/b = 0$) i.e., the medium behaves as a Winkler medium.

Hidden page

Hidden page

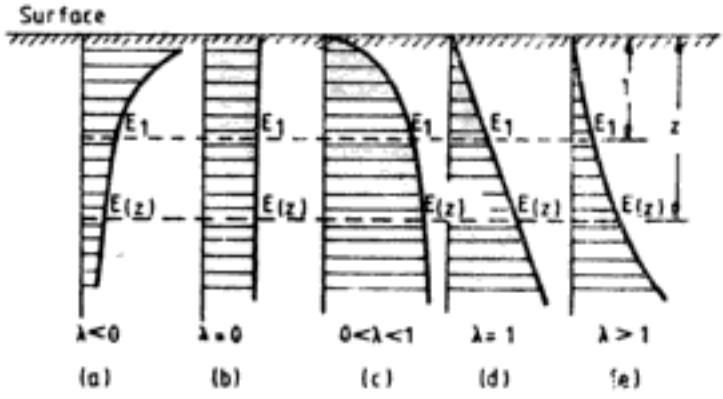

Fig. 13.109 Types of variation of modulus with depth

13.12.1 Vertical Point Load on the Surface (Fig. 13.2)

According to Holl (1940) the vertical stress at a point is given by,

$$\sigma_z = \frac{nQz^n}{2\pi R^{n+2}} \tag{13.98}$$

Equation 13.98 is valid for $n > 2$.

13.12.2 Uniform Vertical Loading on Circles and Rectangles on the Surface (Figs 13.15 and 13.20)

The ratio of vertical stress to the uniform pressure on the surface (σ_z/q) for points below the centre of circle and for points below the centre of rectangle are given in Table 13.47.

Table 13.47 Values of σ_z/q Below Centre of Loaded Areas

$$n = 1 + 1/\mu$$

n	z/a	Circle radius $=a$	Rectangle ($m = b/a$) ($2a \times 2b$) $m=1$	$m=2$	$m=3$	$m=10$	Infinite strip $m=\infty$
4	0	1	1	1	1	1	1
	0.25	0.996	0.942	0.950	0.957	0.970	0.984
	0.5	0.960	0.792	0.824	0.852	0.876	0.884
	1	0.750	0.426	0.547	0.581	0.603	0.625
	1.5	0.518	0.255	0.372	0.404	0.437	0.457
	2	0.360	0.142	0.230	0.281	0.316	0.357
	3	0.109	0.074	0.135	0.175	0.214	0.245
	5	0.077	0.025	0.048	0.063	0.125	0.150
5	0	1	1	1	1	1	1
	0.25	0.998	0.984	0.987	0.988	0.991	0.993
	0.5	0.982	0.859	0.830	0.902	0.922	0.925
	1	0.817	0.508	0.625	0.657	0.676	0.686
	1.5	0.591	0.298	0.404	0.443	0.480	0.510
	2	0.429	0.164	0.249	0.294	0.333	0.411
	3	0.229	0.089	0.150	0.192	0.243	0.282
	5	0.096	0.032	0.062	0.088	0.141	0.162

After Klein, 1956.

Hidden page

Hidden page

Hidden page

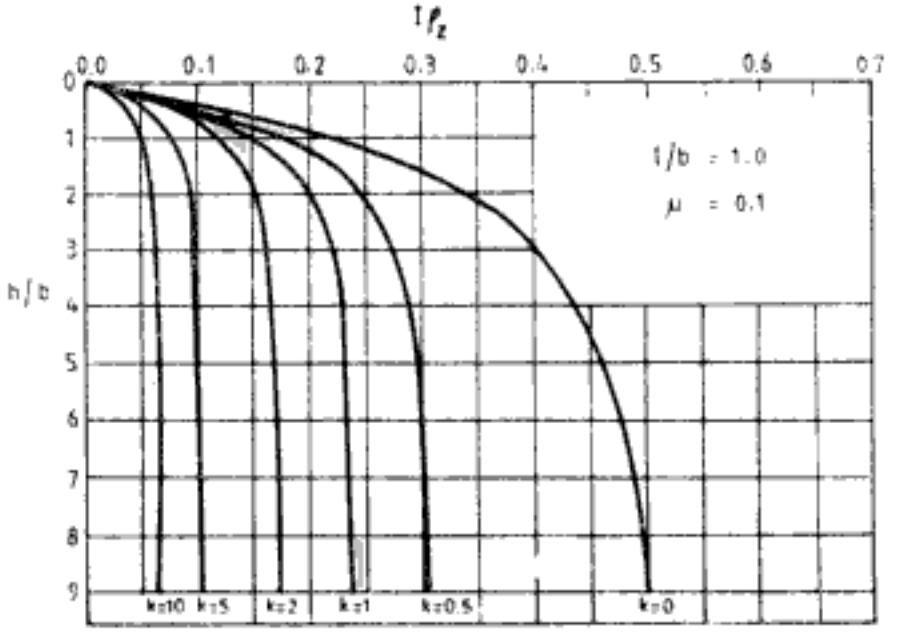

Fig. 13.116 Displacement factor for corner of rectangle: $l/b = 1$, $\mu = 0.1$ (After Butler, 1975)

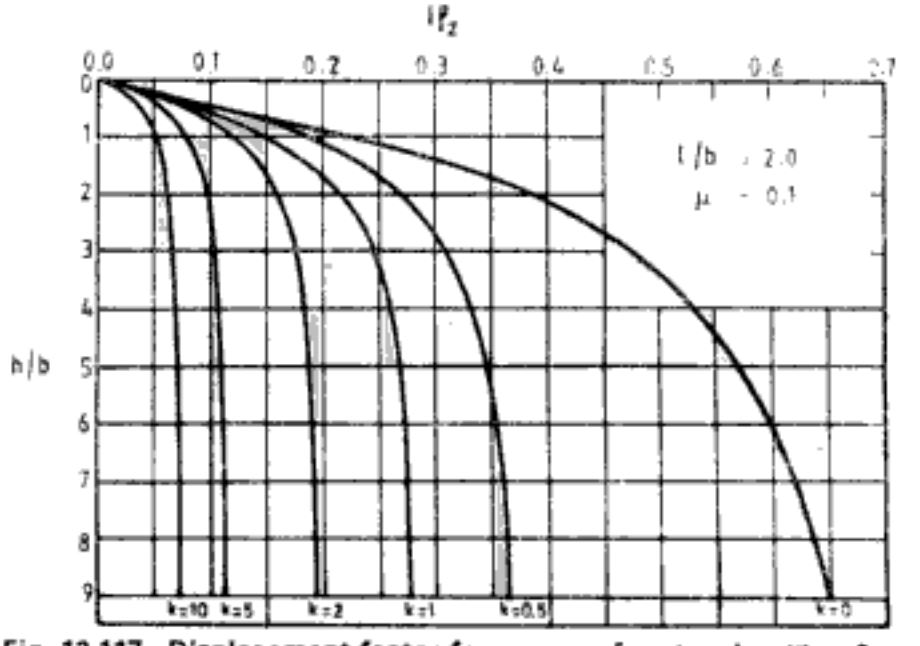

Fig. 13.117 Displacement factor for corner of rectangle: $l/b = 2$, $\mu = 0.1$ (After Butler, 1975)

13.14 APPROXIMATE DETERMINATION OF STRESS DISTRIBUTION

In the approximate method, at any depth the total load is assumed to be distributed over an area of the same shape of the loaded area but with dimensions increasing by an amount equal to the depth below the loaded area (Fig. 13.119).

The method is useful for rough and preliminary calculations. The discrepancy between the approximate method and rigorous method decreases as the depth considered in relation to the size of the loaded area increases.

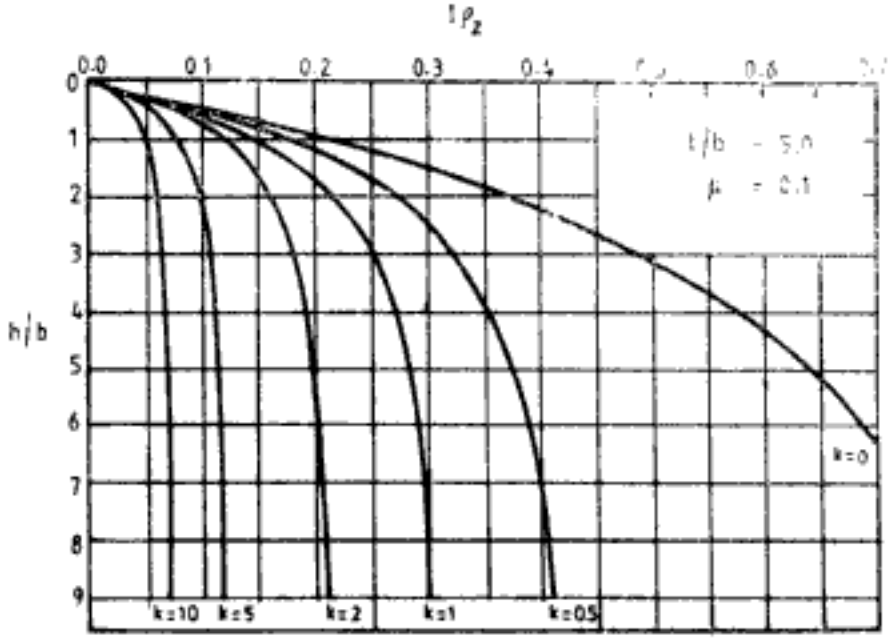

Fig. 13.118 Displacement factor for corner of rectangle; $l/b = 5$, $\mu = 0.1$ (After Butler, 1975)

The approximate method can be used in stratified soil as shown in Fig. 13.120. In order to determine the stress distribution in the clay deposit below sand layer, a reduced uniform vertical pressure on an enlarged size of footing using the principle of approximate method in Fig. 13.119 is considered on the top of the clay deposit. The rigorous analyses and solutions can be now used for stress distribution and displacement in the clay deposit.

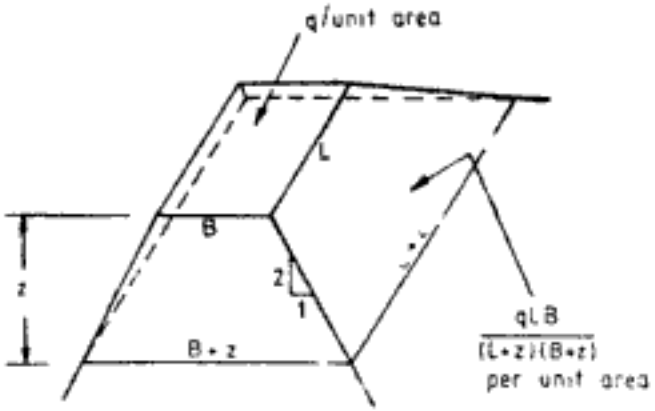

Fig. 13.119 Approximate method of determination of vertical stress in soil

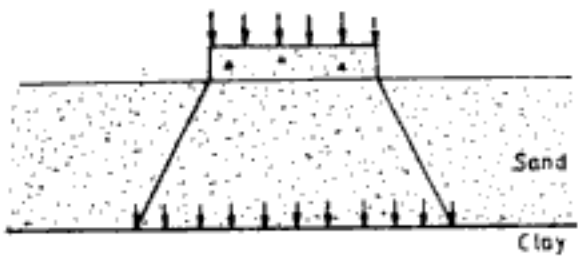

Fig. 13.120 Approximate method for stress distribution in stratified soil

14

SETTLEMENT OF SHALLOW FOUNDATIONS

14.1 COMPONENTS OF TOTAL SETTLEMENT

Figure 14.1 shows the time versus settlement relationship for a loaded area. The settlement increases with time and the ultimate total vertical settlement, ρ_t can be expressed as

$$\rho_t = \rho_i + \rho_c + \rho_s + \rho_{cr} \tag{14.1}$$

where ρ_i = the immediate or elastic settlement, which occurs immediately (or within a short time) after application of the load

ρ_c = settlement due to primary consolidation of the soil, which occurs due to dissipation of excess pore water pressure in the soil. In the process some pore-water is expelled, voids within the soil decrease in size and effective stress increases

ρ_s = settlement due to secondary consolidation of soil. The settlement occurs under constant effective stress, with change in volume of soil, due to yielding, compressing and rearrangement of particles.

ρ_{cr} = settlement due to creep of soil which occurs at constant effective stress and at constant volume.

t_{100} is the time when the excess pore water pressure is completely dissipated indicative of the completion of primary consolidation and the beginning of secondary consolidation and creep settlements.

The time-settlement relationship shown in Fig. 14.1 is applicable to all soils. However, the time scale and the relative magnitudes of the components of settlement differ for different soil types. For example, in sand the immediate settlement forms nearly 100 per cent of the total settlement. In inorganic normally consolidated clays, primary consolidation settlement is the largest component. In the case of organic clays, total settlement is largely composed of secondary consolidation settlement.

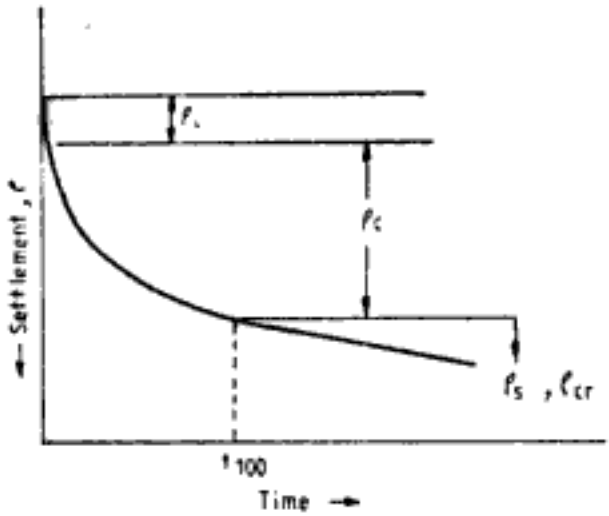

Fig. 14.1 Time-settlement relationship in soils

14.2 CLASSIFICATION OF SETTLEMENT COMPUTATION PROCEDURES

The settlement computation procedures can be classified as follows:

1. *Elastic displacement method:* In this case the solutions are derived by the integration of displacement due to elementary force. There is no need to compute the stresses in this method. The displacement formulae given in Ch. 13 come under this category.

2. *Elastic strain summation method*: This method is based on the theoretical relationship between stresses and vertical strain ϵ_z, i.e.,

$$\epsilon_z = \frac{1}{E}[\sigma_z - \mu(\sigma_x + \sigma_y)] \tag{14.2}$$

and thus $$\rho_z = \Sigma \epsilon_z \Delta h$$

In Eq. 14.2 stresses are entered from stress distribution theories. Under identical boundary conditions methods (i) and (ii) give the same solution since the underlying principle is the same. However, for complex boundary conditions method (ii) is more suitable.

It is also a common practice in this method to assume $\mu = 0$ (i.e., a one-dimensional vertical compression) in the calculation of ϵ_z.

3. *Based on laboratory or field test results*: The use of the formulae or equation in this method cannot be separated from laboratory or field testing of the deformation characteristics of the soil. Whereas in methods (i) and (ii) the deformation characteristics are determined separately.

4. *Simplified procedures:* These are not based on rigorous theories. Based on empirical observation they are found to give adequate results.

5. *Finite element method:* A procedure which is generally computer-oriented and requires data on stress-strain characteristics of the soil.

14.3 SETTLEMENT OF SHALLOW FOUNDATIONS IN INORGANIC CLAY

In inorganic types of deposits, the secondary consolidation and creep effects are either

negligible or absent. Hence total settlement is given by,

$$\rho_t = \rho_i + \rho_c \tag{14.3}$$

The details of computation of ρ_i and ρ_c are explained here.

14.3.1 Computation of Immediate Settlement, ρ_i

The most common practice of calculation of immediate settlement is to use the appropriate equation or formula for elastic displacement explained in Ch. 13. Thus, for example, the immediate settlement of a rigid circular concrete footing can be obtained from Eq. 13.71 if the footing rests on or near the surface of a homogeneous deep soil deposit. Thus it is assumed that the immediate displacement can be obtained from theory of elasticity.

Further, because of the very nature of the phenomenon, the elastic constants E and μ correspond to undrained conditions of loading. Thus $E = E_u$ (i.e., Young's modulus of soil under undrained conditions of loading) is used in the displacement equations.

The different procedures of determination of E and μ for such situations are explained in Sec. 9.8.

14.3.2 Computation of Primary Consolidation Settlement, ρ_c

1. *Elastic displacement method*

Here again, the *total* settlement can be first computed using the appropriate equation or formula for elastic displacement explained in Ch. 13. The primary consolidation settlement can be obtained as the difference of total and immediate settlement of the foundation. However, for total settlement calculations it is necessary to use the Young's modulus E_d appropriate to drained loading and the μ of the mineral skeleton.

This method is not, however, so popular as in the case of immediate settlement. The reason being, the immediate settlement is reasonably elastic in nature whereas total or primary consolidation settlement is not.

2. *Primary consolidation settlement computations using compressibility characteristics of soil obtained from oedometer tests*

Typical test results (e-log $\bar{\sigma}$ curve, Fig. 7.9) and compressibility characteristics (a_v, m_v, C_c) that can be obtained from one-dimensional consolidation tests on high quality undisturbed samples are explained in Sec. 7.1. The concept of normally, over- and under-consolidated soils (Fig. 7.42) is also described in Ch. 7. In order to use the data from oedometer experiments it is first necessary to ascertain the preconsolidation pressure of the soil. By comparing the preconsolidation pressure with the effective vertical overburden pressure at various depths, the nature or type of deposit could be determined (Fig. 7.42). With a knowledge of the stress increase in the soil due to foundation loading and the type of the deposit, appropriate procedure can be used for the determination of primary consolidation settlement. The stress increase can be calculated using equations or formulae given in Ch. 13. The method of obtaining preconsolidation pressure is as follows.

(a) *Determination of preconsolidation pressure*

Among the many methods that have been suggested, Casagrande's (1936) graphical technique is the widely used method. Indian Standards Code (IS: 8009, Part I, 1976) also recommends this method. Other graphical methods include those due to Burmister (1951) and Schmertmann (1955). Only Casagrande's procedure is explained here.

Standard one-dimensional consolidation test is carried out on a high quality undisturbed soil sample. The e versus log $\bar{\sigma}$ curve is plotted (Fig. 14.2). On this curve the point O corresponding to the minimum radius of curvature or maximum curvature is chosen. At this point a horizontal line (OA) is drawn. Also a tangent (OB) to the curve at point O is drawn. A bisector (OC) to the angle AOB is then drawn. The straight line portion of the e-log $\bar{\sigma}$ curve is projected backwards which intersects the bisector OC at point D. The $\bar{\sigma}$ value corresponding to this point of intersection D is the maximum preconsolidation pressure $\bar{p}_c$ which the soil has experienced in the past.

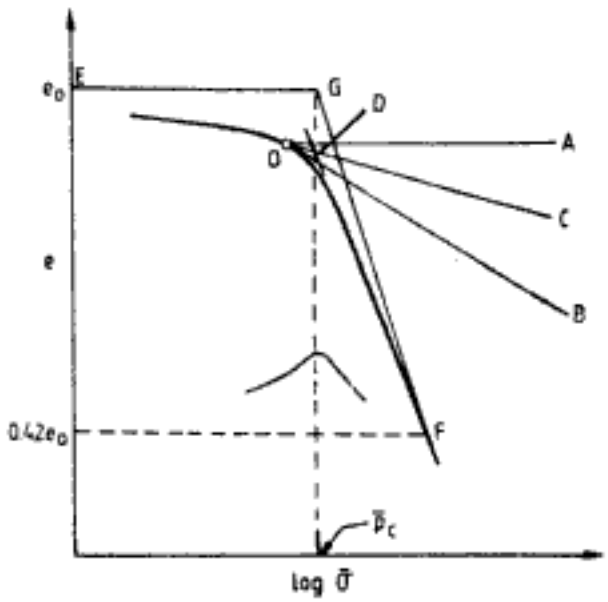

Fig. 14.2 Determination of preconsolidation pressure

In this procedure the point of maximum curvature O is chosen by visual judgement. The following procedure can be used to ascertain the correctness of this arbitrary selection.

The sample has an initial void ratio e_0. This is marked as point E in Fig. 14.2. From this point a horizontal line is drawn. On the horizontal line from E the point G corresponding to $\bar{p}_c$ determined earlier is located. On the e-log $\bar{\sigma}$ curve the point F corresponding to $0.42\,e_0$ is located. F and G are connected by a straight line. The vertical distance between EGF and the e-log $\bar{\sigma}$ curve is plotted along log $\bar{\sigma}$ axis. If this plot is nearly a symmetrical curve about $\bar{p}_c$ then it may be concluded that the point O has been chosen correctly. Otherwise a new point is chosen and the procedure is repeated.

The procedure of determination of preconsolidation pressure is illustrated in Q 14.1.

Q 14.1: Consolidation test data on an undisturbed soil sample recovered at a depth of 23 m at Farakka are as follows:

$\bar{\sigma}$ kg/cm²	0.05	0.1	0.2	0.5	1.0	2.0	1.0	0.5
e	0.717	0.716	0.714	0.709	0.693	0.665	0.668	0.672
$\bar{\sigma}$ kg/cm²	0.2	0.1	0.2	0.5	1.0	2.0	4.0	8.0
e	0.678	0.683	0.682	0.681	0.674	0.663	0.628	0.574

To determine the preconsolidation pressure.

Ans: The preconsolidation pressure determined using Casagrande's method is shown in Fig. 14.3. $\bar{p}_c = 1.5$ kg/cm^2.

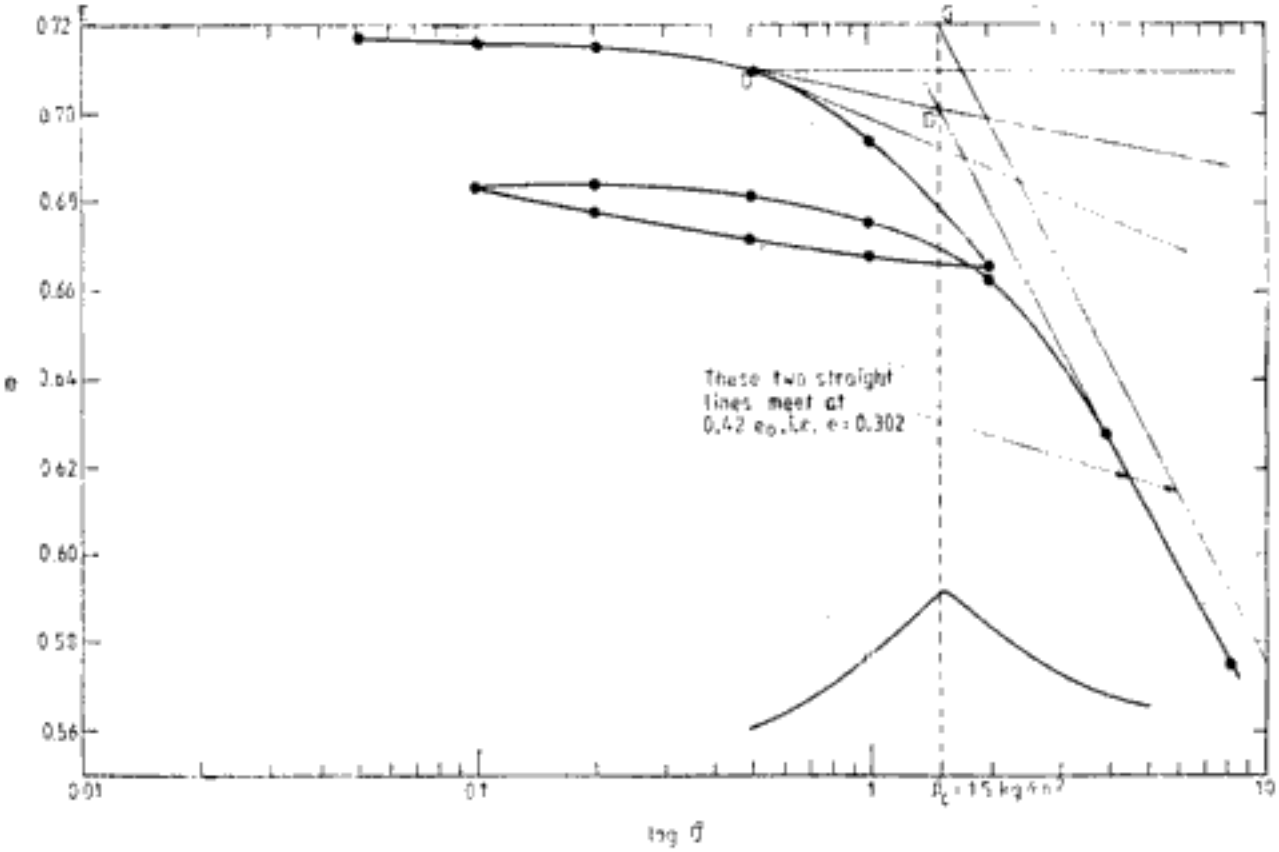

Fig. 14.3 Q 14.1

(b) *Reconstruction of field compression curve from e-log $\bar{\sigma}$ curve determined in the laboratory*
The *e*-log $\bar{\sigma}$ curve so far described which is obtained from consolidation experiments does not fully represent the actual behaviour of the soil sample had it undergone the same stress changes in the field. The reason is that the operations like extraction of sample, insertion in consolidation ring, cutting and trimming of sample, etc., even at the best of conditions tend to disturb the true state of *in situ* soil and consequently its deformation characteristics in the laboratory experiments are somewhat affected. However, the true field compression of the soil can be reconstructed by using empirical procedures evolved by Schmertmann (1955).

In order to use these procedures, the *e*-log $\bar{\sigma}$ curve from experiments is first plotted. The preconsolidation pressure, $\bar{p}_c$, is then determined. The existing vertical effective stress, $\bar{p}_0$, in field at the level of the sample is computed from a knowledge of depth, soil densities, ground water level, etc.

If $\bar{p}_0 = \bar{p}_c$, the soil is normally consolidated
If $\bar{p}_0 < \bar{p}_c$, the soil is overconsolidated
If $\bar{p}_0 > \bar{p}_c$, the soil is underconsolidated (see also Fig. 7.42).

The following procedures can then be used to determine the respective field compression curves.

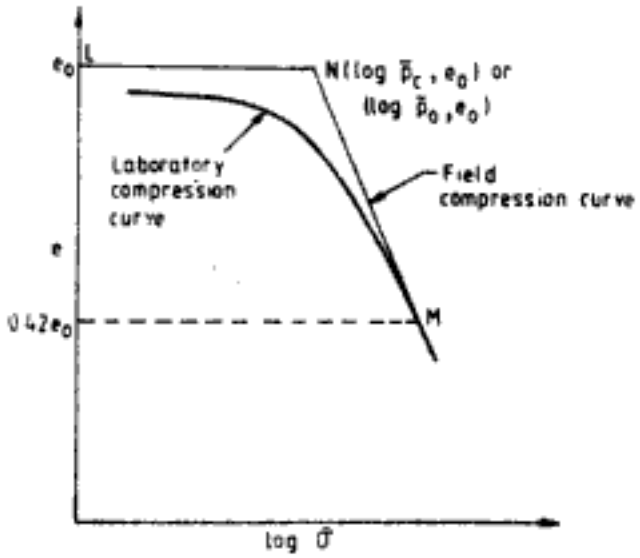

Fig. 14.4 Field and laboratory compression curves for normally consolidated clay

Normally consolidated clays (Fig. 14.4)

The following steps are carried out:

(i) A horizontal line at constant void ratio of $e = e_0$ (e_0 = initial void ratio of sample) is drawn.
(ii) On this horizontal line, point N having ordinates (log $\bar{p}_c$, e_0) or (log $\bar{p}_0$, e_0) is located.
(iii) On the laboratory compression curve point M corresponding to 0.42 e_0 is located.
(iv) A straight line connecting N and M is drawn.

LNM then represents the field compression curve.

Overconsolidated clays (Fig. 14.5).

The following steps are to be followed:

(i) A horizontal line at constant void ratio of $e = e_0$ is drawn.
(ii) On this horizontal line point L having ordinates as (log $\bar{p}_0$, e_0) is located.
(iii) Through the point L a line parallel to the mean slope of the recompression cycle loop is drawn which intersects log $\bar{p}_c$ at M.
The recompression cycle is obtained by loading the sample slightly beyond $\bar{p}_c$ and then unloading it to slightly less than $\bar{p}_0$ and then reloading it.
(iv) On the laboratory compression curve point N corresponding to 0.42 e_0 is located.
(v) A straight line connecting M and N is drawn.

$KLMN$ represents the field compression curve.

Underconsolidated clays (Fig. 14.6)

The following steps are to be followed:

(i) A horizontal line at constant void ratio of $e = e_0$ is drawn.
(ii) On this horizontal line point M having ordinates (log $\bar{p}_c$, e_0) is located.

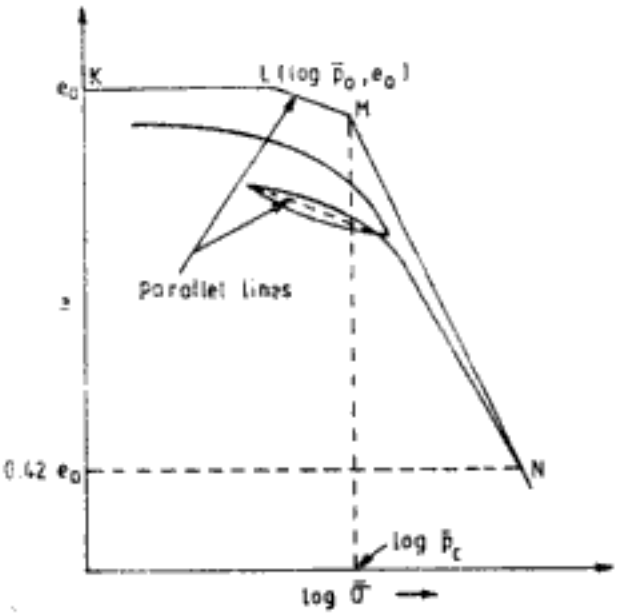

Fig. 14.5 Field and laboratory compression curves for overconsolidated clay

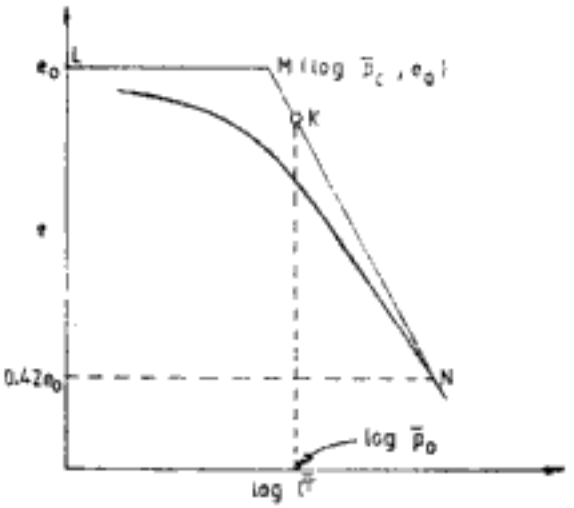

Fig. 14.6 Field and laboratory compression curves for underconsolidated clay

(iii) On the laboratory compression curve point N corresponding to 0.42 e_0 is located.
(iv) A straight line connected M and N is drawn.

LMN represents the field compression curve.

On the straight line portion MN, the point K corresponding to log $\bar{p}_0$ represents the condition that would be obtained when the soil becomes normally consolidated under the existing overburden pressure.

Calculation of primary consolidation settlement

The procedure common for all types of clays is as follows:

(i) The compressible layer is split into a number of small thickness layers (Fig. 14.7).

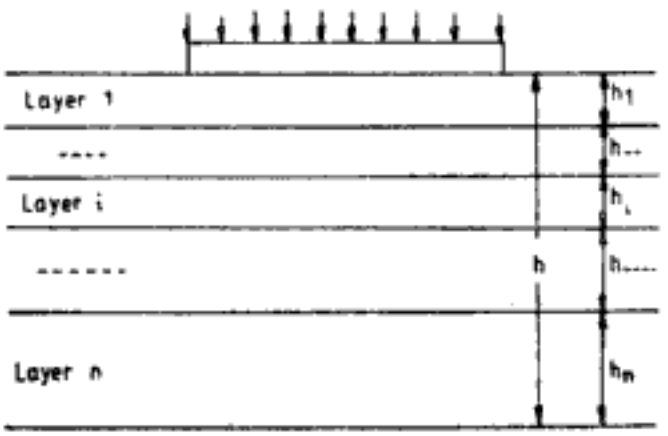

Fig. 14.7 Division of clay deposit into layers for calculation of consolidation settlement

(ii) The consolidation settlement of each layer is computed by the appropriate procedure depending on the type of clay.

(iii) The sum of the settlement of all layers gives the total consolidation settlement.

The precision of calculation increases with the increase in the number of layers. The layers need not be of equal thickness. Since a significant portion of the settlement (about 90 to 95 per cent will occur within a depth of about twice the breadth of the footing, it is preferable to have the thickness of layers small in this zone.

The procedure of calculation in each type of deposit is described below.

Normally consolidated clay: In all types of clay it is assumed that the footing is flexible. Thus the average pressure transmitted by the footing can be computed. For the flexible footing, the settlement can be computed in the following way.

(i) The vertical stress increases below the centre of footing at the middle of layer i is calculated using an appropriate formula given in Ch. 13. Let this increase in stress be $\Delta\sigma_{zi}$.

(ii) In the field compression curve (Fig. 14.8) the point A corresponds to the existing conditions ($\bar{p}_{0i}$ = existing effective overburden pressure in the middle of layer i; e_{oi} = initial void ratio in the middle of layer i). Point B corresponds to the equilibrium conditions that would be ultimately obtained due to vertical stress increase i.e., the effective stress will become ($\bar{p}_{0i} + \Delta\sigma_{zi}$).

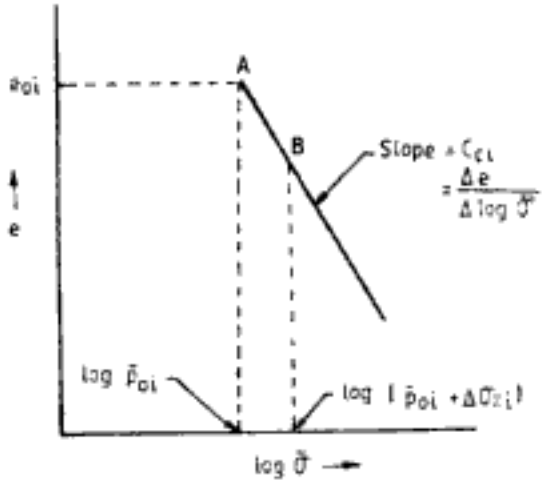

Fig. 14.8 Calculation of ρ_c in normally consolidated clay

(iii) The value of compression index C_{ci} i.e., the slope of the field compression curve is determined. If the entire thickness of soil is homogeneous and normally consolidated the C_c value of all layers will be the same.

(iv) The primary consolidation deformation of layer i can then be worked out from the following formula:

$$\rho_{c-i} = \frac{C_{ci}}{1 + e_{0i}} \log_{10}\left(\frac{\bar{p}_{0i} + \Delta\sigma_{zi}}{\bar{p}_{0i}}\right) h_i \qquad (14.4)$$

(v) The primary consolidation settlement is obtained as the sum of deformation of all layers.

$$\rho_c = \sum_{i=1}^{n} \left[\frac{C_{ci}}{1 + e_{0i}} \log_{10} \left(\frac{\bar{p}_{0i} + \Delta\sigma_{zi}}{\bar{p}_{0i}} \right) h_i \right] \tag{14.5}$$

Underconsolidated clay:

(i) Step (i) described for normally consolidated clay is carried out.

(ii) In the field compression curve point *A* (Fig. 14.9) corresponds to the existing conditions ($\bar{p}_{ci}$ = preconsolidation pressure in the middle of layer i; e_{0i} = initial void ratio in the middle of layer i). Point *B* corresponds to the equilibrium conditions that would be ultimately reached. Point *C* represents the equilibrium conditions that would be ultimately reached in the absence of any loading imposed by the foundation or in other words when the soil becomes normally consolidated under the existing overburden of soil.

(iii) Step (iii) described for normally consolidated clay is carried out.

(iv) The primary consolidation settlement of layer i is determined as,

$$\rho_{c-i} = \frac{C_{ci}}{1 + e_{0i}} \log_{10} \left(\frac{\bar{p}_{0i} + \Delta\sigma_{zi}}{\bar{p}_{ci}} \right) h_i \tag{14.6}$$

(v) The settlement in the total deposit is,

$$\rho_c = \sum_{i=1}^{n} \left[\frac{C_{ci}}{1 + e_{0i}} \log_{10} \left(\frac{\bar{p}_{0i} + \Delta\sigma_{zi}}{\bar{p}_{ci}} \right) h_i \right] \tag{14.7}$$

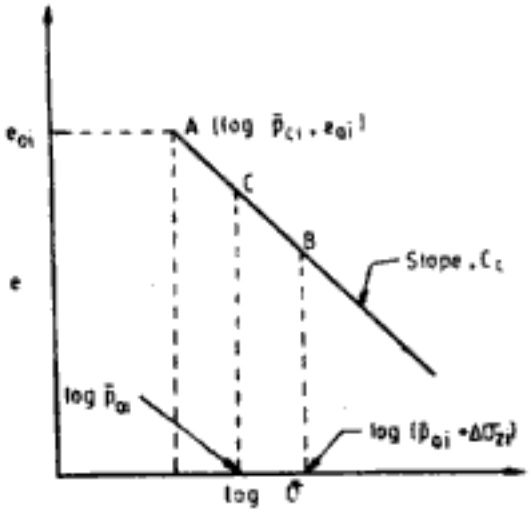

Fig. 14.9 Calculation of ρ_c in underconsolidated clay

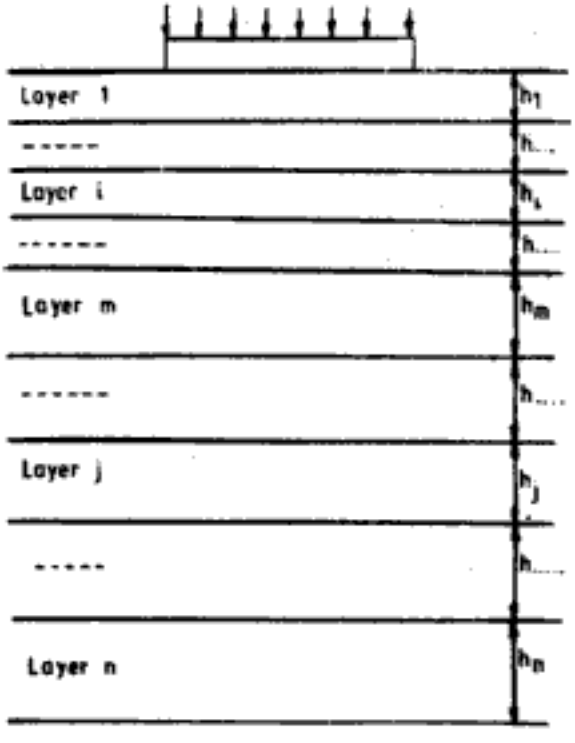

Fig. 14.10 Division of overconsolidated soil into layers for calculation of settlement

Overconsolidated clay

(i) Step (i) described for normally consolidated clay is carried out. With reference to Fig. 14.10, it can be expected in a general situation that in layers close to the footing the net effective stress due to foundation loading will exceed the preconsolidation pressure. Whereas in the deep layers the vertical stress increase will be very small and the net effective stress will be less than the preconsolidation pressure. These two situations are depicted in Figs. 14.11 and 14.12 respectively. Let layers 1 to m be the layers in which the net effective stress exceeds the preconsolidation pressure. Layer i belongs to this category. And, let layers $m + 1$ to n be the layers in which the net effective stress is less than the preconsolidation pressure. Layer j belongs to this category.

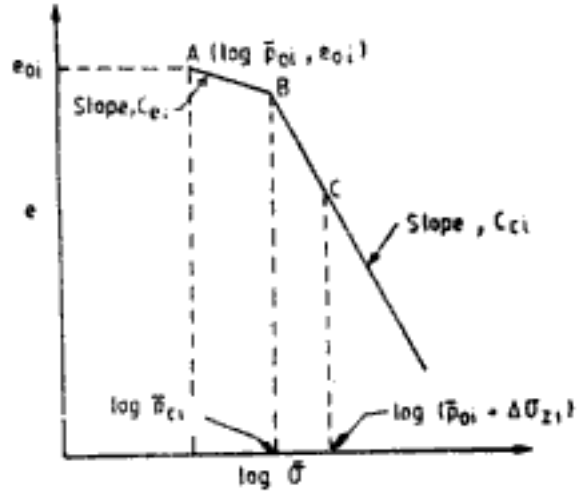

Fig. 14.11 Case of vertical stress being more than preconsolidation pressure

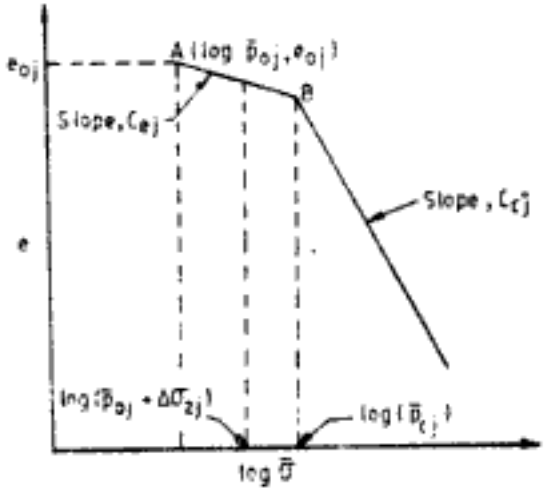

Fig. 14.12 Case of vertical stress being less than preconsolidation pressure

(ii) In Figs. 14.11 and 14.12 point A corresponds to the existing field conditions in the middle of layer i and j respectively. Point B corresponds to the equilibrium conditions that would be ultimately reached if the stress increase is equal to the difference of preconsolidation pressure and the present effective overburden pressure. Point C represents the equilibrium conditions that would be ultimately reached under the stress increase due to foundation loading.

(iii) The slopes of the field compression curves, C_{ei}, C_{ci} (Fig. 14.11) C_{ej}, C_{cj} (Fig. 14.12) are determined.

(iv) The primary consolidation settlement of layer i is given as,

$$\rho_{c-i} = \frac{C_{ei}}{1 + e_{0i}} \log_{10}\left(\frac{\bar{p}_{ci}}{\bar{p}_{0i}}\right) h_i + \frac{C_{ci}}{1 + e_{0i}} \log_{10}\left(\frac{\bar{p}_{0i} + \Delta\sigma_{zi}}{\bar{p}_{ci}}\right) h_i \tag{14.8}$$

(v) The primary consolidation settlement of layer j is given as,

$$\rho_{c-j} = \frac{C_{ej}}{1 + e_{0j}} \log_{10}\left(\frac{\bar{p}_{0j} + \Delta\sigma_{zj}}{\bar{p}_{0j}}\right) h_j \tag{14.9}$$

(vi) The total primary consolidation settlement is then obtained as,

$$\rho_c = \sum_{i=1}^{m} \left[\frac{C_{ci}}{1 + e_{0i}} \log_{10} \left(\frac{\bar{p}_{ci}}{\bar{p}_{0i}} \right) h_i + \frac{C_{ci}}{1 + e_{0i}} \log_{10} \left(\frac{\bar{p}_{0i} + \Delta\sigma_{zi}}{\bar{p}_{ci}} \right) h_i \right] + \sum_{j=m+1}^{n} \left[\frac{C_{cj}}{1 + e_{0j}} \log_{10} \left(\frac{\bar{p}_{0j} + \Delta\sigma_{zj}}{\bar{p}_{0j}} \right) h_j \right] \quad (14.10)$$

Q 14.2: A multi-storey building is to be constructed on the soil profile shown in Fig. 14.13. The structure rests on a mat foundation (12 m × 30 m) which is assumed to distribute the loads uniformly on the surface of the soil. To determine the primary consolidation settlement of the foundation in the homogeneous normally consolidated clay layer, q is the net increase in pressure.

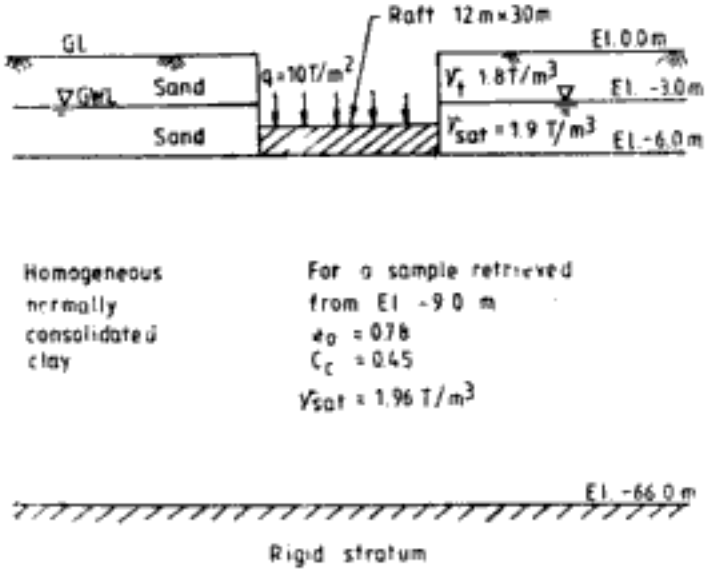

Fig. 14.13 Q 14.2

Ans: The problem will be first solved dividing the normally consolidated deposit into three layers. In the second trial the deposit will be divided into six layers.

Solution I: Column 2 of Table 14.1 gives the elevations of the three layers.
Column 3 gives the thickness of each layer.
Column 4 gives the effective overburden stress at the middle of each layer.

Table 14.1

Layer (1)	Elevation, m (2)	h_i, m (3)	$\bar{p}_{0i}$, T/m² (4)	e_{0i} (5)	$\Delta\sigma_{zi}$, T/m² (6)	ρ_{ci}, m (7)		$(\rho_{ci}/\rho_c) \times 100$ (8)	
Layer 1	−6 to −18	12	13.86	0.734	7.92	0.611	0.783	71	91
Layer 2	−18 to −30	12	25.38	0.616	3.20	0.172		20	
Layer 3	−30 to −66	36	48.42	0.490	0.80	0.077		9	
						ρ_c = 0.86 m			

Column 5 gives the initial void ratio in the middle of each layer. This is arrived at from the known value of e_0 at El. −9 m and the value of C_c. Since the soil is a homogeneous normally consolidated clay, value of C_c is constant for the whole deposit. From a knowledge

of $\bar{p}_0$ at El. -9 m ($= 10.98$ T/m^2) and value of C_c ($= 0.45$), the $e - \log \bar{\sigma}$ plot can be made, from which the e_0 value corresponding to $\bar{p}_0$ value at the middle of a layer can be obtained. Alternatively the value of e_0 at any depth z below the base of the foundation can be expressed from the definition of C_c as (since C_c is constant),

$$C_c = \frac{(e_0)_{-9} - (e_0)_z}{\log_{10} \bar{p}_{0z} - \log_{10} \bar{p}_{0(-9)}} \tag{14.11}$$

where $(e_0)_{-9}$ = value of e_0 at El. -9 m $= 0.78$

$(e_0)_z$ = value of e_0 at z below base of foundation

$\bar{p}_{0z}$ = effective overburden stress at z below base of foundation

$\bar{p}_{0(-9)}$ = effective overburden stress at El. -9 m $= 10.98$ T/m^2

On simplification, Eq. 14.11 becomes,

$$(e_0)_z = 1.2483 - 0.45 \log_{10} \bar{p}_{0z} \tag{14.12}$$

Column 6 gives the vertical stress increase below the centre of foundation at the middle of each layer obtained using Fig. 13.21. To use this figure, z is considered to be the depth to the middle of a layer from the base of the foundation.

Column 7 reports the settlement calculation using Eq. 14.4.

Column 8 gives the proportion of settlement occurring in each layer.

Solution II: The results are given in Table 14.2.

Table 14.2

Layer (1)	Elevation, m (2)	h_i, m (3)	$\bar{p}_{0i}$ T/m^2 (4)	e_{0i} (5)	$\Delta\sigma_{zi}$, T/m^2 (6)	ρ_{ci}, m (7)	$(\rho_{ci}/\rho_c) \times 100$ (8)
Layer 1	-6 to -12	6	10.98	0.780	9.20	0.401	45.8
Layer 2	-12 to -18	6	16.74	0.698	6.40	0.224	25.5
						0.807	92
Layer 3	-18 to -24	6	22.50	0.640	4.00	0.117	13.3
Layer 4	-24 to -30	6	28.26	0.595	2.60	0.065	7.4
Layer 5	-30 to -48	18	39.78	0.528	1.20	0.068	7.8
						0.07	8
Layer 6	-48 to -66	18	57.06	0.458	0.06	0.002	0.2
						$\rho_c = 0.877$ m	

Remarks: In Solutions I and II the following points are noteworthy.

(i) The primary consolidation settlement at the centre of the flexible foundation is about 0.9 m.

(ii) More than 90 per cent of the settlement occurs within a depth of twice the breadth of the foundation.

(iii) The conventional approach has been used in vertical stress increase calculations. The depth of embedment and limited thickness of clay deposit have not been considered. The depth of embedment has been considered only in effective overburden stress calculation. The soil is assumed to be a semi-infinite mass. But settlement computations are limited to the thickness of the deposit.

3. *Primary consolidation settlement calculation using coefficient of volume compressibility, m_v*
In the various types of clays, the primary consolidation settlement of a soil layer is determined using the procedures below:

Normally consolidated clay: In this case,

$$\rho_{ci} = m_{vi}\Delta\sigma_{zi}h_i \tag{14.13}$$

in which, m_{vi}, i.e., m_v of the ith layer is determined in a stress range of $\bar{p}_{0i}$ and $(\bar{p}_{0i} + \Delta\sigma_{zi})$.

Underconsolidated clay: Here,

$$\rho_{ci} = m_{vi}(\bar{p}_{0i} - \bar{p}_{ci} + \Delta\sigma_{zi})h_i \tag{14.14}$$

m_{vi}, in this case is determined in the stress range of $\bar{p}_{ci}$ and $(\bar{p}_{0i} + \Delta\sigma_{zi})$.

Overconsolidated clay: In the layers close to the base of foundation, where the net effective stress is greater than the preconsolidation pressure,

$$\rho_{ci} = m_{vi1}(\bar{p}_{ci} - \bar{p}_{0i})h_i + m_{vi2}(\bar{p}_{0i} + \Delta\sigma_{zi} - \bar{p}_{ci})h_i \tag{14.15}$$

where m_{vi1} is obtained in the stress range of $\bar{p}_{0i}$ and $\bar{p}_{ci}$, and m_{vi2} is obtained in the stress range of $\bar{p}_{ci}$ and $(\bar{p}_{0i} + \Delta\sigma_{zi})$.

In the layers deep below the footing, where the net effective stress is less than the preconsolidation pressure,

$$\rho_{cj} = m_{vj}\Delta\sigma_{zj}h_j \tag{14.16}$$

where m_{vj} is determined in the stress range of $\bar{p}_{0j}$ and $\bar{p}_{cj}$.

The total consolidation settlement in the whole deposit is obtained by summing up settlement of all layers as explained in the case of obtaining settlement using field compression curve.

To the primary consolidation settlement thus computed using either C_c or m_v, corrections for three-dimensional consolidation effect and foundation rigidity are applied as explained in the subsequent sections.

14.3.3 Correction for Three-dimensional Consolidation Effect

In the primary consolidation settlement computations explained so far, one-dimensional consolidation theory has been used. That is, the increase in the pore water pressure due to foundation loading is assumed to be equal to the increase in the vertical stress. But in a three-dimensional consolidation situation this assumption is not valid. The correction proposed by Skempton and Bjerrum (1957) is widely used in practice today. Accordingly,

$$\rho_{c(3D)} = \mu\rho_{c(1D)} \tag{14.17}$$

where $\rho_{c(3D)}$ = primary consolidation settlement corrected for three-dimensional effects

$\rho_{c(1D)}$ = primary consolidation settlement computed from one-dimensional consolidation theory

μ = correction factor dependent on the type of clay (i.e., governed here by A-factor) and foundation geometry

Values of μ as given by Scott (1963) are shown in Fig. 14.14. This procedure of correction is also recommended by Indian Code of Practice, IS: 8009, Part I, 1976.

Hidden page

Hidden page

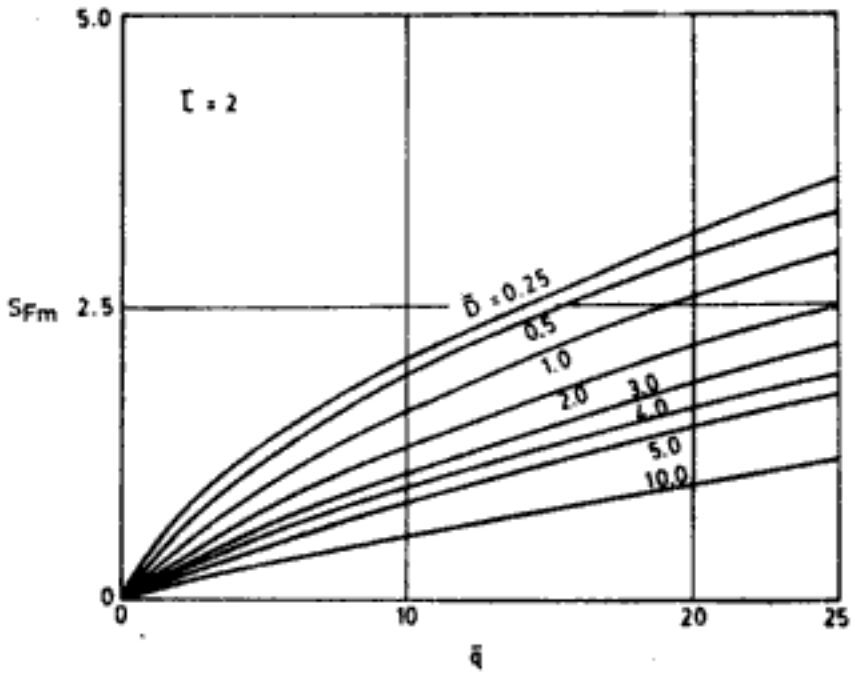

Fig. 14.17 Mean settlement factor for rectangle ($L/B = 2$) using Boussinesq stress distribution (After Kaniraj, 1974)

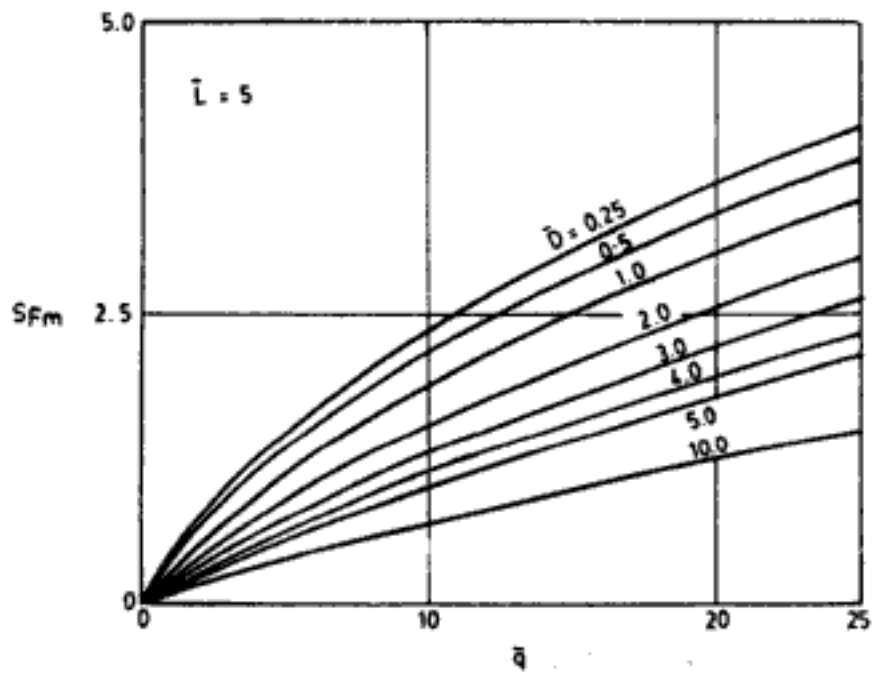

Fig. 14.18 Mean settlement factor for rectangle ($L/B = 5$) using Boussinesq stress distribution (After Kaniraj, 1974)

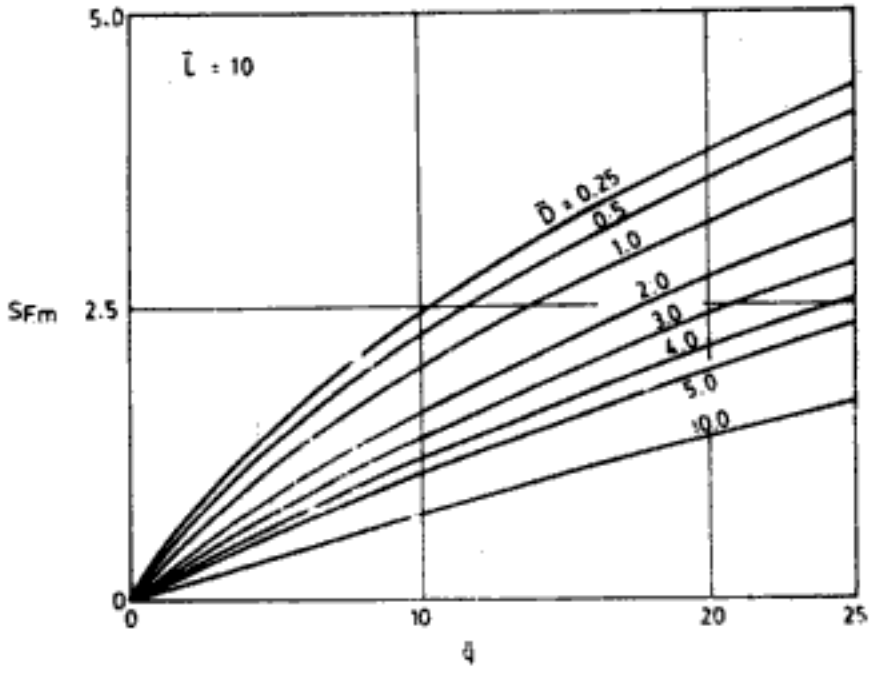

Fig. 14.19 Mean settlement factor for rectangle (L/B = 10) using Boussinesq stress distribution (After Kaniraj, 1974)

$$\bar{D} = \frac{2D}{B} \tag{14.21}$$

$$\bar{q} = \frac{2q}{\gamma B} \tag{14.22}$$

where L = length of foundation
B = breadth of foundation
D = depth of embedment of foundation
q = load intensity on foundation
γ = effective density of soil

$\bar{L}$, $\bar{D}$ and $\bar{q}$ are non-dimensional parameters.

These S_{Fm} values are applicable for semi-infinite normally consolidated clay deposits or where the thickness of the deposit is fairly large compared to breadth of the foundation. In the computation of S_{Fm} values shown in Figs 14.16 to 14.19 the conventional approach for vertical stress increase has been followed. That is, the depth of embedment is considered only in effective stress calculation, otherwise for vertical stress increase Boussinesq's solution is assumed taking the level of the base of the foundation as the surface of semi-infinite half space. The use of the curves is demonstrated in Q 14.4. The average primary consolidation settlement of a rigid strip foundation is also given by Eq. 14.19. The values of S_{Fm} obtained for strip foundations are shown in Fig. 14.20.

Q 14.4: To determine the mean primary consolidation settlement of a rigid foundation as shown in Fig. 14.13 using Kaniraj's design curves in Figs. 14.16 to 14.19.

Ans: The significant zone is considered as El. — 6 m to El. — 30 m (i.e., 2B below base of foundation and the average initial void ratio over this zone, is taken as equal to e_0 at the middle of this zone.

Hidden page

Fox's correction factor (Fig. 13.39): Fox's depth correction factor for average elastic settlement of flexible footing (or settlement of rigid footing) can be used in the same manner as for primary consolidation settlement. It must be, however, noted that for soils when consolidation occurs $\mu < 0.5$.

Q 14.5: To apply correction for depth effects to mean settlement obtained in Q 14.3 using Fox's curves.

Ans: $l/b = 30/12 = 2.5$

$h/\sqrt{lb} = 6/\sqrt{12 \times 30} = 0.316$

From Fig. 13.39, depth correction factor $\simeq 0.91$
From Q 14.3 mean settlement without depth correction $= 0.72$ m
$\therefore$ primary consolidation settlement $= 0.91 \times 0.72 = 0.655$ m.

Kaniraj's procedure: Kaniraj (1974) computes primary consolidation settlement of footings in normally consolidated clay using Skopek's expression (Eq. 13.44) in computations for vertical stress increase. This automatically incorporates the effect of depth of embedment. The average settlement in this case is again given by Eq. 14.19. Appropriate values of S_{Fm} (using Skopek's expression) are shown in Figs 14.21 to 14.24. S_{Fm} values for strip foundations are given in Fig. 14.25.

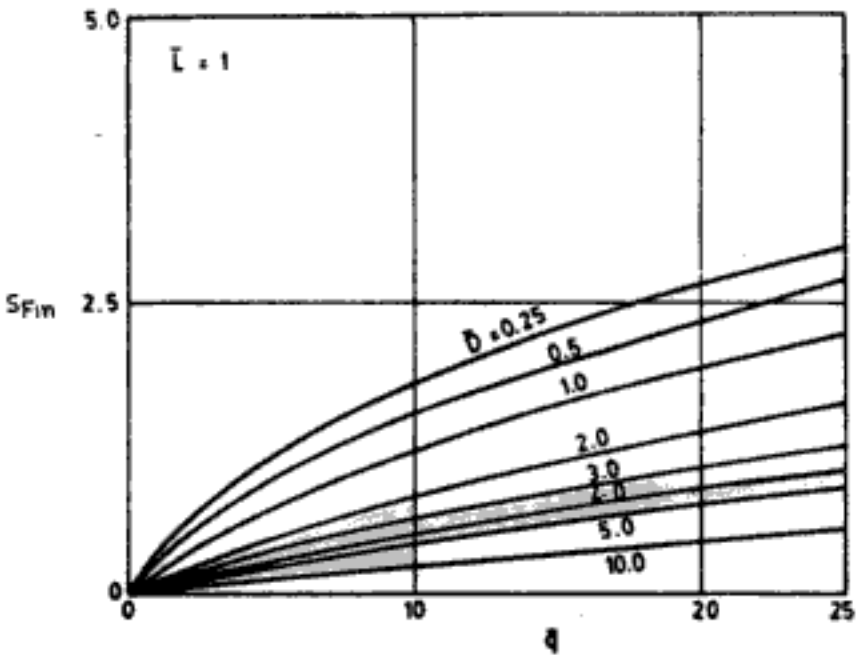

Fig. 14.21 Mean settlement factor for square foundation considering depth of embedment in stress distribution (After Kaniraj, 1974)

Q 14.6: To re-do Q 14.4 using Kaniraj's design curves in Figs. 14.21 to 14.24.

Ans: Parameters L, D, q, C and γ are computed as in Q 14.4. From Figs 14.21 to 14.24,

$$S_{Fm} \simeq 0.33$$

Hence, average primary consolidation settlement

$$= \frac{12}{2 \times 3.702} \times 0.33 = 0.535 \text{ m}$$

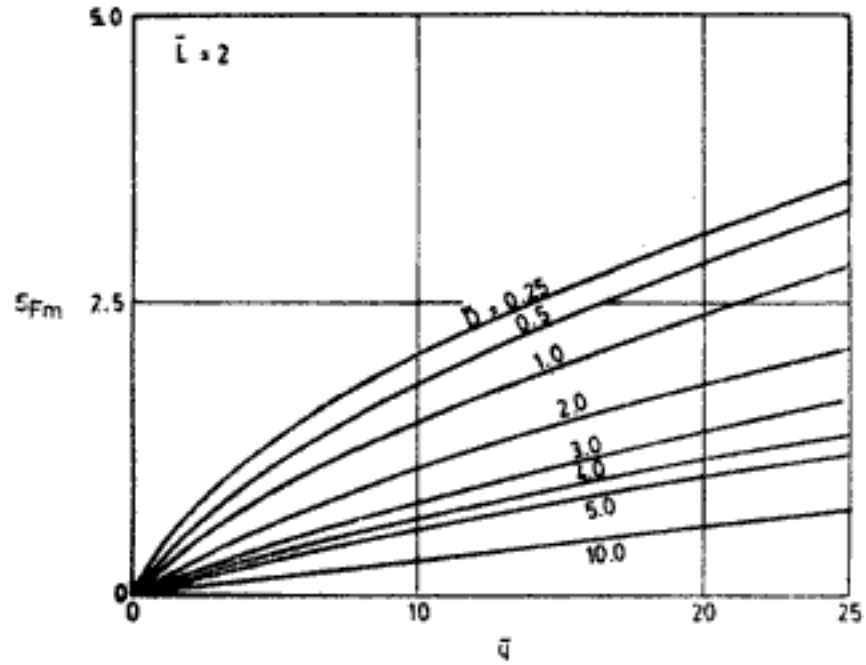

Fig. 14.22 Mean settlement factor for rectangle ($L/B = 2$) considering depth of embedment in stress distribution (After Kaniraj, 1974)

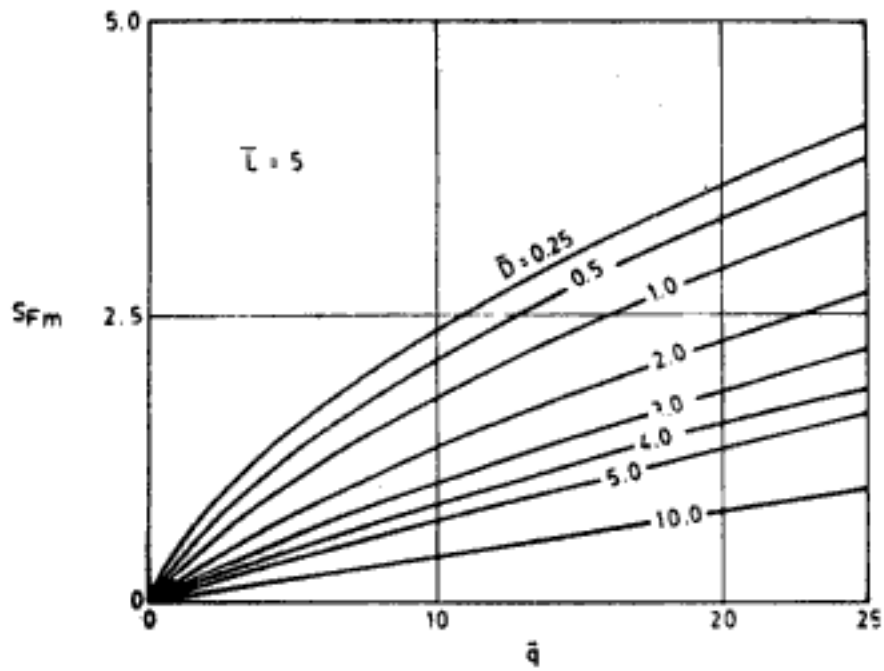

Fig. 14.23 Mean settlement factor for rectangle ($L/B = 5$) considering depth of embedment in stress distribution (After Kaniraj, 1974)

Hidden page

14.3.6 Correction for Depth of Embedment and Limited Thickness of Compressible Clay Layer

The recommendation in Sec. 14.3.5 for correction for depth of embedment is applicable strictly when the depth of clay is fairly large in relation to the width of the foundation. When the thickness of the clay layer below the base of the foundation is finite the following procedure may be used.

Janbu et al.'s solutions: Janbu *et al.*'s solutions for average elastic displacement of embedded rectangular areas in limited thickness deposits are given in Eq. 13.55 and Fig. 13.62. Ignoring the error due to assuming $\mu = 0.5$, the procedure to be followed is explained in Q 14.7.

Q 14.7: To apply correction for effects due to depth of embedment and limited thickness of clay layer, to the average primary consolidation settlement obtained in Q 14.3 using Janbu *et al.*'s solutions.

Ans: Using Janbu *et al.*'s solution, the ratio of the average settlement of a footing embedded at depth D and having a clay layer of thickness H below the footing to the average settlement of the same footing resting on the surface of clay layer of thickness H, can be expressed as,

$$\frac{\rho_{c-D}}{\rho_{c-S}} = \frac{(\mu_0\mu_1)_D}{(\mu_0\mu_1)_S} \tag{14.23}$$

where subscripts D and S refer to embedded and surface footings respectively.

For embedded footing: $D/B = 6/12 = 0.5$ $\quad\therefore\ \mu_0 = 0.87$ (for $L/B = 2.5$)

and $H/B = 60/12 = 5$ $\quad\therefore\ \mu_1 = 0.9$

For surface footing: $D/B = 0$ $\quad\therefore\ \mu_0 = 1$

$H/B = 60/12 = 5$ $\quad\therefore\ \mu_1 = 0.9$

$$\therefore \quad \frac{\rho_{c-D}}{\rho_{c-S}} = \frac{0.87 \times 0.9}{1 \times 0.9} = 0.87$$

$\rho_{c-S} = 0.72$ m from Q 14.3

The average primary consolidation settlement of the embedded footing on limited thickness layer $= 0.72 \times 0.87 = 0.626$ m.

The primary consolidation settlement of rectangular loaded areas in normally consolidated clay deposits of finite thickness has been investigated by Kaniraj (1976). The mean settlement in this case is expressed again in the form of Eq. 14.19. Kaniraj also gives the design curves for mean settlement factor.

14.4 SECONDARY CONSOLIDATION SETTLEMENT IN ORGANIC CLAYS

The important points to be noted regarding secondary consolidation settlement are:

1. Organic soils exhibit pronounced secondary consolidation effects.
2. Many soils show a linear relationship between settlement (or void ratio) and log time during secondary consolidation phase for a considerable period (Fig. 14.26). However, this relationship cannot hold indefinitely.

Hidden page

Hidden page

Table 14.3 gives the results of secondary consolidation settlement. In this table, Cols. 1 to 3 are same as in Table 14.2.

Column 4 gives the net effective stress in the middle of layer at time t_{100}. In this particular case $\bar{p}_{fi} = \bar{p}_{0i} + \Delta\sigma_{zi}$.

Column 5 gives the void ratio in the middle of the layer at time $t_{100} = 6$ y.

Column 6 gives the secondary consolidation settlement in each layer and the total secondary consolidation settlement, at time $t = 25$ y.

Table 14.3

Layer (1)	Elevation, m (2)	h_i, m (3)	$\bar{p}_{fi}$ T/m² (4)	e_{1i} (5)	ρ_{si}, m (6)
1	−6 to −12	6	20.18	0.661	0.022
2	−12 to −18	6	23.14	0.634	0.023
3	−18 to −24	6	26.50	0.608	0.023
4	−24 to −30	6	30.86	0.578	0.024
					ρ_s = 0.092 m

The secondary consolidation settlement at $t = 25$ y is approximately 0.1 m. It may be noted that unlike primary consolidation settlement which decreases with the depth of layers from the base of foundation, the secondary consolidation settlement of all layers is nearly equal. This is because secondary settlement is not influenced by stress increase and $C_{\alpha i}$ also has been assumed to be constant for all layers.

14.5 COMPUTATION OF SETTLEMENT IN SAND

In deposits like sand, the coefficient of permeability is so high compared to fine grained soils that it is normally assumed that the total settlement is instantaneous. Before the description of the different methods of settlement computation in sand a brief explanation about the various factors which affect the settlement of foundations in sand is appropriate.

14.5.1 Factors Influencing Settlement in Sand

Jorden (1977) discusses the various factors which influence settlement in sand. The settlement is generally influenced by (i) loading intensity on the foundation, (ii) size and shape of the loaded area, (iii) relative density of sand, (iv) grain shape, (v) grain size distribution, (vi) mineralogy, (vii) *in situ* state of stresses in the seat or significant depth of settlement, and (viii) depth of embedment of loaded area.

Of these several factors, for a particular loading intensity the most important factors are, the size and shape of the loaded area, relative density, depth of embedment, and *in situ* state of stress. The *in situ* state of stress in turn depends on factors like depth, loading history, i.e., normally or overconsolidated, and the location of the water-table.

14.5.2 Underlying Philosophy and General Approach to Settlement Computation in Sand

Sutherland (1975) gives an excellent description of the philosophy. Following are some of the excerpts from his paper suitably adapted for this book.

Hidden page

where ρ_1 = settlement of footing of width B embedded at depth D_1

ρ_2 = settlement of the same footing embedded at depth D_2

n = a constant $\simeq 0.5$

For the case when $D_1 = 0$,

$$\frac{\rho_2}{\rho_1} = \left[\frac{1}{1 + D_2/B}\right]^n \tag{14.32}$$

Question 14.9 illustrates the use of plate load test results in calculating settlement of foundations.

Q 14.9: The results of a load test carried out on a plate of size 30 cm × 30 cm are given in Table 14.4. The load test was carried out at a depth of 2.5 m, below ground surface. From the test results determine the settlement of an actual foundation of size 3.5 m × 3.5 m carrying a total load of 200 T and located at a depth of 3.5 m below the ground surface. The soil profile is fairly homogeneous silty sand at the site.

Table 14.4 Results of Plate Load Test

Load intensity, kg/cm²	0.496	0.992	1.488	1.984	2.48	2.976	3.472	3.968	4.464	4.96
Settlement, mm	0.5	1.0	1.8	2.75	4.4	5.4	9.8	12.5	17.0	28.7

Ans: The load settlement curve of the test plate is shown in Fig. 14.28. The loading intensity on the actual foundation is

$$= \frac{200}{3.5 \times 3.5}$$

$$= 16.32 \text{ T/m}^2 = 1.632 \text{ kg/cm}^2$$

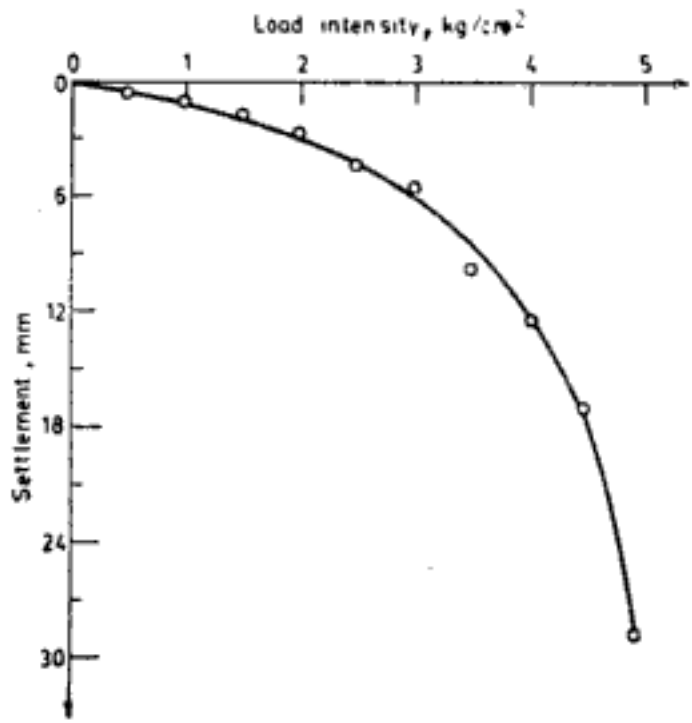

Fig. 14.28 Q 14.9

From Fig. 14.28 the settlement of the plate corresponding to a load intensity of 1.632 kg/cm² is 1.95 mm.

From Eq. 14.30 the settlement of a 3.5 m wide foundation is

$$\rho_B = 1.95 \times \left(\frac{2 \times 350}{350 + 30}\right)^2 = 6.62 \text{ mm}$$

To this value a depth correction must be applied. In applying the depth correction it will be assumed that the depth of embedment will be reckoned only from the level at which the plate load test was done. Thus for depth correction factor calculations the depth of embedment of footing = 3.5 − 2.5 = 1 m.

(a) According to Fox's curves, $h/\sqrt{LB} = 1/\sqrt{3.5 \times 3.5} = 0.286$

$$L/B = 1$$

From Fig. 13.39 depth correction factor = 0.93

Settlement of actual foundation = 0.93 × 6.62 = 6.16 mm

(b) Using Ramasamy's recommendation (Eq. 14.32)

$$D_1 = 0 \qquad D_2 = 1 \text{ m}$$

$$\text{depth correction factor} = \left[\frac{1}{1 + (1/3.5)}\right]^{0.5} = 0.88$$

Settlement of foundation = 0.88 × 6.62 = 5.82 mm

14.5.4 Methods Based on Standard Penetration Test

A number of investigators have proposed procedures and empirical relationship for determination of settlement based on standard penetration test results. Some of these which are important and useful for practical applications will be described here.

1. *IS Code recommendation:*

IS: 2131–1981 makes the following recommendations:

The observed value of N is corrected first for two effects, namely, (i) effect of overburden pressure, and (ii) effect of dilatancy.

Correction for overburden pressure: The corrected value is given by,

$$N' = C_N N \tag{14.33}$$

In Eq. 14.33,

N' = corrected value of observed N

C_N = correction factor recommended by Peck, Hanson and Thornburn (Fig. 19.8)

Correction for dilatancy: Dilatancy correction is to be applied for observations below water-table in the case of fine sand, silty sand and silt. When N' obtained after overburden correction exceeds 15, it is to be further corrected as follows:

$$N'' = 15 + 0.5(N' - 15), \qquad \text{if } N' > 15 \tag{14.34}$$

where N'' is the final corrected value used in design. And when $N' \leqslant 15$,

$$N'' = N' \qquad \text{if } N' \leqslant 15 \tag{14.35}$$

Having applied the corrections to the measured N values, the average of N'' values within a depth of B (breadth of foundation) below the base of the footing is worked out and used in design. With the average N'' value Fig. 14.29 (IS: 8009, Part I, 1976) is used to compute the settlement. Figure 14.29 is for a load intensity of 1 kg/cm² on the footing. The settlement at any other pressure may be computed by assuming the settlement to be proportional to the intensity of pressure. Figure 14.29 is for use in dry cohesionless soils. When water-table is near the foundation level, as shown in Fig. 14.30, a correction is to be applied as follows:

$$\text{Settlement} = \frac{\text{settlement from Fig. 14.29}}{\text{correction factor}} \tag{14.36}$$

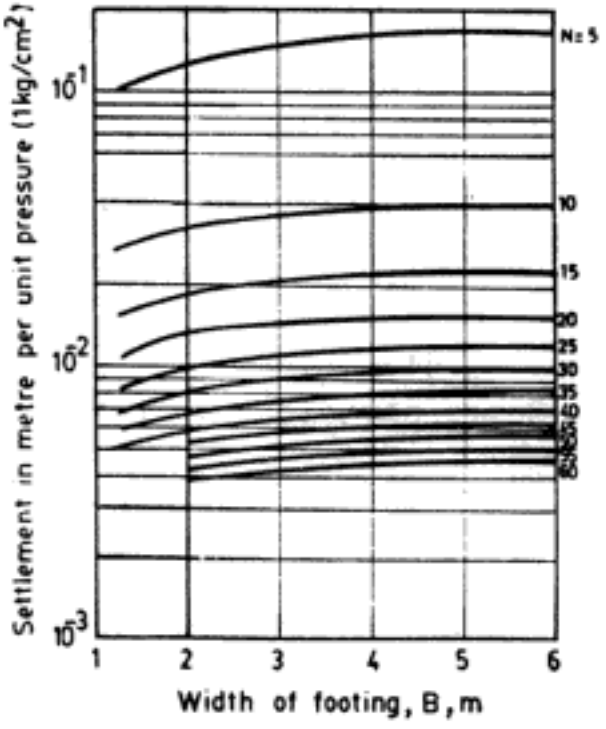

Fig. 14.29 Settlement of foundations in sand (After IS: 8009, Part I, 1976; reprinted by permission of Indian Standards Institution, New Delhi)

The correction factor is given in Fig. 14.31. For water-table at or above base of footing, correction factor = 0.5. When water-table is at B or more than B below base of footing, correction factor = 1.

Q 14.10: The results of standard penetration tests carried out at a site made up of sandy silt and silty sand are as given below:

Elevation (m)	−1.5	−3.0	−4.5	−6.0
N	5	4	4	7

The groundwater level is at El. −1.5 m. The total density of soil above GWL is 1.76 T/m³ and the submerged density of soil below GWL is 0.96 T/m³. To determine the settlement of a 1.5 m wide strip footing embedded at El. −1.2 m and carrying a total vertical load of 10 T/m run. Elevation of ground surface is 0.0 m.

Ans: Table 14.5 shows the corrections for observed values of N. The average values of N'' within a zone of approximately B below the base of footing = (7 + 5)/2 = 6

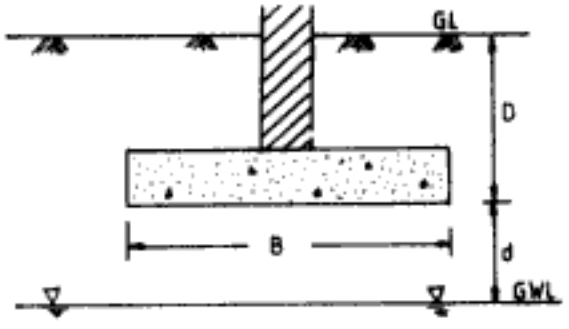

Fig. 14.30 Water-table near foundation level

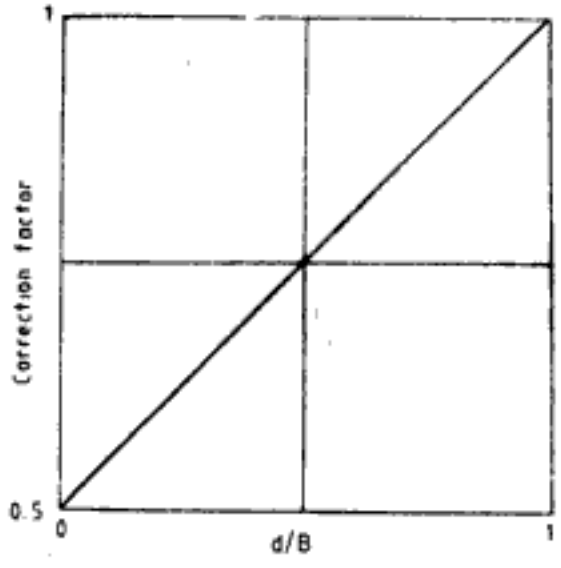

Fig. 14.31 Correction factor for water-table

Table 14.5

Elevation m	N	$\bar{p}_o$ kg/cm²	C_N	N'	N''
−1.5	5	0.264	1.45	7	7
−3.0	4	0.408	1.3	5	5
−4.5	4	0.552	1.2	5	5
−6.0	7	0.696	1.12	8	8

From Fig. 14.29 the settlement of the footing for a load intensity of 1 kg/cm² = 8.0 cm (approx.)

The actual load intensity of footing = $10/(1.5\times 1) = 6.67$ T/m² = 0.667 kg/cm²

For $d/B = 0.3/1.5 = 0.2$, the water-table correction factor, from Fig. 14.30 = 0.6

The settlement of the footing = $\dfrac{0.667\times 8}{0.6} = 8.9$ cm

2. *Settlement from empirical correlation between SPT values and safe bearing pressure*:

The empirical correlations, explained in Ch. 12, between SPT values and safe bearing pressure can be used to compute the settlement of foundations. These correlations are for a specified value of settlement, usually 25 mm. Assuming that settlement is proportional to the bearing pressure, the settlement of a foundation can be extrapolated.

Questions 14.11 to 14.14 illustrate the procedure of using the correlations suggested by Teng, Meyerhof, Bowles, and Peck, Hanson and Thornburn respectively. It may be noted that in all these procedures the value of N to be used in respective equations are the corrected N values as explained in Ch. 12 for respective procedure.

Q 14.11 To determine the settlement of footing in Q 14.10 using Teng's correlation between N and $q_{safe-pr}$.

Ans: According to Teng: $q_{safe-pr} = 3.5(N-3)\left(\dfrac{B+0.3}{2B}\right)^2 R'_w C_D$ (for 25 mm settlement) (12.53)

$N = 7$ obtained as per procedure in Sec. 12.11.6 but averaged over a depth of $2B$ below base of footing i.e. $(9 + 6 + 6)/3 = 7$

$B = 1.5$ m; $R'_w = 0.6$ (From Fig. 12.52 for $d_b/B = \dfrac{0.3}{1.5} = 0.2$)

$$C_D = 1 + \frac{1.2}{1.5} = 1.8$$

Substituting in the equation,

$$q_{safe-pr} = 5.44 \text{ T/m}^2 = 0.544 \text{ kg/cm}^2, \text{ for 25 mm settlement}$$

The settlement of the foundation for an actual load intensity of 0.667 kg/cm²

$$= \frac{25}{0.544} \times 0.667 = 30.1 \text{ mm}$$

Q 14.12: To determine the settlement of footing in Q 14.10 using Meyerhof's correlation between N and $q_{safe-pr}$.

Ans: According to Meyerhof,

$$q_{safe-pr} = 0.81\, N\, K_{D2} \left(\frac{B + 0.3}{B}\right)^2, \text{ for 25 mm settlement} \qquad (12.46)$$

Using corrections in Eq. 19.6 the average value of corrected $N = 7$

$$B = 1.5 \text{ m}; \; K_{D2} = 1 + 0.33 \times \frac{1.2}{1.5} = 1.264$$

Substituting,

$$q_{safe-pr} = 10.32 \text{ T/m}^2 = 1.032 \text{ kg/cm}^2, \text{ for 25 mm settlement}$$

The settlement of the footing for an actual load intensity of 0.667 kg/cm²

$$= \frac{25}{1.032} \times 0.667 = 16.16 \text{ mm}$$

Q 14.13: To determine the settlement of footing in Q 14.10 using Bowles' correlation between N and $q_{safe-pr}$.

Ans: According to Bowles,

$$q_{safe-pr} = 1.25\, N\, K_{D2} \left(\frac{B + 0.3}{B}\right)^2, \quad \text{for 25 mm settlement} \qquad (12.48)$$

Corrected $N = 7$

Substituting the values,

$$q_{safe-pr} = 15.93 \text{ T/m}^2 = 1.593 \text{ kg/cm}^2, \text{ for 25 mm settlement}$$

The settlement of the footing for an actual load intensity of 0.667 kg/cm²

$$= \frac{25}{1.593} \times 0.667 = 10.5 \text{ mm}$$

Q 14.14: To determine the settlement of footing in Q 14.10 using Peck, Hanson, and Thornburn's correlation between $q_{all-net}$ and N.

Ans: Corrected value of $N = 6$

From an examination of Fig. 12.50 and Eq. 12.49 settlement governs design. The pressure for 25 mm settlement = 6.6 T/m². From Eq. 12.50,

Correction for water-table = 0.611

$$\text{Settlement of footing} = \frac{2.5 \times 0.667}{0.66 \times 0.611} = 4.1 \text{ cm}$$

3. *Comparison of empirical calculations using N*:
Table 14.6 presents the results of solutions for Qs 14.10 to Q 14.14.

Table 14.6 Settlement Calculations Using Different Correlations

Method	Settlement, cm	Remarks
Indian Standard Code	8.9	Corrected $N = 6$
Teng	3.0	Corrected $N = 7$
Meyerhof	1.6	Corrected $N = 7$ No water-table correction
Bowles	1.0	Corrected $N = 7$ No water-table correction
Peck, Hanson and Thornburn	4.1	Corrected $N = 6$

From Table 14.6 the following points may be noted:

(a) Indian Standards Code method predicts much higher settlement than other methods and appears to be very conservative.
(b) Meyerhof's and Bowles' procedures predict very low values significantly because no correction is recommended for effect of water-table.
(c) Teng's and Peck, Hanson and Thornburn's procedures give intermediate values and appear to be reasonable. In fact, without correction for presence of water-table these procedures will give values close to settlement predicted by Meyerhof's procedure.
(d) The N values are very low. The bearing capacity considerations may govern the design of foundation in this particular case.

14.5.5 Methods Based on Static Cone Penetration Test

1. *De Beer and Martens' procedure*
In this procedure the static cone penetration diagram is first drawn. From the shape of the diagram the soil can be split into convenient number of layers (Fig. 14.32) and the average value of cone penetration resistance for each layer can be chosen. De Beer and Martens (1957) and De Beer (1965) suggest the following semi-empirical relationship for calculation of the settlement of the ith layer, ρ_i,

$$\rho_i = \frac{2.3}{C_i} \log_{10}\left[\frac{\bar{p}_{0i} + \Delta\sigma_{zi}}{\bar{p}_{0i}}\right] H_i \qquad (14.37)$$

where $\bar{p}_{0i}$ = effective overburden pressure at the middle of the ith layer
$\Delta\sigma_{zi}$ = increase in vertical stress at the middle of ith layer
C_i = a constant of compressibility for ith layer $= \frac{3}{2}\left(\frac{q_{c-i}}{\bar{p}_{0i}}\right)$
q_{c-i} = average static cone resistance in ith layer

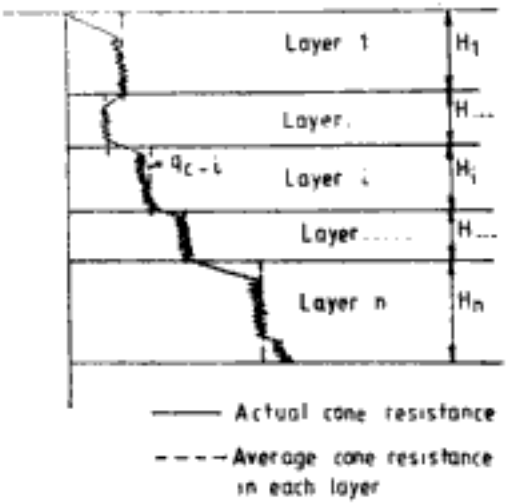

Fig. 14.32 Cone penetration resistance with depth

If there are n layers within the significant zone of, say $2B$ below the footing, the total settlement of the foundation, ρ, is given by,

$$\rho = \sum_{i=1}^{n} \rho_i = \sum_{i=1}^{n} \frac{2.3}{C_i} \log_{10}\left[\frac{\bar{p}_{0i} + \Delta\sigma_{zi}}{\bar{p}_{0i}}\right] H_i \tag{14.38}$$

$\Delta\sigma_z$ in Eqs 14.37 and 14.38 are generally determined by using solutions given in Eq. 13.97 and those given in Table 13.45 with concentration index $n = 4$ (generally referred to as Froehlich's solutions). $\Delta\sigma_z$ is also determined sometimes using Boussinesq's stress distribution theory ($n = 3$, $\mu = 0.5$).

De Beer recommends that at least three penetration tests should be carried out. From these the average settlement and limits of settlement can be calculated. According to De Beer the above procedure is applicable only to normally loaded sands. For pre-compressed sands, a reduction factor is to be applied to the settlement as computed above.

Meyerhof (1965) notes that the procedure explained above overestimates the actual settlement by a factor of about two. Further, the calculated settlement will occur at a loading intensity 50 per cent higher than for what it is calculated. Schmertmann (1970) points out that this modification by Meyerhof amounts to approximately changing the constant of compressibility, C, in Eqs 14.37 and 14.38 as,

$$C = 1.9 \frac{q_c}{\bar{p}_0} \tag{14.39}$$

2. *Schmertmann's method*

Figure 14.33 gives a schematic illustration of Schmertmann's method. In Schmertmann's method the seat of settlement is considered to be a depth $2B$ below the base of the foundation. The static cone penetration diagram within this zone is divided into a number of convenient layers and the average static cone resistance of each layer is determined. The settlement of the foundation is then given by the relationship,

$$\rho = C_1 C_2 q \sum_{i=1}^{n} \frac{I_{z-i}}{E_i} h_i \tag{14.40}$$

Hidden page

Ans: As shown in Fig. 14.34 the significant zone of 3 m below base of footing is divided into two layers.

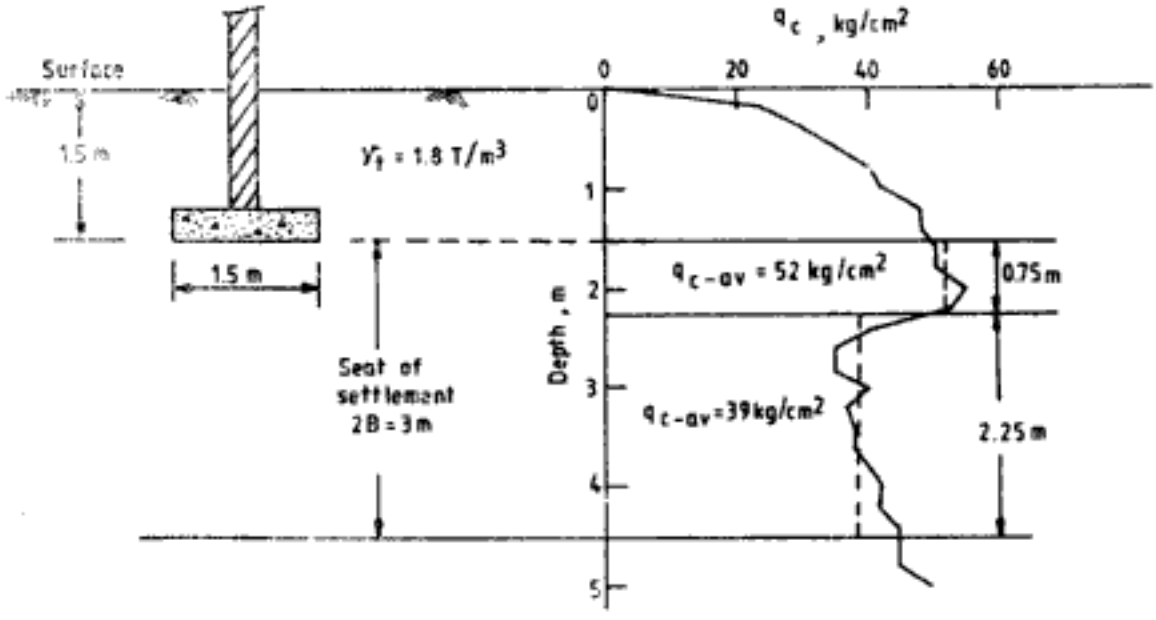

Fig. 14.34 Q 14.15

The first layer of thickness 0.75 m has an average static cone resistance of 52 kg/cm².

The second layer of thickness, 2.25 m has an average static cone penetration resistance of 34 kg/cm²

Settlement of layer 1:

In De Beer and Martens' approach,

$$q_c \text{ for layer} = 52 \text{ kg/cm}^2$$

Effective overburden pressure in the middle of the layer

$$= 1.8 \times (1.5 + 0.375)$$
$$= 3.375 \text{ T/m}^2 = 0.3375 \text{ kg/cm}^2$$

The compressibility constant for the layer $= \frac{3}{2} \times \frac{52}{0.3375} = 231.11$

Using Boussinesq's stress distribution theory (Fig. 13.21 with $m = 1$, $n = 0.5$) the vertical stress increase at the middle of the layer below the centre of footing = 1.892 kg/cm²

$$\text{Settlement of the layer} = \frac{2.3}{231.11} \times \log_{10} \left[\frac{0.3375 + 1.892}{0.3375}\right] \times 0.75$$
$$= 6.12 \times 10^{-3} \text{ m} = 6.12 \text{ mm}$$

Settlement of layer 2:

$$q_c \text{ for layer} = 39 \text{ kg/cm}^2$$

Effective overburden pressure in the middle of the layer

$$= 1.8 \times (1.5 + 0.75 + 1.125) = 6.075 \text{ T/m}^2 = 0.6075 \text{ kg/cm}^2$$

The compressibility constant for the layer

$$= \frac{3}{2} \times \frac{39}{0.6075} = 96.3$$

Using Boussinesq's stress distribution theory, the increase in vertical stress at the middle of the layer below the centre of footing = 0.51 kg/cm²

$$\text{Settlement of the layer} = \frac{2.3}{96.3} \times \log_{10}\left[\frac{0.6075 + 0.51}{0.6075}\right] \times 2.25$$

$$= 14.22 \times 10^{-3} \text{ m} = 14.22 \text{ mm}$$

Hence the total settlement in two layers = 6.12 + 14.22 = 20.34 mm. To this value of settlement corrections for rigidity of foundation and depth of embedment must be applied.

Rigidity correction: Using a rigidity correction factor of 0.8,

Average or mean settlement = 0.8 × 20.34 = 16.27 mm

Correction for depth of embedment: Using Fox's depth correction factor (Fig. 13.39)

$$\frac{h}{\sqrt{LB}} = \frac{1.5}{\sqrt{1.5 \times 1.5}} = 1$$

Depth correction factor = 0.725

The total mean settlement of footing = 0.725 × 16.27 = 11.8 mm

Alternatively, using Ramasamy's recommendation for depth correction, depth correction factor

$$= \left[\frac{1}{1 + 1.5/1.5}\right]^{0.5} = 0.707$$

Hence, the total mean settlement of footing = 0.707 × 16.27 = 11.5 mm

In the above calculations Boussinesq's stress distribution theory has been used. But more appropriate would be to use Froehlich's solutions (Table 13.47, $n = 4$). Using this table,

Vertical stress increase in the middle of layer 1 = 1.584 kg/cm²

Vertical stress increase in the middle of layer 2 = 0.216 kg/cm²

Using these values the settlement can be computed. Table 14.7 presents the results of all computations. It may be noted that the accuracy of the solutions can be improved by splitting the two layers into more number of layers. From the results in Table 14.7 it may be

Table 14.7

Stress distribution theory	Settlement without corrections (mm)	Total settlement corrected for rigidity (rigidity factor = 0.8) (mm)	Total settlement corrected for rigidity and depth of embedment using	
			Fox's curves (mm)	Ramasamy's Eq. (mm)
Boussinesq (Fig. 13.21)	Layer 1 = 6.12 Layer 2 = 14.22 Total = 20.34	16.27	11.8	11.5
Froehlich (Table 13.47, $n = 4$)	Layer 1 = 5.64 Layer 2 = 7.1 Total = 12.74	10.19	7.39	7.2

concluded that from De Beer and Martens' approach the settlement of the footing is approximately 9.5 mm.

Q 14.16: To re-do Q 14.15 using Meyerhof's recommendation for compressibility constant.

Ans: The results of calculations are shown in Table 14.8. It may be noted that in order to get the values in Table 14.8 it requires only to multiply their respective values in Table 14.7 by a factor, (1.5/1.9) = 0.789.

Table 14.8

Stress distribution theory	Settlement without corrections (mm)	Total settlement corrected for rigidity (rigidity factor = 0.8) (mm)	Total settlement corrected for rigidity and depth of embedment using	
			Fox's curves (mm)	Ramasamy's Eq. (mm)
Boussinesq (Fig. 13.21)	Layer 1 = 4.83 Layer 2 = 11.22 Total = 16.05	12.84	9.31	9.07
Froehlich (Table 13.47)	Layer 1 = 4.45 Layer 2 = 5.60 Total = 10.05	8.04	5.83	5.68

It may be concluded from values shown in Table 14.8, that using Meyerhof's modification, the total settlement of the footing is approximately 7.5 mm.

Q 14.17: To re-do Q 14.15 using Schmertmann's method. Assume there is no time dependent settlement, i.e., $C_2 = 1$.

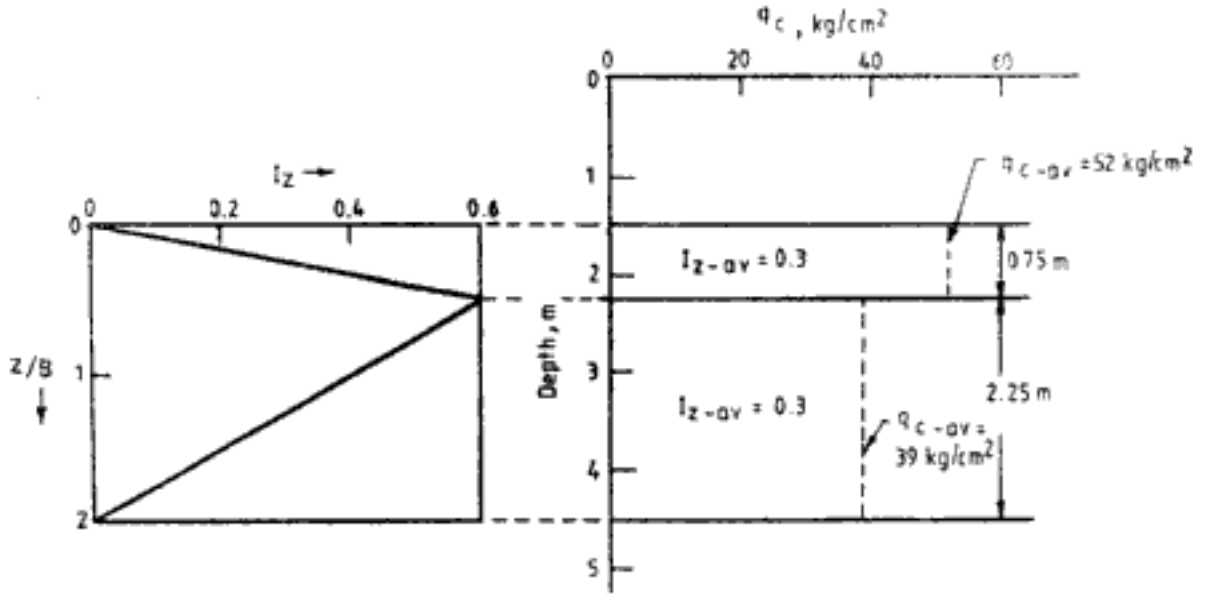

Fig. 14.35 Q 14.17

Ans: Figure 14.35 gives the details of division of layers, the influence factor diagram and the average influence factor for each layer.

Hidden page

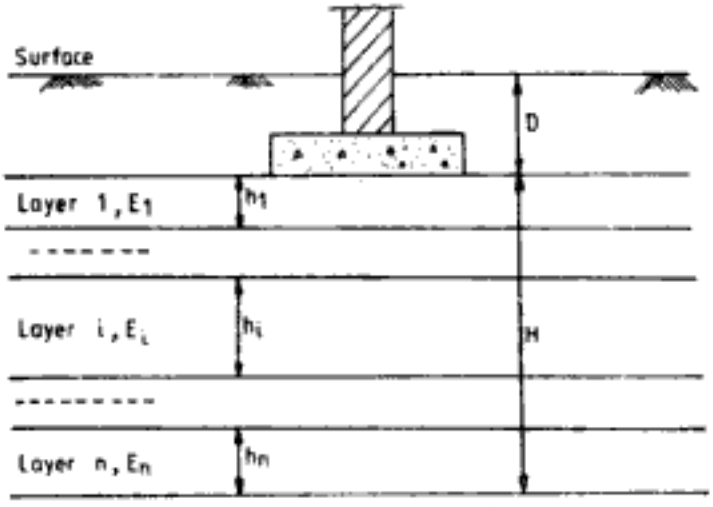

Fig. 14.36 Egorov's method

where M = correction factor depending on the thickness of the compressible layer

$M = 1.5$ for $0 < H/(B/2) \leqslant 0.5$

$M = 1.4$ for $0.5 < H/(B/2) \leqslant 1$

$M = 1.3$ for $1 < H/(B/2) \leqslant 2$

$M = 1.2$ for $2 < H/(B/2) \leqslant 3$

$M = 1.1$ for $3 < H/(B/2) \leqslant 4$

$M = 1$ for $4 < H/(B/2) \leqslant \infty$

K_i = dimensionless coefficient for the ith layer to be taken from Table 14.9 or 14.10 In Tables 14.9 and 14.10,

$$m \text{ (for } i\text{th layer, for } K_i) = \left[\sum_{j=1}^{i} h_j\right]/(B/2)$$

$$n = L/B$$

E_i = modulus of deformation of soil for ith layer

m_E = correction factor that takes into account the large dimensions of the foundation in the plan view

$m_E = 1.35$ for $10 \text{ m} < B \leqslant 15 \text{ m}$

$m_E = 1.5$ for $B > 15 \text{ m}$

Correction factor m_E, in fact, increases the modulus of deformation of the soils and has been introduced into the formula to take into account the structural strength of the soils with depth.

Q 14.18: To determine the average total settlement of a raft foundation 25 m × 45 m, embedded at a depth of 3 m below ground surface in a sandy soil profile. The loading intensity on foundation is 3 kg/cm². The details of soil layers are as in Fig. 14.37.

Ans: From Eq. 14.41, the thickness of compressible layer below foundation is,

$$H = 4\sqrt{25 \times \frac{3^2}{3^2}} = 20 \text{ m}$$

i.e., the compressible layer lies between El. −3 m and El. − 23 m.

Hidden page

Hidden page

Hidden page

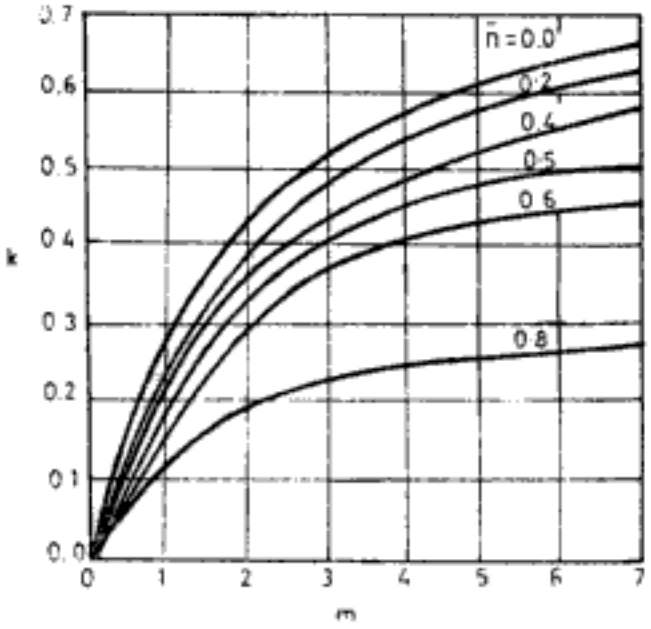

Fig. 14.39 Value of K in Eq. 14.45 (After Egorov *et al.*, 1977)

where i' = inclination
μ = Poisson's ratio
M_w = wind load moment
E_m = average deformation modulus within compressible layer
K_m = dimensionless coefficient defined in Table 14.11

Table 14.11 Values of K_m

$\bar{H}/r_2$	0.25	0.5	1.0	2.0	> 2.0
K_m	0.26	0.43	0.63	0.74	0.75

$\bar{H}$ = height of tower.
After Egorov *et al*., 1977.

Q 14.19: To determine the average total settlement of a ring foundation of external radius 45 m and internal radius 25 m. The foundation is embedded at a depth of 3 m below ground surface in a sandy silt soil profile. The net loading intensity on foundation is 2 kg/cm². The details of soil layers are as shown in Fig. 14.40. The wind load moment acting on foundation is 20,000 tonne metres. Height of tower is 95 m.

Ans: From Eqs 14.43 and 14.44 the thickness of the compressible layer is approximately taken as

$$H = 0.75 r_2$$
$$= 0.75 \times 45 = 33.75 \text{ m}$$

This compressible layer is divided into the following four layers:

Layer 1: between El. −3 m and El. −12 m
Layer 2: between El. −12 m and El. −18 m

Hidden page

From Table 14.11, $K_m = 0.75$

Substituting the values in Eq. 14.46, the inclination of tower is,

$$i' = \frac{1 - 0.35^2}{1.5 \times 292.52} \times 0.75 \times \frac{20{,}000 \times 10^5}{45^3 \times 10^6}$$
$$= 3.29 \times 10^{-5} \text{ radians}$$

14.7 SOME SIMPLE APPROXIMATE PROCEDURES

Quick computations of settlement are often required, for instance in preliminary designs, to compare orders of magnitude of settlement of alternative plans, etc. In such cases some simplified form of stress distribution could be assumed, on the basis of which simple enough expressions for settlement could be arrived at. Following are some such simple procedures for quick and approximate determination of settlement.

14.7.1 Szechy and Varga's Recommendations

Assuming a stress dispersion as shown in Fig. 14.41 Szechy and Varga (1978) recommend the following equations. The average settlement of a circular foundation is,

$$\rho_{mean} = \frac{q}{E} \frac{BH}{(B + 2H \tan \alpha)} \tag{14.47}$$

where H = thickness of compressible soil

The average settlement of a strip foundation, of width B, is given by,

$$\rho_{mean} = \frac{qB}{2E \tan \alpha} \log_e \left(\frac{B + 2H \tan \alpha}{B} \right) \tag{14.48}$$

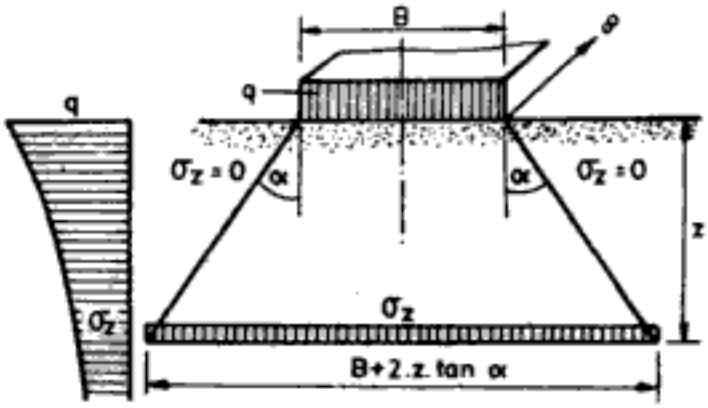

Fig. 14.41 Stress dispersion in soil

14.7.2 Hansen and Lundgren's Recommendations

According to Hansen and Lundgren (1960) the average settlement of a rectangular foundation, $L \times B$, $(L > B)$ is,

$$\rho_{mean} = \frac{qLB}{E(L - B)} \log_e \left(\frac{B + H}{L + H} \times \frac{L}{B} \right) \tag{14.49}$$

Hidden page

Hidden page

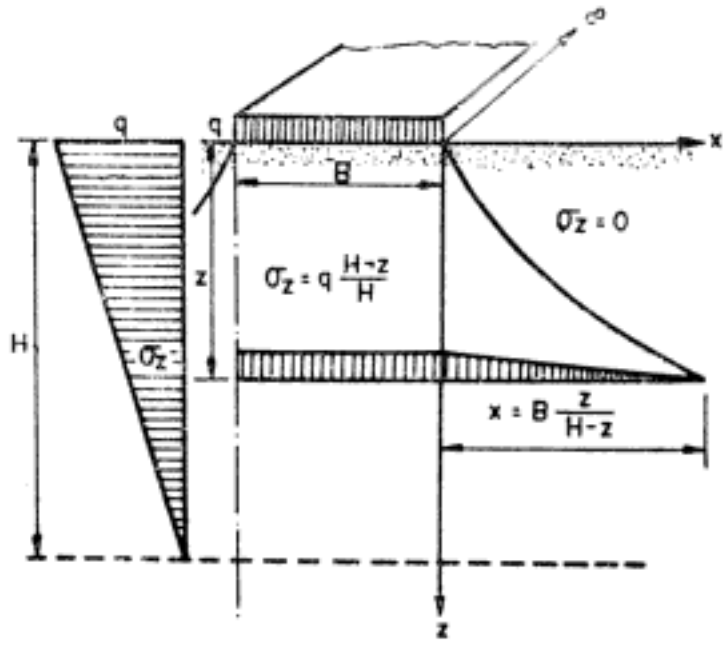

Fig. 14.43 Stress dispersion in soil according to Jaky

With reference to Fig. 14.44 the settlement of the ith layer is given by,

$$\rho_{\text{mean}-i} = \frac{q}{H}\frac{\zeta_i h_i}{E_i} \tag{14.56}$$

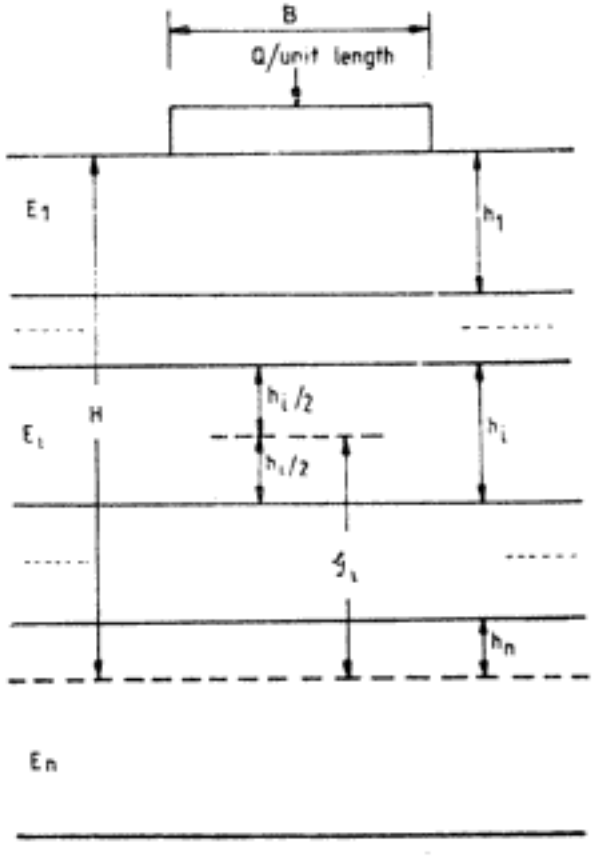

Fig. 14.44 Settlement calculation by Jaky's limit depth method

where $q = Q/B$
$H = 2B$
h_i = thickness of ith layer
E_i = deformation modulus of ith layer
ζ_i = see Fig. 14.44

The total average settlement of foundation is given by,

$$\rho_{mean} = \frac{q}{H} \sum_{i=1}^{n} \frac{\zeta_i h_i}{E_i} \tag{14.57}$$

In homogeneous soil, $n = 1$, $\zeta = H/2$ and the average settlement of foundation is,

$$\rho_{mean} = \frac{qH}{2E} = \frac{qB}{E} = \frac{Q}{E} \tag{14.58}$$

Q 14.22: To determine the average total settlement of a 2.5 m wide strip footing carrying a load of 25 T/m. The footing rests on the surface of a sandy soil profile having a modulus of deformation, $E = 200$ kg/cm².

Ans: From Eq. 14.58,

$$\rho_{mean} = \frac{25}{2000} = 0.0125 \text{ m} = 1.25 \text{ cm}$$

Q 14.23: To determine the average settlement of a 2.5 m wide surface strip footing shown in Fig. 14.45 using Jaky's limit depth assumption.

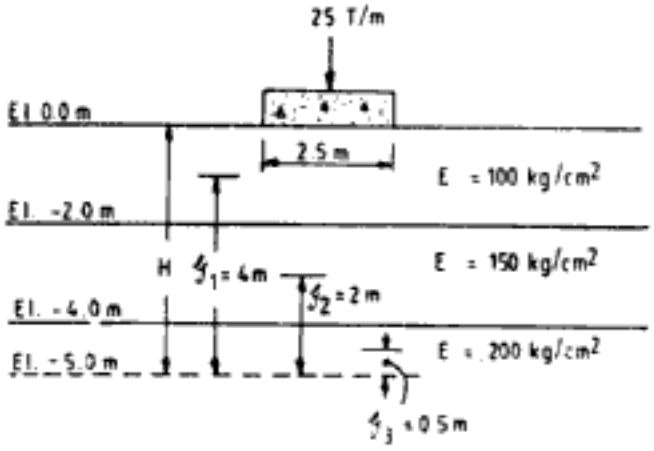

Fig. 14.45 Q 14.23

Ans: Thickness of compressible soil, $H = 2 \times 2.5 = 5$ m
The compressible soil can be divided into three layers with the following details.

Layer 1: $h_1 = 2$ m $\quad \zeta_1 = 4$ m $\quad E_1 = 100$ kg/cm²
Layer 2: $h_2 = 2$ m $\quad \zeta_2 = 2$ m $\quad E_2 = 150$ kg/cm²
Layer 3: $h_3 = 1$ m; $\quad \zeta_3 = 0.5$ m $\quad E_3 = 200$ kg/cm²

Substituting the values in Eq. 14.57 the average settlement of the foundation is,

$$\rho_{mean} = \frac{25/2.5}{5} \times \left[\frac{4 \times 2}{1000} + \frac{2 \times 2}{1500} + \frac{0.5 \times 1}{2000}\right]$$
$$= 0.022 \text{ m} = 2.2 \text{ cm}$$

Hidden page

Table 14.13 Coefficient ω for Calculating the Depth of Active Zone

L/B	$\mu = 0.3$		$\mu = 0.4$	
	I	II	I	II
1	1.17	1.08	1.71	1.58
2	1.60	1.49	2.34	2.20
3	1.89	1.76	2.75	2.59
4	2.09	1.97	3.06	2.90
5	2.25	2.11	3.29	3.10
6	2.41		3.53	
7	2.51		3.67	
8	2.61		3.82	
9	2.69		3.92	
10	2.77		4.05	
Circle	1.04	0.96	1.53	1.41

Note: I is for calculating the average settlement of a flexible base; II is for calculating settlements of rigid foundations.
After Tystovich, 1951.

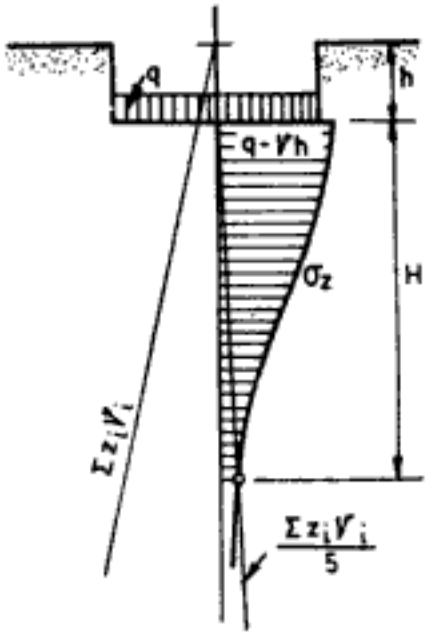

Fig. 14.46 Graphical method for determining the depth of active zone

It must be noted that for very broad foundation (compared to thickness of soil) the net increase in vertical stress will be uniform or constant with depth or nearly so (e.g., one-dimensional consolidation). In such cases values obtained from Eqs 14.59 and 14.60 should be halved.

14.9 DIFFERENTIAL SETTLEMENT AND ANGULAR DISTORTION

The previous sections discuss the total settlement that a foundation may undergo due to the imposed load. A building is not likely to suffer structural damage if it settles down uniformly. There are instances where buildings have settled down so much that what was once a ground floor is now a basement and the building is now short by one storey. In some other buildings where one climbed up steps in the past to enter the building now has to descend down a few steps. These buildings are still operational and are in serviceable condition. Uniform settlement thus does not cause any structural distress, but may call for frequent maintenance of utility and service connections such as water supply and sewarage lines, electricity connections, etc. But, if one part of building settles relatively more than or less than the other part it will be a cause for concern. This relative movement between parts of the building is known as *differential settlement*. Differential settlement between any two points is the difference in their total settlement. *Angular distortion* is the ratio of differential settlement to the distance between the two points. *Tilt* is another form of non-uniform settlement of foundations where one side of building settles more than the other thus affecting the verticality of the building. A classical example of tilt is the Leaning Tower of Pisa. When differential settlement, angular distortion and tilt exceed some maximum levels the building is likely to suffer varying degrees of distress. Figure 14.47 illustrates differential settlement ($\Delta\rho$), angular distortion ($\Delta\rho/l$) and tilt.

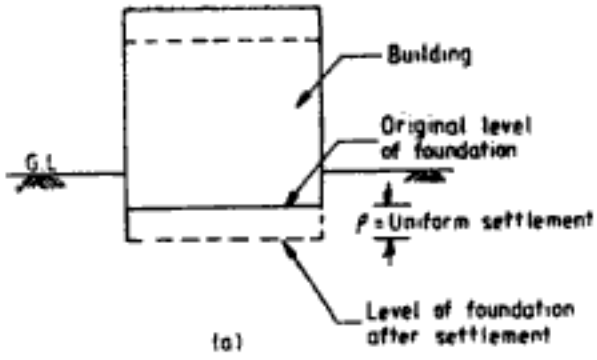

(a)

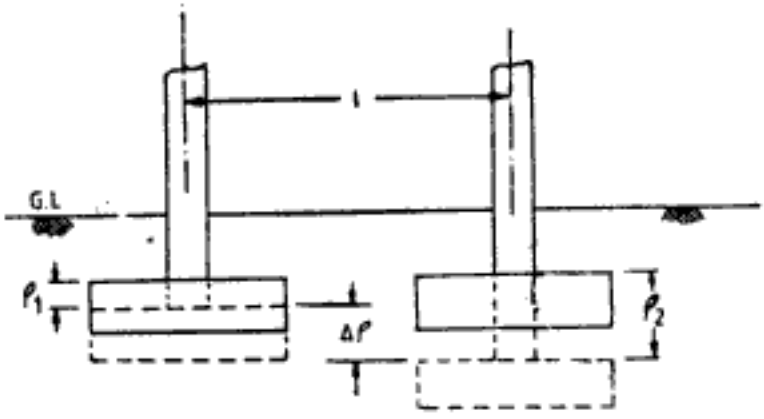

$\Delta\rho = \rho_2 - \rho_1$

angular distortion = $\Delta\rho / l$

(b)

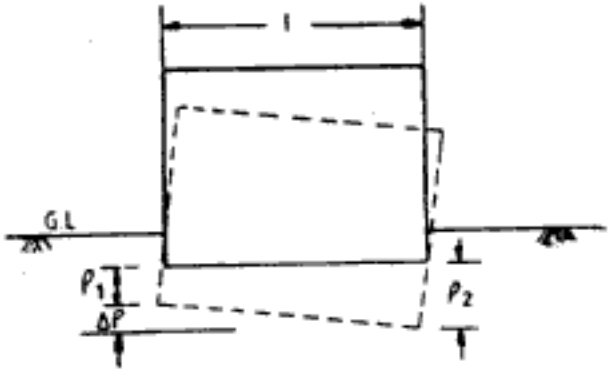

$\Delta\rho = \rho_2 - \rho_1$

angular distortion = $\Delta\rho / l$

(c)

Fig. 14.47 (a) Uniform settlement (b) angular distortion (c) tilt

14.9.1 Relationship Between Total Settlement and Differential Settlement

Generally differential settlement is less than total settlement. The relationship between the two is dependent upon soil type. In case of sand the maximum differential settlement is

Hidden page

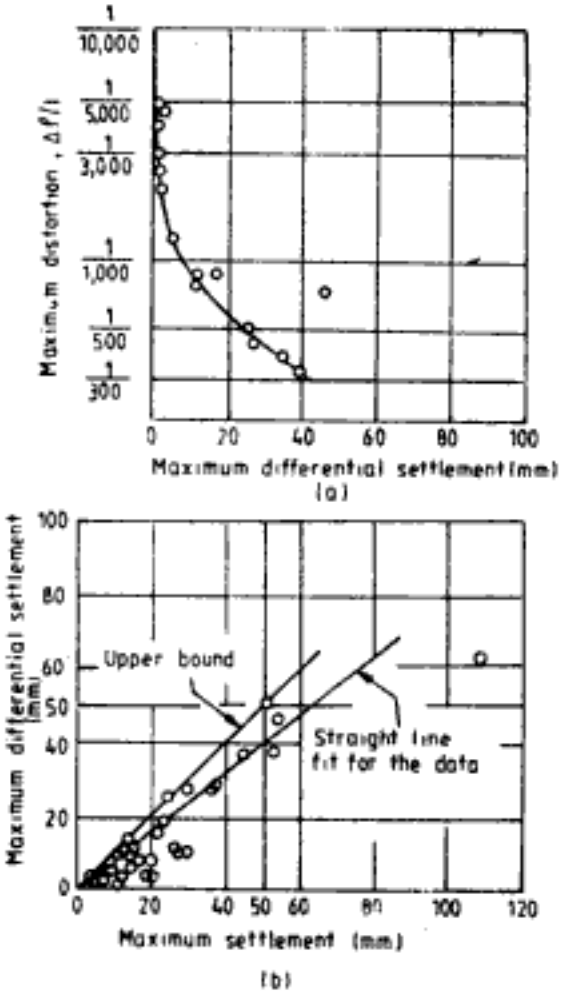

Fig. 14.49 Settlement of structures on sand (After Bjerrum, 1963a and 1963b; from Lambe and Whitman, 1979; with permission of John Wiley and Sons Inc., New York)

14.10 PERMISSIBLE LIMITS OF TOTAL SETTLEMENT, DIFFERENTIAL SETTLEMENT, AND ANGULAR DISTORTION

Based on investigations on buildings many investigators have proposed permissible limits of total and differential settlement and angular distortion. These limits have been studied for different criteria of performance of structure. Building codes also stipulate the allowable limits of settlement and angular distortion. Figure 14.50 and Tables 14.14 to 14.19 present the permissible limits that have been compiled from published literature.

Q 14.24 For a rigid concrete frame structure on clay determine the allowable maximum settlement so that no cracking of building occurs.

Ans: From Fig. 14.50 $\Delta p/l = 1/500 = 0.002$
From Table 14.14 $\Delta p/l = 0.0025$ to 0.004

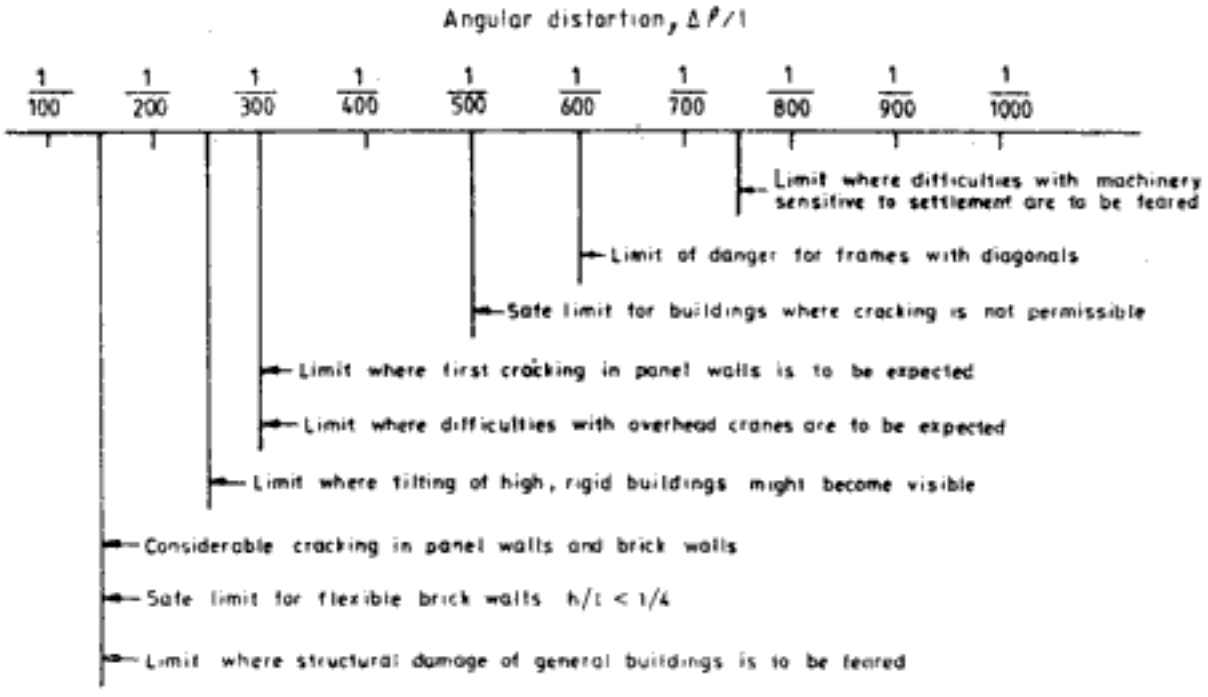

Fig. 14.50 Limits of angular distortion

From Table 14.15 $\Delta\rho/l = 1/300 = 0.0033$
Adopt $(\Delta\rho/l)_{max} = 0.0025$
From Fig. 14.48 $\Delta\rho_{max} = 3$ cm
$\rho_{max} = 6.5$ cm

14.11 PROPORTIONING OF FOUNDATIONS

If the estimated settlement of foundation exceeds prescribed permissible limits then the foundation must be redesigned to bring its settlement down to the permissible limits. The redesign can be done in the following ways, (i) by increasing depth of embedment, (ii) by increasing the bearing area of foundation, and (iii) by making the foundation more oblong. Either any one of these three ways or a combination of any two or all the three ways can be adopted.

Kaniraj (1977), and Kaniraj and Ranganatham (1977b) present analyses to quantify the effects of depth of embedment, bearing area and shape of foundation on the immediate settlement of foundations and on the consolidation settlement of foundations in normally consolidated clay. The results are briefly presented here.

14.11.1 Immediate Settlement

The analysis for immediate settlement is based on Fox's equation for mean elastic settlement (Eq. 13.46).

The effect of varying the depth of settlement can be evaluated using Fig. 13.39. Equation 13.46 indicates that immediate settlement is dependent upon Poisson's ratio. Its

Hidden page

Table 14.16 Permissible Differential Building Slopes by the USSR Code on Both Unfrozen and Frozen Ground

All values to be multiplied by L = length between two adjacent points under consideration. H = height of wall above foundation

Structure	On sand or hard clay	On plastic clay	Average max. settlement, cm
Crane runway	0.003	0.003	
Steel and concrete frames	0.0010	0.0013	10
End rows of brick-clad frame	0.0007	0.001	15
Where strain does occur	0.005	0.005	
Multistorey brick wall			8 $(L/H) \geqslant 2.5$
L/H to 3	0.003	0.004	10 $(L/H) \leqslant 1.5$
Multistorey brick wall			
L/H over 5	0.005	0.007	
One-storey mill buildings	0.001	0.001	
Smokestacks, water towers,			
ring foundations	0.004	0.004	30
	Structures on permanent		
Reinforced concrete frames	0.002-0.0015		15 at 4 cm/year†
Masonry, precast concrete	0.003-0.002		20 at 6 cm/year
Steel frames	0.004-0.0025		25 at 8 cm/year
Timber	0.007-0.005		40 at 12 cm/year

After Mikhejev *et al.*, 1961 and Polshin and Tokar, 1957.
†not to exceed this rate per year.

influence on settlement, however, is not very significant. Immediate settlement increases as μ decreases. The maximum increase because of change in μ from 0.5 to 0 is only 33 per cent for surface footings. This will be still less for embedded footings.

To evaluate the effect of bearing area on immediate settlement, computations for ratio R' defined by Eq. 14.63 are carried out.

$$R' = \frac{\text{immediate settlement of loaded area } Y}{\text{immediate settlement of loaded area } X} \tag{14.63}$$

The area of Y is $(1 + p)$ times that of X where,

$$p = \frac{\text{area of } Y - \text{area of } X}{\text{area of } X} \tag{14.64}$$

X and Y have the same shape. Figure 14.51 shows the variation of R' with p. The accuracy of the average curve in the figure is more than 95 per cent of the actual values. It is evident from this figure that immediate settlement is reduced by 25 per cent when load bearing area is doubled.

Figure 14.52 shows the influence of plan shape on immediate settlement for square foundations. In this,

$$R'' = \frac{\text{immediate settlement of rectangular foundation}}{\text{immediate settlement of square foundation}} \tag{14.65}$$

Table 14.17 Allowable Total and Differential Settlements (Angular Distortion) of Foundations Calculated Without Consideration of the Stiffness of the Structure

Class of building and structure	Type of building or structure	Maximum allowable final settlement (mm)	Maximum allowable angular distortion calculated for three, collinear, adjoining points or foundations of a structure
1	Massive structures of considerable rigidity about horizontal axes founded on rigid mass concrete foundations or cellular or rigid reinforced concrete rafts	150-200	maximum differences of settlements at various points of the structure should not cause tilting of the foundation greater than 1/100 – 1/200 of the ratio of the smallest dimension of the foundation in plan to the height of the structure
2	Statically determinate structures with actual pin joints (three pinned arches, single-span steel trusses, etc.) and timber structures	100-150	$\frac{1}{100} - \frac{1}{200}$
3	Statically indeterminate steel structures and load bearing brickwork construction with reinforced concrete ring beams at every floor level, with longitudinally reinforced concrete strip foundations and with cross walls of at least 250 mm thickness and spaced at not more than 6 m centres and reinforced concrete frame—structures with columns at less than 6 m centres and funded on strip or raft foundations	80-100	$\frac{1}{200} - \frac{1}{300}$
4	Structures of class 3 but not satisfying one of the stated conditions and reinforced concrete structures founded on isolated footings	60-80	$\frac{1}{300} - \frac{1}{500}$
5	Prefabricated structures consisting of large slab or block elements	50-60	$\frac{1}{500} - \frac{1}{700}$

Note: (1) Smaller values quoted relate to public buildings, dwellings, or buildings with structural members or finishes particularly sensitive to differential settlement; larger values relate to taller buildings of considerable rigidity about horizontal axes or to structures which can accept such movements.

(2) In special cases (such as gantry beams, high-pressure boilers, special storage tanks, silos under differential loading, etc.) allowable maximum or differential settlements or both should be taken as specified by service or mechanical engineers or by manufacturers.

After Wilun and Starzewski, 1975.

Table 14.18 Allowable Values of Average Settlement and Banking for Normal Life of Tower Type Structures

The height of smoke stacks (m)	Mean settlement (cm)	Relative banking
$H \leqslant 100$	40	0.005
$100 < H \leqslant 200$	30	$1/2H$
$200 < H \leqslant 300$	20	$1/2H$
$H > 300$	10	$1/2H$

After Egorov, 1977.

Table 14.19 Maximum and Differential Settlements of Buildings

Sl. No.	Type of structure	Isolated foundations						Raft foundations					
		Sand and hard clay			Plastic clay			Sand and hard clay			Plastic clay		
		Maximum settlement	Differential settlement (mm)	Angular distortion	Maximum settlement	Differential settlement (mm)	Angular distortion	Maximum settlement	Differential settlement (mm)	Angular distortion	Maximum settlement	Differential settlement (mm)	Angular distortion
(i)	Steel structure	50	$0.0033L$	1/300	50	$0.0033L$	1/300	75	$0.0033L$	1/300	100	$0.0033L$	1/300
(ii)	Reinforced concrete structure	50	$0.0015L$	1/666	75	$0.0015L$	1/666	75	$0.002L$	1/500	100	$0.002L$	1/500
(iii)	Plain brick walls in multi-storeyed buildings												
	(a) For $L/H \leqslant 3$	60	$0.00025L$	1/4000	80	$0.00025L$	1/4000	←——Not likely to be encountered——→					
	(b) For $L/H \geqslant 3$	60	$0.00033L$	1/3000	80	$0.00033L$	1/3000						
(iv)	Water towers and silos	50	$0.0015L$	1/666	75	$0.0015L$	1/666	100	$0.0025L$	1/400	125	$0.0025L$	1/400

Note: The values given in the table may be taken only as a guide and the permissible settlement and differential settlement in each case should be decided as per requirements of the designer.

L denotes the length of deflected part of wall/raft or centre-to-centre distance between columns.

H denotes the height of wall from foundation/footing.

After National Building Code of India, 1983. Reprinted by permission of Indian Standards Institute, New Delhi.

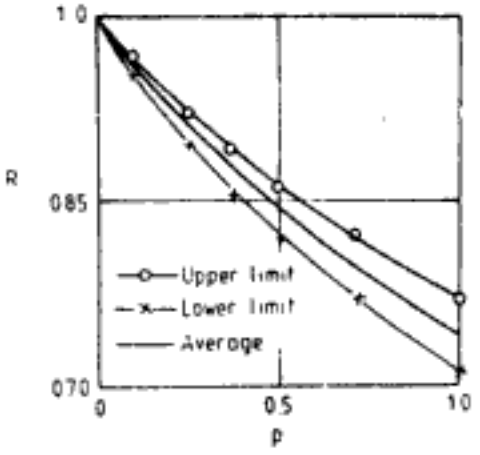

Fig. 14.51 Variation of R' with p
(After Kaniraj, 1977)

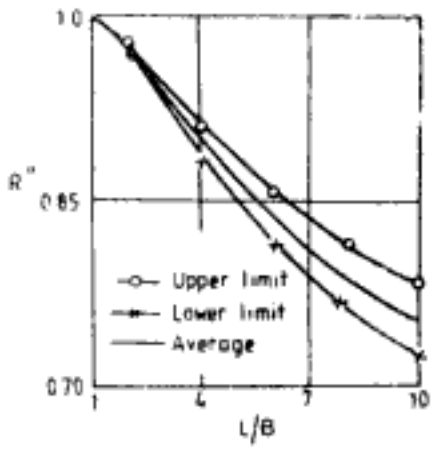

Fig. 14.52 Variation of R'' with L/B
(After Kaniraj, 1977)

The rectangular and square foundations have the same bearing area. Here, also the accuracy of the average curve is more than 95 per cent of actual values. It can be inferred from Fig. 14.52 that the settlement of a square loaded area decreases on the average by 25 per cent when it is changed into a rectangle (with no change in bearing area) with sides ratio of 1 : 10. However, if it is changed into a rectangle with sides ratio of 1 : 3, the usually adopted maximum ratio, the average reduction is only of the order of 7 per cent.

14.11.2 Primary Consolidation Settlement

The effect of increasing the depth of embedment is found to significantly decrease the consolidation settlement also. For example, if the depth of embedment of square footings is increased from $0.5B$ to $1.5B$ (B is the side of footing) the reduction in settlement is of the order of 30 to 50 per cent.

Figure 14.53 shows the effect of bearing area on settlement. R_c' is defined as,

$$R_c' = \frac{\text{primary consolidation settlement of loaded area } Y}{\text{primary consolidation settlement of loaded area } X} \tag{14.66}$$

Loaded area X and Y here have the same shape. Area of Y is $(1 + p)$ times that of X and p is given by Eq. 14.64. In Fig. 14.53 the average curve represents the variation mostly with an accuracy greater than 90 per cent of actual values. It is evident from this curve that settlement reduces by 25 per cent when the load bearing area doubles.

The influence of shape of foundation on settlement is shown in Fig. 14.54. R_c'' is given by,

$$R_c'' = \frac{\text{primary consolidation settlement of rectangular foundation}}{\text{primary consolidation settlement of square foundation}} \tag{14.67}$$

The rectangular and square foundations have the same bearing area. Settlement of a loaded area decreases on the average by 25 per cent when the loaded area is changed from a square into a rectangle with sides ratio of 1 : 10. However, if the square foundation is changed into a rectangular foundation with sides ratio of 1 : 3 the average reduction in settlement is very small and amounts to 6 per cent.

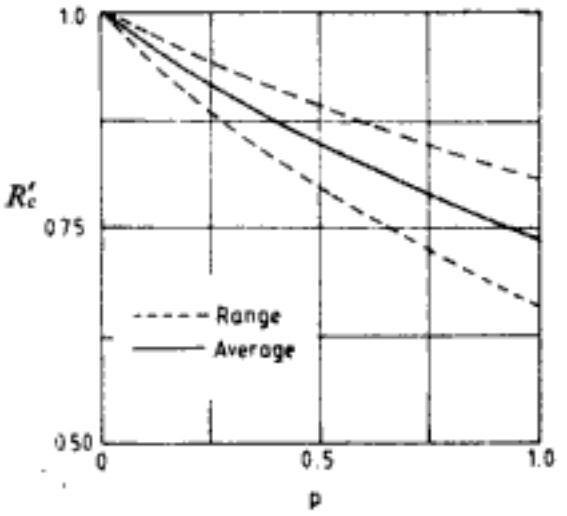

Fig. 14.53 Variation of R_c' with p (After Kaniraj and Ranganatham, 1977b)

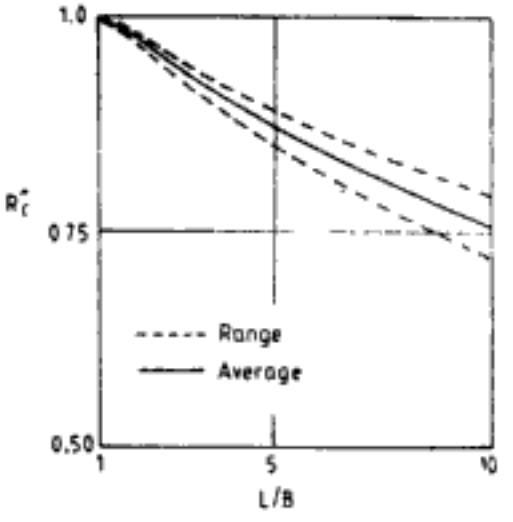

Fig. 14.54 Variation of R_c'' with L/B (After Kaniraj and Ranganatham, 1977b)

14.12 RATE OF SETTLEMENT

The total settlement in pervious soils like sand occurs almost instantaneously. The differential settlement too then occurs rapidly and when excessive causes damage to the building. In clayey soils only the immediate settlement occurs instantaneously but the consolidation settlement occurs over a long period of time. The building has time to adjust to the differential movements, and hence higher differential settlement in clay than in sand is permissible. For these very reasons one must take into account temporary and transient loads also in determination of settlement in sand, but these loads will not cause any significant settlement in clayey soils where it is adequate to consider only the permanent loads for settlement computation.

The amount of primary consolidation settlement at any time since the beginning of application of load can be determined by knowing the average degree of consolidation (see Ch. 7) at that instant. The settlement at time t after the load has been imposed is given by,

$$\rho_{c-t} = U_{av,T}\rho_c \tag{14.68}$$

where ρ_c = total primary consolidation settlement

ρ_{c-t} = primary consolidation settlement at time t

$U_{av,T}$ = average degree of consolidation at time t

Average degree of consolidation can be determined by procedures described in Ch. 7.

Q 14.25: For the problem in Q 7.2 determine the amount of primary consolidation settlement if at the end of consolidation ρ_c is 63 cm.

Ans: For 400 days, $U_{av,T} = 70\%$

$$\rho_{c-400\text{days}} = 0.7 \times 63 = 44.1 \text{ cm}$$

For time dependent loading shown in Fig. 7.28 apart from Olsen's procedure explained in Ch. 7 the following approximate procedure of Taylor (1948) can also be used.

The primary consolidation settlement at any time during construction; i.e., $t < t_c$:

$$\rho_{c-t} = \text{(settlement for instantaneous loading computed using } 0.5\,t) \times \text{(fraction of final load in place)} \quad (14.69)$$

The settlement at any time t greater than construction period t_c ($t > t_c$), is given by,

$$\rho_{c-t} = \text{settlement for instantaneous loading computed using } (t - 0.5\,t_c) \quad (14.70)$$

Q 14.26: For the problem in Q 7.4 determine the amount of settlement 60 days and 450 days after the beginning of construction. The total primary consolidation settlement of layer is 97 cm.

Ans:

(a) *Using Olsen's solutions (Fig. 7.30)*

for $t = 60$ days, $U_{av,T} = 7\%$, from Q 7.4

$$\rho_{c-60\text{ days}} = 0.07 \times 97 = 6.79 \text{ cm}$$

for $t = 450$ days, $U_{av,T} = 67\%$, from Q 7.4

$$\rho_{c-450\text{ days}} = 0.67 \times 97 = 65 \text{ cm}$$

(b) *Using Taylor's procedure*

for $t = 60$ days

$$0.5\,t = 30 \text{ days}$$

$$\text{time factors for 30 days } T = \frac{1.65 \times 10^{-3} \times 30 \times 24 \times 60 \times 60}{375 \times 375}$$

$$= 0.03$$

$$\text{Using Eq. 7.29,} \qquad U_{av,T} = \sqrt{4 \times 0.03/\pi}$$

$$= 0.195$$

$$\text{Fraction of load in place at 60 days} = \frac{t}{t_c} = \frac{60}{150} = 0.4$$

Using Eq. 14.69,

$$\rho_{c-60\text{ days}} = (0.195 \times 97) \times 0.4$$

$$= 7.6 \text{ cm}$$

for $t = 450$ days

$$t - 0.5\,t_c = 450 - (0.5 \times 150) = 375 \text{ days}$$

$$\text{time factor for 375 days } T = \frac{1.65 \times 10^{-3} \times 375 \times 24 \times 60 \times 60}{375 \times 375}$$

$$= 0.38$$

Using Fig. 7.18 $U_{av,T} = 0.67$

$$\rho_{c-400\text{ days}} = 0.67 \times 97 = 65 \text{ cm}$$

from Eq. 14.70

The procedures described in this chapter to determine settlement of foundations give fairly good results. Settlements computed by theory have been found to be comparable with the actually recorded values of settlement. However, the rate of settlement predicted by theory is usually in great error. Even thin seams of pervious layers in compressible deposits or greater coefficient of permeability of soil in horizontal direction than in vertical direction can greatly accelerate the rate of consolidation and settlement. This is evident from a

comparison of results in Q 14.27 and Q 14.28. Similarly any blockage in drainage layers can reduce the rate of settlement appreciably.

Q 14.27: Determine the primary consolidation settlement of the layered soil deposit in Q 7.5, if the settlement of each layer after completion of consolidation is as below:

Layer 1 = 15 cm
Layer 2 = 30 cm
Layer 3 = 18 cm

Ans: Settlement of the deposit at the end of consolidation

$$= 15 + 30 + 18 = 63 \text{ cm}$$

For 1250 days, $U_{av,T} = 45\%$, from Q 7.5

$$\rho_{c-1250 \text{ days}} = 0.45 \times 63 = 28.35 \text{ cm}$$

Q 14.28: Determine the primary consolidation settlement of the layered soil deposit in Q 7.5 but with thin seams of effective drainage layers present at the interface of layers 1 and 2 and also of layers 2 and 3. The final consolidation settlement of each layer is same as given in Q 14.27.

Ans: In this case the three layers consolidate independently of each other (Fig. 7.34).

In Layer 1: This belongs to Case 2 (Sec. 7.2.4).

$$H = 1.25 \text{ m}$$

$$T = \frac{3.85 \times 10^{-4} \times 1250 \times 24 \times 60 \times 60}{125 \times 125} = 2.66$$

From Eq. 7.30,

$$U_{av,T} = \left[1 - \frac{8}{\pi^2} \exp\left(1 - \frac{\pi^2 \times 2.66}{4}\right)\right] = 0.999$$

amount of consolidation in 1250 days in first layer

$$= 0.999 \times 15 = 14.985 \text{ cm}$$

In Layer 2: This again belongs to Case 2 (Sec. 7.2.4).

$$H = 1.5 \text{ m}$$

$$T = \frac{1.65 \times 10^{-3} \times 1250 \times 24 \times 60 \times 60}{150 \times 150} = 7.92$$

From Eq. 7.30 $U_{av,T} \simeq 1.00$

$$\text{settlement} = 30 \text{ cm}$$

In Layer 3: This belongs to Case 3 (Sec. 7.2.4).

$$H = 2 \text{ m}$$

$$T = \frac{1.1 \times 10^{-3} \times 1250 \times 24 \times 60 \times 60}{200 \times 200} = 2.97$$

From Eq. 7.30, $U_{av,T} = 0.999$

$$\text{settlement} = 0.999 \times 18 = 17.982 \text{ cm}$$

Total settlement for 1250 days,

$$= 14.985 + 30 + 17.982$$
$$= 62.967 \text{ cm}$$

Comparing results of Q 14.27 and Q 14.28 it can be easily appreciated that presence of thin seams of pervious layers have almost achieved full consolidation whereas in their absence the average degree of consolidation is only 45 per cent.

15

PILE FOUNDATIONS

The definition of shallow foundations and deep foundations is given in Ch. 11. Also therein explained are the differences between the two categories of foundation in terms of foundation geometry, mechanism of load transfer and changes induced in the soil during installation of the foundation. Pile foundation belongs to the category of deep foundation. As shown in Fig. 15.1 a pile is a slender columnar structure buried inside the earth. It serves to transmit the load to deeper lying firm strata when the soil at shallow depth cannot provide adequate support to the load. Apart from this, pile foundations are also commonly used under the following circumstances:

1. when the structure is expected to carry large uplift loads
2. when large lateral loads act on the foundation
3. when foundation is subjected to large eccentric loads, inclined loads, and moments

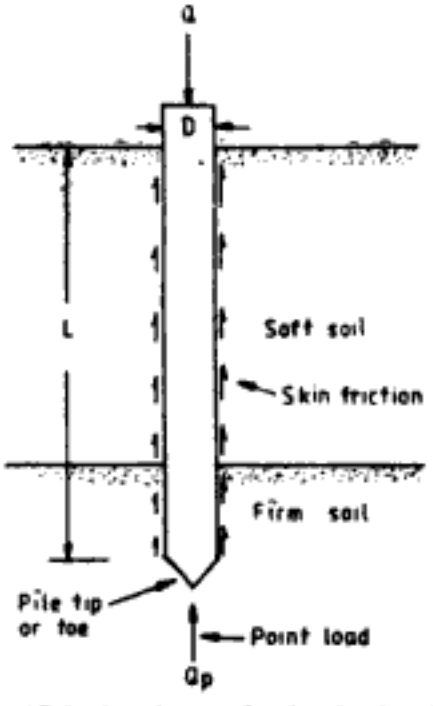

Fig. 15.1 Load transfer in single pile

4. when the soil near the surface undergoes large volume change depending upon environmental factors and the superstructure has to be supported on a deeper stable zone
5. when scouring of soil, immediately below the foundation, is expected to occur
6. when a future construction with deep excavation is anticipated in the adjacent area

Figure 15.1 is only a general representation of a pile foundation. For, the shape of pile can be of different forms, such as, straight sided, tapered, corrugated, fluted, with enlarged base, etc. Similarly in cross-section also a pile can be circular, hexagonal, square, H-section, etc. The array of available pile types is so numerous that a detailed and systematic cataloguing of them will be a mindboggling exercise. Table 15.1 presents a concise categorisation of different types of piles. It is evident that several combinations of different types for different factors are possible.

Table 15.1 Types of Piles Based on Different Factors

Material	Shape	Cross-section	Load transfer	Method of forming	Method of installation	Use	Length
Timber	Cylindrical	Circular	Friction	Cast-*in-situ*	Bored	Load bearing	Short
Steel	Tapered	Square	Bearing	Pre-cast	Driven	Load test	Long
Concrete	Under-reamed	Hexagonal	Uplift	Prestressed	Jacked	Offshore	Slender
Composite	Corrugated	Octagonal			Vibrated	Compac-tion	Large diameter
		I-section			Jetted		
		H-section			Tremie		
		Pipe					

In uniform diameter and straight sided pile the notations adopted to describe the pile are given in Fig. 15.1. D is the diameter or the smallest dimension of the pile. L is the length of the pile embedded inside the soil. In piles which are totally buried inside the soil the length of the pile is reckoned from the cut-off level to the tip of the pile.

15.1 CLASSIFICATION OF PILES

Different criteria have been used in the past to classify the piles, mostly, based on the factors that are listed in Table 15.1. But such classifications serve a very limited purpose. Of late the criterion adopted to classify piles is the *influence of installation of pile on the soil.* Based on this criterion, piles can be classified as

1. Displacement piles
2. Non-displacement piles

A large volume of soil is displaced laterally and upwards during the installation of displacement piles. Consequently, in clays, the soil is remoulded to a distance of about 2 diameters of pile. Near the periphery of pile very high excess pore water pressures are developed. This excess pore water pressure dissipates over a period of time and the soil regains its initial shear strength. In case of loose sands installation of displacement piles compacts the sand which increases the load carrying capacity of the pile. Kishida (1967) suggests that the value

of angle of shearing resistance $\bar{\phi}$ in sands after pile driving varies as shown in Fig. 15.2. If the initial value of angle of shearing resistance ($\bar{\phi}_1$) is less than 40° the increase in $\bar{\phi}$ is given by a linear relationship over a distance of 3.5D from the centre of pile. Beyond this distance the value of $\bar{\phi}_1$ is not affected. $\bar{\phi}_2$ in the figure is given by

$$\bar{\phi}_2 = \frac{\bar{\phi}_1 + 40^\circ}{2} \tag{15.1}$$

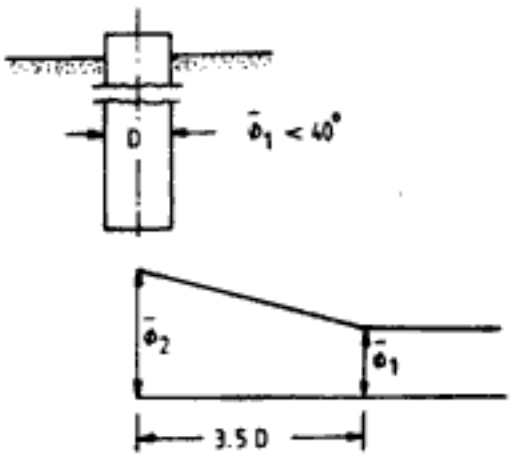

Fig. 15.2 Variation of ϕ in sands due to installation of displacement piles

For $\bar{\phi}_1 = 40^\circ$ there is no change in the angle of shearing resistance. In fact, in very dense soils $\bar{\phi}$ will decrease due to dilation effects. Also large lateral stresses will be set up on the surface of the pile in sand.

While all solid precast driven piles can be cited as examples of displacement piles, there are some piles which can be classified as *small displacement* piles. Pipe piles and H-section piles come under such category which because of their smaller cross-section produce small displacement of soil.

Non-displacement piles involve no displacement of soil. A void space created in soil is refilled with the pile. Bored cast-*in-situ*, and bored pre-cast piles are examples of this type. During installation of non-displacement piles the soil on the sides of borehole softens due to migration of water, due to absorption of water from wet concrete, or due to water used to expedite or facilitate boring operation. The softening of soil reduces its shear strength. To minimise this, the time lag between boring and completing the pile should be kept as small as possible. The lateral stresses on the pile surface will be reduced in non-displacement piles. In sands there will be loosening of soil around the shaft and the base.

The details of classification of piles are illustrated in Fig. 15.3.

15.2 SELECTION OF PILE TYPE

Pile foundation is chosen for a structure generally when other alternatives of shallow foundations are not feasible or are uneconomical. Pile foundation is relatively more expensive than shallow foundation and requires special skills and equipment for construction.

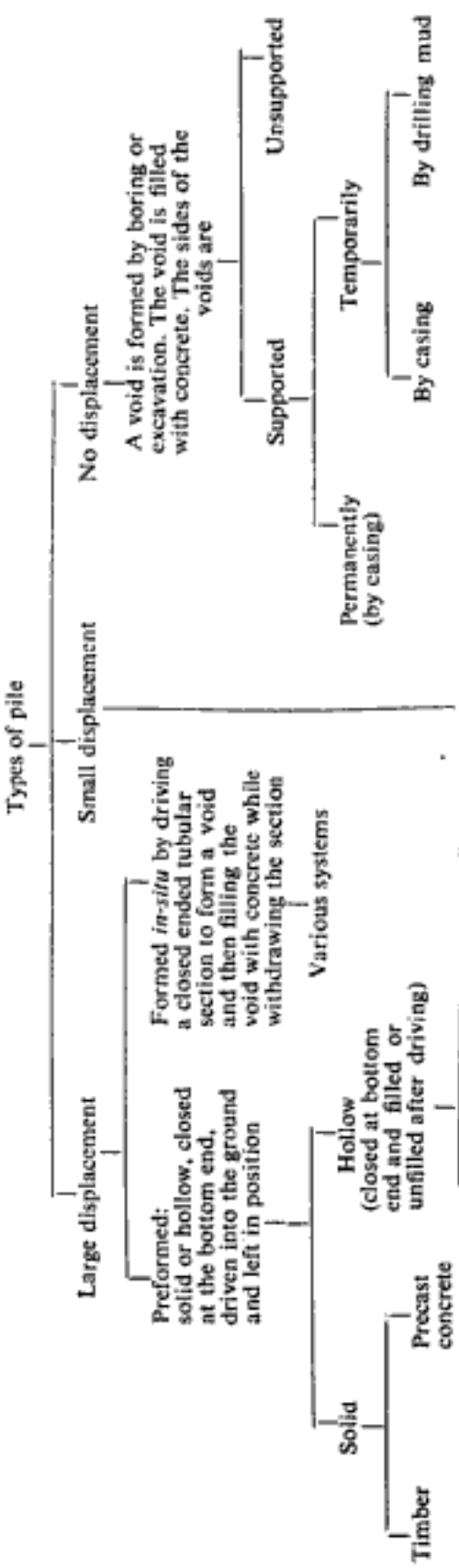

Fig. 15.3 Classification of piles (After Simons and Menzies, 1975; with permission)

Hidden page

Hidden page

The typical arrangement for pile driving operation is shown in Fig. 15.4. The different types of hammers used to drive the piles are: (i) drop hammers, (ii) single acting hammers, (iii) double acting hammers, (iv) differential acting hammers, and (v) diesel hammers. In drop hammers the impact on the pile is due to the free fall of the hammer under gravity. The impact energy is transmitted to the pile through an arrangement of cap block, helmet and cushion as shown in Fig. 15.4. Single acting hammers are lifted by steam or air pressure and they deliver the impact through free fall under gravity. Double acting and differential acting hammers are lifted up and forced down by steam or air pressure and thus usually have a higher energy rating than single acting hammers. Differential acting hammers maintain more control over constant steam or air pressure than double acting hammers. Diesel hammers compress the air-fuel mixture during their downward travel. The mixture explodes producing pile driving energy and also simultaneously lifting the ram or hammer up.

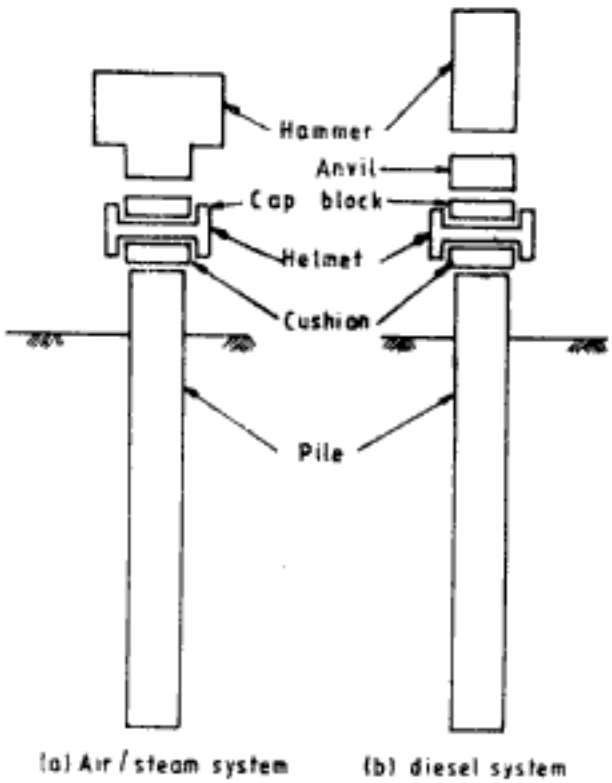

Fig. 15.4 Pile driving arrangement, (a) air/steam system, (b) diesel system

The energy delivered by the hammer is partly used in the penetration of the pile into the ground and the rest is wasted in losses. This is the basic premise in the development of any pile driving formula. The loss of energy occurs in many forms such as, elastic compression of pile, compression of soil, losses in helmet and cushion, etc. There are a vast number of driving formulae in existence. According to Smith (1960) there are 450 such formulae. Investigations reveal that only a few of these have some limited use. These formulae are presented here. The following are the notations used in the formulae:

A = cross-sectional area of pile
E_p = modulus of elasticity of pile

e_h = hammer efficiency
E_h = energy rating for hammer
H = height of fall of hammer
K_1 = elastic compression of cap block and pile cap
K_2 = elastic compression of pile
K_3 = elastic compression of soil
L = length of pile
n = coefficient of restitution
Q_u = ultimate capacity of pile
s = the amount of penetration of the pile point per blow of hammer, called *set*
W_h = weight of hammer
W_p = weight of pile including weight of pile cap, cap block and driving shoe

According to *Engineering News formula*,

$$Q_u = \frac{e_h E_h}{s + C} \tag{15.3}$$

$C = 2.5$ cm for drop hammer
$C = 0.25$ cm for single acting steam hammer
$C = 0.25 \frac{W_p}{W_h}$ cm for steam hammer on very heavy piles

In Eq 15.3 consistent units are used. If efficiency of hammer is assumed to be equal to unity and E_h for hammer is taken as $W_h H$, then Eq. 15.3 can be written as,

$$Q_u = \frac{W_h H}{s + C} \tag{15.4}$$

Engineering News formula has been modified recently and the modified versions can be written as follows:

$$Q_u = \frac{e_h E_h}{s + 0.25} \frac{W_h + n^2 W_p}{W_h + W_p} \tag{15.5a}$$

and,

$$Q_u = \frac{1.25 e_h E_h}{s + 0.25} \frac{W_h + n^2 W_p}{W_h + W_p} \tag{15.5b}$$

With these modified formulae the recommended factor of safety to be used is 6.

Another well-known driving formula is Hiley's formula (1930). This is given by,

$$Q_u = \frac{e_h W_h H}{s + \frac{1}{2}(K_1 + K_2 + K_3)} \frac{W_h + n^2 W_p}{W_h + W_p} \tag{15.6}$$

From recommendations of Chellis (1961) values of K_1 can be tabulated as in Table 15.3. K_2 in Eq. 15.6 can be computed as,

$$K_2 = \frac{Q_u L}{A E_p} \tag{15.7}$$

Table 15.3 Values of K_1 (Eq. 15.6)

Material to which blow is applied	K_1 in mm for driving stresses (P/A) of			
	35 kg/cm²	70 kg/cm²	105 kg/cm²	140 kg/cm²
Directly on head of steel piling or pipe	0	0	0	0
Directly on head of timber pile	1.0	2.0	3.0	5.0
5 mm fibre disk between two 10 mm steel plates	0.5	1.0	1.5	2.0
Steel covered cap containing wood packing for steel H or pipe piling	1.0	2.0	3.0	4.0
Precast concrete pile with 75-100 mm packing inside cap	3.0	6.0	9.0	12.5

After Chellis, 1961. By permission of McGraw-Hill Book Company, New York.

which means that Q_u by Hiley's equation will have to be computed by trial and error iterative procedure. K_3 can be taken as,

$$K_3 = 0 \quad \text{for hard soil}$$
$$K_3 = 2.5 \text{ to } 5 \text{ mm} \quad \text{for other soils}$$

The factor of safety to be applied to Hiley's solution is 3. Janbu's formula for Q_u is given by,

$$Q_u = \frac{E_h}{K_u s} \tag{15.8}$$

where $K_u = C_d\left(1 + \sqrt{1 + \frac{\lambda}{C_d}}\right)$

$$\lambda = \frac{E_h L}{A E_p s^2}$$

$$C_d = 0.75 + 0.15 \frac{W_p}{W_h}$$

Consistent units must be used in Janbu's formula. The factor of safety to be used with the formula varies from 3 to 6.

Another useful formula is the Danish formula which expresses Q_u as,

$$Q_u = \frac{e_h E_h}{s + C_1} \tag{15.9}$$

where $C_1 = \sqrt{\frac{e_h E_h L}{2AE_p}}$ (in the same units of s)

A factor of safety of 3 to 6 is used with Danish formula. Table 15.4 gives the values of e_h that may be used in the driving formulae. Similarly Tables 15.5 and 15.6 give the values of coefficient of restitution, n. While using pile driving formulae the following points must be kept in mind.

Table 15.4 Values of e_h

Hammer type	e_h
Drop hammer released by trigger	1.00
Drop hammer actuated by rope and friction winch	0.75
Single acting hammer	0.75–0.85
Double acting hammer	0.85
Differential acting hammer	0.75
Diesel hammer	1.00

Table 15.5 Values of Coefficient of Restitution, n

Material	n
Broomed wood	0
Wood pile (non-deteriorated end)	0.25
Compact wood cushion on steel pile	0.32
Steel-on-steel anvil on either steel or concrete pile	0.50
Cast-iron hammer on concrete pile without cap	0.40

After ASCE, 1941.

Table 15.6 Values of Coefficient of Restitution, n

Pile type	Head condition	Drop, single-acting or diesel hammers	Double-acting hammers
Reinforced concrete	Helmet with composite plastic or greenheart dolly and packing on top of pile	0.4	0.5
	Helmet with timber dolly*, and packing on top of pile	0.25	0.4
	Hammer direct on pile with pad only	—	0.5
Steel	Driving cap with standard plastic or greenheart dolly	0.5	0.5
	Driving cap with timber dolly*	0.3	0.3
	Hammer direct on pile	—	0.5
Timber	Hammer direct on pile	0.25	0.4

*not greenheart.
After Whitaker, 1970. Reprinted by permission of Pergamon Books Ltd , Oxford.

(a) The formulae are applicable for point bearing piles and not if significant skin friction is mobilised along the pile.

(b) The Q_u is a dynamic and instantaneous value. The actual static ultimate resistance will be significantly different if soil conditions around the pile change over time after pile driving. This is typically the case in clays where soil around pile gets remoulded during driving and regains its strength over time.

(c) From works of several investigators (Agerschou, 1962; Flaate, 1964; Michigan State Highway Commission, 1965; Olsen and Flaate, 1967; Sorensen and Hansen, 1957) it can be concluded that the Janbu, Danish and Hiley formulae are generally more reliable than the other driving formulae. Hiley's formula is reasonably good for timber piles and Janbu's formula gives good results in timber, steel and concrete piles. Engineering News formula is generally unreliable and does not give satisfactory results.

(d) In general, almost all the driving formulae have been discredited and are unreliable. They are not recommended for design purposes. Still they are widely used in practice. The pile driving record may be useful for control of piling operation in the field but cannot be entirely depended on for ultimate load capacity of pile.

Q 15.1: Determine the ultimate load carrying capacity of a driven pipe pile given the following data: W_h (drop hammer) = 10 T; H = 1.5 m; OD of pipe = 430 mm; ID of pipe = 400 mm; L = 20 m; $E_p = 2.1 \times 10^6$ kg/cm²; density of steel = 7.9 T/m³; $e_h = 0.75$; $n = 0.3$; number of blows for last 30 cm penetration = 10; weight of cap block and helmet = 500 kg.

Ans: Area of pipe, $A = \pi\left(\frac{43^2}{4} - \frac{40^2}{4}\right) = 195.56 \text{ cm}^2$

$$W_p = (195.56 \times 10^{-4} \times 20 \times 7.9) + 0.5 = 3.59 \text{ T}$$

$$s = 30/10 = 3 \text{ cm}$$

Using Janbu's formula (Eq. 15.8)

$$\lambda = \frac{10 \times 10^3 \times 150 \times 20 \times 100}{195.56 \times 2.1 \times 10^6 \times 3^2} = 0.81$$

$$C_d = 0.75 + 0.15 \times \frac{3.59}{10} = 0.804$$

$$K_u = 0.804\left(1 + \sqrt{1 + \frac{0.81}{0.804}}\right) = 1.943$$

$$Q_u = \frac{10 \times 150}{1.943 \times 3} = 257 \text{ T}$$

Using a factor of safety of 4,

$$Q_{safe} = \frac{257}{4} = 64 \text{ T}$$

Using Danish formula (Eq. 15.9)

$$C_1 = \sqrt{\frac{0.75 \times 10 \times 10^3 \times 150 \times 20 \times 100}{2 \times 195.56 \times 2.1 \times 10^6}} = 1.655 \text{ cm}$$

$$Q_u = \frac{0.75 \times 10 \times 150}{3 + 1.655} = 242 \text{ T}$$

With a factor of safety of 4,

$$Q_{safe} = \frac{242}{4} = 60 \text{ T}$$

Hidden page

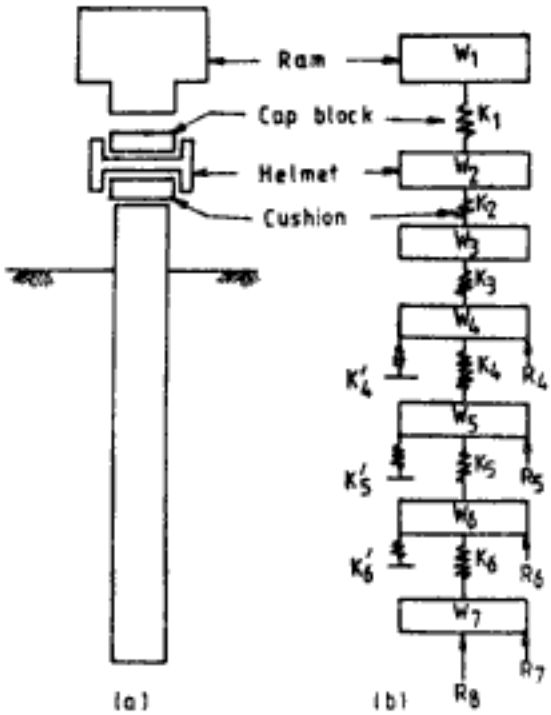

Fig. 15.5 Wave equation analysis: (a) actual pile, (b) idealisation of pile
W_1 to W_7—weight of pile segments
R_4 to R_7—soil reactions
R_8—pile point reaction
K'_4 to K'_6—soil springs

Wave equation analysis can be used:

(a) to determine ultimate load capacity of a pile, by plotting the load v. set curve. Here again, the ultimate load is only a dynamic resistance of the pile;
(b) for the selection of suitable hammer and pile combinations so that the pile can be driven to the required depth of penetration;
(c) to analyse for the driving stresses over the entire length of pile and to thus ensure that no section of the pile is overstressed during driving.

4. *Finite element method*: Finite element method is rarely used as a routine procedure in the design office. Often its use is limited to research investigations or to those rare instances where a complete and more detailed information on the behaviour of pile is required. Given the amount of variation in the natural soil conditions and the complexities introduced due to pile installation operations, the results of finite element analysis can be only as accurate as the parameters used in the analysis in spite of their mathematical rigour and sophistication. The method requires data collected from carefully conducted extensive field and laboratory testing programme. Obviously time and cost dimensions are more in this exercise.

5. *Static formulae*: The determination of ultimate load capacity using static formulae is also called the *soil mechanics approach* since it is based on the principles of soil

mechanics. For the load transfer mechanism suggested in Fig. 15.1 the static formulae assume that,

$$Q_u = Q_{su} + Q_{pu} \tag{15.11}$$

where Q_{su} = ultimate skin frictional load

Q_{pu} = ultimate point load

It is thus assumed that at the instant of ultimate load capacity of the pile the ultimate point and skin friction loads are mobilised simultaneously. In fact this does not occur. Very small relative movement between pile and soil is required to mobilise full skin friction. This movement is of the order of 13 to 25 mm or some investigators say is about one per cent of the pile diameter. When the relative movement exceeds this value the skin frictional resistance drops. The movement required for the full mobilisation of point resistance is significantly higher and depends on the size of pile and method of installation. For example, in clays, and for driven piles in sand the movement required is about 10 per cent of the diameter of the pile. For piles buried in sand the required movement is as high as 25 to 30 per cent of the pile diameter. This leads to two inferences:

(a) When the ultimate skin friction resistance is mobilised only a fraction of the ultimate point load is mobilised.

(b) When the ultimate point load is mobilised the skin friction resistance has reduced to a lower value than its peak.

Hence, a true total ultimate state in the soil mechanics sense lies between these two states. Despite this we will persist with our definition of ultimate load by Eq. 15.11 for reasons of simplicity and the demonstrated utility of such a simplification without being grossly in error. Since static formulae are dependable and more convenient to use in design office these are discussed in more detail in the following sections.

Ultimate Load Capacity by Static Formulae

1. Piles in clay

(a) *Driven piles—skin friction*

Three different approaches are suggested for the calculation of ultimate skin frictional capacity of piles driven into clay. These are:

α-method (or total stress approach)
β-method (or effective stress approach)
λ-method (or pseudo-effective stress approach)

α-method: In the α-method unit skin friction resistance on the pile f_s is expressed as the adhesion between pile and soil, c_a.

$$f_s = c_a = \alpha c_u \tag{15.12}$$

where c_u = undrained cohesion or undrained strength (S_u) of soil

α = a factor called adhesion factor

Thus the correlation between f_s and c_u is through the adhesion factor α. In this total stress approach skin friction is expressed in terms of undrained cohesion on the basis that considerable time is required for the excess pore water pressure to dissipate in case of clays and stability under undrained conditions is critical. The value of adhesion factor α depends on

Hidden page

Hidden page

The skin friction is expressed in this method as,

$$f_s = \bar{\sigma}_z K \tan \delta \tag{15.14}$$

where $\bar{\sigma}_z$ = effective vertical stress

K = coefficient of lateral earth pressure, often K_0 is used

δ = effective friction angle between pile and the soil, generally δ is assumed to be equal to the effective angle of shearing resistance

β is defined as,

$$\beta = K \tan \delta \tag{15.15}$$

Thus the skin friction at any depth is directly proportional to the vertical effective stress at that depth. For normally consolidated clays the *lower limit* for value of β can be expressed as,

$$\beta = (1 - \sin \bar{\phi}) \tan \bar{\phi} \tag{15.16}$$

From Eq. 15.16, for normally consolidated clay β varies from 0.25 to 0.29. There are evidences to indicate that value of β decreases for very long piles, otherwise very high skin-frictional resistance will be indicated at large depth. β could be as low as 0.15 for piles exceeding 60 m length. Bowles (1982) recommends that the β value should be multiplied by a correction factor which has been modified by the author as follows:

$$\text{Correction factor for } \beta = \log_{10}\left(\frac{180}{L}\right) \not< 0.5 \tag{15.17}$$

where L is in metres.

For piles in stiff overconsolidated soils the *lower limit* of β is given as,

$$\beta = (1 - \sin \bar{\phi})\sqrt{\text{OCR}} \tan \bar{\phi} \tag{15.18}$$

where OCR = overconsolidation ratio

λ-method: This is a pseudo-effective stress approach developed by Vijayavergia and Focht (1972) who suggest an empirical relationship for average skin friction, f_{s-av}, from analysis of load test results on steel pipe piles. f_{s-av} is given by,

$$f_{s-av} = \lambda(\bar{\sigma}_{zm} + 2\, c_{um}) \tag{15.19}$$

where $\bar{\sigma}_{zm}$ = average effective vertical stress between the ground surface and pile tip

c_{um} = average undrained shear strength along the length of the pile

λ = an empirical factor which depends on the length of pile as shown in Fig. 15.8

The ultimate skin frictional load is determined from,

$$Q_u = f_{s-av} CL \tag{15.20}$$

This method gives reliable results when piles penetrate deep into homogeneous (non-layered) clays.

(b) *Driven piles—point bearing*

In the total stress approach the ultimate point load of piles driven into clays is given by,

$$Q_{pu} = c_{ub} N_c A_b \tag{15.21}$$

Hidden page

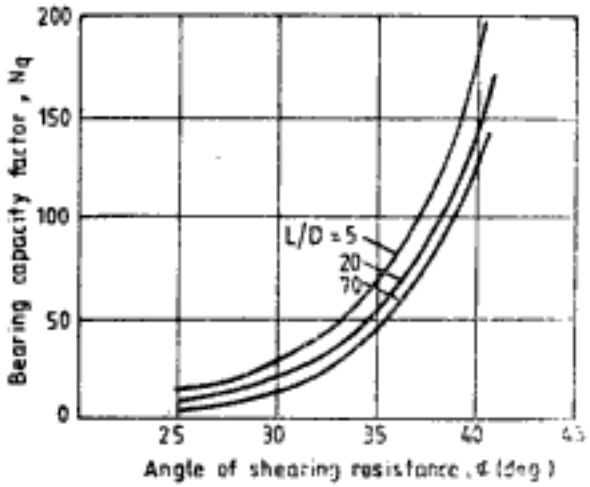

Fig. 15.9 Berezantzev's bearing capacity factor, N_q (After Berezantzev *et al.*, 1961)

Q 15.2: Determine the ultimate load capacity of a driven circular pipe pile. The following are the pile and soil data. $D = 45$ cm; $L = 22$ m; $c_u = 0.4$ kg/cm²; $\phi_u = 0°$; $\gamma_{sat} = 1.85$ T/m³. The soil is deep homogeneous clay and the groundwater is at the level of the ground surface.

Ans: $L/D = 22/0.45 = 48.89$

Using α-method:

$c_u = 0.4$ kg/cm² ($= 4$ T/m²), is medium clay (Table 9.10). From Fig. 15.6 using Tomlinson's curve, $\alpha = 0.8$. But from Fig. 15.7c, $\alpha = 1$ for stiff clay. Therefore, for medium clay also $\alpha = 1$ is more appropriate.

From Eq. 15.13 $$Q_{su} = \pi \times 0.45 \times 22 \times 1 \times 4$$
$$= 124 \text{ T}$$

From Eq. 15.21 $$Q_{pu} = 4 \times 9 \times \pi \times 0.45^2/4 \simeq 6 \text{ T}$$
$$Q_u = 124 + 6 = 130 \text{ T}$$

Using λ-method: From Fig. 15.8, for $L = 22$ m, $\lambda \simeq 0.17$

$$\bar{\sigma}_{zm} = \frac{0.85 \times 22}{2} = 9.35 \text{ T/m}^2$$

$$c_{um} = 4 \text{ T/m}^2$$

From Eq. 15.19 $$f_{s-av} = 0.17(9.35 + 2 \times 4)$$
$$= 2.95 \text{ T/m}^2$$
$$Q_{su} = 2.95 \times \pi \times 0.45 \times 22 = 92 \text{ T}$$
$$Q_u = 92 + 6 = 98 \text{ T}$$

Note: α-method and λ-method differ in the determination of Q_u. λ-method is based on the presence of a stiff upper crust. With $\alpha = 0.8$ as obtained from Fig. 15.6, Q_{su} is 99 T and $Q_u = 105$ T which is nearer to the value calculated by λ-method. Hence, Q_u here may be taken nearly as 100 T.

Hidden page

Hidden page

Point load capacity:

$$\text{gross area of base} = 0.356 \times 0.3755 = 0.134 \text{ sq. m}$$

$$Q_{pu} = 4 \times 9 \times 0.134 \simeq 5 \text{ T}$$

$$\therefore \quad Q_u = 66 + 5 = 71 \text{ T}$$

Note: For allowable pile load the pile stresses will, however, have to be checked on the basis of actual area of pile section.

(c) *Bored and cast-in-situ piles*

During the time lag between boring of a shaft and the installation of the pile there is some softening of the soil along the sides of the borehole due to migration of water and stress release.

To determine skin-frictional capacity by α-method, an average value of $\alpha = 0.45$ is recommended by Tomlinson in firm to stiff clays. However, the unit skin frictional resistance thus obtained should not be more than 1 kg/cm^2. If the pile is short and the clay is heavily fissured α may be taken as 0.3. In soft and very soft clays α may be nearer to 1 a considerable time after pile installation when the remoulded soil regains its strength.

For point resistance, value of $N_c = 9$ can be used in calculations provided the pile penetrates a minimum distance of five diameters into the bearing stratum. In the case of fissured clays the undrained cohesion at the level of base must represent the fissured strength.

(d) *Driven and cast-in-situ piles*

If a steel tube is driven and then the concrete is poured inside the tube without extracting the tube the same procedure explained for precast driven piles can be used. However, if the tube is withdrawn during concreting, the conditions are intermediate between driven piles and bored piles. If the concrete is compacted properly, good bond between pile surface and soil can be expected. Then the procedures explained for driven piles can be used. If compaction results in an increase in the size of the base or the diameter of the pile the enlarged dimensions must be used in the calculations.

2. Piles in sand

(a) *Driven piles—skin friction*

For piles driven into sand the unit skin friction is given by Eq. 15.14. Table 15.8 gives the values of K recommended by Broms (1966). Values of $K \tan \delta (= \beta)$ determined by Vesic (1967) for steel tube piles are shown in Fig. 15.11 and those given by Meyerhof (1976) are shown in Fig. 15.12. Equation 15.14 suggests that f_s increases continuously with depth. But there are evidences to indicate that skin friction does not increase continuously with depth. It reaches a maximum value at a depth of about 15 pile diameters. The variation of this critical depth (z_c) for steel pipe piles reported by Vesic is shown in Fig. 15.13. The reason for this is attributed to the vertical stress near the pile becoming constant after the critical depth due to arching action.

The procedures discussed so far for straight sided piles will require modifications for other shapes. In the case of tapered piles, unit skin friction is written as,

$$f_s = F_a \bar{\sigma}_z K \tan \delta \qquad (15.23)$$

where F_a = a correction factor for tapered piles

Hidden page

Hidden page

Skin friction resistance can also be computed using empirical relationships suggested by Meyerhof (1956) which make use of static cone penetration test data. For displacement piles,

$$f_{s\text{-av}} = \frac{q_{c\text{-av}}}{200} \tag{15.24}$$

and for H-section piles,

$$f_{s\text{-av}} = \frac{q_{c\text{-av}}}{400} \tag{15.25}$$

where $q_{c\text{-av}}$ = average cone resistance (in kg/cm²) over the length of pile under consideration. Similarly in terms of standard penetration number, Meyerhof gives for displacement piles,

$$f_{s\text{-av}} = \frac{N_{av}}{5} \tag{15.26}$$

and for H-piles,

$$f_{s\text{-av}} = \frac{N_{av}}{10} \tag{15.27}$$

where N_{av} = average value of N along length of pile. $f_{s\text{-av}}$ is in T/m².
The maximum value of $f_{s\text{-av}}$ is 10 T/m² for displacement piles and 5 T/m² for H-piles.

(b) *Driven piles—point bearing*
The ultimate point load of driven piles in sand is given by Eq. 15.22. Figure 15.9 shows the variation of bearing capacity factor N_q with ϕ. In using this chart for N_q, Tomlinson recommends that the *in-situ* angle of shearing resistance ($\bar{\phi}$) may be used as the value of ϕ. Whereas Poulos and Davis (1980) recommend that to account for soil compaction due to driving, value of ϕ may be taken as,

$$\phi = \frac{\bar{\phi} + 40^\circ}{2} \tag{15.28}$$

where $\bar{\phi}$ is the *in-situ* angle of shearing resistance of sand. The value of unit point resistance ($q_p = \bar{\sigma}_{zb} N_q$) does not increase continuously with depth. It tends to become constant after a depth of penetration of 15 diameters into sand, because the vertical stress becomes constant after this depth due to arching effects. The maximum value of q_p is, however, limited to 110 kg/cm² in normal silica sand. In calcareous sands the limiting value is 50 kg/cm². For H-piles the ultimate point load should be calculated on the basis of the net cross-sectional area of the steel only. For tapered piles the area at the base must be used. Equation 15.22 is applicable when the pile penetrates at least a distance of five diameters into the bearing stratum and there is no weak soil below the bearing stratum. Meyerhof suggests that if the weak soil is at a depth of more than $10D$ below the pile base there is no reduction in point load capacity. If the depth to weak soil is less than $10D$ then the ultimate point resistance can be considered to decrease linearly from the value at $10D$ above the weak layer to the value at the surface of the weak layer. Based on Eqs 15.22 and 15.28, Figs 15.9 and 15.13, and the limiting value of point resistance, Poulos and Davis give a dimensionless plot of Q_{pu} as shown in Fig. 15.16 for piles in uniform sand.

Q 15.6: A 45 cm diameter concrete pile is driven into an uniform sand deposit of saturated density 1.85 T/m³. The length of the pile is 15 m. The groundwater table is at the surface. Determine the ultimate load capacity of the pile.

$\bar{\phi} = 40^\circ$

Hidden page

Hidden page

Hidden page

Hidden page

Calculations for l_p in this manner can result in very large depths of penetration. However, from practical considerations the pile should be driven at least five diameters into the bearing stratum but not more than 20 diameters, or not deeper than the level at which point resistance of 1100 T/m^2 can be attained as indicated by static cone resistance diagram.

The empirical relationship between unit point resistance and standard penetration number for driven piles in sand including *H*-pile is as follows:

$$q_p = 39.1 N_b \quad \text{T/m}^2 \tag{15.30}$$

where N_b is the value of N at the level of pile base.

(c) *Bored and cast-in-situ piles*

The load carrying capacity of bored and cast-in-situ pile is significantly less than the capacity of driven pile. It also depends on the method of construction. For preliminary estimates one-third of f_s and one-half of q_p calculated for driven piles can be used for unit skin friction and unit point resistance, respectively.

Tomlinson recommends the following. For piles formed by shelling or baling Eq. 15.23 may be used for skin friction and Eq. 15.22 for point resistance. However, loose soil conditions must be assumed to account for boring operations. For piles installed by rotary drilling under bentonite slurry the same formulae may be used with angle of shearing resistance of in-situ undisturbed soil.

In another approach it is assumed that the angle of shearing resistance is reduced by 3° due to loosening of soil. Then Figs 15.11, 15.15 and 15.16 can be used in conjunction with the equations explained for driven piles to determine the ultimate load of the pile. The variation of $K \tan \delta$ suggested by Meyerhof for bored piles is shown in Fig. 15.12. To use this figure the in-situ angle of shearing resistance $\bar{\phi}$ must be used.

(d) *Driven and cast-in-situ piles*

A steel tube is driven into the ground and then the concrete is poured inside the tube. If the tube is not extracted out but left inside the ground, the design approach discussed earlier for driven piles can be used to compute the load carrying capacity. If the tube is extracted while pouring the concrete, then the construction technique significantly influences the method of calculation of ultimate load. The skin friction depends upon the amount of compaction given to the concrete, for depending on that the soil can be in loose or dense state. If no compaction is done loose conditions may be assumed and where the concrete is compacted well, medium dense conditions can be assumed. For point resistance the enlarged dimensions of the bulb must be used if one were to be formed by compacting the concrete.

3. Piles in c - ϕ soils

For piles constructed in soils having both cohesion and friction the superposition of the procedures explained for clays and sands can be adopted. An example of this procedure is given in Q 15.3 where the calculations have been carried out using total stress approach for c and effective stress approach for ϕ.

4. Safe compressive load on piles

For piles in sand with shaft diameter less than 600 mm a factor of safety of 2.5 on Q_u computed using static formulae is satisfactory.

Thus, the safe load Q_{safe} is given by,

$$Q_{safe} = \frac{Q_u}{2.5} = \frac{Q_{su} + Q_{pu}}{2.5} \tag{15.31}$$

When piles are driven to refusal in very dense sand or gravel or rock the safe load on the pile is governed by the strength of the pile as a structural member than by the ultimate resistance provided by the soil.

In case of clays ultimate skin-frictional load is calculated in the following two ways: (i) using *average* shear strength and adhesion factors in Fig. 15.7 say Q'_{su}, and (ii) using *lowest range* of shear strength and adhesion factors in Fig. 15.7, say Q''_{su}, then according to Tomlinson the safe load Q_{safe} is the smaller of the two values given by Eqs 15.32 and 15.33.

$$Q_{safe} = \frac{Q'_{su} + Q_{pu}}{2.5} \tag{15.32}$$

$$Q_{safe} = \frac{Q''_{su}}{1.5} + \frac{Q_{pu}}{3} \tag{15.33}$$

15.3.2 Load Capacity in Tension

Piles used in foundation for structures like chimneys, tall towers, dry docks and off-shore structures are required to resist uplift loads and overturning moments. The uplift capacity of piles is calculated based on static approach similar to that explained for piles in compression.

1. Piles in clay

The ultimate uplift capacity of piles, Q_{tu}, depends on the shape of the pile base. For uniform diameter piles Q_{tu} is given by,

$$Q_{tu} = f_{st} A_s + W_p \tag{15.34}$$

where f_{st} = unit skin friction in tension
A_s = area of pile shaft
W_p = weight of pile

For undrained conditions, f_{st} is equal to the unit skin friction in compression f_s obtained by α-method. For sustained loading f_{st} is, however, only about half the value for undrained conditions.

In order to increase the uplift load capacity often the base of the pile is enlarged. Meyerhof and Adams (1968) suggest that the uplift capacity of enlarged piles in clay under undrained conditions is calculated as the smaller of the values given by Eqs 15.35 and 15.36. Equation 15.35 is based on failure taking place through mobilisation of skin friction along the cylindrical surface formed by the base diameter. The failure mechanism for Eq. 15.36 is one of bearing failure of the base.

$$Q_{tu} = c_u \bar{A}_s K + W_s + W_p \tag{15.35}$$

where $\bar{A}_s$ = surface area of the vertical cylinder above the base
$= \pi D_b L$
D_b = diameter of base
K = a factor
W_s = weight of soil in the annulus between pile shaft and vertical cylinder above the base

Hidden page

Hidden page

Therefore the uplift capacity of pile is

$$Q_{tu} = 242 \text{ T}$$

15.3.3 Ultimate Lateral Load Capacity

Many structures transmit large lateral loads. Retaining walls, bridge piers, and tall structures under wind and seismic activity are typical examples. When the lateral loads are small vertical piles can be used to resist them. Building codes generally suggest that the safe lateral load on vertical pile is 10 per cent of the safe axial load. McNulty's (1956) recommended values for safe lateral load on vertical piles are shown in Table 15.11. Den Norske Pelekomite's (1973) recommendations are given in Tables 15.12 and 15.13. Where lateral loads are large, inclined (also called batter or raker) piles will be necessary. Berezantzev *et al.* (1961) give the following recommendations: If the inclination, i, of the load to vertical is less than 5°, vertical piles can be used. For values of i between 5° and 15° batter piles in one direction can be used. When i is more than 15° piles inclined in two directions are required. These recommendations are shown in Fig. 15.20. In this section the discussions will be confined to lateral load capacity of vertical piles. The lateral load capacity depends on (i) the type of soil, (ii) the condition of the pile head, viz., whether free or fixed, (iii) the mechanism of failure depending upon whether the pile is long or short, and (iv) the pile dimensions and its properties. The two theories generally used to determine the ultimate lateral load capacity Q_{hu} of a vertical pile are (i) Hansen's theory for short piles and (ii) Broms' theory for short and long piles. These are explained in detail.

Table 15.11 Values of Safe Lateral Load on Vertical Piles

Type of pile	Diameter (cm)	Safe lateral load (T)		
		Medium sand	Fine sand	Medium clay
Timber pile—free head	30	0.7	0.7	0.7
Timber pile—fixed head	30	2.3	2.0	1.8
Concrete pile—free head	40	3.2	2.5	2.3
Concrete pile—fixed head	40	3.2	2.5	2.3

After McNulty, 1956. By permission of American Society of Civil Engineers, New York.

Table 15.12 Safe Horizontal Load on the Top of Timber or Concrete Pile for Short Term Loading in Clays

Pile area (m^2)	Maximum bending moment (T·m)	Safe short term load in clays (T)		
		$S_u = 1$ T/m^2	$S_u = 2.5$ T/m^2	$S_u = 5$ T/m^2
0.04	0.45	0.7	1.5	2
0.06	0.85	1	2	3
0.09	1.50	1.5	3	4

After Den Norske Pelekomite, 1973.

Hidden page

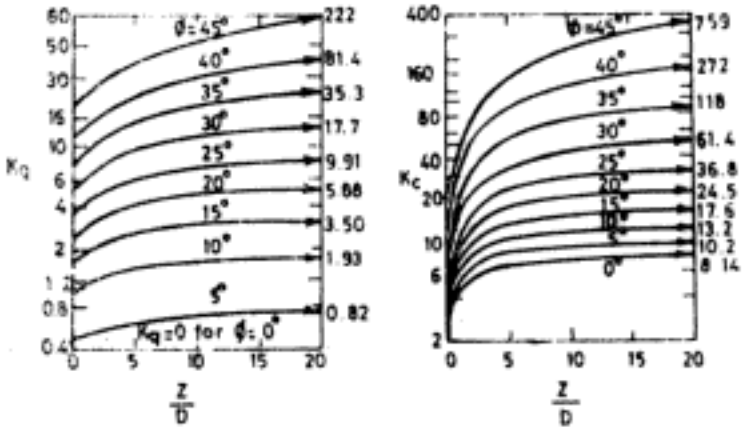

Fig. 15.22 Coefficients K_q and K_c (After Hansen, 1961)

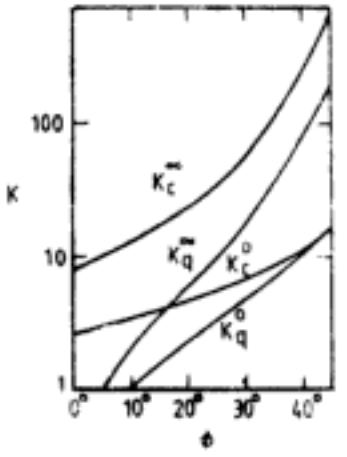

Fig. 15.23 Coefficients K_c and K_q at surface (K^0_c, K^0_q) and at great depth (K^{∞}_c, K^{∞}_q) (After Hansen, 1961)

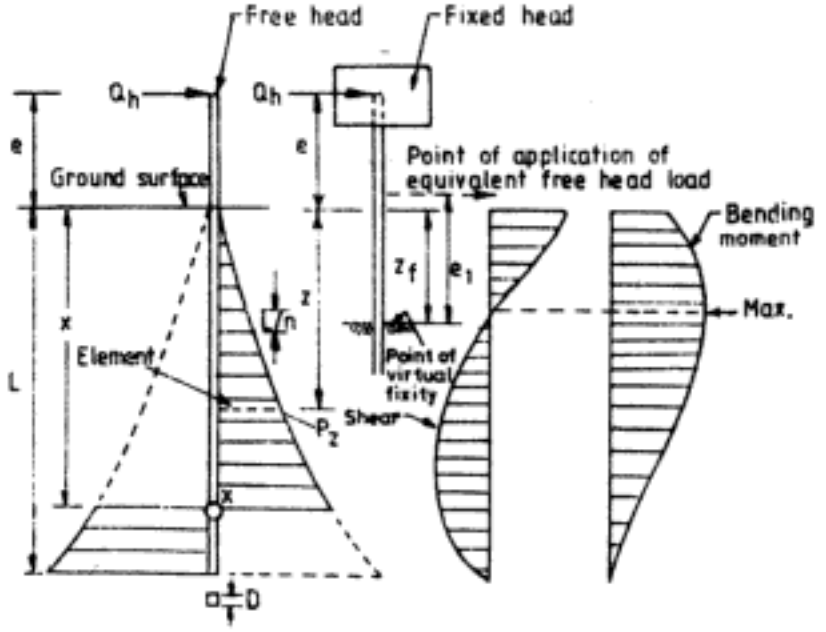

Fig. 15.24 Hansen's method for calculation of ultimate lateral resistance of short piles

(b) Draw the passive resistance distribution with depth and divide this into a number of small equal elements n. The total passive resistance on each horizontal element of the pile is,

$$p_z \times \left(\frac{L}{n}\right) \times D$$

(c) Determine the sum of the moments due to total passive resistance of each element about the point of application of horizontal load Q_h. The equation of the sum of the moments is given as,

$$\Sigma M = \sum_{z=0}^{x} p_z \left(\frac{L}{n}\right) D(e + z) - \sum_{z=x}^{L} p_z \left(\frac{L}{n}\right) D(e + z) \qquad (15.42)$$

Hidden page

Hidden page

Hidden page

Equations 15.45, 15.49 and 15.50 can be solved to obtain Q_{hu} of the pile and the other unknowns f and g. The maximum bending moment at depth $(1.5D + 0.5f)$ given by Eq. 15.46 should not exceed M_y, otherwise failure mechanism for long piles is applicable.
For long piles,

$$Q_{hu} = \frac{2M_y}{1.5D + 0.5f} \tag{15.51}$$

where f is given by Eq. 15.45. Solutions for Q_{hu} in dimensionless form for fixed head piles are shown in Fig. 15.26 in broken lines.

(b) *Piles in sands*

The following are the assumptions in the analysis: the active earth pressure on the back of the pile is neglected; the distribution of passive pressure along the front of the pile is equal to three times Rankine earth pressure; the shape of the pile section has no influence on the ultimate lateral resistance or on the ultimate earth pressure distribution; the full lateral resistance is mobilised at the movements considered.

(i) *Free head piles*: Figure 15.28 shows the failure mechanism, soil reaction and bending moment diagrams for short and long piles. For short piles the ultimate lateral load is given by,

$$Q_{hu} = \frac{0.5\gamma DL^3K_p}{e + L} \tag{15.52}$$

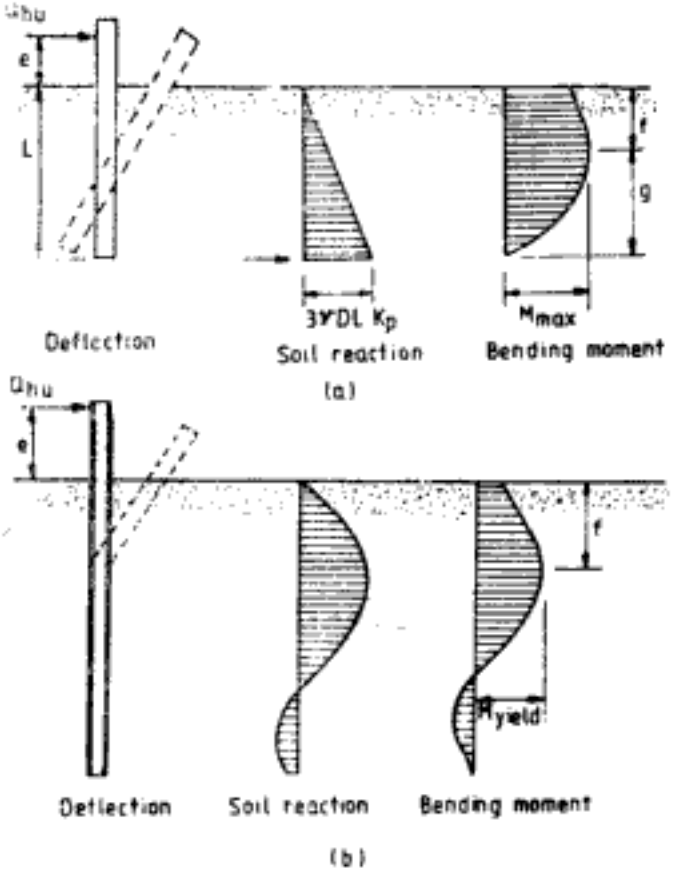

Fig. 15.28 Failure mechanisms of free head piles in sand: (a) short piles, and (b) long piles (After Broms, 1964b; with permission of American Society of Civil Engineers, New York)

where $K_p = \dfrac{1 + \sin\phi}{1 - \sin\phi}$

The maximum moment, M_{max}, occurs at a depth f below the ground surface, given by,

$$f = 0.82\sqrt{\frac{Q_{hu}}{K_p \gamma D}} \tag{15.53}$$

and the maximum moment is given by,

$$M_{max} = Q_{hu}(e + 0.67f) \tag{15.54}$$

If M_{max} exceeds the pile yield moment the pile will behave as a long pile. For long piles,

$$Q_{hu} = \frac{M_y}{e + 0.67f} \tag{15.55}$$

f is given by Eq. 15.53. Solutions for ultimate lateral load in dimensionless form are shown in Fig. 15.29.

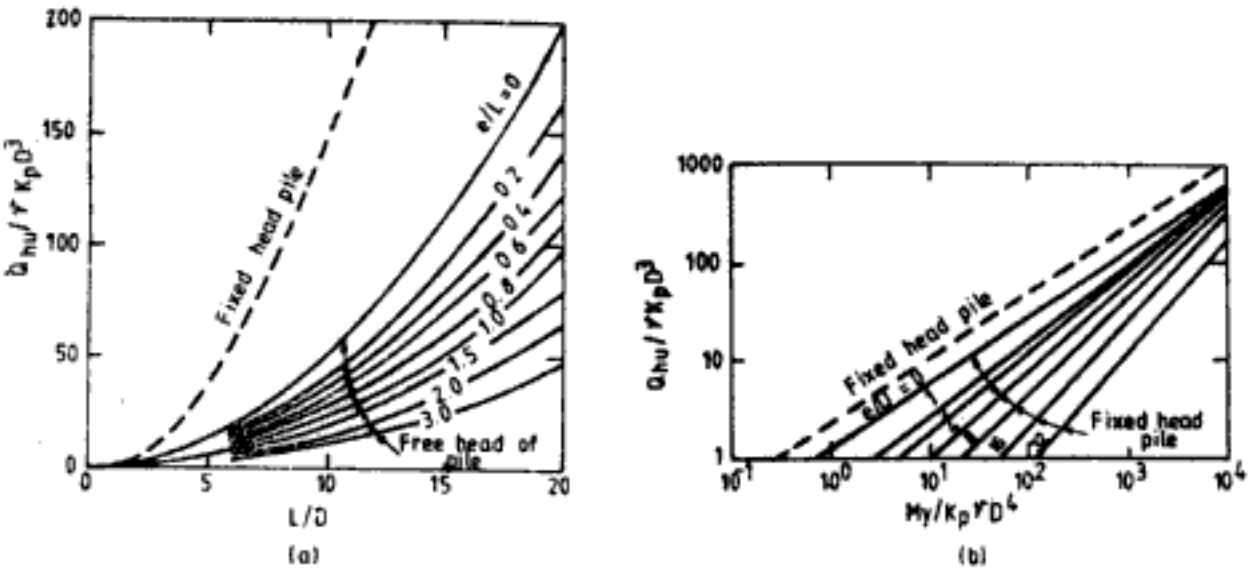

Fig. 15.29 Ultimate lateral load in sands: (a) short piles, (b) long piles (After Broms, 1964b; with permission of American Society of Civil Engineers, New York)

(ii) *Fixed head piles*: The failure mechanism, soil reaction and bending moment diagrams for short, intermediate, and long piles are shown in Fig. 15.30.

For short piles, the ultimate lateral load is given by,

$$Q_{hu} = 1.5\gamma D K_p L^2 \tag{15.56}$$

and maximum bending moment by,

$$M_{max} = 0.67 Q_{hu} L \tag{15.57}$$

If M_{max} exceeds M_y then failure mechanism for intermediate piles should be considered.

For intermediate piles,

$$Q_{hu} = \frac{0.5\gamma D K_p L^3 - M_y}{L} \tag{15.58}$$

The maximum bending moment at depth f should not exceed M_y and f is given by Eq. 15.53.

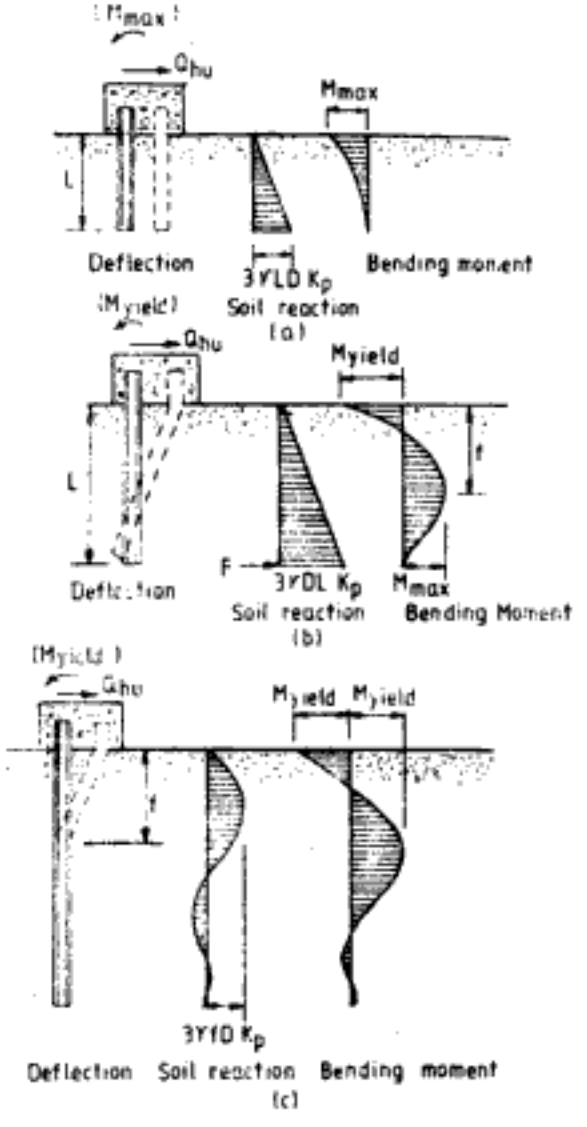

Fig. 15.30 Failure mechanisms of fixed head piles in sand: (a) short piles, (b) intermediate piles, (c) long piles (After Broms, 1964b; with permission of the American Society of Civil Engineers, New York)

If M_{max} exceeds M_y then the pile behaves as a long pile. For long piles,

$$Q_{hu} = \frac{2M_y}{e + 0.67f} \tag{15.59}$$

Dimensionless solutions for short and long fixed head piles are shown in Fig. 15.29 in broken lines.

15.3.4 Settlement and Lateral Deflection of Single Piles

Pile foundations like shallow foundations, should be designed to satisfy the twin criteria, namely, (i) they should have an adequate factor of safety against soil failure, and (ii) the deformation under working load should be within permissible limits. Hence, it is necessary to calculate the movement of piles under vertical and lateral loads.

1. Settlement of single piles

Conventional methods of calculating the consolidation settlement of single piles in clay assume some form of skin friction distribution along the length of the pile and use Terzaghi's

one-dimensional consolidation theory. On these principles Kaniraj (1974), and Kaniraj and Ranganatham (1979) present solutions for single piles and pile groups in normally consolidated clay. In the analysis the following assumptions are made: (i) the pile load is resisted by a uniform skin friction along the length of the pile, (ii) the normally consolidated clay deposit is very deep, (iii) the pile is rigid and its elastic compression is negligible.

For stress distribution in soil, Mindlin's theory is used. The consolidation settlement of a single pile ρ_s is expressed as,

$$\rho_s = \frac{D}{C} S_{Fs} \tag{15.60}$$

where S_{Fs} = dimensionless single pile settlement factor

$C = \dfrac{1 + e_0}{C_c}$ assumed a constant

e_0 = in-situ void ratio

C_c = compression index

S_{Fs} depends on the L/D ratio of the pile and the dimensionless pile load factor $\bar{Q}_p$ given by

$$\bar{Q}_p = \frac{Q_p}{\gamma' D^3} \tag{15.61}$$

where Q_p = load on pile

γ' = effective density of soil

The variation of S_{Fs} with L/D and $\bar{Q}_p$ is shown in Fig. 15.31.

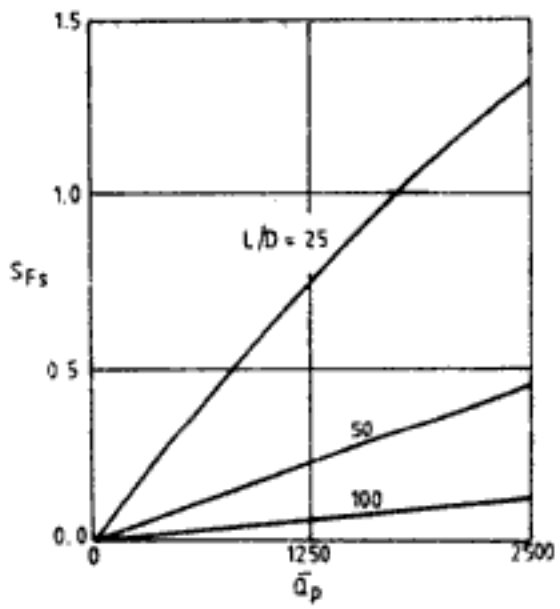

Fig. 15.31 Variation of settlement factor S_{Fs} with load parameter $\bar{Q}_p$ (After Kaniraj, 1974; Kaniraj and Ranganatham, 1979)

More rigorous and sophisticated procedures are available in literature using which the load vs. settlement curve of the pile can be plotted and the load or skin friction distribution along the pile can be obtained. These methods can be classified into three categories as follows:

(i) Load-transfer method
(ii) Methods based on theory of elasticity
(iii) Numerical methods

An elaborate discussion of these methods is given by Poulos and Davis (1980).

2. Lateral deflection of piles

The lateral deflection of piles is generally computed using the *modulus of subgrade reaction* approach. The other approach, namely *elastic approach* is explained by Poulos and Davis (1980). Only the modulus of subgrade reaction method is presented here.

(a) *Modulus of subgrade reaction*

The lateral pressure p at any point within the soil medium is assumed to be proportional to the lateral deflection ρ at that point. The constant of proportionality is called the modulus of subgrade reaction. Thus,

$$p = k_h \rho \tag{15.62}$$

where k_h = horizontal modulus of subgrade reaction

It is commonly assumed that k_h is constant with depth for clays which is true for overconsolidated clays. For granular soils like sands, and for soft and stiff normally consolidated clays, k_h is assumed to increase linearly with depth and is given by,

$$k_h = n_h \left(\frac{z}{D}\right) \tag{15.63}$$

where n_h = coefficient of subgrade reaction

z = depth below ground surface

The values of subgrade reaction in cohesive soils k_{h1} for square plates of breadth equal to 0.3 m are given in Table 15.14. Similarly the values of n_h for granular soils are presented in Table 15.15 and for cohesive soils in Table 15.16.

Table 15.14 Values of k_{h1} in Cohesive Soils

Undrained strength, S_u (kg/cm²)	1-2	2-4	>4
k_{h1} (kg/cm³)	1.8-3.6	3.6-7.2	>7.2

Table 15.15 Values of n_h for Sand

Relative density	Loose	Medium	Dense
n_h for dry or moist sand (kg/cm³)	0.25	0.75	2
n_h for submerged sand (kg/cm³)	0.14	0.50	1.22

Table 15.16 Values of n_h for Cohesive Soils

Soil type	n_h (T/m^3)
Soft normally consolidated clay	17–350
Normally consolidated organic clay	11–83
Peat	3–11
Loess	800–1110

(b) *Lateral deflection of piles in soils having constant modulus of subgrade reaction with depth*
The lateral deflection of the pile depends on the dimensionless quantity βL, where

$$\beta = \left(\frac{k_h D}{4E_p I_p}\right)^{1/4} \tag{15.64}$$

E_p = modulus of elasticity of pile

I_p = moment of inertia of pile section

k_h can be taken as equal to the values of k_{h1} in Table 15.14. Broms (1964a) gives the following relationship when plate load test results with plates loaded vertically are available.

$$k_h = \frac{1.67E_s}{D} \tag{15.65}$$

where, E_s = secant modulus at half the ultimate stress (at failure) on the plate
k_h can also be obtained from undrained triaxial shear test results. Skempton (1951) assuming the secant modulus of soil to be equal to 50 to 200 times the undrained shear strength suggests that,

$$k_h = \frac{80c_u}{D} \text{ to } \frac{320c_u}{D} \tag{15.66}$$

Davisson (1970) suggests the relationship as,

$$k_h = 67\,\frac{c_u}{D} \tag{15.67}$$

For a free head pile subjected to a horizontal load Q_h at an eccentricity e above the ground surface the lateral displacement ρ_0 and rotation θ_0 at the ground surface can be computed through the following steps:

(i) Determine βL. The value of βL will represent the behaviour of a pile either as a short pile or as a long pile.
(ii) If βL is less than 1.5 the pile behaves as a short pile, in which case

$$\rho_0 = \frac{4Q_h\left(1 + 1.5\frac{e}{L}\right)}{k_h DL} \tag{15.68}$$

$$\theta_0 = \frac{6Q_h\left(1 + 2\frac{e}{L}\right)}{k_h DL} \tag{15.69}$$

(iii) If βL is more than 2.5 the pile behaves as an infinitely long pile. In this case,

$$\rho_0 = \frac{2Q_h\beta(e\beta + 1)}{n_1 n_2 k_h D} \tag{15.70}$$

$$\theta_0 = \frac{2Q_h\beta^2(1 + 2e\beta)}{k_h D} \tag{15.71}$$

n_1 and n_2 in Eq. 15.70 (and also Eq. 15.73) are shown in Tables 15.17 and 15.18 respectively.

Table 15.17 Values of n_1

Unconfined compressive strength, kg/cm²	n_1
<0.50	0.32
0.5–2.0	0.36
>2.0	0 40

After Broms, 1964a.

Table 15.18 Values of n_2

Pile material	n_2
Steel	1.00
Concrete	1.15
Wood	1.30

After Broms, 1964a.

Similarly for fixed head piles which are free to translate but not free to rotate the steps in the calculations are

(i) Compute βL.

(ii) For βL less than 0.5 the pile is a short pile and

$$\rho_0 = \frac{Q_h}{k_h D L} \tag{15.72}$$

(iii) For βL more than 1.5 the pile is a long pile and

$$\rho_0 = \frac{Q_h}{n_1 n_2 k_h D} \tag{15.73}$$

Dimensionless solutions for horizontal displacement of free head and fixed head piles are shown in Fig. 15.32.

Barber (1953) presents solutions for deflection and rotation at the ground surface of laterally loaded piles. For free head piles subjected to a lateral load Q_h and moment M_0 ($= Q_h e$) at the ground level,

$$\rho_0 = \left(\frac{Q_h}{k_h D L}\right) I_{\rho h} + \left(\frac{M_0}{k_h D L^2}\right) I_{\rho M} \tag{15.74}$$

$$\theta_0 = \left(\frac{Q_h}{k_h D L^2}\right) I_{\theta h} + \left(\frac{M_0}{k_h D L^3}\right) I_{\theta M} \tag{15.75}$$

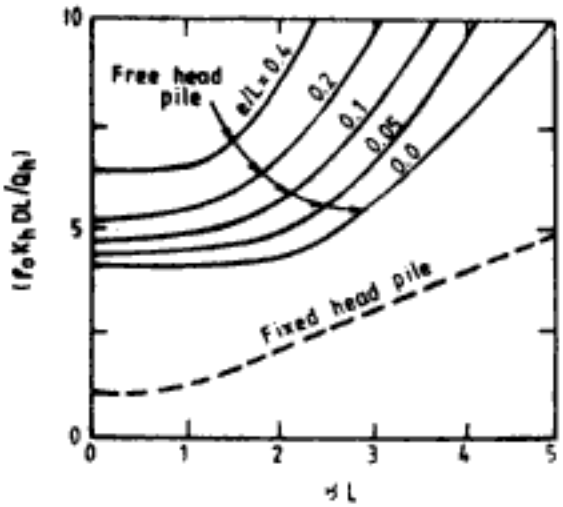

Fig. 15.32 Lateral deflection of piles in soils having constant k_h (After Broms, 1964a; with permission of American Society of Civil Engineers, New York)

where I_{ph} = displacement influence factor for lateral load
I_{pM} = displacement influence factor for moment
$I_{\theta h}$ = rotation influence factor for lateral load
$I_{\theta M}$ = rotation influence factor for moment
and $I_{\theta h} = I_{pM}$

In Eqs 15.74 and 15.75 the moment M_0 tends to move the pile in the same direction as Q_h. If the moment acts in the opposite direction—M_0 should be used in the equations. For fixed head piles not free to rotate,

$$\rho_0 = \frac{Q_h}{k_h DL} I_{pF} \tag{15.76}$$

where I_{pF} = displacement influence factor for fixed head pile

Figure 15.33 gives values of displacement and rotation influence factors.

Hetenyi (1946) gives solutions for horizontal displacement ρ_z, slope θ_z, moment M_z, and shear Q_z at depth z below ground level for a free head pile subjected to horizontal load Q_h and moment M_0 at the ground surface. These solutions are as follows:

$$\rho_z = \frac{2Q_h}{k_h D} K_{ph} + \frac{2M_0\beta^2}{k_h D} K_{pM} \tag{15.77}$$

$$\theta_z = \frac{2Q_h\beta^2}{k_h D} K_{\theta h} + \frac{4M_0\beta^3}{k_h D} K_{\theta M} \tag{15.78}$$

$$M_z = \frac{Q_h}{\beta} K_{Mh} + M_0 K_{MM} \tag{15.79}$$

$$Q_z = -Q_h K_{Qh} - 2M_0\beta K_{QM} \tag{15.80}$$

where K_{ph}, K_{pM}, $K_{\theta h}$, $K_{\theta M}$, K_{Mh}, K_{MM}, K_{Qh}, and K_{QM} are dimensionless influence factors. Table 15.19 gives the values of these influence factors for different values of βL and z/L.

Table 15.19 Influence Factors for Constant k_h

βL	z/L	K_{ph}	$K_{\phi h}$	K_{Mh}	K_{Qh}	K_{pM}	$K_{\phi M}$	K_{MM}	K_{QM}
2.0	0.	1.1376	1.1341	0.0000	1.0000	−1.0762	1.0762	1.0000	0.
	0.0625	0.9964	1.1200	0.1080	0.7333	−0.8807	0.9518	0.9836	0.1256
	0.1250	0.8586	1.0828	0.1848	0.5015	−0.6579	0.8314	0.9397	0.2214
	0.1875	0.7264	1.0298	0.2347	0.3035	−0.4644	0.7178	0.8751	0.2913
	0.2500	0.6015	0.9673	0.2620	0.1377	−0.2982	0.6133	0.7959	0.3387
	0.3125	0.4848	0.9004	0.2704	0.0021	−0.1569	0.5192	0.7073	0.3669
	0.3750	0.3764	0.8333	0.2637	−0.1054	−0.0376	0.4366	0.6138	0.3788
	0.4375	0.2763	0.7695	0.2452	−0.1868	0.0624	0.3658	0.5191	0.3771
	0.5000	0.1838	0.7115	0.2180	−0.2442	0.1463	0.3068	0.4262	0.3639
	0.5625	0.0981	0.6610	0.1851	−0.2793	0.2168	0.2591	0.3379	0.3411
	0.6250	0.0182	0.6192	0.1491	−0.2937	0.2767	0.2220	0.2564	0.3101
	0.6875	−0.0571	0.5865	0.1125	−0.2887	0.3286	0.1946	0.1834	0.2722
	0.7500	−0.1288	0.5628	0.0776	−0.2654	0.3747	0.1757	0.1208	0.2282
	0.8125	−0.1981	0.5474	0.0468	−0.2245	0.4171	0.1640	0.0698	0.1787
	0.8750	−0.2659	0.5389	0.0222	−0.1665	0.4572	0.1578	0.0318	0.1241
	0.9375	−0.3330	0.5356	0.0059	−0.0916	0.4963	0.1554	0.0082	0.0645
	1.0000	−0.3999	0.5351	0.0000	−0.0000	0.5351	0.1551	0.0000	0.0000
3.0	0.0000	1.0066	1.0004	0.0000	1.0000	−1.0004	1.0038	1.0000	0.
	0.0625	0.8210	0.9695	0.1543	0.6575	−0.6589	0.8183	0.9690	0.1545
	0.1250	0.6459	0.8919	0.2508	0.3829	−0.3854	0.6433	0.8913	0.2514
	0.1875	0.4882	0.7870	0.3018	0.1709	−0.1743	0.4857	0.7862	0.3029
	0.2500	0.3515	0.6698	0.3184	0.0141	−0.0184	0.3493	0.6684	0.3202
	0.3125	0.2371	0.5514	0.3101	−0.0956	0.0905	0.2352	0.5491	0.3127
	0.3750	0.1444	0.4394	0.2850	−0.1664	0.1607	0.1429	0.4360	0.2887
	0.4375	0.0716	0.3389	0.2496	−0.2063	0.2002	0.0710	0.3339	0.2544
	0.5000	0.0164	0.2528	0.2091	−0.2223	0.2162	0.0168	0.2458	0.2150
	0.5625	−0.0242	0.1823	0.1673	−0.2205	0.2147	−0.0222	0.1728	0.1744
	0.6250	−0.0529	0.1271	0.1272	−0.2057	0.2011	−0.0489	0.1148	0.1353
	0.6875	−0.0727	0.0864	0.0908	−0.1819	0.1793	−0.0661	0.0709	0.0995
	0.7500	−0.0861	0.0584	0.0594	−0.1619	0.1524	−0.0763	0.0396	0.0684
	0.8125	−0.0953	0.0411	0.0340	−0.1178	0.1227	−0.0816	0.0189	0.0426
	0.8750	−0.1021	0.0321	0.0154	−0.0807	0.0916	−0.0839	0.0069	0.0225
	0.9375	−0.1077	0.0287	0.0039	−0.0414	0.0599	−0.0846	0.0014	0.0083
	1.0000	−0.1130	0.0282	0.	−0.0000	0.0282	−0.0847	0.0000	0.

Hidden page

Hidden page

For free head short pile (ηL or $Z_{max} < 2$)

$$\rho_0 = \frac{18Q_h(1 + 1.33\,e/L)}{L^2 n_h} \tag{15.85}$$

$$\theta_0 = \frac{24Q_h(1 + 1.5\,e/L)}{L^3 n_h} \tag{15.86}$$

For free head infinitely long piles (ηL or $Z_{max} > 4$)

$$\rho_0 = \frac{2.4Q_h}{(n_h)^{3/5}(E_pI_p)^{2/5}} + \frac{1.6Q_he}{(n_h)^{2/5}(E_pI_p)^{3/5}} \tag{15.87}$$

$$\theta_0 = \frac{1.6Q_h}{(n_h)^{2/5}(E_pI_p)^{3/5}} + \frac{1.74Q_he}{(n_h)^{1/5}(E_pI_p)^{4/5}} \tag{15.88}$$

For fixed head short piles (ηL or $Z_{max} < 2$)

$$\rho_0 = \frac{2Q_h}{L^2 n_h} \tag{15.89}$$

For fixed head long piles (ηL or $Z_{max} > 4$)

$$\rho_0 = \frac{0.93Q_h}{(n_h)^{3/5}(E_pI_p)^{2/5}} \tag{15.90}$$

Solutions for lateral deflection at the ground level, ρ_0, are given in dimensionless form in Fig. 15.34. Barber's solutions for deflection and rotation are in terms of influence factors. For free head piles subjected to a lateral load Q_h and moment M_0,

$$\rho_0 = \left(\frac{Q_h}{n_hL^2}\right)I_{\rho h} + \left(\frac{M_0}{n_hL^3}\right)I_{\rho M} \tag{15.91}$$

$$\theta_0 = \left(\frac{Q_h}{n_hL^3}\right)I_{\theta h} + \left(\frac{M_0}{n_hL^4}\right)I_{\theta M} \tag{15.92}$$

For fixed head piles not free to rotate,

$$\rho_0 = \frac{Q_h}{n_hL^2}\,I_{\rho F} \tag{15.93}$$

Values of influence factors $I_{\rho h}$, $I_{\rho M}$, $I_{\rho F}$, $I_{\theta h}$ and $I_{\theta M}$ are presented in Fig. 15.35. Reese and Matlock (1956) present comprehensive solutions for lateral displacement (ρ_z), slope (θ_z), moment (M_z), shear (Q_z), and soil reaction (p_z) at depth z below ground surface for a free head pile subjected to horizontal load Q_h and moment M_0 at the ground surface. These solutions are given in Eqs 15.94 to 15.98.

$$\rho_z = A_\rho\frac{Q_hT^3}{E_pI_p} + B_\rho\frac{M_0T^2}{E_pI_p} \tag{15.94}$$

$$\theta_z = A_\theta\frac{Q_hT^2}{E_pI_p} + B_\theta\frac{M_0T}{E_pI_p} \tag{15.95}$$

$$M_z = A_MQ_hT + B_MM_0 \tag{15.96}$$

$$Q_z = A_QQ_h + B_Q\frac{M_0}{T} \tag{15.97}$$

$$p_z = A_p\frac{Q_h}{T} + B_p\frac{M_0}{T^2} \tag{15.98}$$

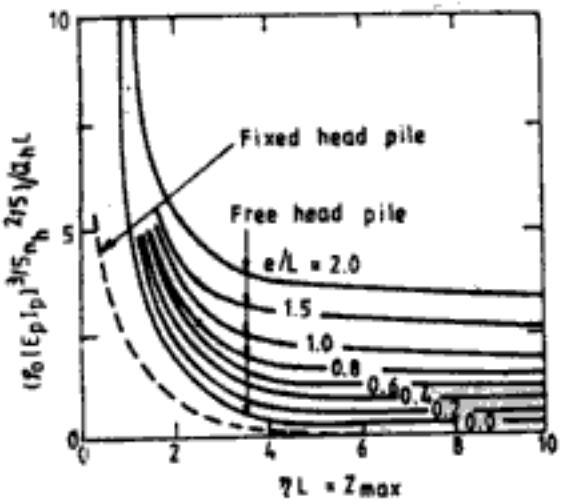

Fig. 15.34 **Lateral deflection of piles in soils with increasing modulus with depth** (After Broms, 1964b; with permission of American Society of Civil Engineers, New York)

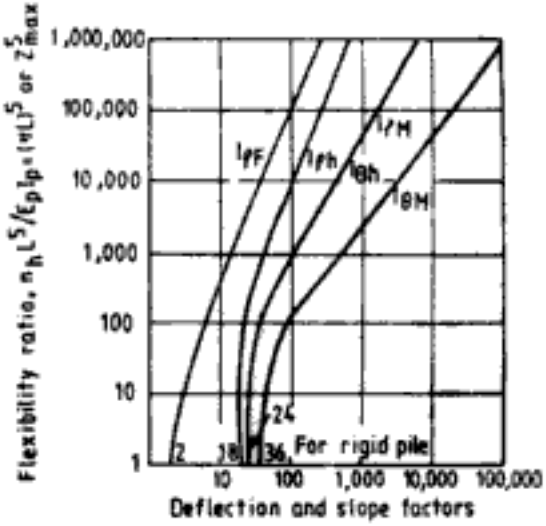

Fig. 15.35 **Top deflection and rotation for lateral loads on vertical piles for subgrade reaction increasing linearly with depth** (After Barber, 1953; with permission of ASTM, Philadelphia)

In Eqs 15.94 to 15.98, T is defined by Eq. 15.84 and the coefficients A and B depend on the length of pile Z_{max} and depth z/T. For long piles, i.e., $Z_{max} > 4$, it has been found that coefficients A and B do not vary significantly. For piles whose length is governed by compression load, generally Z_{max} is greater than 4. Values of coefficients A and B given in Tables 15.20 and 15.21 respectively, can therefore be used for all long piles. Equation 15.94 can be written as follows,

$$\rho_z = C_\rho \frac{Q_h T^3}{E_p I_p} \tag{15.99}$$

where $C_\rho = A_\rho + B_\rho \dfrac{M_0}{Q_h T}$

Similarly Eq. 15.96 can be expressed as,

$$M_z = C_M Q_h T \tag{15.100}$$

where $C_M = A_M + B_M \dfrac{M_0}{Q_h T}$

Equations for rotation, shear, and soil reaction can also be expressed in similar form. Figure 15.36 shows the variation of coefficient C_ρ with z/T and $M_0 Q_h/T$ for long piles. Similarly the variation of C_M is shown in Fig. 15.37.

For a free head pile subjected to only Q_h at the ground surface the value of $M_0/Q_h T$ is zero. When a moment M_0 acts in the direction of Q_h on the free head pile the value of $M_0/Q_h T$ is positive and the value is negative when the moment M_0 acts in the opposite direction to Q_h. For fixed head pile not free to rotate the value of $M_0/Q_h T$ is -0.93. For such fixed head piles, in Eq. 15.99

$$C_\rho = A_\rho - 0.93 B_\rho \tag{15.101}$$

Hidden page

Hidden page

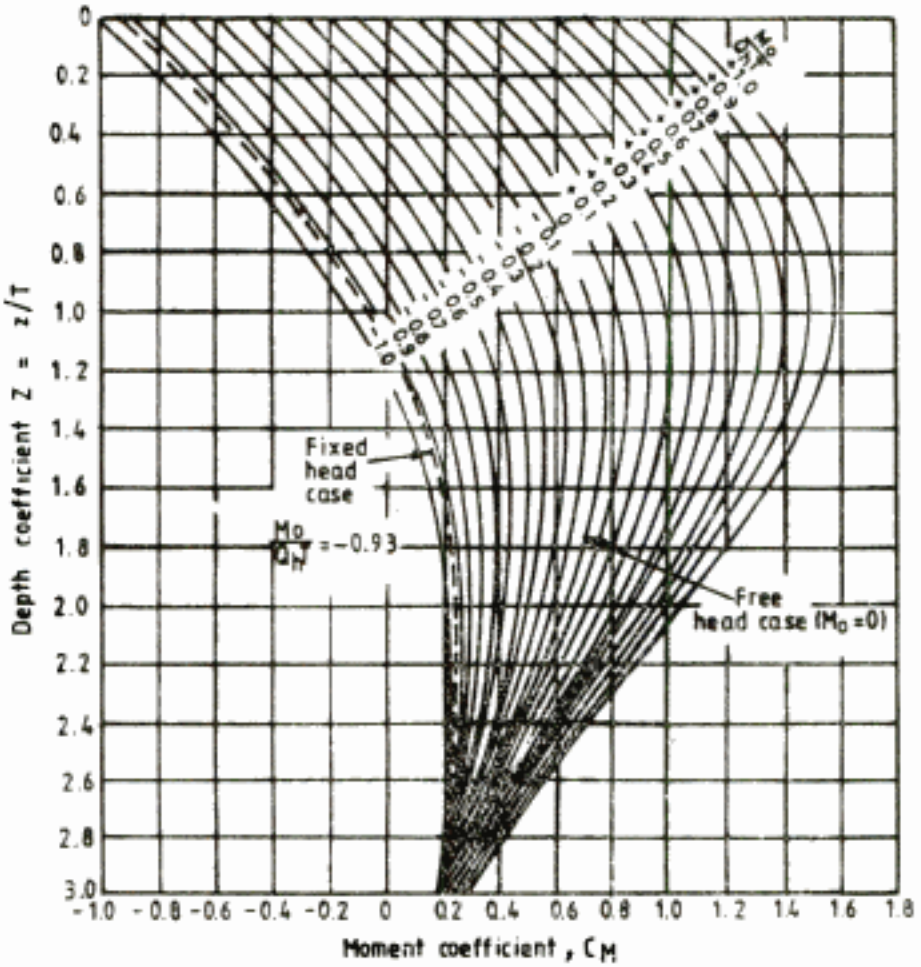

Fig. 15.37 Curves of moment coefficient C_M for long piles (After Matlock and Reese, 1961)

(d) *General observations on the lateral deflection of piles*

(i) It is difficult to evaluate the value of k_h or n_h precisely. Back figured values of n_h and k_h from pile load tests indicate that they vary with pile deflection. Values of n_h and k_h decrease as pile deflection increases.

(ii) The soil near the ground surface, for example, the upper three to five metres, governs the lateral deflection behaviour of the pile to a large extent. It is sufficient to consider variations in k_h to a depth of $\beta L = 2$ for free head piles, and $\beta L = 1$ for restrained piles when the piles are long. Soil within a depth of $0.4R$, where

$$R = \left(\frac{E_p I_p}{k_h D}\right)^{1/4} = \frac{1}{\beta} \tag{15.105}$$

must be investigated thoroughly to determine the modulus of subgrade reaction. A stiff surface layer in this zone will help to reduce pile deflection and moment considerably.

(iii) The modulus of subgrade decreases by about 30 per cent for cyclic or repeated load on the pile. Lateral deflection increases by 100 per cent for 50 cycles or more of repetition and the pile moments also increase.

(iv) Consolidation increases the lateral deflection of the piles. Broms (1964) suggests that to account for consolidation effects reduced values of k_h may be used in the calculations. The effective values (k_{h-eff}) suggested are

$$k_{h-eff} = \frac{1}{2}k_h \text{ to } \frac{1}{4}k_h$$

for stiff to very stiff clay

$$k_{h-eff} = \frac{1}{3}k_h \text{ to } \frac{1}{6}k_h$$

for soft and very soft clays

$$k_{h-eff} = k_h$$

for sands

(v) The maximum bending moment on the pile occurs within a few pile diameters below the ground surface. For short durations of loading the maximum bending moment occurs at depths between 0.5 m and 1.5 m and for long term loading this depth is between 1 and 1.5 m.

(vi) The lateral load analysis of piles embedded in soils with modulus of subgrade reaction increasing linearly with depth can be carried out approximately by using the procedures for k_h constant with depth in the following manner:
For short piles if subgrade reaction increases with depth the value at a depth of $0.25L$ for a free head pile and at a depth of $0.5L$ for a fixed head pile, may be taken as the equivalent constant value of k_h. For long piles the value of subgrade reaction at the depth corresponding to $\beta L = 0.4$ may be taken as the equivalent constant value of k_h.

(vii) The lateral load analysis of piles embedded in soils having uniform k_h with depth can be carried out approximately by using the procedures for modulus of subgrade reaction proportional to depth in the following manner:
The modulus of elasticity of soil E_s is determined. A value of n_h is assumed and using the analysis for subgrade reaction linearly increasing with depth, the depth of z_0 to the point of zero deflection is calculated. $n_h z_0$ is computed. If $n_h z_0$ is not equal to $2E_s$ a new value of n_h is assumed and the procedure is repeated. The analysis of the pile is carried out with the value of n_h which satisfies the condition that $n_h z_0 = 2E_s$.

15.3.5 Pile Load Tests

In spite of the many rigorous and sophisticated analytical procedures available for the determination of pile load capacity, in most situations a pile load test still remains the acid test for the actual performance of the piles at the site. Pile load test can be initial test or routine test. Initial load test is carried out on test piles which is generally made for the purpose of determining the safe load and/or ultimate load capacity of the pile. Routine tests are regular checks which are carried out on working piles to determine the displacement at the safe load and check the integrity of the piles. Indian Code of Practice (IS: 2911, Part 4, 1985) specifies that if there is a lack of information about strata and of experience with the soil at the site, a minimum of two initial tests must be performed. The number of routine tests may generally be one-half per cent of the total number of piles. However, this may vary depending upon the importance of the structure and the variation in the soil strata. For very

important structures and in erratic soil deposits the number of routine tests can be as high as 2 per cent of the total number of piles or even more.

The different types of load tests that may be conducted on piles are (i) vertical load test (compression), (ii) pull-out test, and (iii) lateral load test. Indian Code of Practice (IS: 2911, Part 4, 1985) describes the guidelines for all three types of tests. Only salient features of these tests are discussed here.

1. *Vertical load test (compression)*

The test can be carried out in three different manners, namely, (i) maintained load test, (ii) constant rate of penetration test and (iii) equilibrium method of test. Of these, however, the maintained load test is the most commonly used, as it is believed to give the load-settlement relationship of the pile.

In the maintained load test the pile is subjected to a series of load increments. Each increment of load is about 20 per cent of the assumed safe load. Each stage of loading is maintained till the rate of movement becomes negligibly small. IS Code specifies that each stage of load is maintained till the rate of movement of the pile top is either 0.1 mm in first 30 minutes, or 0.2 mm in first one hour, or till 2 hours whichever occurs first. The estimated safe load is recommended to be maintained for 24 hours. For each stage of loading the movement of the pile is recorded using minimum two dial gauges of sensitivity 0.01 mm. In the case of routine test the load increment is continued up to a maximum test load of one and half times the working load, the maximum settlement, however, not exceeding 12 mm. For initial test, the maximum test load may be higher and may correspond to ultimate load at failure.

The load-settlement data can be used to plot curves from which the ultimate load capacity of the pile can be determined. Figure 15.38 shows the form of a load vs. settlement graph, in which the coordinate points are plotted to ordinary scale. The shape of the curve greatly depends on the scale used for the diagram, as shown in Fig. 15.38. Hence, improper selection of scale can lead to ambiguous interpretations from the curve. Figure 15.39 shows another form of plotting the load test data. In this plot there is a distinct change in the slope of the curve at the ultimate load of the pile. The load on the pile corresponding to a settlement of 10 per cent of the pile diameter is also commonly considered as the ultimate load of the pile. But this may not be true for non-displacement piles in sand where a pile settlement exceeding 20 per cent of the pile diameter will be required to mobilise ultimate load.

Several recommendations concerning the determination of safe load on the pile from load test data are found in literature. According to Indian Code of Practice the safe load is the least of the following:

(a) Two-thirds of the final load at which the total settlement is 12 mm, unless a value different from 12 mm is specified depending upon the nature and type of structure.

(b) The load at which the total permissible settlement is reached.

(c) Fifty per cent of the load at which total settlement is equal to 10 per cent of the pile diameter in case of uniform diameter piles and 7.5 per cent of bulb diameter in case of under-reamed piles.

The load test must be carried out at the intended cut-off level. If for any reason the test is carried out at a level different from the cut-off level, due care must be taken in the pile load test, or suitable adjustments must be made in the interpretation of load test data.

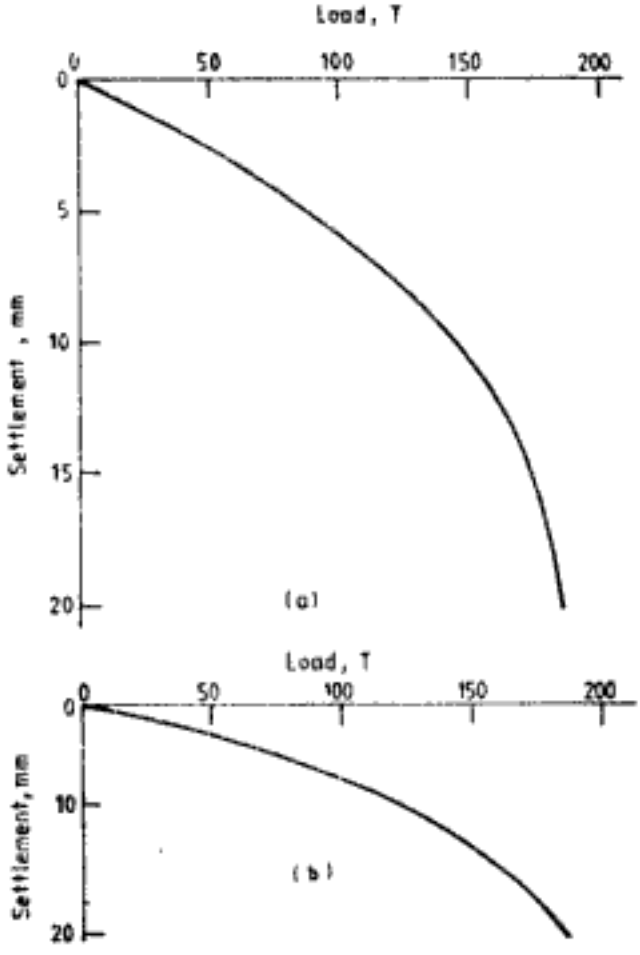

Fig. 15.38 Load vs. settlement curves plotted to different scales

2. *Pull-out test*

The application of load increments and the observations for displacement of pile can be performed in the same manner as explained for vertical or compression load test. The initial test can be carried out up to twice the estimated safe load or until the load-displacement curve shows a distinct break. The maximum load applied in routine test is $1\frac{1}{2}$ times the allowable load or load required for 12 mm upward movement of pile, whichever is smaller. According to Indian Code of Practice, the safe load is the least of the following:

(a) Two-thirds of the load at which total upward displacement is 12 mm,
(b) The load corresponding to a specified permissible uplift,
(c) Fifty per cent of the load at which the load-displacement curve shows a clear break.

3. *Lateral load test*

Lateral load test is usually conducted by inserting a hydraulic jack between two piles and thrusting them apart. The test pile and the reaction pile must be sufficiently spaced to avoid mutual interference. The load is applied in increments of about 20 per cent of the estimated safe load. The load at any stage is maintained till the rate of displacement becomes nearer to 0.1 mm per 30 minutes. Lateral displacements are read by using minimum two dial gauges of 0.01 mm sensitivity and spaced 30 cm vertically. The displacement at the load axis and at the cut-off level of the pile can be determined by using the procedure shown

Hidden page

15.4 PILE GROUPS

Single piles are rarely used as foundation members. A cluster of piles, connected together at top either by a beam or a slab called *pile cap*, is invariably used. Such an arrangement called *pile group* is necessary for the stability and integrity of the foundation system. There are two different types of pile groups, namely, (i) free-standing pile groups, and (ii) piled foundations.

In a free-standing pile group the pile cap stands clearly above the ground level as shown in Fig. 15.41a. Free-standing pile groups may be used as a necessity in some situations, for example, in expansive soils to prevent the swelling pressure from acting on the pile cap. Or certain situations may impose free-standing pile group action, such as the condition where the soil below and around the pile cap is scourable by water current.

A piled foundation as shown in Fig. 15.41b rests on the soil. It may be partly or completely buried below the ground level. Depending upon the soil conditions, the pile cap can also serve to transmit a part of the load imposed on the foundation.

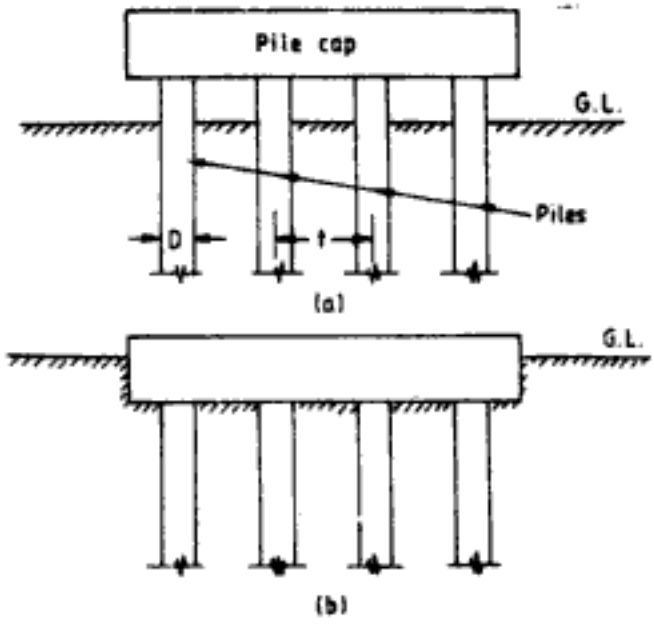

Fig. 15.41 (a) Free-standing pile group
(b) Piled foundation

The behaviour of a pile group differs from that of a single pile. However, the behaviour of a single pile is usually taken as the guiding post for the behaviour of the pile group. As in the case of shallow foundations, pile groups should be analysed for bearing capacity and settlement criteria.

15.4.1 Ultimate Load Capacity of Pile Groups

1. *Pile Groups in Compression*

The ultimate load capacity of a pile group is generally not equal to the sum of the individual load capacities of the piles which constitute that pile group. The ultimate load capacity of pile group Q_{ug} is often correlated to the ultimate load capacity of an individual representative

Hidden page

type of failure can occur at very close pile spacings. For block failure the ultimate load of the pile group is given as,

$$Q_{ug} = B_b L_b c_{u-b} N_c + 2(B_b + L_b) L c_{u-av} \tag{15.107}$$

where B_b = breadth of the block (see Fig. 15.42)
L_b = length of the block (see Fig. 15.42)
L = height of block = length of pile
c_{u-b} = undrained cohesion at base of the block
c_{u-av} = average undrained cohesion along the depth of the block
N_c = bearing capacity factor (determined from Fig. 15.43)

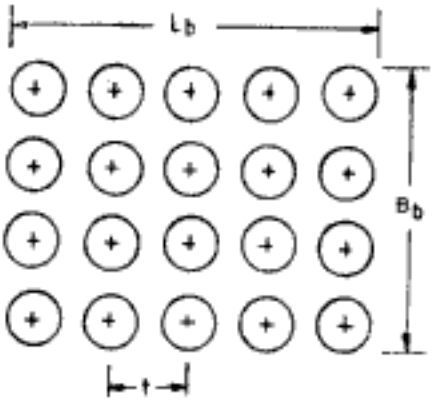

Fig. 15.42 Plan view of piles in a pile group

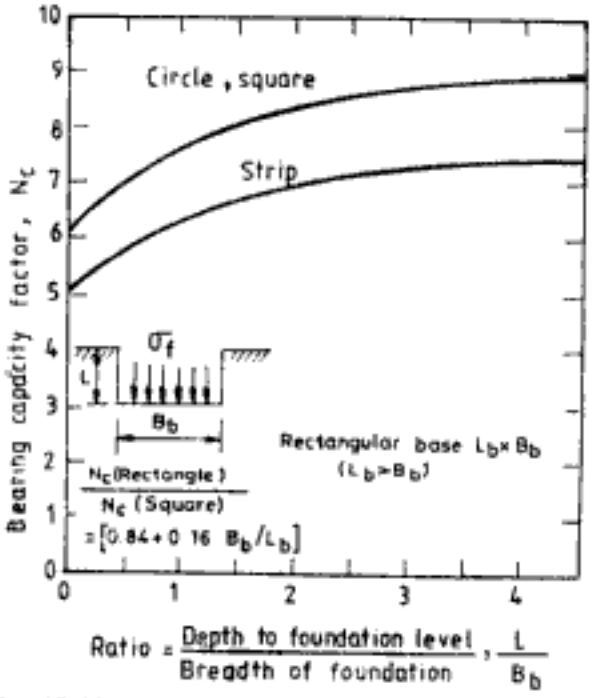

Fig. 15.43 Bearing capacity factors for foundations in clay, $\phi = 0$. (After Skempton, 1951)

For large spacing, the surface area of the block increases and individual pile failure is more feasible. In this case,

$$Q_{ug} = nQ_u \tag{15.108}$$

For piled foundations in clay, again the two different failure mechanisms are considered. The ultimate load capacity is the smaller of the two values computed for these two mechanisms. The two ultimate loads computed are:

(i) the ultimate load capacity of a block encompassing the piles (Eq. 15.107) *plus* the ultimate load capacity of that portion of the pile cap outside the perimeter of the block,

(ii) the sum of the individual pile capacities plus the ultimate load capacity of the pile cap, which gives,

$$Q_{ug} = nQ_u + c_{u-c} N_c \left(B_c L_c - \frac{n\pi D^2}{4} \right) \tag{15.109}$$

where c_{u-c} = undrained cohesion beneath pile cap
B_c = breadth of pile cap, $< L_c$
L_c = length of pile cap
$N_c = 5.14(1 + 0.2B_c/L_c)$

It is reported that eccentricity of load, even up to half the breadth of pile group (B_b), has no effect on the ultimate load capacity of the pile group, except where the breadth of pile group is of the same order of magnitude as the pile length. In such a case Meyerhof (1963) recommends that the shaft resistance of piles may be ignored and the ultimate load can be taken as equal to the base resistance computed on an effective base as explained for shallow foundations.

If a weak clay layer underlies the bearing clay stratum a load distribution as shown in Fig. 15.44 is assumed and the stability of the equivalent footing resting on top of the weak clay deposit is determined.

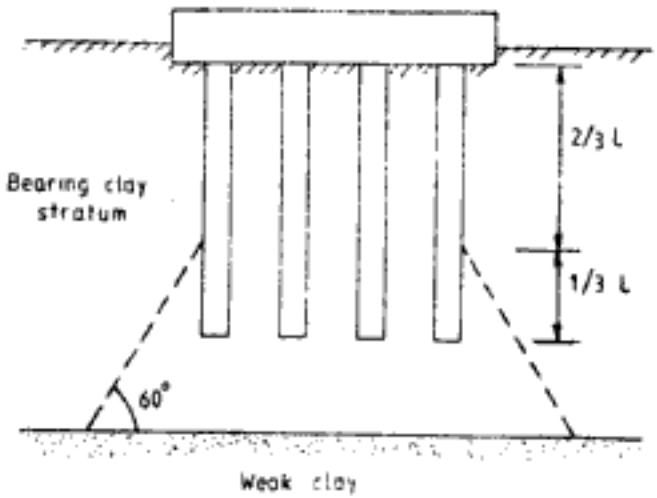

Fig. 15.44 Spread of load from bearing clay stratum to weak clay stratum

(b) *Pile groups in sand*

The group efficiency of free-standing pile groups in sand is generally believed to be more than 1 at closer spacing, due to compaction of sand by pile driving operation. But this is true only in loose sand. In medium dense and very dense sand the group efficiency is less than 1 (Kaniraj 1974, Ranganatham and Kaniraj 1978, Ranganatham and Kaniraj 1983). For design purposes group efficiency is usually taken as 1; in other words, the load capacity of free-standing pile group is equal to the sum of individual pile load capacities.

For piled foundation the pile cap obtains considerable reaction from soil. However, the amount of movement required to mobilise this reaction will be very large and may exceed the permissible limit of settlement. Compaction of the soil around the pile group to a depth influenced by the pile cap will reduce the movement required for mobilising soil reaction.

If a weak clay layer underlies the sand stratum, the stability of the equivalent footing resting on top of the weak soil deposit must be ensured. The assumed load spread diagram is shown in Fig. 15.45.

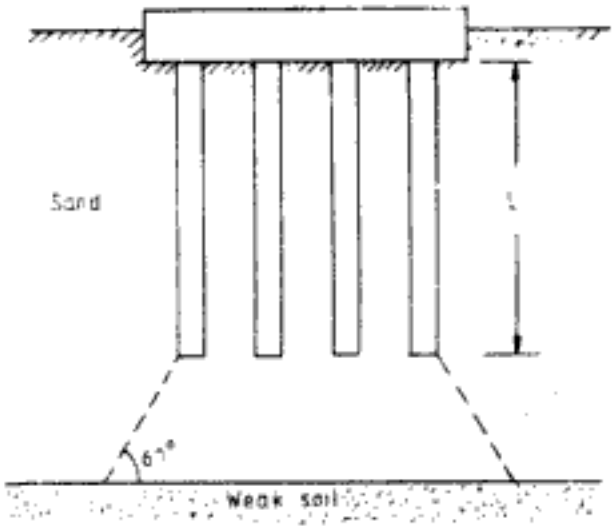

Fig. 15.45 Spread of load from bearing sand stratum to weak stratum

2. *Uplift Load Capacity of Pile Groups*

From the inferences made for footings by Meyerhof and Adams (1968), the uplift load capacity of pile groups may be calculated as the smaller of the following two values: (i) the sum of the uplift capacity of individual piles, and (ii) the uplift capacity of the equivalent block formed by the pile group including the weight of the block.

3. *Lateral Load Capacity of Pile Groups*

The group efficiency for lateral loading is less than 1. The lateral load capacity of pile groups is recommended to be computed as the smaller of the following two values: (i) the sum of the lateral load capacity of the individual piles, and (ii) the lateral load capacity of the equivalent block formed by the piles and the soil within the pile group.

If Broms' theory is used to calculate the lateral load capacity of the equivalent block, Poulos and Davis (1980) recommend that in clay, soil reaction may be assumed to be zero to a depth of $0.1L$ (Figs 15.25 and 15.27). For fixed head pile groups with massive pile caps, the ultimate load capacity for block failure can be calculated as the sum of the resistance of a short restrained pile and the shear resistance at the base area of the block. Some allowance may be made for the shear resistance at the sides of the block.

15.4.2 Vertical Settlement of Pile Groups

The settlement of a pile group is more than the settlement of a single pile even when the loads on the single pile and on each individual pile of the pile group are the same. This is primarily because of the difference in the size of zone of soil influenced by the single pile and the pile group (Fig. 15.46). The zone of influence for a pile group is much larger and deeper than for a single pile. In case of driven piles in sand, the zone of influence for pile group is more compressible also. The soil in the zone of influence for single pile is already *precompressed* or *prestressed* due to pile driving operations. Whereas, the sand in the larger zone of pile group is essentially undisturbed, except for the small zone surrounding each individual pile.

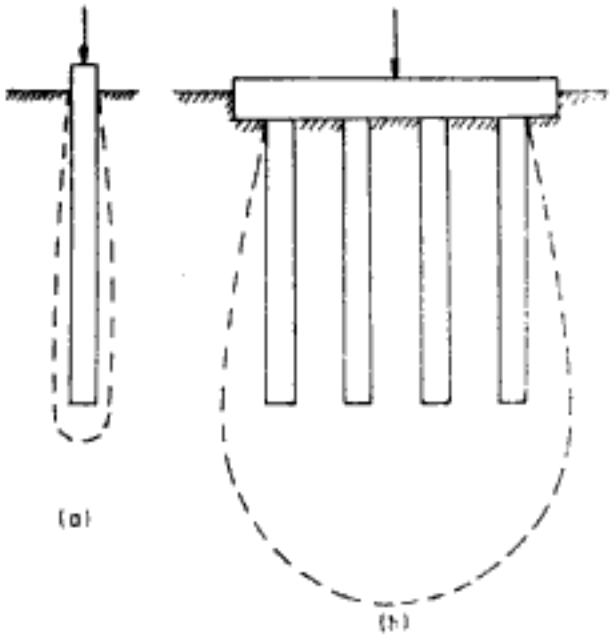

Fig. 15.46 Zone of influence: (a) Single pile (b) Pile group

The settlement of pile group is correlated to settlement of a single pile through a parameter called *settlement ratio*, R_s defined as

$$R_s = \frac{\rho_g}{\rho_s} \tag{15.110}$$

where ρ_s = settlement of single pile at load Q

ρ_g = settlement of the pile group at the same average load Q per pile, i.e. at the total pile group load of nQ

1. *Pile groups in clay*

Settlement of pile groups in clay can be determined by rigorous analytical procedures (Poulos and Davis 1980, Kaniraj and Ranganatham 1979) which consider the interaction between the piles in a pile group. With these procedures it is possible to compute the settlement of a single pile and the settlement ratio of the pile group. Using Eq. 15.110 the settlement of pile group can be determined. But the most common approach to calculate settlement of pile groups in clay is the *equivalent footing approach*. In the equivalent footing approach a fictitious footing is assumed at some arbitrary depth inside the soil and the settlement of this footing is calculated using procedures explained in Ch. 14. The settlement of this pile group is assumed to be equal to the settlement of the fictitious footing. Some commonly used assumptions for equivalent footings are shown in Fig. 15.47. It is evident that the calculated value of settlement depends upon the assumptions made for the depth of the equivalent footing and the load spread.

For a specified permissible value of settlement, Simons and Menzies (1975) point out that the length of the piles determined by using approximation in Fig. 15.47a is 50 per cent more than that obtained by using approximation in Fig. 15.47c. For displacement piles they recommend Fig. 15.47a and for bored piles Fig. 15.47c. Tomlinson (1980) recommends

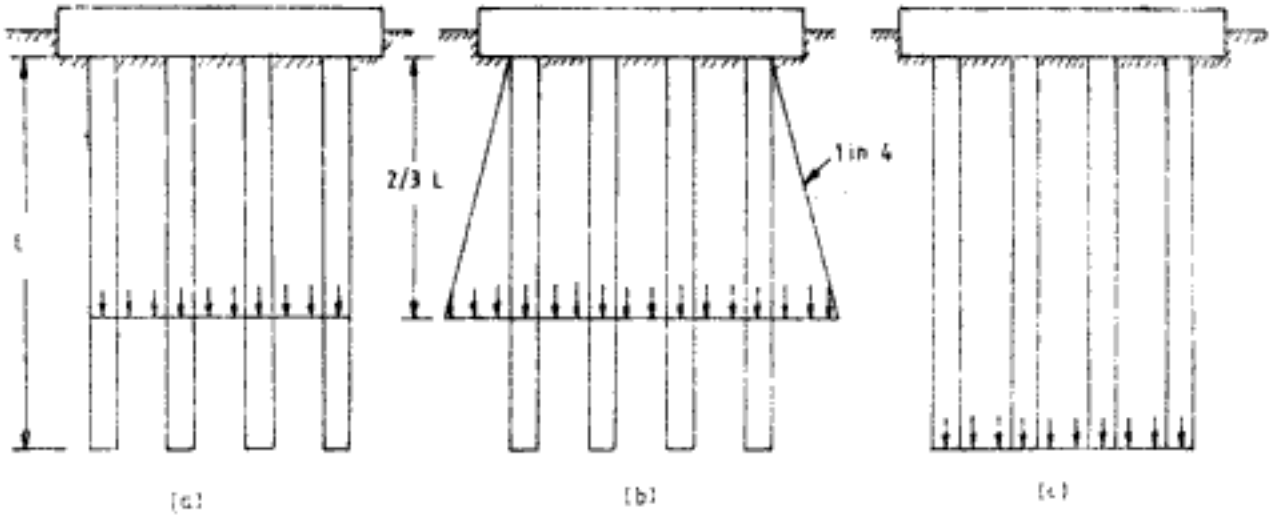

Fig. 15.47 Equivalent footing approximations for calculation of settlement

Fig. 15.47b, in general. Kaniraj and Ranganatham (1974, 1977b) point out that the use of conventional Boussinesq theory for stress distribution instead of the more appropriate Mindlin's theory results in conservative prediction of settlement. For a square footing, embedded at depth equal to the side of the footing, the difference in the computed settlements by the two theories is about 30 per cent.

2. *Pile groups in sand*

Empirical relationships for pile foundations are available. For pile groups made of driven piles, Skempton (1953) gives the relationship for settlement ratio as,

$$R_s = \left(\frac{4B + 9}{B + 12}\right)^2 \tag{15.111}$$

where, B = width of pile group in feet. Equation 15.111 is expressed with B in terms of metres as,

$$R_s = \left(\frac{4B + 2.7}{B + 3.6}\right)^2 \tag{15.112}$$

Figure 15.48 shows the variation of R_s according to Eq. 15.112. It can be inferred from Eq. 15.111 or Eq. 15.112 that according to Skempton's suggestion R_s will not exceed 16, which means the settlement of pile group will not be more than 16 times the settlement of the single pile irrespective of the width of the pile group.

Another empirical relationship for square pile groups with driven piles is due to Meyerhof (1959). According to him,

$$R_s = \frac{s(5 - s/3)}{(1 + 1/r)^2} \tag{15.113}$$

where s = ratio of pile spacing to diameter of pile = t/D

r = number of rows for square groups

In order to calculate the pile group settlement using the empirical relationships, the settlement of single pile must be known which can be obtained from pile load test results.

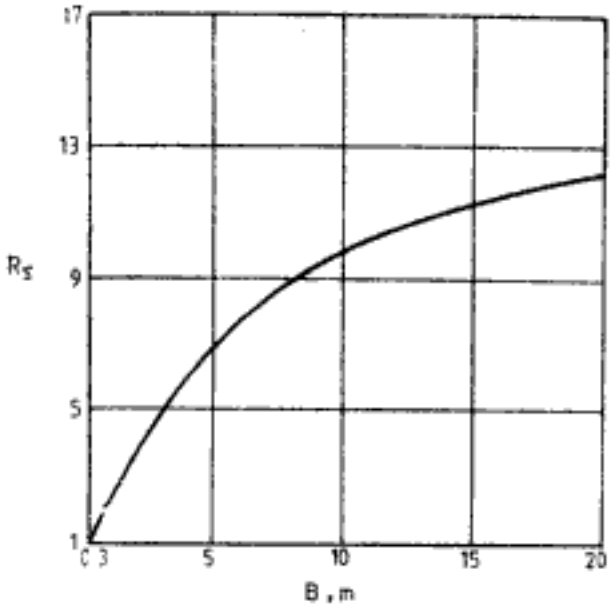

Fig. 15.48 Skempton's empirical relationship for pile foundation in sand

The USSR and Poland national building codes make use of the equivalent raft area for single pile A_s and for pile group A_g (Tomlinson, 1977). The equivalent raft area is determined in the manner shown in Fig. 15.49. The settlement ratio is given by,

$$R_s = \frac{A_g}{A_s}$$

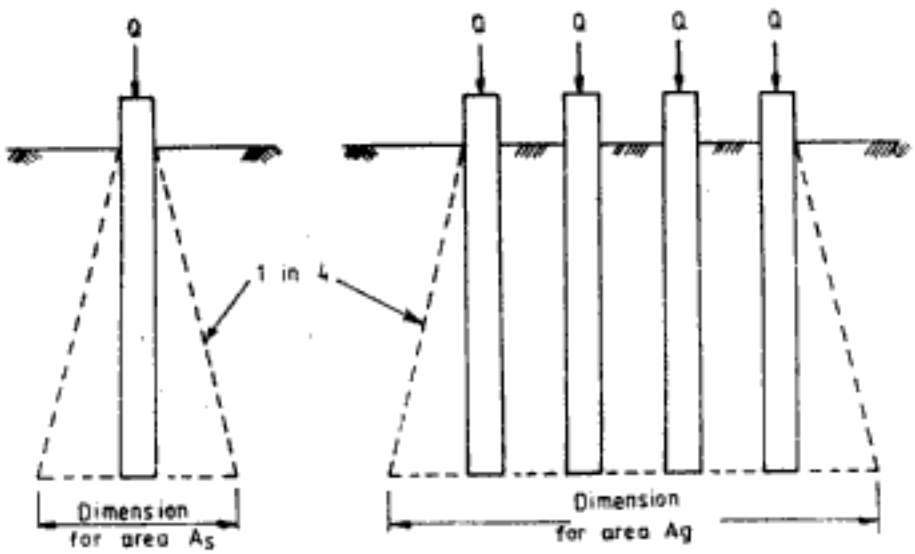

Fig. 15.49 Equivalent raft area for determination of settlement of pile groups in sand

Two observations of Berezantzev *et al.*, (1961) are worth noting here: (i) the settlement of piled foundations is proportional to the load transmitting area, (ii) pile foundations with equal load transmitting area at the level of the pile base but with different number of piles have practically equal settlements under equal loads.

The common procedure for calculation of settlement is again the *equivalent footing approach* explained for clay. Tomlinson recommends the approximation shown in Fig. 15.47b.

If the pile is driven into sand through an overlying clay stratum the equivalent footing must be considered as shown in Fig. 15.50.

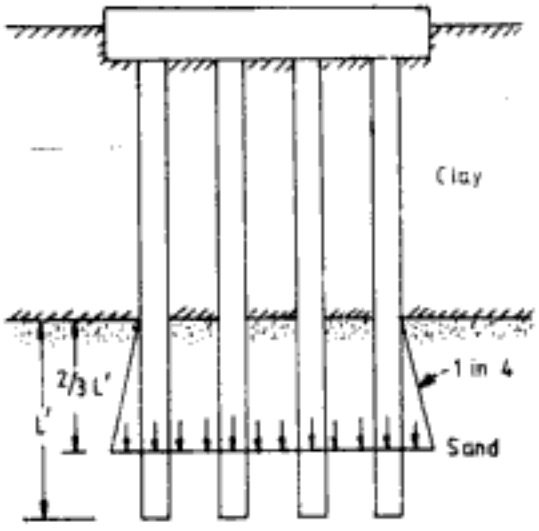

Fig. 15.50 Equivalent footing approximation for pile group driven through clay into sand

15.4.3 Lateral Displacement of Pile Groups

The lateral deflection of pile groups can be calculated using modulus of subgrade reaction approach explained for single piles. To account for the effects due to interaction between the piles, a reduced value of modulus of subgrade reaction k_{eff}, is used in the analysis. For normal spacings, Poulos and Davis (1980) recommend the following values of k_{eff}.

$k_{eff} = 0.5k_h$ for two piles
$k_{eff} = 0.33k_h$ for three or four piles
$k_{eff} = 0.25k_h$ for five or more piles

Rigorous elastic solutions for pile groups are given by Poulos and Davis (1980).

15.4.4 Load Distribution

The load and moment shared by each pile in a pile group should be analysed to safeguard against the possibility of overstressing any portion of the pile group. The methods of analysis are broadly,

(i) Simple statical analysis
(ii) Equivalent bend method
(iii) Elastic continuum approach

Simple static analysis considers the pile group as a simple statically-determinate structural system and ignores the presence of soil altogether. The joint between pile and pile cap is considered as a pin-joint and the pile group can be analysed graphically or analytically. By virtue of the assumption of pin-joint at the pile head the moment carried by each pile is zero which is not realistic. But the simple static analysis is the traditional method commonly used in practice. Only simple static analysis is discussed here for this reason. Details on the

equivalent bend method and elastic continuum approach are given by Poulos and Davis (1980).

1. *Simple static analysis*

Figure 15.51 shows a pile group acted upon by a vertical load V and a horizontal load H. The resultant R intersects the bottom of the pile cap at a distance e away from neutral axis. The pile group is in effect subjected to vertical load V at the centre of the pile group, an anti-clockwise moment $M = Ve$, and a horizontal load H at the bottom of the pile cap. As long as the resultant R intersects the bottom of the pile cap, the vertical load Q_v on a pile can be computed from,

$$Q_v = \frac{V}{n} + \frac{Mx}{\Sigma x^2} \tag{15.114}$$

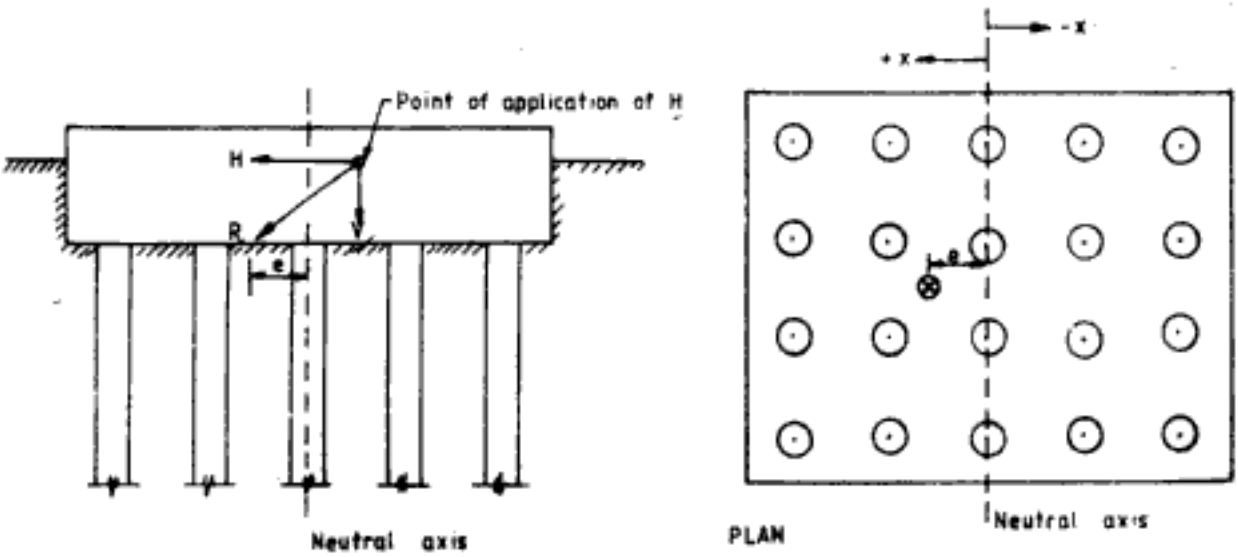

Fig. 15.51 Pile group subjected to vertical and horizontal load

where $M = Ve$

n = number of piles in the pile group

x = the distance of pile from neutral axis. The positive and negative directions of x are shown in Fig. 15.51

When the load is eccentric in two directions as shown in Fig. 15.52 the vertical load on each pile is given by,

$$Q_v = \frac{V}{n} + \frac{M_x x}{\Sigma x^2} + \frac{M_y y}{\Sigma y^2} \tag{15.115}$$

where $M_x = Ve_x$

$M_y = Ve_y$

e_x and e_y are eccentricities in x and y directions respectively. For pile groups made of vertical piles as in Fig. 15.51, the horizontal load, Q_h, per pile is,

$$Q_h = \frac{H}{n} \tag{15.116}$$

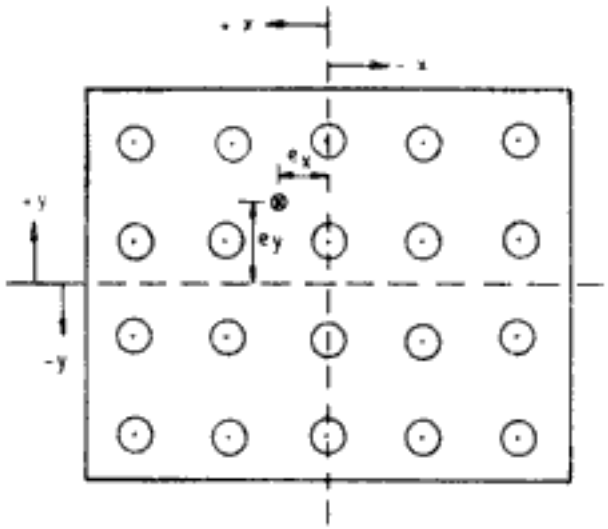

Fig. 15.52 Two-way eccentric load on pile group

When the pile group consists of inclined piles, graphical analysis as shown in Fig. 15.53 can be used. Assuming pin-joint at the pile heads the vertical reaction on each pile is first computed using Eq. 15.115. Then a force polygon is constructed by drawing lines parallel to the resultant R and parallel to the direction of the piles. The residual horizontal load, H is taken to be shared equally by all the piles of the pile group.

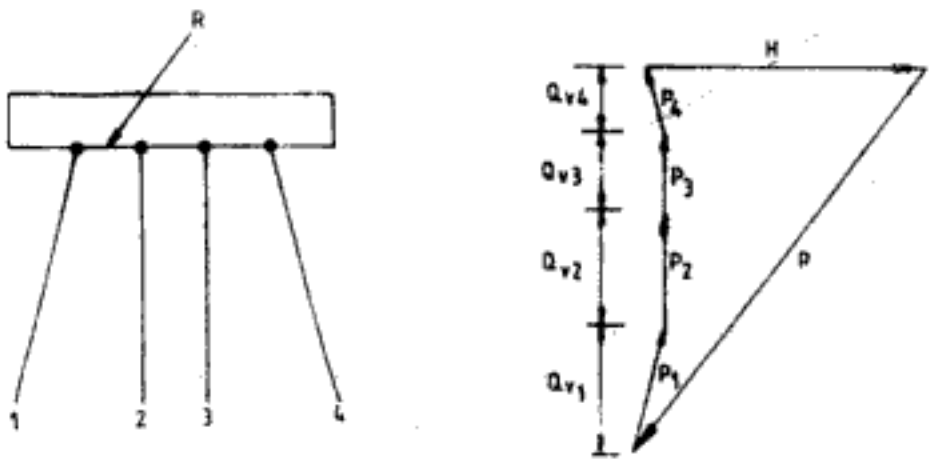

Fig. 15.53 Graphical analysis of pile loads using force polygon

15.5 NEGATIVE SKIN FRICTION/DOWNDRAG

When the soil sorrounding the pile shaft moves downwards relative to the pile, downward shear stresses are developed along the pile shaft. This is known as downdrag or negative skin friction. Downdrag on piles may be caused by: (i) consolidation of soils under the weight of recently placed fills, (ii) land subsidence due to lowering of groundwater table, (iii) regional subsidence due to underconsolidated nature of the deposits, such as reclaimed land, and (iv) reconsolidation of soil around the pile, disturbed by pile driving action.

Negative skin friction causes adverse effects on the foundation and is even referred to as the *silent enemy* of foundations (Van Veele, 1964). Negative skin friction imposes additional load on the pile. Thereby it decreases the ultimate load capacity of the pile. The settlement of pile foundation becomes excessive due to downdrag. A number of analytical and empirical procedures for the determination of drag load on piles (Kaniraj 1974, Kaniraj and Ranganatham 1977a, Broms 1979, Poulos and Davis 1980, Hora 1981) have been suggested by various investigators. The most common ones are presented here.

The *limiting* value of unit negative skin friction f_n can perhaps be taken as equal to the undrained shear strength of soil. Terzaghi and Peck (1948) assuming full mobilisation of soil shear strength at the pile-soil interface along the entire length of the pile recommend,

$$f_n = c_u \tag{15.117}$$

The maximum value of total downdrag load Q_n on a single pile is then given by

$$Q_n = c_u C L \tag{15.118}$$

where, C = the perimeter of the pile. Assuming that the negative skin friction on pile groups will be mobilised on the vertical sides of the block formed by the perimeter of the pile group, and the soil within the block will hang on the piles, the limiting downdrag load on pile group, Q_{ng}, is given by,

$$Q_{ng} = C_g c_u L + W_b \tag{15.119}$$

where C_g = perimeter of pile group

W_b = weight of soil block within the pile group

The most popular method to determine negative skin friction on single piles is the *β-method*. The unit negative skin friction in this method is expressed as,

$$f_n = \beta \bar{\sigma}_v \tag{15.120}$$

where $\beta = K \tan \bar{\phi}_a$, a coefficient which depends on the soil type

$\bar{\phi}_a$ = effective friction angle between pile material and soil

K = an earth pressure coefficient

$\bar{\sigma}_v$ = vertical effective stress

Baligh and Vivatrat (1975) give a procedure for β-method, which has been slightly modified and presented below.

1. Estimate the settlement at the ground surface after installation of pile. If it is large, say more than 2.5 to 5 cm, the downdrag load should be computed.
2. Establish the pile parameters like, perimeter, and elevations of pile tip and the pile top.
3. Establish the soil profile, the soil layers, their total density, and the water table level.
4. Compute the vertical effective stress $\bar{\sigma}_v$ at the midheight of those soil layers in which the soil settles more than the pile.
5. Determine the value of unit negative skin friction in each layer using Eq. 15.120. β can be obtained from Table 15.23 or Table 15.24.
6. Compute the downdrag force in each layer and sum them up to get the total downdrag load Q_n on the pile.

According to USSR Building Code (1978), downdrag forces need not be considered if the settlement after construction is less than the settlement which the structure can tolerate

Table 15.23 Values of β

Soil type	β
Clay	0.20 to 0.25
Silt	0.25 to 0.35
Sand	0.35 to 0.50

After Garlanger, 1974. By permission of Transportation Research Board, National Research Council, Washington, D.C.

Table 15.24 Values of β

Soil type	β
Rock fill	0.40
Sand and gravel	0.35
Silt or normally consolidated clay with low to medium plasticity (PI < 50)	0.30
Normally consolidated clay with high plasticity (PI > 50)	0.20

After Broms, 1976.

without damage. The unit negative skin friction depends on the height of fill around the structure and on the liquidity index I_L of the soil. When height of fill is more than 5 m, negative skin friction values shown in Table 15.25 are to be used. For peat, a constant value of 0.05 kg/cm^2 is recommended for f_n. When the height of fill is between 2 and 5 m, f_n can

Table 15.25 Limiting Values of Unit Negative Skin Friction

Average depth of layer below ground surface (m)	Limiting values of f_n for different I_L (kg/cm^2)								
	$I_L = 0.2$	0.3	0.4	0.5	0.6	0.7	0.8	0.9	1.0
1	0.35	0.23	0.15	0.12	0.08	0.04	0.04	0.03	0.02
2	0.42	0.30	0.21	0.17	0.12	0.07	0.05	0.04	0.04
3	0.48	0.35	0.25	0.20	0.14	0.08	0.07	0.06	0.05
4	0.53	0.38	0.27	0.22	0.16	0.09	0.08	0.07	0.05
5	0.56	0.40	0.29	0.24	0.17	0.10	0.08	0.07	0.06
6	0.58	0.42	0.31	0.25	0.18	0.10	0.08	0.07	0.06
8	0.62	0.44	0.33	0.26	0.19	0.10	0.08	0.07	0.06
10	0.65	0.46	0.34	0.27	0.19	0.10	0.08	0.07	0.06
15	0.72	0.51	0.38	0.28	0.20	0.11	0.08	0.07	0.06
20	0.79	0.56	0.41	0.30	0.20	0.12	0.08	0.07	0.06
25	0.86	0.61	0.44	0.32	0.20	0.12	0.08	0.07	0.06
30	0.93	0.66	0.47	0.34	0.21	0.12	0.09	0.08	0.07
35	1.00	0.70	0.50	0.36	0.22	0.13	0.09	0.08	0.07

After USSR Building Code, 1978.

Hidden page

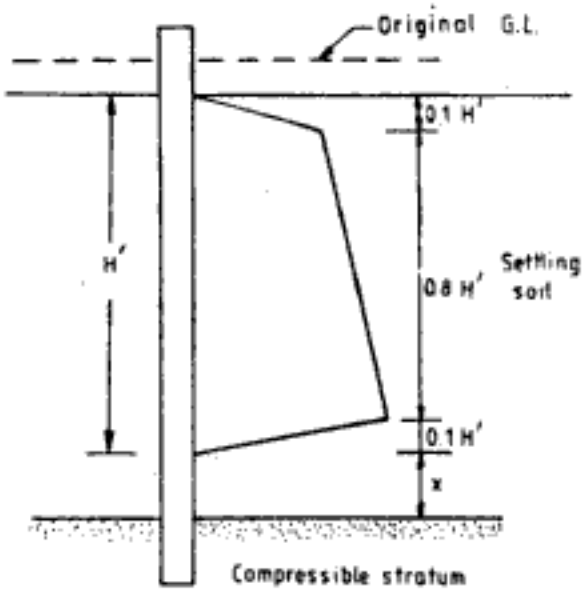

Fig. 15.55 Negative skin friction distribution for piles with tip in compressible stratum
(After Tomlinson 1980)

is suggested. In the diagram x is the zone in which the pile settles more than the soil. Q_n is given by,

$$Q_n = 0.45H'(\tau_p + \tau_r)C \tag{15.122}$$

where H' = depth to neutral point

The calculated value of downdrag load is added to the working load Q on the pile. The factor of safety is then defined as,

$$\text{Factor of safety} = \frac{\text{ultimate load capacity}}{Q + Q_n} \tag{15.123}$$

A lower factor of safety than what is normally used for working load alone is adopted.

Downdrag can be significantly reduced in precast piles by coating the pile surface with bitumen. Enlarged pile points should be used to avoid damage to bitumen coating. However, the skin frictional capacity is also greatly reduced because of the bitumen coating. Batter piles should be avoided where downdrag is expected because of the large bending moments that will be induced in the piles.

16

LATERAL EARTH PRESSURE

Some structures are designed and constructed predominantly to resist lateral earth pressure acting on them. Figures 16.1 and 16.2 show examples of two such structures. The retaining wall shown in Fig. 16.1 prevents the outward movement of the soil. The soil which the wall retains bears upon the wall and exerts a lateral thrust on it.

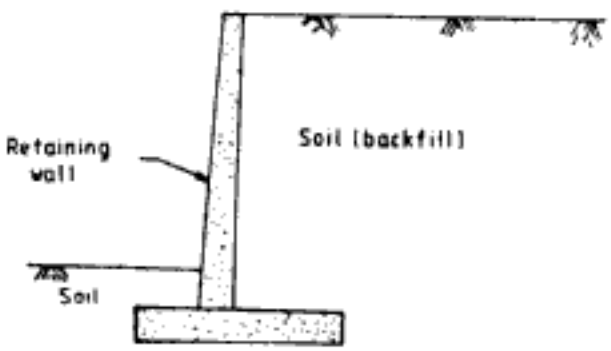

Fig. 16.1 Retaining wall

Figure 16.2 shows a braced excavation. The sheet piles and the braces support the sides of excavation and prevent their collapse. And in this process they are called upon to resist the lateral forces from the soil.

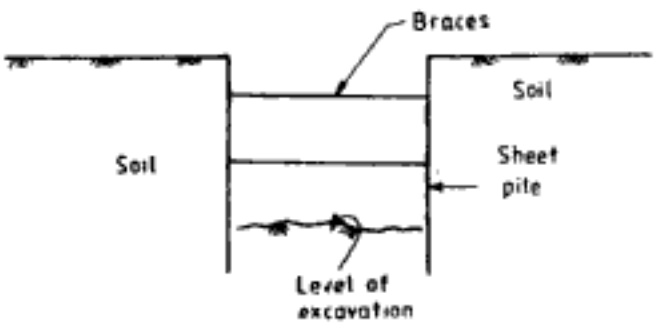

Fig. 16.2 Braced sheet pile for excavation

16.1 ACTIVE EARTH PRESSURE

Consider the sheet pile AB shown in Fig. 16.3. Let it translate to a new position $A'B'$ or rotate about A away from the soil to position AB''. In either of the two cases or a combination of them the lateral support to the soil decreases. When sufficient movement of the sheet pile has occurred, the decrease in the lateral support becomes high enough that the soil behind the sheet pile is no longer a stable mass. A wedge of soil ABC as shown in the figure fails and slides along the failure plane AC. The lateral earth pressure exerted by soil at this stage of failure is known as *active earth pressure*.

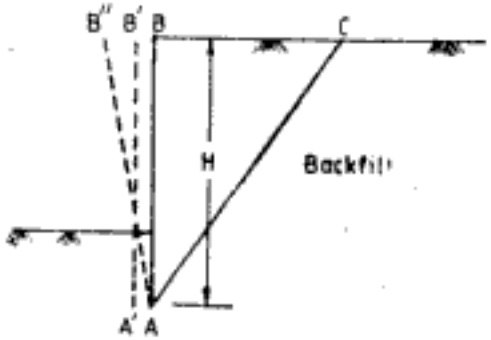

Fig. 16.3 Movement of sheet pile

Very little movement of the earth retaining structure is required to reach active state of earth pressure. The movements are grossly exaggerated in Fig. 16.3. Table 16.1 gives typical values of movements required to reach active state. Such small movements are often realised in structures like retaining walls, sheet piles, bridge abutments, and wing walls, that they are usually designed for active earth pressure.

Table 16.1 Amount of Movement and Strain Required to Reach Active State

Soil	Amount of translation at top	Amount of horizontal strain
Cohesionless, dense	$0.001H$-$0.002H$	Less than (−) 0.5 per cent is required. Horizontal strain is defined as the ratio of the amount of movement to the length BC (Fig. 16.3) of failure wedge.
Cohesionless, loose	$0.002H$-$0.004H$	
Cohesive, firm	$0.01H$ -$0.02H$	
Cohesive, soft	$0.02H$ -$0.05H$	
(H is the height of retaining structure)		

16.2 PASSIVE EARTH PRESSURE

Figure 16.3 shows the sheet pile movement to occur away from the soil. Now, if the sheet pile movement is in the reverse direction, it will press more against the soil. As the sheet pile is moved more and more against the soil the pressure will continue to increase until a stage is reached when a wedge of soil mass fails and slides along a failure plane. The lateral earth pressure on the sheet pile at this stage of failure is known as *passive earth pressure*.

The magnitude of movement or horizontal strain required to reach passive state is many times larger than that required to reach the active state. However, very little horizontal strain, about 0.5 per cent, is required to reach 50 per cent of the maximum passive resistance. Much more horizontal strain, about 2 per cent, is required to reach full passive resistance. For loose sands, the horizontal strain required to reach maximum passive resistance may be as high as 15 per cent.

Passive resistance is typically mobilised by anchor plates or anchor blocks. The anchor rod or cable pulls the anchor against the soil and develops passive resistance. Structures like retaining walls, bridge abutments and sheet piles are not designed for passive pressure. Even the passive resistance offered by the soil in front of the wall due to embedment of the base is often ignored in design or taken into account after applying a suitable reduction factor (or factor of safety).

16.3 EARTH PRESSURE AT REST

When the soil deposit is formed by transportation followed by sedimentation, at any point within the soil mass the state of stress will be as shown in Fig. 16.4. There will be a vertical stress σ_{vz} due to the weight of overburden above that point and there will be a corresponding lateral stress σ_{hz}. σ_{hz} is called as the lateral stress at rest and the summation of the stresses over a vertical plane above the point is known as the lateral earth pressure at rest. In practice, the earth pressure on a retaining structure will correspond to *at rest* condition when the following two requirements are satisfied:

1. the retaining structure is absolutely non-yielding, and
2. the backfill is very carefully placed to simulate natural deposition of soil.

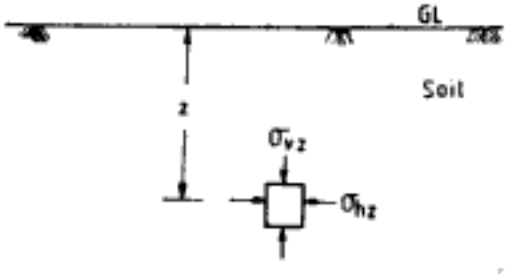

Fig. 16.4 Stresses on soil element

16.4 COEFFICIENTS OF LATERAL EARTH PRESSURE

16.4.1 Coefficient of Earth Pressure at Rest (K_0)

The coefficient of earth pressure at rest K_0, is defined as the ratio of the horizontal effective stress ($\bar{\sigma}_h$) to the vertical effective stress ($\bar{\sigma}_v$) in soil. Thus,

$$K_0 = \frac{\bar{\sigma}_h}{\bar{\sigma}_v} \tag{16.1}$$

The value of K_0 depends on the soil type and its stress history. From experiments and observations, several authors have proposed empirical relations for K_0.

For *normally consolidated sands and cohesionless soils*, the well-known expression for K_0 is due to Jaky (1944, 1948) which is as follows,

$$K_0 = 1 - \sin \phi \tag{16.2}$$

Brooker and Ireland (1965) propose the following relationship for *normally consolidated clays*,

$$K_0 = 0.95 - \sin \phi \tag{16.3}$$

For *normally consolidated clays* Alpan (1967) gives a relationship for K_0 in terms of plasticity index, as

$$K_0 = 0.19 + 0.233 \log_{10} (\text{PI}) \tag{16.4}$$

where PI = plasticity index in per cent.

In overconsolidated soils value of K_0 is more than that for normally consolidated soils. In these cases,

$$K_{0(\text{OC})} = K_{0(\text{NC})} \text{OCR}^n \tag{16.5}$$

where $K_{0(\text{OC})}$ = K_0 for overconsolidated soil
$K_{0(\text{NC})}$ = K_0 for normally consolidated soil
OCR = overconsolidation ratio
n = an empirical constant

For sands, the value of n in Eq. 16.5 can be obtained from Fig. 16.5. For overconsolidated cohesive soil n can be obtained from Eq. 16.6 in which PI must be entered in per cent.

$$n = 0.54 \times 10^{-(\text{PI}/281)} \tag{16.6}$$

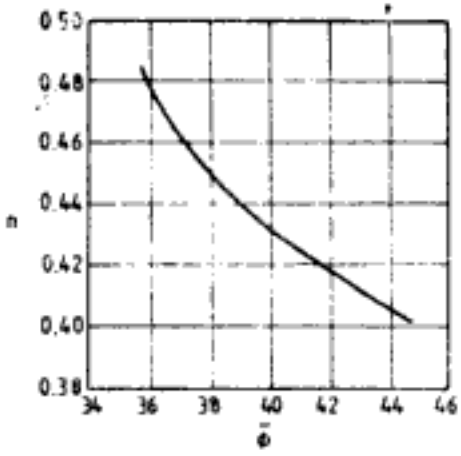

Fig. 16.5 Variation of n with $\bar{\phi}$ (After Alpan, 1967)

Wroth (1975) gives the following relationship for *overconsolidated soil*,

$$K_{0(\text{OC})} = \text{OCR} \times K_{0(\text{NC})} - \left(\frac{\bar{\mu}}{1 - \bar{\mu}}\right)(\text{OCR} - 1) \tag{16.7}$$

where, $\bar{\mu}$ = Poisson's ratio in terms of effective stresses.
For overconsolidated soils with OCR < 5, $\bar{\mu}$ is given by the relationship,

$$\bar{\mu} = 0.23 + 0.003 \text{ PI} \tag{16.8}$$

with value of PI in per cent in Eq. 16.8.

Similarly in the case of *normally consolidated soils*,

$$K_0 = \frac{\mu}{1 - \mu} \tag{16.9}$$

Q 16.1: Determine K_0 for a normally consolidated sand deposit having $\phi = 38°$.

Ans: From Eq. 16.2, $K_0 = 1 - \sin 38° = 0.38$

Q 16.2: Determine the value of K_0 for a overconsolidated sand deposit with $\phi = 38°$ and OCR = 5.

Ans: From Fig. 16.5, $n = 0.45$
From Q 16.1, $K_{0(NC)} = 0.38$
Substituting in Eq. 16.5,

$$K_{0(OC)} = 0.38 \times 5^{0.45} = 0.78$$

Q 16.3: Determine the value of K_0 for a normally consolidated clay deposit with the following properties:
$\phi = 28°$, PI = 16%

Ans: Using Eq. 16.3, $K_0 = 0.95 - \sin 28° = 0.48$
Using Eq. 16.4, $K_0 = 0.19 + 0.233 \log_{10} 16 = 0.47$

Q 16.4: Determine the value of K_0 for an overconsolidated clay deposit having the following properties:
$\phi = 28°$; PI = 16%; OCR = 5

Ans: First, K_0 is determined using Eq. 16.5.
From Eq. 16.6, $n = 0.54 \times 10^{-(16/281)}$
$= 0.474$
From Q16.3, $K_{0(NC)} = 0.47$
Substituting in Eq. 16.5

$$K_{0(OC)} = 0.47 \times 5^{(0.474)} = 1.01$$

Alternatively K_0 is determined using Eq. 16.7.
From Eq. 16.8, $\bar{\mu} = 0.23 + 0.003\,(16) = 0.278$
Substituting in Eq. 16.7,

$$K_{0(OC)} = 5 \times 0.47 - \frac{0.278}{1 - 0.278} \times (5 - 1)$$
$$= 0.81$$

The K_0 value of the overconsolidated clay deposit may be taken as the average of the two values. Thus,

$$K_0 = (1.01 + 0.81)/2 = 0.91$$

16.4.2 Coefficients of Active Earth Pressure K_a and Passive Earth Pressure K_p

The state of stress at the interface of the retaining structure at the active conditions and passive conditions defines the respective earth pressure coefficients. K_a and K_p are again defined by Eq. 16.1, but $\bar{\sigma}_h$ is now the horizontal effective stress on the sheet pile or retaining structure. K_a and K_p depend on a number of parameters like wall friction δ, inclination of the back of the wall α, slope of the back fill β, and angle of shearing resistance of the soil ϕ. Typical expressions for K_a and K_p will be discussed in the sections to follow.

Hidden page

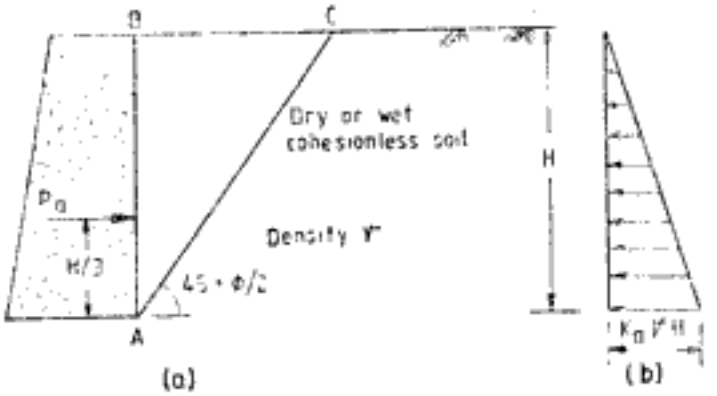

Fig. 16.7 Rankine's solution for active earth pressure

$$P_a = \frac{\gamma H^2}{2} K_a \tag{16.10}$$

where $K_a = (1 - \sin \phi)/(1 + \sin \phi)$

In Fig. 16.7, ABC is the failure wedge. The failure plane AC is inclined at $45 + \phi/2$ to the horizontal. The active thrust P_a acts horizontally since there is no wall friction. P_a acts at a distance of $H/3$ from the base of the wall since the lateral stress distribution on the wall is triangular as shown in Fig. 16.7b.

The passive lateral thrust, P_p, is given by,

$$P_p = \frac{\gamma H^2}{2} K_p \tag{16.11}$$

where $K_p = (1 + \sin \phi)/(1 - \sin \phi)$

The failure plane AC in this case is inclined at an angle $45 - \phi/2$ to the horizontal. P_p acts horizontally and at a height of $H/3$ from the base for reason explained in the case of active thrust.

Table 16.3 gives values of K_a and K_p for use in Eqs 16.10 and 16.11 respectively.

Q. 16.5: Determine the active and passive lateral thrust per metre run on the wall shown in Fig. 16.8 using Rankine's theory.

Ans: Active lateral thrust on the wall, from Eq. 16.10,

$$P_a = \frac{1}{2} \times 1.7 \times 7^2 \times \frac{1 - \sin 34^\circ}{1 + \sin 34^\circ}$$

$$= 11.8 \text{ T/m run of wall}$$

Table 16.3 Values of K_a and K_p for Use in Eqs 16.10 and 16-11

ϕ°	K_a	K_p
10	0.703	1.42
15	0.589	1.70
20	0.490	2.04
25	0.406	2.46
30	0.333	3.00
35	0.271	3.66
40	0.217	4.60
45	0.171	5.83

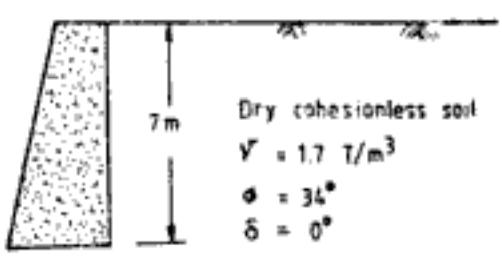

Fig. 16.8 Q 16.5

Passive lateral thrust on wall, from Eq. 16.11,

$$P_p = \frac{1}{2} \times 1.7 \times 7^2 \times \frac{1 + \sin 34^\circ}{1 - \sin 34^\circ}$$

$$= 147.4 \text{ T/m run of wall}$$

The active and passive thrust act horizontally at a height of 2.33 m from the base of the wall.

Coulomb's solutions

In a general situation the surface of retaining wall is not smooth, the backfill can be inclined and the back of the wall is also not always vertical. Figure 16.9 shows such a case which also shows the direction of action of active lateral thrust, P_a. Coulomb's solution for active thrust, P_a, in this ease is given by,

$$P_a = \frac{\gamma H^2}{2} K_a \tag{16.12}$$

where $$K_a = \left[\frac{\sin (\alpha + \phi)}{\sin \alpha \{ \sqrt{\sin (\alpha - \delta)} + \sqrt{\frac{\sin (\phi + \delta) \sin (\phi - \beta)}{\sin (\alpha + \beta)}} \}} \right]^2$$

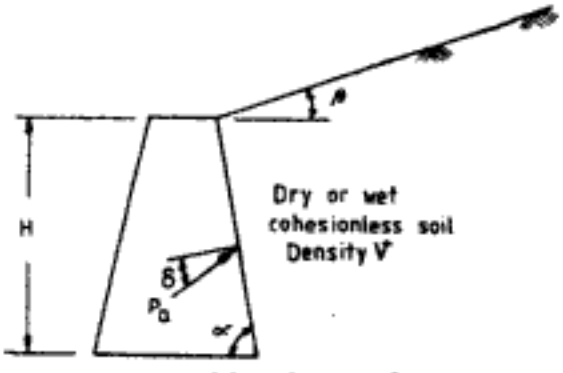

Fig. 16.9 Coulomb's solution for earth pressure

Tables 16.4 and 16.5 give values of K_a for a few combination of parameters. Similarly Coulomb's solution for passive thrust, P_p, is given by,

$$P_p = \frac{\gamma H^2}{2} K_p \tag{16.13}$$

where $$K_p = \left[\frac{\sin (\alpha - \phi)}{\sin \alpha \left\{ \sqrt{\sin (\alpha + \delta)} - \sqrt{\frac{\sin (\phi + \delta) \sin (\phi + \beta)}{\sin (\alpha + \beta)}} \right\}} \right]^2$$

Table 16.6 gives the values of K_p for use in Eq. 16.13. For vertical wall with horizontal backfill and no wall friction Rankine's solution and Coulomb's solution are identical.

Q 16.6: Determine the active and passive lateral thrust on a 7 m high wall retaining dry cohesionless backfill. Given the following data: $\gamma = 1.7$ T/m^3; $\phi = 34^\circ$; slope of backfill $\beta = 10^\circ$; the back of the wall is vertical ($\alpha = 90^\circ$). Determine the lateral thrust, when

(a) the wall is smooth, i.e. $\delta = 0$, and
(b) the wall is rough and $\delta = (2/3)\phi$

Hidden page

Table 16.6 Values of K_p for a Vertical Wall ($\alpha = 90°$), Eq. 16.13

				$\beta = 0°$				
$\delta°$	$\phi° = 26$	28	30	32	34	36	38	40
0	2.561	2.770	3.000	3.255	3.537	3.852	4.204	4.599
16	4.195	4.652	5.174	5.775	6.469	7.279	8.230	9.356
17	4.346	4.830	5.385	6.025	6.767	7.636	8.662	9.882
20	4.857	5.436	6.105	6.886	7.804	8.892	10.194	11.771
22	5.253	5.910	6.675	7.574	8.641	9.919	11.466	13.364
				$\beta = 5°$				
$\delta°$	$\phi° = 26$	28	30	32	34	36	38	40
0	2.943	3.203	3.492	3.815	4.177	4.585	5.046	5.572
16	5.250	5.878	6.609	7.464	8.474	9.678	11.128	12.894
17	5.475	6.146	6.929	7.850	8.942	10.251	11.836	13.781
20	6.249	7.074	8.049	9.212	10.613	12.321	14.433	17.083
22	6.864	7.820	8.960	10.334	12.011	14.083	16.685	20.011
				$\beta = 10°$				
$\delta°$	$\phi° = 26$	28	30	32	34	36	38	40
0	3.385	3.713	4.080	4.496	4.968	5.507	6.125	6.841
16	6.652	7.545	8.605	9.876	11.417	13.309	15.665	18.647
17	6.992	7.956	9.105	10.492	12.183	14.274	16.899	20.254
20	8.186	9.414	10.903	12.733	15.014	17.903	21.636	26.569
22	9.164	10.625	12.421	14.659	17.497	21.164	26.013	32.602

After Bowles, 1982. Reprinted by permission of McGraw-Hill Book Company, New York.

Ans: Coulomb's solutions will be used to determine the lateral thrust on the wall.

(a) From Table 16.5, $K_a = 0.314$

Substituting in Eq. 16.12,

$$P_a = \tfrac{1}{2} \times 1.7 \times 7^2 \times 0.314 = 13.1 \text{ T/m}$$

The distribution of lateral stress on the wall is shown in Fig. 16.10. P_a acts at a distance of $H/3$ (= 2.33 m from the base of the wall and is parallel to the slope of the backfill since $\delta = 0°$. For passive thrust on the wall, from Table 16.6,

$$K_p = 4.968$$

Substituting in Eq. 16.13,

$$P_p = 206.9 \text{ T/m}$$

Comments: Comparison of the solutions with values calculated in Q 16.5 indicate the following.

(i) In smooth walls the lateral earth pressure is more when the backfill has a (positive) slope than when the backfill is horizontal.

(ii) The increase in earth pressure due to slope of backfill is more in case of passive pressure than active pressure. In this example the active pressure increases by 11 per cent whereas the increase in passive pressure is 40 per cent

(b) $\delta = (2/3)\phi = (2/3) \times 34° = 22° 40'$

From Eq. 16.12, $K_a = 0.287$

$P_a = 11.95$ T/m

Hidden page

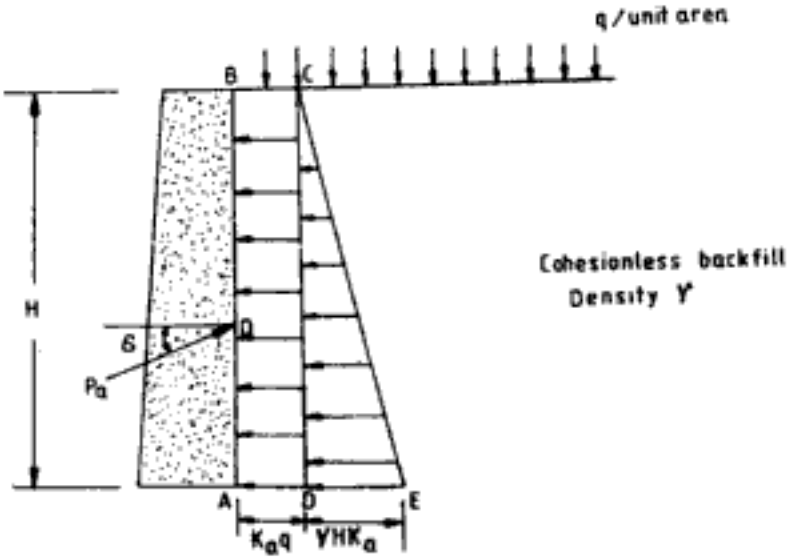

Fig. 16.12 Uniform surcharge pressure on cohesionless backfill

Ans: $K_a = 0.283$

The lateral stress over the wall due to uniform surcharge pressure is

$$= 0.283 \times 5 = 1.415 \text{ T/m}^2$$

The total active thrust due to surcharge, $P_1 = 1.415 \times 7$

$$= 9.9 \text{ T/m}$$

The active thrust due to backfill, P_2, has been already computed in Q 16.5. Figure 16.13 shows the lateral stress distribution. In Fig. 16.13, P_1 acts through the centroid of *ABCD* and P_2 through the centroid of *CDE*. The total active thrust,

$$P_a = P_1 + P_2$$
$$= 9.9 + 11.8 = 21.7 \text{ T/m}$$

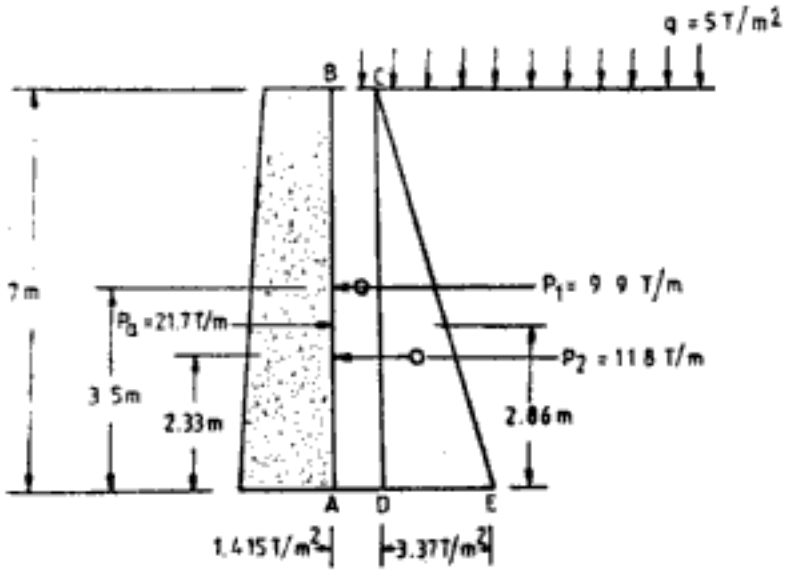

Fig. 16.13 Q 16.7

Hidden page

acts at $\bar{y}$ from A along AB with the same inclination as P_1 and P_2. To compute $\bar{y}$, taking moment of forces about A,

$$40 \times \bar{y} = 18.8 \times 3.625 + 21.2 \times 2.42$$

Solving, $\bar{y} = 2.99$ m

Note: Since all the forces P_1, P_2 and P_a are inclined at the same angle and are parallel to each other, there is no need in this case to consider normal or horizontal component of forces in the computation of moments.

16.6.3 Cohesionless Soil with Water-table

A general situation of presence of water-table in earth retaining structures is shown in Fig. 16.16.

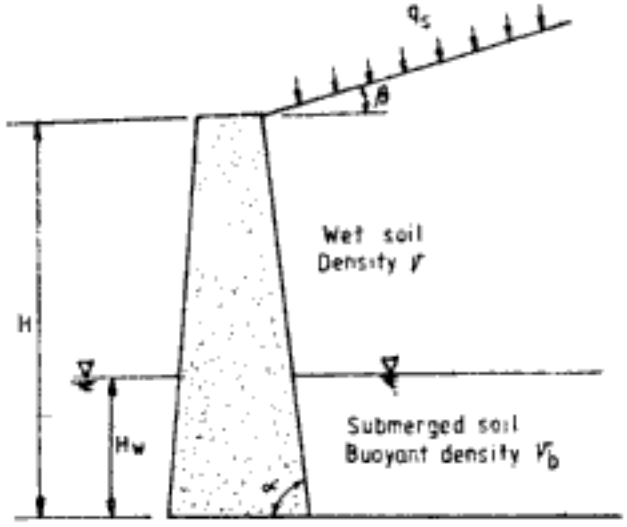

Fig. 16.16 Partial submergence of retaining wall

The water-table is at a height of H_W above the base of the retaining wall.
The active lateral stress diagram is shown in Fig. 16.17. K_a in the diagram is computed from solutions explained in Sec. 16.6.1 for dry/wet cohesionless soils. From Fig. 16.17 the total active lateral thrust on the wall can be computed as,

$$P_a = qHK_a + \tfrac{1}{2}\gamma(H - H_W)^2K_a + \gamma(H - H_W)H_WK_a + \tfrac{1}{2}\gamma_bH_W^2K_a$$

which on simplification gives,

$$\begin{aligned} P_a &= qHK_a + \tfrac{1}{2}\gamma H^2K_a - \tfrac{1}{2}(\gamma - \gamma_b)H_W^2K_a \qquad (16.14)\\ &= (P_1) \quad + \quad (P_2) \quad - \quad (P_3) \end{aligned}$$

From the form of Eq. 16.14 the location of P_a can be computed from the following considerations:

1. the thrust computed in first term ($P_1 = qHK_a$), acts at the mid-height of the wall,
2. the thrust computed in second term ($P_2 = \tfrac{1}{2}\gamma H^2K_a$), acts at 1/3 height above the base of the wall, and
3. the thrust computed in third term [$P_3 = \tfrac{1}{2}(\gamma - \gamma_b)H_W^2K_a$], is opposite in direction to forces in 1 and 2 above and acts at $H_W/3$ above the base of the wall.

Hidden page

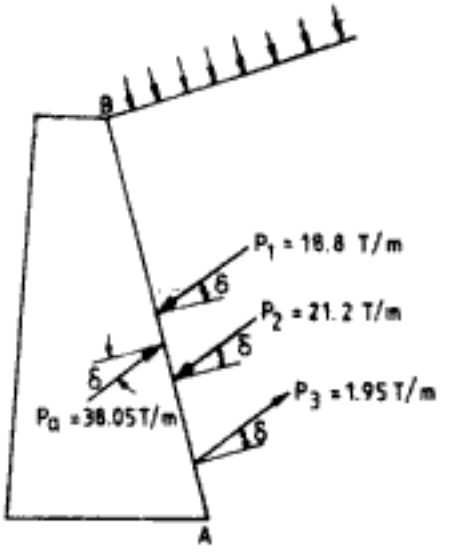

Fig. 16.18 Q 16.9

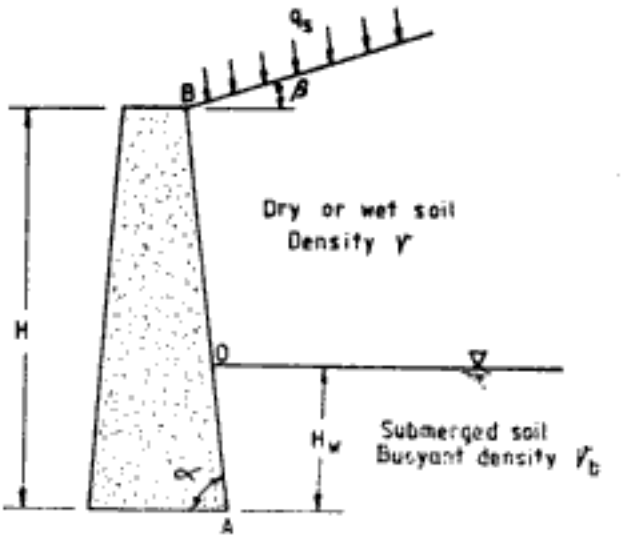

Fig. 16.19 Perched water-table in retaining wall

Q 16.10: Compute the total lateral thrust on the wall in Q 16.9 when water-table is present only in backfill at 3 m above the base of the wall.

Ans: Active thrust is calculated using Eq. 16.15. Computations for P_1, P_2, and P_3 are shown in answer to Q 16.8 or Q 16.9. For P_4 in Eq. 16.15,

$$P_4 = \frac{1}{2} \times \frac{1 \times 3^2}{\sin 75^\circ} = 4.66 \text{ T/m}$$

which acts at 1.03 m from A along AB. Figure 16.20 shows the forces on the wall. Total active lateral thrust,

$$P_t = [(4.66 + 38.05 \cos 22°40')^2 + (38.05 \sin 22°40')^2]^{1/2}$$
$$= 42.4 \text{ T/m}$$

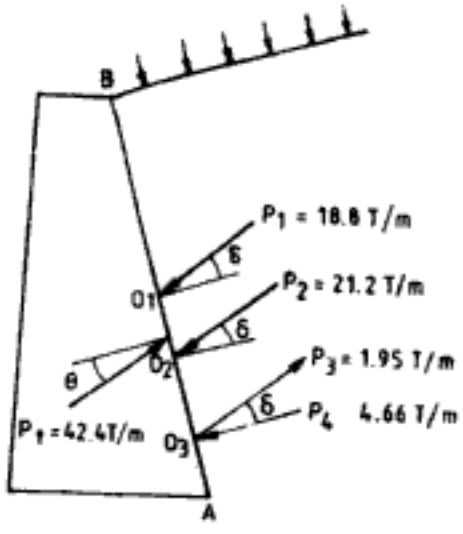

Fig. 16.20 Q 16.10

Inclination of P_t with respect to normal of the face of the wall,

$$\theta = \tan^{-1}\left(\frac{38.05 \sin 22°40'}{4.66 + 38.05 \cos 22°40'}\right)$$
$$= 20°14'$$

Let P_t act at $\bar{y}$ from A along AB. In this case all forces are not in the same direction. Considering the components of forces normal to the wall,

$$P_t \cos\theta \times \bar{y} = P_1 \cos\delta \times AO_1 + P_2 \cos\delta \times AO_2 - P_3 \cos\delta \times AO_3 + P_4 \times AO_3$$

$$\bar{y} = \frac{\{(18.8 \times \cos 22°40' \times 3.625) + (21.2 \cos 22°40' \times 2.42) - (1.95 \cos 22°40' \times 1.03) + (4.66 \times 1.03)\}}{42.4 \times \cos 20°14'}$$

i.e., $\bar{y} = 2.84$ m

Comments: Comparison of solutions in Q 16.8, Q 16.9 and Q 16.10 indicates the following:

(i) Presence of water-table on both sides of the retaining wall decreases the active earth pressure.

(ii) Presence of perched water-table in the backfill alone increases the total lateral thrust.

16.6.4 Stratified Cohesionless Soils

Figure 16.21 shows a typical two-layer stratification in the backfill. Let us assume no wall friction. In Fig. 16.21,

$$K_{a1} = \frac{1 - \sin\phi_1}{1 + \sin\phi_1},$$

and

$$K_{a2} = \frac{1 - \sin\phi_2}{1 + \sin\phi_2}$$

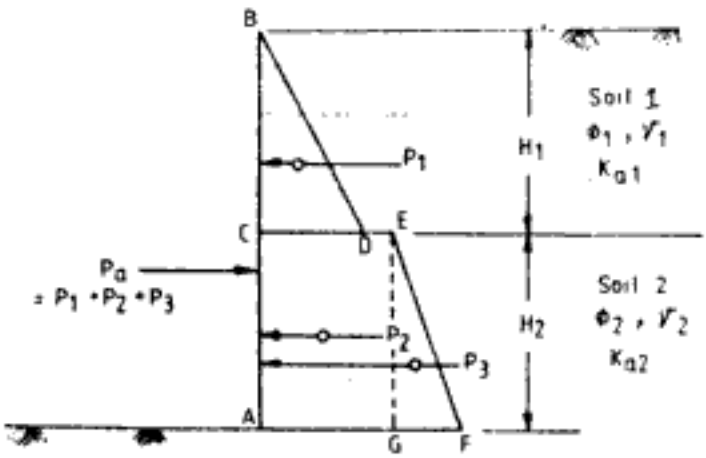

Fig. 16.21 Earth pressure in stratified cohesionless soils

In layer 1 the lateral pressure is computed using K_{a1}. Thus, at depth H_1 the lateral stress is equal to $K_{a1}\gamma_1 H_1$. CD in the figure represents this value. However, the interface between two layers is also at depth H_1. If the depth of soil, H, is considered as a uniform surcharge

Hidden page

$P_4 = 1.78 \times 2 = 3.56$ T/m

$P_5 = \frac{1}{2} \times 0.44 \times 2 = 0.44$ T/m

$P_6 = \frac{1}{2} \times 4 \times 4 = 8$ T/m

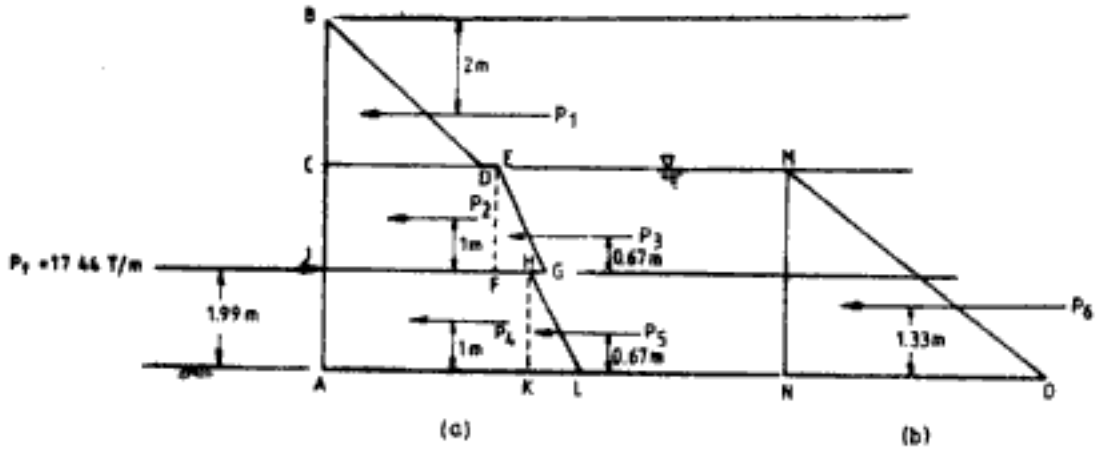

Fig. 16.23 Lateral pressure distribution in Q 16.11: (a) due to soil, and (b) due to water

The active thrust due to soil $= P_1 + P_2 + P_3 + P_4 + P_5 = 9.44$ T/m. The total thrust including water pressure, $P_t = 9.44 + 8 = 17.44$ T/m. If P_t acts at y above A along AB,

$$y = (2.05 \times 5 + 2.94 \times 3 + 0.45 \times 2.67 + 3.56 \times 1 + 0.44 \times 0.67 + 8 \times 1.33)/17.44$$

$$= 1.99 \text{ m}$$

In Secs. 16.6.2, 16.6.3, and 16.6.4 above, only active pressure has been considered. Discussions on passive pressure have not been included, for the following reasons:

1. most of the earth retaining structures are designed for active pressure and not for passive pressure,
2. a large movement is required to mobilise passive pressure,
3. while the validity of solutions for active pressure has been established by observations on earth retaining structures, it has not been done so in the case of passive pressure.

Nevertheless, the passive pressure can be determined in Secs. 16.6.2, 16.6.3 and 16.6.4 also using the principles explained in Sec. 16.6.1.

16.7 EARTH PRESSURE IN COHESIVE SOILS

Consider a vertical sheet pile shown in Fig. 16.24 supporting a clayey backfill. The lateral stress σ_h on the sheet pile at depth z below the surface of backfill is given by,

$$\sigma_h = \gamma z K_a - 2c\sqrt{K_a} \tag{16.17}$$

where $K_a = \dfrac{1 - \sin \phi}{1 + \sin \phi}$

In clayey soils due to drying tension cracks will develop as shown in Fig. 16.24. The tension crack can form adjacent to sheet pile wall also. The depth of tension crack H_t is determined by equating Eq. 16.16 to zero. Thus,

$$H_t = \frac{2c}{\gamma\sqrt{K_a}} \tag{16.18}$$

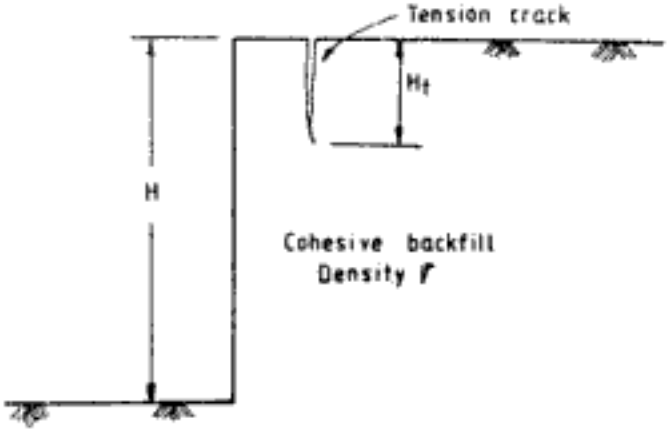

Fig. 16.24 Sheet pile with cohesive backfill

In Fig. 16.25, *ABCD* gives the stress distribution according to Eq. 16.17. There is negative stress (tension) above *O*. This diagram *BCO* of negative stress is ignored in active earth pressure calculations. The tension crack might be filled with water which can exert lateral pressure on the sheet pile. Active earth pressure in case of cohesive backfill is then calculated using the following alternative procedures:

1. Ignore negative stress diagram *BCO* and include water pressure over depth of tension crack
2. Modify the lateral stress diagram as *ABD* (*BD* shown in broken line in Fig. 16.25) and calculate the active earth pressure

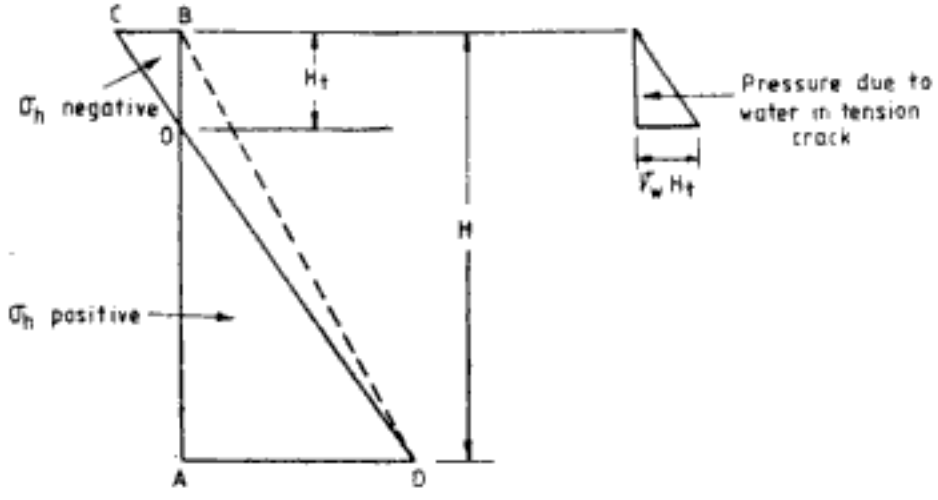

Fig. 16.25 Lateral stress distribution on sheet pile with cohesive backfill

Q 16.12: Compute the active earth pressure on the sheet pile shown in Fig. 16.26 retaining a cohesive backfill.

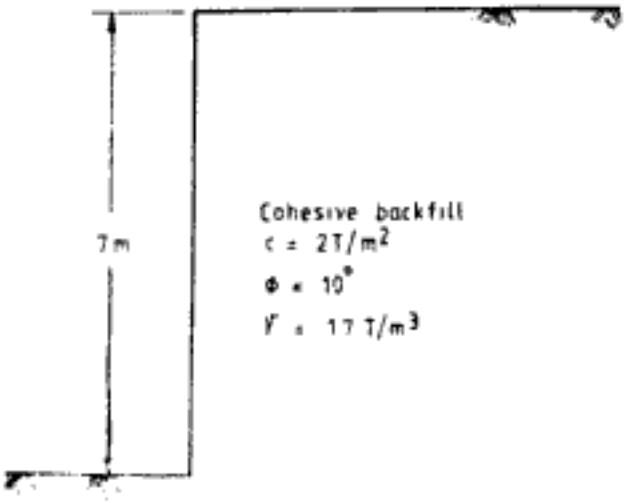

Fig. 16.26 Q 16.12

Ans: $$K_a = \frac{1 - \sin 10^\circ}{1 + \sin 10^\circ} = 0.704$$

$$H_t = \frac{2 \times 2}{1.7\sqrt{0.704}} = 2.8 \text{ m}$$

From Eq. 16.17,

At $z = 0$ m, $\sigma_h = -2 \times 2 \times \sqrt{0.704} = -3.36$ T/m²

At $z = 7$ m, $\sigma_h = 1.7 \times 7 \times 0.704 - 2 \times 2 \times \sqrt{0.704} = 5.02$ T/m²

At $z = 2.8$ m, $\sigma_h = 0$

The pressure distribution diagram is shown in Fig. 16.27.

Alternative (a)

Referring to Fig. 16.25 and ignoring OCB, active earth pressure from OAD

$= \frac{1}{2} \times 5.02 \times (7 - 2.8) = 10.54$ T/m which acts at $(7 - 2.8)/3$ m above A

Water pressure in tension crack $= \frac{1}{2} \times 1 \times 2.8 \times 2.8 = 3.92$ T/m which acts at

$$\left(7 - 2.8 + \frac{2.8}{3}\right) \text{m} \quad \text{above } A$$

Total lateral thrust, $P_t = 10.54 + 3.92$

$= 14.46$ T/m

P_t acts at a distance of Y above A, where

$$Y = \frac{10.54 \times (7 - 2.8/3) + 3.92 \times (7 - 2.8 + 2.8/3)}{14.46}$$

$= 2.41$ m

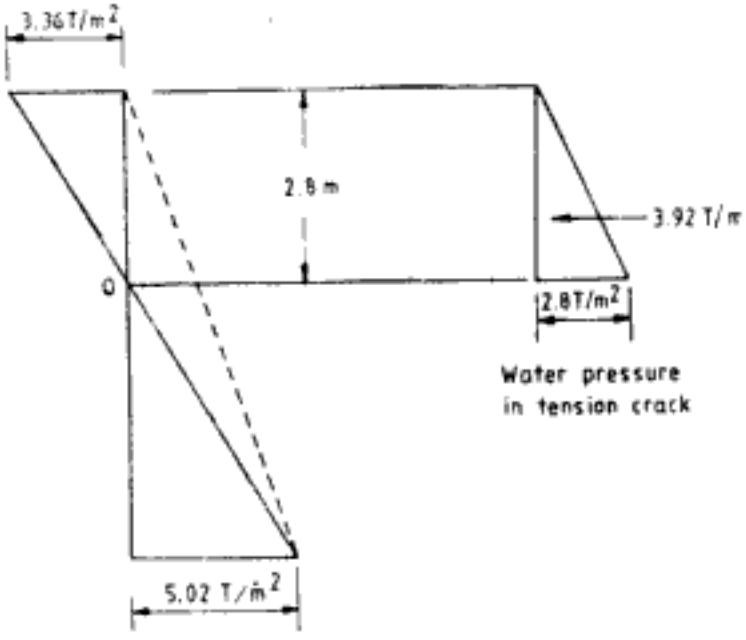

Fig. 16.27 Lateral pressure distribution diagram for sheet pile in Q 16.12

Moment of force about $A = 14.46 \times 2.41$

$= 34.85$ T m/m

Alternative (b)

Considering the diagram ABD in Fig. 16.25

$P_a = \frac{1}{2} \times 5.02 \times 7 = 17.57$ T/m which acts at 7/3 m above A

Moment of force about $A = 17.5 \times \frac{7}{3} = 40.94$ T m/m

Solution obtained by alternative (b) is conservative, and estimates higher pressure and moment than solution by alternative (a).

Q 16.13: Determine the active earth pressure for sheet pile in Q 16.12 when a uniform surcharge of 5 T/m² acts on the backfill.

Ans: At $z = 0$ m, $\sigma_h = 5 \times 0.704 - 3.36 = 0.16$ T/m²

At $z = 7$ m, $\sigma_h = 5 \times 0.704 + 5.02 = 8.54$ T/m²

The lateral stress diagram is shown in Fig. 16.28. Since the clayey soil is up to the surface of backfill it can be assumed that tension cracks will form and can be filled with water.

Lateral pressure due to $ABCD$ in Fig. 16.28,

$$= \frac{0.16 + 8.54}{2} \times 7 = 30.45 \text{ T/m}$$

which acts at 2.38 m above A

Water pressure = 3.92 T/m

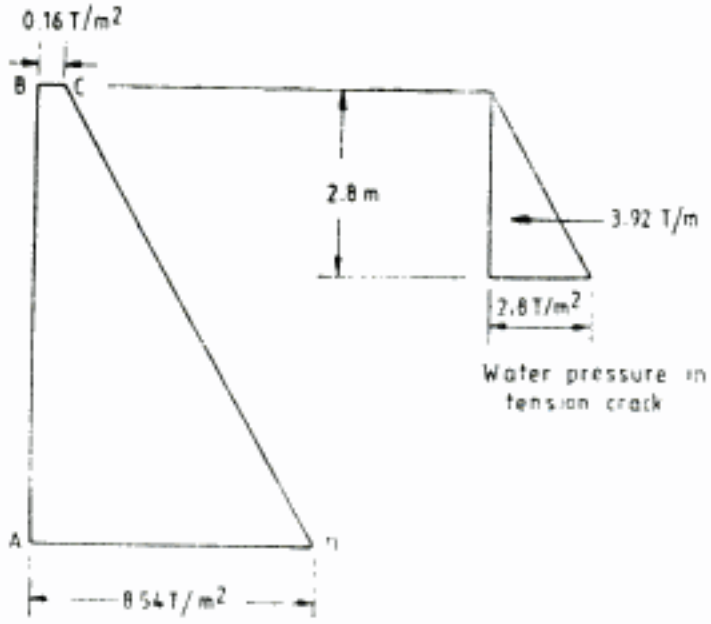

Fig. 16.28 Lateral pressure distribution diagram for sheet pile in Q 16.13

Total lateral thrust $P_t = 30.45 + 3.92 = 34.37$ T/m. P_t acts at y above A, and

$$y = \frac{30.45 \times 2.38 + 3.92 \times (7 - 2.8 + 2.8/3)}{34.37} = 2.69 \text{ m}$$

When the cohesive layer does not extend up to the surface of backfill and the overlying material is of sufficient thickness, formation of tension cracks will be restricted.

16.8 MODIFICATIONS TO EARTH PRESSURE THEORIES TO ACCOUNT FOR EFFECTS DUE TO WALL GEOMETRY

The earth pressure theories discussed till now consider the back of wall as vertical or inclined and not interfering with the rupture zone. But where the base of the wall interferes with the failure zone some simple approximations will be made in the calculation of earth pressure.

16.8.1 Rupture Zone

Figure 16.29 shows the rupture surface for a wall not interfering with the rupture zone. The rupture zone is inclined at ρ to horizontal. ρ is given by the expression,

$$\sin 2\rho = \frac{x_2 x_3 \pm \{x_1 \sqrt{x_1^2 + x_2^2 - x_3^2}\}}{x_1^2 + x_2^2} \tag{16.19}$$

where $x_1 = \cos(2\alpha - \phi - \delta) - \dfrac{\sin(\phi + \delta)}{\sin(\phi - \beta)} \cos(\phi + \beta)$

$$x_2 = \sin(2\alpha - \phi - \delta) + \frac{\sin(\phi + \delta)}{\sin(\phi - \delta)} \sin(\phi + \beta)$$

$$x_3 = \frac{\sin(\beta + \delta)}{\sin(\phi - \beta)}$$

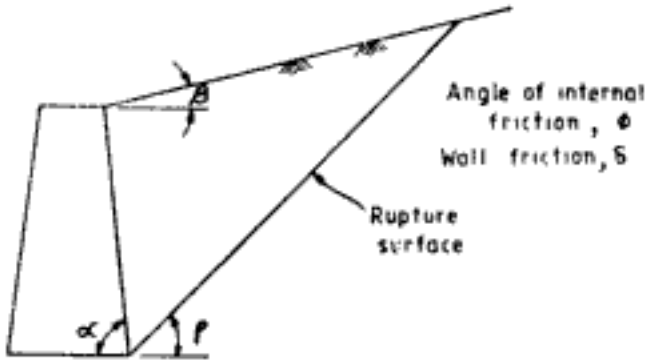

Fig. 16.29 Rupture zone in backfill

In Eq. 16.19 use +ve sign for active earth pressure and −ve sign for passive earth pressure. For horizontal backfill and vertical smooth wall Eq. 16.19 gives

$$\rho = 45 \pm \phi/2$$

16.8.2 Interference with Rupture Zone

Figure 16.30 shows a retaining wall with an enlarged base. For earth pressure calculations with Rankine's solution the earth pressure is computed on an imaginary vertical plane AB as shown in the figure. When Coulomb's solution is used, the inclination of the wall is extended to the base as shown by CD in Fig. 16.30. The projection $OCDA$ is then ignored. The weight of soil W lying above CO will be used in the stability analysis of wall.

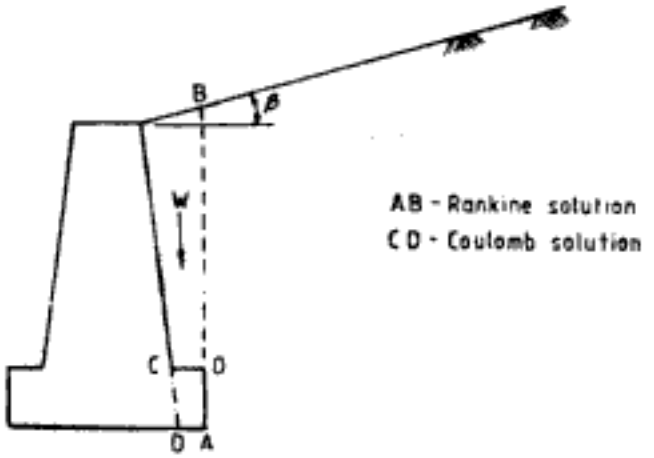

Fig. 16.30 Retaining wall with enlarged base

In the case of cantilever and counterfort retaining walls (Fig. 16.31) the heel of the wall interferes with the rupture zone. The earth pressure in such cases is calculated on a imaginary vertical plane AB as shown in Fig. 16.31. If the heel is very long then rupture planes may be formed on both sides of AB as shown in Fig. 16.32. Then active pressure P_a is computed on AB. P_a acts at an angle of β for Rankine's solution and at an angle of δ for Coulomb's solution. The weight of soil lying on the heel above CO will be used in the stability analysis of the retaining wall.

Hidden page

Hidden page

Hidden page

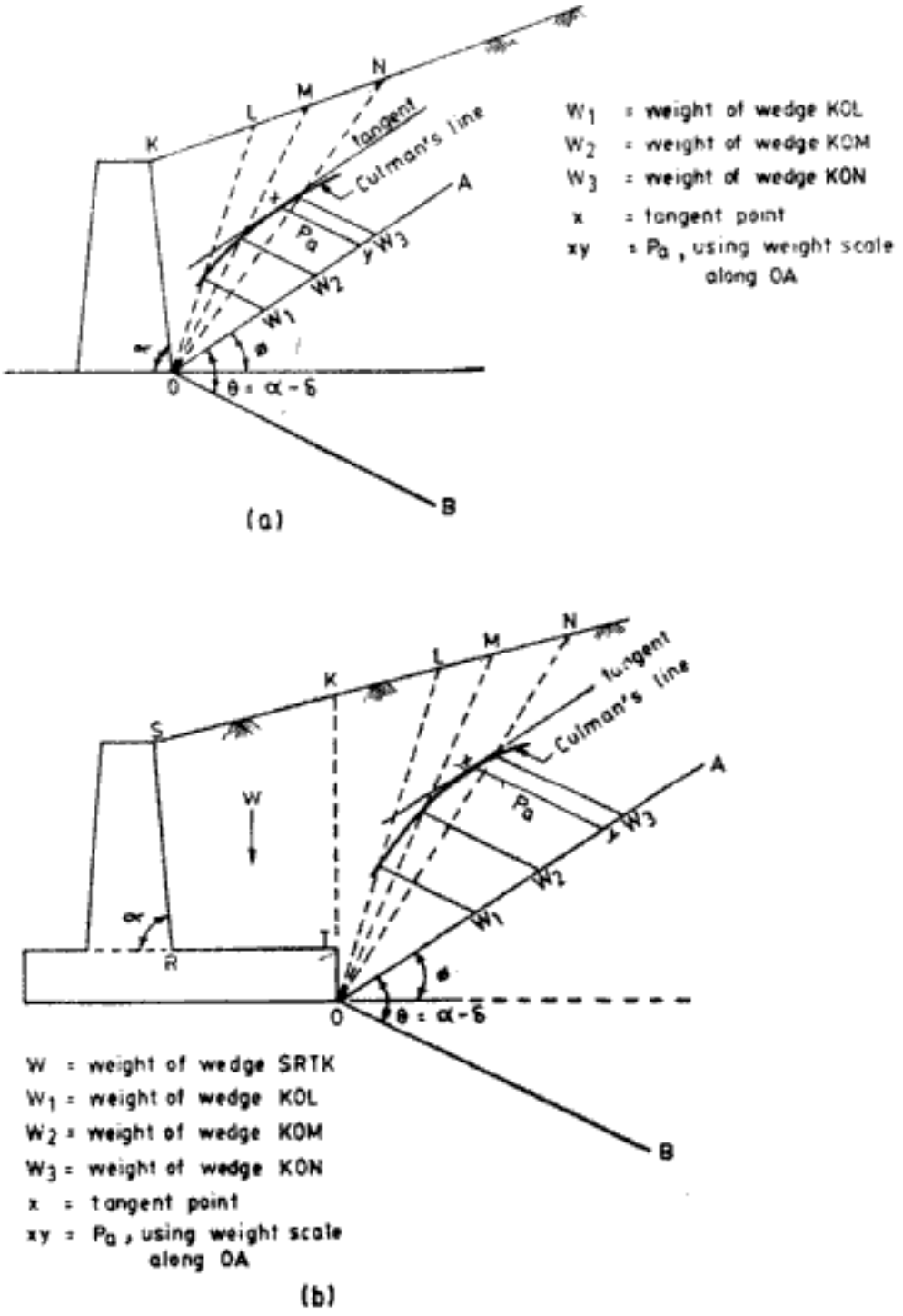

Fig. 16.34 Culman's method for determination of active earth pressure

to failure surface which intersects OK at F. The point of application of P_a is $EF/3$ from E.

Case C *Concentrated or line load outside failure wedge (Fig. 16.35c)*

Draw a line from point of application of load parallel to OA to intersect OK at E. The point of action of P_a lies at $EO/3$ from E.

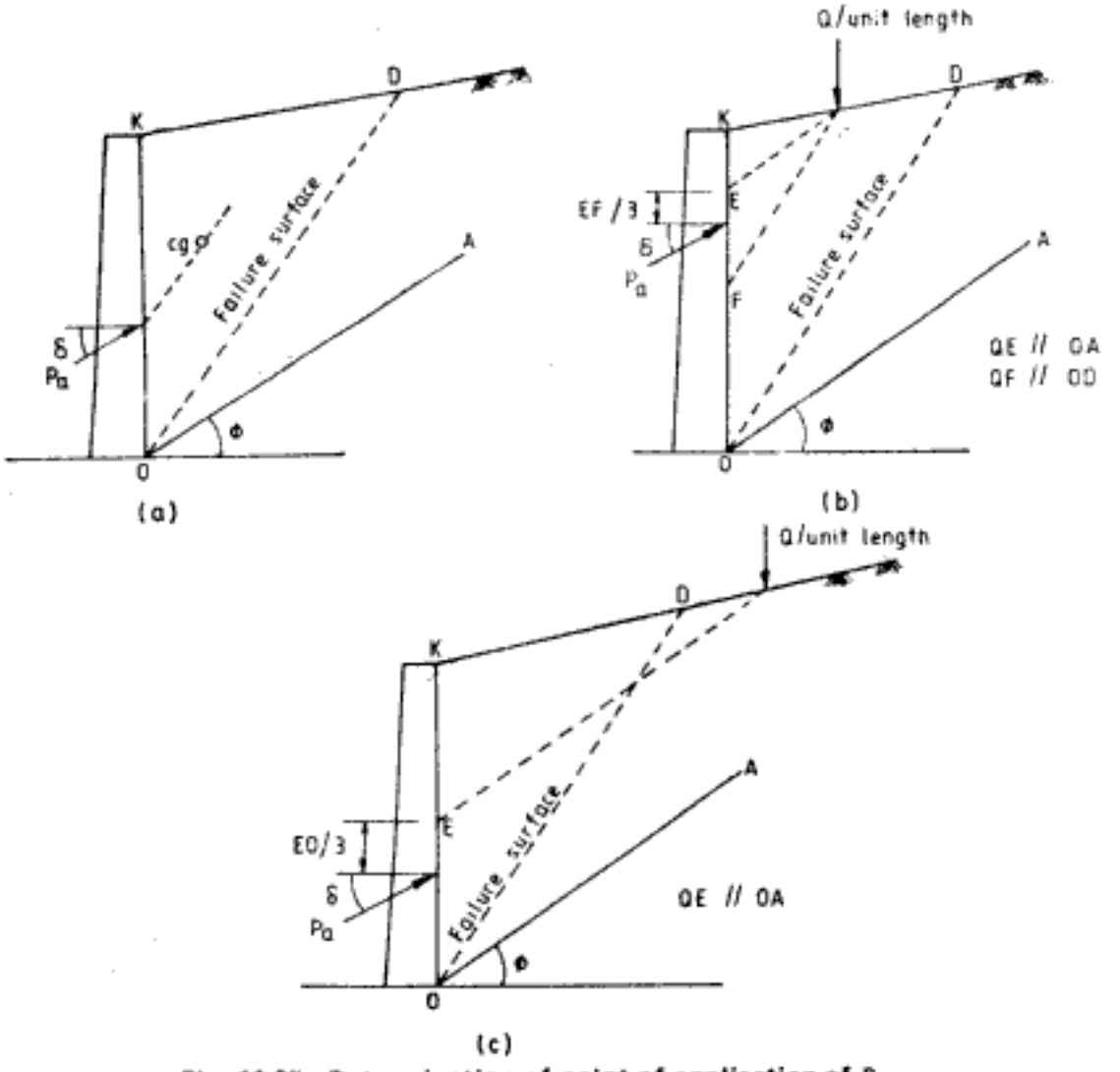

Fig. 16.35 Determination of point of application of P_a

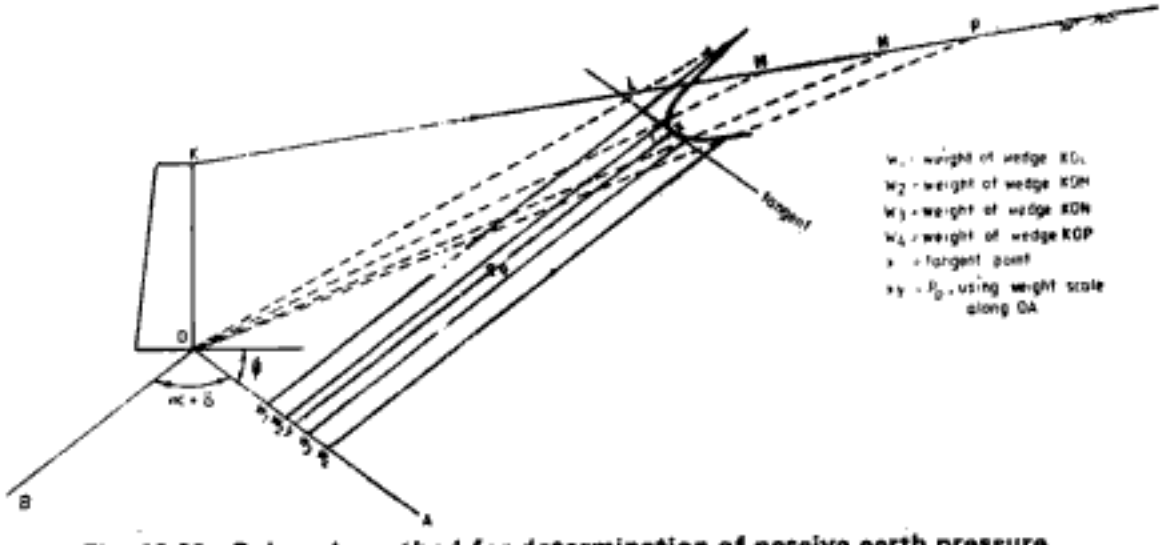

Fig. 16.36 Culman's method for determination of passive earth pressure

The determination of passive earth pressure by Culman's method is shown in Fig. 16.36. The following steps are to be carried out.

Step 1: Draw the retaining wall and the backfill to a convenient scale.

Step 2: Select point O at the heel of the wall as described for determination of active pressure.

Step 3: From O draw a straight line OA downwards inclined at ϕ to the horizontal. Draw another straight line OB downwards such that angle AOB is $(\alpha + \delta)$.

Step 4 to Step 8 are same as described for determination of active earth pressure.

Step 9: From tangent points draw lines parallel to OB to intersect OA. Select the shortest of these lines and convert it to force using weight scale used along OA to plot weight of soil wedges. This is the value of passive thrust P_p. A straight line drawn from O to backfill through the point of tangency corresponding to passive thrust gives the failure surface.

16.10.2 Trial Wedge Method for Cohesive Soils

This method involves considering a number of soil wedges and drawing the force polygon to determine P_a. The method is shown in Fig. 16.37 in which the following steps are to be carried out.

Step 1: Draw the retaining wall and backfill to a convenient scale.

Step 2: Compute the depth of tension crack H_t, using

$$H_t = \frac{2c}{\gamma\sqrt{K_a}} \tag{16.18}$$

Plot the value of H_t at a sufficient number of points vertically below backfill and establish the tension crack profile

Step 3: Select point O at the heel of the retaining wall as described in Culman's method. Lay off trial wedges such as OLL_1K_1, OMM_1K_1, etc.

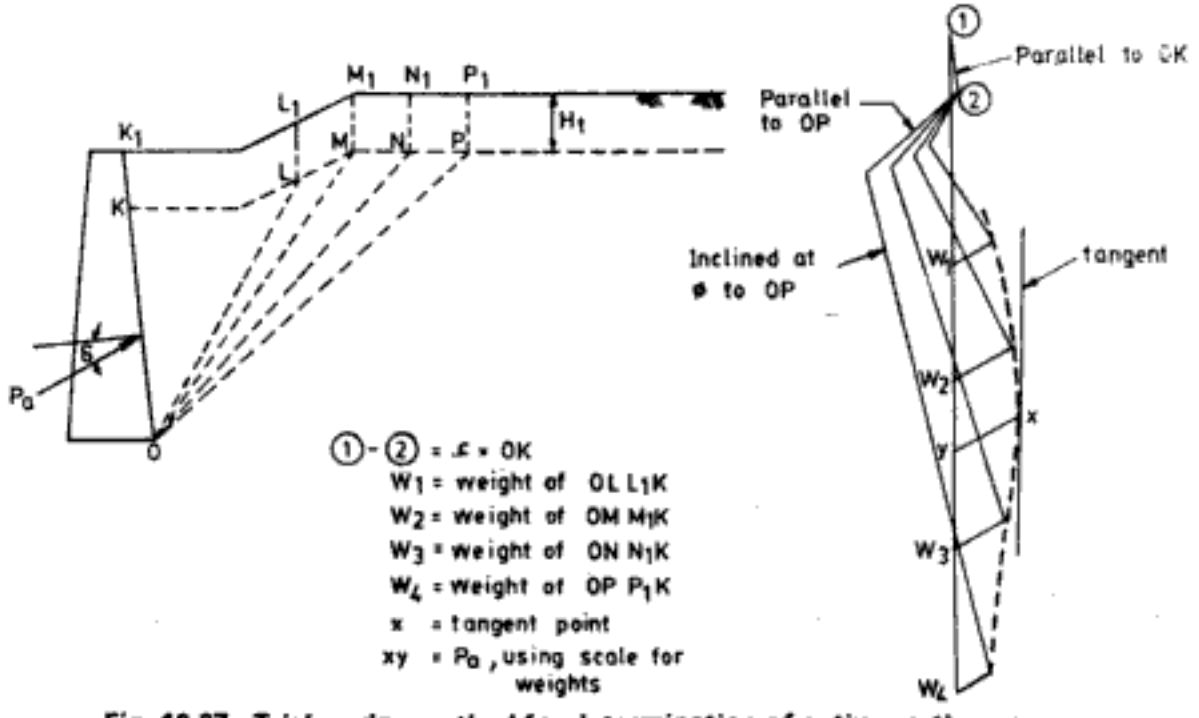

Fig. 16.37 Trial wedge method for determination of active earth pressure

Hidden page

Hidden page

Table 16.7 Values of I_1 ($\mu = 0.5$)

n \ m	0.5	0.6	0.7	0.8	0.9	1.0
0	0	0	0	0	0	0
0.1	0.252	0.121	0.069	0.041	0.026	0.017
0.2	0.726	0.382	0.233	0.144	0.090	0.063
0.3	1.013	0.604	0.400	0.262	0.177	0.123
0.4	1.027	0.696	0.505	0.354	0.251	0.181
0.5	0.885	0.674	0.535	0.402	0.301	0.227
0.6	0.702	0.590	0.508	0.408	0.322	0.253
0.7	0.535	0.488	0.452	0.385	0.320	0.262
0.8	0.402	0.392	0.385	0.346	0.301	0.257
0.9	0.301	0.310	0.320	0.301	0.273	0.242
1.0	0.227	0.243	0.262	0.257	0.242	0.221
n at which I_1 is maximum	0.354	0.424	0.495	0.566	0.636	0.707
$I_{1(max)}$	1.049	0.728	0.535	0.410	0.324	0.262

Table 16.8 Values of I_2 ($\mu = 0.5$)

n	0	0.1	0.2	0.3	0.4	0.5	0.6	0.7	0.8	0.9	1.0
I_2	0	0.570	1.400	1.613	1.367	1.016	0.717	0.500	0.350	0.248	0.179

Maximum value of I_2 occurs at $n = 0.283$. Maximum value of I_2 is 1.620.

Ans: $x = 5$ m $\quad H = 10$ m $\quad z = 5$ m

$m = 5/10 = 0.5$

$n = 5/10 = 0.5$

Since $m > 0.4$, Eq. 16.23 and Table 16.7 will be used in solution.

(a) From Table 16.7, $I_1 = 0.885$

$$\text{Substituting in Eq. 16.23, } \sigma_h = \frac{0.885 \times 5 \times 1000}{(10 \times 100)^2}$$

$$= 4.425 \times 10^{-3} \text{ kg/cm}^2$$

(b) $\tan \alpha = 6/5$

$\alpha = 50.19°$

From Eq. 16.25,

$$\sigma_{hz} = 4.425 \times 10^{-3} \cos^2 (1.1 \times 50.19°)$$

$$= 1.44 \times 10^{-3} \text{ kg/cm}^2$$

16.11.2 Line Load on Backfill

Figure 16.38 also shows line load acting on the surface of backfill. Using the same notations as for point load, expressions for lateral stresses are as given below:

For $m > 0.4$ and $\mu = 0.5$,

$$\sigma_h = \frac{4}{\pi} \frac{q}{H} \frac{m^2 n}{(m^2 + n^2)^2} \tag{16.26}$$

which can be written as,

$$\sigma_h = \frac{\bar{q}}{H} I_1 \tag{16.27}$$

where $I_1 = \frac{4}{\pi} \frac{m^2 n}{(m^2 + n^2)^2}$

For $m \leqslant 0.4$ and $\mu = 0.5$,

$$\sigma_h = \frac{\bar{q}}{H} \frac{0.203n}{(0.16 + n^2)^2} \tag{16.28}$$

which can be expressed as,

$$\sigma_h = \frac{\bar{q}}{H} I_2 \tag{16.29}$$

where $I_2 = \frac{0.203n}{(0.16 + n^2)^2}$

Tables 16.9 and 16.10 give values of I_1 and I_2. Maximum value of I_1 is reached at $n = m/\sqrt{3}$. The tables report the maximum values also.

Table 16.9 Values of I_1 ($\mu = 0.5$)

n \ m	0.5	0.6	0.7	0.8	0.9	1.0
0	0	0	0	0	0	0
0.1	0.471	0.335	0.250	0.193	0.153	0.125
0.2	0.757	0.573	0.444	0.352	0.285	0.235
0.3	0.826	0.679	0.556	0.459	0.382	0.321
0.4	0.757	0.678	0.591	0.509	0.438	0.378
0.5	0.637	0.616	0.570	0.514	0.459	0.407
0.6	0.513	0.531	0.518	0.489	0.452	0.413
0.7	0.407	0.444	0.455	0.447	0.427	0.401
0.8	0.321	0.367	0.391	0.398	0.392	0.379
0.9	0.255	0.301	0.332	0.349	0.354	0.350
1.0	0.204	0.248	0.281	0.303	0.315	0.318
n at which I_1 is maximum	0.289	0.346	0.404	0.462	0.520	0.577
$I_{1(\max)}$	0.827	0.689	0.591	0.517	0.459	0.413

Table 16.10 Values of I_2 ($\mu = 0.5$)

n	0	0.1	0.2	0.3	0.4	0.5	0.6	0.7	0.8	0.9	1.0
I_2	0	0.702	1.015	0.974	0.793	0.604	0.450	0.336	0.254	0.194	0.151

Maximum of I_2 occurs at $n = 0.231$.
Maximum value of I_2 is 1.030.

Q 16.15: A line load of 2.5 T/m due to a concrete pipe running parallel to the retaining wall acts at a distance of 4 m from the wall. The height of the wall is 10 m. Determine the lateral stress on the wall due to the line load at a depth of 2 m below the surface.

Ans: $x = 4$ m $H = 10$ m $z = 2$ m

$$m = \frac{4}{10} = 0.4$$

$$n = \frac{2}{10} = 0.2$$

From Table 16.10,

$$I_2 = 1.015$$

Using Eq. 16.29,

$$\sigma_h = \frac{2.5 \times 1000 \times 1.015}{100 \times 1000} = 2.5375 \times 10^{-2} \text{ kg/cm}^2$$

16.11.3 Strip Load on Backfill

In the case of strip load on backfill the lateral stress at any depth is given by,

$$\sigma_h = \frac{2q}{\pi}(\beta - \sin\beta \cos 2\alpha) \qquad (16.30)$$

where α and β are explained in Fig. 16.40.

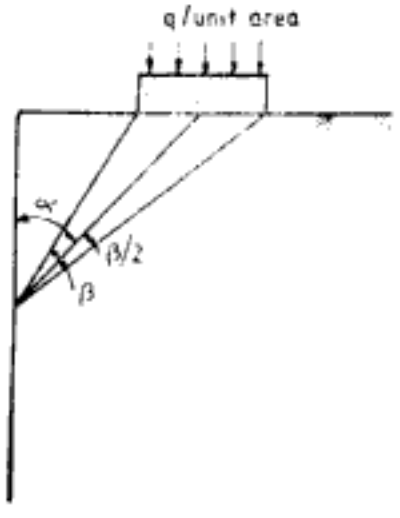

Fig. 16.40 Strip load on backfill

16.11.4 Uniformly Distributed Load on Regular and Irregular Shaped Areas

Newmark's chart shown in Fig. 16.41 can be used in this case. The procedure of use is similar to the procedure for Newmark's chart explained in Ch. 13 for determination of vertical stress.

The loaded area is drawn to the depth scale indicated in the chart. The point where stress is required is kept on the chart to coincide with the origin. The lateral stress is obtained from the equation,

$$\sigma_h = IMq \qquad (16.31)$$

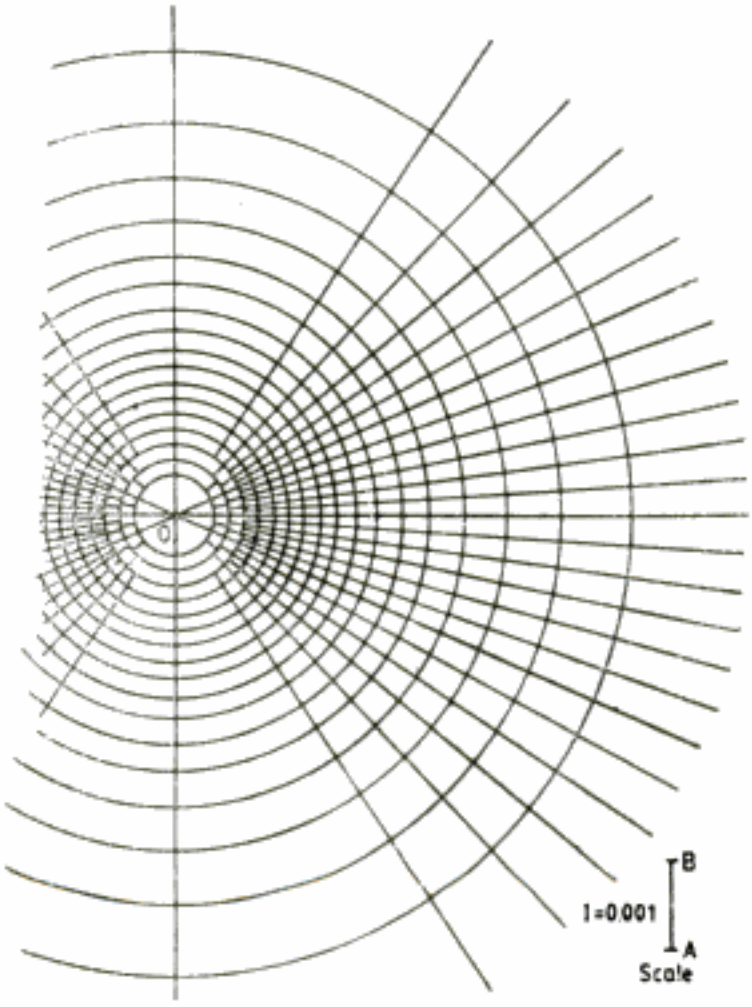

Fig. 16.41 Influence chart for computing lateral pressure at point 0 for any type of loading in the influence field, $\mu = 0.5$. (After Newmark, 1942; drawn after Bowles, 1982)

where I = influence value

M = number of influence blocks covered by the loaded area

For rigid retaining wall the value obtained by Eq. 16.31 should be doubled.

The distribution of lateral stress due to surcharges can be determined using the procedures explained here. The point of application of resultant of this distribution can be determined. This can be added to the active earth pressure due to backfill. The net lateral thrust and its point of application can be determined by considering moment of forces about the heel of retaining wall. The point of application thus determined will be more accurate than that determined by graphical procedures.

16.12 APPROXIMATE DETERMINATION OF EARTH PRESSURE

Peck, Hanson and Thornburn (1974) contend that the designer is rarely aware of the type of

Hidden page

17

EARTH RETAINING STRUCTURES

Earth retaining structures may be broadly grouped into two categories, namely, rigid retaining structures and flexible retaining structures. Rigid retaining structures are usually permanent structures. But some of the flexible retaining structures are used only for temporary purposes. The analysis of both types of structures makes use of earth pressures calculated based on the principles of earth pressure theories discussed in Ch. 16.

17.1 RIGID RETAINING STRUCTURES

Gravity retaining wall, cantilever retaining wall, counterfort retaining wall, building basement wall, and bridge abutment are examples of rigid retaining structures. Some of these are shown in Fig. 17.1. The retaining structures must be analysed and designed from the following two considerations:

1. Stability considerations
2. Structural considerations

The structure must be safe against both. To analyse for stability requirements, the actual earth pressure on structure, and the resistance offered by structure due to its weight and other reactions will be taken into account. To ensure safety against structural failure, moment and shear force are computed at various sections and proper structural design is carried out. In this case, load factor will be used for the earth pressure acting on the wall. The earth pressure considered for stability analysis can be different from that considered for structural analysis and design. This chapter concerns mostly with stability analysis of retaining structures. The gravity retaining wall is of such large dimensions that the stresses induced on it due to external loading are very small and well within permissible limits. Cantilever and counterfort retaining walls and bridge abutments are ordinarily made of reinforced concrete. Their structural design is available in many standard text-books on design of reinforced concrete structures.

17.1.1 Stability Analysis of Retaining Walls

The stability analysis of all retaining walls involves the following sequence of steps:

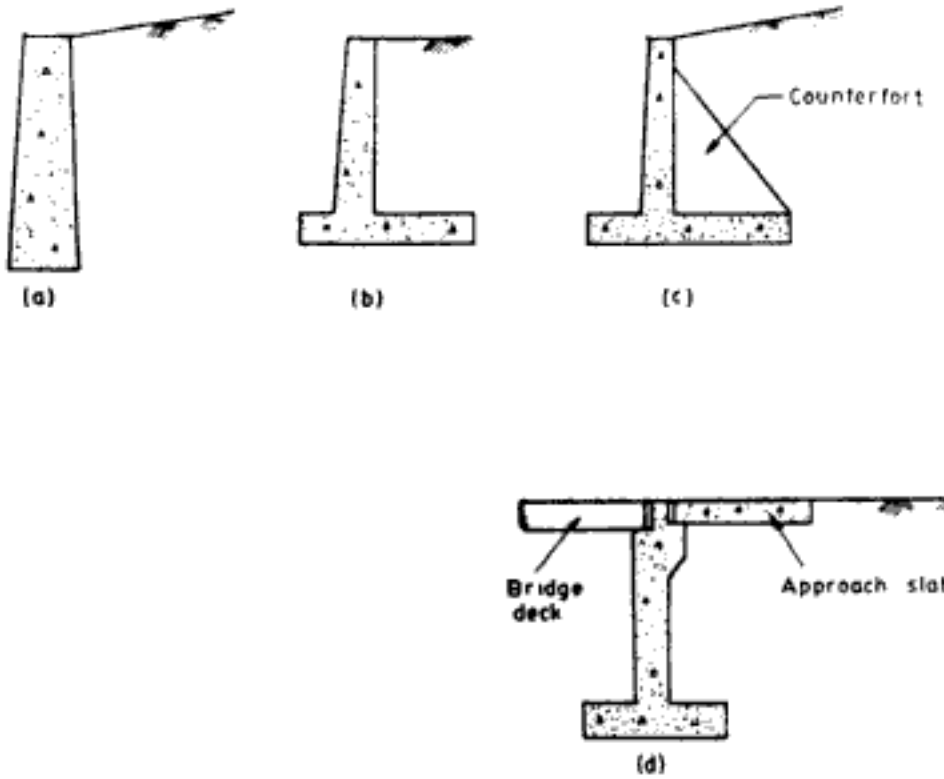

Fig. 17.1 Rigid retaining structures: (a) gravity retaining wall, (b) cantilever retaining wall, (c) counterfort retaining wall, and (d) abutment

Step 1: Select tentative dimensions of retaining wall. Some useful guidelines are given in this chapter.

Step 2: Compute the forces involved in the stability analysis. Check whether the chosen profile of retaining wall meets the requirements of allowable bearing pressure.

Step 3: Check for stability against overturning.

Step 4: Check for stability against sliding.

Step 5: If necessary check for shear failure of soil through the backfill.

Steps 1 to 5 are explained in detail in the following paragraphs.

1. *Guidelines for dimensions of retaining walls*

(a) *Cantilever retaining walls*

Figure 17.2 shows the terminologies and notations used with cantilever retaining walls. Typical proportions of the dimensions are as below:

$$B = 0.4\,H \text{ to } 0.7\,H \tag{17.1}$$

When the foundation soil is firm the lower value is applicable. But, if the foundation is soft and the lateral thrust is very high then the higher value is to be used.

$$t_0 = 200 \text{ mm minimum but } 300 \text{ mm is preferable for ease of casting}$$
$$t_b = H/12 \text{ to } H/10 \tag{17.2}$$

However, it may be noted that t_b is dependent upon the position of stem on the base (i.e. L_t).

$$t_s = H/12 \text{ to } H/8 \tag{17.3}$$

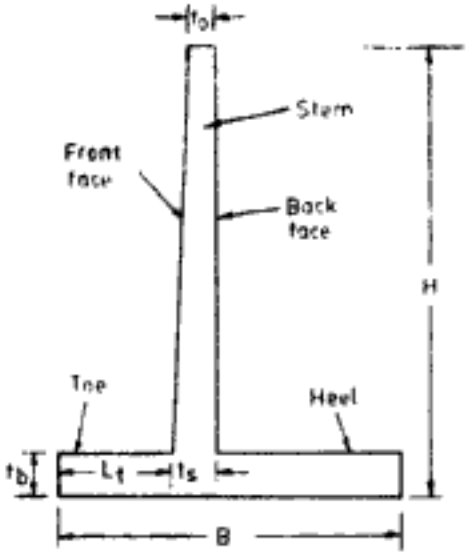

Fig. 17.2 Terminology and notations for cantilever retaining wall

$$L_t = 0.2\ B \text{ to } 0.4\ B \tag{17.4}$$

The front face is usually sloped and the batter varies from 1 : 48 (1 horizontal to 48 vertical) minimum to 1 : 16.

Krishna and Jain (1966) make recommendations for proportions of walls retaining cohesionless backfill. These are,

(i) *When resultant of forces lies within the middle third of base*

Horizontal backfill: ($\beta = 0°$)

$$B = 0.95H \sqrt{\frac{K_a}{(1 - m)(1 + 3m)}} \tag{17.5}$$

where K_a = coefficient of active earth pressure

$$m = \frac{L_t}{B} = 1 - \frac{4}{9\omega}$$

$$\omega = \frac{\gamma(H - t_b)}{q_{all-net}}$$

$q_{all-net}$ = allowable bearing pressure

γ = density of backfill

Inclined backfill: ($\beta > 0°$)

$$B = H \sqrt{\frac{K_a \cos \beta}{(1 - m)(1 + 3m)}} \tag{17.6}$$

where $m = 1 - \frac{3}{8\omega}$

ω is same as given for horizontal backfill (Eq. 17.5).

Hidden page

Hidden page

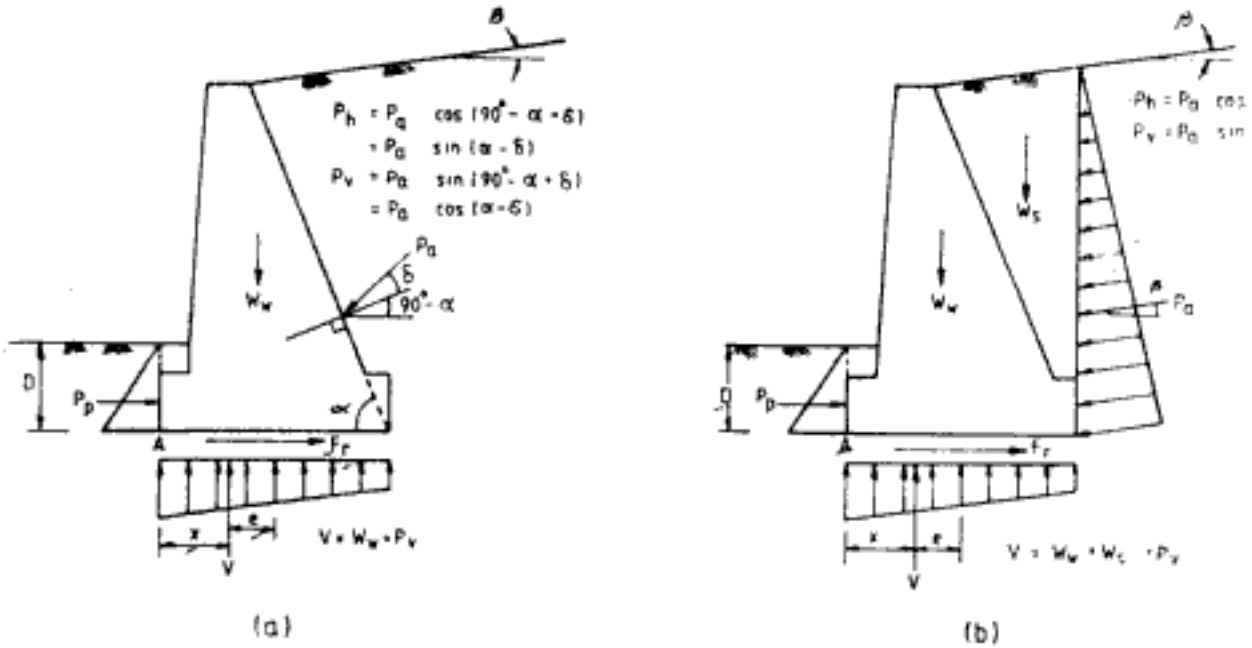

Fig. 17.5 Forces on gravity retaining wall: (a) lateral pressure by Coulomb's method, and (b) earth pressure by Rankine's method

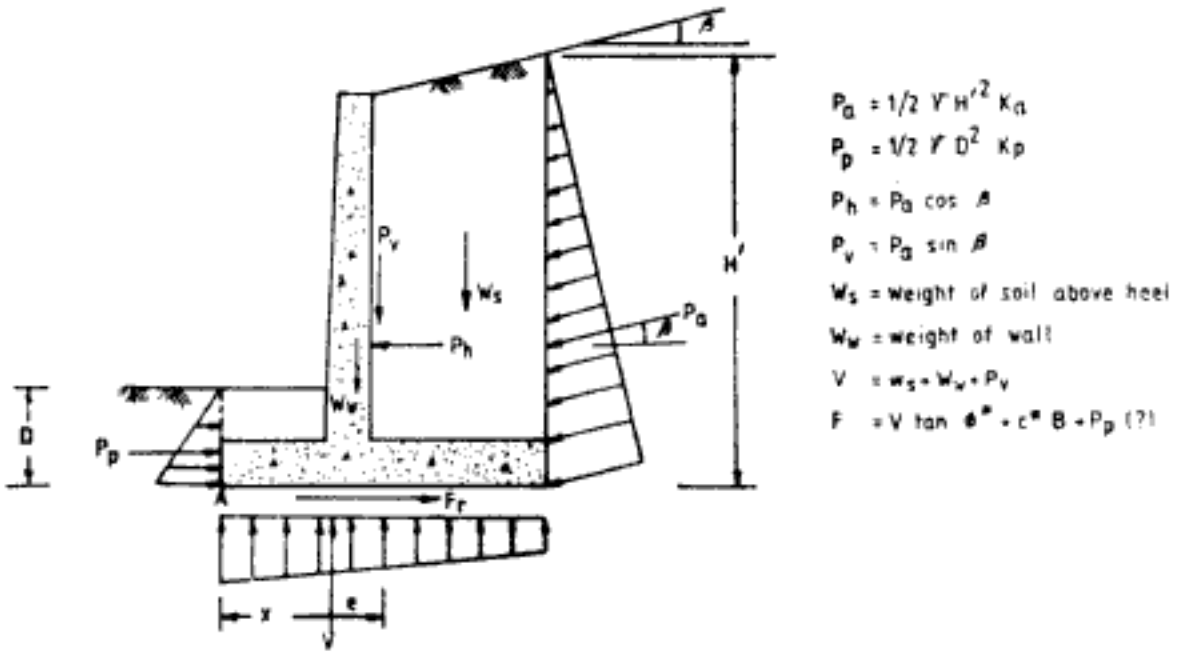

$P_a = \frac{1}{2} \gamma H'^2 K_a$

$P_p = \frac{1}{2} \gamma D^2 K_p$

$P_h = P_a \cos \beta$

$P_v = P_a \sin \beta$

W_s = weight of soil above heel

W_w = weight of wall

$V = W_s + W_w + P_v$

$F = V \tan \phi^* + c^* B + P_p$ (?)

Fig. 17.6 Forces on cantilever and counterfort retaining walls

this conservatively estimated value in stability analysis reasoning that large movement of wall is required to mobilise full passive resistance whereas only very small movement is required to mobilise half the passive resistance. There are still others who include the full value of conservatively estimated passive resistance in the stability analysis. A compromise seems to have been worked out for these different approaches by prescribing different values of factor of safety for each approach. Thus an analysis which ignores the passive resistance completely

will have to satisfy a lower factor of safety than the analysis which includes also the passive resistance. A retaining wall is considered safe when it satisfies at least one of these safety factors.

The sliding resistance at the base F_r of the retaining wall is given by the equation,

$$F_r = V \tan \phi^* + c^* B \tag{17.17}$$

where V = total vertical reaction

$\tan \phi^* = \tan \phi$ to $0.67 \tan \phi$

$c^* = 0.5\ c$ to $0.75\ c$

Vertical reaction V acts on the base eccentrically at a distance e from the centre. If we consider the moments of forces about the toe, that is about point A in Figs. 17.5 and 17.6,

$$e = \frac{B}{2} - x \tag{17.18}$$

where $$x = \frac{\Sigma M_A}{V} \tag{17.19}$$

ΣM_A = moment of forces about A and P_p is not usually considered

The soil reaction below the base is considered to vary linearly along breadth. If the resultant of forces falls within the middle third of the base the reaction at all points on the base is compression. To ensure this then eccentricity of V must be limited to,

$$e < \frac{B}{6} \tag{17.20}$$

If the resultant lies within the middle third of the base the soil reaction is computed using equation,

$$q_s = \frac{V}{B}\left(1 \pm \frac{6e}{B}\right) \tag{17.21}$$

$+$ sign is used for maximum and $-$ sign for minimum soil reaction. When the lateral thrust is very large the resultant may fall outside the middle third of the base. Also when the wall rests on very hard stratum, like rock, higher eccentricity is permissible. If eccentricity is more than $B/6$ the whole of the base is not under compression. The soil reaction is as shown in Fig. 17.7. In this figure,

$$\frac{y}{3} = \frac{B}{2} - e \tag{17.22}$$

and the maximum soil reaction is given by,

$$q_{s\text{-max}} = \frac{2V}{3B\left(\frac{B}{2} - e\right)} \tag{17.23}$$

It must be ensured that the maximum soil reaction computed using Eqs 17.21 and 17.23 must not exceed the allowable bearing pressure.

Q 17.2: Determine the forces acting on the wall, the tentative dimensions of which have been determined in Q 17.1.

Hidden page

The moment due to P_p is not considered in calculations.

$$V = 39.393 \text{ T/m}$$

$$\Sigma M_A = 99.63 - 29.67 = 69.96 \text{ T m/m}$$

$$x = \frac{69.96}{39.393} = 1.776 \text{ m}$$

$$e = 2 - 1.776 = 0.224 < 0.67 \text{ m} = 4/6$$

The resultant lies within the middle third of the base.

From Eq. 17.17

$$F_r = 39.393 \tan 38^\circ = 30.78 \text{ T/m}$$

Maximum soil reaction (Eq. 17.21),

$$q_{s-\max} = \frac{39.393}{4}\left(1 + \frac{6 \times 0.224}{4}\right) = 13.16 \text{ T/m}^2$$

$$q_{s-\min} = \frac{39.393}{4}\left(1 - \frac{6 \times 0.224}{4}\right) = 6.54 \text{ T/m}^2$$

The procedures to determine allowable bearing pressure are explained in Ch. 12. It must be ensured that $q_{s-\max}$ does not exceed this value.

3. *Stability against overturning*

The wall tends to rotate or overturn about toe, point A (Figs. 17.5 and 17.6). The stability against overturning must therefore be ensured. Factor of safety against overturning is defined as,

$$FS_t = \frac{\text{sum of resisting moment about toe}}{\text{sum of overturning moment about toe}} \tag{17.24}$$

Factor of safety against overturning must be more than 1.5 for cohesionless soils and must be more than 2 for cohesive soils. The passive resistance in the front of the wall is not taken into consideration in calculation of moment about toe.

Q 17.3: Check the stability of the wall chosen in Q 17.1 against overturning.

Ans: The forces against the wall are given in Q 17.2.

From Table 17.1,

Sum of resisting moment about $A = 99.63$ T m/m

Sum of overturning moment about $A = 29.67$ T m/m

$$FS_t = \frac{99.63}{29.67} = 3.36 > 1.5 \quad O.K.$$

4. *Stability against sliding*

The retaining wall must have adequate resistance against sliding. Factor of safety against sliding is defined as,

$$FS_s = \frac{\text{sum of resisting horizontal forces}}{\text{sum of disturbing horizontal forces}} \tag{17.25}$$

Bowles (1982) recommends a minimum factor of safety of 1.5 in cohesionless soils and 2 in cohesive soils, without taking passive resistance into account. Peck, Hanson and Thornburn

(1974) also ignore passive resistance and recommend a minimum factor of safety of 1.5. Lambe and Whitman (1979) recommend a minimum factor of safety of 1.5 when passive resistance is disregarded and 2 when half of the passive resistance is taken into account.

Q 17.4: Determine the stability against sliding of the wall chosen in Q 17.1.

Ans: (a) Without considering passive resistance:
Sum of resisting forces = 30.78 T/m
Sum of disturbing forces = 12.11 T/m

$$FS_s = \frac{30.78}{12.11} = 2.54 > 1.5 \quad \text{O.K.}$$

(b) Considering half of passive resistance:
Sum of resisting forces = 30.78 + 4.14 = 34.92 T/m

$$FS_s = \frac{34.92}{12.11} = 2.88 > 2 \quad \text{O.K.}$$

From questions 17.2, 17.3 and 17.4 it appears that to get an economical design the dimensions of wall could be reduced purely from the point of view of stability of wall. However the structural safety should also be considered.

17.1.2 Construction Details

Drainage: To avoid large lateral thrust proper provisions for drainage must be made behind retaining walls. Vertical and longitudinal drain pipes can be provided. Weep holes of minimum 10 cm diameter can be provided in the wall itself. Weep holes and drain pipes must be protected by providing graded filters. Wherever possible the backfill must be of free draining cohesionless material and cohesive material must be avoided. In instances where this cannot be done economically at least a small zone of cohesionless material must be provided immediately behind the wall throughout its entire depth and length.

Wall joints: *Construction joints* will be required both horizontally and vertically. These may be provided in the form of keys. Due to shrinkage, cracks will develop in concrete. To avoid haphazard formation of cracks and disfiguration of the appearance of wall *contraction joints* can be provided vertically at regular intervals along the length of wall. These are purposely built weakened planes to localise the cracking along these planes. Contraction joints are typically spaced at 8 m to 12 m intervals. Similarly in order to provide scope for expansion of wall, expansion joints are necessary. These are also vertical joints separating one portion of wall from another. The reinforcement must be freed of bond by greasing and sheathing the end of bars. Spacing of expansion joints varies from 18 to 30 m. The gap for expansion, g_e, to be provided at the expansion joint can be theoretically evaluated from,

$$g_e = \alpha T L \tag{17.26}$$

where α = thermal coefficient for concrete which may be taken as 5×10^{-6} per degree F or 17×10^{-6} per degree C

T = change in temperature from construction temperature

L = spacing of expansion joints

Hidden page

17.2 FLEXIBLE RETAINING STRUCTURES

Cantilever sheet pile walls, anchored bulkheads, and braced supports for excavation are some examples of flexible retaining structures. The stability of cantilever sheet piles and anchored bulkheads depends on the passive resistance on the embedded portion of these structures. For this reason the factor of safety of these structures is generally defined in two different ways: (i) the computed depth of embedment is increased by 20 per cent to 40 per cent, (ii) the passive pressure coefficient and cohesion used in the determination of depth of embedment are reduced by a factor of safety varying from 1.5 to 2.

17.2.1 Cantilever Sheet Pile Walls

Figure 17.10 shows the deflection pattern of cantilever sheet pile wall. From top to the point of rotation, active pressure is exerted on the back face of the pile. From point of rotation to the bottom of the pile, passive resistance is mobilised at the back face, whereas, over the same length soil exerts active pressure in the front face of pile. Below dredge line and up to the point of rotation passive resistance is mobilised on the front face of the pile. The resulting net pressure diagram is complicated. But, for the sake of simplicity modified pressure diagrams are generally used which are adequate for practical purposes.

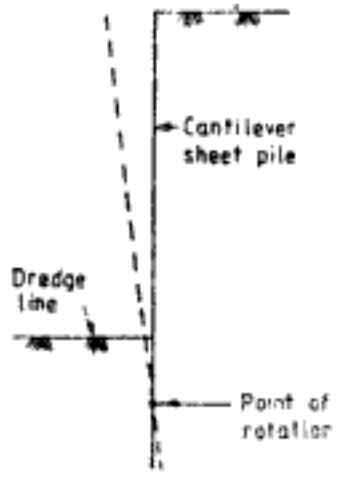

Fig. 17.10 Cantilever sheet pile

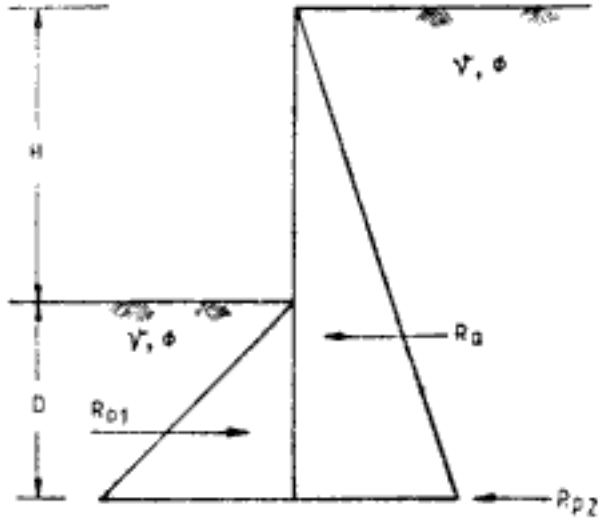

Fig. 17.11 Earth pressure diagram for sheet pile in cohesionless soil

1. *Sheet piles in cohesionless soils*

A simplified earth pressure distribution for sheet piles with cohesionless backfill and embedded in cohesionless soil is shown in Fig. 17.11. Active pressure is assumed throughout the back face and passive pressure throughout the front face of embedded portion of sheet pile. The passive resistance on the back face below the point of rotation is represented by a total passive thrust R_{p2} acting at the bottom of the pile as shown in Fig. 17.11. This assumption will give good enough results if the point of rotation is not very far from the bottom of pile. It is further assumed that the active and passive thrusts act horizontally even though wall friction may be taken into account in computation of earth pressure coefficients. The depth

of embedment D for the type of pressure distribution in Fig. 17.11 to satisfy the equilibrium of forces and moments is given by,

$$D = \frac{H \sqrt[3]{K_a/K_p}}{1 - \sqrt[3]{K_a/K_p}} \tag{17.27}$$

The shear force on the sheet pile is zero at a depth d below dredge line, consequently the moment at this point is maximum. d is given by,

$$d = \frac{\sqrt{K_a/K_p}\, H}{1 - \sqrt{K_a/K_p}} \tag{17.28}$$

Q 17.5: Determine the depth of embedment for sheet pile and the maximum design moment given the following data:

height of cohesionless backfill above dredge line = 7 m

$\gamma = 1.80$ T/m³

$\phi = 38°$

$\delta = 20°$

Solve the problem by applying factor of safety of (a) 1.3 to depth of embedment, and (b) 2 to passive earth pressure coefficient.

Ans: (a) From Table 16.5, $K_a = 0.217$, and from Table 16.6, $K_p = 10.194$

From Eq. 17.27, $D = \dfrac{7\sqrt[3]{0.217/10.194}}{1 - \sqrt[3]{0.217/10.194}} = 2.68$ m

Depth of embedment required $= 1.3 \times 2.68 = 3.48$ m

From Eq. 17.28,

$$d = \frac{7\sqrt{0.217/10.194}}{1 - \sqrt{0.217/10.194}} = 1.20 \text{ m}$$

$$\text{Maximum moment} = \tfrac{1}{2} \times 0.217 \times 1.8 \times 8.2^2 \times \frac{8.2}{3} - \tfrac{1}{2} \times 10.194 \times 1.8 \times 1.2^2 \times \frac{1.2}{3}$$

$$= 30.6 \text{ T m/m}$$

(b) $K_a = 0.217$, $K_p = 10.194/2 = 5.097$

$$D = \frac{7\sqrt[3]{0.217/5.097}}{1 - \sqrt[3]{0.217/5.097}} = 3.76 \text{ m}$$

$$d = \frac{7\sqrt{0.217/5.097}}{1 - \sqrt{0.217/5.097}} = 1.82 \text{ m}$$

$$\text{Maximum moment} = \tfrac{1}{2} \times 0.217 \times 1.8 \times 8.82^2 \times \frac{8.82}{3} - \tfrac{1}{2} \times 5.097 \times 1.8 \times 1.82^2 \times \frac{1.82}{3}$$

$$= 35.45 \text{ T m/m}$$

When the point of rotation is well above the bottom of pile the pressure distribution diagram in Fig. 17.12 can be used, which gives a more rigorous representation of net pressure inten-

sities with depth. *ABCGE* in the figure gives the earth pressure distribution. The figure also shows the other construction lines. In Fig. 17.12,

$$a = \frac{p_a}{\gamma(K_p - K_a)} \tag{17.29}$$

$$P_{p1} = \gamma(K_p - K_a)X \tag{17.30}$$

$$P_{p0} = \gamma(H + a)K_p - \gamma a K_a \tag{17.31}$$

$$P_{p2} = P_{p0} + P_{p1} \tag{17.32}$$

$$y = (H + 2a)/3 \tag{17.33}$$

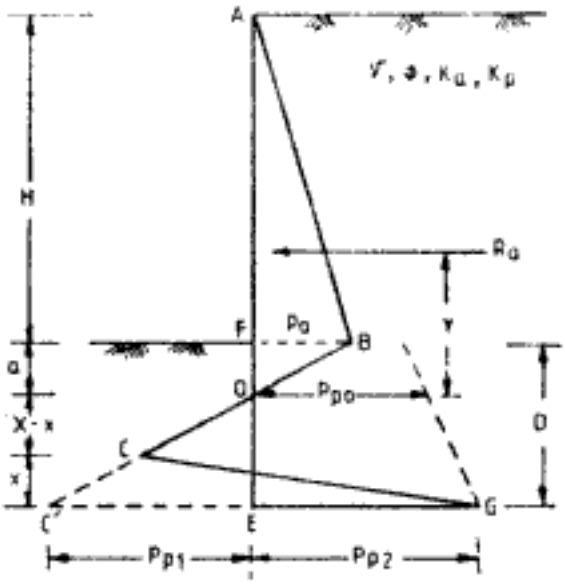

Fig. 17.12 Earth pressure distribution for sheet pile in cohesionless soil

Value of X can be obtained by solving the following equation,

$$X^4 + X^3\frac{P_{p0}}{C} - X^2\frac{8R_a}{C} - X\left[\frac{6R_a}{C^2}(2yC + P_{p0})\right] - \frac{6R_a y P_{p0} + 4R_a^2}{C^2} = 0 \tag{17.34}$$

where $C = \gamma(K_p - K_a)$

R_a = total active thrust for diagram ABO

Equation 17.34 is solved by trial and error procedure. Depth of pile below dredge line is,

$$D = X + a \tag{17.35}$$

Q 17.6: Re-do Q 17.5 using earth pressure distribution shown in Fig. 17.12.

Ans: (a) $K_a = 0.217, \quad K_p = 10.194$

$$p_a = 1.8 \times 0.217 \times 7 = 2.73 \text{ T/m}^2$$

$$a = \frac{2.73}{1.8(10.194 - 0.217)} = 0.152 \text{ m}$$

$$C = 1.8(10.194 - 0.217) = 17.96 \text{ T/m}^3$$

$$P_{p0} = 1.8 \times (7 + 0.152) \times 10.194 - 1.8 \times 0.152 \times 0.217 = 9.76 \text{ T/m}^2$$
$$R_a = \tfrac{1}{2} \times 7.152 \times 2.73 = 9.76 \text{ T/m}$$
$$y = \frac{7 + 0.304}{3} = 2.435 \text{ m}$$

Substituting the values in Eq. 17.34 and simplifying,

$$X^4 + 7.3X^3 - 4.35X^2 - 39.69X - 59.17 = 0$$

Choosing different values for X the LHS of the equation can be computed.

X	LHS
2.4 m	−45.39
2.5 m	−32.46
2.6 m	−17.77
2.7 m	−1.21
2.71 m	0.55 → O.K. Value of X = 2.71 m

$$D = 2.71 + 0.152 = 2.862 \text{ m}$$

Depth of embedment required $= 1.3 \times 2.862 = 3.72$ m

(b) $K_a = 0.217$, $K_p = 10.194/2 = 5.097$

$p_a = 2.73$ T/m² from (a) above

$$a = \frac{2.73}{1.8(5.097 - 0.217)} = 0.311 \text{ m}$$
$$C = 1.8(5.097 - 0.217) = 8.78 \text{ T/m}^3$$
$$P_{p0} = 1.8 \times (7 + 0.311) \times 5.097 - 1.8 \times 0.311 \times 0.217 = 66.95 \text{ T/m}^2$$
$$R_a = \tfrac{1}{2} \times 7.311 \times 2.73 = 9.98 \text{ T/m}$$
$$y = \frac{7 + 0.622}{3} = 2.54 \text{ m}$$

Substituting the values in Eq. 17.34 and simplifying,

$$X^4 + 7.625X^3 - 9.09X^2 - 86.65X - 137.26 = 0$$

X	LHS
3.7 m	−8.66
3.72 m	−1.36 → O.K.

Depth of embedment required = 3.72 + 0.311 = 4 m (say)

Frequently in situations where sheet pile is used, water-table is found on both sides. The backfill may also be layered. Figure 17.13 shows the modified diagram of Fig. 17.11 for presence of water-table on both sides or for layered backfill. If the water-table does not affect the angle of shearing resistance, then $\phi_1 = \phi_2$, $K_{a1} = K_{a2}$, and $K_{p1} = K_{p2}$. For homogeneous conditions $\phi_1 = \phi_2 = \phi$, $K_{a1} = K_{a2} = K_a$ and $K_{p1} = K_{p2} = K_p$. In Fig. 17.13, D is obtained by solving the following equation,

$$D^3 - aD^2 - bD - c = 0 \qquad (17.36)$$

Hidden page

The coefficients now are,

$$a = 1.201$$
$$b = 9.738$$
$$c = 24.946$$

Therefore,

$$D^3 - 1.201D^2 - 9.738D - 24.946 = 0$$

Solving, $D = 4.55$ m, the depth of embedment required.

Figure 17.14 gives a more rigorous representation of earth pressure distribution for the case represented in Fig. 17.13. In Fig. 17.14,

$$a = \frac{p_a}{\gamma_2(K_{p2} - K_{a2})} \tag{17.37}$$

$$P_{p1} = \gamma_2(K_{p2} - K_{a2})X \tag{17.38}$$

$$P_{p0} = \gamma_1 h_1 K_{p2} + \gamma_2 K_{p2}(h_2 + a) - \gamma_2 a K_{a2} \tag{17.39}$$

$$P_{p2} = P_{p0} + P_{p1} \tag{17.40}$$

$$p_a = K_{a2}(\gamma_1 h_1 + \gamma_2 h_2) \tag{17.41}$$

$$R_a = \tfrac{1}{2}[K_{a1}\gamma_1 h_1^2 + K_{a2}\gamma_1 h_1 h_2 + p_a(h_2 + a)] \tag{17.42}$$

$$y = \frac{K_{a1}\gamma_1 h_1^2(3h_2 + 3a + h_1) + 2K_{a2}\gamma_1 h_1 h_2^2 + 3K_{a2}\gamma_1 h_1 h_2 a + p_a(h_2 + a)(h_2 + 2a)}{6R_a} \tag{17.43}$$

X can be obtained by solving Eq. 17.34 in which $C = \gamma_2(K_{p2} - K_{a2})$.

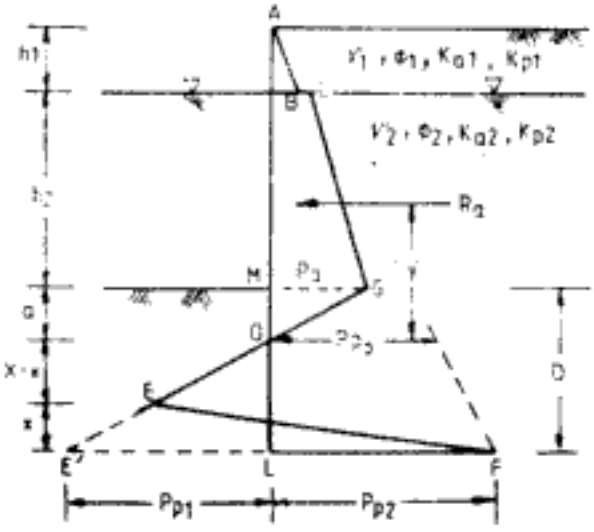

Fig. 17.14 Modified figure of Fig. 17.12 for presence of water-table or for layered backfill

Q 17.8: Re-do Q 17.7 using earth pressure distribution shown in Fig. 17.14.

(a) Using the data in Q 17.7,

$$C = 0.9(10.194 - 0.217) = 8.98 \text{ T/m}^3$$

$$p_a = 0.217(1.8 \times 2 + 0.9 \times 5) = 1.758 \text{ T/m}^2$$

$$a = 1.758/8.98 = 0.196 \text{ m}$$

$$P_{p0} = 1.8 \times 2 \times 10.194 + 0.9 \times 10.194 \times (5 + 0.196) - 0.9 \times 0.196 \times 0.217$$
$$= 84.33 \text{ T/m}^2$$

$$R_a = \tfrac{1}{2}[0.217 \times 1.8 \times 4 + 0.217 \times 1.8 \times 2 \times 5 + 1.758 \times 5 + 0.196] = 7.30 \text{ T/m}$$

$$y = [0.217 \times 1.8 \times 4 \times (3 \times 5 + 3 \times 0.196 + 2) + 2 \times 0.217 \times 1.8 \times 2 \times 25 + 3 \times 0.217 \times 1.8 \times 2 \times 5 \times 0.196 + 1.758 \times (5 + 0.196) \times (5 + 2 \times 0.196)]/(6 \times 7.3)$$
$$= 2.7 \text{ m}$$

Substituting the values in Eq. 17.34 and simplifying,

$$X^4 + 9.39X^3 - 6.5X^2 - 72.14X - 126.31 = 0$$

Solving by trial and error,

X	LHS	
3 m	−66.7	
3.3 m	20.88	
3.2 m	−11.16	
3.25 m	4.49	O.K.

$$D = 3.25 + 0.196 = 3.446 \text{ m}$$

Depth of embedment required $= 1.3 \times 3.446 \simeq 4.8$ m

(b) $K_{p1} = K_{p2} = 10.194/2 = 5.097$

$$C = 0.9(5.097 - 0.217) = 4.39 \text{ T/m}^3$$

$$R_a = 7.3 \text{ T/m}$$

$$p_a = 1.758 \text{ T/m}^2$$

$$a = 1.758/4.39 = 0.4 \text{ m}$$

$$P_{p0} = 1.8 \times 2 \times 5.097 + 0.9 \times 5.097 \times (5 + 0.4) - 0.9 \times 0.4 \times 0.217$$
$$= 43.04 \text{ T/m}^2$$

$$y = [0.217 \times 1.8 \times 4 \times (3 \times 5 + 3 \times 0.4 + 2) + 2 \times 0.217 \times 1.8 \times 2 \times 25 + 3 \times 0.217 \times 1.8 \times 2 \times 5 \times 0.4 + 1.758 \times (5 + 0.4) \times (5 + 2 \times 0.4)]/(6 \times 7.3)$$
$$= 2.90 \text{ m}$$

Substituting in Eq. 17.34,

$$X^4 + 9.8X^3 - 13.3X^2 - 155.68X - 294.73 = 0$$

X	LHS	
4.5 m	38.47	
4.4 m	−27.6	
4.45 m	4.85	O.K.

Depth required $= 4.45 + 0.4 = 4.85$ m

Hidden page

Hidden page

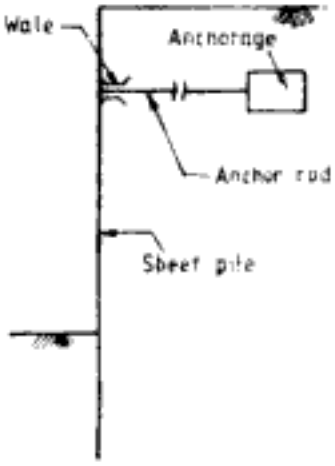

Fig. 17.18 Anchored bulkhead

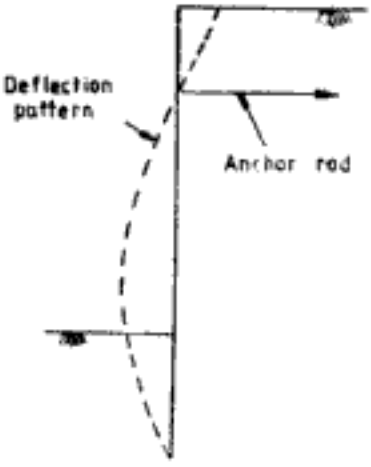

Fig. 17.19 Free-earth support—deflection pattern

1. *Free earth support method*

When the depth of embedment of sheet pile is small, free earth support can be assumed. The bottom of pile is not fixed, but free to deflect or rotate. The deflection pattern for sheet pile under such condition is shown in Fig. 17.19. The earth pressure distribution for analysis is shown in Figs 17.20 and 17.24 for bulkheads in cohesionless and purely cohesive soils, respectively.

(a) *Cohesionless soils*

In Fig. 17.20,

$$p_p = CX \tag{17.47}$$

$$C = \gamma_2(K_{p2} - K_{a2}) \tag{17.48}$$

$$R_p = CX^2/2 \tag{17.49}$$

$$a = p_a/C \tag{17.50}$$

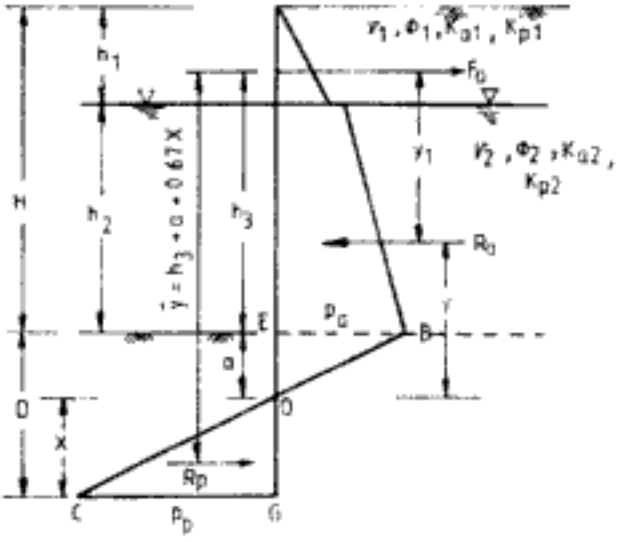

Fig. 17.20 Free earth support—earth pressure distribution in cohesionless soil

p_a and R_a are given by Eqs 17.41 and 17.42 respectively.

$$y_1 = h_3 + a - y \tag{17.51}$$

where y is as given in Eq. 17.43. X is determined by solving the following equation,

$$2X^3 + 3X^2(h_3 + a) - \frac{6R_a y_1}{C} = 0 \tag{17.52}$$

Force in the anchor rod, F_a, is given by

$$F_a = R_a - R_p \tag{17.53}$$

To check the analysis, the moment about anchor point on sheet pile is zero.

$$R_p \bar{y} - R_a y_1 = 0 \tag{17.54}$$

To locate the point of maximum bending moment, the point of zero shear can be determined and moment of forces about this point gives the maximum bending moment. Rowe (1952, 1957) from experimental observations pointed out that due to the flexibility of sheet piles reduction factors should be applied to moments computed on the basis of free earth support method. Rowe's moment reduction factors are given in Fig. 17.21 for sheet piles in sand and clay. Bowles (1982), however, recommends that in loose sands due to their high compressibility and in clays due to consolidation deformation, the moment reduction factors should not be applied. Application of the moment reduction factor is done through the following steps:

(i) For cohesionless granular soils determine relative density

(ii) For cohesive soils determine stability number, S_n, defined as,

$$S_n = \frac{1.25c}{\gamma L} \tag{17.55}$$

where L = total length of sheet pile = $H + D$

(iii) Determine flexibility number, ρ, defined as,

$$\rho = \frac{1113L^4}{EI} \tag{17.56}$$

where L is in metres

E = modulus of elasticity of sheet pile, in kg/cm^2

I = moment of inertia for a unit width, in cm^4/m

(iv) Determine α and β as,

$$\alpha = H/L \tag{17.57}$$

$$\beta = h_a/L \tag{17.58}$$

where H = height of sheet pile above dredge line

h_a = depth of anchor below surface of backfill.

(v) From appropriate curve (or by interpolation) in Fig. 17.21 determine the value of M/M_0.

(vi) Compute M/M_0 for sheet pile sections. M is the moment capacity of section and M_0 is the moment computed by free earth support method. M = allowable stress × section modulus/unit width. Select sheet pile section having M/M_0 value equal to or more

Hidden page

than the M/M_0 value determined in Step 5. Closer the two values, more economical is the section.

Q 17.10: For the anchored bulkhead shown in Fig. 17.22 determine the depth of embedment by free earth support method using a factor of safety of 1.3 for depth of embedment. Determine also the anchor force.

Ans: $\gamma_1 = 1.8$ T/m^3 $\quad \gamma_2 = 0.9$ T/m^3

$\phi_1 = \phi_2 = 38°$

From Tables 16.5 and 16.6, $K_{a1} = K_{a2} = 0.217$

$K_{p1} = K_{p2} = 10.194$

$C = 0.9(10.194 - 0.217) = 8.98$ T/m^3

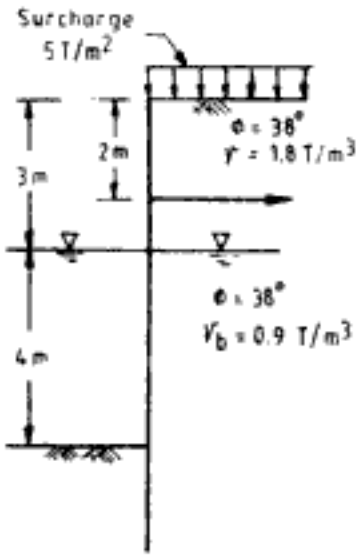

Fig. 17.22 Q 17.10

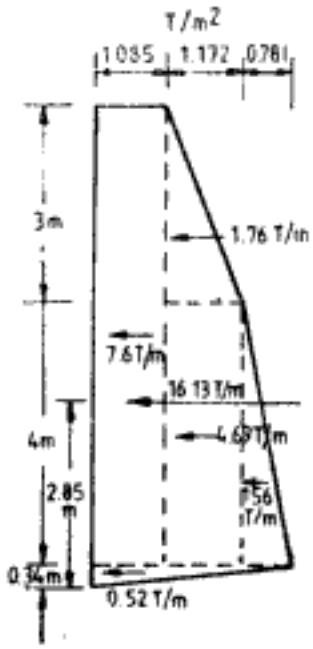

Fig. 17.23 Earth pressure distribution for sheet pile in Q 17.10

Active earth pressure distribution on the back face of sheet pile is shown in Fig. 17.23 from which $p_a = 3.04$ T/m^2.

$$R_a = 16.13 \text{ T/m}$$

$$a = \frac{3.04}{8.98} = 0.34 \text{ m}$$

$$y = (7.6 \times 3.84 + 1.76 \times 5.34 + 4.69 \times 2.34 + 1.56 \times 1.67 + 0.52 \times 0.67 \times 0.34)/16.13$$

$$= 3.24 \text{ m}$$

$$y_1 = 5 + 0.34 - 3.24 = 2.10 \text{ m}$$

Substituting the values in Eq. 17.52,

$$2X^3 + 16.02X^2 - 22.63 = 0$$

Hidden page

$M/M_0 = 31.8/10.77 = 2.95$, which is much higher than 0.85 determined from chart. The section is satisfactory but not economical. A search for suitable lighter sections can be made.

(b) *Purely cohesive soils* ($\phi = 0$)

When the sheet pile is embedded in purely cohesive soil below dredge line earth pressure distribution will be as shown in Fig. 17.24. D is computed using equation,

$$D = -h_3 + \sqrt{h_3^2 + \frac{2R_a y_1}{4c - \bar{q}}} \tag{17.59}$$

$$y_1 = h_3 - y \tag{17.60}$$

$\bar{q}$ is the effective surcharge pressure at the level of dredge line.

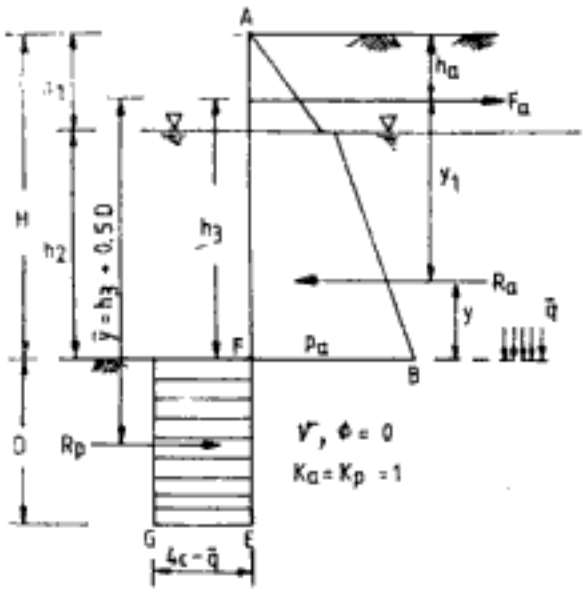

Fig. 17.24 Free earth support method—sheet pile embedded in purely cohesive soil

Q 17.12: Re do Q 17.10 if the sheet pile is embedded below dredge line in purely cohesive soil having $c = 6$ T/m^2. Use a factor of safety of 1.5 on cohesion.

Ans: $c = 6/1.5 = 4$ T/m^2

$\bar{q} = 1.8 \times 3 + 0.9 \times 4 + 5 = 14$ T/m^2

Active earth pressure diagram is same as Fig. 17.23, but the portion below dredge level should be omitted.

$$R_a = 16.13 - 0.52 = 15.61 \text{ T/m}$$

$$y = \frac{7.6 \times 3.5 + 1.76 \times 5 + 4.69 \times 2 + 1.56 \times 1.33}{15.61}$$

$$= 3.00 \text{ m}$$

$$y_1 = 5 - 3 = 2 \text{ m}$$

Hidden page

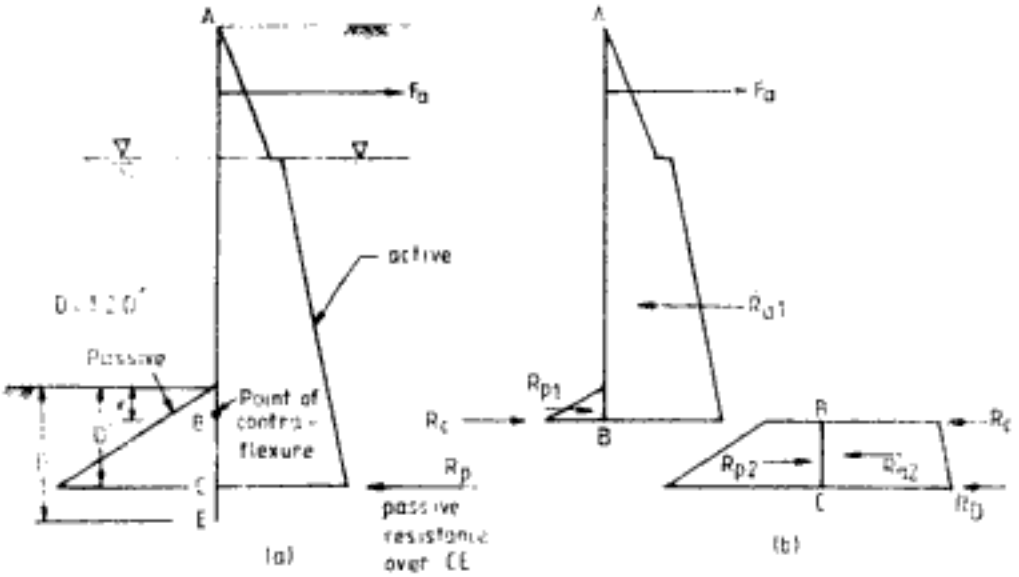

Fig. 17.26 Fixed earth support method: (a) earth pressure distribution and forces on sheet pile, and (b) equivalent beam method

Table 17.2 Variation of x with ϕ for Equivalent Beam Method

ϕ	x
20	$0.25H$
25	$0.15H$
30	$0.08H$
35	$0.025H$
40	0

(iii) The part below the hinge, BC, can also be treated as a simply supported beam with reactions R_C and R_D of which R_C is known. The span $D' - x$ is not known which can be determined by taking moment of known forces on BC about C and equating to zero. Depth of embedment D is $1.2\ D'$.

(iv) The maximum bending moment generally occurs above dredge level. The location of zero shear can be determined and the maximum bending moment about this point can be calculated.

Q 17.13: For the anchored bulkhead in Fig. 17.22 but with no surcharge on backfill determine the depth of embedment by fixed earth support method. Also determine the anchor force and the maximum bending moment in the sheet pile.

Ans: From Table 17.2 for $\phi = 38°$, $x \simeq 0$. Hence, the hinge is assumed at dredge level. Equivalent beams AB and BC are shown in Fig. 17.27 with the forces on them. On AB the values of forces and their leverage about anchor rod are as below:

Force No.	*Force*, T/m	*Leverage about anchor rod*, m
I	1.76	0
II	4.69	3.00
III	1.56	3.67
R_C	Unknown	5

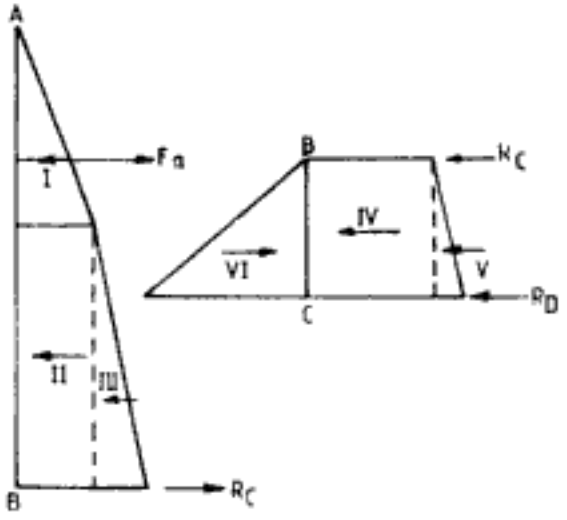

Fig. 17.27 Equivalent beams for bulkhead in Q 17.13

Total active thrust is sum of forces I to III = 8.01 T/m

$$F_a + R_C = 8.01 \tag{a}$$

Taking moment of forces about anchor rod,

$$R_C \times 5 = 1.76 \times 0 + 4.69 \times 3 + 1.56 \times 3.67$$

Solving, $R_C = 3.96$ T/m

From Eq. a, anchor force is,

$$F_a = 4.05 \text{ T/m}$$

The span of beam BC is D' and unknown. The forces on BC are,

Force No.	*Force*, T/m	*Leverage about C*, m
IV	$1.95\,D'$	$D'/2$
V	$0.098\,D'^2$	$D'/3$
VI	$4.59\,D'^2$	$D'/3$
R_C	3.96	D'

Taking moment of forces about point C and simplifying the expression,

$$1.4973D'^2 - 0.975D' - 3.96 = 0$$

Solving, $D' = 1.98$ m

Depth of embedment, $D = 1.2 \times 1.98 = 2.4$ m

Let the maximum bending moment occur at a point between water level and dredge level at a distance $\bar{x}$ below water level. The shear force at this point is zero.

i.e., $4.05 - 1.76 - 0.217 \times 1.8 \times 3 \times \bar{x} - \frac{1}{2} \times 0.217 \times 0.9 \times \bar{x}^2 = 0$

Simplifying, $2.29 - 1.1718\bar{x} - 0.09765\bar{x}^2 = 0$

Solving, $\bar{x} = 1.71$ m

This satisfies the assumption for the location of maximum bending moment.

Maximum bending moment

$$= 4.05 \times 2.71 - 1.76 \times 2.71 - 0.217 \times 1.8 \times 3 \times \frac{172^2}{2} - \frac{1}{2} \times 0.217 \times 0.9 \times \frac{1.71^3}{3}$$

$$= 4.33 \text{ T m/m}$$

3. *Tschebotarioff's method*

Tschebotarioff (1951) assumes the hinge at the dredge line. His procedure is shown in Fig. 17.28. In his procedure, active earth pressure coefficient is taken as,

$$K_a = \left(1 - \frac{h_a}{f'H}\right) 0.33 f^* \tag{17.61}$$

where f' = ranges from 1.5 to 3.5 with larger values preferred, a factor which takes into account uncertainty about passive pressure above anchor rod and capillary tension above water level

f^* = 0.9, a factor which takes into account effect of wall friction on active pressure

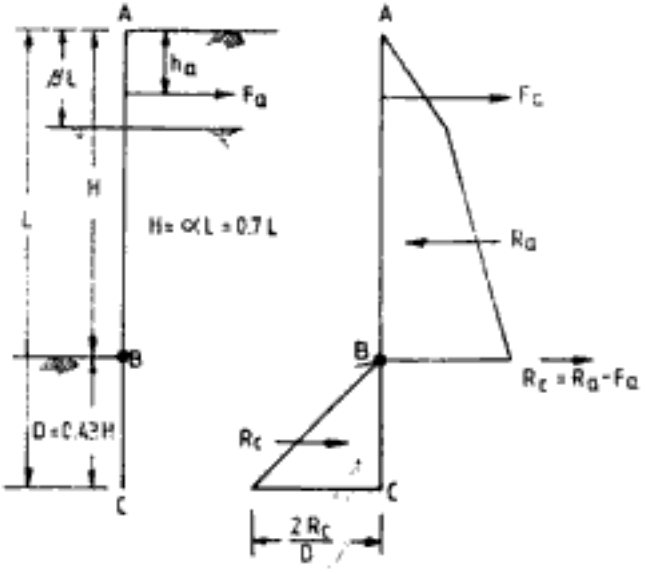

Fig. 17.28 Tschebotarioff's method for anchored bulkheads

The depth of embedment of sheet pile is taken as $0.43H$. It is enough to analyse span AB only to determine anchor force and maximum bending moment as in most of the cases the maximum bending moment occurs above dredge line. Where the soil below dredge level is different from backfill material, then the passive resistance offered by the soil over span BC may be investigated. It is recommended that anchor should be designed for a force of F_a^* given as,

$$F_a^* = \frac{F_a}{(1 - h_a/f'H)f''} \tag{17.62}$$

where f'' = 1 for granular soil

Q17.14: Re do Q 17.13 using Tschebotarioff's method.

Ans: The depth of embedment $= 0.43 \times 7 = 3.00$ m

$$K_a = \left(1 - \frac{2}{3.5 \times 7}\right)^2 \times 0.33 \times 0.9 = 0.273$$

The forces acting on span AB are as shown in Fig. 17.27 but the values are,

Force No.	*Force*, T/m
I	2.21
II	5.9
III	1.96

Proceeding in the same manner as in Q 17.13,

$$R_c = 4.98 \text{ T/m}$$

$$F_a = 5.09 \text{ T/m}$$

$$\bar{x} = 1.71 \text{ m}$$

Maximum bending moment $= 5.8$ T m/m

design force in another rod, $F_a^* = \dfrac{5.09}{1 - \dfrac{2}{3.5 \times 7}} = 5.54$ T/m

4. *Anchorages*

Common types of anchorages for bulkheads are shown in Fig. 17.29.

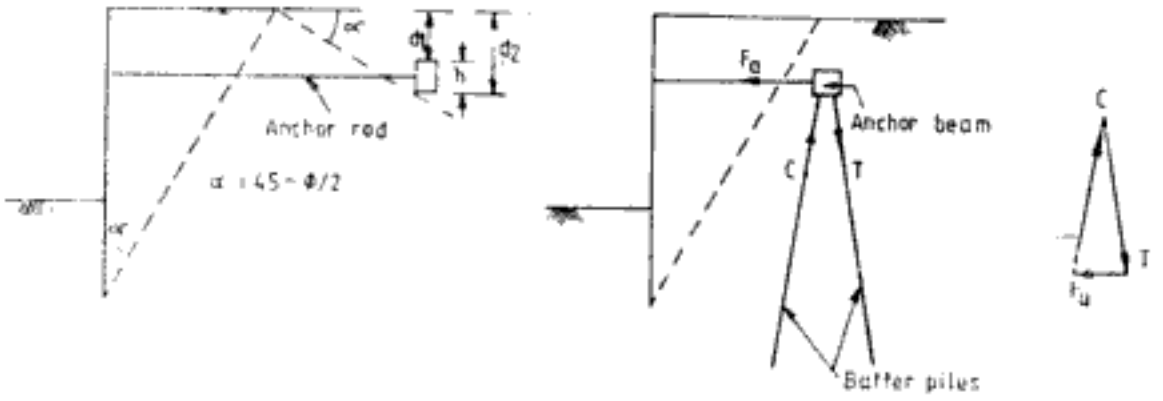

(a) (b)

Fig. 17.29 Anchorages for bulkhead: (a) deadman anchorage, and (b) anchor beam on batter piles

Deadman anchors depend upon passive resistance for their stability. They must be located in a zone within the backfill as shown in Fig. 17.29a. If the anchor is considerably long and the depth from surface of backfill to top of anchor wall (d_1) is less than 0.5 to 0.7 times the depth from surface of backfill to bottom of anchor wall (d_2), the anchor wall can be considered to extend up to the top of the backfill. Then the resistance of deadman anchor is the net of active and passive resistance behind and in front of the wall. For strong anchorage the minimam factor of safety is 2.5. The ultimate resistance Q_u is given by,

$$Q_u = (P_p - P_a)L \qquad (17.63)$$

Anchorages, like in Fig. 17.29b, can be located closer to the bulkhead than the deadman anchors. The forces on the piles can be determined by constructing a force polygon.

Hidden page

If backfill material is cohesive it must be removed at least to a distance of H from the back of sheet pile and replaced with sand. This is done in order to reduce earth pressure on sheet pile. While filling backfill it must be done from sheet pile end to prevent mud waves damaging pile frames and squeezing in a cohesive layer behind the sheet pile. The sheet pile can be analysed as though it retains sand.

In the analyses presented, active earth pressure distribution has been assumed on the back face of sheet pile. This may be realistically achieved in a *fill bulkhead*, where the bulkhead is first installed and the backfill is then filled up. In the case of *dredge bulkheads*, where bulkhead is first driven into soil and the soil in front of sheet pile is dredged out, the earth pressure distribution will be more or less uniform with depth. If the anchorage is very stiff and does not allow any movement at the anchorage point the earth pressure at the top will be more than the value determined by active earth pressure distribution. The procedures recommended for braced cuts can be used here.

Structural failure of sheet pile is rare. But anchorage failures are often reported. One reason is the under-estimation of anchor force. Where softer deposits underlie the backfill, the soil undergoes consolidation. The anchors are forced to carry the weight of overlying soil which causes bending stresses in the anchor rod. To prevent this, anchor rods may be surrounded by corrugated pipes embedded in backfill. When backfill settles, due to clearance available between the pipe and anchor rod no load is transferred to the anchor rod.

17.3 BRACED CUTS

Deep excavations in soil are often required, for example, for the construction of basements. The sides of the excavation should be properly supported to ensure safety of excavation and construction. Sheet piles are used against the sides which are joined by a set of wales running across them. The earth pressure acting on sheeting is resisted by horizontal struts (Figs. 16.2 and 17.30a), or by inclined struts (Fig. 17.34), or by the tie back braces (Fig. 17.30b). The struts and braces must be designed for the forces which act upon them.

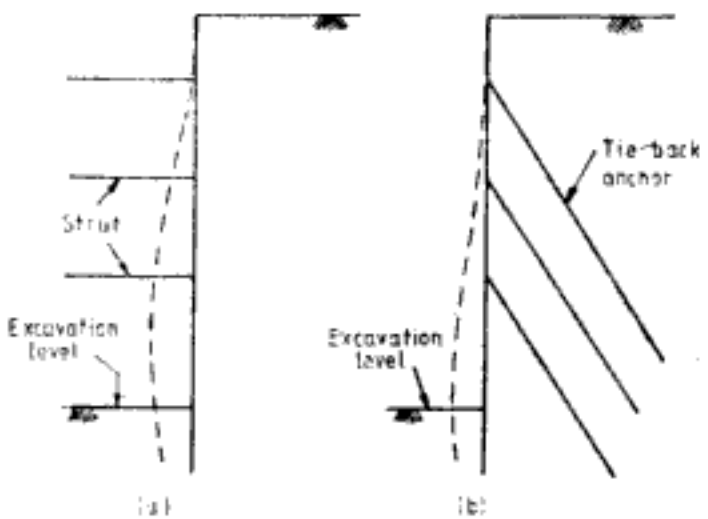

Fig. 17.30 Deflection pattern of braced cuts

Figure 17.30 shows typical deflection pattern of braced cuts. As a result of restricted deformation near the braces at the top active earth pressure distribution behind the sheeting cannot be assumed. Based on a number of experiments and measurements of earth pressure in braced cuts for actual excavations investigators have proposed earth pressure distribution diagrams which will be discussed here.

17.3.1 Recommendations for Earth Pressure Distribution in Sand

Figure 17.31 shows the various recommendations for earth pressure distribution behind sheeting. In these diagrams H is the height of excavation. K_a is the coefficient of active earth pressure distribution with wall friction angle as zero ($\delta = 0°$).

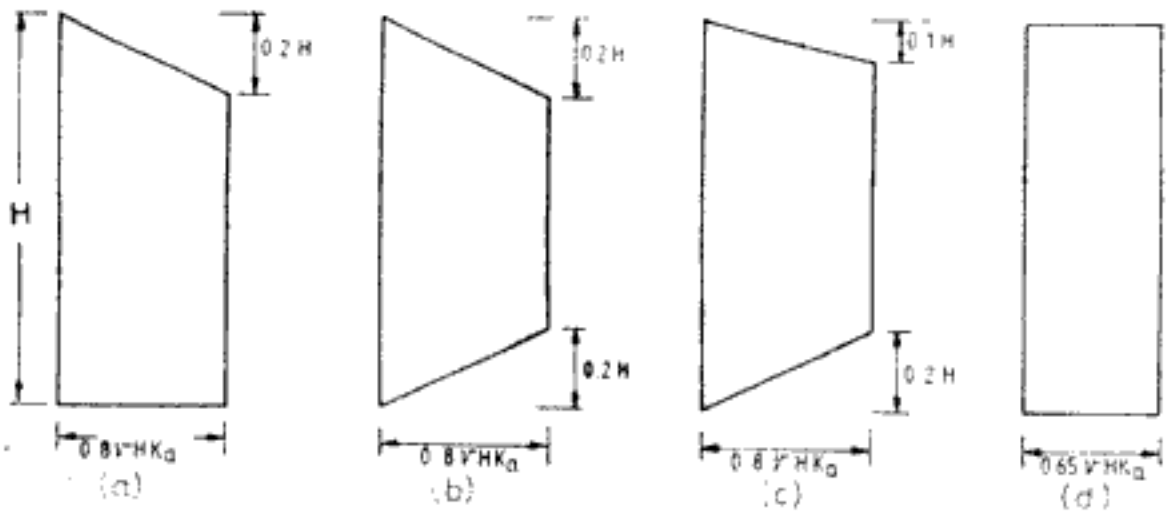

Fig. 17.31 Earth pressure distribution in sand for braced cuts due to: (a) Terzaghi and Peck—for loose sand, (b) Terzaghi and Peck—for dense sand, (c) Tschebotarioff, and (d) Peck, Hanson, and Thornburn—for moist and dry sands

17.3.2 Recommendations for Earth Pressure Distribution in Clay

Figure 17.32 shows the different recommendations in case of clay. In the diagrams, c is the average undrained cohesion of soil over the depth of excavation. γ is the average total density.

Braced excavations in clay may become unstable due to the heave of bottom. To ensure the stability of braced systems $\gamma H/c_b$ must be kept less than 6, where c_b is the undrained shear strength of soil below base or excavation level. Figure 17.32d can be used for $\gamma H/c$ value as large as 10 to 12, but $\gamma H/c_b$ must be less than 6.

17.3.3 Loads on Braces

Figure 17.33 explains the two methods of analysis for loads in horizontal struts. In tributary area method (Fig. 17.33a) the load on a strut is equal to the load resulting from pressure distribution over the tributary area for that strut. For example, strut load P_B in Fig. 17.33a is the total load on tributary area 1–2–3–4. In the equivalent beam method of analysis (Fig. 17.33b) the entire depth is split into segments of simply supported beam and the reactions can then be determined by standard procedures. In both the methods of analysis, P_S is the soil reaction in the embedded portion of sheet piles or soldier piles.

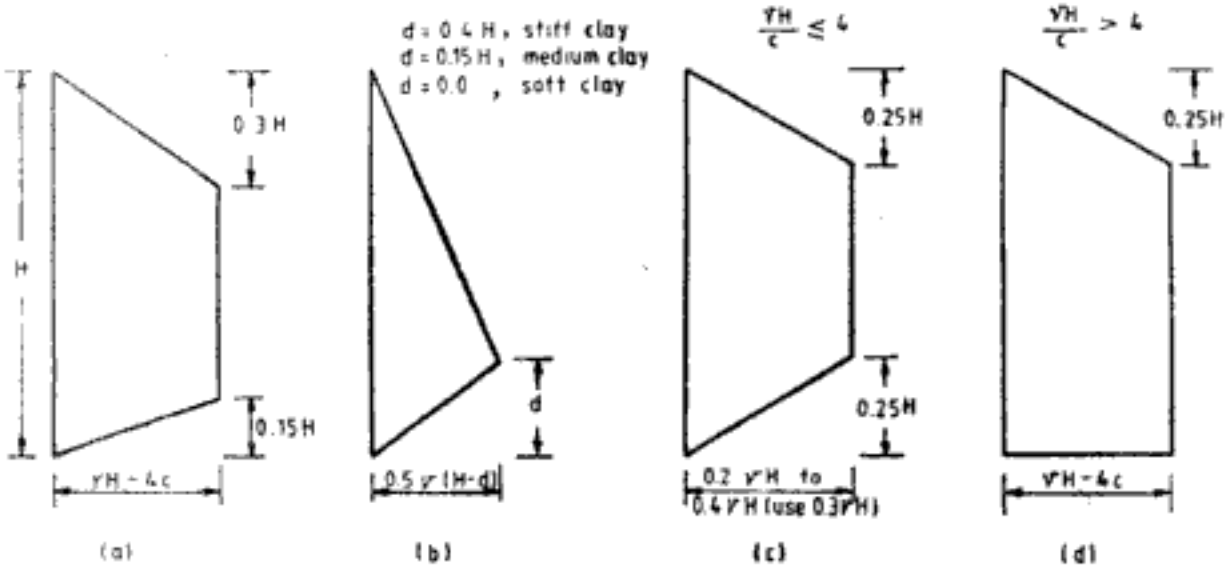

Fig. 17.32 Earth pressure distribution for braced cuts in clay: (a) for plastic clay by Peck, (b) neutral earth pressure ratio method by Tschebotarioff, (c) Peck, Hanson, and Thornburn's diagram when $\gamma H/c \leq 4$, (d) Peck, Hanson and Thornburn's diagram when $\gamma H/c > 4$

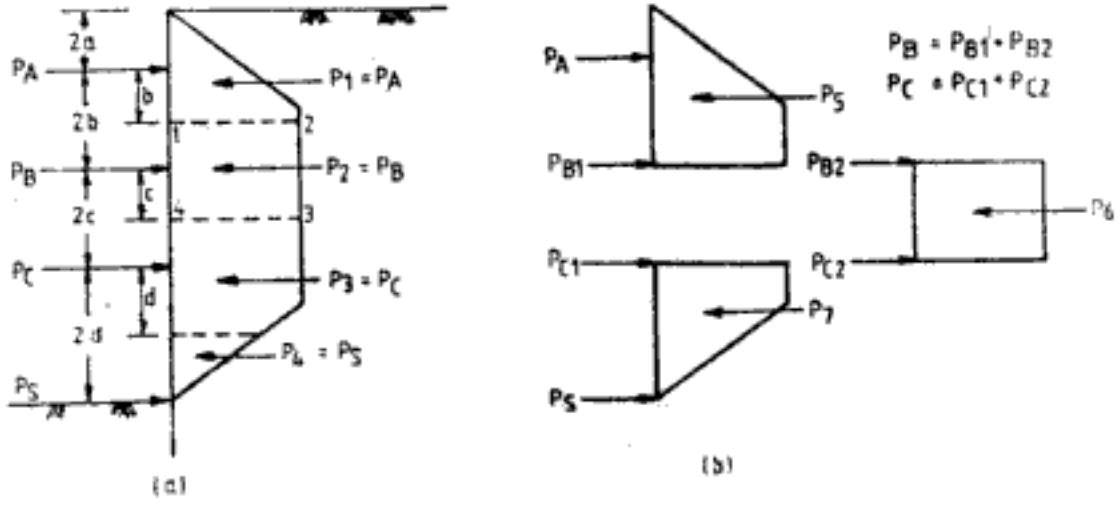

Fig. 17.33 Loads on horizontal struts (a) tributary area method, (b) equivalent beam method

If inclined struts are used, after determining the horizontal component of strut load by procedures mentioned above, the axial load can be determined by constructing a force polygon as shown in Fig. 17.34. In this case there is a component of uplift load also. The depth of embedment of sheet pile must be sufficient enough to provide reaction against the total uplift load. When the area of excavation is large inclined braces will be advantageous. The reaction for strut load is provided through kicker block embedded in base of excavation. The base of kicker block may be either inclined or horizontal as shown in Fig. 17.35.

The ultimate bearing capacity q_{ult} of kicker block can be determined using the following equations:

$$q_{ult} = cN_{cq} \text{ in purely cohesive soils, i.e. } \phi = 0^\circ \qquad (17.67)$$

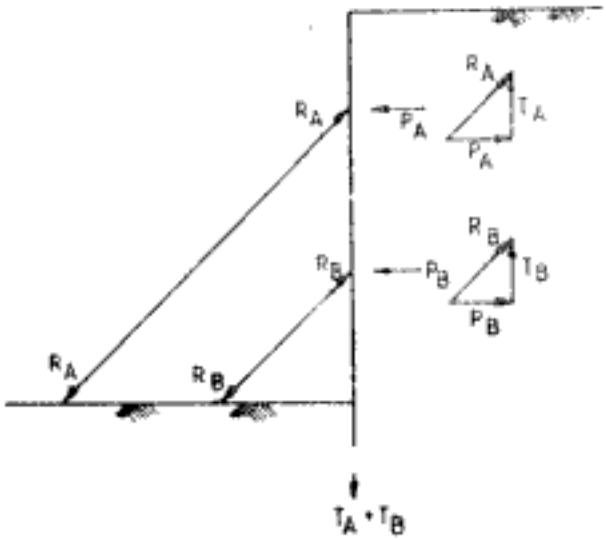

Fig. 17.34 Loads on inclined struts

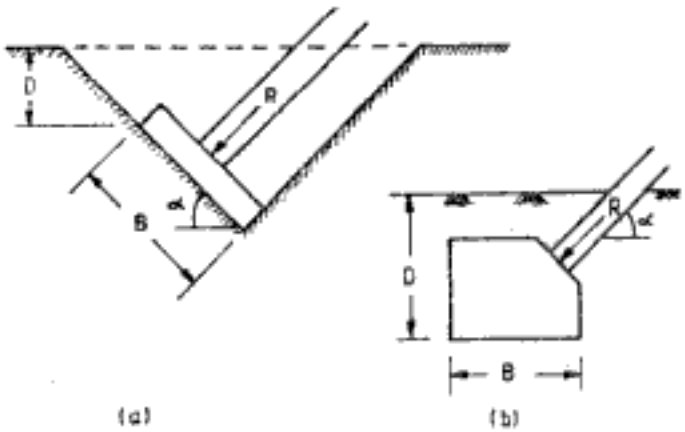

Fig. 17.35 (a) Inclined kicker block. (b) horizontal kicker block

$$q_{ult} = \frac{\gamma B}{2} N_{\gamma q} \quad \text{in cohesionless soils, i.e., } c = 0 \tag{17.68}$$

$$q_{ult} = cN_{cq} + \frac{\gamma B}{2} \quad N_{\gamma q} \text{ in } c - \phi \text{ soils} \tag{17.69}$$

Figure 17.36 gives the bearing capacity factors N_{cq} and $N_{\gamma q}$ which are also dependent on inclination of load α. A factor of safety of 3 must be used in purely cohesive soils and in cohesionless soils the minimum factor of safety must be 2.5.

Tie-back braces provide obstacle-free working space in the excavated area. Where possible tie back bracing system can be used. But infringement against underground utility lines and other structures must be properly investigated. The tie back braces have another advantage that each anchor is pretested for capacity during installation. The axial pull in the anchor

Hidden page

Ans: The strut loads will be determined using different earth pressure distributions, by both tributary area method and equivalent beam method. The different pressure distribution diagrams used in the solution are,

(a) Peck, Hanson and Thornburn's diagram (Fig. 17.31d)
(b) Terzaghi and Peck's diagram for dense sand (Fig. 17.31b)
(c) Tschebotarioff's diagram (Fig. 17.31c)

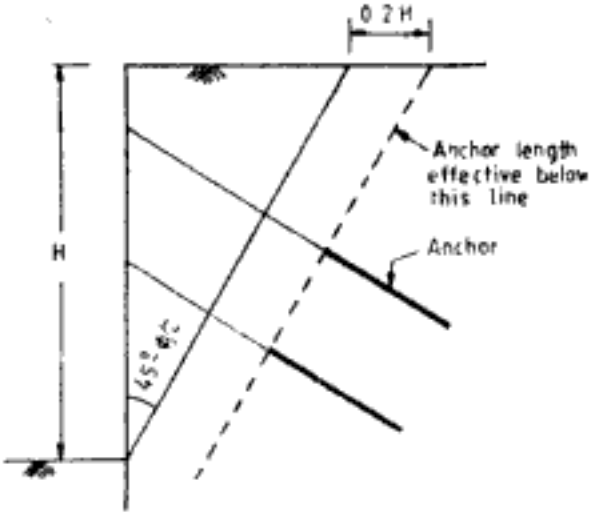

Fig. 17.37 Effective anchorage in tie-back bracing system

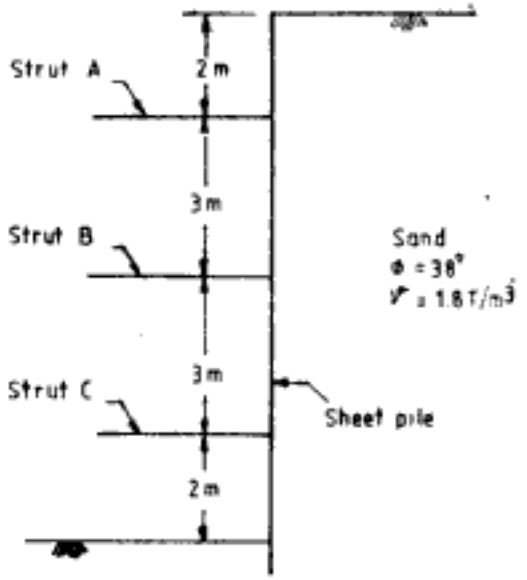

Fig. 17.38 Q 17.16

Solution by tributary area method using Peck, Hanson and Thornburn's diagram

$$K_a = 0.238$$

The uniform pressure over the depth of sheet pile is

$$= 0.65 \times 1.8 \times 10 \times 0.238 = 2.785 \text{ T/m}^2$$

The diagram for analysis of strut loads is shown in Fig. 17.39 from which,

$$P_A = 2.785 \times 3.5 = 9.75 \text{ T/m}$$
$$P_B = 2.785 \times 3 = 8.36 \text{ T/m}$$
$$P_C = 2.785 \times 2.5 = 6.96 \text{ T/m}$$
$$P_S = 2.785 \times 1 = 2.785 \text{ T/m}$$

Depending on the spacing of struts along the length of excavation the load per strut can be computed as,

Load per strut = load on strut per unit length × spacing of struts

Solution by equivalent beam method using Peck, Hanson and Thornburn's diagram

Figure 17.40 gives the analysis for strut loads using equivalent beam method. From analysis it can be shown that,

$$P_A = 11.6 \text{ T/m}$$
$$P_{B1} = 2.32 \text{ T/m}$$

Hidden page

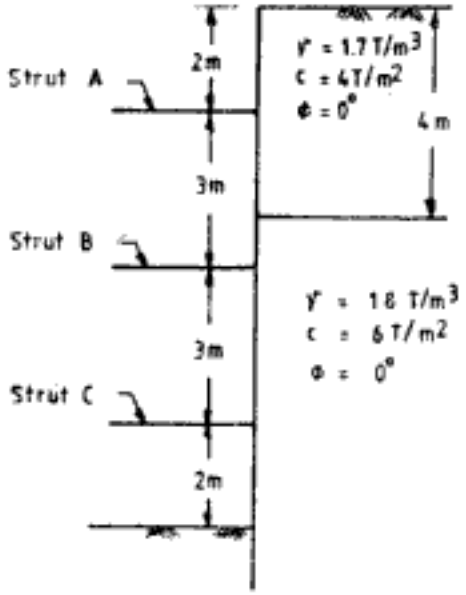

Fig. 17.41 Q 17.17

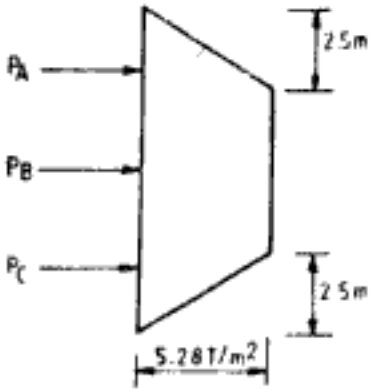

Fig. 17.42 Peck, Hanson, and Thornburn's pressure diagram for Q 17.17

undrained strength below base, $c_b = 6$ T/m²

$$\frac{\gamma H}{c_b} = \frac{1.76 \times 10}{6} = 2.93 < 6 \quad \text{O.K.}$$

Since, $\frac{\gamma H}{c} = \frac{1.76 \times 10}{5.2} = 3.38 < 4$, Peck, Hanson, and Thornburn's diagram (Fig. 17.32c) can be used.

$$0.3\gamma H = 0.3 \times 1.76 \times 10 = 5.28 \text{ T/m}^2$$

The pressure diagram is as shown in Fig. 17.42. The diagram can be analysed by tributary area method and equivalent beam method as explained in Q 17.16. The results of the analysis are shown in Table 17.4.

Table 17.4 Forces on Struts for Q 17.17

Force	Tributary area method T/m	Equivalent beam method T/m
P_A	11.88	12.83
P_B	15.84	14.88
P_C	10.82	10.48
P_S	1.06	1.41

Q 17.18: Instead of horizontal struts in Q 17.16, inclined struts at an inclination of 35° to horizontal are used. Horizontal kicker blocks of 1 m width embedded 1 m deep in soil provide reaction to the struts. Investigate the stability of kicker block for inclined strut *A*.

Ans: $D/B = 1$

From Fig. 17.36c, for $\alpha = 35^\circ$ and $\phi = 38^\circ$, $N_{\gamma q} \simeq 40$

From Eq. 17.68, $q_{ult} = \frac{1}{2} \times 1.8 \times 1 \times 40 = 36$ T/m²

Ultimate load, $q_{ult} = 36 \times 1 = 36$ T/m

From a perusal of Table 17.3, an average value of horizontal load of 10 T/m for strut A is chosen.

$$\text{Axial load in inclined strut, } R = \frac{10}{\cos 35} = 12.2 \text{ T/m}$$

$$\text{Factor of safety for kicker block} = \frac{36}{12.2} = 2.95 \quad \text{O.K.}$$

Q 17.19: In Q 17.17 instead of horizontal struts inclined struts are used. The struts are inclined at 35° to horizontal. 2 m wide kicker blocks embedded 2 m deep in soil provide reaction to the struts. Investigate the stability of kicker block for inclined strut A.

Ans: $D/B = 2/2 = 1$

From Fig. 17.36a, for $\alpha = 35^\circ$, $N_{cq} = 3$

From Eq. 17.67, $q_{ult} = 6 \times 3 = 18$ T/m²

Ultimate load, $Q_{ult} = 18 \times 2 = 36$ T/m

From Table 17.4 an average value of 12 T/m can be chosen for the horizontal load on strut A.

$$\text{Axial load in inclined strut, } R = \frac{12}{\cos 35} = 14.65 \text{ T/m}$$

$$\text{Factor of safety for kicker block} = 36/14.65 = 2.46 < 3 \quad \text{not O.K.}$$

The width of kicker block should be increased.

17.3.4 Some Other Considerations in Braced Cuts

For cuts in sands below water level, it is necessary to lower the water level both in the excavation and behind the sheet pile for stability of the bracing system. If water level is lowered only in the excavation and not behind the sheet pile, the resulting upward flow of water into excavation from behind sheet pile will cause quick condition in sand. The sheet piles will then become unstable.

In clays, if soil is soft for considerable depth below excavation level, driving of sheet pile deep below excavation level will not have much of beneficial effect. But if a firm stratum is available at a shallow depth below excavation level driving of sheet pile into firm stratum will have significant influence in reducing the movement of soil.

If braces or struts are spaced very much apart the lateral movement of sheet pile will be excessive. The adjacent ground surface also goes down inducing a drag force on sheet pile. To prevent large lateral movements in plastic clays the vertical distance between struts should not exceed $2c/\gamma$ where c is the average undrained shearing strength of clay for a depth of about $B/2$ below the level of the preceding strut and B is the width of the cut.

18

STABILITY OF EARTH SLOPES

Slopes can be natural or man-made. Slopes can be formed by addition of material on natural soil, like construction of earth dams and embankments. Or slopes can be formed by removal of material, like excavation in road/railway construction, for basement construction, etc. The slope in its final position must remain stable. The stability of slopes is governed by several factors which differ from case to case. For example, the stability of an embankment slope and that of a slope in an excavation will have to be analysed from different considerations. The conditions which govern the stability of the upstream slope of an earth dam are different from the conditions which govern the stability of the downstream slope of the same earth dam. Therefore, the various methods for the analysis of stability of slopes is presented first. The use of appropriate method for typical situations is discussed subsequently.

18.1 INFINITE SLOPES

18.1.1 Dry or Submerged Sand Slopes

Figure 18.1 shows a submerged infinite sand slope. Evidently, as the angle of inclination, i, becomes more and more the slope tends to become unstable. In cases of both dry and submerged infinite sand slopes, the slope becomes unstable when $i > \phi$. The failure surface is parallel to the slope and a thin mass of material starts sliding down. The thickness of the unstable mass is small compared to thickness of sand. The factor of safety (F) in infinite slopes in sand is defined as,

$$F = \frac{\tan \phi}{\tan i} \tag{18.1}$$

Fig. 18.1 Infinite sand slope

In practice F can be determined with $\phi = \phi_r$ where ϕ_r is the residual angle of shearing resistance and $F = 1$ will be adequate.

18.1.2 Infinite Sand Slope with Seepage Parallel to Slope

Seepage as shown in Fig. 18.2 can occur near the toe of natural slopes. The flow generally tends to reduce stability. Factor of safety in this case is given by,

$$F = \frac{\gamma_b}{\gamma_t} \frac{\tan \phi}{\tan i} \tag{18.2}$$

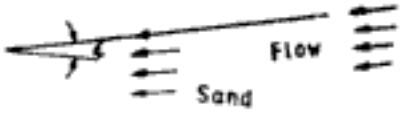

Fig. 18.2 Seepage in infinite sand slope

That is, when there is flow parallel to the slope, the stable slope angle is nearly reduced to half its value without flow.

18.1.3 Infinite Slopes in Clay

When there is no seepage but the slope is submerged as in Fig. 18.1, then at the instant of failure,

$$\frac{\bar{c}}{\gamma_b H_c} = \cos^2 i \, (\tan i - \tan \bar{\phi}) \tag{18.3}$$

where, H_c is the depth measured vertically to failure plane.
And if there is seepage parallel to the slope (Fig. 18.3),

$$\frac{\bar{c}}{\gamma_t H_c} = \cos^2 i \left(\tan i - \frac{\gamma_b}{\gamma_t} \tan \bar{\phi} \right) \tag{18.4}$$

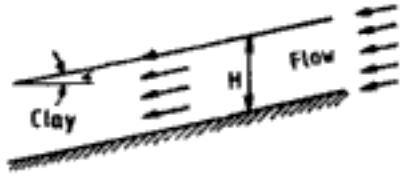

Fig. 18.3 Infinite clay slope

Equations 18.3 and 18.4 are useful where clay overlies firm stratum at a shallow depth. Unlike sand, in clay inclination of slope can be more than angle of shearing resistance of soil, $\bar{\phi}$, provided the depth of soil is less than the critical value H_c.

Hidden page

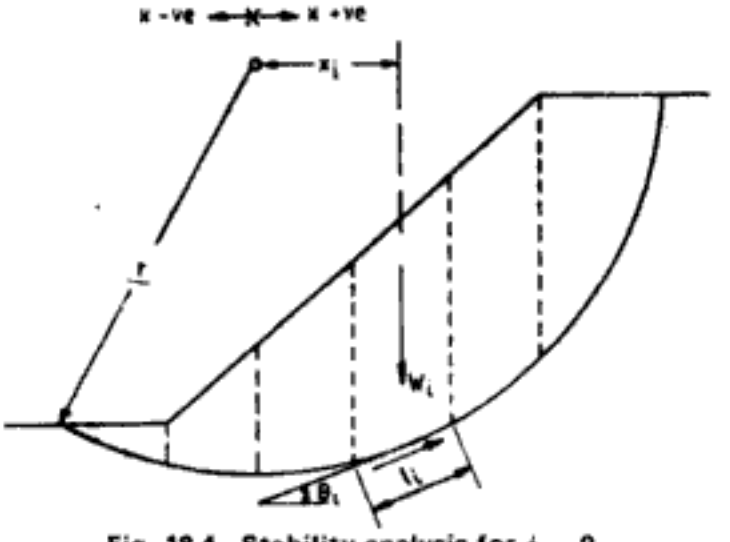

Fig. 18.4 Stability analysis for $\phi = 0$

Step 4: Determine the moment arm of weight of each slice to the centre of the circular arc. The moment arm will be positive to the right and negative to the left of centre for conditions shown in Fig. 18.4 (x_i is the moment arm of ith slice).

Step 5: Compute the moment due to weight of each slice about the centre of the circular arc and find the sum of moments for all slices. This gives the total disturbing moment. In Fig. 18.4, $W_i x_i$ is the moment for ith slice and $\sum_{i=1}^{n} W_i x_i$ is the total disturbing moment.

Step 6: Determine the maximum available shear resistance at the base of each slice. When $\phi = 0$ either c_u (undrained cohesion) or S_u (undrained strength) can be used. $c_{ui} l_i$ ($= S_{ui} l_i$) is the resistance for ith slice.

Step 7: Compute the moment due to shear resistance of each slice about the centre of arc and find the sum, for all slices. This gives the total resisting moment. $c_{ui} l_i r$ is the resisting moment for ith slice.

Step 8: Find the factor of safety from definition,

$$F = \frac{\text{total resting moment}}{\text{total disturbing moment}} \tag{18.5}$$

that is,

$$F = \frac{r \sum_{i=1}^{n} c_{ui} l_i}{\sum_{i=1}^{n} W_i x_i} \tag{18.6}$$

If the shear strength of soil is constant,

$$F = \frac{r c_u R_a}{\sum_{i=1}^{n} W_i x_i} \tag{18.7}$$

where, R_a is the length of the failure arc. It can be noted that $x_i = r \sin \theta_i$, from Fig. 18.4 where θ_i is the inclination of the base of the slice. In terms of θ_i, Eq. 18.6 can be written as,

$$F = \frac{\sum_{i=1}^{n} c_{ui} l_i}{\sum_{i=1}^{n} W_i \sin \theta_i} \tag{18.8}$$

For several trials of failure surface the factor of safety can be computed from which the minimum factor of safety and the corresponding failure surface can be obtained. The nearest approach to the true factor of safety is given by the lowest value of F obtained with any circular arc. The method explained so far does not take into account the possibility of occurrence of tension crack or any other external loading on the slope. But these also can be easily accounted for by adding their respective component to disturbing or resisting moment in the equation for factor of safety. When there is a tension crack the failure arc is terminated at the bottom of the tension crack as shown in Fig. 18.5. The height of tension crack, z_c, is given by,

$$z_c = \frac{1.33c_u}{\gamma_t} \tag{18.9}$$

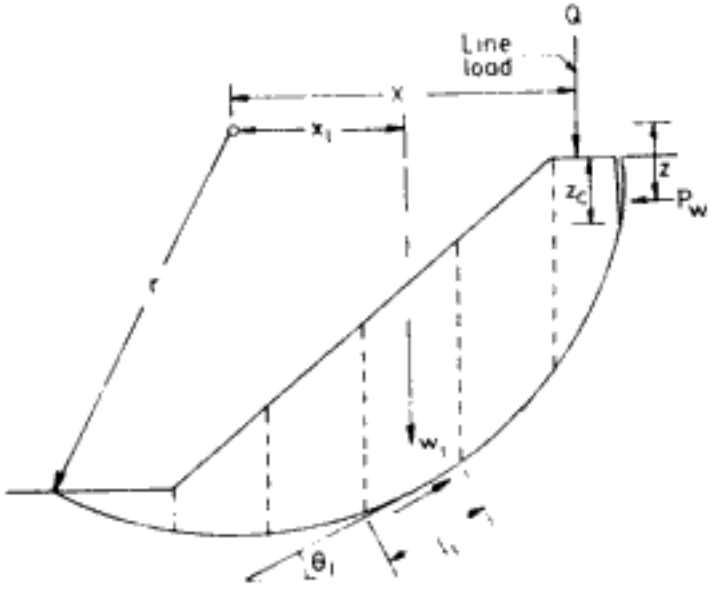

Fig. 18.5 Slope with tension crack and external loading

P_w is the hydrostatic pressure which may be exerted by water in the tension crack. P_w has a moment arm of z with respect to centre of failure arc. There is a line loading of Q per unit length at the top of the slope with a moment arm of x. P_w and Q both contribute to disturbing moment. Under these conditions, factor of safety is given by,

$$F = \frac{r \sum_{i=1}^{n} c_{ui} l_i}{\left\{\sum_{i=1}^{n} W_i x_i\right\} + QX + P_w z} \tag{18.10}$$

Likewise any other loading on the slope can be considered in the determination of factor of safety.

Q 18.2: The height of a clay slope is 12 m and has a slope of 1 : 1.5 (1 vertical to 1.5 horizontal). The undrained strength of soil is 6 T/m^2. The total and submerged densities are 1.9 T/m^3 and 0.9 T/m^3 respectively. The depth of water at the toe is 4 m. Determine the factor of safety of the slope for the failure surface shown in Fig. 18.6 under undrained conditions.

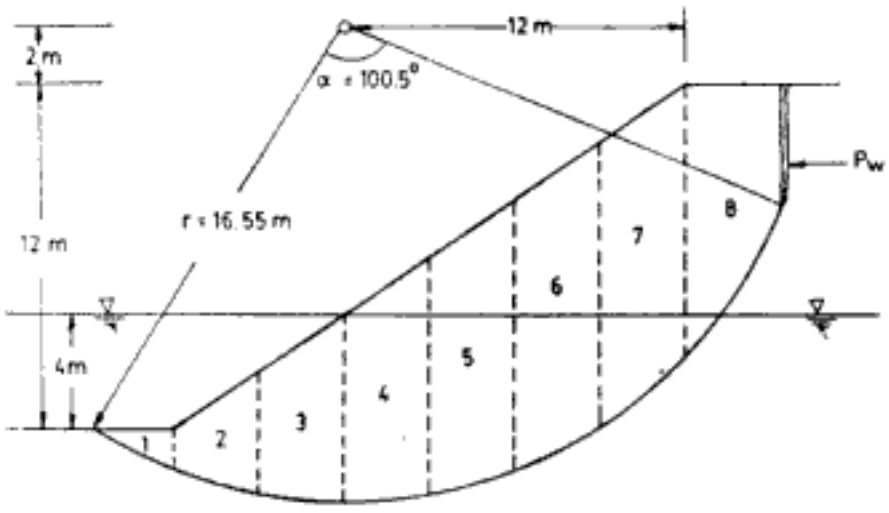

Fig. 18.6 Q 18.2

Ans: Tension crack will be assumed to occur and the depth of tension crack z_c is given by Eq. 18.9.

$$z_c = \frac{1.33 \times 6}{1.9} = 4.2 \text{ m}$$

The failure surface is divided into eight slices as shown in Fig. 18.6. Calculated values of weight and moment of each slice are given in Table 18.1. In the calculation of weight submerged unit weight is taken below water level for all slices. In the determination of moment arm the weight of trapezoidal slice is assumed to act in the middle of the slice. The error due to this assumption can be minimised by considering thinner slices in analysis.

Table 18.1 Calculations for Q 18.2

Slice No. i	Weight of slice W_i (T/m)	Moment arm of slice, x_i (m)	Moment $W_i x_i$ (T m/m)
1	1.890	−6.93	−13.0977
2	7.830	−4.50	−35.2350
3	14.715	−1.50	−22.0725
4	23.115	1.50	34.6725
5	32.895	4.50	148.0275
6	41.055	7.50	307.9125
7	47.055	10.50	494.0775
8	45.368	13.70	621.5416
			Σ = 1535.8264

Water pressure, P_w, in the tension crack $= \frac{1}{2} \times 1 \times 4.2^2$

$= 8.82$ T/m

Moment arm for $P_W = 2 + \frac{2}{3} \times 4.2$

$= 4.8$ m

Moment due to $P_W = 8.82 \times 4.8$

$= 42.336$ T m/m

Total disturbing moment $= 1535.8264 + 42.336 = 1578.1624$ T m/m

Length of failure surface, $R_a = \frac{\pi \times 16.55 \times 100.5}{180} = 29.03$ m

Total resisting moment $= 6 \times 29.03 \times 16.55 = 2882.679$ T m/m

Factor of safety $= \frac{2882.679}{1578.1624} = 1.83$

2. *Taylor's stability numbers*

For simple slopes of uniform undrained strength (c_u or S_u) the factor of safety can be quickly evaluated using Taylor's stability chart shown in Fig. 18.7.

Taylor (1948) defines stability number N as,

$$N = \frac{c_u}{F\gamma_t H} \tag{18.11}$$

The value of N for failure surface depends on depth to hard stratum. The distance between toe of slope and toe of failure surface is expressed in terms of coefficient n. In Fig. 18.7a for Case A the full lines of the chart must be used and for Case B the lower broken lines must be used. The diagonal broken lines give values of n.

When depth to hard stratum is very large ($D \to \infty$) value of N is same for all values of slope inclination less than 54° (Fig. 18.7b) and is equal to 0.181.

If the slope inclination is greater than 54° all critical failure surfaces pass through the toe of the slope, and the stability number does not depend on D but only on i. Values of N can be obtained from Fig. 18.7b or Table 18.2.

Table 18.2 Values of N for $i > 54°$

i	60°	65°	70	75°	80°	85°	90°
N	0.191	0.199	0.208	0.219	0.232	0.246	0.261

Taylor's stability charts are based on friction circle method using total stress analysis. They must be used only for $\phi = 0$ case. The charts are valid only for geometrically similar failure surfaces. Hence, presence of tension crack will have to be ignored. Only two cases as shown in Fig. 18.7a can be analysed using the charts.

Q 18.3: Determine the stability of slope in Q 18.2 when there is no water at the toe. Assume no tension cracks. Find the factor of safety using Taylor's stability chart when the depth to hard stratum is (a) very large ($D \to \infty$), and (b) twice the height of slope ($D = 2$).

Ans: $i = \tan^{-1} \frac{1}{1.5} = 33.69°$

(a) When D is large, $N = 0.181$

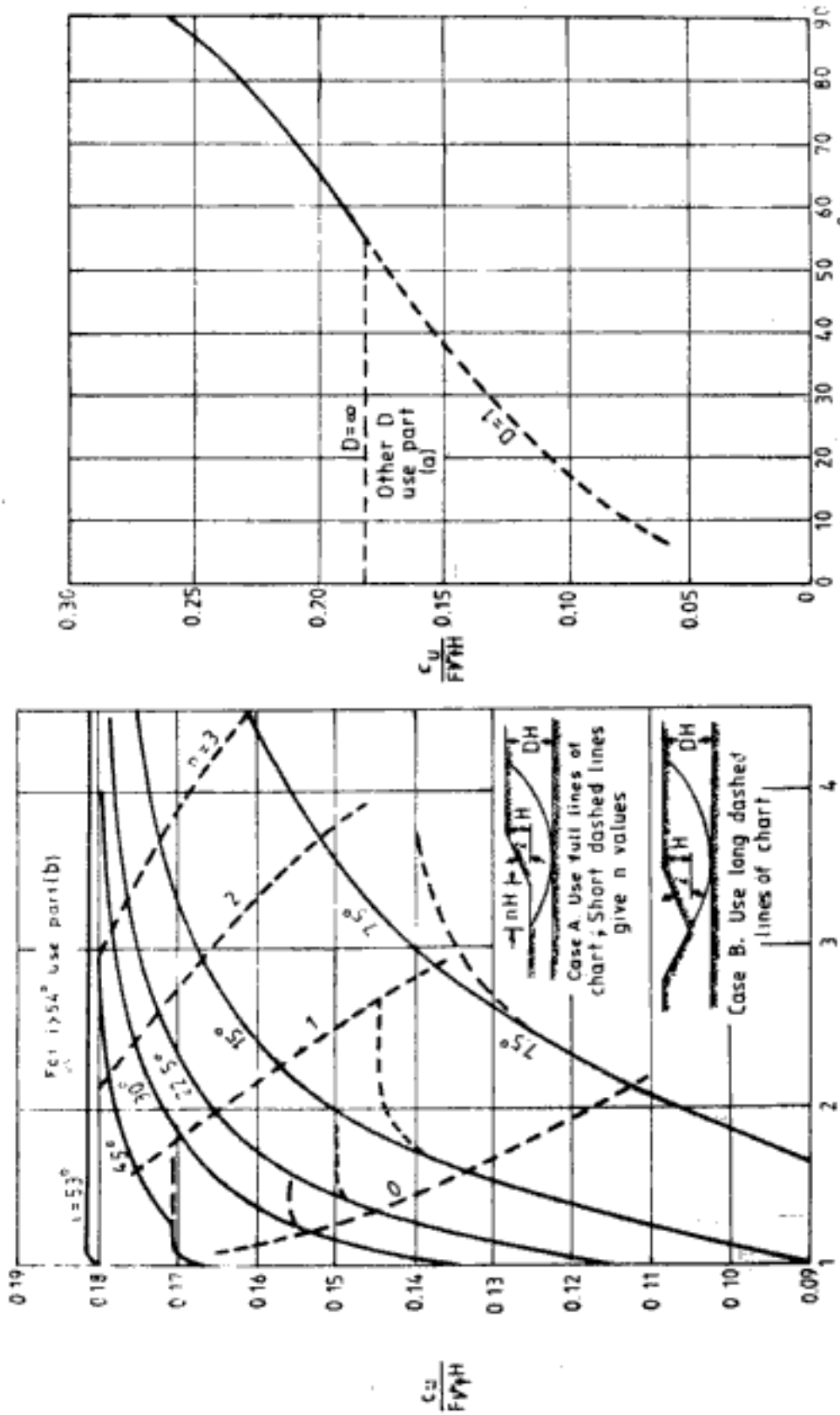

Fig. 18.7 Stability charts for $\phi = 0$ (After Taylor, 1948; with permission of John Wiley and Sons, Inc., New York)

Hidden page

the following equation,

$$\tau = \frac{\tau_f}{F} = \frac{c}{F_c} + \frac{\sigma \tan \phi}{F_\phi} \tag{18.12}$$

where τ = shear stress

τ_f = shear stress at failure or shear strength

F_c and F_ϕ are factors to be determined by trial and error such that $F = F_c = F_\phi$. The forces to be considered in the friction circle method are shown in Fig. 18.8a. The forces are:

(a) The weight of the soil in failure zone, W.

(b) The hydrostatic force P_W due to water in tension crack.

S is the resultant of W and P_W.

(c) Sum of the cohesive forces parallel to chord AB along the failure surface. This is designated by C and given by,

$$C = \frac{c}{F_c} \times \text{length of chord } AB \tag{18.13}$$

Value of C is not known but its direction (parallel to AD) and location are known. C acts at a distance L from the centre of the circular arc. L is given by,

$$L = r \frac{\text{length of arc } AB}{\text{length of chord } AB} \tag{18.14}$$

(d) The resultant of frictional forces along the failure surface, R. Value of R is not known but its direction and position are known. R passes through the intersection of forces S and C. R is also tangential to a circle drawn with centre as 0 and radius as $r \tan \phi$. This circle is called *friction circle*. ϕ is obtained from,

$$\tan \phi = \frac{\tan \phi}{F_\phi} \tag{18.15}$$

The force polygon for the set of forces is given in Fig. 18.8b. The following are the steps in the use of friction circle method.

Step 1: For a chosen failure surface determine the value and location of W and P_W. Determine the point of intersection of their resultant S with the known line of action of C

Step 2: Assume the value of F_ϕ. From Eq. 18.15 determine $\tan \phi$. Draw a circle at 0 with radius $r \tan \phi$. The direction of R can then be established.

Step 3: Draw the force polygon as in Fig. 18.8b from which value of C can be determined. From Eq. 18.13 calculate the value of F_c.

Step 4: If $F_c \neq F_\phi$ repeat steps 2 and 3 with new value for F_ϕ until F_c and F_ϕ are equal.

Step 5: Repeat Steps 1 to 4 for different failure surfaces to get the minimum factor of safety of the slope.

Q 18.5: Re-do Q 18.2 by friction circle method if $c = 4$ T/m^2 and $\phi = 16°$. Other data remain the same.

Ans: Tension crack is assumed to develop. Depth of crack is,

$$z_c = 1.33 \times 4/1.9 = 2.8 \text{ m}$$

Water pressure in tension crack is,

$$P_W = \tfrac{1}{2} \times 1 \times 2.8^2 = 3.92 \text{ T/m}$$

Figure 18.9 gives the failure surface in which $W = 212.597$ T
Length of chord $AB = 26.4$ m

$$\text{Length of arc } AB = \frac{\pi \times 16.55}{180} \times 105 = 30.33 \text{ m}$$

C acts parallel to chord AB at L from centre of arc,

$$L = 16.55 \times \frac{30.33}{26.4} = 19.01 \text{ m}$$

Let $F_\phi = 1.8$

$$\tan \psi = \frac{\tan 16^\circ}{1.8} = 0.1593$$

from which, $\sin \psi = 0.1573$

radius of friction circle is $= 16.55 \times 0.1573 = 2.6$ m

Figure 18.9 shows the location and direction of forces and the force polygon.

$$C = 51 \text{ T/m}$$

$$F_c = \frac{4 \times 26.4}{51} = 2.07$$

With the next assumption for $F_\phi = 1.95$ the analysis can be repeated.

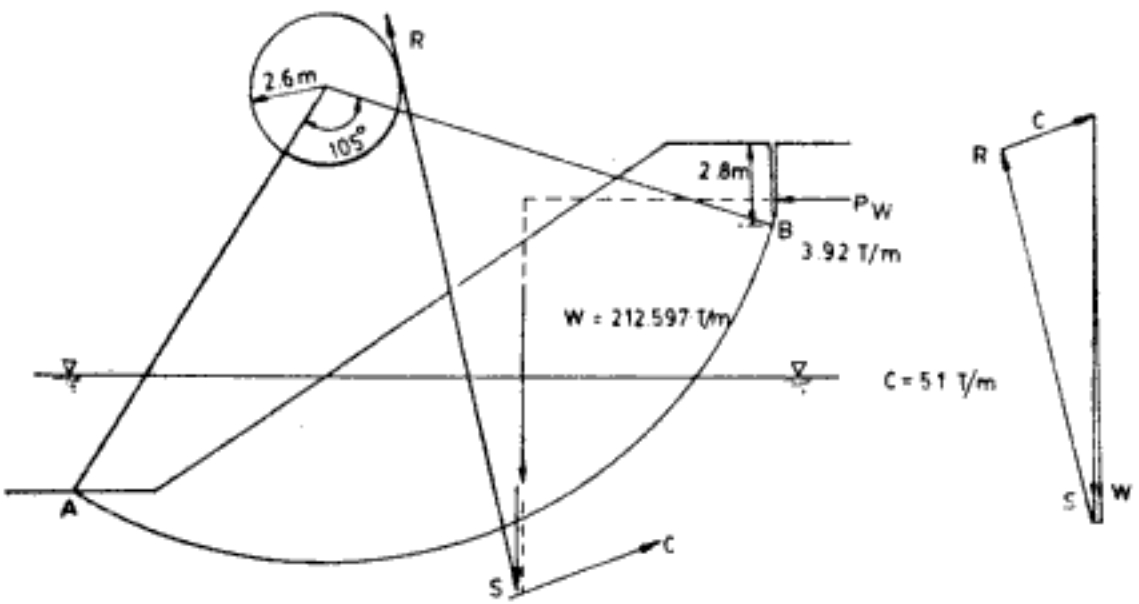

Fig. 18.9 Q 18.5

18.2.2 Effective Stress Method

Friction circle described for total stress method can be adapted for effective stress analysis also. However the most common method of effective stress analysis is the *method of slices.* In this method, the failure zone above circular arc is divided into a number of vertical slices

Hidden page

Hidden page

Hidden page

Trial and error procedure is required to evaluate F by simplified Bishop's method. A trial value of F is chosen and used to determine values of M_θ in Eq. 18.21. With these values of M_θ, F is determined from Eq. 18.20. If the two values of F are significantly different, a new value of F is chosen and the procedure is repeated. The convergence is rapid and fairly accurate results can be obtained in two or three iterations. M_θ can be also determined from Fig. 18.13 which represents Eq. 18.21.

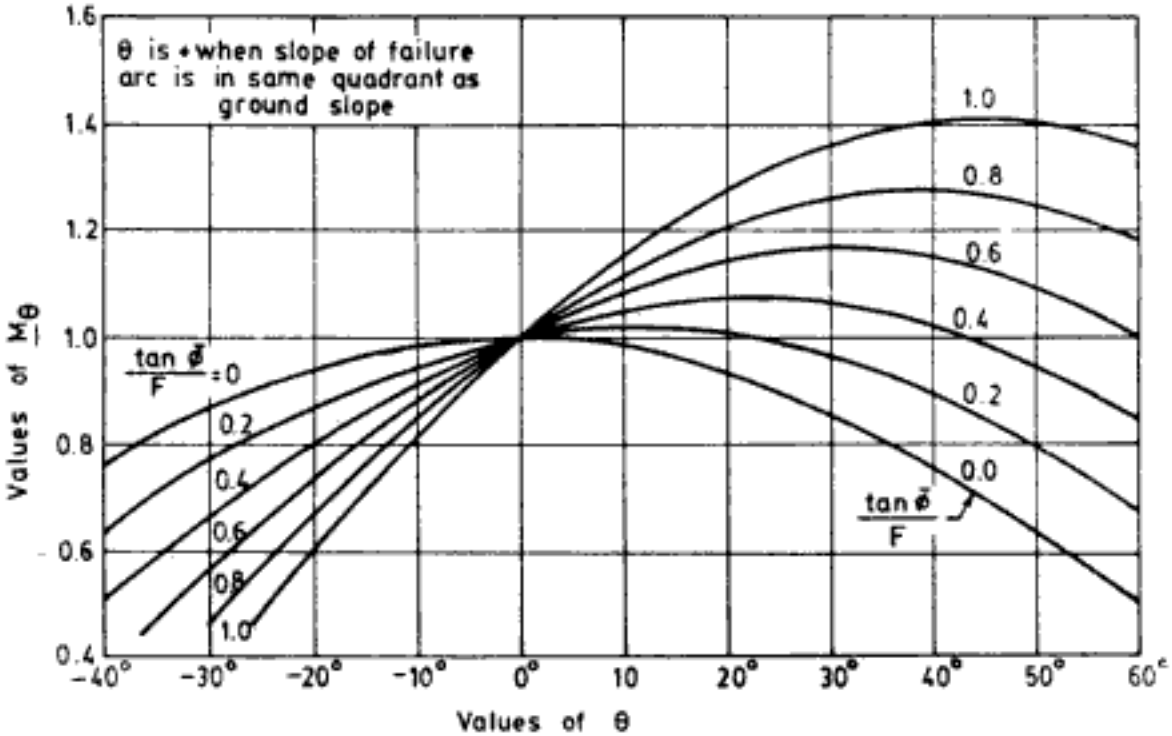

Fig. 18.13 Graph for determination of M_θ (After Janbu *et al.*, 1956; with permission of Norwegian Geotechnical Institute, Oslo)

Simplified Bishop's method yields results which are fairly accurate and adequate enough for practical purposes. Hence, this method is commonly used in slope stability analysis. Q 18.7 presents an example of analysis using Bishop's simplified method.

(c) *Bishop and Morgenstern's effective stress stability coefficients*

Bishop and Morgenstern (1960) developed effective stress stability coefficients similar to Taylor's stability numbers for total stress analysis. These coefficients, namely, m and n are presented in Fig. 18.14. The factor of safety is defined as,

$$F = m - nr_u \tag{18.22}$$

where r_u for a slice is defined as,

$$r_u = \frac{ub}{W} \tag{18.23}$$

The factor of safety is not sensitive to value of D (for D see Fig. 18.7) and m, n values are shown for $D = 1$, 1.25, and 1.5.

F also varies linearly with $\bar{c}/\gamma H$ and with r_u. The following is the procedure of determining F using the stability coefficients.

Hidden page

Hidden page

Hidden page

Hidden page

Hidden page

Hidden page

Hidden page

If drawdown is fast and time taken to reach new equilibrium is long, effective stress method can be used with pore water pressures calculated according to Bishop's (1954) equations. Alternatively, total stress method can be used using undrained strength evaluated according to procedure suggested by Lowe and Karafiath (1960).

If drawdown is slow and time to reach new equilibrium is small then the condition immediately after drawdown is critical. Effective stress method must be used for stability analysis using pore water pressure determined from flow net for transient conditions.

2. *Excavation slopes*

The excavation slopes should be analysed for two situations explained below:

(a) The stability of the slope, immediately after excavation, must be analysed by total stress method.

(b) For long-term stability effective stress method must be used. Pore water pressure must be estimated by the natural groundwater elevations at the site.

Immediately after excavation the slopes are generally stable because of presence of negative pore water pressure. But, over time the pore water pressure increases, effective stress decreases, and the soil may also deteriorate. Thus, for excavation slopes long-term stability is usually the controlling factor.

18.2.4 Determination of Minimum Factor of Safety

The minimum factor of safety of a slope is determined by trial and error process. For several possible failure surfaces the factor safety is computed using an appropriate procedure. The centre of the failure arc is chosen in grid-like fashion as shown in Fig. 18.16. The factor of safety for failure surfaces is marked against respective grid points. From these grid values, contours of equal factor of safety can be drawn. Figure 18.16 shows contours for $F = 1.7$, and $F = 1.6$. From this the centre of failure arc for minimum factor of safety can be

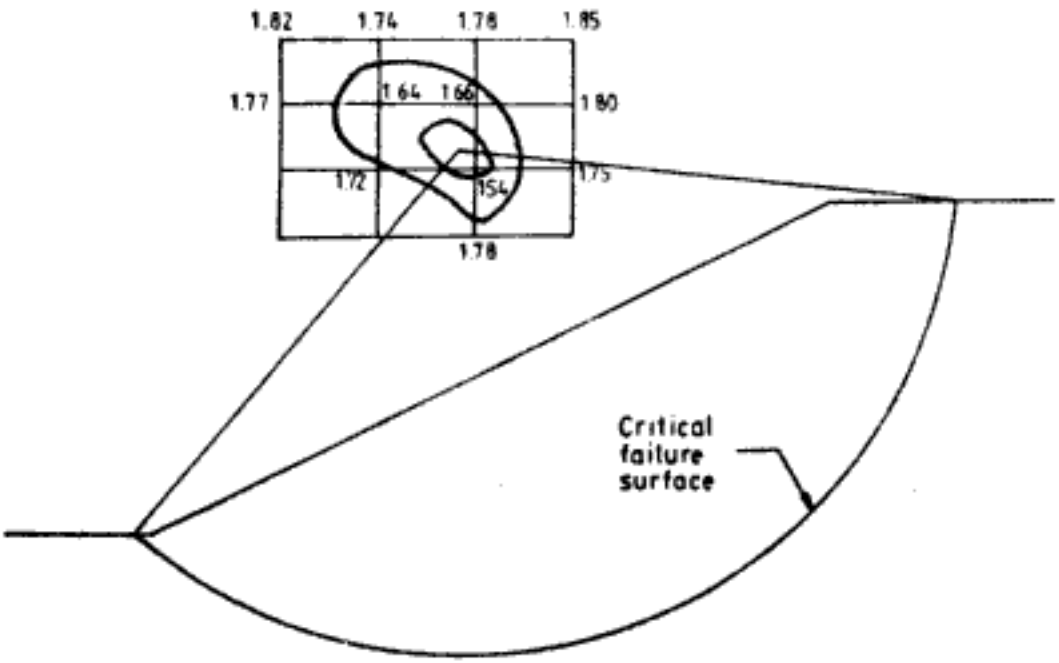

Fig. 18.16 Determination of minimum factor of safety for a slope

located. Drawing the failure arc the minimum factor of safety can be computed or can be approximated from the contours drawn with the grid values.

18.2.5 Analysis of Three-Dimensional Slopes

The methods explained so far treat the stability of one particular cross-section of two-dimensional slopes. For three-dimensional slopes no rigorous procedure is available. Approximate procedures must be used. Figure 18.17a shows the plan view of a three-dimensional slope. For three typical cross-sections of the slope A–A, B–B, and C–C, their respective minimum factors of safety are determined. The overall factor of safety of the three-dimensional slope is given by,

$$F = \frac{F_1A_1 + F_2A_2 + F_3A_3}{A_1 + A_2 + A_3} \tag{18.24}$$

where F_1, F_2, F_3 = minimum factor of safety of cross-sections A–A, B–B and C–C, respectively.

A_1, A_2, A_3 = weight of soil in the failure zone in cross-sections A–A, B–B and C–C, respectively

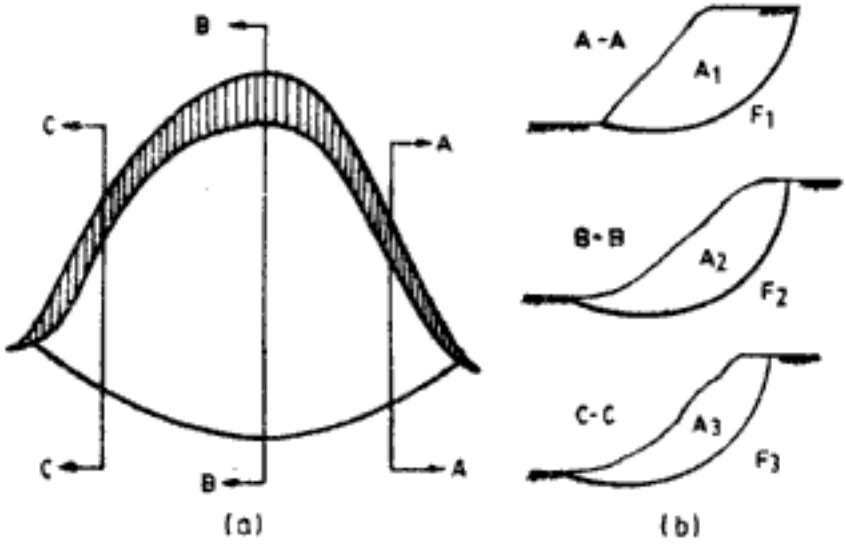

Fig. 18.17 (a) Plan view of three-dimensional slope and (b) cross-sectional views through sections A–A, B–B, and C–C

18.2.6 Wedge Method

Circular arc like failure surfaces may not be reasonable assumption when slopes lie over firm strata or over weak planes. A typical situation is shown in Fig. 18.18 with the earth slope on a firm strata and having a sloping clay core. Another example is a natural soil slope lying on inclined rock material. In such situations failure surface can be approximated by two or three segments of straight lines and the soil in the failure zone can be considered in the form of two or three slices or wedges. Figure 18.18 shows two wedges, namely, ABE and $BCDE$. AB and BC are the straight line failure surfaces. Fairly accurate results can be

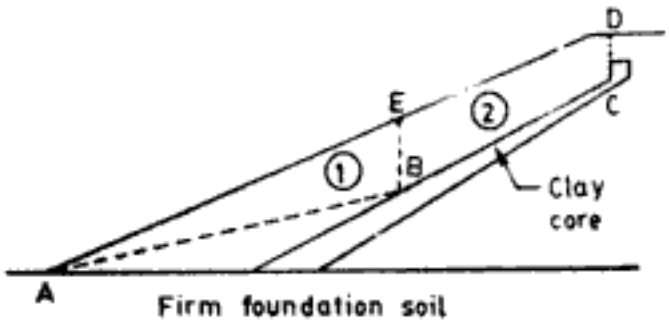

Fig. 18.18 Wedge method of analysis

obtained by considering the equilibrium of the assumed wedges. Figure 18.19 shows the forces acting on the two slices. The different forces are,

W_1, W_2 = weight of the slices
T_1, T_2 = shear forces on failure surfaces
N_1, N_2 = total normal forces on failure surfaces
$\bar{N}_1, \bar{N}_2$ = effective normal forces on failure surfaces
U_1, U_2 = forces due to pore water pressure
U_0 = interslice forces due to pore water pressure
$\bar{P}$ = interslice effective forces

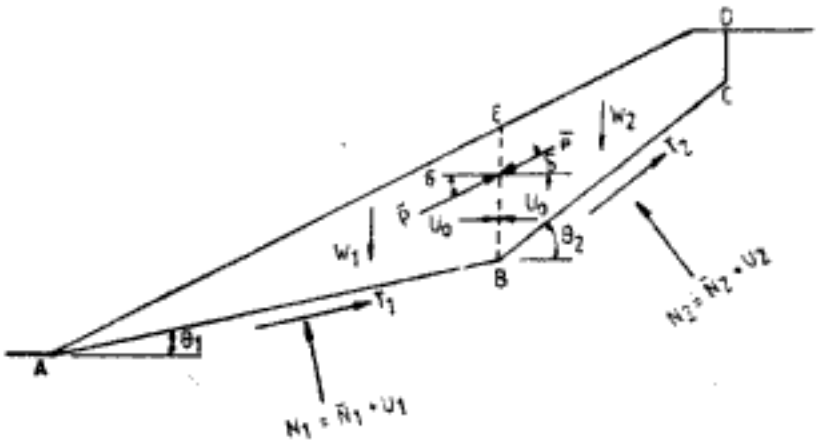

Fig. 18.19 Forces on wedges

To determine the factor of safety for the two slices approximation in Fig. 18.19 the following two equations are set up.

$$\frac{1}{F}\frac{\bar{c}_1 l_1 + (W_1 \sec\theta_1 - U_1 + \bar{P}\sin\delta)\tan\bar{\phi}}{M_{\theta 1}} = (W_1 + \bar{P}\sin\delta)\tan\theta_1 - \bar{P}\cos\delta - U_0 \tag{18.25}$$

$$\frac{1}{F}\frac{\bar{c}_2 l_2 + (W_2 \sec\theta_2 - U_2 - \bar{P}\sin\delta)\tan\bar{\phi}}{M_{\theta 2}} = (W_2 - \bar{P}\sin\delta)\tan\theta_2 + \bar{P}\cos\delta + U_0 \tag{18.26}$$

In Eqs 18.25 and 18.26 M_ϕ is defined by Eq. 18.21. In the two equations the unknowns are F, $\bar{P}$, and δ. Hence, in order to solve the two equations to determine F, generally the value of δ is assumed. Common assumptions for δ are,

$$\tan \delta = \frac{\tan \bar{\phi}}{F} \tag{18.27}$$

and

$$\delta = \text{inclination of slope} \tag{18.28}$$

Factor of safety computations differ very little if either assumption is made. From the form of Eqs 18.25 and 18.26 it is evident that F has to be determined by reiterative procedure as in the case of simplified Bishop's method.

19

SUBSURFACE INVESTIGATION

The nature and extent of subsurface investigation depends upon the ultimate use to which the results of the investigation will be applied. For example, for structures which transmit heavy load on the soil, the aim of subsurface investigation is to provide data which will help in the selection of proper types of foundation, in the determination of location of foundations and in the design of foundations. In highway construction the aim of subsurface investigation may vary from one place to another such as from determining the suitability of soil as construction material to getting data for design of foundations for structures like bridges. For earth dams, subsurface investigation is needed to determine the hydraulic characteristics of the foundation material and to assess the suitability of soil as construction material. The discussions in this chapter, however, are mostly on subsurface investigation for load transmitting structures.

The subsurface investigation can be conducted in the following three phases:

1. Reconnaissance survey
2. Preliminary exploration
3. Datailed exploration

In *reconnaissance survey* no exploratory field observations are carried out but the general details regarding the site are collected from published literature such as journals, reports, geological maps, soil survey maps prepared for agricultural purposes, highway construction purposes, etc. The engineers and consultants usually visit the site to familiarise themselves with the terrain and its geological features. Information is collected locally by examining the structures in the nearby area, by talking to local residents regarding their experience with the soil, and by observing the water level in the wells.

In the *preliminary exploration* stage a few boreholes may be selectively sunk at the site to know the soil profile and the depth to bed rock. A few soil samples are also collected for laboratory testing. For relatively light and unimportant structures decisions can be based on the information available at this stage itself. Whereas, for important structures the information helps to establish the feasibility of using the site and to plan the detailed exploration programme.

Depending on the information available from preliminary exploration stage and the details of the structure, a *detailed exploration* programme is designed and carried out. A fairly

large number of boreholes are drilled from which representative and undisturbed soil samples are collected for laboratory testing. Some field tests are also carried out. These operations are explained in detail in the sections to follow. The conditions where the detailed soil exploration tends to be very elaborate and the conditions where it is not so elaborate is explained in Table 19.1. The total activities to be performed in the completion of a subsurface investigation programme are shown schematically in Fig. 19.1.

Table 19.1 Detailed Soil Exploration

Detailed soil exploration is limited where	Detailed soil exploration is very elaborate where
1. The soil deposit is very erratic. In this case the final design will be conservatively based on the properties of poor soils.	1. The soil deposit is uniform. A systematic analysis of the behaviour of soil under foundation loads is possible here.
2. The structure is relatively unimportant and inexpensive. Associated losses due to failure of structure are small.	2. The structure is very important and expensive. Associated losses due to failure of structure are very high.
3. Good experience with soil similar to the one at the site exists. Data regarding soil are already available.	3. Experience regarding the soil at site is lacking. Very little data are available about the soil.
4. The structure transmits very light loads on the soil.	4. The structure transmits very heavy loads on the soil.
5. It is possible to place the structure on sound rock available at reasonable depth.	5. It is not possible to place the structure on sound rock.

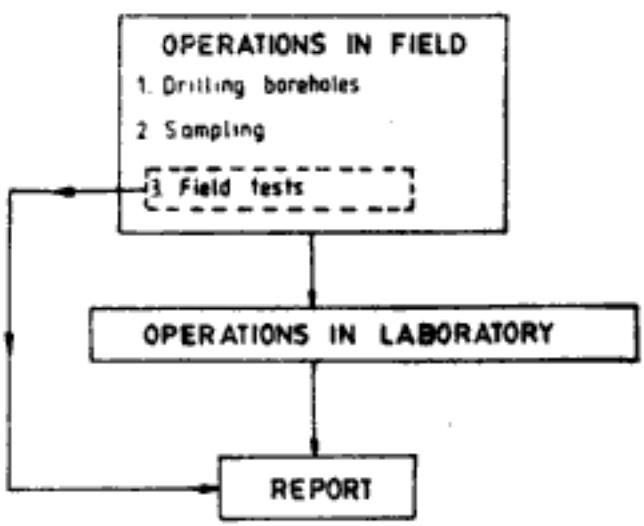

Fig. 19.1 Activities in subsurface investigation

19.1 OPERATIONS IN FIELD

19.1.1 Drilling Boreholes

A borehole is a narrow vertical shaft drilled into the ground. Borehole may be drilled manually or using power driven equipments. The common methods used in drilling a borehole are, (i) auger boring, (ii) wash boring, (iii) rotary drilling, and (iv) percussion drilling.

In auger boring the common tools used are helical auger and post-hole auger (Fig. 19.2). The auger is pressed into the soil and twisted. After the auger blades in this way are completely inserted into the soil, the auger is pulled out and the soil in the blades is removed. Extension rods can be connected to the auger to increase the reach of auger inside the borehole. This method of removal of soil to advance the borehole using auger is possible only in soils having some cohesion. In sandy soils a device called bailer is used. The bailer is a heavy cylindrical metallic barrel with a flap valve at the bottom. It is open at the top and is provided with a hook for lifting purposes. The bailer is repeatedly lifted and dropped on the soil by rope or steel wire attached to the hook. The sandy material enters into the barrel and the flap valve would not allow it to go out. The penetration of the bailer into the soil becomes easier due to increasing weight of bailer as more and more soil gets into it. When the bailer is filled with soil it is lifted up to the ground surface and emptied of soil through the top opening. While the use of bailer is essential for advancing boreholes in cohesionless material it is commonly used in cohesive soils also, frequently with bailers employed for constructing bored piles.

It is possible to use auger and bailer manually for boreholes to depth of 30 m. But the pace of drilling slows down due to the weight of extension rods connected to the auger. They are well suited for depths up to 10 m. Use of bailer to greater depths can be facilitated using power driven winches for lifting and dropping operations. Power driven flight augers are useful for fast investigations extending to depths of 60 m and more. However, these are not very commonly used in India.

The apparatus for wash boring is shown in Fig. 19.3. Up to a shallow depth the borehole is drilled using auger. Then a casing is inserted into the borehole. A chopping bit connected to drill rods is inserted. The drill rod is connected at the top to a pump through a swivel. Water is forced down through the drill pipe. The water emerges at the bottom and flows upward through the annular space between drill rods and casing, carrying along with it the soil removed by the chopping bit. The muddy water flows out through the T-connection at the top in the casing. The water is recirculated for further washing operations. Additional lengths of casing pipe and drill rod can be added whenever required.

If soil is highly resistant to augering and wash boring methods of drilling, rotary drilling can be used. In this method the fast rotating drilling bits cut and grind the soil. This soil is removed to the surface by using water or drilling fluid as explained for wash boring method.

For very hard materials like rock, percussion drilling is used. Here, a heavy drilling bit is repeatedly lifted and dropped on the hard material. The slurry which accumulates at the bottom can be removed using a bailer.

Some features common to the different methods of drilling are as below:

1. The diameter of borehole varies from 10 cm to 20 cm. However, in rock the diameter is considerably small. Larger diameter boreholes require relatively more effort and time for completion and thus are expensive.
2. The soil around the borehole may not be self-supporting and collapses in cohesionless soils. In such situations casing pipe is used in the upper reaches of borehole to provide support to soil. Bentonite slurry stabilisers can also be used. The slurry is heavier than water and has thixotropic characteristics. It also seals off the pores in soil on the surface of borehole. It is important that the level of bentonite slurry inside the borehole be maintained always above the natural groundwater level.

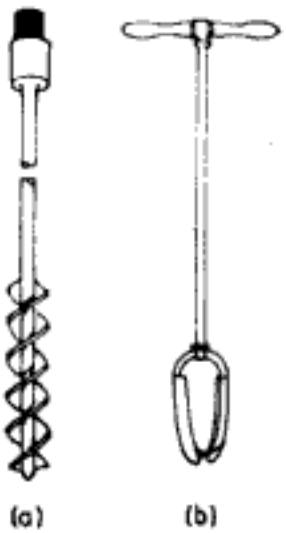

Fig. 19.2 (a) Helical auger
(b) Post-hole auger

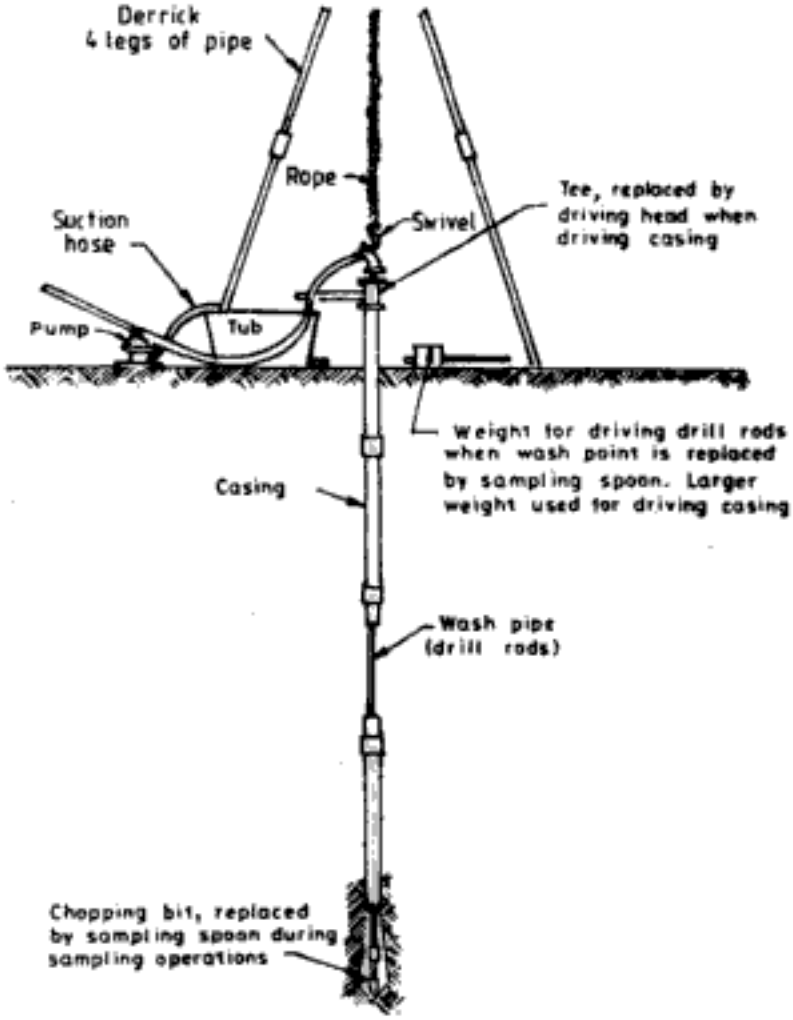

Fig. 19.3 Wash boring method of drilling borehole

3. The borehole is not drilled continuously without interruption. At several pre-identified stages and also when there is variation in subsurface soils, samples must be collected from borehole and standard penetration tests (SPT) are also to be carried out.
4. Guidelines regarding depth of boreholes are given in Table 19.2.

Table 19.2 Guidelines for Depth of Boring

1. Where possible at least one borehole must be taken down to the level of bed rock.
2. If bedrock is expected to provide support to the load at least one borehole must be drilled 3 m into bedrock to establish whether bedrock does actually exist or merely a boulder has been encountered.
3. At least one borehole should extend to a depth of twice the width of anticipated largest size foundation.
4. The boreholes should be drilled minimum to a depth beyond which the increase in stress due to foundation loading is not significant.
5. For purposes of highway and airport pavement construction the depth of exploration is in the range of 4 to 5 m.
6. The depth of exploration depends upon the extent of likely damage in the event of inadequate soil investigation and also on features that are peculiar to the site and the structure.

Hidden page

The area ratio of sampler should be less than 10 per cent. The cutting edge of the sampler is slightly smaller than the inside diameter of the sampling tube. This is meant to reduce friction between soil sample and the sampler when the soil enters the tube. The side friction will otherwise compress the soil sample. *Inside clearance ratio*, C_r is defined as,

$$C_r = \frac{D_i - D_e}{D_e} \quad 100 \tag{19.2}$$

where D_i = inner diameter of tube

If the inside clearance is very large then the soil tends to expand laterally. To prevent this, the inside clearance ratio should be between 1 and 3 per cent.

A measure of determining sample disturbance is the *recovery ratio*, L_r.

$$L_r = \frac{\text{recovered length of sample}}{\text{penetration length of sampler}} \tag{19.3}$$

L_r has to be observed during sampling operations. $L_r = 1$ indicates a good recovery, $L_r < 1$ means the soil is compressed and $L_r > 1$ indicates swelling in the soil sample. For very high quality undisturbed soil sample piston samplers can be used. These are used only in extremely important projects.

In rocks, rotary drilling is used to take samples. A core barrel which does the function of both drilling and retaining the sample is attached to drilling rods as shown in Fig. 19.5. The cutting edge called coring bit is impregnated with diamonds, chilled shot, tungsten carbide inserts or steel cutters. The coring bit grinds the rock and leaves an annular space around a cylindrical core of sample. The pulverised rock substance is removed by forcing drilling fluid through drill rods which flows out through the casing. The cylindrical rock core

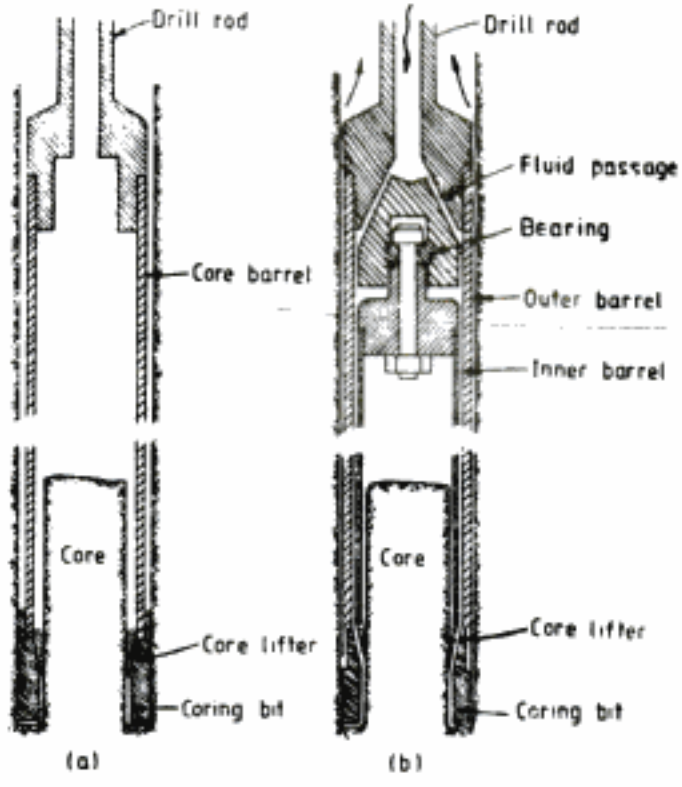

Fig. 19.5 Core barrels: (a) single tube, and (b) double tube

is retained in the core lifter. In the single tube core barrel the sample is considerably disturbed and is contaminated by the circulating drilling fluid. In a double tube core barrel these effects are reduced. Size of rock cores ranges from 31 mm to 150 mm diameter. The various sizes of drill rods, casings and core barrels are given in Table 19.3.

Table 19.3 Standard Sizes of Core Barrels, Drill Rods, and Compatible Casings[a]

Symbol	Core barrel		Drill rod		Compatible casing		
	Hole diameter (approx. in.)	Core diameter (approx. in.)	Symbol	Outside diameter (in.)	Symbol	Outside diameter (in.)	Inside diameter (in.)
EWX[b], EWM[c]	$1\frac{1}{2}$	$1\frac{3}{16}$	*E*	$1\frac{5}{16}$	—	—	—
AWX, AWM	$1\frac{15}{16}$	$1\frac{3}{16}$	*A*	$1\frac{5}{8}$	EX[d]	$1\frac{13}{16}$	$1\frac{1}{2}$
BWX, BWM	$2\frac{3}{8}$	$1\frac{5}{8}$	*B*	$1\frac{7}{8}$	AX	$2\frac{1}{4}$	$1\frac{29}{32}$
NWX, NWM	3	$2\frac{1}{8}$	*N*	$2\frac{3}{8}$	BX	$2\frac{7}{8}$	$2\frac{3}{8}$
$2\frac{3}{4} \times 3\frac{7}{8}$	$3\frac{7}{8}$	$2\frac{11}{26}$	—	—	NX	$3\frac{1}{2}$	3

[a]As standardized by the Diamond Core Drill Manufacturer's Association, Bulletin No. 2 (ASTM D 2113)
[b]Symbol *X* indicates single-tube barrel
[c]Symbol *M* indicates double-tube barrel
[d]EX casing will fit into a hole drilled by AWX or AWM barrel and EWX or EWM barrels will fit inside EX casing

The diameter of the core should be preferably not less than 54 mm (NWX, NWM).

The length of rock sample recovered inside the core barrel is a measure of the soundness of the rock. *Rock quality designation, RQD* is defined as

$$RQD = \frac{L_c}{L_a} \times 100 \tag{19.4}$$

where L_c = total length of intact pieces which are more than 100 mm long. Obvious breaks due to drilling are ignored.

L_a = total length of core advance

Table 19.4 gives the description of rock based on RQD from which the *in-situ* (field) modulus of elasticity and compression strength of rock mass also can be assessed based on laboratory tests on rock cores.

19.1.3 Field Tests

The field tests serve the purpose of substantiating and supplementing the results obtained from laboratory testing of soil samples. In fact, in many instances the laboratory tests are

Table 19.4 Rock Description Based on RQD

RQD per cent	Rock description	E_f/E_{lab} or q_f/q_{lab}
< 25	Very poor	0.15
25–50	Poor	0.20
50-75	Fair	0.25
75–90	Good	0.3 to 0.70
90-100	Excellent	0.7 to 1.0

E_f, E_{lab} = field and laboratory modulus respectively
q_f, q_{lab} = field and laboratory compressive strength respectively

minimum and the analysis and design of foundations are based on the information obtained from field tests itself. The field tests commonly associated with subsurface investigation are:

1. Penetrometer tests
   (a) Standard penetration test (SPT)
   (b) Dynamic cone penetration test (DCPT)
   (c) Static cone penetration test (SCPT)
2. Vane shear test
3. Plate load test
4. Geophysical investigation
   (a) Seismic survey
   (b) Resistivity survey

These field tests are described in detail below.

1. *Penetrometer Tests*

Of the three such tests, standard penetration test is carried out in the borehole whereas dynamic cone test and static cone penetration test are carried out without drilling a borehole. The feature common to all these tests is the measurement of resistance to penetration of the penetrometer which is considered to be an indicator of the soil characteristics.

(a) *Standard penetration test*

Of the different penetrometer tests the most commonly used test in India is the standard penetration test. The test is carried out using a split spoon sampler shown in Fig. 19.6. The assembly consists of three parts, namely, the driving shoe, the split barrel (which is split into two parts), and the coupling or adaptor. The standard procedure of carrying out standard penetration test is as follows:

(i) The borehole is drilled to the required depth and the bottom is cleaned.
(ii) The split spoon sampler already fitted to the string of drill rods is lowered into the borehole and rested at the bottom.
(iii) The split spoon sampler is driven into the soil to a distance of 450 mm using a monkey weight of 65 kg falling freely from a height of 750 mm. While driving, the number of blows required to penetrate every 75 mm are recorded. The total number of blows required for the last 300 mm is entered as the *N value* at that particular depth of the borehole.

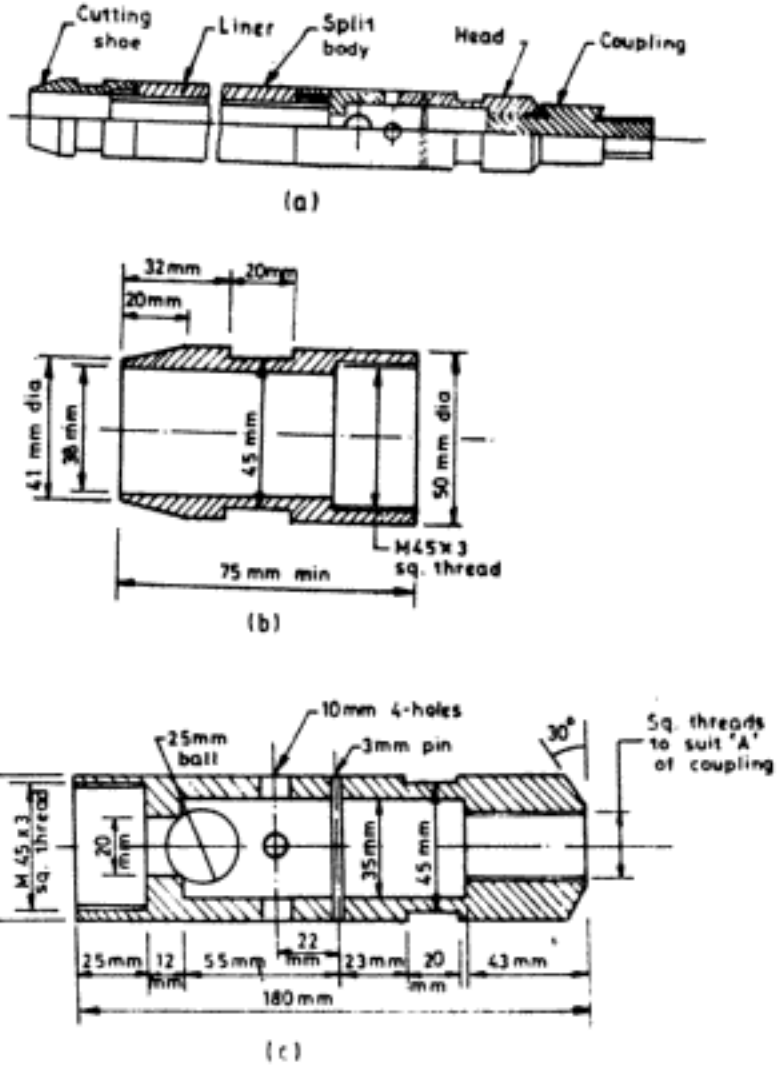

Fig. 19.6 Split spoon sampler (After IS: 9640-1970)

(iv) The sampler is removed to the surface and detached from the drill rods. The split barrel is disconnected from the cutting shoe and the adaptor. The soil inside the split barrel is collected for laboratory tests.

The following are some more points pertinent to standard penetration test.

(i) At shallow depths SPT is carried out at intervals of 75 cm. At greater depths this interval can be increased to 150 cm.

(ii) Sometimes a thin *liner* in the form of a thin tube is inserted inside the split barrel. At the end of the SPT, the liner with the soil sample is sealed at both ends with wax and transported to the laboratory.

(iii) Due to presence of boulders or rock it may not be possible to drive the sampler through a distance of 450 mm. If the sampler is driven less than 450 mm then the penetration resistance is recorded for the last 300 mm of penetration. If less than 300 mm is penetrated in 50 blows, it is entered in borelog as *refusal* and the penetration obtained and number of blows are recorded.

Hidden page

The measured N values are multiplied by a correction factor C_N given by,

$$C_N = 0.77 \log_{10} \frac{20}{\bar{p}_o} \tag{19.5}$$

where, $\bar{p}_o$ = effective overburden pressure, in kg/cm²

Equation 19.5 is valid for $\bar{p}_o > 0.25$ kg/cm². The variation of C_N with $\bar{p}_o$ is shown in Fig. 19.7. For $\bar{p}_o$ less than 0.25 kg/cm² Eq. 19.5 gives very high values of C_N. Hence, for $\bar{p}_o < 0.25$ kg/cm², C_N must be obtained from Fig. 19.7 and not from Eq. 19.5. It is evident from Eq. 19.5 and Fig. 19.7 that measured N values for sand are decreased at greater depths, ($\bar{p}_o > 1$ kg/cm²) but are increased at shallow depths ($\bar{p}_o < 1$ kg/cm²) the maximum increase being twice the measured value.

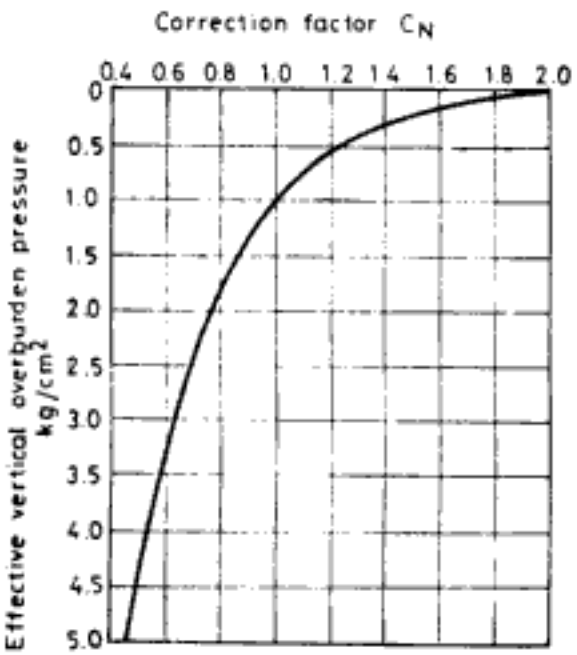

Fig. 19.7 Chart for correction of N values in sand for influence of overburden pressure (After Peck, Hanson and Thornburn, 1974)

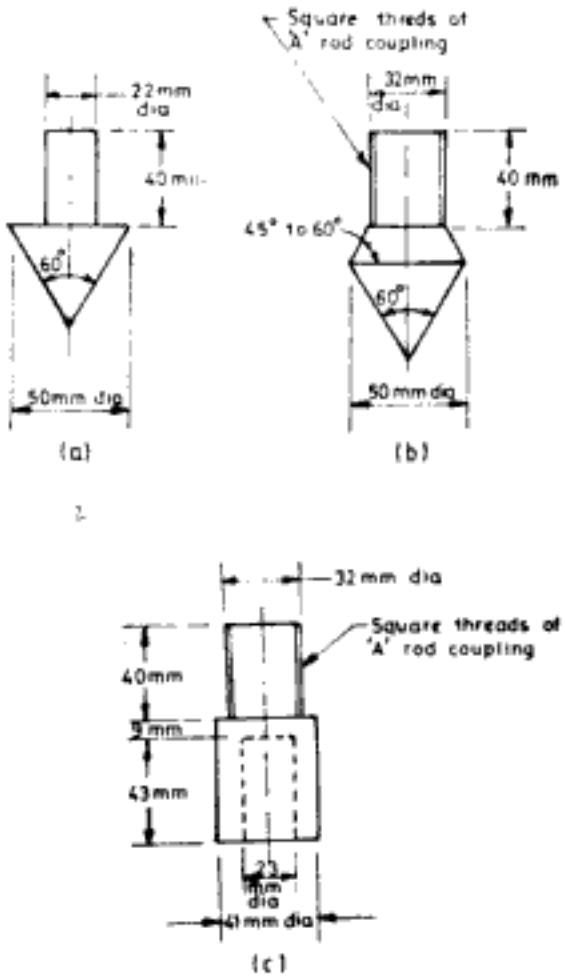

Fig. 19.8 Dynamic cone penetrometer (After IS: 4968, Part I, 1976)

Yet another correction for overburden pressure is due to Bazarra (1967). His recommendations are as follows:

$$C_N = \frac{4}{1 + 4\bar{p}_o} \qquad \text{for } \bar{p}_o \leqslant 0.75 \text{ kg/cm}^2 \tag{19.6}$$

and $$C_N = \frac{4}{3.25 + \bar{p}_o} \quad \text{for } \bar{p}_o \geqslant 0.75 \text{ kg/cm}^2 \tag{19.7}$$

Equations 19.6 and 19.7 also suggest that measured values are increased at shallow depths but decreased at greater depths.

In saturated fine sands and silts Terzaghi and Peck recommended dilatancy correction when recorded N is greater than 15. N is corrected as N' using the following equation,

$$N' = 15 + \tfrac{1}{2}(N - 15), \quad N > 15 \tag{19.8}$$

Bazarra's recommendation for dilatancy correction is,

$$N' = 0.6N, \quad \text{for } N > 15 \tag{19.9}$$

The reason for dilatancy correction may be stated as follows: $N > 15$ indicates dense deposit. Due to the fast penetration of split sampler negative pore water pressure is developed in dense silty sands and fine sands as dilation occurs. The resistance measured in SPT is therefore more than the actual value.

(b) *Dynamic cone penetration test*

The typical details of dynamic cone penetrometer are shown in Fig. 19.8. A cone is attached to drill rods and driven into the ground using the same monkey weight and height of fall used in standard penetration test. The blow count required for successive penetration of 75 mm is continuously recorded. The cone is slightly larger in diameter at the base than the outer diameter of the drill rod to reduce skin friction that will act on the drill rod. The cone is driven till refusal and then the drill rods are withdrawn leaving the cone in the ground.

Dynamic cone test gives a continuous record of the penetration resistance of the cone with depth. But no sample is obtained in the test.

Dynamic cone test is a quick test and helps to understand the uniformity or variability in the subsoil profile of a large area under investigation more economically. Drilling of boreholes and carrying out standard penetration test are time consuming and expensive. Dynamic cone tests can be carried out near a few borehole locations. The blowcounts from DCPT and SPT can be compared and approximate correlations can be established for the site. With the aid of these correlations, the data from DCPT tests at other locations can be deduced to know the values of N or variation in penetration resistance with depth at those locations. Such type of work is very useful in the preliminary exploration for extensive sites, and will be adequate for relatively small structures.

(c) *Static cone penetration test*

Figure 19.9 shows the typical assembly for static cone penetrometer. The cone at the bottom has a base area of 10 cm^2 and an apex angle of 60°. Either manually or using a power mechanism the cone alone is pushed into the soil using the rod inside the casing. The cone is advanced to a distance of 10 cm at the rate of 2 cm/s. The resistance required for the penetration of cone referred to as q_c is recorded. Following the penetration of cone the sleeve around the drill rod is pushed down to the level of cone. The resistance due to friction on the sleeve can thus be separately measured. The cone resistance variation with depth can be plotted as shown in Fig. 19.10 from which the different strata can be identified. Typical uses of cone resistance diagram are explained in Chaps 13 and 14. Static cone penetration test gives a continuous record of variation of penetration resistance with depth. But no

Hidden page

Hidden page

Hidden page

Hidden page

Hidden page

Hidden page

ready. There is even a tendency to limit the total soil exploration programme. These may prove to be costly errors, if one considers the following reasons.

1. The total cost of subsurface exploration generally ranges from 0.5 per cent to 1.0 per cent of construction costs. There will not be any saving in this cost if the exploration programme is delayed, conversely the cost will be more due to urgency of the work. Also it must be realised that it may not be possible to carry out the investigations at all times. Climatic conditions, for example, can prevent any work at the site during specific periods. The exploration programme must be planned well ahead of time.

2. A significant proportion of the disputes in construction works arises out of inadequate soil data. Costly and prolonged legal battles ensue. Heavy overrun in the budget, delay in execution of project and in deriving the benefits thereof, do naturally follow. Expenses in soil exploration programme must not be viewed in isolation but should be considered from the overall view of the implications.

3. Sometimes *it is too late to mend*. For, after subsurface investigation it may be realised that the design of the superstructure will have to be drastically changed or even the whole project may have to be abandoned in view of the site conditions.

Another noteworthy point is the soil consultant's role in the construction project. The soil consultant's role begins in the very early phases of the project and must continue till most of the civil construction works are over. In special cases it must be maintained for some time after construction is over to monitor the post-construction performance of the structure. It is a good practice to involve the soil consultant in the planning of the investigation programme, rather than requiring the consultant to undertake an arbitrarily chosen programme. The professional standing of the firm, its previous experience, its ability to carry out the work are also some of the important factors other than cost which the client must consider in the selection of soil consultant. The consultant's recommendations based on subsurface investigation are many times diagnostic rather than prescriptive, particularly in large and important projects. Because, earth can spring many a surprise within a very short distance. The client's need for continuous association with the soil consultant in such cases is obvious.

Hidden page

Hidden page

Hidden page

Hidden page

Hidden page

Hidden page

Hidden page

then the above three cases of free vibration are defined as follows:

$D > 1$, system is overdamped

$D = 1$, system is critically damped

$D < 1$, system is underdamped

and the damped circular frequency in Eq. 20.24 can be expressed as

$$\omega_d = \sqrt{1 - D^2}\ \omega_n \tag{20.26}$$

Figure 20.7 shows the nature of vibratory motion for the three cases. It can be seen that eventually the damped system under free vibration returns to static equilibrium condition. The system returns to its original position in the minimum time when it is critically damped. For underdamped system the damping factor can be determined by experimentally measuring successive amplitudes of motion as shown in Fig. 20.8. *Logarithmic decrement* δ is defined as,

$$\delta = \log_e \left(\frac{A_1}{A_2}\right) \tag{20.27}$$

and its relationship with damping factor is given by

$$\delta = \frac{2\pi D}{\sqrt{1 - D^2}} \tag{20.28}$$

If D is very small, Eq. 20.28 can be written as

$$\delta \simeq 2\pi D \tag{20.29}$$

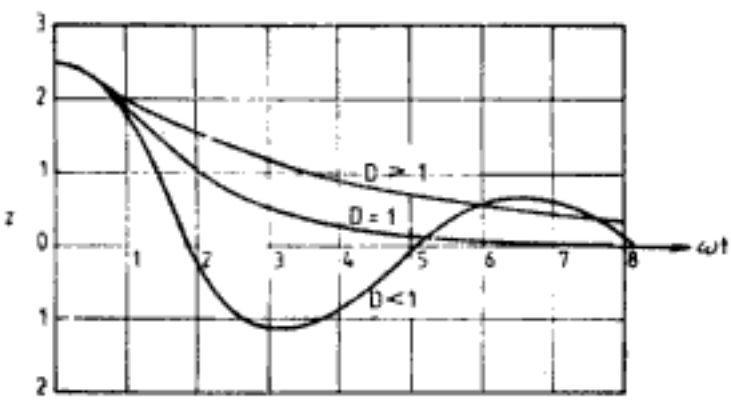

Fig. 20. 7 Vibratory motions for damped systems under free vibration

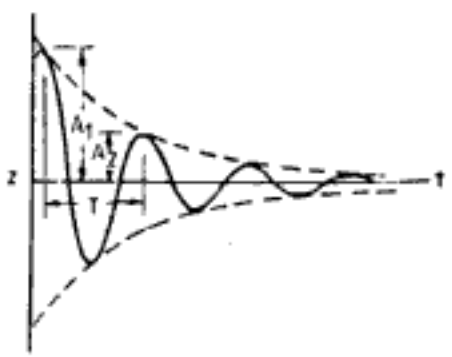

Fig. 20.8 Vibratory motion of under-damped system under free vibration

If D is very small the amplitudes of motion can be measured for a number of cycles and then δ is given by,

$$\delta = \frac{1}{n} \log_e \left(\frac{A_0}{A_n}\right) \tag{20.30}$$

where n = number of cycles

A_0 = amplitude of motion in the beginning of first cycle

A_n = amplitude of motion at the end of nth cycle

Hidden page

Hidden page

Hidden page

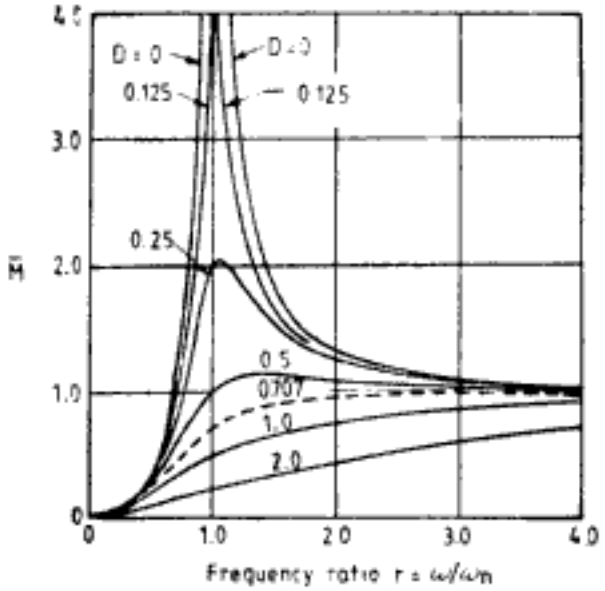

Fig. 20.11 **Magnification factor for variable force excitation**

(d) For all values of D, $\bar{M}$ tends to 1 at large value of ω/ω_n. Phase angle ϕ is given by Eq. 20.39 and therefore the variation of ϕ is same as in Fig. 20.10.

20.1.4 Vibration Due to Motion of Support

Many times the vibration is not due to the forces directly impressed upon the system. It is often due to transmission of vibration through the support or the foundation. Typical examples are vibrations induced due to traffic and construction operations. Care must be taken to safeguard very sensitive equipments against such ground transmitted vibrations.

Figure 20.12 shows the system where the support motion z_1 is defined as $z_s \sin \omega t$. The resulting absolute motion z of mass m is given as,

$$z = z_0 \sin (\omega t - \phi) \tag{20.34}$$

where $z_0 = M_s z_s$ (20.45)

M_s = magnification factor of support motion for absolute motion of mass

$$= \left\{ \frac{1 + (2Dr)^2}{(1 - r^2)^2 + (2Dr)^2} \right\}^{1/2} \tag{20.46}$$

$$\tan \phi = \frac{2Dr^3}{1 - r^2(1 - 4D^2)} \tag{20.47}$$

Variation of M_s and phase angle ϕ with r and D are shown in Figs 20.13 and 20.14 respectively. If we define relative motion z_r as,

$$z_r = z - z_1 \tag{20.48}$$

then the relative motion of mass is given by

$$z_r = \bar{z}_0 \sin (\omega t - \phi) \tag{20.49}$$

where $\bar{z}_0 = M_r z_s$ (20.50)

Hidden page

Hidden page

Q 20.2: A foundation block weighs 2500 kg. It has a stiffness (from soil support) of 20,000 kg/cm. The value of damping coefficient is 250 kg s/cm. If an excitation force of 250 sin 31.4t (kg) acts on the block causing it to vibrate vertically determine (a) whether the system is underdamped, overdamped or critically damped, (b) the natural circular frequency, the natural frequency, and the period, (c) the amplitude of vertical displacement, and (d) the amplitude of force transmitted to the support.

Ans: (a) $W = 2500$ kg; $m = \dfrac{2500}{981} = 2.55$ kg s^2/cm

$k = 20{,}000$ kg/cm

$c = 250$ kg s/cm

From Eq. 20.22, $c_c = 2\sqrt{2 \times 10^4 \times 2.55} = 452$ kg s/cm

From Eq. 20.25, $D = 250/452 = 0.533 < 1$

The system is underdamped.

(b) From Eq. 20.13 $\omega_n = \sqrt{\dfrac{2 \times 10^4}{2.55}} = 88.6$ rad/s

From Eq. 20.14 $f_n = \dfrac{88.6}{2\pi} = 14.1$ cps

f_n can also be determined as below

From Eq. 20.10, $\delta_{st} = \dfrac{2500}{2 \times 10^4} = 0.125$ cm

From Eq. 20.17, $f_n = \dfrac{5}{\sqrt{0.125}} = 14.1$ cps

From Eq. 20.15, $T_n = \dfrac{1}{14.1} = 0.071$ s

(c) *Amplitude of displacement*

From Eq. 20.36, $r = \dfrac{31.4}{88.6} = 0.354$

$$M = \frac{1}{\sqrt{(1 - 0.354^2)^2 + (2 \times 0.354 \times 0.553)^2}}$$

$$= \frac{1}{0.959} = 1.043$$

$$z_{st} = \frac{250}{20000} = 0.0125 \text{ cm} = 0.125 \text{ mm}$$

From Eq. 20.35, $z_0 = 1.043 \times 0.125 = 0.13$ mm

(d) *Transmitted force*

From Eq. 20.54, $\text{TR} = \left\{\dfrac{1 + (2 \times 0.533 \times 0.354)^2}{(1 - 0.354^2)^2 + (2 \times 0.553 \times 0.354)^2}\right\}^{1/2}$

$= 1.12$

$P_0 = 1.12 \times 250 = 280$ kg

Hidden page

The solution gives four values for ω, of which only two are real and positive. These two frequencies are called the natural frequencies of the system. The lower of the two natural frequencies is called the *first mode* of natural frequency, ω_I. The higher of the two is the *second mode* at natural frequency, ω_{II}. The two natural frequencies can be obtained by drawing Mohr's circle as explained below.

Let
$$\omega_A^2 = \frac{k_1 + k_3}{m_1} \tag{20.60}$$

$$\omega_B^2 = \frac{k_2 + k_3}{m_2} \tag{20.61}$$

$$\omega_{AB}^2 = \frac{k_3}{\sqrt{m_1 m_2}} \tag{20.62}$$

The frequency equation (Eq. 20.58) can be now written as

$$\omega^4 - \omega^2(\omega_A^2 + \omega_B^2) + (\omega_A^2\omega_B^2 - \omega_{AB}^4) = 0 \tag{20.63}$$

Mohr's circle is drawn as shown in Fig. 20.18 from which ω_I and ω_{II} are read off. It is also of interest to note that the ratio of the two amplitudes of motion is

$$\lambda = \frac{A_2}{A_1} = \frac{k_1 + k_3 - m_1\omega^2}{k_3} = \frac{k_3}{m_2\omega^2 - k_2 - k_3} \tag{20.64}$$

Substitution of ω_I for ω in the above equation gives always positive values for $\lambda = \lambda_I$ thereby meaning that the two motions are in phase. When ω_{II} is used for ω, values of $\lambda = \lambda_{II}$ are always negative indicating that the two motions are 180° out of phase.

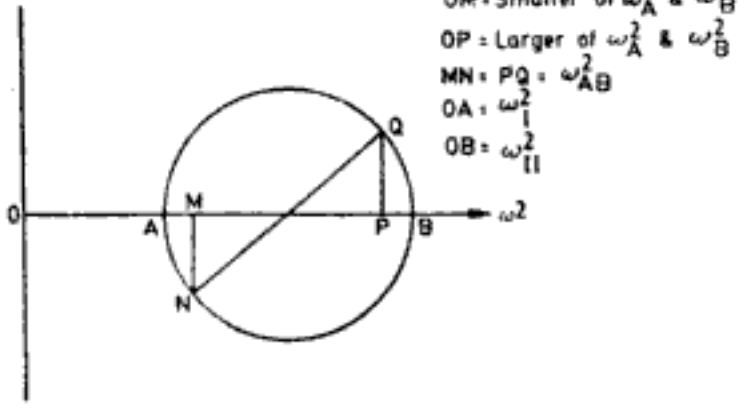

Fig. 20.18 Mohr circle for determination of natural frequencies

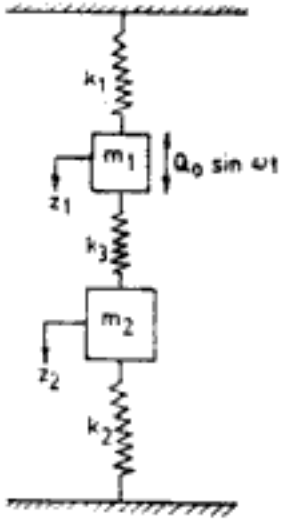

Fig. 20.19 Forced vibration of two degree freedom system

2. *Forced vibrations*

For the two degree system shown in Fig. 20.19 the excitation force acts on mass m_1. The motion of the two masses is defined as,

$$z_1 = A_{1f} \sin \omega t \tag{20.65}$$

$$z_2 = A_{2f} \sin \omega t \tag{20.66}$$

The amplitudes of vibration under forced vibration are,

$$A_{1f} = \frac{Q_0(k_2 + k_3 - m_2\omega^2)/m_1m_2}{(\omega - \omega_I)(\omega - \omega_{II})} \tag{20.67}$$

$$A_{2f} = \frac{Q_0k_3/m_1m_2}{(\omega - \omega_I)(\omega - \omega_{II})} \tag{20.68}$$

The denominator in Eqs 20.67 and 20.68 can be replaced by LHS of frequency equation (Eq. 20.58)

Similarly, when Q_0 sin ωt acts on mass m_2 the motions are still defined by Eqs 20.65 and 20.66 with the following expressions for amplitudes of displacement.

$$A_{2f} = \frac{Q_0(k_1 + k_3 - m_1\omega^2)/m_1m_2}{(\omega - \omega_I)(\omega - \omega_{II})} \tag{20.69}$$

$$A_{1f} = \frac{Q_0k_3/m_1m_2}{(\omega - \omega_I)(\omega - \omega_{II})} \tag{20.70}$$

When m_1 is acted upon by Q_1 sin ωt and m_2 by Q_2 sin ωt,

$$A_{1f} = \frac{\{Q_1(k_2 + k_3 - m_2\omega^2)/m_1m_2\} + (Q_2k_3/m_1m_2)}{(\omega - \omega_I)(\omega - \omega_{II})} \tag{20.71}$$

$$A_{2f} = \frac{(Q_1k_3/m_1m_2) + \{Q_2(k_1 + k_3 - m_1\omega^2)/m_1m_2\}}{(\omega - \omega_I)(\omega - \omega_{II})} \tag{20.72}$$

20.2 FOUNDATIONS SUBJECTED TO VIBRATION

Machine foundations can be broadly grouped into the following four categories.

Block foundation which consists of a pedestal of concrete on which the machine rests.

Box or caisson foundation is of the shape of a hollow concrete block supporting machinery at the top.

Wall foundation consists of a pair of walls which support the machinery at the top.

Frame foundation consists of vertical columns on a base slab. The columns support at their top a horizontal framework of beams and deck slab on which machinery is supported.

Based on their operating speed machines can be grouped into the following three categories:

(a) Low to medium frequencies—less than 500 rpm
(b) Medium to high frequencies—300 to 1000 rpm
(c) Very high frequencies—more than 1000 rpm

Reciprocating engines which operate within a speed range of 50 to 250 rpm, compressors and large blowers come under the category of low to medium speed machines. These are usually supported on block foundations having a large contact area with soil. Medium size reciprocating engines, such as diesel and gas engines are examples of medium to high frequency machines. High speed internal combustion engines, electric motors and turbogenerator machines are very high speed machines. Turbogenerators are, as a rule, supported on frame foundations. Other high speed machines are placed on block foundations.

Hidden page

Hidden page

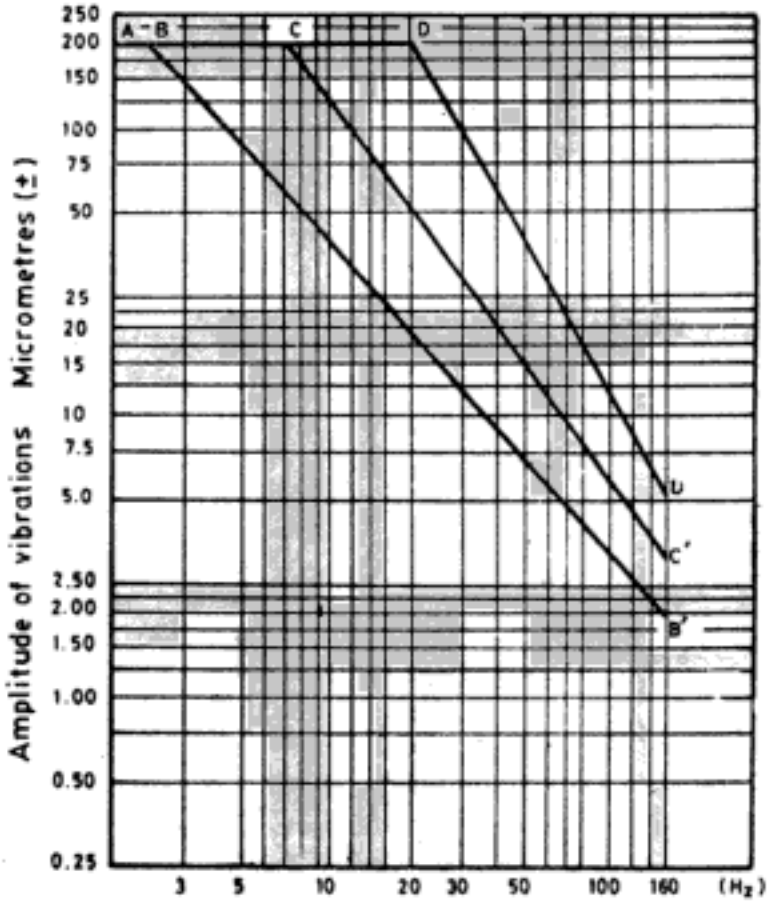

LINE ADD' LIMIT TO AVOID DAMAGE TO BUILDINGS
LINE ACC' LIMIT TO AVOID SERIOUS DISCOMFORT TO PERSONS
LINE ABB' LIMIT TO ENSURE REASONABLE COMFORT TO PERSONS
NOTE - THESE LIMITS DO NOT INCLUDE ANY FACTOR OF SAFETY

Fig. 20.21 Displacement amplitude limits of foundation block (After IS : 2974, Part I, 1982; reprinted by permission of Indian Standards Institution, New Delhi)

Table 20.1 Barkan's Recommendations for Permissible Amplitude of Displacement

Type of machine	Permissible amplitude of displacement (mm)
1. Low speed machinery (500 rpm)	0.20–0.25
2. Hammer foundations	1.00–1.20
3. High speed machinery	
(a) 3000 rpm	
vertical vibration	0.02–0.03
horizontal vibration	0.04–0.05
(b) 1500 rpm	
vertical vibration	0.04–0.06
horizontal vibration	0.07–0.09

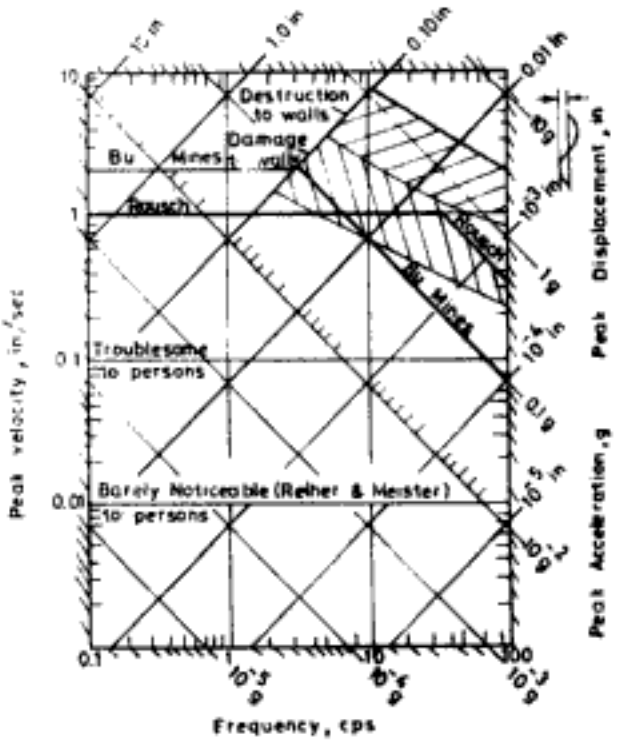

Fig. 20.22 Response spectra (After Richart *et al.*, 1970)

Q 20.3: For the vibration in Q 20.2 determine the response of persons.

Ans: The operating frequency of the force $= \frac{31.4}{2\pi} = 5$ cps

$= 300$ rpm

The amplitude of displacement as determined in Q 20.2 = 0.13 mm = 0.0051 in = 130 μm.

Using Richart's recommendations in Fig. 20.20, for 300 rpm and amplitude of displacement of 0.0051 in, the point lies in the zone troublesome to persons.

Using ISI diagram in Fig. 20.21, for 5 Hz and amplitude of displacement of 130 μm the point lies above the limit of ensuring reasonable comfort to persons and below the limit of avoiding serious discomfort to persons which in other words can be just troublesome to persons.

20.3 DYNAMIC ANALYSIS OF BLOCK FOUNDATIONS

A block foundation in general has six degees of freedom, of which three are translational modes and the other three are rotational modes. The six modes of vibration or degrees of freedom are shown in Fig. 20.23. However, the principles of analysis must be understood for four modes of vibration since these principles are the same for rocking and pitching (rocking is rotation about longer axis, pitching is rotation about shorter axis) and similarly for longitudinal and lateral motions. For a circular footing or cylindrical foundation the

Hidden page

where f_n = in cycles per second
γ = density of soil, pcf
G = shear modulus of soil, psi
P_d = maximum dynamic load, lb
W_v = static weight of vibrator or machine, lb
r_0 = radius of the vibrator base plate or of an equivalent circular area in the case a rectangular base plate, in

2. *Newcomb's method*
This method is based on rewriting Eq. 20.17 with δ_{st} in mm as,

$$f_n = \frac{15.8}{\sqrt{\delta_{st}}} \tag{20.74}$$

where, f_n is in cps, δ_{st} is the elastic deflection in mm. δ_{st} is obtained from plate load test or from empirical figure suggested by Newcomb for four different types of soil.

3. *Tschebotarioff's method*
Tschebotarioff (1953) defines a term *reduced natural frequency*, f_{nr} as

$$f_{nr} = f_n \sqrt{\sigma_{st}} \tag{20.75}$$

where σ_{st} = static pressure on soil = W/A
W = weight of machine and foundation
A = contact area of foundation with soil
f_n = natural frequency, cpm

The variation of f_{nr} with A for four different soil types is shown in Fig. 20.24.

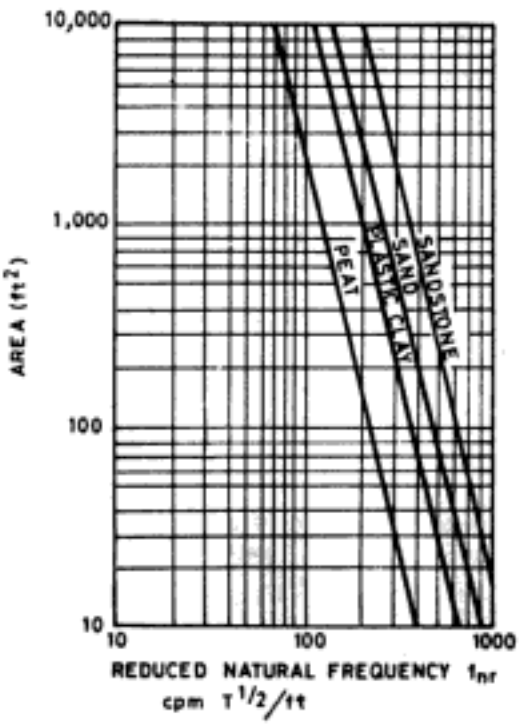

Fig. 20.24 Variation of reduced natural frequency with base area
(After Tschebotarioff, 1953).

4. *Alpan's method*

Alpan (1961) suggests the following equation for natural frequency based on Tschebotarioff's data.

$$f_n = \frac{\alpha}{\sqrt{W}} A^{1/4} \tag{20.76}$$

where W = weight of machine and foundation, kg

A = contact area, m^2

α = a constant

= 3900 for peat

= 69,000 for plastic clay

= 82,000 for sand

= 111,000 for sandstone

f_n = natural frequency, cpm

Q 20.4: A foundation block with machine weighs 12000 kg and has a base area of 10 m^2. If the block rests on sand, determine its natural frequency in vertical mode of vibration using Tschebotarioff's method and Alpan's method.

Ans: (i) *Tschebotarioff's method*

$$W = 12000 \text{ kg} = 12 \text{ T}$$

$$A = 10 \text{ m}^2 = 107.64 \text{ ft}^2$$

$$\sigma_{st} = 12/10 = 1.2 \text{ T/m}^2 \simeq 0.12 \text{ T/ft}^2$$

From Fig. 20.24

$$f_{nr} = 450 \text{ cpm } \text{T}^{1/2}/\text{ft}$$

$$f_n = \frac{450}{\sqrt{0.12}} = 1300 \text{ cpm} \simeq 22 \text{ cps}$$

(ii) *Alpan's method*

$$\alpha = 82000$$

$$f_n = \frac{82000}{\sqrt{12000}} 10^{1/4} = 1331 \text{ cpm} \simeq 22 \text{ cps}$$

20.3.2 Soil-as-spring Approach

Some of the general features of this approach are:

(a) As the name implies this approach considers the soil as spring.

(b) The damping in the system is neglected, leading to conservative solutions.

(c) It is considered that the total mass of the system includes, in addition to the mass of the foundation and the machine, mass of the *in-phase* soil assumed to vibrate together with the machine-foundation system. Several investigators have suggested procedures for calculating this mass of soil (Pauw 1953, Balakrishna Rao and Nagaraj 1960). But Barkan has shown that the mass of the participating soil is maximum 23 per cent of mass of machine and foundation when $\mu = 0.5$. For other values

Hidden page

The vertical motion is,

$$z = A_z \sin \omega t \tag{20.79}$$

and the amplitude of motion A_z is

$$A_z = \frac{Q_z}{m(\omega_{nz}^2 - \omega^2)} \tag{20.80}$$

Q 20.5: A machine weighing 1250 kg runs at a speed of 1000 rpm inducing vertical vibration. It is supported on a concrete block of plan dimensions 6 m × 1.5 m and thickness 3 m. The other data are: $C_u = 1.67$ kg/cm³; $m_e e = 65$ g s²; unit weight of concrete = 2.52 g/cm³. For satisfactory performance of the machine it is desired that the resonant frequency be less than 0.5 times the operating speed (500 cpm) or more than 1.5 times the operating speed (1500 cpm) and also that the amplitude of displacement during operation be less than 0.015 mm. Check the adequacy of the foundation.

Ans: For high speed machines, such as the one here, the natural/resonant frequency is kept significantly lower than the operating frequency.

$$C_u A = k_z = 1.67 \times 600 \times 150/1000 = 150.3 \text{ T/cm}$$

Weight of concrete block $= 6 \times 1.5 \times 3 \times 2.52 = 68.04$ T

$$\text{Total mass, } m = \frac{68.04 + 1.25}{981} = 0.0706 \text{ T s}^2/\text{cm}$$

$$\omega_{nz} = \sqrt{\frac{150.3}{0.0706}} = 46.14 \text{ rad/s}$$

$$f_{nz} = 46.14/2\pi = 7.34 \text{ cps} = 441 \text{ cpm} < 500 \text{ cpm O.K.}$$

$$\omega = 1000 \times 2\pi/60 = 104.72 \text{ rad/s}$$

Amplitude of force at operating speed,

$$Q_0 = m_e e \omega^2 = 65 \times 10^{-6} \times (1000 \times 2\pi/60)^2 = 0.713 \text{ T}$$

From Eq. 20.80, amplitude of displacement at 1000 rpm,

$$A_z = \frac{0.713}{0.0706(46.14^2 - 104.72^2)} = -0.00114 \text{ cm}$$

$$= -0.0114 \text{ mm} < 0.015 \text{ mm O.K.}$$

The negative sign indicates that the displacement is out of phase with excitation force by 180°. The foundation block meets both requirements. Hence, it is adequate. However, during starting and stopping of the machine the system will momentarily pass through resonance.

2. *Sliding vibration*

In Fig. 20.26 the horizontal excitation force is assumed to act at the level of the base of the foundation. Only when the foundation block is a very thin disc pure sliding vibration is possible and a single degree freedom system can be assumed for sliding. Generally, the foundation block is very thick and the horizontal excitation force acts considerably above the base level. Then both sliding and rocking will be induced and this coupled mode should be analysed by a two degree freedom system. This analysis is considered on p. 651. Analysis for pure sliding is as follows:

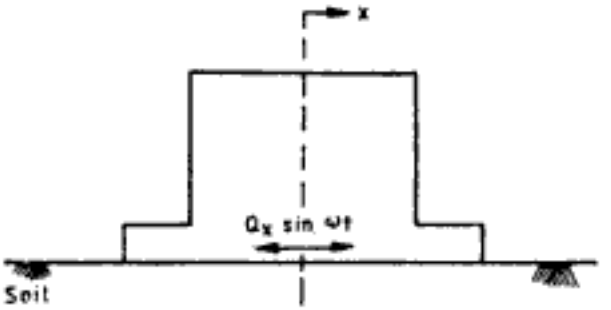

Fig. 20.26 Sliding vibration of block foundation

Spring constant in sliding vibration k_x is,

$$k_x = C_\tau A \tag{20.81}$$

where, C_τ = coefficient of elastic uniform shear

The natural circular frequency ω_{nx} is,

$$\omega_{nx} = \sqrt{\frac{C_\tau A}{m}} \tag{20.82}$$

The sliding motion is given by,

$$x = A_x \sin \omega t \tag{20.83}$$

Amplitude of sliding motion A_x is,

$$A_x = \frac{Q_x}{m(\omega_{nx}^2 - \omega^2)} \tag{20.84}$$

3. *Rocking vibration*

In the analysis of pure rocking vibration the following assumptions are necessary:

(a) The centroid of the base area and the centre of gravity of the foundation lie on a vertical line lying in the plane of rocking moment. The centre of gravity is located at a distance L above the centroid as shown in Fig. 20.27.

(b) Only rocking occurs and the other modes are constrained not to take place. This makes the analysis possible with a single degree freedom system. Generally, rocking and sliding vibrations are coupled together.

Rotational spring constant for rocking k_ϕ is given by

$$k_\phi = C_\phi I \tag{20.85}$$

where C_ϕ = coefficient of elastic non-uniform compression

I = moment of inertia of foundation area about the axis of rotation passing through the centroid of the base area

For notations shown in Fig. 20.28 the expression for moment of inertia is,

$$I = \frac{ba^3}{12} \tag{20.86}$$

b and a are sides parallel and perpendicular to the axis of rotation, respectively.

The natural circular frequency of the foundation in pure rocking $\omega_{n\phi}$ is given by

$$\omega_{n\phi} = \sqrt{\frac{C_\phi I}{M_{m0}}} \tag{20.87}$$

Hidden page

Hidden page

Hidden page

Hidden page

Hidden page

Hidden page

The mass moment of inertia of the foundation and machine can be calculated as follows.

(i) For each element calculate the mass moment of inertia about its own centroidal axis say w_1 to w_n. Table 20.4 gives the expressions for regular geometrical shapes shown in Fig. 20.33.

Table 20.4 Mass Moment of Inertia About Centroidal Axes

Geometrical shape of mass m	Mass moment of inertia about		
	x-axis	y-axis	z-axis
Rectangular prism	$\frac{m}{12}(l_y^2 + l_z^2)$	$\frac{m}{12}(l_x^2 + l_z^2)$	$\frac{m}{12}(l_x^2 + l_y^2)$
Solid circular cylinder	$\frac{m}{12}\left(\frac{3}{4}D^2 + l^2\right)$	$\frac{m}{8}D^2$	$\frac{m}{12}\left(\frac{3}{4}D^2 + l^2\right)$

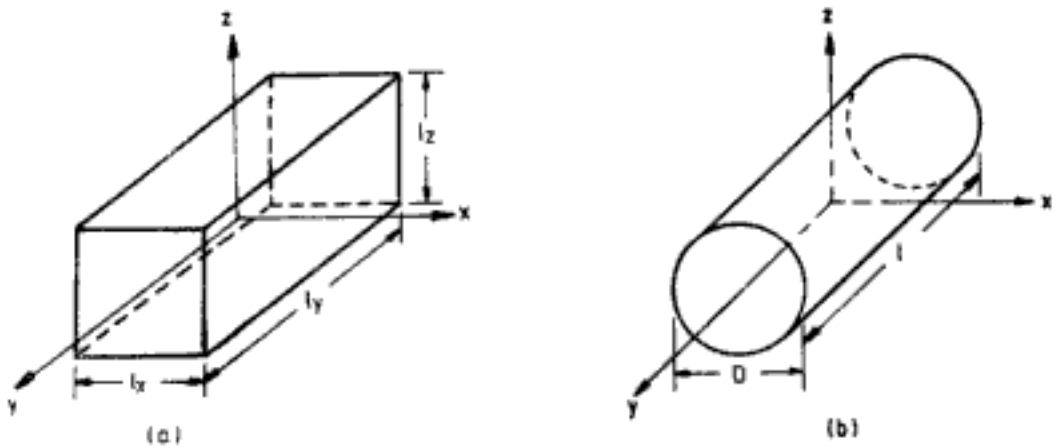

Fig. 20.33 Regular geometrical shapes: (a) Rectangular prism (b) Solid circular cylinder

(ii) The mass moment of inertia of any element about a parallel axis is given by,

$$w_{i0} = w_i + m_i S_i^2 \tag{20.123}$$

where w_{i0} = mass moment of inertia of ith element about a parallel axis at a distance of S_i from the centre of gravity of the element

w_i = mass moment of inertia of ith element about its own centroidal axis

(iii) Mass moment of inertia about a common axis is the sum of mass moment of inertia of all elements about the same axis.

With reference to Fig. 20.34 the expressions for moment of inertia of base area are as follows:

about x-axis

$$I_x = \frac{ab^3}{12} \tag{20.124}$$

Hidden page

Hidden page

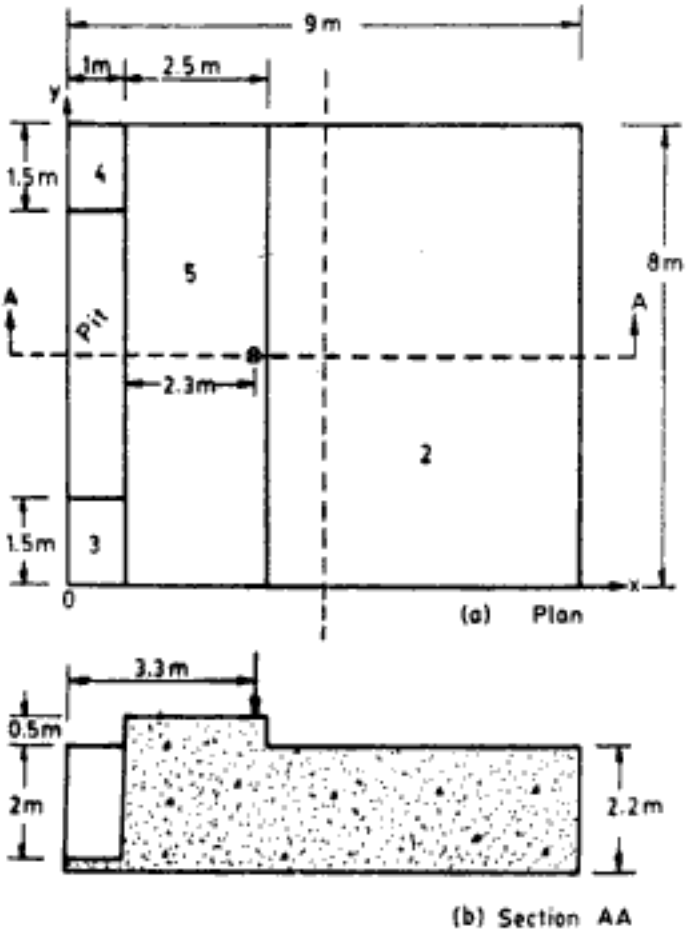

● Point of action of engine weight and vertical dynamic force

Fig. 20.35 Q 20.6

The eccentricities are within the allowable limit of 5 per cent. The dynamic excitation can be now considered to be made of two components, namely

(i) Vertical excitation with a force amplitude Q_z of 15 T
(ii) Rocking moment excitation of maximum moment

$$M_\phi = 15\ (4.497 - 3.3) = 17.955\ \text{T m}$$

The vertical motion can be analysed independently of rocking.

Analysis for rocking motion

Operating circular frequency $= \omega = 2\pi \times 180/60$

$= 18.55$ rad/s

Moment of inertia of base area about y-axis passing through centroid (Fig. 20.34)

$$I_y = \frac{8 \times 9^3}{12} = 486\ \text{m}^4$$

Hidden page

From Eq. 20.110

$$A_x = \frac{2.5\times10^3\times9\times8\times1.31}{72.945\times10^{10}}\times17.955$$

$$= 58.04\times10^{-7}\text{ m} = 0.0058\text{ mm}$$

From Eq. 20.111

$$A_\phi = \frac{2.5\times10^3\times9\times8 - 42.422\times3.55\times10^2}{72.945\times10^{10}}\times17.955$$

$$= 4.06\times10^{-6}\text{ rad}$$

The lateral movement of the centroid of base area is, from Eq. 20.115

$$x_0 = 0.0058 - 1.31\times10^3\times4.06\times10^{-6}$$

$$= 0.00048\text{ mm}$$

As already seen when only rocking moment is acting and operating frequency is very small compared to ω_{nx}, no sliding occurs at the base.
The horizontal movement at the top of foundation

$$= 0.0058 + (2.2 - 1.31)\times10^3\times4.06\times10^{-6}$$

$$= 0.0094\text{ mm}$$

Analysis for vertical motion
From Eq. 20.78

$$\omega_{nz} = \left(\frac{5\times10^3\times9\times8}{42.422}\right)^{1/2} = 92.12\text{ rad/s}$$

$$\omega_{nz}^2 = 84.86\times10^2\text{ (rad/s)}^2$$

From Eq. 20.80 amplitude of vertical displacement of centre of gravity

$$A_z = \frac{15}{42.422\times(84.86\times10^2 - 3.55\times10^2)} = 4.35\times10^{-5}\text{ m}$$

$$=0.0435\text{ mm}$$

Vertical movement of the edge of foundation due to rocking (Eq. 20.90)

$$= \frac{9}{2}\times10^3\times3.189\times10^{-6} = 0.0144\text{ mm}$$

Total vertical movement of the edge of the foundation

$$= 0.0144 + 0.0435 = 0.0579\text{ mm}$$

20.3.3 Elastic Half-space Approach

Some of the general features of elastic half-space approach are as follows:

(a) The soil is considered as a semi-infinite elastic medium and the foundation is assumed to rest on the surface of the medium.
(b) The soil parameters needed for the analysis are dynamic shear modulus G, Poisson's ratio μ, and total density γ.

Hidden page

Hidden page

Hidden page

Hidden page

Hidden page

where $\bar{B}_\phi = n_\phi B_\phi$

B_ϕ = mass ratio in rocking $= \dfrac{3(1-\mu)}{8}\dfrac{M_{m0}}{\rho r_0^5}$ (20.144)

M_{m0} = mass moment of inertia of a cylinder of height h and radius r_0 about an axis through its base

$$= m\left(\frac{r_0^2}{4} + \frac{h^2}{3}\right)$$

The values of n_ϕ for different B_ϕ are given in Table 20.9. α_ϕ is the depth of embedment factor for damping factor expressed as,

$$\alpha_\phi = \frac{1}{\sqrt{\eta_\phi}}\left\{1 + 0.7(1-\mu)\left(\frac{h}{r_0}\right) + 0.6(2-\mu)\left(\frac{h}{r_0}\right)^3\right\} \quad (20.145)$$

(v) The rocking motion can now be analysed from theory of vibrations. Table 20.10 gives the expressions for resonance conditions for circular footings at surface ($\alpha_\phi = \eta_\phi = 1$).

Table 20.9 Variation of n_ϕ with B_ϕ

B_ϕ	0.2	0.5	0.8	1.0	2.0	3.0	5.0
n_ϕ	1.600	1.378	1.251	1.219	1.143	1.100	1.079

Table 20.10 Rocking Vibration—Expressions for Analog Model for Circular Foundations

Quantity	Constant moment excitation $M_\phi \sin \omega t$	Variable moment excitation $m_e e\omega^2 z \sin \omega t$
natural frequency $\omega_{n\phi} = \sqrt{k_\phi / I_\phi}$	$\dfrac{1}{r_0}\sqrt{\dfrac{G}{\rho B_\phi}}$	$\dfrac{1}{r_o}\sqrt{\dfrac{G}{\rho B_\phi}}$
resonant frequency $\omega_{\phi m}$	$\dfrac{1}{r_0}\sqrt{\dfrac{G}{\rho \bar{B}\phi}}\left\{1 - \dfrac{0.045}{\bar{B}_\phi(1+\bar{B}_\phi)^3}\right\}$	$\dfrac{1}{r_0}\sqrt{\dfrac{G}{\rho B_\phi}\left\{1 - \dfrac{0.045}{\bar{B}_\phi(1+\bar{B}_\phi)^3}\right\}}$
resonant amplitude of rotation $A_{\phi m}$	$\dfrac{M_\phi}{k_\phi}\left\{\dfrac{(1+\bar{B}_\phi)^3\bar{B}_\phi}{0.3\sqrt{(1+\bar{B}_\phi)^3\bar{B}_\phi - 0.0225}}\right\}$	$\dfrac{m_e e z}{M_{m0}} \times \left\{\dfrac{0.3\sqrt{(1+\bar{B}_\phi)^3\bar{B}_\phi - 0.0225}}{(1+\bar{B}_\phi)^3\bar{B}_\phi}\right\}$

Note: z is the vertical distance between centroid of base area and the horizontal force $m_e e\omega^2 \sin \omega t$.

(d) *Torsional vibration*: Following are the steps in the analysis of torsional vibration:

(i) Compute the mass of the system m.

(ii) For rectangular foundations determine the equivalent radius r_0 from the equation,

$$r_0 = \sqrt[4]{\frac{2I_z}{\pi}} = \sqrt[4]{\frac{BL(B^2+L^2)}{6\pi}} \quad (20.146)$$

where I_z = moment of inertia of base area about axis of rotation (Eq. 20.126)

Hidden page

20.4 DETERMINATION OF DYNAMIC PROPERTIES OF SOIL

The soil properties required for the analysis of the dynamic response of the foundation can be determined in many ways. Broadly they may be classified into two categories of tests as (i) field tests and (ii) laboratory tests. The different types of tests within these two categories and the parameters obtained from these tests are given in Table 20.12. For a complete description of these tests reference may be made to publications on soil dynamics (Prakash, 1981, Srinivasulu and Vaidyanathan, 1976, IS: 5249-1977 Richart, Hall and Woods, 1970).

Table 20.12 Field and Laboratory Tests for Determination of Dynamic Soil Properties

Type of test	Parameters obtained
Field tests	
Block vibration test	C_u, C_τ, D
Cyclic plate load test	C_u
Wave propagation test	E, G, μ
Laboratory tests	
Repeated load triaxial test	E, G
Wave propagation test	E, G
Resonant column test	E, G, D

Values for C_u recommended by Barkan (1962) are presented in Table 20.2. Table 20.13 gives some representative values of dynamic shear modulus for different soil types. Following are some of the empirical equations suggested by different investigators for maximum value of dynamic shear modulus. According to Hardin and Richart (1963), and Hardin and Black (1968), for round grained soils when *in situ* void ratio e is less than 0.8,

$$G = \frac{697(2.17 - e)^2}{1 + e}(\bar{\sigma}_0)^{0.5} \quad \text{kg/cm}^2 \tag{20.151}$$

Table 20.13 Representative Values of Dynamic Shear Modulus, G

Soil type	G (kg/cm^2)
Clean dense quartz sand	125 to 210
Micaceous fine sand	160
Loamy sand	105
Dense sand-gravel	700
Wet soft silty clay	90 to 140
Dry soft silty clay	175 to 210
Dry silty clay	280 to 350
Medium clay	140 to 280
Sandy clay	140 to 280

For angular grained soils with void ratio greater than 0.6 and clays of modest activity, G is estimated using,

$$G = \frac{326(2.97 - e)^2}{1 + e}(\bar{\sigma}_0)^{0.5} \quad \text{kg/cm}^2 \tag{20.152}$$

In terms of overconsolidation ratio (OCR) Hardin and Drnevich (1972) suggest the following relationship,

$$G = \frac{326(2.97 - e)^2}{1 + e} (\text{OCR})^n (\bar{\sigma}_0)^{0.5} \quad \text{kg/cm}^2 \tag{20.153}$$

where, n is a coefficient which depends on the value of plasticity index (PI) as shown in Table 20.14. For sands Iwasaki and Tatsuoka (1977) recommend the following relationship for G.

$$G = \frac{328(2.17 - e)^2}{1 + e} (\bar{\sigma}_0)^{0.38} \quad \text{kg/cm}^2 \tag{20.154}$$

Table 20.14 Variation of n with Plasticity Index

PI	0	20	40	60	80	> 100
n	0	0.18	0.30	0.41	0.48	0.50

In Eqs 20.151 to 20.154

$\bar{\sigma}_0$ = mean principal effective stress, kg/cm^2

$$= \frac{\bar{\sigma}_1 + \bar{\sigma}_2 + \bar{\sigma}_3}{3}$$

$$= \frac{\bar{\sigma}_1(1 + 2K_0)}{3} \quad \text{for } \textit{in situ} \text{ soils}$$

For Poisson's ratio μ Indian Standard Code (IS: 5249-1977) recommends the following values,

clay — 0.5
sand — 0.3 to 0.35
rock — 0.15 to 0.25

Bowles (1982) recommends values of $\mu = 0.3$ for cohesionless soil and $\mu = 0.4$ for cohesive soil.

The relationship between E, G and μ is given by

$$G = \frac{E}{2(1 + \mu)} \tag{20.155}$$

The relationship between C_u and E is given as

$$C_u = \frac{1.13E}{1 - \mu^2} \sqrt{A} \tag{20.156}$$

where A = base area of foundation

The relationship between C_u and E is based on the assumption that E is constant with depth.

REFERENCES

The following abbreviations for Conferences, Journals and Organisations have been used. A comprehensive list of Indian Standard Codes on soil mechanics, foundation engineering and other related areas in geotechnical engineering appears on Pages 683–691.

ARC —*Asian Regional Conference*
ASCE —*American Society of Civil Engineers*
ASME —*American Society of Mechanical Engineers*
ASTM —*American Society for Testing and Materials*
CGJ —*Canadian Geotechnical Journal*
HRB —*Highway Research Board*
HRR —*Highway Research Record*
ICSMFE—*International Conference on Soil Mechanics and Foundation Engineering*
IGJ —*Indian Geotechnical Journal*
JGED —*Journal of Geotechnical Engineering Division*
JSMFD —*Journal of Soil Mechanics and Foundations Division*
STP —*Special Technical Publication*

Agerschou, H.A. (1962), "Analysis of the Engineering News Pile Formula", *JSMFD, ASCE*, Vol. 88, SM5, pp 1-11.

Ahlvin, R.G. and Ulery, H.H. (1962), "Tabulated Values for Determining the Complete Pattern of Stresses, Strains and Deflections Beneath a Uniform Load on a Homogeneous Half Space", *HRB Bulletin 342*, pp 1-13.

Alpan (1961), "Machine Foundations and Soil Resonance", *Geotechnique*, Vol. 11.

Alpan, I. (1967). "The Empirical Evaluation of the Coefficient K_o and K_{oR}", *Soils and Foundations*, Vol. 7, No. 1, pp. 31-40.

ASCE (1941), Pile Driving Formulas, *Proceedings ASCE*, Vol. 67, No. 5, pp. 853-866.

Azzouz, A.S. *et al.* (1976), "Regression Analysis of Soil Compressibility", *Soils and Foundations*, Vol. 16, No. 2, pp. 19-29.

Babu Shankar, N. (1977), "Stress Distribution Under Embedded Circular Footings", *IGJ*, Vol. 7, No. 2, pp. 178-181.

Baligh, M.M. and Vivatrat, V. (1975), "A Manual on Prediction of Pile Downdrag on End-Bearing Piles", *Research Report R 75-38, Geotechnical Publication 518*, Department of Civil Engineering, M.I.T., Cambridge, Mass., U.S.A.

Barber, E.S. (1953), Discussion to Paper by S.M. Gleser, *ASTM, STP 154*, pp. 96-99.

Barkan, D.D. (1962), *Dynamics of Bases and Foundations*, McGraw-Hill, New York.

Bazarra, A.R. (1967), "Use of the Standard Penetration Test for Estimating Settlements of Shallow Foundations on Sand", *Ph.D. Thesis*, University of Illinois, Urbana,

Berezantzev, V.G., Khristoforov, V. and Golubkov, V. (1961), "Load Bearing Capacity and Deformation of Piled Foundations", *5th ICSMFE*, Paris, Vol. 2, pp. 11-15.

Bishop, A.W. (1955), "The Use of Slip Circle in the Stability Analysis of Earth Slopes", *Geotechnique*, Vol. 5, pp. 7-17.

Bishop, A.W. and Morgenstern, N. (1960), "Stability Coefficients for Earth Slopes", *Geotechnique*, Vol. 10, pp. 129-150.

Bishop, A.W. (1961), "The Measurement of Pore Pressure in the Triaxial Test", *Pore Pressure and Suction in Soils*, Butterworths.

Bishop, A.W. and Henkel, D.J. (1962), *The Measurement of Soil Properties in the Triaxial Test*, Edward Arnold Ltd., London, Second Edition.

Bjerrum, L. (1963a), *Discussions to European Conference on Soil Mechanics and Foundation Engineering*, Wiesbaden, Vol. II, p. 135.

Bjerrum, L. (1963b), "Generelle Krav til fundamentering av forskjellige byggverk; tillatte setninger", Den Norske Ingenirforening, Kurs i fundamentering, Oslo.

Bjerrum, L. (1972), "Embankments on Soft Ground", *Proceedings Speciality Conference on Performance of Earth and Earth Supported Structures, ASCE*, Vol. 2, pp. 1-54.

Blum, H. (1931), "Einspannings verhaeltnisse bei Bohlwerken", Wilhelm, Ernst and Sohn, K.G. Berlin.

Borowica, H. (1943), "Uber ausmittig belaste starre platten auf elastich-isotropem untergrund", *Ingenieur-Archiv*, Berlin, Vol. 1, pp. 1-8.

Bowles, J.E. (1982), *Foundation Analysis and Design*, McGraw-Hill International Book Company, Third edition.

British Standards 1377 (1967), *Methods of Testing Soils for Civil Engineering Purposes*, British Standards Institution, London.

Broms, B.B. (1964a), "Lateral Resistance of Piles in Cohesive Soils", *JSMFD, ASCE*, Vol. 90, SM2, pp. 27-63.

Broms, B.B. (1964b), "Lateral Resistance of Piles in Cohesionless Soils", *JSMFD, ASCE*, Vol. 90, SM3, pp. 123-156.

Broms, B.B. (1966), "Methods of Calculating Ultimate Bearing Capacity of Piles—A Summary", *Sols-Soils*, Vol. 5, pp. 21-31.

Broms, B.B. (1979), "Negative Skin Friction", *6th ARC*, Singapore, Vol. 2, pp. 41-75.

Brooker, E.W. and Ireland, H.O. (1965), "Earth Pressure at Rest Related to Stress History", *CGJ*, Vol. 2, No. 1, pp. 1-15.

Brown, P.T. and Gibson, R.E. (1972), "Surface Settlement of a Deep Elastic Stratum Whose Modulus Increases Linearly with Depth", *CGJ*, Vol. 9, No. 4.

Burmister, D.M. (1943), "The Theory of Stresses and Displacements in Layered Systems and Applications to the Design of Airport Runways", *HRB*, Vol. 23, pp. 127-148.

Burmister, D.M. (1945), "The General Theory of Stresses and Displacements in Layered Soil Systems", *Journal of Applied Physics*, Vol. 16, No. 2, pp. 89-96; No. 3, pp. 126-127; No. 5, pp. 296-302.

Burmister, D.M. (1951), "The Application of Controlled Test Methods in Consolidation Testing", *Symposium on Consolidation Testing of Soils, ASTM STP 126*, p. 83.

Burmister, D.M. (1956), "Stress and Displacement Characteristics of a Two-Layer Rigid Base Soil System: Influence Diagrams and Practical Applications", *HRB*, Vol. 35, pp. 773-814.

Burmister, D.M. (1962), "Application of Layered System Concepts and Principles to Interpretations and Evaluations of Asphalt Pavement Performances and to Design and Construction", *Proceedings of the International Conference on Structural Design of Pavements*, University of Michigan, pp. 441-453.

Burmister, D.M. (1965), "Influence Diagrams for Stresses and Displacements in a Two-Layer Pavement System for Airfields", *Contract NBY 13009*, Department of the Navy, Washington, D.C.

Butler, F.G. (1975), "Heavily Overconsolidated Clays", *Settlement of Structures*, Conference Organised by British Geotechnical Society, Pentech Press, London, pp. 531-578.

Butterfield, R. and Banerjee, P.K. (1971), "A Rigid Disc Embedded in an Elastic Half Space", *Geotechnical Engineering*, Vol. 2, No. 1, pp. 35-52.

Button, S.J. (1953), "The Bearing Capacity of Footings on a Two-Layer Cohesive Subsoil", *3rd ICSMFE*, Zurich, Vol. 1, p. 332.

Bycroft, G.N. (1956), "Forced Vibration of a Rigid Circular Plate on a Semi-Infinite Elastic Space and on an Elastic Stratum", *Philosophical Transactions*, Royal Society, London, Series A, Vol. 248, pp. 327-368.

Casagrande, A. (1936), "The Determination of Preconsolidation Load and Its Practical Significance", *1st ICSMFE*, Cambridge, Massachusetts, Vol. 3, p. 60.

Casagrande, A. and Fadum, R.E. (1940), "Notes on Soil Testing for Engineering Purposes", *Harvard Univ. Graduate School of Engg.*, Publication No. 8.

Chellis, R.D. (1961), *Pile Foundations*, 2nd ed., McGraw-Hill Book Company, New York.

Chen, W.F. (1975), *Limit Analysis and Soil Plasticity*, Elsevier, Amsterdam.

Christian, J.T. and Carrier III, W.D. (1978), "Janbu, Bjerrum and Kjaernsli's Chart Reinterpreted", *CGJ*, Vol. 15, No. 1, pp. 124-128.

Coulomb, C.A. (1776), "Essai sur une application des regles des maximis et minimis à quelques problemes de statique relatif à l'architecture", *Mem. Acad. Royoal Pres. Divers Sav.*, Paris.

CRRI (1953), "A Suggested Classification of Black Cotton Soils of India", *Road Research Notes*, No. 6, New Delhi.

D'Appolonia, D.J., D'Appolonia, E.E. and Brissette, R.F. (1968), "Settlement of Spread Footings on Sand", *JSMFD, ASCE*, Vol. 94, No. SM3, pp. 735-760.

D'Appolonia, D.J., Whitman, R.V. and D'Appolonia, E. (1969), "Sand Compaction with Vibratory Rollers", *JSMFD, ASCE*, Vol. 95, SM1, pp. 263-284.

Das, B.M. (1983), *Advanced Soil Mechanics*, Hemisphere Publishing Corporation, McGraw-Hill Book Company.

Davis, E.H. and Taylor, H. (1962), "The Movement of Bridge Approaches and Abutments on Soft Foundation Soils", *Proceedings First Biennial Conference*, Australian Road Research Board, p. 740.

Davisson, M.T. (1970), "Lateral Load Capacity of Piles", *HRR No. 333*, pp. 104-112.

De Beer, E. and Martens, A. (1957), "Method of Computation of an Upper Limit for the Influence of Heterogeneity of Sand Layers in Settlement of Bridges", *4th ICSMFE*, London, Vol. 1, pp. 275-281.

De Beer, E. (1965), "Bearing Capacity and Settlement of Shallow Foundations on Sand", *Proceedings of Symposium on Bearing Capacity and Settlement of Foundations*, Duke University, pp. 15-33.

De Beer, E.E. (1970), "Experimental Determination of the Shape Factors and the Bearing Capacity Factors of Sand", *Geotechnique*, Vol. 20, No. 4,

Den Norske Pelekomite (1973), "Veiledning ved pelefundamentaring", Norwegian Geotechnical Institute, Veiledning No. 1.

Egorov, K.E. and B.P. Popov (1957), "The Observed Settlements of Buildings as Compared with Preliminary Calculation", *4th ICSMFE*, London, Vol. 1, pp. 291-296.

Egorov, K.E. (1965), "Calculation of Bed for Foundation with Ring Footing", *6th ICSMFE*, Montreal, Vol. 2, pp. 41-45.

Egorov, K.E. and T.A. Malikova (1975), "Settlement of Foundation Slabs on Compressible Base", *5th ARC*, Bangalore, Vol. 1, pp. 187-190.

Egorov, K.E., Konovalov, P.A., Kitaykina, O.V., Salnikov, L.F. and A.V. Zinovyev (1977), "Soil Deformations under Circular Footing", *9th ICSMFE*, Tokyo, Vol. 1, pp. 489-492.

Fadum, R.E. (1948), "Influence Values for Estimating Stresses in Elastic Foundations", *2nd ICSMFE*, Rotterdam, Vol. 3, pp. 77-84.

Fenske, C.W. (1900), "Influence Charts for Vertical Stress Distribution by Westergaard's Equation", *Univ. of Texas Cir. 21.*

Flaate, K.S. (1964), "An Investigation of the Validity of Three Pile Driving Formulae in Cohesionless Material", *Publication No. 56, Norwegian Geotechnical Institute*, Oslo, Norway.

Foott, R. and Koutsoftas, D. (1984), "Settlement of Natural Ground Under Static Loading", *Ground Movements and Their Effects on Structures*, Attewell, P.B. and R.K. Taylor (Eds), Surrey University Press.

Foster, C.R. and Ahlvin, R.G. (1954), "Stresses and Deflections Induced by a Uniform Circular Load", *HRB*, Vol. 33, pp. 467-470.

Fox, L. (1948a) "Computations of Traffic Stresses in a Simple Road Structure", *2nd ICSMFE*, Rotterdam, Vol. 2, pp. 236-246.

Fox, L. (1948b) "The Mean Elastic Settlement of a Uniformly Loaded Area at a Depth Below the Ground Surface", *2nd ICSMFE*, Rotterdam, Vol. 1, p. 129.

Fredlund, D.G. and Krahn, J. (1977), Comparison of Slope Stability Methods of Analysis", *CGJ*, Vol. 14, No. 3, pp. 429-439.

Garlanger, J.E. (1974), "Measurement of Pile Downdrag beneath a Bridge Abutment", Highway Research Board, *Transportation Research Record No. 517*, pp. 61-69.

Gibson, R.E. (1967), "Some Results Concerning Displacements and Stresses in a Nonhomogeneous Elastic Half Space", *Geotechnique*, Vol. 17, pp. 58-67.

Gibson, R.E., Brown, P.T. and Andrews, K.R.F. (1971), "Some Results Concerning Displacements in a Nonhomogeneous Elastic Layer", *ZAMP*, Vol. 22, Fasc. 5, pp. 855-864.

Giroud, J.P. (1968), "Settlement of Linearly Loaded Rectangular Area", *JSMFD, ASCE*, Vol. 94, No. SM4, pp. 18-35.

Gray, H. (1936), "Stress Distribution in Elastic Solids", *1st ICSMFE*, Cambridge, Massachusetts, Vol. 2, pp. 157-168.

Grasshoff, H. (1955), "Setzungsberechnungen starrer Fundamente mit Hilfe des Kennzeichnenden Punktes", *Bauingenieur*, p. 53.

Groth, N.N. and Chapman, C.R. (1969), "Computer Evaluation of Deformation due to Subsurface Loads in a Semi-infinite Elastic Medium", *B.E. Thesis*, Univ. of Sydney, Australia.

Hansen, J.B. (1957), "Foundations of Structures: General Report", *4th ICSMFE*, London, Vol. 2, pp. 441-447.

Hansen, J.B. and H. Lundgren (1960), *Hauptprobleme der Bodenmechanik*, Springer Verlag, Berlin.

Hansen, J.B. (1961), "The Ultimate Resistance of Rigid Piles against Transversal Forces", *Danish Geotechnical Institute Bulletin No. 12*, pp. 5-9.

Hansen, J.B. (1970), "A Revised and Extended Formula for Bearing Capacity", *Danish Geotechnical Institute Bulletin No. 28*, Copenhagen, 22 pp.

Hardin, B.O. and Richart, F.E. (Jr.) (1963), "Elastic Wave Velocities in Granular Soils", *JSMFD, ASCE*, Vol. 89, SM1, pp. 33-65.

Hardin, B.O. and Black, W.L. (1968), "Vibration Modulus of Normally Consolidated Clay", *JSMFD, ASCE*, Vol. 94, SM2, pp. 27-42.

Hardin, B.O. and Drnevich, V.P. (1972), "Shear Modulus and Damping in Soils: Design Equations and Curves", *JSMFD, ASCE*, Vol. 98, SM7, pp. 667-692.

Harr, M.E. (1966), *Foundations of Theoretical Soil Mechanics*, McGraw-Hill, New York.

Hetenyi, M. (1946), *Beams on Elastic Foundations*, Ann Arbor, Michigan, University of Michigan Press.

Hiley, A. (1930), "Pile Driving Calculations with Notes on Driving Forces and Ground Resistances", *Structural Engineer*, London, Vol. 8, pp. 246-259, 278-288.

Holl, D.L. (1940), "Stresses Transmission in Earths", *HRB*, Vol. 20, pp. 709-721.

Hora, P. (1981), "Effect of Pile Shape on Downdrag—An Experimental Study", *M. Tech. Thesis*, Indian Institute of Technology, Delhi.

Hough, B.K. (1957), *Basic Soil Engineering*, The Ronald Press Company, New York.

Ismael, N.F. and Vesic, A.S. (1981), "Compressibility and Bearing Capacity", *JGED, ASCE*, Vol. 107, No. GT12, Proc. Paper 16718, pp. 1677-1691.

Iwasaki, T. and Tatsuoka, F. (1977), "Dynamic Soil Properties with Emphasis on Comparison of Laboratory Tests with Field Measurements", *Proc. Sixth World Conf. on Earthquake Engg., New Delhi*, Vol. 1, pp. 153-158.

Jaky, J. (1944a) "Stress Distribution Under Rigid Footings" (In Hungarian), *Technika*.

Jaky, J. (1944b), "The Coefficient of Earth Pressure at Rest", *Journal of the Society of Hungarian Architects and Engineers*, pp. 355-358.

Jaky, J. (1948), "Pressure in Silos", *2nd ICSMFE*, Rotterdam, Vol. 1, pp. 103-107.

Janbu, N., Bjerrum, L. and Kjaernsli, B. (1956), "Veiledning ved Losning av Fundamenteringsoppgaver", *Norwegian Geotechnical Institute, Publication 16*, Oslo.

Johnson, S.M. and T.C. Kavanagh (1968), *The Design of Foundations for Buildings*, McGraw-Hill Book Company.

Jones, A. (1962), "Tables of Stresses in Three-Layer Elastic Systems", *HRB Bulletin 342*, pp. 176-214.

Jorden, E.E. (1977), "Settlement in Sand—Methods of Calculating and Factors Affecting", *Ground Engineering*, Vol. 10, No. 1.

Jumkis, A.R. (1967), *Soil Mechanics*, Affiliated East-West Press Pvt. Ltd., New Delhi.

Jurgenson, L. (1934), "The Application of Theories of Elasticity and Plasticity to Foundation Problems", *Contributions to Soil Mechanics, 1925-1940*, Boston Society of Civil Engineers.

Kaniraj, S.R. (1974), "Settlement of Pile Foundations and Drag Load on Piles", *Ph.D. Thesis*, Indian Institute of Science, Bangalore.

Kaniraj, S.R. and Ranganatham, B.V. (1974), "Settlement of Buried Loaded Areas in Normally Consolidated Clay", *Soils and Foundations*, Vol. 14, No. 2, pp. 95-103.

Kaniraj S.R. (1976), "Settlement of Buried Loaded Areas in Normally Consolidated Clay Deposits of Finite Thickness", *IGJ*, Vol. 6, No. 4, pp. 246-254.

Kaniraj, S.R. (1977), "Limiting of Immediate Settlement of Shallow Foundations", *IGJ*, Vol. 7, No. 3, pp. 235-247.

Kaniraj, S.R. and Ranganatham, B.V. (1977a), "Drag Load on Piles in Normally Consolidated Clay", *IGJ*, Vol. 7, No. 2, pp. 83-105.

Kaniraj, S.R. and Ranganatham, B.V. (1977b), "Limiting of Settlement of Shallow Foundations in Normally Consolidated Clay", *IGJ*, Vol. 7, No. 2, pp. 161-177.

Kaniraj, S.R. and Ranganatham, B.V. (1979), "Settlement of Piles and Pile Groups in Normally Consolidated Clay", *IGJ*, Vol. 9, No. 3, p. 279.

Kany, M. (1959), Berechnung von Flachengrundengen, W. Ernst, Berlin.

Karisson, R. and Viberg, L. (1967), "Ratio c/p' in Relation to Liquid Limit and Plasticity Index with Special Reference to Swedish Clays", *Proc. Geotech Conf.*, Oslo, Norway, Vol. 1, pp. 43-47.

Kenney, T.C. (1959), Discussion, *Proceedings ASCE*, Vol. 85, No. SM3, pp. 67-69.

Kishida, H. (1967), "Ultimate Bearing Capacity of Piles Driven into Loose Sand", *Soils and Foundations*, Vol. 7, No. 3, pp. 20-29.

Klein G.K. (1956), "Calculation of Non-homogeneous Distribution of Deformation and Other Mechanical Properties of Soils for Estimating Construction of Compressible Bases", *Sb Tr. No. 14, Gos. Izd. Lit. Stroit, i Arkh.*

Kondner, R.L. (1963), "Hyperbolic Stress-Strain Response; Cohesive Soils", *JSMFD, ASCE*, Vol. 89, SM 1, pp. 115-143.

Kozeny, J. (1933), Theorie and Berechnung der Brunnen, *Wasserkr Wasserwritsch*, Vol. 28, p. 104.

Krishna, J. and Jain O.P. (1966), *Plain and Reinforced Concrete*, Nem Chand and Bros, Roorkee.

Kul Bhushan and Haley, C.S. (1976), "Stress Distribution for Heavy Embedded Structures", *JGED, ASCE*, Vol. 102, No. 7, pp. 807-810.

Ladd, C.C. and Foot R. (1974), "New Design Procedure for Stability of Soft Clays", *JGED, ASCE*, Vol. 100, No. GT 7, pp. 763-786.

Lambe, T.W. and Whitman, R.V. (1979), *Soil Mechanics SI Version*, John Wiley and Sons.

Laursen, E.M. and Toch, A. (1956), "Scour Around Bridge Piers and Abutments", *Iowa Highway Research Board Bulletin*, No. 4.

Lee, I.K. (1962), "Bearing Capacity of Foundations with Particular Reference to the Melbourne Area", *Journal of Institution of Engineers, Australia*, Vol. 34, pp. 283-291.

Lee, K.L. and Singh, A. (1971), "Relative Density and Relative Compaction", *JSMFD, ASCE*, Vol. 97, No. SM 7, pp. 1049-1052.

Luscher, U. (1965), Discussion, *JSMFD, ASCE*, Vol. 91, No. SM 1, pp. 190-195.

Matlock, H. and Reese, L.C. (1961), "Foundation Analysis of Offshore Pile Supported Structures", *5th ICSMFE*, Paris, Vol. 2, pp. 91-97.

Matlock, H. and Reese, L.C. (1962), "General Solutions for Laterally Loaded Piles", *Transactions ASCE*, Vol. 127, Part 1, pp. 1220-1247.

McClelland, B. (1974), "Design of Deep Penetration Piles for Ocean Structures", *JGED ASCE*, Vol. 100, No. GT 7, 705-747.

McDonald, D.H. and Skempton, A.W. (1955), "A Survey of Comparisons between Calculated and Observed Settlements of Structures on Clay", *Institution of Civil Engineers*, London.

McNulty, J.F. (1956), "Thrust Loading on Piles", *JSMFD, ASCE*, Vol. 82, No. SM 4, paper 1081.

Meyerhof, G.G. (1951), "The Ultimate Bearing Capacity of Foundations", *Geotechnique*, Vol. 2, No. 4, pp. 301-331.

Meyerhof, G.G. (1953), "The Bearing Capacity of Foundations under Eccentric and Inclined Loads", *3rd ICSMFE*, Zurich, Vol. 1, p. 660.

Meyerhof, G.G. (1956), "Penetration Tests and Bearing Capacity of Cohesionless Soils", *JSMFD, ASCE*, Vol. 82, SM 1, pp. 1-19.

Meyerhof, G.G. (1957), "The Ultimate Bearing Capacity of Foundations on Slopes", *4th ICSMFE*, London, Vol. 1, pp. 384-386.

Meyerhof, G.G. (1959), "Compaction of Sands and Bearing Capacity of Piles", *JSMFD, ASCE*, Vol. 85, SM 6, pp. 1-29.

Meyerhof, G.G. (1963), "Some Recent Research on Bearing Capacity of Foundations", *CGJ*, Vol. 1, No. 1, pp. 16-26.

Meyerhof, G.G. (1965), "Shallow Foundations", *JSMFD, ASCE*, Vol. 91, SM 2, pp. 21-31.

Meyerhof, G.G. and J.D. Brown (1967), "Discussion: Bearing Capacity of Footings on Layered Clays", *JSMFD, ASCE*, Vol. 93, SM 5, Part 1, pp. 361-363.

Meyerhof, G.G. and Adams, J.I. (1968), "The Ultimate Uplift Capacity of Foundations", *CGJ*, Vol. 5, No. 4, pp. 225-244.

Meyerhof, G.G. (1974), General Report: Outside Europe, *Proc. Conf. on Penetration Testing*, Stockholm, Vol. 2, pp. 40-48.

Meyerhof, G.G. (1976), "Bearing Capacity and Settlement of Pile Foundations", *JGED, ASCE*, Vol. 102, No. GT 3, pp. 195-228.

Michigan State Highway Commission (1965), *A Performance Investigation of Pile Driving Hammers and Piles*, Lansing, Michigan, 338 pp.

Milovic, D.M. (1970), "Contraintes et deplacements dans une couche elastique d'epaisseur limitee, produits par une fondation circulaire", *Le Genie Civil*, T. 147, No. 5, pp. 281-285.

Milovic, D.M. and Tournier, J.P. (1971), "Stresses and Displacements Due to Rectangular Load on a Layer of Finite Thickness", *Soils and Foundations*, Vol. 11, No. 1, pp. 1-27.

Mikhejev, V.V. *et al.* (1961), "Foundation Design in the USSR", *5th ICSMFE*, Paris, Vol. 1, pp. 753-757.

Muki, R. (1961), "Asymmetric Problems of the Theory of Elasticity for a Semi-infinite Solid and a Thick Plate", *Progress in Solid Mechanics*, Vol. 1, North Holland Publishing Co., Amsterdam.

Newcomb, W.K. (1951), "Principles of Foundation Designs for Engines and Compressors", *Transactions ASME*, Vol. 73.

Newmark, N.M. (1942), "Influence Charts for Computation of Stresses in Elastic Foundations", *University of Illinois Experiment Station Bull. 338.*

Newmark, N.M. (1947), "Influence Charts for Computation of Vertical Displacements in Elastic Foundations", *Univ. of Illinois Eng. Expt. Station, Bulletin No. 367.*

Nishida, Y. (1966), "Vertical Stress and Vertical Deformation of Ground Under a Deep Circular Uniform Pressure in the Semi-infinite", *Proc. 1st Congress of International Society for Rock Mechanics*, Vol. 2, pp. 493-498.

Nordlund, R.L. (1963), "Bearing Capacity of Piles in Cohesionless Soils", *JSMFD, ASCE*, Vol. 98, SM 12, pp. 1291-1310.

Odemark, N. (1949), "Investigations as to the Elastic Properties According to the Theory of Elasticity", *Statens Vagunstitut*, Stockholm, Middleland 77.

Olsen, R.E. and Flaate, K.S. (1967), "Pile Driving Formulas for Friction Piles in Sands", *JSMFD, ASCE*, Vol. 93, SM 6, pp. 279-296.

Olson, R.E. (1977), "Consolidation under Time-dependent Loading", *JGED, ASCE*, Vol. 103, No. GT 1, pp. 55-60.

Osterberg, J.O. (1957), "Influence Values for Vertical Stresses in Semi-infinite Mass due to Embankment Loading", *4th ICSMFE*, London, Vol. 1, pp. 393-394.

Osterman, J. (1959), "Notes on Shearing Resistance of Soft Clays", *Acta Polytechnica Scandinavica*, No. 263.

Palmer, L.A. and Barber, E.S. (1940), "Soil Displacement under a Circular Loaded Area", *HRB*, Vol. 20, pp. 279-286; Discussion pp. 319-332.

Palmer, L.A. (1953), *Soil Mechanics and Earth Structures*, U.S. Navy, Bureau of Yards and Docks.

Pauw, A. (1953), "A Dynamic Analogy for Foundation-Soil System", *ASTM Special Technical Publication No. 156.*

Peck, R.B. (1943), "Earth Pressure Measurements in Open Cuts, Chicago Subway", *Transactions ASCE*, pp. 1008-1036.

Peck, R.B., Hanson, W.E. and Thornburn, W.H. (1974), *Foundation Engineering*, 2nd Edition, John Wiley and Sons.

Polshin, D.E. and Tokar, R.A. (1957), "Maximum Allowable Non-uniform Settlement of Structures", *4th ICSMFE*, London, Vol. 1, pp. 402-405.

Poulos, H.G. (1967a), "The Use of the Sector Method for Calculating Stresses and Displacements in an Elastic Mass", *Proc. 5th Aust-New Zealand Conference on Soil Mechanics and Foundation Engineering*, pp. 198-204.

Poulos, H.G. (1967b), "Stresses and Displacements in an Elastic Layer Underlain by a Rough Rigid Base", *Geotechnique*, Vol. 17, pp. 378-410.

Poulos, H.G. (1968), "The Behaviour of a Rigid Circular Plate Resting on a Finite Elastic Layer", *Civil Engineering Transactions, Institution of Engineers*, Australia, Vol. CE 10, pp. 213-219.

Poulos, H.G. and Davis, E.H. (1974), *Elastic Solutions for Soil and Rock Mechanics*, John Wiley and Sons, Inc.

Poulos, H.G. and Davis, E.H. (1980), *Pile Foundation Analysis and Design*, John Wiley and Sons.

Prakash, S. (1981), *Soil Dynamics*, McGraw-Hill Book Company.

Prandtl L. (1920), "Uber die Harte Plastischer Korper", *Nachr. Kgl. Gas Wiss. Gottingen Math. Phys. Kl.*

Proctor, E.R. (1933), "Design and Construction of Rolled Earth Dams", *Engineering News Record*, pp. 245-284, 286-289, 348-351, 372-376.

Ramasamy, G., Rao, A.S.R. and Prakash, C. (1982), "Effect of Embedment on Settlement of Footings on Sand", *IGJ*, Vol. 12, No. 4, pp. 112-131.

Rankine, W.J.M. (1857), "On the Stability of Loose Earth", *Philosophical Transactions of The Royal Society*, London, Vol. 147,

Ranganatham, B.V. and Kaniraj, S.R. (1978), "Settlement of Model Pile Foundations in Sand", *IGJ*, Vol. 8, No. 1, pp. 1-26.

Ranganatham, B.V. and Kaniraj, S.R. (1983), "Experiments on Pile Groups in Sand", *7th ARC*, Haifa.

Reddy, A.S. and R.J. Srinivasan (1967), "Bearing Capacity of Footings on Layered Clays", *JSMFD, ASCE*, Vol. 93, SM 2, pp. 83-99.

Reese, L.C. and Matlock, H. (1956), "Non-dimensional Solutions for Laterally Loaded Piles with Soil Modulus Assumed Proportional to Depth", *Proceedings 8th Texas Conf. on SMFE, Special Publication 29*, Bureau of Engineering Research, Univ. of Texas, Austin.

Reissner, H. (1924), Zum Erddruckproblem, *Proc. 1st. Int. Conf. App. Mech.*, Delft.

Reissner, E. and Sagoci, H.F. (1944), "Forced Torsional Oscillations of an Elastic Half Space", *Journal of Applied Physics*, Vol. 15, pp. 652-662.

Richart, F.E. (Jr.) (1962), "Foundation Vibration", *Transactions ASCE*, Vol. 127, Part I, pp. 863-898.

Richart, F.E. (Jr.), Hall J.R. (Jr.) and Woods, R.D. (1970), *Vibration of Soils and Foundations*, Prentice-Hall, Englewood Cliffs, New Jersey, U.S.A.

Rowe, P.W. (1952), "Anchored Sheet Pile Walls", *Proceedings of Institution of Civil Engineers*, Vol. 1, Part 1, pp. 27-70.

Rowe, P.W. (1957), "Sheet Pile Walls in Clay", *Proceedings of Institution of Civil Engineers*, Vol. 7, pp. 629-654.

Schiffman, R.L. and Aggarwala, D.B. (1961), "Stresses and Displacements Produced in a Semi-infinite Elastic Solid by a Rigid Elliptical Footing", *5th ICSMFE*, Paris, Vol. 1, pp. 795-801.

Schleicher, F. (1926), "Zur Theorie des Baugrundes", *Bauingenieur*, Vol. 7, pp. 931-935, 949-952.

Schmertman, J.M. (1955), "The Undisturbed Consolidation of Clay", *Transactions ASCE*, Vol. 120, pp. 1201.

Schmertmann, J.H. (1970), "Static Cone to Compute Static Settlement Over Sand", *JSMFD, ASCE*, Vol. 96, SM 3, pp. 1011-1043.

Schmertmann, J.H. (1975), "The Measurement of In-situ Shear Strength", *Speciality Conf. on In-situ Measurement of Soil Properties*, Vol. 2, pp. 57-138.

Scott, R.F. (1963), *Principles of Soil Mechanics*, Addison-Wesley.

Scott, R.F. and Schoustra, J.J. (1968), *Soil Mechanics and Engineering*, McGraw-Hill Book Co.

Scott, C.R. (1980), *An Introduction to Soil Mechanics and Foundations*, Third edition, Applied Science Publishers Ltd., London.

Sethi, H.K.L. (1960), "River Training and Control for Bridges", *Technical Paper No. 335*, Research Designs and Standards Organisation, Ministry of Railways, Lucknow.

Shields, D.H., Scott, J.D., Bauer, J.E., Deschenes, J.H. and Barsvary, A.K. (1977), "Bearing Capacity of Foundations Near Slopes", *9th ICSMFE*, Tokyo, Vol. 1, pp. 715-720.

Simons, N.E. (1975), "Normally Consolidated and Lightly Over Consolidated Cohesive Materials", *Settlement of Structures*, Conference Organised by British Geotechnical Society, Pentech Press, London, pp. 500-530.

Simons, N.E. and Menzies, B.K. (1975), *A Short Course in Foundation Engineering*, Butterworths.

Sivaram, B. and Swamee, P. (1977), "A Computational Method for Consolidation Coefficient", *Soils and Foundations*, Vol. 17, No. 2, pp. 48-52.

Skempton, A.W. (1951), "The Bearing Capacity of Clays", *Building Research Congress*, London, Institution of Civil Engineers, Division I: 180.

Skempton, A.W. (1953a), "The Colloidal Activity of Clays", *3rd ICSMFE*, Zurich, Vol. 1, p. 57.

Skempton, A.W. (1953b), "Discussion: Piles and Pile Foundations, Settlement of Pile Foundations", *3rd ICSMFE*, Zurich, Vol. 3, p. 172.

Skempton, A.W. (1954), "The Pore Pressure Coefficients A and B", *Geotechnique*, Vol. 4, pp. 143-147.

Skempton, A.W. (1957), Discussion: The Planning and Design of New Hong Kong Airport, *Proc. Institution of Civil Engineers*, Vol. 7, pp. 305-307.

Skempton, A.W. and Bjerrum, L. (1957), "A Contribution to the Settlement Analysis of Foundations on Clay", *Geotechnique*, Vol. 7, p. 168.

Skempton, A.W. (1964), "Long-term Stability of Clay Slopes", *Geotechnique*, Vol. 14. pp. 77-102.

Skopek, J. (1961), "The Influence of Foundation Depth on Stress Distribution", *5th ICSMFE*, Paris, Vol. 1, p. 815.

Smith, E.A.L. (1960), "Pile Driving Analysis by the Wave Equation", *JSMFD, ASCE*, Vol. 86, SM 4, pp. 35-61.

Sneddon, I.N. (1946), "Boussinesq's Problem for a Flat-ended Cylinder", *Proceedings of Cambridge Philosophical Society*, Vol. 42, Part 1, pp. 29-39.

Sorensen, T. and Hansen, B. (1957), "Pile Driving Formulae, an Investigation Based on Dimensional Considerations and a Statistical Analysis", *5th ICSMFE*, Paris, Vol. 2, pp. 61-65.

Sovinc, I. (1969), "Displacements and Inclinations of Rigid Footings Resting on a Limited Elastic Layer of Uniform Thickness", *7th ICSMFE*, Mexico City, Vol. 1, pp. 385-389.

Sowers, G.F. (1962), "Shallow Foundations", Chapter 6, *Foundation Engineering*, edited by Leonards, G.A., McGraw-Hill.

Spangler, M.G. (1973), *Soil Engineering*, 2nd edition, International Text Book Company, Scranton, Pennsylvania.

Srinivasulu, P. and Vaidyanathan, C.V. (1976), *Handbook of Machine Foundations*, Tata McGraw-Hill Publishing Company Ltd., New Delhi.

Stamatopoulos, C. (1959), "Linearly Variable Load Distribution on a Rectangular Foundation", *Proceedings ASCE*, Dec., SM, p. 137.

Steinbrenner, W. (1934), "Tafeln zur setzungberechnung", *Die Strasse*, Vol. 1, p. 121.

Steinbrenner, W. (1936), "Bodenmechanik und neuzeitlicher Strassenbau", *Symposium by 24 authors*, Volk und Reich Verlag, Berlin.

Su, H.L. (1958), "Procedures for Rapid Consolidation Test", *JSMFD, ASCE*, Vol. 95, Proc. Paper 1729.

Sutherland, H.B. (1975), "Granular Materials", *Settlement of Structures*, Conference Organised by British Geotechnical Society, Pentech Press, London, pp. 473-499.

Szechy, K. and Varga, L. (1978), *Foundation Engineering*, Akademiai Kiado, Budapest.

Taylor, D.W, (1942), "Research on Consolidation of Clays", *Massachusetts Institute of Technology, Publication No. 82.*

Taylor, D.W. (1948), *Fundamentals of Soil Mechanics*, Wiley and Sons, New York.

Teng, W.C. (1962), *Foundation Design*, Prentice-Hall, Inc. Englewood Cliffs, New Jersey.

Terzaghi, K. (1925), *Erdbaumechanik auf Boudenphysikalischer Grundlage*, Deuticke, Vienna.

Terzaghi, K. (1935), "Relation Between Soil Mechanics and Foundation Engineering: Presidential Address", *Ist ICSMFE*, Cambridge, Massachusetts, Vol. 3, pp. 13-18.

Terzaghi, K. (1943), *Theoretical Soil Mechanics*, Wiley, New York.

Terzaghi, K. and Peck, R.B. (1948), *Soil Mechanics in Engineering Practice*, 1st edn., Wiley, New York.

Thenn de Barros (1966), "Deflection Factor Charts for Two- and Three-Layer Elastic Systems", *HRR*, No. 145, pp. 83-108.

Tomlinson, M.J. (1970), "Some Effects of Pile Driving on Skin Friction", *Conference on Behaviour of Piles*, Institution of Civil Engineers, London, pp. 59-66.

Tomlinson, M.J. (1977), *Pile Design and Construction Practice*, A Viewpoint Publication.

Tomlinson, M.J. (1980), *Foundation Design and Construction*, Pitman Publishing Ltd., London.

Tschebotarioff, G.P. (1949), "Large Scale Earth Pressure Tests with Model Flexible Bulkheads", *Final Report to U.S. Navy, Bureau of Yards and Docks*, Princeton University, Princeton, N.J.

Tschebotarioff, G.P. (1951), *Soil Mechanics, Foundations and Earth Structures*, McGraw-Hill Book Co., New York.

Tschebotarioff, G.P. (1953), "Performance Records of Engine Foundations", *ASTM Special Technical Publication No. 156.*

Tystovich, N.A. (1951), *Mechanika gruntov*, Moscow.

Tystovich, N.A. (1968), "To the Problem of the Effect on Natural Compaction of Clayey Soils on the Magnitude of the Active Zone of Compression", *Donau-Europaische Konf. Generalberichte*, p. 23.

U.S. Bureau of Reclamation, Department of Interior, *Design of Small Dams*, U.S. Government Printing Office, Washington DC, 1961.

U.S. Department of the Navy, Naval Facilities Engineering Command, *Design Manual—Soil Mechanics, Foundations and Earth Structures*, NAVFAC DM-7, Washington DC, 1971.

Ueshita, K. and Meyerhof, G.G. (1967), "Deflection of Multilayer Soil Systems", *JSMFD, ASCE*, Vol. 93, No. SM 5, pp. 257-282.

Ueshita, K. and Meyerhof, G.G. (1968), "Surface Displacement of an Elastic Layer under Uniformly Distributed Loads", *HRR*, No. 228, pp. 1-10.

Van Veele, A.F. (1964), "Negative Skin Friction on Pile Foundations in Holland", *Proceedings of the Symposium on Bearing Capacity of Piles*, Roorkee, Vol. 1, pp. 1-10.

Vesic, A.S. (1963), Discussion—Session III, *Proceedings of the First International Conference on Structural Design of Asphalt Pavements*, University of Michigan, pp. 283-290.

Vesic, A.S. (1967), "A Study of Bearing Capacity of Deep Foundations", *Final Report, Project B-189*, School of Civil Engineering, Georgia Institute of Technology, USA.

Vesic, A.S. (1974), "Bearing Capacity of Shallow Foundation", Chapter 3, *Handbook of*

Foundation Engineering, Winterkorn, H.F. and Fang, H. (Eds), Von Nostrand, New York.

Vijayvergiya, V.N. and Focht, J.A. (1972), "A New Way to Predict Capacity of Piles in Clay", *Proceedings of the Offshore Technology Conference*, Dallas, Vol. 2, pp. 865-871.

Wagner, A.A. (1957), "The Use of Unified Soil Classification System by the Bureau of Reclamation", *4th ICSMFE*, London, Vol. I, p. 125.

Westergaard, H.M. (1938), "A Problem of Elasticity Suggested by a Problem in Soil Mechanics: Soft Materials Reinforced by Numerous Strong Horizontal Sheets", *Contributions to the Mechanics of Solids, Stephen Timoshenko 60th Anniversary Volume*, The Macmillan Co., N.Y., pp. 268-277.

Whitaker, T. (1970), *The Design of Pile Foundations*, Oxford, Pergamon.

Whitman, R.V. and Richart, F.E. (1967), "Design Procedures for Dynamically Loaded Foundations", *JSMFD, ASCE*, Vol. 93, No. SM 6, pp. 169-193.

Wilun, Z. and Starzewski, K. (1975), *Soil Mechanics in Foundation Engineering*, Vol. 2, *Theory and Practice*, Second Edition, Surrey University Press, London.

Wroth, C.P. (1975), "In-situ Measurement of Initial Stresses and Deformation Characteristics", *Proceedings of Speciality Conference on Analysis and Design in Geotechnical Engineering*, ASCE, Univ. of Texas, Vol. 2, pp. 181-230.

Yegorov, K.E. and Nitchiporovich, A.A. (1961), "Research on the Deflection of Foundations", *5th ICSMFE*, Paris, Vol. 1, pp. 861-866.

INDIAN STANDARD CODES ON SOIL MECHANICS, FOUNDATION ENGINEERING AND OTHER RELATED AREAS IN GEOTECHNICAL ENGINEERING

The following is a list of Indian Standard Codes on soil mechanics, foundation engineering and other related areas in geotechnical engineering. The codes are listed under seven major categories. These standards are available for sale from the Bureau of Indian Standards, New Delhi and its regional branches and inspection offices at Ahmedabad, Bangalore, Bhopal, Bhubaneshwar, Bombay, Calcutta, Chandigarh, Hyderabad, Jaipur, Kanpur, Madras, Patna, Pune and Trivandrum. The list is adapted from *The Indian Geo-guide, 1986-87*. published by the Indian Geotechnical Society, New Delhi.

Abbreviation COP stands for Code of Practice.

1. GENERAL

1.1 Terminology

IS: 2809-1972	Glossary of terms and symbols relating to soil engineering
IS: 2810-1979	Glossary of terms relating to soil dynamics
IS: 4410	Glossary of Terms relating to River Valley Projects: Part VII-1968 Engineering Geology Part XI-Section 6 Ground Water Part XX-1968 Tunnels
IS: 4988	Glossary of terms and classification of earth moving machinery: Part I-1969 General terms Part II-1968 Dozers Part III-1968 Motor and towed scrappers Part IV-1968 Excavators Part V-1968 Motor graders
IS: 6427-1972	Glossary of terms relating to pile driving equipment

IS: 7314-1974 Glossary of terms relating to port and harbour engineering
IS: 7422 Symbols and abbreviations for use in geological maps, sections and subsurface exploratory logs:
Part I-1974 Abbreviations
Part II-1974 Igneous Rocks
Part III-1974 Sedimentary Rocks
Part IV-1985 Metamorphic Rocks

2. SITE INVESTIGATION

2.1 General

IS: 1892-1979 COP for subsurface investigations of foundations
IS: 4453-1980 Subsurface exploration by pits, trenches, drafts and shafts
IS: 5510-1969 Guide for soil surveys for river valley projects
IS: 6955-1973 COP for subsurface exploration for earth and rockfill dams
IS: 10042-1981 COP for site investigations for foundation in gravel, boulder deposits
IS: 10060-1981 COP for subsurface investigations for power house sites
IS: 10290-1982 COP for photogeological interpretation and mapping river valley project site

2.2 Probings (Soundings)

IS: 4968 Subsurface sounding:
Part I-1976 Dynamic method using 50 mm cone without bentonite slurry
Part II-1976 Dynamic method using cone and bentonite slurry
Part III-1976 Static cone penetration test
IS: 10589-1983 Equipment for determination of subsurface sounding of soils

2.3 Boring Techniques and Equipment

IS: 4464-1967 COP for presentation of drilling information and core description in foundation
IS: 5313-1980 Guide for core drilling observations
IS: 6926-1973 COP for diamond core drilling for site investigation for river valley projects
IS: 10442-1983 Earth augers

2.4 Sampling

IS: 2132-1986 COP for thin walled tube sampling
IS: 8763-1978 Undisturbed sampling of sands and sandy soils
IS: 9640-1980 Split spoon sampler
IS: 10108-1982 COP for sampling by thin wall sampler with stationary piston

2.5 Measurement of Field Conditions

IS: 6935-1973 Determination of water level in a bore hole.

2.6 Field Testing

IS: 1888-1982 Load test
IS: 2131-1981 SPT (Standard Penetration Test)
IS: 2720 Part 32-1970 North Dakota cone test
IS: 4434-1978 COP for in-situ vane shear test

IS: 5529 COP for in-situ permeability tests:
Part I-1969 Test in overburden
Part II-1973 Test in bedrocks
IS: 9214-1979 Determination of modulus of subgrade reaction in the field

3. SOIL PROPERTIES: LABORATORY AND IN-SITU DETERMINATIONS

3.1 Classification and Description of Soils

IS: 1498-1970 Classification and identification
IS: 2720 Tests for soil:
Part 1-1983 Preparation of dry soil samples
Part 5-1985 Determination of liquid and plastic limit
Part 6-1972 Determination of shrinkage factors
Part 20-1966 Determination of linear shrinkage
IS: 9259-1979 Liquid limit apparatus
IS: 10077-1982 Equipment for determination of shrinkage factors
IS: 11196-1985 Equipment for determination of liquid limit-cone penetration method

3.2 Physico-Chemical Properties

IS: 2720 Tests for soil:
Part 24-1976 Determination of cation exchange capacity
Part 26-1973 Determination of pH value

3.3 Composition, Structure, Density, and Water Content

IS: 2720 Tests for soils:
Part 2-1973 Water content
Part 3-Section 1-1980 Specific gravity—fine grained soils
Section 2-1980 Specific gravity—fine, medium and coarse grained soils
Part 4-1985 Grain size analysis
Part 14-1983 Determination of density index (relative density of cohesionless soils)
Part 18-1964 Field moisture equivalent
Part 19-1964 Centrifuge moisture equivalent
Part 21-1977 Determination of organic matter
Part 23-1976 Determination of calcium carbonate
Part 25-1982 Determination of silica-sesquioxide ratio
Part 27-1977 Determination of total soluble sulphates
Part 28-1974 Dry density in place by the sand replacement method
Part 29-1975 Dry density in place by the core cutter method
Part 33-1971 Density in place by the ring and water replacement method
Part 34-1972 Density in place by rubber balloon method
Part 37-1976 Sand equivalent values of soils and fine aggregates
IS: 10837-1984 Moulds for determination of relative density and its accessories

3.4 Hydraulic Properties

IS: 2720 Tests for soils:
Part 17-1986 Determination of permeability
Part 36-1975 Determination of permeability of granular soils (constant head)

3.5 Compressibility and Swelling

IS: 2720 Tests for soils:
- Part 15-1986 Consolidation properties
- Part 40-1977 Free swell index of soils
- Part 41-1977 Swelling pressure of soils

IS: 11550-1985 COP for field instrumentation of swelling pressure in expansive soils

3.6 Shear Deformation and Strength Properties

IS: 2720 Tests for soils:
- Part 10-1973 Unconfined compressive strength
- Part 11-1971 Shear strength parameters (UU without pore water pressure measurement)
- Part 12-1981 Shear strength parameters of soil from consolidated undrained test with measurement of pore water pressure
- Part 13-1986 Direct shear test
- Part 16-1979 Laboratory determination of CBR
- Part 30-1980 Laboratory vane shear test
- Part 31-1969 Field determination of California Bearing Ratio
- Part 35-1974 Measurement of negative pore water pressure
- Part 39-Sec. 1-1977 Direct shear test for soils containing gravel: laboratory test
  Sec. 2-1979 Direct shear test for soils containing gravel: in-situ test

IS: 4332 Tests for stabilized soils:
- Part V-1970 Unconfined compressive strength of stabilized soils
- Part VI-1972 Flexural strength of soil-cement using simple beam with third-point loading

IS: 9669-1980 CBR mould and its accessories

IS: 11229-1985 Shear box for testing of soils

3.7 Dynamic Properties

IS: 5249-1977 Test for the determination of dynamic properties of soil

3.8 Compactibility

IS: 2720 Tests for soils:
- Part 7-1980 Water content-dry density relation using light compaction
- Part 8-1983 Water content-dry density relation using heavy compaction
- Part 9-1971 Dry density-moisture content relation by constant weight of soil method
- Part 38-1976 Compaction control test

IS: 9198-1979 Compaction rammer for soil testing

IS: 10084-1982 Compaction mould assembly for light and heavy compaction

IS: 10379-1982 COP for field control of moisture and compaction of soils for embankment and sub-grade

3.9 Properties of Soil-Additive Mixtures

IS: 4332 Tests for stabilized soils:
- Part I-1967 Sampling and preparation of stabilized soils
- Part II-1967 Moisture content of stabilized soil mixtures
- Part III-1967 Moisture content-dry density relation
- Part IV-1968 Wetting and drying and freezing and thawing tests for compacted soil-cement mixtures
- Part V-1970 Unconfined compressive strength
- Part VI-1972 Flexural strength using simple beam with third point loading

Hidden page

Hidden page

Hidden page

Hidden page

IS: 9401 Method of measurement of works in river valley projects (dams and appurtenant structures):
Part 3-1980 Grouting

7.4 Earthworks and Rock Excavations Processing and Transportation

IS: 1200 Measurement of building and civil engineering works:
Part 1-1974 Earthwork
IS: 2431-1963 Steel wheel barrows single wheel type
IS: 3764-1966 Safety code for excavation work
IS: 4081-1967 Safety code for blasting and related drilling operations
IS: 4184-1967 Steel wheel barrows with two wheels
IS: 9401 Method of measurement of works in river valley projects (dams and appurtenant structures):
Part 1–1982 Excavation of foundation

7.5 Soil Stabilization and Erosion Control

IS: 1725-1982 Soil based blocks used in general construction

7.6 Piles, Pile Driving and Anchors

IS: 2110-1980 COP for in-situ construction of walls, in building with soil-cement
IS: 7113-1973 COP for soil cement lining of canals
IS: 1200-1977 Method of measurement of building and civil engineering works:
Part 23-1977 Piling
IS: 5121-1969 Safety code for piling and other deep foundations
IS: 6426-1972 Pile driving hammer
IS: 6428-1972 Pile frame
IS: 10270-1982 Design and construction of prestressed rock anchors

7.7 Construction of Caissons and Deep Piers

IS: 1200 Measurement of building and civil engineering works:
Part 24-1983 Well foundations

INDEX

Hidden page

Hidden page

Design Aids in Soil Mechanics and Foundation Engineering

The book caters to the interests and needs of designers, teachers and students of civil engineering. It provides the designers with specific design procedures and the relevant background material to understand the theory and methodology behind the procedures, their limitations and their relevance to the problem on hand. For teachers, this is a good resource book to teach more than one course in geotechnical engineering, both at the undergraduate and postgraduate levels. The students will find the book a good reference for several courses in geotechnical engineering and in their future professional career.

About one-fourth of the book is devoted to principles of soil mechanics. This will aquaint the reader with the engineering properties of soils, their evaluation and selection for the solution of the problem on hand. The remaining part of the book, on soil engineering, covers all important problems typically met with in civil engineering practice. Applications of procedures are illustrated with numerous solved examples. Instances where the designer must use his own judgement are also brought out. A useful and exhaustive list of Indian Standard Codes on soil mechanics, foundation engineering and other related areas in geotechnical engineering is given at the end of the book.

Shenbaga R Kaniraj is presently Professor, Department of Civil Engineering Indian Institute of Technology, Delhi. He graduated in Civil Engineering in 1967 from PSG College of Technology, Coimbatore, then affiliated to the Madras University. He obtained an ME degree in Soil Mechanics and Foundation Engineering from the Indian Institute of Science, Bangalore, in 1969. He was awarded a Ph D degree in 1975 by the same institute for his research work on "Settlement of Pile Foundations and Drag Load on Piles" In 1983 he obtained an M Tech degree in Management and Systems at the Indian Institute of Technology, Delhi.

Dr Kaniraj worked at the Birla Institute of Science and Technology, Pilani, during 1974-75. He joined the Indian Institute of Technology, Delhi, in 1975. During 1983-84 he worked at the Military Technical College, Baghdad, Iraq. In 1987 he carried out research on Reinforced Soil and Geotextiles at the University of Oxford, UK on an Indo-British Technical Cooperation Award. From December 1989 to April 1991, he worked at the University of Calgary, Canada, on a visiting assignment. He has published several papers in national and international journals and conferences. He was the editor of the *IGS Newsletter* during 1986-87 and earlier was a co-editor of the *Indian Geotechnical Journal*.

Dr Kaniraj is an active consultant in geotechnical engineering, and a popular lecturer.

Tata McGraw-Hill
Publishing Company Limited
7 West Patel Nagar, New Delhi 110 008
Visit our website at : www.tatamcgrawhill.com